DYNA

Journal of the Facultad de Minas, Universidad Nacional de Colombia - Medellin Campus

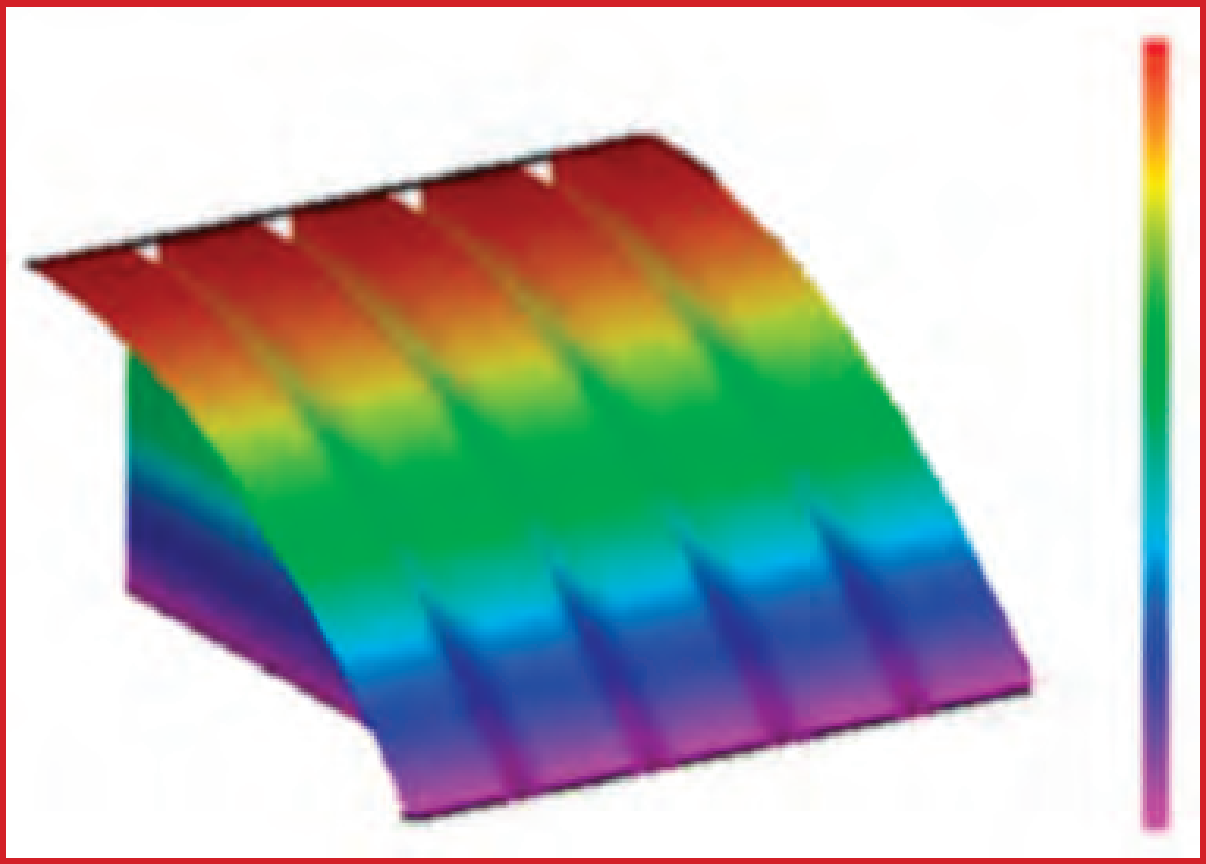

DYNA 83 (196), April, 2016 - ISSN 0012-7353
Tarifa Postal Reducida No. 2014-287 4-72
La Red Postal de Colombia, Vence 31 de Dic. 2016.

UNIVERSIDAD NACIONAL DE COLOMBIA
SEDE MEDELLÍN
FACULTAD DE MINAS

UNIVERSIDAD NACIONAL DE COLOMBIA
SEDE MEDELLÍN
FACULTAD DE MINAS

DYNA
http://dyna.medellin.unal.edu.co/

DYNA is an international journal published by the Facultad de Minas, Universidad Nacional de Colombia, Medellín Campus since 1933. DYNA publishes peer-reviewed scientific articles covering all aspects of engineering. Our objective is the dissemination of original, useful and relevant research presenting new knowledge about theoretical or practical aspects of methodologies and methods used in engineering or leading to improvements in professional practices. All conclusions presented in the articles must be based on the current state-of-the-art and supported by a rigorous analysis and a balanced appraisal. The journal publishes scientific and technological research articles, review articles and case studies.

DYNA publishes articles in the following areas:

Organizational Engineering
Civil Engineering
Materials and Mines Engineering
Geosciences and the Environment
Systems and Informatics
Chemistry and Petroleum
Mechatronics
Bio-engineering
Other areas related to engineering

Publication Information

DYNA (ISSN 0012-73533, printed; 2346-2183, online) is published by the Facultad de Minas, Universidad Nacional de Colombia, with a bimonthly periodicity (February, April, June, August, October, and December). Circulation License Resolution 000584 de 1976 from the Ministry of the Government.

Contact information
Web page: http://dyna.unalmed.edu.co
E-mail: dyna@unal.edu.co
Mail address: Revista DYNA
Facultad de Minas Universidad Nacional de Colombia - Medellín Campus
Carrera 80 No. 65-223 Bloque M9 - Of.:107
Telephone: (574) 4255068 Fax: (574) 4255343
Medellín - Colombia

© Copyright 2016. Universidad Nacional de Colombia
The complete or partial reproduction of texts with educational ends is permitted, granted that the source is duly cited. Unless indicated otherwise.

Notice
All statements, methods, instructions and ideas are only responsibility of the authors and not necessarily represent the view of the Universidad Nacional de Colombia. The publisher does not accept responsibility for any injury and/or damage for the use of the content of this journal.
The concepts and opinions expressed in the articles are the exclusive responsibility of the authors.

Institutional Exchange Request
DYNA may be requested as an institutional exchange through the e-mail canjebib_med@unal.edu.co or to the postal address:

Biblioteca Central "Efe Gómez"
Universidad Nacional de Colombia, Sede Medellín
Calle 59A No 63-20
Teléfono: (57+4) 430 97 86
Medellín - Colombia

Indexing and Databases

DYNA is admitted in:

The National System of Indexation and Homologation of Specialized Journals CT+I-PUBLINDEX, Category A1

Science Citation Index Expanded
Web of Science - WoS, Thomson Reuters
Journal Citation Reports - JCR
SCImago Journal & Country Rank - SJR
Science Direct
SCOPUS
Chemical Abstract - CAS
Scientific Electronic Library on Line - SciELO
GEOREF
PERIÓDICA Data Base
Latindex
Actualidad Iberoaméricana
RedALyC - Scientific Information System
Directory of Open Acces Journals - DOAJ
PASCAL
CAPES
UN Digital Library - SINAB
CAPES
EBSCO Host Research Databases

Publisher's Office
Juan David Velásquez Henao, Director
Mónica del Pilar Rada T., Editorial Coordinator
Catalina Cardona A., Editorial Assistant
Amilkar Álvarez C., Diagrammer
Byron Llano V., Editorial Assistant
Landsoft S.A., IT

Reduced Postal Fee
Tarifa Postal Reducida # 2014-287 4-72. *La Red Postal de Colombia,* expires Dec. 31st, 2016

UNIVERSIDAD NACIONAL DE COLOMBIA
SEDE MEDELLÍN
FACULTAD DE MINAS

DYNA

UNIVERSIDAD NACIONAL DE COLOMBIA

SEDE MEDELLÍN

FACULTAD DE MINAS

UNIVERSIDAD NACIONAL DE COLOMBIA
SEDE MEDELLÍN
FACULTAD DE MINAS

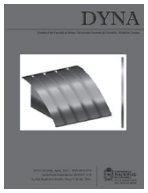

DYNA
http://dyna.medellin.unal.edu.co/

COUNCIL OF THE FACULTAD DE MINAS

Dean
Pedro Nel Benjumea Hernández PhD

Vice-Dean
Ernesto Pérez González, PhD

Vice-Dean of Research and Extension
Santiago Arango Aramburo, PhD

Director of University Services
Carlos Alberto Graciano, PhD

Academic Secretary
Francisco Javier Díaz Serna, PhD

Representative of the Curricular Area Directors
Carlos Jaime Franco Cardona, PhD

Representative of the Curricular Area Directors
Eliana Isabel Arango Zuluaga, PhD

Representative of the Basic Units of Academic-Administrative Management
Rosa Elvira Correa Gutiérrez, PhD

Representative of the Basic Units of Academic-Administrative Management
Rafael Esteban Ribadeneira Paz, PhD

Professor Representative
Luis Hernán Sánchez Arredondo, MSc

Delegate of the University Council
León Restrepo Mejía, PhD

Student representative (alternate) undergraduate at the Faculty Council
Sergio Esteban Ospina Rendón

FACULTY EDITORIAL BOARD

Dean
Pedro Nel Benjumea Hernández, PhD

Vice-Dean of Research and Extension
Santiago Arango Aramburo, PhD

Members
Oscar Jaime Restrepo Baena, PhD
Juan David Velásquez Henao, PhD
Jaime Aguirre Cardona, PhD
Mónica del Pilar Rada Tobón, MSc

JOURNAL EDITORIAL BOARD

Editor-in-Chief
Juan David Velásquez Henao, PhD
Universidad Nacional de Colombia, Colombia

Editors
George Barbastathis, PhD
Massachusetts Institute of Technology, USA

Tim A. Osswald, PhD
University of Wisconsin, USA

Juan De Pablo, PhD
University of Wisconsin, USA

Hans Christian Öttinger, PhD
Swiss Federal Institute of Technology (ETH), Switzerland

Patrick D. Anderson, PhD
Eindhoven University of Technology, the Netherlands

Igor Emri, PhD
Associate Professor, University of Ljubljana, Slovenia

Dietmar Drummer, PhD
Institute of Polymer Technology University Erlangen-Nürnberg, Germany

Ting-Chung Poon, PhD
Virginia Polytechnic Institute and State University, USA

Pierre Boulanger, PhD
University of Alberta, Canadá

Jordi Payá Bernabeu, Ph.D.
Instituto de Ciencia y Tecnología del Hormigón (ICITECH)
Universitat Politècnica de València, España

Javier Belzunce Varela, Ph.D.
Universidad de Oviedo, España

Luis Gonzaga Santos Sobral, PhD
Centro de Tecnología Mineral - CETEM, Brasil

Agustín Bueno, PhD
Universidad de Alicante, España

Henrique Lorenzo Cimadevila, PhD
Universidad de Vigo, España

Mauricio Trujillo, PhD
Universidad Nacional Autónoma de México, México

Carlos Palacio, PhD
Universidad de Antioquia, Colombia

Jorge Garcia-Sucerquia, PhD
Universidad Nacional de Colombia, Colombia

Juan Pablo Hernández, PhD
Universidad Nacional de Colombia, Colombia

John Willian Branch Bedoya, PhD
Universidad Nacional de Colombia, Colombia

Enrique Posada, Msc
INDISA S.A, Colombia

Oscar Jaime Restrepo Baena, PhD
Universidad Nacional de Colombia, Colombia

Moisés Oswaldo Bustamante Rúa, PhD
Universidad Nacional de Colombia, Colombia

Hernán Darío Álvarez, PhD
Universidad Nacional de Colombia, Colombia

Jaime Aguirre Cardona, PhD
Universidad Nacional de Colombia, Colombia

UNIVERSIDAD NACIONAL DE COLOMBIA
SEDE MEDELLÍN
FACULTAD DE MINAS

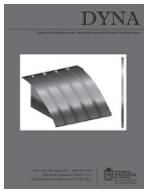

DYNA
http://dyna.medellin.unal.edu.co/

DYNA 83 (199), April, 2016. Medellín. ISSN 0012-7353 Printed, ISSN 2346-2183 Online

CONTENTS

Variation in risk category in methods of calculation of the modified fire load density 9
Cristina Maria Paulo Cadete-Pires, Rui António de Carvalho-Veiga & Maria Isabel Simões-Miguel

Application of the Delphi Method for the inclusion of externalities in occupational safety and health analysis 14
Delfina Ramos, Pedro Arezes & Paulo Afonso

Occupational risk assessment at Olive Oil Mills: Limitations and new perspectives 21
Matilde A. Rodrigues, Juan C. Rubio-Romero, Pedro Arezes & Manuel Soriano-Serrano

Absenteeism and presenteeism costs from occupational accidents with WRMSDs in a Portuguese hospital 27
Maria Emília Queiroz-Lima & Florentino Serranheira

Identification of areas of intervention for public safety policies using multiple correspondence analysis 31
Jesús Antonio Carrillo-Castrillo, Juan Carlos Rubio-Romero, José Guadix & Luis Onieva

A qualitative analysis on occupational health and safety conditions at small construction projects in the Brazilian construction sector 39
Haroldo Pereira Gomes, Pedro Miguel Ferreira Martins Arezes & Luiz Carlos Fadel de Vasconcellos

Emerging risk in the construction industry: Recommendations for managing exposure to nanomaterials 48
Beatriz María Díaz-Soler, María Dolores Martínez-Aires & Mónica López-Alonso

Differences in muscular activity between obese and non-obese workers during manual lifting 55
Ana Colim, Pedro Arezes, Paulo Flores & Ana Cristina Braga

Impact of a workplace exercise program on neck and shoulder segments in office workers 63
Mariana Machado-Matos & Pedro Miguel Arezes

Occurrence of a skarn-type mineralogy found in Ciénaga Marbles, located in the NW foothills of the Santa Marta Massif (Colombia) 69
Oscar Mauricio Castellanos-Alarcón, Carlos Alberto Ríos-Reyes & Luis Carlos Mantilla-Figueroa

Decontamination of industrial textile wastewater using photocatalysis 80
José Herney Ramírez-Franco & Hugo Ricardo Zea-Ramírez

Nutritional composition of meals at work and its relationship with manufacturing workers' anthropometric profile and energy expenditure 86
Eliana Aparecida Queiroz Bortolozo, Luiz Alberto Pilatti, Maria Helene Canteri & Pedro Arezes

Study of a repair technique in carbonated blended mortars: Electrochemical re-alkalization 93
Ana María Aguirre, Ruby Mejía-de Gutiérrez, Jean Paul Restucci & Alexander Alvarado

The manufacture of a maxillofacial prosthesis from an axial tomography using simulation technologies with a virtual machine tool and four-axis machining 100
Jorge Andrés García-Barbosa, José Manuel Arroyo-Osorio & Ernesto Córdoba-Nieto

The influence of design methodology on a designer's emotional parameters and on design results 106
Vicente Chulvi & Mª Carmen González-Cruz

Computational simulation of laminar heat convection of nanofluids in a circular tube and squared duct 113
Diego Andrés Vasco-Calle, Daming Chen b & Jorge Acevedo-Cabello

Viscoelastic behavior of yellow pitahaya treated with 1-MCP 119
Laura Sofía Torres-Valenzuela, Alfredo Adolfo Ayala-Aponte & Liliana Serna-Cock

Adopting Ecodesign Management Systems in the construction sector. Analysis from the perspective of stakeholders 124
Beñat Landeta-Manzano, Germán Arana-Landín, Patxi Ruiz de Arbulo-López & Pablo Díaz de Basurto-Uraga

Numerical experimentation for the optimal design of reinforced rectangular concrete beams for singly reinforced sections 134
Arnulfo Luevanos-Rojas

A study of co-movements between U.S. and Latin American stock markets: A cross-bicorrelations perspective 143
Semei Coronado, Omar Rojas, Rafael Romero-Meza & Francisco Venegas-Martínez

A comparative study for the design of rectangular and circular isolated footings using new models 149
Arnulfo Luévanos-Rojas

Developing a self-regulating soldering iron based on induction heating 159
Cuauhtémoc Mazón-Valadez, Luis Héctor Quintero-Hernández, Ernesto Edgar Mazón-Valadez, Alfonso Hernández-Sámano, José Ávila-Paz & Mario Eduardo Cano-González

UNIVERSIDAD NACIONAL DE COLOMBIA
SEDE MEDELLÍN
FACULTAD DE MINAS

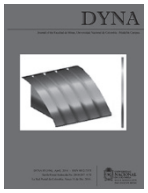

DYNA
http://dyna.medellin.unal.edu.co/

Microstructure and electrical properties of solid electrolytes of fully stabilized zirconia with rare earth mixed oxides 168
Rodrigo Arbey Muñoz-Meneses, Paola Cristina Cajas-Daza, Jose Luis Narvaez-Semanate & Cosme Roberto Moreira-da Silva

Analysis of working nanofluids for a refrigeration system 176
Diana C. Hernández, César Nieto-Londoño & Zulamita Zapata-Benabithe

Synthesis and modification of beta zeolite for use in toluene disproportionation reaction 184
Santiago Mesa, Johana Arboleda & Adriana Echavarría

Effect of a dual tire pressure on the design parameters of thick asphalt pavements using finite element freeware 194
Myriam Rocío Pallares-Muñoz & Julián Andrés Pulecio-Díaz

Collaborative goods distribution using the IRP model 204
Martín Darío Arango-Serna, Carlos Andrés-Romano & Julián Andrés Zapata-Cortés

Baseflow analysis using master recession curves and numerical algorithms in mountain basins: Suratá's river and Oro's river (Santander, Colombia) 213
Sully Gómez-Isidro & Viviana Lucía Gómez-Ríos

Study of the adsorption capacity of Fe(II) dissolved in water by using a mineral rich in Manganese Dioxide (MnO_2) from Colombia 223
Jhonnathan Machado-Infante, Gustavo Ramírez-Caballero & Martha Barajas-Meneses

Preliminary studies on hydrated cement for its reuse in geopolymers 229
Yasna Pamela Segura-Sierpe, María Victoria Borrachero-Rosado, José María Monzó-Balbuena & Jordi Payá-Bernabeu

Our cover
Image alluding to Article:
Effect of a dual tire pressure on the design parameters of thick asphalt pavements using finite element freeware

Authors:
Myriam Rocío Pallares-Muñoz & Julián Andrés Pulecio-Díaz

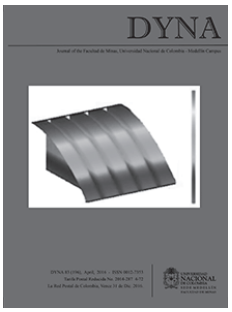

UNIVERSIDAD NACIONAL DE COLOMBIA
SEDE MEDELLÍN
FACULTAD DE MINAS

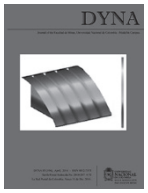

DYNA
http://dyna.medellin.unal.edu.co/

DYNA 83 (196), April, 2016. Medellín. ISSN 0012-7353 Printed, ISSN 2346-2183 Online

CONTENIDO

Variación de la categoría de riesgo en los métodos de cálculo de la densidad de carga de fuego ponderada 9
Cristina Maria Paulo Cadete-Pires, Rui António de Carvalho-Veiga & Maria Isabel Simões-Miguel

Aplicación del método Delphi para la inclusión de las externalidades en análisis de seguridad y de salud laboral 14
Delfina Ramos, Pedro Arezes & Paulo Afonso

Evaluación de riesgos laborales en Almazaras: Limitaciones y nuevas perspectivas 21
Matilde A. Rodrigues, Juan C. Rubio-Romero, Pedro Arezes & Manuel Soriano-Serrano

Costos de accidentes de trabajo con TMOL consecuencia de absentismo y presentismo en un hospital portugués 27
Maria Emília Queiroz-Lima & Florentino Serranheira

Identificación de aéreas de intervención de políticas públicas en seguridad laboral usando análisis de correspondencias múltiple 31
Jesús Antonio Carrillo-Castrillo, Juan Carlos Rubio-Romero, José Guadix & Luis Onieva

Un análisis cualitativo de las condiciones de salud y seguridad en el trabajo en pequeños proyectos de construcción en el sector de la construcción brasileña 39
Haroldo Pereira Gomes, Pedro Miguel Ferreira Martins Arezes & Luiz Carlos Fadel de Vasconcellos

Riesgo emergente en la industria de la construcción: Recomendaciones para controlar la exposición a nanomateriales 48
Beatriz María Díaz-Soler, María Dolores Martínez-Aires & Mónica López-Alonso

Diferencias en la actividad muscular entre trabajadores obesos y no obesos durante la elevación manual de cargas 55
Ana Colim, Pedro Arezes, Paulo Flores & Ana Cristina Braga

Impacto de un programa de ejercicio en el trabajo en los segmentos de cuello y hombros en los trabajadores de oficina 63
Mariana Machado-Matos & Pedro Miguel Arezes

Ocurrencia de una mineralogía tipo skarn reconocida en los Mármoles de Ciénaga, estribaciones NW del Macizo de Santa Marta (Colombia) 69
Oscar Mauricio Castellanos-Alarcón, Carlos Alberto Ríos-Reyes & Luis Carlos Mantilla-Figueroa

Descontaminación de aguas de desecho de la industria textil usando Fotocatálisis 80
José Herney Ramírez-Franco & Hugo Ricardo Zea-Ramírez

La alimentación de los trabajadores en la industria y su relación con los datos antropométricos y el gasto energético 86
Eliana Aparecida Queiroz Bortolozo, Luiz Alberto Pilatti, Maria Helene Canteri & Pedro Arezes

Estudio de una técnica de reparación aplicada a morteros adicionados carbonatados: Realcalinización electroquímica 93
Ana María Aguirre, Ruby Mejía-de Gutiérrez, Jean Paul Restucci & Alexander Alvarado

Manufactura de una prótesis maxilofacial, a partir de una tomografía axial, usando tecnologías de simulación en una máquina herramienta virtual y maquinado de cuatro ejes 100
Jorge Andrés García-Barbosa, José Manuel Arroyo-Osorio & Ernesto Córdoba-Nieto

Influencia de la metodología de diseño en los parámetros emocionales del diseñador y en los resultados del diseño 106
Vicente Chulvi & Mª Carmen González-Cruz

Simulación computacional de convección de calor laminar de nanofluidos en tubo circular y ducto cuadrado 113
Diego Andrés Vasco-Calle, Daming Chen b & Jorge Acevedo-Cabello

Comportamiento viscoelástico de pitahaya amarilla tratada con 1-MCP 119
Laura Sofía Torres-Valenzuela, Alfredo Adolfo Ayala-Aponte & Liliana Serna-Cock

Adopción de Sistemas de Gestión de Ecodiseño en el sector de la construcción. Análisis de la perspectiva de los diferentes agentes involucrados 124
Beñat Landeta-Manzano, Germán Arana-Landín, Patxi Ruiz de Arbulo-López & Pablo Díaz de Basurto-Uraga

Experimentación numérica para el diseño óptimo de vigas rectangulares de concreto reforzado para secciones simplemente reforzadas 134
Arnulfo Luevanos-Rojas

Un estudio de comovimientos entre las bolsas de valores de Estados Unidos de Norteamérica y América Latina: Una perspectiva de la bicorrelación cruzada 143

UNIVERSIDAD NACIONAL DE COLOMBIA
SEDE MEDELLÍN
FACULTAD DE MINAS

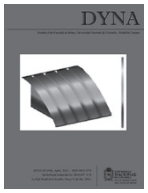

DYNA
http://dyna.medellin.unal.edu.co/

Semei Coronado, Omar Rojas, Rafael Romero-Meza & Francisco Venegas-Martínez

Un estudio comparativo para diseño de zapatas aisladas de forma rectangular y circular usando nuevos modelos 149
Arnulfo Luévanos-Rojas

Desarrollo de un cautín autorregulable basado en calentamiento por inducción 159
Cuauhtémoc Mazón-Valadez, Luis Héctor Quintero-Hernández, Ernesto Edgar Mazón-Valadez, Alfonso Hernández-Sámano, José Ávila-Paz & Mario Eduardo Cano-González

Microestructura y propiedades eléctricas de electrólitos sólidos de circonia totalmente estabilizada con óxidos mixtos de tierras raras 168
Rodrigo Arbey Muñoz-Meneses, Paola Cristina Cajas-Daza, Jose Luis Narvaez-Semanate & Cosme Roberto Moreira-da Silva

Análisis de nanofluidos para un sistema de refrigeración 176
Diana C. Hernández, César Nieto-Londoño & Zulamita Zapata-Benabithe

Síntesis y modificación de la zeolita beta para su uso en la reacción de desproporción de tolueno 184
Santiago Mesa, Johana Arboleda & Adriana Echavarría

Efecto de la presión de contacto de una carga dual sobre los parámetros de diseño de pavimentos asfalticos gruesos usando software libre de elementos finitos 194
Myriam Rocío Pallares-Muñoz & Julián Andrés Pulecio-Díaz

Distribución colaborativa de mercancías utilizando el modelo IRP 204
Martín Darío Arango-Serna, Carlos Andrés-Romano & Julián Andrés Zapata-Cortés

Análisis de flujo base usando curvas maestras de recesión y algoritmos numéricos en cuencas de montaña: Cuenca del río Suratá y cuenca del Río de Oro (Santander, Colombia) 213
Sully Gómez-Isidro & Viviana Lucía Gómez-Ríos

Estudio de la capacidad de adsorción de Fe(II) disuelto en agua usando un mineral rico en Dióxido de Manganeso (MnO_2) de origen colombiano 223
Jhonnathan Machado-Infante, Gustavo Ramírez-Caballero & Martha Barajas-Meneses

Estudios preliminares sobre cemento hidratado para su reutilización en geopolímeros 229
Yasna Pamela Segura-Sierpe, María Victoria Borrachero-Rosado, José María Monzó-Balbuena & Jordi Payá-Bernabeu

Nuestra carátula
Imagen alusiva al artículo:
Efecto de la presión de contacto de una carga dual sobre los parámetros de diseño de pavimentos asfalticos gruesos usando software libre de elementos finitos

Autores:
Myriam Rocío Pallares-Muñoz & Julián Andrés Pulecio-Díaz

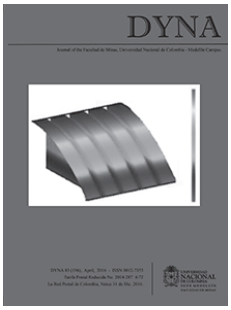

UNIVERSIDAD NACIONAL DE COLOMBIA
SEDE MEDELLÍN
FACULTAD DE MINAS

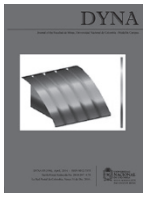

DYNA
http://dyna.medellin.unal.edu.co/

Variation in risk category in methods of calculation of the modified fire load density

Cristina Maria Paulo Cadete-Pires [a] , Rui António de Carvalho-Veiga [b]& Maria Isabel Simões-Miguel [c]

[a] *Graduate in Occupational Safety Engineering– ISLA, Santarém – Portugal. cadete.pires@gmail.com*
[b] *Specialist Teacher in Safety and Health at work – ISLA, Santarém – Portugal. rveiga.sht@gmail.com*
[c] *Assistant professor of Human Resources Management - ISLA Santarém – Portugal. isabel.miguel@unisla.pt*

Received: December 7th, 2015. Received in revised form: February 20th, 2016. Accepted: March 07th, 2016.

Abstract
The management of fire safety in buildings is conducted in accordance with the type of use-risk category (Building occupancy code). For Building type XI "libraries and archives" and XII "industrial, workshops and warehouses", the determination of the risk category involves the calculation of the modified fire load density, which can be done by two methods used interchangeably by the technician: deterministic and probabilistic. This study aims to investigate variation results obtained with the calculation of the modified fire load density using two methods and the classification of the Building occupancy code. The performed calculations referred to real buildings of type XII, with defined and distinct materials and activities. The different results determine a variation in the risk category, which consequently, will define the technical criteria to be applied to the Building occupancy code in the implementation for Building Fire Safety measures.

Keywords: Fire Safety in Buildings; fire load; deterministic; probabilistic.

Variación de la categoría de riesgo en los métodos de cálculo de la densidad de carga de fuego ponderada

Resumen
La gestión de seguridad contra incendios en los edificios se efectúa de acuerdo a la categoría de riesgo dependiendo del tipo de utilización (TU). Para el TU XI «bibliotecas y archivos» y XII «industrias, talleres y almacenes», la determinación de la categoría de riesgo implica el cálculo de la densidad de la carga modificada del incendio, que puede ser efectuada mediante dos métodos, utilizados de forma indistinta por el técnico: determinístico y probabilístico. Este estudio, tiene como objetivo investigar la variación de los resultados obtenidos del cálculo de la densidad de la carga modificada del incendio por dos métodos y la clasificación TU. Los cálculos efectuados hacen referencia a dos TU XII reales con distintos materiales y actividades definidas. La diferencia de los resultados obtenidos por los métodos determina la variación de la categoría de riesgo, que consecuentemente, va a definir cuáles son los criterios técnicos a aplicar sobre la TU en la implementación de medidas de SCIE.

Palabras clave: Riesgo de incendio, densidad de carga de fuego.

1. Introduction

The main objective of fire safety regulations developed and implemented in most countries is the protection of workers and the reduction of losses in organizations [10].

Buildings' fire safety, in Portugal, walks hand in hand it with the technical and technological changes that accompany the construction process of buildings making it possible to evolve and adapt during construction. Increasingly, the concern with fire safety is left is not only to protect but nowadays, and increasingly, also to prevent [8].

With the implementation of the current legal regime for Fire Safety in Buildings, any project or self-protection measure necessarily implies the classification of buildings according to their uses (Building occupancy code). The determination of the classification of risk categories applicable to Building type XI "libraries and archives" and XII "industrial, workshops and warehouses" implies the calculation of the modified fire load density [1]. The Legal Portuguese Regime of Fire Safety in Buildings refers to the

© The author; licensee Universidad Nacional de Colombia.

concept of fire load and modified fire load density for measuring those calculations [2].

The fire load corresponds to the probable volume of heat to be released by the complete combustion of all elements in a space, including the lining of walls, partitions, floors and ceilings. The modified fire load density is the fire load density affected by coefficients referred to the degree of danger and the fuel activation rate as mentioned in article 2 of Decree-Law 220/2008 of 12th November-Portugal [2].

The technical criteria for determining the modified fire load density is defined in the legal technical regulation Nr. 2074/2009, of 15th January-Portugal [3]. This Law Decree, points out two calculation methods that can be used interchangeably. The deterministic method, based on prior knowledge of the quantity and quality of existing materials in the studied section, and the probabilistic method based on statistical results of the type of activity in the studied section [3].

The calculations were made using any of the methods for determination of the modified fire load density of a site or group of sites belonging to the same fire compartment, i.e. the part of a building, comprising one or more spaces, rooms or floors enclosed by the building elements with suitable resistance to fire for a certain period of time to ensure the protection of the building or to prevent the spread of fire to the rest of the building, or even the fire load to fractionate [4].

Although the calculations are simple, it is important to have adequate knowledge to be able to apply the presented formulas and obtain real consistent values. The complexity of the legislation requires that only skilled technicians can prepare projects and measures of self-protection [5].

1.1. Objectives

To conduct studies in the field of fire safety in buildings based on the results of the calculation of the fire load density modified by two different methods and the risk category classification. The following precise objectives were established:

1st - Determine if it is indifferent to method selection of calculation of the modified fire load density to classify risk category of Buildings type XI and XII;

2nd – Analyse if a definition of criteria is required when a method is selected in order to standardize procedures in the implementation of the measures of Portuguese Fire Safety in Buildings.

2. Materials and methods

In the study, two real Building types are described with defined materials and activities, modified fire load density is calculated using two methods and the Buildings are classified in risk category based on the obtained results.

The facilities of the first Building have no fireguard, despite being divided into pavilions, it is considered in terms of foreclosure as a single building, and the calculations were made for the covered space and outdoors. Later, the same calculations were made considering the subdivided building with fireguard.

The second Building has fireguard and all areas are covered.

The modified fire load density (qs) corresponds to the heat energy that can be released in case of fire, presented in megajoules per square meter (MJ/m2) and can be determined from the presented formulas in the legal technical regulation Nr. 2074/2009 15th January-Portugal [3,7]And also referred to the NTP 766 - Technical Notes of Prevention [9]: Deterministic calculation eq. (1)

$$q_s = \frac{\sum_{i=1}^{N_c} M_i H_i C_i R_{ai}}{S} \quad (1)$$

Where:

M_i = Mass in kg, of fuel constituent (i);

H_i = Lower heating value in MJ/m^2, of fuel constituent (i);

C_i = Dimensionless coefficient of combustibility of fuel constituent (i);

R_{ai} = Dimensionless coefficient of activation of fuel constituent (i);

S = Useful area of fireguard compartment in m^2.

Probabilistic calculation: manufacturing eq.(2), storage eq.(3) and total Building eq (4)

$$q_s = \frac{\sum_{i=1}^{N_a} q_{si} S_i C_i R_{ai}}{\sum_{i=1}^{N_a} S_i} \quad (2)$$

Where:

q_{si} = Fire load density for the type of activity (i) em MJ/m^2;

S_i = Activity zone area (i) in m^2;

C_i = Dimensionless coefficient fuel constituent of combustibility with higher risk of combustibility present in the activity zone (i);

N_a = Number of distinct activities areas.

$$q_s = \frac{\sum_{i=1}^{N_{ar}} q_{vi} h_i S_i C_i R_{ai}}{\sum_{i=1}^{N_{ar}} S_i} \quad (3)$$

Considering the parameters of the previous equation (1 and 2) except for the following:

q_{vi} = Fire load density per unit volume on the storage area (i) in MJ/m^3;

h_i = Storage height of the storage area (i) in m;

N_{ar} = Number of distinct storage areas.

$$q = \frac{\sum_{k=1}^{N} q_{sk} S_k}{\sum_{k=1}^{N} S_k} \quad (4)$$

Where:

q_{sk}= Modified fire load Density, in MJ/m^2, each compartment fireguard (k);

S_k = Useful area of each compartment fireguard (k) inm^2;

N = Number of fireguard sections.

In the legal technical regulation Nr. 2074/2009 of 15th January-Portugal [3] are the specifications for featured formulas and in its annex are published tables with the coefficients needed for the calculations.

2.1. Deterministic method

It requires knowledge of the quantity and quality of materials, so an inventory was made of all products and their respective quantities (kg) of the studied Buildings.

2.2. Probabilistic method

This is based on statistical results for the type of activity in the mentioned fireguard compartments.

2.2. Classification of Risk Category

After the calculation of the modified fire load in the Building under study it was determined as a type XII risk category according to the X framework of Annex III of Decree Nr. 220/2008 of 12th November-Portugal [2].

3. Study Case

This study was based in two type XII Buildings with distinct activities, manufacture and storage and they were designated as Building 1 and Building 2.

Building 1 has storage and does refining of oils, and all products are manufactured and stored in tanks with the maximum capacity of 80% tank volume.

The stored products and subjected to refining are mainly made from cooking oil. Referring to Table 1 of the legal Technical Regulation Nr. 2074 / 2009 January 15th [3] it is stated that in order to calculate the calorific fuel power (Hi), the material that has similar characteristics may be Flaxseed Oil (Hi = 37.2 MJ/kg) and fat (Hi = 42MJ/kg). In order to demonstrate if this choice influenced the value of the modified fire load, calculations were made using the two values.

Building 2 is dedicated to drying, storage and processing of grain. All products are stored in silos, verifying the maximum capacity of 100%.

4. Results

In the first phase of the study it was verified that calculation results of Building 1 differed significantly, if they were based on constituent fuel fat or linseed oil. The calculations performed by the deterministic method revealed the results represented in Table 1.

Once verified that there is no significant difference in the results, the remaining calculations were made with fat component.

Table 1.
Density of the modified fire load table - deterministic method (fat and linseed oil).

Constituent fuel	Useful Area m2 compartment	Covered /Outdoor	q_s=MJ/m²	Risk Category
Fat	1.186,82	Covered	50.239	4ª RC
	4.468,91	Outdoor	39.003	4ª RC
Linseed oil	1.186,82	Covered	44.580	4ª RC
	4.468,91	Outdoor	35.014	4ª RC

Source: The Authors

Table 2.
Modified fire load density - Probabilistic Method.

Constituent fuel	Useful Area m2 compartment	Covered / Outdoor	q_s= MJ/m²	Risk Category
Fat	1.186,82	Covered	14.236	3ª RC
	4.468,91	Outdoor	14.022	3ª RC

Source: The Authors

First, and because, according to the organization, this is what corresponds to the stored and manufactured products and secondly because it has higher H_i, thus being the most prudent calculation [6].

In the second phase we calculated the density of the modified fire load by the probabilistic method (Table 2).

In the third phase, we proceeded equally, the calculation of the fire load density per shed by deterministic and probabilistic method to determine whether there were significant differences, if the spaces of the building had fireguard and we extended our study to Building 2 that had a fireguard (Table 3 and Table 4).

Table 3.
Modified fire load density - deterministic method Building 1 and Building 2.

	Compartment	Area m²	Covered/ Outdoor	q_s= MJ/m²	Risk Category
Building 1	Pavilion Nr. 1	421	Covered	79.640	4ª RC
	Pavilion Nr. 2	274	Covered	42.680	4ª RC
	Pavilion Nr. 3	269	Covered	16.917	4ª RC
	Pavilion Nr. 4	223	Covered	44.159	4ª RC
	Pavilion Nr. 4	400	Outdoor	82.381	4ª RC
	Outdoor Park	4.068	Outdoor	34.738	4ª RC
Building 2	Cereals line	990	Covered	101	1ª RC
	A. Packaging	490	Covered	1.584	2ª RC
	A. Peel	230	Covered	13.069	3ª RC
	Silos 1 to 10	365	Covered	41.178	4ª RC
	silo 11	403	Covered	808.064	4ª RC
	silo 12	403	Covered	683.746	4ª RC

Source: The Authors

Table 4.
Modified fire load density - probabilistic method Building 1 and Building 2.

	Compartment	Area m²	Covered /Outdoor	q_s= MJ/m²	Risk Category
Building 1	Pavilion Nr. 1	421	Covered	20.344	4ª RC
	Pavilion Nr. 2	274	Covered	27.698	4ª RC
	Pavilion Nr. 3	269	Covered	4.055	2ª RC
	Pavilion Nr. 4	223	Covered	6.675	3ª RC
	Pavilion Nr. 4	400	Outdoor	56.842	4ª RC
	Outdoor Park	4.068	Outdoor	11.163	3ª RC
Building 2	Cereals line	990	Covered	4.200	2ª RC
	A. Packaging	490	Covered	29.183	4ª RC
	A. Peel	230	Covered	30.600	4ª RC
	Silos 1 to 10	365	Covered	244.800	4ª RC
	Silo 11	403	Covered	265.200	4ª RC
	Silo 12	403	Covered	265.200	4ª RC

Source: The Authors

Table 5.
Modified fire load density - Building 1.

Method	Covered / Outdoor	q_s= MJ/m²	Risk Category
Deterministic	Covered	50.239	4ª RC
	Outdoor	39.003	4ª RC
Probabilistic	Covered	14.236	3ª RC
	Outdoor	14.022	3ª RC

Source: The Authors

Table 6.
Comparison of results between methods - Building 1.

Compartment	Area m²	Covered /Outdoor	q_s= MJ/m²	Risk Category
Pavilion Nr. 1	Deterministic	Covered	79.640	4ª RC
	Probabilistic	Covered	20.344	4ª RC
Pavilion Nr. 2	Deterministic	Covered	42.680	4ª RC
	Probabilistic	Covered	27.698	4ª RC

Pavilion Nr. 3	Deterministic	Covered	16.917	4ª RC
	Probabilistic	Covered	4.055	2ª RC
Pavilion Nr. 4	Deterministic	Covered	44.159	4ª RC
	Probabilistic	Covered	6.675	3ª RC
	Deterministic	Outdoor	82.381	4ª RC
	Probabilistic	Outdoor	56.842	4ª RC
Outdoor Park	Deterministic	Outdoor	34.738	4ª RC
	Probabilistic	Outdoor	11.163	3ª RC

Source: The Authors

Table 7.
Comparison of results between methods - Building 2.

Compartment	Area m²	Covered /Outdoor	q_s= MJ/m²	Risk Category
Cereals line	Deterministic	Covered	101	1ª RC
	Probabilistic	Covered	4.200	2ª RC
A. Packaging	Deterministic	Covered	1.584	2ª RC
	Probabilistic	Covered	29.183	4ª RC
A. Peel	Deterministic	Covered	13.069	3ª RC
	Probabilistic	Covered	30.600	4ª RC
Silos 1 to 10	Deterministic	Covered	41.178	4ª RC
	Probabilistic	Covered	244.800	4ª RC
Silo 11	Deterministic	Covered	808.064	4ª RC
	Probabilistic	Covered	265.200	4ª RC
Silo 12	Deterministic	Covered	683.746	4ª RC
	Probabilistic	Covered	265.200	4ª RC

Source: The Authors

During the fourth phase, summary tables were elaborated to facilitate the comparison of results and classification of risk categories between methods (Table 5).

Finally the obtained results were compared using two methods of calculation for the Building 1 and Building 2 with fireguard (Table 6 and Table 7).

5. Discussion

In Building 1, the use of distinct fuel constituents in the calculation resulted in no significant change in the results (Table 1). However, we consider that further studies should broaden the base of the study sample and validate the now obtained conclusion.

The comparative analysis made between the two methods for Building 1 (Table 5) provided a value of the modified fire load density (qs) different between the deterministic and the probabilistic method. The difference in the results is significant, causing changes in the Building occupancy risk category (Table 1 and Table 2).

When we considered Building 1 with fireguard and we extended our study to Building 2, it was possible to perceive significant differences in the modified fire load density of the respective compartments (Table 3 and Table 4).

In the comparative analysis made between the two methods for Building 1 and Building 2 (Table 6 and Table 7), the differences found changed the risk category.

When we studied Building 1, we noticed that the deterministic method always presented higher values. However, with Building 2, the deterministic method only showed higher values when the constituent fuel occupied the entire fireguard compartment (Table 7 - Silos 11 and 12).

This study considers Building 1 with fireguard compartment. When we extended the study to Building 2, it presented greater disparity in values between the deterministic and probabilistic methods.

For Building type XI, “libraries and archives”, and XII, “industrial, workshops and warehouses”, the value of the modified fire load density is an important factor in determining the risk category. This will later define the technical requirements that should be adopted according to the Legal Regime of Portuguese Fire Safety in Buildings. This difference between building types will change the technical and specific conditions required by the regulation for the building’s occupancy code.

A range of results were obtained by the modified method of the deterministic fire load density of 16 917 MJ/m2 and 82 381 MJ/m2 for the Building 1 and 41 178 MJ/m2 and 808 064 MJ/m2 for the Building 2. We questioned the value shown in Table X, of the Law Decree Nr. 220/2008 of 12th November [2] for the 4th RC> 15,000 MJ/m2 (integrated in buildings) and> 30,000 MJ/m2 (outdoor) is not adjusted, and should be changed a superior limit.

The Law Decree values were based on the work undertaken by Engineer Max Gretener in the 60s, and the activities and storage made at that time does not reflect the current reality [4].

Compared to 2009, in 2015 the organizations already have IT tools allowing the calculation of fire load density that best reflects the reality of the organization - deterministic method.

6. Conclusions

In this study, we conclude that the calculation method used for the classification of type XII Building risk category makes a difference. The legislator does not define which method to use and therefore leaves it up to each technician to select and determine the building occupancy risk category. Thus the goal as stated in the Legal Regime of Portuguese Fire Safety in Buildings, which is to standardize the level of demand in the implementation of Fire Safety in Buildings measures cannot be achieved. It is also necessary to define criteria for method selection, in order to standardize the level of demand in the implementation of Fire Safety measures for Buildings.

In later studies, we intend to investigate the criteria to be used in the method selection, which will standardize the risk classification results, regardless of the used calculation method.

References

[1] Castro, C.F. e Abrantes, J.B., Manual de Segurança contra Incêndio em Edifícios, Vol. I, 2ª ed., E.N. Bombeiros, Sintra, Portugal, 2009, 46 P.

[2] Decreto-Lei n.º 220/2008, 12 de Novembro de 2008, alterado pelo Decreto-Lei nº 224/2015, 9 de Outubro de 2015, Regime Jurídico da Segurança Contra Incêndios em Edifícios, Diário da República, Portugal.

[3] Despacho nº 2074/2009, 15 de Janeiro de 2009, Critérios técnicos para determinação da densidade de carga de incêndio modificada, Diário da República, 2ª Série nº 10.

[4] Miguel, M. e Silvano, P., Regulamento de segurança em tabelas, fábrica das letras, Lisboa, Portugal, 2009, pp. 337-338.

[5] Almeida, J.E., Segurança contra incêndios em armazéns. [Online]. [Consulta, 2 de Agosto de 2014], Disponível em: http://www.avantec.net/artigos/APAT73_armazens.pdf.
[6] Arezes, P., Baptista, J.S., Barroso, M.P., Carneiro, P., Cordeiro, P., Costa, N., et al., Occupational Safety and Hygiene SHO2015, Sociedade Portuguesa de Segurança e Higiene Ocupacionais (SPOSHO), Guimarâes, Portugal, 2015, pp. 270-272.
[7] GEPRIX. Cálculo da carga de incêndio modificada. [Online]. [Consulta 1 de Novembro de 2015], Disponível em: http://www.geprix.com/mediateca/c%C3%A1lculo-da-densidade-de-carga-de-inc%C3%AAndio-modificada
[8] G-Rodrigues, A.D., Comparação das medidas de autoproteção exigíveis, face ao enquadramento legal na área de segurança contra incêndio em edifícios, Tese de Mestrado. Obtido de Universidade de Lisboa-Sistema Integrado de Bibliotecas. [Online]. [Consulta de 30 de Outubro de 2015]. Disponível em: http://hdl.handle.net/10400.5/3889
[9] Trabajo, I.N., NTP 766 - Notas Técnicas de Prevención. Carga de fuego ponderada: Parámetros de cálculo, 2007.
[10] NFPA 557: Standard for Determination of Fire Loads for Use in Structural Fire Protection design. National Fire Protection Association, 2010.

C.M. Cadete-Pires, has a graduation in Engineering in Safety, Quality and Environmental Management from the Instituto Superior de Línguas e Administração - ISLA Santarém, Portugal. She currently works as a trainer and consultant in Hygiene and Safety at Work and Quality, Environment and Safety.
ORCID ID: 0000-0001-5244-6002

R.A. Carvalho-Veiga, has an academic education in Hygiene and Safety at work, Human Resource Management and Social Policy from the University of Leon, España, the Instituto Superior de Línguas e Administração - ISLA Santarém, Protugal and Social Service Institute of Lisbon, Portugal. He is a teacher at ISLA and at the European University. He works also as a trainer and consultant in the area of hygiene and safety at work. He is a co-author and coordinator of several publications of Hygiene and Safety at Work and author of multiple articles.
ORCID ID: 0000-0001-9515-9978

M.I. Simões-Miguel, is PhD student in Business Management at the University of Coimbra, Portugal. She has a MSc. in Human Resource Management. She is certified in School Libraries Management and E-Learning system, and has an English Language Teacher Certification from the University of Cambridge and a Degree in Modern Languages and Literature from the University of Lisbon. She is Assistant Professor and Trainer at ISLA Santarém, Portugal and co-author of multiple articles in the area of knowledge management and consultancy.
ORCID ID: 0000-0003-4233-225X

UNIVERSIDAD NACIONAL DE COLOMBIA
SEDE MEDELLÍN
FACULTAD DE MINAS

Área Curricular de Ingeniería Administrativa e Ingeniería Industrial

Oferta de Posgrados

Especialización en Gestión Empresarial
Especialización en Ingeniería Financiera
Maestría en Ingeniería Administrativa
Maestría en Ingeniería Industrial
Doctorado en Ingeniería - Industria y Organizaciones

Mayor información:

E-mail: acia_med@unal.edu.co
Teléfono: (57-4) 425 52 02

UNIVERSIDAD NACIONAL DE COLOMBIA
SEDE MEDELLÍN
FACULTAD DE MINAS

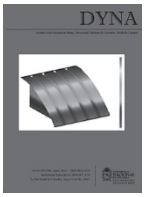

DYNA
http://dyna.medellin.unal.edu.co/

Application of the Delphi Method for the inclusion of externalities in occupational safety and health analysis

Delfina Ramos [ab], Pedro Arezes [b] & Paulo Afonso [b]

[a] *Technology School, Polytechnic Institute of Cávado and Ave, Barcelos, Portugal gramos@ipca.pt*
[b] *Center Algoritmi, University of Minho, Guimarães, Portugal. parezes@dps.uminho.pt; psafonso@dps.uminho.pt*

Received: November 30th, 2015. Received in revised form: February 29th, 2016. Accepted: March 07th, 2016.

Abstract
Organizations should regularly conduct an assessment of their occupational hazards in order to design and implement preventive measures that are necessary and sufficient to deal with the level of risk, the costs of prevention and the safety at levels considered acceptable by the organization. Furthermore, the selection of measures to be implemented in an organization should take into account both internal and external costs. Externalities are of great importance in terms of the costs of accidents at work; nevertheless, they are not often properly addressed by the organizations. In this paper we describe an application of the Delphi method to understand how externalities can be included in Occupational Safety and Health.

Keywords: Occupational Safety and Health; Externalities, Economic perspective, Delphi Method.

Aplicación del método Delphi para la inclusión de las externalidades en análisis de seguridad y de salud laboral

Resumen
Las organizaciones deben realizar periódicamente una evaluación de sus riesgos laborales con el fin de diseñar y poner en práctica medidas preventivas que sean necesarias y suficientes para mantener e l nivel de riesgo, los costos de la prevención y la seguridad en los niveles considerados aceptables por la organización. Por otra parte, la selección de las medidas a aplicar en una organización debe tener en cuenta tanto los costes internos como externos. Las externalidades son de gran importancia en términos de los costos de los accidentes de trabajo; sin embargo, a menudo no se tratan adecuadamente por las organizaciones. En este artículo se describe una aplicación del método Delphi para entender cómo los factores externos pueden ser incluidos en la Seguridad y Salud Laboral.

Palabras clave: Seguridad y Salud Ocupacional; Externalidades, Economía, Método Delphi.

1. Introduction

Economists tend to emphasize the costs and economic benefits of additional safety, which is in contrast to safety experts, who generally have a particular focus on safe working conditions and in designing safe products [1]. Certainly, the organization's financial costs and benefits involved in Occupational Safety and Health (OSH) are an important aspect of economic analysis; however, society-at-large's perspective is far more important. This perspective includes workers, their families and their communities as well as enterprises, and it recognizes that not all the effects of ill-health show up in monetary transactions.

Both individuals and society lose emotionally and financially from injuries and accidents. Individuals can be understood to make their own best safety decisions if they have good information and the correct incentives. In this context, society may subsidize risk taking in many ways, thereby discouraging safety. Thus, regulation is required to deal with such externalities [2].

According to Agénor and Dinh [3], as defined by Putnam in 1993, there is a "social capital" that consists of "those features of social organization, such as networks of individuals or households, and the associated norms and values that create externalities for the community as a whole". Although a number of economists initially questioned the validity of classifying

© The author; licensee Universidad Nacional de Colombia.

social interactions as a form of capital, an increasing number of them now acknowledge that social capital shares at least some similarities with physical and human capital in its inter-temporal dimension and its ability to generate external effects and future benefits. These externalities include information sharing among individuals and firms; and the matching of people to economic opportunities, mutual aid and insurance, which may affect expectations and individual behavior, as well as effective collective action. Social capital also enables agents to cope with market imperfections or imperfect institutions.

According to Varian [4], the definition of externality is that the action of an agent affects the living conditions of another agent not involved in that action. Externalities can also be defined as: "the uncompensated impact of actions of one person over the welfare of a spectator" [5]. The focus on human welfare, primarily used as a synonym for human utility, is due to the traditional utilitarianism of economics.

Samuelson and Nordhaus [6] state that externalities occur when companies or individuals impose costs or benefits on others who are not involved in the market. In the same way, Van Beukering et al. [7] consider that an externality occurs when an economic decision has an impact on the welfare of another economic agent not directly involved in the process. This results from the fact that the possibility of impact has not been properly addressed or has been disregarded. In general, an externality is present when the welfare function (Y) of some economic agent (utility or profit) includes real variables whose values are chosen directly by others (X), without special attention paid to the effect on the welfare of agent Y. Usually, externalities generated are only taken into consideration when a project needs or deserves an evaluation by a public entity. According to Cullis and Jones [8], externalities consist of social costs or benefits that manifest themselves beyond the realm of the project and influence the welfare of third parties without any monetary compensation.

The evaluation of projects of a private nature does not consider the effects on third parties arising from associated externalities. Indeed, the externalities generated by projects are in many cases difficult to quantify. This is the case, for example, with calculations that relate to the "value" of human life.

For Rebitzer et al. [9], externalities can be divided into the internalized externalities and the non-internalized externalities. According to Mann and Wüstemann [10], there are economic textbooks that suggest that externalities must be internalized in order to achieve a situation that is Pareto optimum.

Externalities are also important in the domain of OHS for both public and private organizations. Indeed, governments are usually concerned about the effect of negative externalities, not only in relation to the environment, which is the most typical external impact, but also to the area of occupational safety.

According to Dorman [1], broadly speaking, there are three general ways in which economics can be useful for OSH. Firstly, identifying and measuring the economic costs of occupational injury and disease can motivate governments to take these problems more seriously. This is true at all levels; the enterprise may be only dimly aware of the toll that worker ill-health takes on its performance, and national governments may not realize the impact of OSH problems on economic growth and development. Secondly, understanding the connections between the way firms and markets function and the types of OSH problems that arise are crucial for the success of public policies. Finally, the author considers that the protection of worker health and wellbeing is not the only objective of OHS in a modern society. Economic analysis can help to show when safeguarding working conditions are also complementary to other social goals, and it can enlighten any trade-offs, if indeed there are any.

Furthermore, when an organization performs a risk analysis that is integrated into the assessment of its OSH management system, several steps are suggested in order to solve the problems that are identified. Usually, the organization makes a detailed analysis of the monetary impact (positive or negative) for the organization in terms of each of the considered measures. However, it is also important to perform an analysis of the impact that those measures have on society, i.e., to measure the associated externalities. Indeed, as was previously explained, the measures taken by an organization in risk prevention may have an indirect positive effect (positive externality) on society, while no action, due to the costs for the organization, may have significant negative effect for society (negative externality). It follows that these effects should be duly considered in the decision-making process [11].

Externalities are, in fact, of great importance in terms of costs of work accidents [12]. Therefore, it is important to consider them when performing a cost-benefit analysis in OSH. Nevertheless, there are very few studies that allow the externalities related to workplace accidents to be estimated [13].

Furthermore, the quest for economic sustainability of OSH is acquiring greater visibility and strategic weight in corporate management. Thus, the process of calculating or estimating the economic value of OSH is a very relevant topic that needs to be analyzed in greater depth, as confirmed by Cagno et al. [14].

It is clear that different approaches, strategies and policies must be made according to the different consequences of accidents as well as which perspective is considered. It can also be concluded that the role of the workers in the prevention of accidents is essential, especially for the accidents that involve major injuries or death.

Thus, for all of these goals, a central issue is that of costs. On the one side, we have the costs of improving working conditions in order to reduce the incidence of injury and disease. On the other, we have the costs of not reducing the level of accidents; these are both tangible and intangible costs. For example, suppose, as a result of a catastrophic industrial accident, a firm loses half of its market share. This constitutes an enormous private cost to the firm. However, if sales are t still made by other firms, not all this private cost will be translated in a social cost. If the firm suffering the accident were more efficient than its competitors then the increase in the cost to society of supplying the goods would qualify as social. Second, not all social costs appear as private costs. For instance, a significant portion of the medical cost of occupational injury and disease in industrialized countries is indemnified by social insurance systems [1].

One of the priorities for research related to OSH in Europe during the period 2013-2020, undertaken by the European Agency for Safety and Health at Work [15], is to strengthen the research on the economic dimension of OSH, including estimating the socioeconomic costs of the consequences of poor or no OSH, and an analysis of costs and benefits of OSH prevention in order to support evidence-based policies and decision-making on society and enterprise levels.

The purpose of this paper is to contribute to the economic analysis that should be made in order to increase our understanding and management of OSH, with special emphasis on externalities resulting from work accidents.

2. Materials and methods

2.1. Delphi Methodology

The Delphi method is a particularly suitable research technique when there is an incomplete understanding of the subject under consideration: as is the case for externalities in occupational safety [16,17]. The method was developed by [18] of RAND Corporation in 1950 for a project sponsored by the U.S. Army. It was created as part of a post-war movement concerned with the prediction of possible effects of technological development in economic and social regeneration. The objective of the original study was to "obtain the most reliable consensus of opinion by a group of experts using a series of intensive questionnaires interspersed with controlled opinion feedback" [19].

The Delphi method may be characterized as a method for structuring a group communication process so that the process is effective in allowing a group of individuals, as a whole, to deal with a complex problem [19].

This method is defined as a structured, interactive group communication and judgmental forecasting process which has the purpose of facilitating a systematic exchange of informed opinions among a panel of experts in order to develop a consensual understanding on a topic [19,20]. This is particularly the case in situations that are characterized by uncertainty, i.e., when objective, fact-based quantitative information is scarce or not reliable. It this context the Delphi method has proven to be effective [19].

Thus, the Delphi methodology is an exploratory study that allows the views of a panel of experts -which is called the Delphi panel- to be gathered. This process is carried out by conducting a series of questionnaires in, typically two or three rounds, on the subject under study [17]. In this research method, the results depend strongly on the quality of the questionnaire and the selection of experts [21].

The dimensions of heterogeneity for the purposes of a Delphi survey are manifold. For instance, individuals can differ in their age, gender, cultural and educational background, knowledge base, profession, values, attitudes, or tenure [22]. Furthermore, the Delphi methodology is characterized by the anonymity of the participants, the statistical representation of the distribution of results and the use of the feedback from the group to review the answers in a later round.

In this research method, the results depend strongly on the quality of the questionnaire and the selection of experts [16].

Although the method foresees several successive rounds of questionnaires, it can often be limited to two rounds without affecting the quality of the results, as has already been demonstrated in many studies [23,24].

According to Geist [25], the Delphi method can be used to determine important issues and also be used as a precursor or a first approach to the development of research.

Nevertheless, it is also important to be aware of its limitations, namely it is a laborious and time-consuming technique and it may be characterized by poor internal consistency and reliability of opinions among experts. This can lead to low reproducibility of forecasts based on the results obtained. Sensible results are obtained with respect to the ambiguity and reactivity of respondents; however, it is difficult to assess the participating experts' degree of knowledge.

2.2. Delphi Panel

For this study, a panel of experts specialized in the area of OSH has been chosen. Initially, 29 experts, including 13 academic experts, 8 technical/professional experts and 8 experts in consulting/audit have been contacted.

The 29 potential participants were contacted and formally invited by email to participate in research. Of these 29 experts, 20 have shown interest in participating, and thus these experts will constitute the panel: 8 academic experts, 8 technical/professional experts and 4 experts in consulting/auditing.

The questionnaire has been developed for the purpose of being applied to a panel of experts with different backgrounds. It was expected that with three rounds it would be possible to obtain important conclusions and to have a better understanding of the importance of the externalities in occupational safety [17].

2.3. Delphi Questionnaire

The questionnaire has a total of 11 questions related to externalities. For each question, the expert was asked to choose the answer on a scale of between 1 and 5 (1=very low, 2=low, 3=medium, 4=high, 5=very high); the possibility of having "no opinion" was also permitted. The variables studied are discrete, categorical and qualitative of ordinal type. The detailed structure of the questionnaire was presented in a previous publication [17]. The questionnaire was previously validated with three experts before being sent to all members of the expert panel. The questions are presented in Table 1 (section Results and Discussion).

The questionnaire was prepared as a PDF file in Adobe Acrobat and was then sent by email to each expert. After filling in the questionnaire, the expert just had to click on the "Submit Form" button and then the questionnaire was immediately transmitted electronically. This platform is user-friendly and allows the direct uploading of the answers in an Excel file for statistical analysis.

2.4. Methodology for the analysis of the answers

The questionnaires were used to reduce the "interquartile interval" (IQR), a measure of the deviation of the opinion of an expert from the opinion of the whole panel (median). The

aim of the first questionnaire was then to calculate this deviation. If one or more rounds are performed, a higher consensus is to be expected on each issue [16,22,23]. According to Skulmoski et al. [26], the process can be considered as being concluded when the answers are near the consensus, according to appropriate statistical methods.

Quantifying the degree of consensus among Delphi panelists is an important component of Delphi data analysis and interpretation [27], but reaching consensus (as measured by a certain pre-defined threshold value) is not the general aim of a Delphi survey [28,29]. Among others, the IQR is often used as a measure for consensus in Delphi literature due to its robustness as a statistical measure [29,30]. The IQR is the range in which the middle 50% of the provided evaluations are located [31]. The inter-quartile range is the difference between the 3rd and 1st quartile in which 50% of core values lie. The IQR and the presentation of the quartiles allow an assessment of the degree of convergence of the answers. The quartiles can be used to help measuring the variability or dispersion of the observed data. The first quartile is a variable value such that the number of observations for lower values is 25% and upper 75%, i.e., the first inter-quartile (Q1) refers to 25% agreement between the experts, and the third quartile (Q3) refers to 75% agreement [32,33]. According to Bryman and Cramer [34], this measurement is more robust and less sensitive to isolated cases. It is also applicable in the case of ordinal variables, which are contained in the applied questionnaire.

There are many criteria to establish the moment the experts reached a consensus [35]. Indeed, depending on the scales used, different thresholds for the IQR can be defined to indicate that consensus among the experts has been achieved [28,32]. In the current study, the adopted criterion of consensus was when an IQR≤1 was achieved.

Thus, in this research, an IQR less than 1 means that more than 50% of all opinions fall on a certain point on the scale; this shows that they have reached consensus [32]. An IQR of zero indicates a perfect consensus among panel members: the higher the IQR, the greater the dispersion of the data.

For all the 11 questions, the following statistical parameters have been calculated: mean, median, standard deviation and inter-quartile range.

The median is a better measure of the degree of group support for each factor; if it is high, we can conclude that there is a high level of support from the group. The standard deviation permits us to see the dispersion of results, which is directly related to the IQR.

The questionnaire sent to the experts for the second Delphi round included the treated results from the first round. In this second round, the "zone of agreement" was indicated with a red rectangle (see Fig. 1), considering the median value of the responses of the panel with a deviation of plus or minus one level. The answer given by the corresponding expert in the previous round has also been presented by using a red dot (see Fig. 1).

Fig. 1 shows an example of an extract from a second round questionnaire sent to the experts.

The experts have been invited to indicate their agreement or disagreement with respect to the median answer. The following alternatives were possible for each expert:

a) keep the original answer,
b) re-evaluate the initial answer and change it.

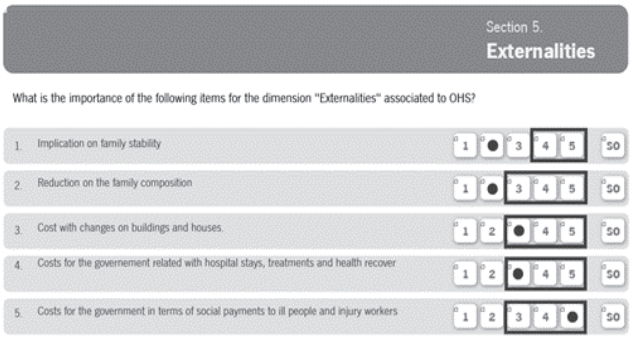

Figure 1. Extract of the questionnaire used in the second round.
Source: The authors

In case the final answer of the expert was outside the range of consensus, he/she was requested to briefly indicate the main reason(s) that led him/her to keep the same response. They should do this by using the text box that was available for this purpose at the end of the questionnaire.

In the third round questionnaire, the experts' comments have also been included in order to help respondents to eventually re-evaluate the previous answer and change it. This helps to improve the level of consensus.

The statistical analysis of diagrams of extremes and quartiles in the first and third round was undertaken by using the statistical software IBM SPSS v.20.

3. Results and Discussion

3.1. Results of the first Delphi round

In the first round, we had the effective participation of a total of 20 experts from the 29 contacted. The results showed a good agreement (IQR≤1) in 8 of the 11 questions.

Fig. 2 presents the diagram of extreme quartiles and first round "Externalities".

The circle and the asterisk in Fig. 2 represent extreme cases. The circle represents the situation in which the minimum

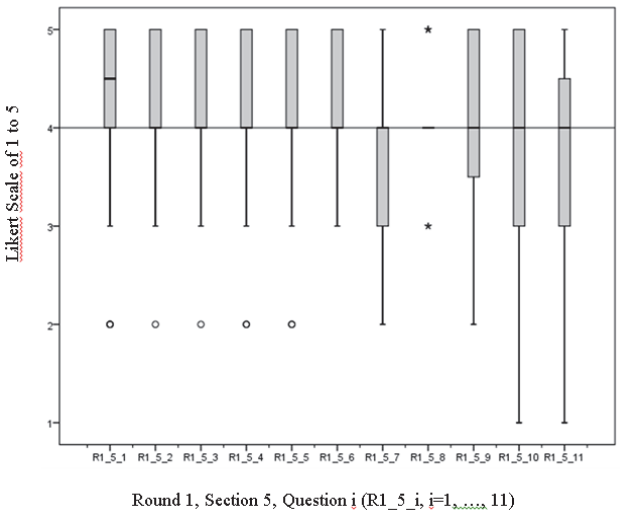

Figure 2. Diagram of extreme quartiles and first round "Externalities"
Source: The authors

or maximum value is lower or higher than 1.5 IQR but less than 3 IQR (case considered as "moderate outlier"). The asterisk represents the extreme cases, which are significantly higher than 3 IQR (called "faroutlier" or "extreme outlier"). This notation follows the standard set in SPSS, as well as other conventional statistics programs (Statistica, SAS, R, etc.).

3.2. Results from the second Delphi round

The second Delphi round was carried out in order to increase the consensus. In this round, there were 9 questions with IQR≤1 (including one with IQR = 0). The diagram of extremes and quartiles is very similar to the first round.

3.3. Results from the third Delphi round

In the third round, the experts were asked to reassess their responses, taking into account the results and also the comments made in the second round. In this round, the number of issues with IQR≤1 increased to 10.

The answers obtained from the panel in the third round are shown in Fig. 3. All the questions obtained a median of at least 4.0 (full line of Fig. 3).

Table 1 presents the statistical treatment of the results from the third (and final) round. For each question the following statistical parameters are presented:

- W: median. Positional statistical parameter: central value of those observed:
- m: mean. Positional statistical parameter: the sum of data values divided by the number of observations;
- s: standard deviation. Dispersion parameter: square root of the mean of the squares of deviations with respect to its median;
- IQR: interquartile interval. Dispersion parameter: difference between third and first quartiles.

3.4. Global discussion of the results

Table 2 presents the evolution of the panel's opinion throughout the three rounds.

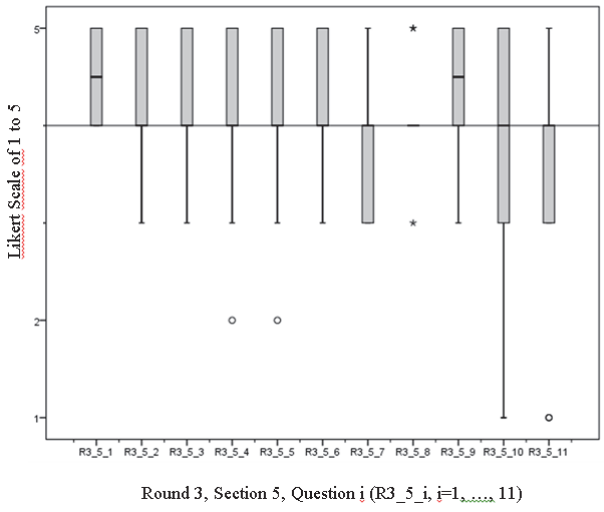

Figure 3. Diagram of extreme quartiles from third round "Externalities." Source: The authors

Table 1.
Summary of statistical results with the inclusion of externalities in OSH after the third round.

Questions	W	m	s	IQR
1. Implications in the family stability.	4.5	4.50	0.52	1.00
2. Reduction of household income.	4.0	4.29	0.73	1.00
3. Expenses of accommodation and adaptation at home.	4.0	4.21	0.58	0.75
4. Costs for society in terms of payment of hospitalization costs, treatments and recovery.	4.0	4.14	0.86	1.00
5. Costs for society in terms of social welfare payments to sick and injured workers.	4.0	4.14	0.86	1.00
6. Costs for society in terms of reintegrating people into the labor market and back in society in general.	4.0	4.29	0.73	1.00
7. Indirect calculation of externalities, based on the costs of the plans and equipment for prevention and safety.	4.0	3.71	0.61	1.00
8. Direct calculation of the externalities based on the damages caused.	4.0	4.07	0.47	0.00
9. Reduction of the negative externalities through public measures (taxes, fines, legislation, etc.).	4.5	4.29	0.83	1.00
10. Reduction of negative externalities through private solutions in terms of the relationship between the company and the worker (codes of conduct, safety rules, etc.).	4.0	3.86	1.17	2.00
11. Reduction of negative externalities through awards/grants/tax deductions for legitimate businesses.	4.0	3.57	1.28	1.00

Source: The authors

Table 2.
Consensus criterion concerning the questions related to Externalities.

Parameter	Round 1	Round 2	Round 3
No. of respondents	20	19	14
No. of questions with IQR ≤ 1	8	9	10

Source: The authors

The number of experts has reduced as the rounds, have gone on, which is normal in Delphi studies and does not invalidate the results. In fact, according to Okoli & Pawlowski [16], 14 is a good number of experts in Delphi studies; these authors suggest between 10 and 18 experts.

After round 3, the expert panel found that questions 1 and 9 in Table 1 were extremely important (median equals to 4.5 or 5) with IQR=1. Question 8 obtained the highest consensus (IQR = 0), with a median of 4.0.

The expert panel recognized the relevance of the implications for family stability, the direct calculation of the externalities based on the damages caused and the reduction of negative externalities through public solutions (taxes, fines, legislation, etc.). There was no consensus among the panel of experts on reducing negative externalities through private solutions in terms of the relationship between the company and the worker.

Translating risks and prevention measures in terms of the costs for companies employees' and for society may be used to support the reduction of negative externalities through public measures such as taxes, fines, legislation, etc. Responses showed a high consensus on the direct calculation of the externalities based on the damages caused.

4. Conclusions

The Delphi method is a suitable research technique when there is an incomplete or vague knowledge of the subject under consideration, as is the case of externalities in OSH.

This methodology allowed the assessment of selected experts to be collected through a questionnaire specifically designed for this purpose. It was then developed in three rounds, in order to increase consensus among the group of experts.

According to the issues highlighted by the expert panel, the externalities can be used to promote, support or to legislate on measures of preventing occupational hazards. Indeed, the incorporation of the effects of risks and preventive measures in terms of cost to the company for the employees and society may be used to support the reduction of negative externalities through public measures such as taxes, penalties and more restrictive laws.

The Delphi Method can be viewed as an important tool to gain a better understanding of the inclusion of externalities in occupational safety and health analysis, highlighting the more relevant aspects to be considered in economic studies in this particular field.

5. Acknowledgments

The authors would like to acknowledge all the experts who have participated in the Delphi panel. The authors also acknowledge the anonymous reviewers who helped to improve the overall quality of the current manuscript. This study was financially supported by FCT-Fundação para a Ciência e Tecnologia of Portugal, under the project ID/CEC/00319/2013.

References

[1] Dorman, P., The Economics of safety, health, and well-being at work: An overview. In Focus Program on SafeWork, International Labour Organisation. The Evergreen State CollegeTechnol, [On line]. 2000 [consulted February 2015]. Available at: http://www.oit.org/wcmsp5/groups/public/---ed_protect/---protrav/---safework/documents/publication/wcms_110382.pdf.

[2] Lave, L.B., Injury as externality: An economic perspective of trauma. Accident Analysis & Prevention,19 (1), pp 29-37, 1987. DOI: 10.1016/0001-4575(87)90015-7

[3] Agénor, P-R. and Dinh, H. T. Social capital, product imitation and growth with learning externalities. Journal of Development Economics 114, pp. 41-54, 2015. DOI: 10.1016/j.jdeveco.2014.11.008

[4] Varian, H.R., Microeconomic Analysis. W.W. Norton & Company, Inc. 3rd Edition, 1992.

[5] Mann, S. and Wüstemann, H., Multifunctionality and a new focus on externalities. The Journal of Socio-Economics, 37, pp. 293-307, 2008. DOI: 10.1016/j.socec.2006.12.031

[6] Samuelson, P.A. and Nordhaus, W.D., Economics. McGraw Hill, 10th Edition, 1999.

[7] van Beukering, P. van Drunen, M., Dornland, K. and Jansen, H., External economic benefits and costs in water and solid waste investments - Methodology, guidelines and case studies. Report number R98/11. IVM/EFTEC. ISBN 90-5383-632-2, 1998.

[8] Cullis, J. and Jones, P., Public finance & Public choice: Analytical perspectives. Third edition. Oxford University Press. Oxford. UK, 2009.

[9] Rebitzer, G., Ekvall, T., Frischknecht, R., Hunkeler, D., Norris, G., Rydberg, T., Schmidt, W.P. Suhh, S., Weidemai, B.P. and Pennington, D.W., Life Cycle Assessment – Part 1: Framework, Goal & Scope Definition, Inventory Analysis, and Applications. Environment International, 30(5), pp. 701-720, 2004. DOI: 10.1016/j.envint.2003.11.005

[10] Mann, S. and Wüstemann, H., Multifunctionality and a new focus on externalities. The Journal of Socio-Economics 37, pp. 293-307, 2008. DOI: 10.1016/j.socec.2006.12.031

[11] Ramos, D., Arezes, P. and Afonso, P., The role of costs, benefits and social impact of injuries and prevention measures on the design of occupational safety programs. In: Arezes et al. (eds), Occupational Safety and Hygiene, Taylor & Francis Group, London, 2013, ISBN 978-1-138-00047-6, pp. 153-157. DOI: 10.1201/b14391-32

[12] HSE – Health and safety executive. Costs to Britain of workplace injuries and work-related ill health: 2010/11 update. HSE Books, UK, 2012.

[13] ILO – International labour organization. Estimating the economic costs of occupational injuries and illnesses in developing countries: Essential Information for Decision-Makers. ISBN 978-92-2-127015-7. Geneva, 2012.

[14] Cagno, E., Micheli, G., Masi, D. and Jacinto, C., Economic evaluation of OSH and its way to SMEs: A constructive review. Safety Science 53, pp. 134-152, 2013. DOI: 10.1016/j.ssci.2012.08.016

[15] European Agency for Safety and Health at Work (EU-OSHA)., Priorities for occupational safety and health research in Europe: 2013-2020. Summary report. ISBN 978-92-9240-316-4, Luxembourg, 2014.

[16] Okoli, C. and Pawlowski, S.D., The Delphi method as a research tool: An example, design considerations and applications. Information & Management 42, pp. 15-29, 2004. DOI: 10.1016/j.im.2003.11.002

[17] Ramos, D., Arezes, P. and Afonso, P., Cost-benefit analysis in occupational health and safety: A proposal model. 11th International Probabilistic Safety Assessment and Management Conference and the Annual European Safety and Reliability Conference, PSAM11 ESREL 2012, 2, pp. 1273-1282.

[18] Dalkey, N.C. and Helmer, O., An experimental application of the Delphi Method to the use of experts. Management Science, 9(3), pp. 458-468, 1963. DOI: 10.1287/mnsc.9.3.458

[19] Linstone, H. and Turrof, M., The Delphi method, techniques and applications. Addison Wesley Publishing, 1975.

[20] Donohoe, H.M. and Needham, R.D., Moving best practice forward: Delphi characteristics, advantages, potential problems, and solutions. International Journal of Tourism Research, 11(5), pp. 415-437, 2009. DOI: 10.1002/jtr.709

[21] Förster, B. and von der Gracht, H., Assessing Delphi panel composition for strategic foresight - A comparison of panels based on company-internal and external participants. Technological Forecasting & Social Change 84, pp. 215-229, 2014. DOI: 10.1016/j.techfore.2013.07.012

[22] Godet, M. Manual de Prospetiva Estratégica. Lisboa: Publicações Dom Quixote, 1993.

[23] Landeta, J., El método Delphi. Barcelona: Ariel, 1999.

[24] Vergara, S., Métodos de pesquisa em administração. São Paulo. Editora Atlas, 2005.

[25] Geist, M.R., Using the Delphi method to engage stakeholders: A comparison of two studies. Evaluation and Program Planning 33, pp. 147-154. 2010. DOI: 10.1016/j.evalprogplan.2009.06.006

[26] Skulmoski, J.G., Hartman, T.F. and Krahn, J., The Delphi method for graduate research. Journal of Information Technology Education, 6, pp. 1-21, 2007.

[27] von der Gracht, H.A., Consensus measurement in Delphi studies: Review and implications for future quality assurance, Technol. Forecast. Soc. Chang. 79, pp. 1525-1536, 2012. DOI: 10.1016/j.techfore.2012.04.013

[28] Linstone, H.A. and Turoff, M., Delphi: A brief look backward and forward, Technol. Forecast. Soc. Chang. 78, pp. 1712-1719, 2011. DOI: 10.1016/j.techfore.2010.09.011
[29] Warth, J., von der Gracht, H.A. and Darkow, I.-L., A dissent-based approach for multi-stakeholder scenario development — the future of electric drive vehicles, Technol. Forecast. Soc. Chang. 80, pp. 566-583, 2013. DOI: 10.1016/j.techfore.2012.04.005
[30] Ray, P.K. and Sahu, S., Productivity management in India: A Delphi study, Int. J. Oper. Prod. Manag. 10, pp. 25-51, 1990. DOI: 10.1108/01443579010005245
[31] De Vet, E., Brug, J., De Nooijer, J., Dijkstra, A. and De Vries, N.K., Determinants of forward stage transitions: A Delphi study, Health Educ. Res. 20, pp. 195-205, 2005. DOI: 10.1093/her/cyg111
[32] von der Gracht, H.A. and Darkow, I.-L., Scenarios for the logistics services industry: A Delphi-based analysis for 2025. International Journal of Production Economics 127, pp. 46-59, 2010. DOI: 10.1016/j.ijpe.2010.04.013
[33] Astigarraga, E., El método Delphi. Universidad de Deusto, Facultad de CC.EE. y Empresariales. ESTE, [On line]. 2005, Available at: http://www.echalemojo.org/uploadsarchivos/metodo_delphi.pdf.
[34] Bryman, A. e Cramer, D., Análise de dados em ciências sociais - Introdução às técnicas utilizando o SPSS. Celta Editora. Oeiras, 1993.
[35] Fink, A., Kosecoff, J., Chassin, M. and Brook RH., Consensus methods: Characteristics and guidelines for use. Am J Public Health, 74(9), pp. 979-83, 1984. DOI: 10.2105/AJPH.74.9.979

D. Ramos, has a PhD in Industrial and Systems Engineering from the University of Minho, Portugal. She is also Professor Honoris Causa of University of Tourism and Management in Skopje. Professor at Polytechnic Institute of Management and Technology (ISLA) and Polytechnic Institute of Cávado and Ave (IPCA). Member of Human Engineering research group – HErg - University of Minho. Member of the Research Center ALGORITMI, at the School of Engineering – University of Minho. Member of group of auditors of SGS Certification Body/ICS - General Society of Superintendence, SA. Health and Safety (OHSAS 18001) and (ISO 9001) area. ORCID: 0000-0003-2862-2883

P. Arezes, has a PhD. in Industrial and Systems Engineering from U.Minho, in Portugal, and is currently a full professor of Ergonomics and Human Factors at the same university. He is also a visiting fellow at MIT's AgeLab in the USA. He leads the Human Engineering research group and he is also the coordinator of Engineering Design and Advanced Manufacturing (EDAM) for the MIT Portugal Program at UMinhoand the chair of the steering board of the PhD program "Leaders for Technical Industries (LTI)" at UMinho. ORCID: 0000-0001-9421-9123

P. Afonso, holds a Diploma in Economics from the ISEG (Economics and Business School) - Technical University of Lisbon (UTL), a MSc. in Industrial Engineering from University of Minho, Portugal and a PhD. in Accounting and Finance from University of Manchester (UK). He is currently an auxiliary professor in the Production and Systems Department at University of Minho (Portugal) and author or co-author of more than 70 articles in international peer-reviewed conferences, books and journals. He is a researcher in Center Algoritmi (CAlg). He has also been a visiting scholar in several universities.
ORCID: 0000-0003-3882-2491

UNIVERSIDAD NACIONAL DE COLOMBIA
SEDE MEDELLÍN
FACULTAD DE MINAS

Área Curricular de Ingeniería Administrativa e Ingeniería Industrial

Oferta de Posgrados

Especialización en Gestión Empresarial
Especialización en Ingeniería Financiera
Maestría en Ingeniería Administrativa
Maestría en Ingeniería Industrial
Doctorado en Ingeniería - Industria y Organizaciones

Mayor información:

E-mail: acia_med@unal.edu.co
Teléfono: (57-4) 425 52 02

UNIVERSIDAD NACIONAL DE COLOMBIA
SEDE MEDELLÍN
FACULTAD DE MINAS

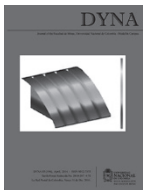

DYNA
http://dyna.medellin.unal.edu.co/

Occupational risk assessment at Olive Oil Mills: Limitations and new perspectives

Matilde A. Rodrigues [a,b], Juan C. Rubio-Romero [c], Pedro Arezes [b] & Manuel Soriano-Serrano [d]

[a] *Department of Environmental Health, Sciences School of the Polytechnic Institute of Porto, Porto, Portugal. mar@estsp.ipp.pt*
[b] *Centre Algoritmi, Department of Production and Systems, Engineering School, University of Minho, Guimarães, Portugal. parezes@dps.uminho.pt*
[c] *School of Industrial Engineering, University of Málaga, Málaga, Spain. juro@uma.es*
[d] *The Centre of Occupational Risk Prevention of Jaén, Government of Andalucía, Jaén, Spain. msoriano@ujaen.es*

Received: December 09th, 2015. Received in revised form: February 29th, 2016. Accepted: March 02nd, 2016.

Abstract
Risk assessment is an essential tool to support risk decisions. However, this process may not always be applied effectively, and this can limit the quality of the preventative action. This is particularly critical in sectors that have a lot of micro and small companies, such as Olive Oil Mills (OOMs). To better understand how to improve the quality of the risk assessment at OOMs, this study aims to analyze the views of Occupational Safety and Health (OSH) practitioners on the key difficulties/limitations in this process and identify some improvements to current practices. This analysis was based on a questionnaire that was developed and given to 13 OSH practitioners working for OOMs. The results showed that the time available to perform the risk assessment is the major limitation. The need for a specific tool for risk assessment in the OOM sector was identified, and the use of accident reports from the entire sector was indicated as an alternative to the absence of data at company level.

Keywords: occupational accidents; Olive Oil Mills; prevention; risk assessment quality; risk assessment.

Evaluación de riesgos laborales en Almazaras: Limitaciones y nuevas perspectivas

Resumen
La evaluación de riesgos es una herramienta esencial para apoyar las decisiones acerca del riesgo. No obstante, este proceso puede no siempre aplicarse con eficacia, y esto puede limitar la calidad de la acción preventiva. Esto es particularmente crítico en sectores que incluyen una gran cantidad de micro y pequeñas empresas, como las Almazaras. Para comprender cómo mejorar la calidad de la evaluación de riesgos en las Almazaras, este estudio tiene como objetivo analizar los puntos de vista de los profesionales de la Prevención de Riesgos Laborales (PRL) acerca de las principales dificultades/limitaciones en este proceso e identificar algunas mejoras en las prácticas actuales. Para este análisis fue desarrollado un cuestionario que fue aplicado a 13 profesionales de la PRL con experiencia en las Almazaras. Los resultados mostraron que el tiempo disponible para el desarrollo de la evaluación del riesgos es la principal limitación. Esta investigación identificó la necesidad de una herramienta específica para la evaluación de riesgos en las Almazaras, siendo identificado el uso de informes de accidentes de todo el sector como una alternativa a la falta de datos a nivel de la empresa.

Palabras clave: accidentes del trabajo; almazaras; calidad de la evaluación de riesgos; evaluación de riesgos; prevención.

1. Introduction

Risk assessment is an essential and systematic process to assess the impact, occurrence and consequences of specific activities in safety and health [1,2]. Quite understandably, it is a critical phase in the overall process of risk management in any organization as it is important to help decision-makers make informed choices and prioritize actions [3].

Despite the importance of risk assessment, it must be understood that it is not a simple process. The obvious problem is that there is no simple, unique method and strategy to undertake the process. There are many ways to perform a risk assessment as different strategies and tools can be selected. Each OSH practitioner can do this differently by selecting and applying different approaches. The degree of depth with which some of the steps of risk assessment are analyzed can change depending

© The author; licensee Universidad Nacional de Colombia.

on the practitioner who is carrying out the process [4]. Moreover, it is important to bear in mind that each sector of activity has particular features that need to be considered when making decisions about how risk should be assessed. This will provide reliable results to support decision-making when risk reduction measures are being undertaken. In fact, selecting which approach will be used is a critical issue in the risk assessment process, since the results will vary significantly as a result of this decision [4]. In view of this, it is essential to use adequate risk assessment strategies and tools that, on the one hand, make it possible to consider limitations in the situation being analyzed and, on the other hand, are capable of providing risk judgment based on complete and transparent risk evaluation [1].

To select a strategy that makes it possible to achieve quality risk assessment, it is essential to be aware of the limitations/problems in the process. Over the years, several problems related to the reliability of the risk assessment process have been identified. Cox [5] indicated five: inaccuracy; incompleteness; difficulty of checking final results; inadequate criteria to evaluate the results; and complexity and laboriousness of the method. Backlund & Hannu [4] pointed out three key problems in the risk assessment process: a vague requirement specification; lack of systematic preliminary hazard analysis; and incomplete documentation of the analysis performed. Specifically, for occupational risks, the lack of reliable data [6-8], time available, quality of the applied methods [9] and the criteria used to support decisions about risk acceptance [10,11] are some of the key problems that determine the reliability of this process. In fact, a lack of sufficient data to apply objective approaches in these settings and the limited time available to spend on this process limit the methodologies that can be applied; this may affect the quality of the results. For example, Carvalho e Melo [12] found that when the risk assessment methodologies usually used to assess occupational risks are applied, different OSH practitioners make different decisions. Furthermore, the use of inappropriate acceptance criteria may result in poor and divergent decisions about risk control and mitigation [11]. Due to these limitations/problems, Pinto et al. [13] suggested that many companies only undertake a superficial analysis of their hazards, just to comply with legal requirements.

Based on this context, it is necessary to understand how the quality of the risk assessment process can be improved in order to provide a reliable basis for decision-making according to the specific characteristics of the sector. This understanding is maybe more important for sectors composed of micro and small companies, as in the case of Olive Oil Mills (OOMs). These types of companies mostly have less resources, and accident prevention management is not a priority. Furthermore, they lack sufficient accident data to support more objective approaches to risk assessment.

The OOM industry is one of the most important sectors in Spain, particularly in the region of Andalusia, which is responsible for 74% of the overall national production [14]. In fact, Spain remains the world's leading producer of olive oil. Close to 23% of olive groves are located in Spain, which is responsible for about 47% of the global olive oil production [15].

The risk management process at OOMs is not straightforward. These industries have particularities that make this process more difficult to carry out. Most of the companies are small and micro companies and the number of workers varies throughout the year [16]. In addition, at most of the companies, the health and safety management system is undertaken by an external prevention service, which does not always cover all the critical areas, such as ergonomics [16]. This can be a critical issue in a sector where most occupational accidents are related to excessive physical effort [17].

Although most of the accidents that occur in this sector are considered to be "basic" risks, such as excessive physical effort and fall-related injuries [17], correct risk assessment needs to be made in order to provide supporting information for the companies' managers and to better define intervention priorities that promote an effective use of resources. In view of this, this study aims to analyze the views of Occupational Safety & Health (OSH) practitioners regarding the risk assessment process in OOMs. The key difficulties/limitations inherent to the risk assessment process at these companies will be identified, as well as some improvements to current practices.

2. Materials and Method

2.1. Sample

A total of 13 OSH practitioners working in the Andalusia region who engaged with OOMs were surveyed. They had, on average, 12.4 years' (SD=5.3) experience undertaking OSH duties and had worked with OOMs for an average of 9.9 years (SD=5.5).

2.2. Analysis of OSH practitioners' views about the risk assessment process at OOMs

An analysis was undertaken of OSH practitioners' views that dealt with OOMs about the current limitations to the risk assessment process; improvements that could be made to this process were also identified. This process was important in order to better understand the most important features to bear in mind during the risk assessment process and, additionally, when developing new risk assessment methodologies. Thus, a questionnaire was developed and applied.

The questionnaire was divided into two parts. The first part referred to professional characterization, and the OSH practitioners were asked about their qualifications, academic background, years of experience and number of years working with OOMs. The second part was comprised of three questions. In the first question, the OSH practitioners surveyed were asked to classify whether the four factors presented were seen as a limitation to the risk assessment process at OOMs: (1) Accident data available at the companies; (2) Risk acceptance criteria included in the risk assessment methodologies; (3) Risk assessment methods available; (4) Time available for the risk assessment process. Finally, they were asked to comment on their choices. The issues included in this question have been frequently mentioned in previous studies as important limitations to the risk assessment of occupational accidents at SMEs [6, 9].

Despite the fact that the limitations identified may be linked to the risk assessment process, the quality of the process must be guaranteed and some factors need to be considered in order to do so. Pinto et al. [13], for example, have identified some important factors for the quality of the risk assessment process in the construction sector. Some of the factors identified were included in this study, according to their applicability to OOM risk assessment. Therefore, in the second question, OSH practitioners were asked about the importance of several factors to ensure the quality of the risk assessment process: (1) Accident reports; (2) Risk assessment methods adjusted to the needs of the OOM; (3) Risk assessment tools based on a quantitative approach; (4) Structured processes for hazard identification; (5) Identification of the relationship between cause and effect; (6) Identification of safety barriers; and (7) Support for risk decisions based on acceptance criteria that is defined specifically for OOMs. The last question in the survey enquired as to OSH practitioners' perspectives on the applicability of different ways to carry out the risk assessment process at OOMs in order to gain important insights into the development of a new methodology: (1) The use of accident reports from the sector; (2) Severity being assessed as number of days missed as a result of injury; (3) Severity assessed as a qualitative scale; (4) Probability derived from accident frequency; (5) Probability assessed as a qualitative scale; (6) The use of diagrams to establish the relationship between hazard, event, and consequence.

The preliminary version of the questionnaire was given to four OSH practitioners, who examined the questionnaire in terms of the clarity of the meaning of the questions and the linguistic terms, the applicability of the questions, and the scales used to check that the order of the survey questions did not affect the answers. Some improvements related to the language used were suggested and taken into consideration in the final version.

2.3. Data analysis

All statistical analyses were conducted using the IBM SPSS Statistics version 20. statistical software package. To determine differences between the ways of carrying out the risk assessment process at OOMs, the Kruskal-Wallis test was utilized. A $p < 0.05$ significance level was used.

3. Results

Table 1 presents the views of OSH practitioners about the limitations to the risk assessment process at OOMs due to several different factors. The results showed that the main limitation identified was the time available to perform the risk assessment (92.3%), followed by the criteria included in the risk assessment methodologies (30.8%) and then the data of the companies available to support objective risk assessment (30.8%). The risk assessment methods available were not seen as a problematic issue in the risk assessment process in the OOM sector, as only 15.4% of the respondents identified it as a limitation.

The importance of some specific factors in terms of the quality of the risk assessment process was also analyzed and the results are presented in Fig. 1. This information is relevant to be able to better understand how the quality of the risk assessment methodology in this specific sector can be improved in order to provide reliable results.

Table 1.
Limitations to the risk assessment process at OOMs (%)

Factor	Not a limitation	Limitation
Accident data available from the companies	69.2	30.8
Risk acceptance criteria included in the risk assessment methodologies	69.2	30.8
Risk assessment methods available	84.6	15.4
Time available for the risk assessment process	7.7	92.3

Source: The authors

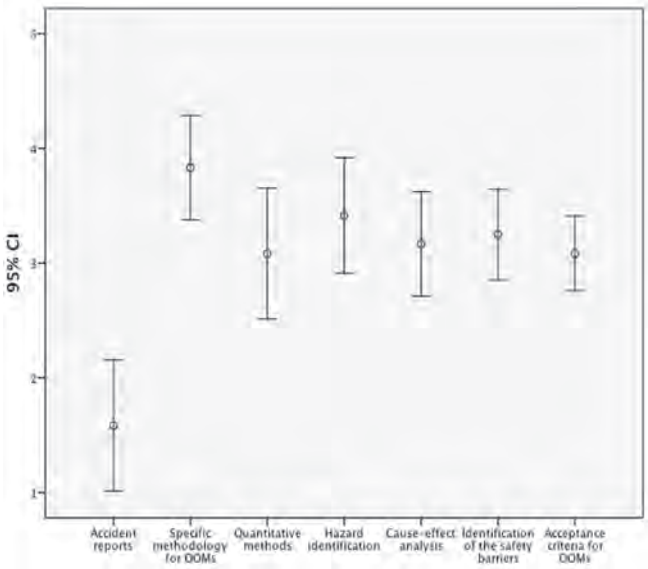

Figure 1. 95% confidence interval for the importance of some factors in the quality of the risk assessment process (5-point Likert scale, "1=Unimportant" to "5 =Extremely important").
Source: The authors

According to the results obtained, most of OSH practitioners consider that the use of statistical accident reports to support a more objective risk assessment process is not an important issue (61.5% of respondents indicate this information as "unimportant"). However, greater importance was attributed to a specific risk assessment methodology for the OOM sector (79.9% of respondents consider this factor to be "highly important"). Respondents assessed the other factors analyzed as "important".

The applicability of different ways of carrying out the risk assessment was also analyzed in order to obtain insights into a new possible strategy to be applied in the sector. Respondents were asked about the use of workdays lost as a measure for severity or whether the use of a qualitative classification was more appropriate. Although no significant differences were found ($p>0.05$), most respondents assessed the use of qualitative measures as being either "applicable" (23.1%) or "highly applicable" (69.2%). The possibility of using accident frequency as a measure for probability was also compared with a qualitative assessment. Significant differences were not found

($p>0.05$); however, most respondents considered the use of accident frequency to be either "applicable" (30.8%) or "highly applicable" (69.2%). Results also show that sector data could be a good solution for supporting risk decisions as most of the OSH practitioners surveyed assessed this possibility to be highly applicable (30.8% "applicable" and 69.2% "highly applicable"). The use of diagrams to establish the relationship between hazard, event, and consequence was also seen as applicable to the risk assessment process at OOMs (38.5% "applicable" and 53.8% "highly applicable").

4. Discussion

According to the results obtained, the time available to carry out the risk assessment at OOM companies is the main limitation for OSH practitioners. The organization of health and safety management at these companies may explain this result. Most OOM companies outsource OSH services to external consultants and only sign comprehensive contracts covering limited prevention actions [16]. Obviously, faced with this scenario, and bearing in mind that all the OSH practitioners surveyed are external consultants in the OOM sector, they do not have much time to spend on the risk assessment process. This can be a major limitation to the quality of risk assessment in this sector. Without sufficient time, a superficial analysis of hazards and risk assessments based on insufficient information may be performed, the only goal being the provision of prevention services to ensure that the companies comply with legal requirements [13,16]. Furthermore, as there is not very much time, it is expected that the approaches used and the results obtained are not presented in the most effective way to the companies' managers. Without due care, the approaches employed and results obtained from risk assessments cannot be easily understood, and, as such, important risk reduction measures may not be implemented [4].

Moreover, most of the OSH practitioners surveyed did not identify the risk assessment methods available as a limitation. To better understand this point of view, we should emphasize several issues. In Spain, the National Institute for Safety and Health at Work (INSHT) (www.insht.es) recommends that a qualitative method be used in small and medium-sized enterprises (SMEs). This method is based on a risk matrix, in which the likelihood of accidents and their expected severity are presented as categorical variables. Based on this idea, and considering the small amount of time available and the lack of statistical accident data, it is expected that most OSH practitioners will apply this method and perform the assessment of occupational risks qualitatively [8]. In fact, qualitative methods have the advantage of requiring less information, time and effort [17]. Therefore, they can be seen as a good approach for companies with little information about past accidents and when the time for performing the risk assessment is limited.

As qualitative methodologies may be used in this sector, it is understandable that OSH practitioners do not see companies' accident reports as a critical limitation to the risk assessment process. However, it is important to bear in mind that, in these conditions, decisions about risk will be based on the knowledge, perception and experience of the decision-makers [18]. This can be a limitation to the quality of risk assessment in the sector. This is particularly critical when only one person performs most of the process. In other industrial sectors, a team of 3 to 5 people is recommended in order to cover all areas of expertise [13]. However, it is important to highlight that some respondents considered the absence of accident data from the companies as a limitation to the risk assessment process. In fact, by using this information, the subjectivity inherent to this process can be reduced and additional important information can be provided [8].

The results also showed that the criteria included in the risk assessment methodologies were seen as a limitation by some respondents. Although most consider the methodologies used to be adequate in the OOM sector, the criteria included may not be the most appropriate in all circumstances. Rodrigues et al. [11] discussed this issue, emphasizing the need to adjust the acceptance criteria included in the risk assessment methodologies to the companies' circumstances. In these cases, when acceptance criteria are not properly adapted, the OSH practitioners may take the initiative to adjust them, and, without guidelines, this process may be based on their own judgment about risk acceptance. In fact, this is a regular practice in several countries such as Portugal. Rodrigues et al. [10], in a study of Portuguese OSH practitioners, found that a significant number adjust the acceptance criteria included in the methodologies, particularly when risk matrices are used.

It is interesting to note that all the respondents agreed that a specific risk assessment methodology in the OOM sector is important. In fact, the features specific to this sector in terms of organization, the particularities of the activities performed at these companies, differences at the worksite, the varying number of workers throughout the year (as most are seasonal), operations in more than one shift, and external staff [16] are all a significant constraint to the risk assessment process. It may be difficult for the OSH practitioner to identify all the hazards and to analyze all the accident mechanisms when they are faced with this type of work organization. This situation is exacerbated by the limited time available to perform the risk assessment and the lack of data about accidents.

The results also indicated that the OSH practitioners surveyed believe that it is important to perform hazard identification in a structured manner, following a systematic process. This process makes it possible to ensure that all the sources of risks have been identified. Furthermore, the analysis of cause and effect, i.e., the analysis of the relationship between hazard, event, and consequence, and the analysis of the safety barriers to prevent or provide protection from risks are also seen as important. These results are in accordance with other studies in other sectors [13].

This study also analyzed how OSH practitioners view the applicability of different ways of carrying out the risk assessment process at OOMs. The results show that respondents see the use of accident reports from the sector as a good alternative to support the risk assessment process. This kind of approach is not new in Spain; Carrillo-Castrillo et al. [8] had already proposed this a method based on the use of sectorial accident reports to support an initial risk assessment of maintenance activities. Furthermore, the OSH practitioners surveyed believe that the use of quantitative measures for probability, such as accident frequency, would

also be useful, although they seemed to prefer assessing severity in a qualitatively. The use of diagrams to establish the relationship between hazard, event, and consequence is also considered to be useful in this sector. In fact, they indicated the importance of the cause and effect analysis to improve the quality of risk assessment. Diagrams can enable the relevant accident's causal pathways and their consequences to be identified, while at the same time identifying the existing or necessary safety barriers [6].

Despite this study's results, it is important to bear in mind that if the questionnaire was applied in other sectors, the results could be different, e.g. in other sectors the lack of accident data on a company level may not be deemed to be an important limitation.

5. Conclusions

The results of the current study provided evidence about the key difficulties/limitations inherent to the risk assessment process at OOMs, and identify some improvements that could be made to current practices. This research is an extension of a previous paper [19], in which a more in-depth analysis of the issue was undertaken.

In general, throughout the study, a need for a new strategy for risk assessment at OOMs was emphasized. This strategy needs to be directed towards the quality of the risk assessment process in order to provide useful and beneficial information for the companies. When the results of the risk assessment are effective, risk reduction measures can be implemented more easily, achieving a suitable level of accomplishment to improve work conditions and, more importantly, to allow the companies go beyond legal requirements. Furthermore, this type of approach can make the companies' managers more risk-conscious and committed to OSH, promoting new models for risk management such as a culture based on people [20]. In this way, companies can change their prevention policy, providing better conditions for OSH practitioners to perform a more quality risk assessment. The companies' managers can hire other types of services that allow for a deeper analysis of hazardous situations, thereby giving more time to OSH practitioners to perform their actions.

The study highlighted the need for a specific tool for risk assessment in the OOM sector. That tool needs to include acceptance criteria adjusted to the OOMs' circumstances and to use risk metrics based on the frequency of accidents as measures to assess accident probability. The use of accident reports from the entire sector was deemed to be a good approach to reduce the subjectivity of the risk assessment process and to help OSH practitioners to focus on the most important circumstances of accidents. Furthermore, a structured process for hazard identification, the identification of the relationship between cause and effect, and the identification of the safety barriers were also considered to be important issues in order to improve the quality of risk assessment in OOMs.

References

[1] van Duijne, F.H., van Aken, D. and van Schouten, E.G., Considerations in developing complete and quantified methods for risk assessment. Safety Science, 46(2), pp. 245-254, 2008.

[2] Hajakbari, M.S. and Minaei-Bidgoli, B., A new scoring system for assessing the risk of occupational accidents: A case study using data mining techniques with Iran's Ministry of Labor data. Journal of Loss Prevention in the Process Industries, 32, pp. 443-453, 2014.

[3] ISO 31000: 2009., Risk management- Principles and guidelines. International Organization for Standardization, 2009.

[4] Backlund, F. and Hannu, J., Can we make maintenance decisions on risk analysis results? Journal of Quality in Maintenance Engineering, 8(1), pp. 77-91, 2002.

[5] Cox, R.A., Improving risk assessment methods for process plant. Journal Of Hazardous Materials, 6, pp. 249-260, 1982.

[6] Jacinto, C. and Silva, C., A semi-quantitative assessment of occupational risks using bow-tie representation. Safety Science, 48(8), pp. 973-979, 2010.

[7] Pinto, A., Ribeiro, R.A. and Nunes, I.L., Fuzzy approach for reducing subjectivity in estimating occupational accident severity. Accident Analysis & Prevention, 45, pp. 281-290, 2012.

[8] Carrillo-Castrillo, J.A., Rubio-Romero, J.C., Guadix, J. and Onievac, L., Risk assessment of maintenance operations: The analysis of performing task and accident mechanism. International Journal of Injury Control and Safety Promotion, 22(3), pp. 267-77, 2015.

[9] Khanzode, V.V., Maiti, J. and Ray, P.K., Occupational injury and accident research: A comprehensive review. Safety Science, 50(5), pp. 1355-1367, 2012.

[10] Rodrigues, M.A., Arezes, P.M. and Leão, C.P., Risk decision in occupational environments: The Portuguese reality, Proceedings of 11th International Probabilistic Safety Assessment and Management Conference and the Annual European Safety and Reliability Conference 2012, PSAM11 ESREL 2012, 2, pp. 1366-1375, 2012.

[11] Rodrigues, M.A., Arezes, P. and Leão, C.P., Defining risk acceptance criteria in occupational settings: A case study in the furniture industrial sector. Safety Science, 80, pp. 288-295, 2015.

[12] Carvalho, F. and Melo, R., Stability and reproducibility of semi-quantitative risk assessment methods within the occupational health and safety scope. Work, 51(3), pp. 591-600, 2015.

[13] Pinto, A., Ribeiro, R.A. and Nunes, I.L., Ensuring the quality of occupational safety risk assessment. Risk Analysis, 33(3), pp. 409-419, 2013.

[14] Agencia de Información y Control Alimentarios., Informe de gestión de la campaña 2012-2013 del aceite de oliva y de la aceituna de mesa, Madrid, Ministério de Agricultura, Alimentación y Medio Ambiente, 2014.

[15] Consejeria de Agricultura, Pesca y Medio Ambiente., Estrategia Andaluza para la investigación de la calidad del aceite de oliva, Andaluzia, Junta de Andaluzia, 2013.

[16] Parejo-Moscoso, J.M., Rubio-Romero, J.C., Pérez-Canto, S. and Soriano-Serrano, M., Health and safety management in olive oil mills in Spain. Safety Science, 51, pp. 101-108, 2013.

[17] Lee, H.-S., Kim, H., Park, M., Teo, E.A.L. and Lee, K.-P., Construction risk assessment using site influence factors. Journal of Computing in Civil Engineering, 26, pp. 319-330, 2012.

[18] Parejo-Moscoso, J.M., Rubio-Romero, J.C. and Pérez-Canto, S., Occupational accident rate in olive oil mills. Safety Science, 50, pp. 285-293, 2012.

[19] Hughes, P. and Ferrett, E., Introduction to health and safety at work. 1st ed. UK: Elsevier, 2007.

[20] Rodrigues, M., Romero, J., Arezes, P., and Soriano-Serrano, M., Limitations and improvements to the risk assessment process in olive oil mills: The views of OSH practitioners, Proceedings of Occupational Safety Hygiene SHO2015, pp. 309-311, 2015.

[21] Formoso, J.A.F., Couce, L.C., Rodriguez, G.I. and Carricoba, M.S., The path to excellence: A management strategy based on people. DYNA, 80(182), pp. 7-14, 2013.

M.A. Rodrigues, is a lecturer in the Department of Environmental Health at the Allied Health Sciences School at the Polytechnic Institute of Porto; Portugal. She received her BSc. in Environmental Health in 2007 from the Polytechnic Institute of Porto; Portugal. She received her MSc. from the University of Minho; Portugal in Human Engineering in 2009 and her PhD in Industrial Engineering and Systems in 2014. Her research interests focus on occupational, safety and health in different domains, particularly risk management, industrial hygiene, risk perception, safety culture and

ergonomics. She is particularly interested in the decision-making process behind occupational accidents.
ORCID: 0000-0001-6175-6934

J.C. Rubio-Romero, is PhD, MSc. and Industrial Engineer and an associate professor of "Safety at Work" in the School of Industrial Engineering of the University of Malaga, Spain. He obtained his PhD in 2000 in occupational health and safety in the industry, and is currently the Chair of Prevention and Social Corporate Responsibility at the University of Malaga as well as the director of the research group, "Operations and Sustainability: Quality, ICT and Risk Prevention at Work". Dr. Rubio has spent over 18 years researching workplace health and safety and has published a wide range of textbooks, reports, and papers, especially on management of workplace health and safety in the manufacturing industry and at construction sites.
ORCID: 0000-0002-5122-7526

P.M. Arezes, received his PhD. in Industrial and Systems Engineering from UMinho, in Portugal. He is a full professor of ergonomics and human factors at the School of Engineering - University of Minho. He is also a visiting fellow at MIT's AgeLab in the USA. He leads the human engineering research group and he is also the UMinho coordinator of the Engineering Design and Advanced Manufacturing (EDAM) area of the MIT Portugal Program, and he is the chair of the steering board on the "Leaders for Technical Industries (LTI)" PhD program at UMinho. He is the (co)author of more than 60 papers published in peer-reviewed international journals, as well as a member of the editorial board of more than 15 international scientific journals.
ORCID: 0000-0001-9421-9123

M. Soriano-Serrano, is a Lawyer, the Director of the Centre of Occupational Risk Prevention in the Government of Andalucía, and a lecturer at the University of Jaén, Spain.

UNIVERSIDAD NACIONAL DE COLOMBIA
SEDE MEDELLÍN
FACULTAD DE MINAS

Área Curricular de Ingeniería Administrativa e Ingeniería Industrial

Oferta de Posgrados

Especialización en Gestión Empresarial
Especialización en Ingeniería Financiera
Maestría en Ingeniería Administrativa
Maestría en Ingeniería Industrial
Doctorado en Ingeniería - Industria y Organizaciones

Mayor información:

E-mail: acia_med@unal.edu.co
Teléfono: (57-4) 425 52 02

UNIVERSIDAD NACIONAL DE COLOMBIA
SEDE MEDELLÍN
FACULTAD DE MINAS

DYNA
http://dyna.medellin.unal.edu.co/

Absenteeism and presenteeism costs from occupational accidents with WRMSDs in a Portuguese hospital

Maria Emília Queiroz-Lima [a] & Florentino Serranheira [b,c]

[a] Centro de Medicina e Reabilitação de Alcoitão - CMRA, Portugal. emilia.lima@cmra.scml.pt
[b] Escola Nacional de Saúde Pública, Universidade NOVA de Lisboa, Portugal. serranheira@ensp.unl.pt
[c] CISP – Centro de Investigação em Saúde Pública, Lisboa, Portugal

Received: December 10th, 2015. Received in revised form: March 01rd, 2016. Accepted: March 07th, 2016.

Abstract
The morbidity associated with WRMSDs leads to productivity losses (absenteeism and presenteeism) in healthcare organizations, which induces a substantive impact (cost).. The present study aimed to evaluate the impact (cost) of WRMSDs for accidents involving nurses and nurses' aides in a small Portuguese hospital. It begins by identifying the workplace accidents (WA) that these occupational groups suffered between 2009 and 2013, which resulted in WRMSDs. Healthcare workers answered a questionnaire with WQL-8 and SPS-6 scales to determine the levels of presenteeism. This study adopted a human capital methodology in order to estimate the indirect costs of lost productivity from WRMSDs. Patient transfers are a major cause of WRMSDs, with most prevalent injuries being in the lumbar region. Between 2009 and 2013 there is a loss of productivity in this institution estimated of €222,015.98 from WA with WRMSDs that lead to absenteeism and presenteeism (€ 189,679.87 absenteeism and € 32,158.86 presenteeism).

Keywords: Ergonomics, Occupational accidents, Productivity losses, Hospitals, Nurses.

Costos de accidentes de trabajo con TMOL consecuencia de absentismo y presentismo en un hospital portugués

Resumen
La morbilidad por trastornos musculoesqueléticos de origen laboral (TMELs) conduce a una pérdida de productividad (absentismo y presentismo) en sistemas de asistencia sanitaria, con substanciales costos. El objetivo del estudio fue evaluar costos de TMELs consecuencia de accidentes en enfermeras y auxiliares de un hospital portugués. Se inició con la identificación de los accidentes de trabajo (AT) que estos grupos ocupacionales sufrieron entre 2009 y 2013. Estos trabajadores respondieron a un cuestionario con las escalas WQL-8 y SPS-6 para determinar los niveles de presentismo. En este estudio se adoptó una metodología de capital humano con el fin de estimar costos indirectos de pérdida de productividad por TMELs. Los traslados de pacientes fueran una importante causa de TMELs, incidiendo estas en la región lumbar. Entre 2009 y 2013 se produjo una pérdida de productividad estimada en 222.015,98€ por AT con TMELs derivando en pérdidas de 189.679,87€ (absentismo) y 32.158,86€ (presentismo).

Palabras clave: Ergonomía, accidentes de trabajo, Pérdidas de productividad, Hospitales, Enfermeras.

1. Introduction

Work-related musculoskeletal disorders (WRMSDs) are a major worldwide problem, principally for healthcare personal [1].

The international research in healthcare confirms the negative productivity impact caused by WRMSDs, in particular by high levels of absenteeism and presenteeism; there is also a decrease in the level of healthcare personals' quality of life. There are several studies that describe nurses and nurses' aides working conditions and their risk of developing musculoskeletal disorders whilst undertaking these tasks [2-7].

Recently in Portugal several authors have focused on WRMSDs [8,9] and also developed several studies in a hospital setting [10-15] that draw attention to working conditions and for the significant WRMSDs risk level for nurses and nurses' aids.

Beyond the effects on quality of life, WRMSDs can cause substantial costs for the society. Work accidents and

© The author; licensee Universidad Nacional de Colombia.

occupational diseases can have severe financial implications, in particular through absenteeism and presenteeism.

Absenteeism is a specific and inevitable cost [16] that the working world has to incur [17]. Cunha et al. [18] report that the simplest and most accepted definition of absenteeism refers to the unexpected absence of an employee at the workplace. The word "unexpected" excludes absences due to vacation, "bank holidays", clearances, special leave of absence (e.g. maternity), or other reasons that are known and / or programmed by the organization.

Empirical research has shown that absenteeism is affected by the employees' professional capacity and their motivation to work, as well as by internal and external factors at work [17]. In fact, absenteeism can be a result of multiple factors interaction, and this problem may have several consequences at the individual, organizational and also at a societal level.

The concept "presenteeism" is used when someone is present at work, but it is difficult to tell when (or how much) the person's illness or medical condition is hindering their performance [7,19].

In general, we can consider expressed productivity losses [20,21] and reduced on-the-job productivity as a result of health issues affecting the overall performance of companies with negative economic implications to be associated with presenteeism. There are two types of presenteeism: the first is associated with acute illness (temporary as a cold or a pregnancy) and the second is associated with chronic diseases (such as musculoskeletal disorders or mental health disorders).

Presenteeism affects productivity, not only in terms of amount of work, but also in terms of quality of work, [19] specifically in nurses' productivity. It may also affect patient safety. The decrease in productivity translates to the inability to perform routine tasks, [22] and may also result in high absence rates due to disease [23]. These phenomena are therefore not only important in terms of the organization's social responsibility, but also in terms of its competitiveness [7].

2. Material and methods

This study was conducted at a public hospital in Lisbon, and we aimed to determine the costs of the lost in productivity, from the employer's perspective, in terms of absenteeism and presenteeism.

All nurses and nurses' aides who suffered work accidents between 2009 and 2013 took part in the study (n = 188 possible participants who had suffered work accidents: 107 nurses and 81 nurses' aids). To take part in this study (inclusion criteria in the sample), the participants had to have a WRMSD as a result of a work accident.

Data collection was first performed in the "human resources department" in the hospital to identify the work accident cases and consequent WRMSDs. We then sent a questionnaire to each healthcare worker that included a socio demographic characterization and identified lost productivity by asking the following two questions (i) the number of days lost due to sick leave with work-related musculoskeletal disorders resulting from work accidents (absenteeism) and (ii) the level of presenteeism, which was assessed using the Work Limitations Questionnaire (reduced - 8 issues) - WLQ [24, 25] and Stanford Presenteeism Scale - SPS-6 [26] scales translated and validated for the Portuguese population [27]. The value of unpaid domestic work, by WRMSDs, was excluded.

The WLQ scale [24] consists of 25 items and assesses four dimensions: time management, ability to perform physical labor, concentration and interpersonal skills, and the ability to achieve goals through the participant's self-assessment. It uses a 5 point Likert scale, where 1 represents "all the time (100%)" and 5 "any time (0%)". We used the small version (WLQ-8) that was adapted by Ozminkowski et al. [25] and consists of 8 items (the original contains 25 items) and evaluates the same four dimensions.

The SPS-6 scale [26] consists of 6 items and assesses two dimensions: (i) work completed (TC), which refers to the amount of work that is carried out when the employee is suffering from the causes of presenteeism, and (ii) avoided distraction (DE) that corresponds to the capacity for concentration that people have when they have symptoms of presenteeism. This is assessed by participant self-assessment, using a Likert scale, where 1 is "strongly disagree" and 5 "strongly agree". According to Koopman et al. [26], the lowest number is associated more with origins of psychological conditions, whereas the latter is manifested by physical causes. Each respondent's total score was on a SPS-6 scale and was obtained after adding scores together in each of the six statements.

To calculate the cost of lost productivity (i.e., the indirect costs of WRMSDs for accidents at work), we opted for the human capital method as it is commonly used in these type of studies, when the potentially productive time lost is valued using the average wages of affected employees [28, 29].

To calculate of the cost of absenteeism (between 2009 and 2013), the following formula used was (1):

$$\text{lost days} \times (\text{Average hourly wage} \times n^{\underline{o}} \text{ hours of daily work}) \times 1.83 \quad (1)$$

The cost of presenteeism was evaluated according to the following formula (2):

$$(\text{Score WLQ}/100) \times \text{Useful working days per year} \times (\text{Average hourly wage} \times n^{\underline{o}} \text{ hours of daily work}) \quad (2)$$

Data analysis was carried out with IBM® SPSS® Statistics software (vs 22).

3. Results and discussion

The present study included 30 nurses and 20 nurses' aides that had a work accident resulting in a WRMSD between 2009 and 2013. A total sample with (n) 50 participants was obtained, in which 72% (n = 36) were female.

Regarding the work accidents that cause work-related musculoskeletal disorders, most were due to "patient transfer" (60%), followed by "health professionals fall" (12%), "patients positioning" (10%) and "patient aggression

Table 1.
Characterization for days lost.

Professional group	2009	2010	2011	2012	2013	Total
Nurses	20	96	32	515	105	768
Nurses' aides	0	93	364	218	106	781
Total	20	189	396	733	211	1.549

Source: The authors

Table 2.
Characterization by level of presentism (second level SPS-6).

Professional group	x̄ total SPS-6	x̄ completed work	x̄ avoided distraction
Nurses	1.95 (sd= 0.96)	1.87 (sd=1.07)	2.03 (sd=1.18)
Nurses' aides	2.28 (sd=0.70)	1.93 (sd=1.07)	2.63 (sd=1.28)

Source: The authors

towards health care worker" (6%). Smaller reasons were due to: "improper positioning of the healthcare professional" (4%), "equipment falling on the health care professional" (4%) and "road accidents whilst at work" (2%). Regarding the body region affected by work accidents, the "spine" (n = 9) had the largest modal value, followed by the "right foot" (n = 6), "right upper limb" (n = 5) and "right shoulder" (n = 5).

Regarding the number of days lost through sick leave due to WRMDs (absenteeism) there was a total loss of 1,549 days (for the 50 participants in the study (n = 50). 768 days were missed by nurses and 781 by nurses' aids) (Table 1). These result show an average loss of 6.20 days (sd = 1.47).

Considering that "patients transfer" was the main cause of work accidents in the present study, we chose to analyze its contribution to the number of days lost due to sick leave. This analysis found that there were 861 days lost due to patient transfer (220 days lost for nurses and 641 days for nurses' aids). This represents about 55.58% (14.20% relative to the nurses and 41.38% for nurses' aids) of all days lost.

Regarding presenteeism and taking into account the overall score of the SPS-6 scale (5-point Likert scale) and mean scores from its two dimensions, we found that both the nurses' aides and the nurses had higher "avoided distraction" mean scores (2.03; 2.63, respectively) compared with the "completed work" (1.87 to 1.93), and nurses' aids had higher levels of presenteeism than nurses in both dimensions (Table 2).

Regarding the presenteeism percentage, and taking into account the outcome of WQL scale, there was an average loss of 19.56% productivity per working day (trimmed mean at 95% of 17.19%). In terms of professional category, nurses had a lower level of presenteeism (14.48%) compared with the operating assistants (27.19%).

To calculate the lost productivity cost (i.e., the costs of WRMSDs due to accidents at work), we decided to adopt the formulas proposed by Mitchell and Bates [30].

The average hourly wage was 12.54€ for nurses and 6.62€ for nurses' aides, according to in the figures from 2013 (Finances Ministry).

In 2013 the costs extrapolation (Table 4) amount to € 6,431.77 (€ 3,229.57for nurses and € 3,202.20for nurses' aides). For five years (2009-2013), extrapolation estimated

Table 3.
Calculation of the cost of absenteeism (2009-2013).

Nurses	=	768	x	(12.54€	x	7)	X	1.83	=	23,411.28€
Nurses' aides	=	781	x	(6.62€	x	7)	X	1.83	=	66,268.59€
Total									=	89,679.87€

Source: The authors

Table 4.
Calculation of the cost of presenteeism (2013).

Nurses	= (14.48% / 100)	x	254	x	(12.54€	x	7) =	3,229.57€
Nurses' aides	= (27.19% / 100)	x	254	x	(6.62€	x	7) =	3,202.20€
Total							=	6,431.77€

Source: The authors

the total amount of costs at around €16,147.85 for the nurses' and € 16,011.00for nurses' aides (Table 3).

The total cost of lost productivity for work-related musculoskeletal disorders due to work accidents during the period 2009-2013 was estimated to be € 221,838.73, taken from adding the total cost of absenteeism (€189,679.87) and the total from presenteeism (€32,158.86).

4. Conclusions

The most important cause of WRMSDs for nurses and nurses' aides were patient transfers, and this injury had a prevalent symptom in the lumbar region (18%), and were predominantly on the right side for shoulders (10%), wrists (8%) and hands (4%), .

The loss of productivity in this institution, for instance in 2013, was (i) €16,866.92 for nurses' absenteeism and €8,989.03 for nurses' aides, and (ii) €3,229.57 for nurses' presenteeism, and €3,202.20 for nurses' aides. The total amount in loss of productivity in 2013 was €64,575.44.

The total estimated cost for 2009-2013 was €222,015.98, which came from absenteeism (€189,679.87) and presenteeism (€32,158.86). The Institution should take these results into consideration for the future occupational management strategies in order to resolve the problem.

In relation to absenteeism in these two professional groups, it was possible to estimate costs by comparing our results with the results from the Ministry of Health's social balance data sheet.

Costs resulting from work accidents from absenteeism due to WRMSDs may be estimated at around 10% of hospital total costs (€1,887,464.05, absenteeism due to occupational accidents or occupational diseases). This is a high value considering the size of the institution, and, thus, justifies the need for preventive measures and the management of this occupational health issue.

Regarding presenteeism and taking into account the overall score of the SPS-6, the dimension "avoid distraction" is the most visible for both nurses' aides and nurses. There is also a decrease in productivity, an increased likelihood of errors occurring, and lapses due to employees performing their duties with less ability to concentrate. Absenteeism and presenteeism lead to increased costs for the institutions and worse health outputs. It is assumed therefore that institutions should periodically undertake a

healthcare personal work health status assessment (particularly in hospitals), which will contribute to prevent and manage this occupational health problem.

The absenteeism and different causes of presenteeism (personal, organizational and social) analysis, the study of the impact of the productivity loss in health institutions, and the establishment of human resources policies to implement solutions should be addressed by further studies in this hospital. This will raise awareness in Occupational Health that should be shared with top hospital managers in order to contribute to a policy that prevents work accidents and work-related musculoskeletal disorders.

Work productivity in hospitals is not well understood and nurses' productivity results should be measured according to a hospital policy that includes (i) costs of absenteeism and presenteeism costs, and (ii) the relation between nurses (and nurses' aides) demands as well as the human resources needed to undertake the healthcare work. If this relation were better understood, managers may implement healthcare personal policies that would avoid an increase in injuries, hospital disease complications, longer hospitalizations, and patient mortality from healthcare outputs. Absenteeism and presenteeism should also be an indicator for patient care if we want to promote patient safety and worker safety in hospitals and other healthcare institutions.

References

[1] Serranheira, F., et al., Lesões musculoesqueléticas ligadas ao trabalho em enfermeiros portugueses: "Ossos do ofício" ou doenças relacionadas com o trabalho? Revista Portuguesa de Saúde Pública, 2012. DOI: 10.1016/j.rpsp.2012.10.001

[2] Trinkoff, A.M., et al., Musculoskeletal problems of the neck, shoulder, and back and functional consequences in nurses. Am J Ind Med, 41(3), pp. 170-178, 2002. DOI: 10.1002/ajim.10048

[3] Alexopoulos, E.C., Burdorf, A. and Kalokerinou, A., Risk factors for musculoskeletal disorders among nursing personnel in Greek hospitals. Int Arch Occup Environ Health, 76(4) pp. 289-294, 2003.

[4] Sherehiy, B., Karwowski, W. and Marek, T., Relationship between risk factors and musculoskeletal disorders in the nursing profession: A systematic review. Occupational Ergonomics, 4(4), pp. 241-279, 2004.

[5] Alexopoulos, E.C., Burdorf, A. and Kalokerinou, A., A comparative analysis on musculoskeletal disorders between Greek and Dutch nursing personnel. International Archives of Occupational and Environmental Health, 79(1), pp. 82-88, 2006. DOI: 10.1007/s00420-005-0033-z

[6] Serranheira, F., Uva, A. e Sousa, P., Ergonomia hospitalar e segurança do doente: Mais convergências que divergências. Revista Portuguesa de Saúde Pública. 2, pp 1-21, 2010.

[7] Letvak, S.A., Ruhm, C.J. and Gupta, S.N., Nurses' presenteeism and its effects on self-reported quality of care and costs. The American Journal of Nursing, 112(2), pp. 30-38, 2012.

[8] Serranheira, F., Lopes, F. e Uva, A., Lesões músculo-esqueléticas (LME) e trabalho: Uma associação muito frequente. Jornal das Ciências Médicas, Tomos CLXVIII, pp. 59-78, 2004.

[9] Serranheira, F., Lesões músculo-esqueléticas ligadas ao trabalho: Que métodos de avaliação do risco?, in Grupo de Disciplinas de Saúde Ambiental e Ocupacional - Escola Nacional de Saúde Pública. Universidade Nova de Lisboa: Lisboa, 2007, 299 P.

[10] Maia, P.M.S., Avaliação da capacidade laboral de enfermeiros em contexto hospitalar. ENSP: Lisboa, 2002.

[11] Fonseca, R. e Serranheira, F., Sintomatologia músculo-esquelética auto-referida por enfermeiros em meio hospitalar. Rev Port Saúde Pública. Volume Temático, pp. 37-44, 2006.

[12] Cotrim, T., et al., Assessing the exposure risk to low back-pain at nurses' related with patient handling using MAPO. In: Proceedings of the 16th World Congress on Ergonomics–Meeting Diversity in Ergonomics, Maastricht, Holanda. 2006.

[13] Barroso, M., Carneiro, P. and Braga, A., Characterization of ergonomic issues and musculoskeletal complaints in a Portuguese District Hospital. In: Proceedings do international symposium Risks for Health Care Workers: prevention challenges, ISSA, Atenas. 2007.

[14] Almeida, C., et al., Caracterização de LMELT em assistentes operacionais de um serviço de apoio hospitalar. saúde & trabalho: Sociedade portuguesa de medicina do trabalho, 8, pp. 131-144, 2012.

[15] Serranheira, F., et al., Nurses, working tasks and MSDs back symptoms: Results from a national survey. Work: A Journal of Prevention, Assessment and Rehabilitation, 41, pp. 2449-2451, 2012.

[16] Ibarra, F.B., Contabilidad de costes y analítica de gestión para las decisiones estratégicas. 1999.

[17] Morales, M.G.G., Silla, J.M.P. y Rodríguez-Molina, I., El absentismo laboral: Antecedentes, consecuencias y estrategias de mejora. Universitat de València, España, 2011.

[18] Cunha, M., et al., Manual de gestão de pessoas e do capital humano, Lisboa, 2008.

[19] Hemp, P., Presenteeism: At work-but out of it. Harvard Business Review, 82(10), pp. 49-58, 2004.

[20] Lofland, J.H., Pizzi, L. and Frick, K.D., A review of health-related workplace productivity loss instruments. Pharmacoeconomics, 22(3), pp. 165-184, 2004. DOI: 10.2165/00019053-200422030-00003

[21] Cooper, C. and Dewe, P., Well-being—absenteeism, presenteeism, costs and challenges. Occupational Medicine, 58(8), pp. 522-524, 2008. DOI: 10.1093/occmed/kqn124

[22] Burton, W.N., et al., The association of health status, worksite fitness center participation, and two measures of productivity. Journal of Occupational and Environmental Medicine, 47(4), pp. 343-351, 2005. DOI: 10.1097/01.jom.0000158719.57957.c6

[23] Grinyer, A. and Singleton, V., Sickness absence as risk-taking behaviour: A study of organisational and cultural factors in the public sector. Health, Risk & Society, 2(1), pp. 7-21, 2000. DOI: 10.1080/136985700111413

[24] Lerner, D., et al., The angina-related limitations at work questionnaire. Quality of life research, 7(1), pp. 23-32, 1997. DOI: 10.1023/A:1008880704343

[25] Ozminkowski, R.J., et al., The application of two health and productivity instruments at a large employer. Journal of Occupational and Environmental Medicine, 46(7), pp. 635-648, 2004. DOI: 10.1097/01.jom.0000131797.52458.c8

[26] Koopman, C., et al., Stanford presenteeism scale: Health status and employee productivity. Journal of Occupational and Environmental Medicine, 44(1), pp. 14-20, 2002. DOI: 10.1097/00043764-200201000-00004

[27] Ferreira, A.I., et al., Tradução e validação para a língua portuguesa das escalas de presentismo WLQ-8 E SPS-6. Avaliação Psicológica, 9(2), pp. 253-266, 2010.

[28] Mitchell, R.J. and Bates, P., Measuring health-related productivity loss. Population health management, 14(2), pp. 93-98, 2011. DOI: 10.1089/pop.2010.0014

[29] Pereira, J. e Mateus, C., Custos indirectos associados à obesidade em Portugal. Revista Portuguesa de Saúde Pública, 3, pp. 65-80, 2003.

[30] Mitchell, R.J. and Bates, P., Measuring health-related productivity loss. Population health management, 14(2), pp. 93-98, 2011. DOI: 10.1089/pop.2010.0014

M.E. Queiroz-Lima, is currently head nurse at Centro de Medicina e Reabilitação de Alcoitão, and she is undertaking a postgraduate degree in Psychomotricity at FMH as well as a qualification in Infant and Pediatric Health Nursing at the Nursing School of São José de Cluny. She has a MSc. degree in Health Management from ENSP/Universidade Nova de Lisboa, Portugal.
ORCID: 000-0003-1499-9823.

F. Serranheira, received his MSc in Ergonomics in 1996 and his MSc degree in Public Health in 2000, and his PhD in Occupational Health/Public Health in 2007 from the Universidade Nova de Lisboa, Portugal. He is currently an assistant professor at ENSP/UNL, Occupational and Environmental Health Department.
ORCID: 0000-0001-7211-2843

UNIVERSIDAD NACIONAL DE COLOMBIA
SEDE MEDELLÍN
FACULTAD DE MINAS

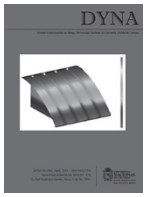

DYNA
http://dyna.medellin.unal.edu.co/

Identification of areas of intervention for public safety policies using multiple correspondence analysis

Jesús Antonio Carrillo-Castrillo [a], Juan Carlos Rubio-Romero [b], José Guadix [c] & Luis Onieva [d]

[a] *Grupo de Investigación en Ingeniería de Organización, Universidad de Sevilla, Sevilla, Spain. jcarrillo@io.us.es*
[b] *Escuela de Ingenieros Industriales, Universidad de Málaga, Málaga, Spain. juro@uma.es*
[a] *Grupo de Investigación en Ingeniería de Organización, Universidad de Sevilla, Sevilla, Spain. guadix@io.us.es*
[a] *Grupo de Investigación en Ingeniería de Organización, Universidad de Sevilla, Sevilla, Spain. onieva@io.us.es*

Received: December 07th, 2015. Received in revised form: March 01rd, 2016. Accepted: March 07th, 2016.

Abstract
Analysis of accident reports has been a useful tool in occupational safety research. According to European Statistics on Accidents at Work framework (ESAW), important variables related to the main circumstances of accidents are being gathered in Europe. The purpose of this paper is to present a method for analysis of accident databases that are coded according to the ESAW and based on Multiple Correspondence Analysis. The method proposed considers the implicit conceptual relationship between the exposure and accident variables in order to identify main areas for public policy intervention. This method is presented by analyzing specific working processes using a dataset of the accidents that were reported in the Andalusian manufacturing over a ten-year period. The method presented allowed easy identification of the main associations candidates for public intervention programs. Each could be object to further detailed research before designing the intervention program. This method could help policy makers when identifying areas for public intervention.

Keywords: occupational safety, accident analysis, risk factors, multiple correspondence analysis, ESAW.

Identificación de aéreas de intervención de políticas públicas en seguridad laboral usando análisis de correspondencias múltiple

Resumen
El análisis de los partes de accidentes ha sido una herramienta útil en la investigación en materia de seguridad laboral. De acuerdo a marco para la elaboración de Estadísticas de Accidentes Laborales en Europa (ESAW), hay importantes variables relacionadas con las principales circunstancias de los accidentes que se están recopilando en Europa. El objetivo de este artículo es presentar in método de análisis de bases de datos de accidentes codificados de acuerdo a ESAW mediante el uso de Análisis de Correspondencias Múltiple. El método propuesto tiene en cuenta las relaciones conceptuales implícitas entre las variables relacionadas con la exposición y las variables relacionadas con el accidente para identificar las áreas de intervención pública de las políticas de seguridad laboral. Este método es presentado analizando procesos específicos de trabajo en la información reportada de los accidentes laborales en el sector industrial de Andalucía en un período de 10 años. El método presentado permite una identificación fácil de las principales asociaciones que puedan ser objeto de programas de intervención pública. Cada una de estas asociaciones puede ser analizada en mayor detalle antes del diseño del programa de intervención. Este método puede ayudar a los responsables de elaborar políticas para identificar áreas de intervención pública.

Palabras clave: seguridad laboral, análisis de accidentes, factores de riesgo, análisis de correspondencias múltiple, ESAW.

1. Introduction

1.1. Accident analysis

Analysis of accident reports have been a useful tool in occupational safety research [1].

Governments have also understood the importance of the quality of accident reports data. For instance, the European Union developed a project denominated European Statistics on Accidents at Work (ESAW hereinafter), launched in 1990 [2]. The main purpose of ESAW is to harmonize data on accidents at work and also to incorporate meaningful variables from accident scenarios.

Over the last decades, most researchers have used statistical analysis to discover the relationships between circumstances and accident occurrence.

© The author; licensee Universidad Nacional de Colombia.

Accident circumstances are usually structured as a flow of events [3] and then analyzed with contingency tables. Also, exploratory techniques [4] and clustering tools [5] have been used to identify sequences of events and their prevalence. Accident analysis has been used for risk assessment as well [6,7].

Also, correspondence methods have been applied to explore relationships among certain variables, such as between deviations and the type of accident injury[8].

All these methods are useful for identifying relation ships between accident circumstances variables; nevertheless, from a prevention and risk assessment perspective, the key factor is to analyze the relationships between the categories of these variables and not just the between-variable relations [9].

An important issue is that accidents need to be analyzed considering their different etiology. A group of accidents from the same scenario share a common internal structure in terms of the exposure and circumstances leading to the accident's occurrence [10].

1.2. Accident notification according to ESAW

In Europe, as harmonized variables and classifications of the circumstances of accidents at work that establish the prevalent situation and conditions at the time of the accident are coded using ESAW, identifying the accident scenarios in accident reports should be undertaken using the ESAW taxonomy.

European Parliament and of the Council regulation (EC) No 1338/2008 of 16th December 2008 on community statistics on public health and health and safety at work sets out obligations to supply statistics on accidents at work to the European Commission, according to the third phase of ESAW (ESAW-III). In the third phase of ESAW [2], the harmonized and common data set to be provided on accidents at work cover new characteristics of the accident, including the sequence of event characterizing the accident's causes and circumstances.

Regarding the quality of the data from accident notification, according to [10] Spain has properly implemented ESAW, which is comparable to most western countries [11]. It is important to highlight that every accident notification is accepted by the mutual insurance system in Spain, which covers the cost of rehabilitation after an accident, and it must be also reviewed by the Labor Authority, which on occasion performs its own accident investigations. In an unpublished report by the Instituto Nacional de Seguridad e Higiene en el Trabajo (the National Institute for Occupational Health and Safety in Spain), the quality of accidents notified from 2003 to 2008 was analyzed. It was concluded that the circumstances of the accidents showed adequate information in more than 90% of those cases [12].

In a deeper analysis, using cross-sectional double-blind design, Molinero-Ruiz et al. (2015) found a moderate agreement reliability coefficient (Kappa index) for most categories with the *Deviation* and *Contact* variables [13].

Analysis of the ESAW data needs to be undertaken with a clear differentiation between the circumstances related to risk exposure and the circumstances related to the accident occurrence [14].

The variables relating to exposure are *Working Process* and *Specific Physical Activity*, and the variables relating to the accident itself are *Deviation* and *Contact*. For each variable there are two levels of coding.

1.3. Paper objective

The purpose of this paper is to present a method to analyze accident databases that are coded according to ESAW and based on Multiple Correspondence Analysis (hereinafter MCA).

The method proposed considers the implicit conceptual relationship between exposure variables and accident variables in order to identify main areas for public policy intervention.

This method is presented analyzing specific working processes using a dataset of the accidents reported in the Andalusian manufacturing sector over a ten-year period.

2. Materials and Methods

2.1. Data

In order to present the method, we have gathered all accidents that have led to at least one day of absence in the Andalusian manufacturing sector, from 2003 to 2012, with a total of 201,311 valid accident notifications.

According to Eurostat, the manufacturing sector uses NACE economic classification. Manufacturing is the sector in Europe with the highest number of annual days of absence due to accidents [15]. In order to limit the analysis to accidents occurring in industrial sites, we used the ESAW variable working environment.

The latest incidence rate for the manufacturing sector published by Eurostat is 3,097 accidents per 100,000 workers, which shows the importance of manufacturing sector accidents for accidents with more than three days' absence in the European Union and Norway in 2007

It is important to add that Andalusia is one of the biggest regions in Europe, represents approximately 12% of the Spanish manufacturing sector, and employs on average more than 200,000 workers.

In Spain, accident reports are electronically collected in "Official Workplace Incident Notification Forms" [16]. All accidents that result in an absence from work for one or more days must be notified.

For each accident, variables related to main circumstances are gathered according to ESAW: *Working Process*, *Specific Physical Activity*, *Deviation* and *Contact*.

2.2. Implicit structure of the accident circumstances

Another important issue is that in-depth analyses of accident circumstances of should only be carried out for accidents classified as fitting the same scenario [6, 10]. The accident scenario is identified by the combination of accident circumstances (see Fig. 1).

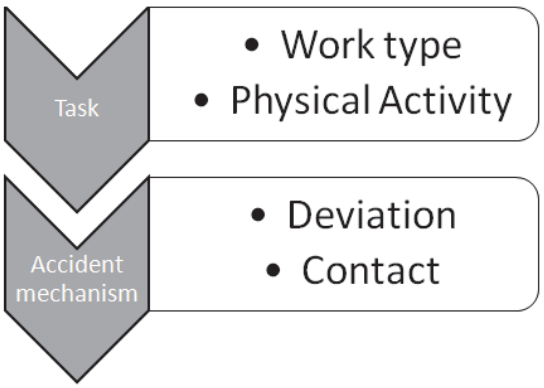

Figure 1. Concepts of task and accident mechanisms in the flow of events. Source [6].

According to previous researchers' findings, and regarding ESAW variables, meaningful concepts underlie the structure of accident reports [6]. In particular, two main concepts are directly linked with flow of events that lead to the accident: *Task* and *Accident Mechanism*.

The *Task* is what the worker was doing. This concept can be used to identify the risk that the worker was exposed to when the accident occurred. Tasks are identified through the ESAW variables *Working Process* and *Specific Physical Activity*.

According to ESAW, *Working Process* is the "main type of work or task (general activity) being performed by the victim at the time of the accident" and *Specific Physical Activity* is "the victim's exact specific physical activity at the instant of the accident."

The *Accident Mechanism* is what happened in the lead-up from normal work to when the accident occurred. The accident mechanism is used to identify each central bow-tie events and it is defined by the combination of the ESAW variables *Deviation* and *Contact* [6,17].

According to ESAW, *Deviation* is "the event that triggers the accident" and *Contact* is "the contact that injured the victim."

2.3. Method

The relationships between the variables and their categories in ESAW can be identified using Multiple Correspondence Analysis (MCA hereinafter).

MCA analysis, as an exploratory technique and provides an intuitive representation of how certain categories are close enough to intuit an association [8]. MCA is also a useful method for presentation purposes as the plots are very intuitive [18].

MCA is a multivariate statistical technique. It is conceptually similar to principal component analysis, but applies to categorical rather than continuous data. In a similar manner to principal component analysis, it provides a means of displaying or summarizing a set of data in two-dimensional graphical form.

The nearest two modalities are in the plot, the stronger one is the evidence of the relationship between them. It must be considered that in the center of the correspondence plot, very little can be said as it represents the average profile.

A group of categories that are close to each other and separated from the rest is called a cluster, and in terms of accident analysis a cluster identifies a scenario of accidents that could be prevented.

The identification of category clusters is subjective. To provide a more objective identification, the Phi coefficient test has been used to identify all significant associations [19]

Table 1.
Most frequent tasks for accidents in Production.

(ESAW code) *Working Process*	(ESAW code) *Specific Physical Activity*	*Task*	Number
(1x) Production, manufacturing, processing, and storing	(4x) Handling of objects (manually)	T1	53,241
	(2x) Working with hand-held tools	T2	26,205
	(6x) Movement (walking, getting in/out, jumping, etc.)	T3	25,088
	(5x) Carrying by hand, transporting	T4	18,189
	(1x) Operating machine	T5	17,582

Source: Elaborated by the authors based on Accidents notified in the Andalusian manufacturing sector 2003-2012

Table 2.
Most frequent accident mechanisms for accidents within the tasks identified in Table 1.

(ESAW code) *Deviation*	(ESAW code) *Contact-Mode of Injury*	*Accident mechanism*	Number
(7x) Body movement under/with physical stress	(7x) Physical or mental stress (includes stress on the musculoskeletal system)	M1	33,968
(4x) Loss of control (total or partial)	(5x) Contact with a sharp, pointed, rough, coarse material agent	M2	9,839
(4x) Loss of control (total or partial)	(4x) Struck by, collision with object in motion	M3	7,989
(5x) Slipping - Stumbling and falling - fall	(3x) Impact with or against a stationary object …	M4	8,369
(6x) Body movement without any physical stress	(7x) Physical or mental stress (includes musculoskeletal system)	M5	7,858
(3x) Breakage, bursting, splitting, (…) of Material	(4x) Struck by, collision with object in motion	M6	5,593
(6x) Body movement without any physical stress	(5x) Contact with sharp, pointed, rough, coarse material agent	M7	5,190
(6x) Body movement without any physical stress	(3x) Impact with or against a stationary object	M8	4,375
(3x) Breakage, bursting, splitting, (…) of Material Agent	(5x) Contact with a sharp, pointed, rough, coarse material agent	M9	3,567

Source: Elaborated by the authors based on Accidents notified in the Andalusian manufacturing sector 2003-2012

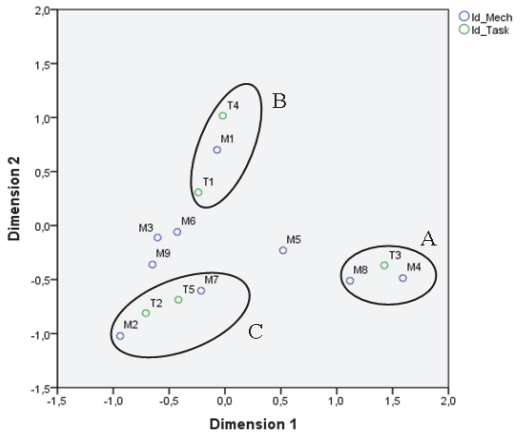

Figure 2. Plot of Task and Accident Mechanism in "Production". The label in each Task and Accident Mechanism from tables 1 and 2 is indicated. Source: Elaborated by the authors

3. Results

3.1. Correspondence analysis of accidents in "production"

In this section we use the ESAW first level of coding. The symbol x is used to identify all possible codes with the same first digit in the code.

The method proposed is used to analyze a specific type of accidents: accidents with code 1x for *Working process* in ESAW. For ESAW, code 1x is used for "Production, manufacturing, processing, and storing", including storing.

The most frequent tasks are presented in Table 1, and the most frequent accident mechanisms are presented in Table 2. Note that in ESAW the codes used for each variable are the same, so depending on the variable in the column title, the meaning of a code can be different.

For those tasks and accident mechanisms, two dimensions captured 98% of the total inertia.

In Fig. 2, there is a representation of the categories after correspondence analysis.

In terms of accident prevention, this association identifies an accident scenario. Main associations, according to Fig. 2, are the following generic accident scenarios:

1. Scenario A: "Movements" tasks (T3) are associated with the accident mechanisms "slipping - stumbling and falling - fall", or with "body movement without any physical stress", which leads to "impact with or against a stationary object" (M4) and (M8).
2. Scenario B: "Handling of objects (manually)" (T1) and "carrying by hand, transporting" (T4) are associated with "body movement under/with physical stress" which leads to "physical or mental stress (including stress on the musculoskeletal system)" (M1).
3. Scenario C: Tasks such as "operating machines" (T2) and "working with hand-held tools" (T5) are associated with "loss of control" accident mechanisms, which leads to "contact with a sharp, pointed, rough, coarse material agent" (M2), and "body movement without any physical stress" accident mechanisms, which leads to "contact with a sharp, pointed, rough, coarse material agent" (M7).

Table 3.
Most frequent tasks for accidents in setting up, preparation, installation, mounting, disassembling, and dismantling.

(ESAW code) *Working Process*	(ESAW code) *Specific Physical Activity*	*Task*	Number
(51) Setting up, preparation, installation, mounting, disassembling, dismantling	(41) Manually taking control of, grasping, seizing, holding, placing - on a horizontal level	T1	4,394
	(61) Walking, running, going up, going down, etc.	T2	2,172
	(21) Working with hand-held tools - manual	T3	1,540
	(51) Carrying vertically - lifting, raising, lowering an object	T4	1,119
	(22) Working with hand-held tools - motorized	T5	963
	(43) Fastening, hanging up, raising, putting up - on a vertical level	T6	933
	(40) Handling of objects - not specified	T7	630
	(67) Movements on the spot	T8	531
	(53) Transporting a load - carried by a person	T9	505
	(42) Tying, binding, tearing off, undoing, squeezing, unscrewing, screwing, turning	T10	488

Source: Elaborated by the authors based on Accidents notified in the Andalusian manufacturing sector 2003-2012

Table 4.
Most frequent accident mechanisms for accidents in setting up, preparation, installation, mounting, disassembling, and dismantling (within the ten tasks identified in Table 3).

(ESAW code) *Deviation*	(ESAW code) *Contact-Mode of Injury*	*Accident mechanism*	Nº cases
(71) Lifting, carrying, standing up	(71) Physical stress - musculoskeletal system	M1	1,546
(64) Uncoordinated movements, spurious or untimely actions	(71) Physical stress - musculoskeletal system	M2	486
(51) Fall of person - to a lower level	(31) Vertical motion, crash on or against	M3	422
(70) Body movement under or with physical stress - not specified	(71) Physical stress - musculoskeletal system	M4	429
(52) Slipping - Stumbling and falling - Fall of person - on the same level	(31) Vertical motion, crash on or against	M5	315
(44) Loss of control (total or partial) - of object	(42) Struck - by falling object	M6	306
(72) Pushing, pulling	(71) Physical stress - musculoskeletal system	M7	279
(33) Slip, fall, collapse of material agent - from above	(42) Struck - by falling object	M8	268
(43) Loss of control (total or partial) - hand-held tool (motorized or not) or of the material being worked by the tool	(51) Contact with sharp material Agent (knife, blade etc.)	M9	230
(74) Twisting, turning	(71) Physical stress - musculoskeletal system	M10	229

Source: Elaborated by the authors based on Accidents notified in the Andalusian manufacturing sector 2003-2012

Table 5.
Most frequent contacts for accidents in setting up, preparation, installation, mounting, disassembling, and dismantling (within the ten tasks identified in Table 3).

(ESAW code) *Contact-Mode of Injury*	*Contact*	Nº cases
(71) Physical stress - musculoskeletal system	C1	4,000
(31) Vertical motion, crash on or against	C2	1,224
(42) Struck - by falling object	C3	1,222
(50) Contact with a sharp, pointed, rough, coarse material agent - not specified	C4	1,039
(51) Contact with a sharp material agent (knife, blade etc.)	C5	902
(32) Horizontal motion, crash on or against	C6	808
(41) Struck - by flying object	C7	517
(40) Struck by object in motion, collision with - not specified	C8	504
(30) Horizontal or vertical impact with or against a stationary object (the victim is in motion) - not specified	C9	392
(52) Contact with a pointed material agent (nail, sharp tool etc.)	C10	293
(43) Struck - by swinging object	C11	288

Source: Elaborated by the authors based on Accidents notified in the Andalusian manufacturing sector 2003-2012

3.2. Correspondence analysis of accidents in "Setting up, preparation, installation, mounting, disassembling, and dismantling"

In this section, the method is used to analyze in-depth a specific type of accident: accidents with code 51 in ESAW for the *Working process* variable, which is used for "Setting up, preparation, installation, mounting, disassembling, and dismantling".

This type of work is part of the manufacturing activities process, but is most of the time related to construction and on-site delivery of pieces of equipment or industrial products. The most frequent tasks are presented in Table 3.

For those tasks, the most frequent accident mechanisms are presented in Table 4, and the most frequent modes of contact are presented in Table 5.

Note that in ESAW the codes used for each variable are the same, so depending on the variable in the column title, the meaning of a code can be different.

3.2.1. Analysis of associations between task and accident mechanisms in "*setting up, preparation, installation, mounting, disassembling, and dismantling*" accidents.

MCA of the Task and Accident Mechanism variables with two dimensions captured 82% of the total inertia and identified at least two scenarios for intervention (see Fig. 3):

1. Scenario D: "Working with hand-held tools – motorized" (T5) tasks are associated with "loss of control (total or partial) - of hand-held tool (motorized or not) or with the material being worked by the tool" accident mechanism, which lead to "contact with a sharp material agent (knife, blade etc.)" (M9).
2. Scenario E: "Walking, running, going up, going down" (T2) tasks are associated with "fall of person - to a lower level" or "Slipping - Stumbling and falling - Fall of person - on the same level" accident mechanisms, which lead to "vertical motion, crash on or against (resulting from a fall)" (M3, M5).

The phi coefficient test identifies the following significant associations (see Table 6):

3.2.2. Analysis of associations between Task and Contact in "setting up, preparation, installation, mounting, disassembling, and dismantling" accidents

MCA for the variables *Task* and *Contact* with two dimensions captured 90% of the total inertia and identified at least four scenarios for intervention (see Fig. 4):

1. Scenario F: "Walking, running, going up, going down, etc." (T2) tasks are associated with "vertical motion, crash on or against" (C2) or "horizontal motion, crash on or against" contacts (C6).

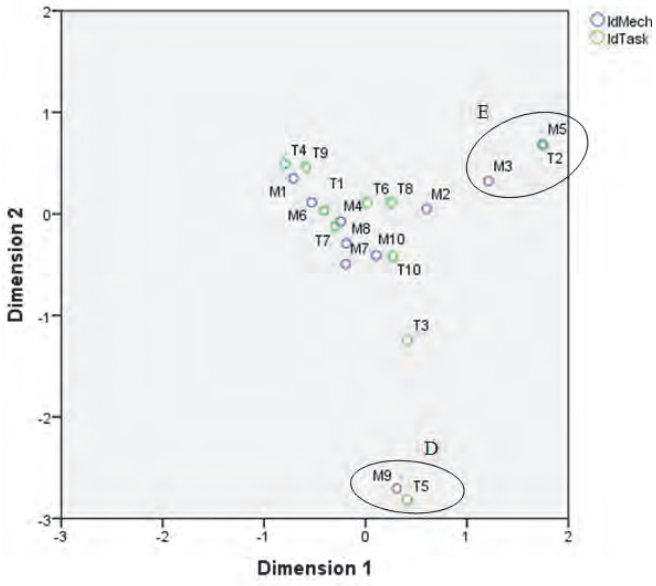

Figure 3. Plot of Task and Accident Mechanisms in "setting up, preparation, installation, mounting, disassembling, and dismantling". The label in each Task and Accident Mechanism from Tables 1 and 2 is indicated. Source: Source: Elaborated by the authors.

Table 6.
Phi coefficient analysis of Task and Accident Mechanisms in "setting up, preparation, installation, mounting, disassembling, and dismantling".

Tas K	M1	M2	M3	M4	M5	M6	M7	M8	M9	M10
T1						#				
T2		#	#		#					
T3									#	
T4	#					#				
T5									#	
T6			#			#		#		
T7				#						
T8		#								#
T9	#					#				
T10		#					#			#

Source: Elaborated by the authors based on Accidents notified in the Andalusian manufacturing sector 2003-2012

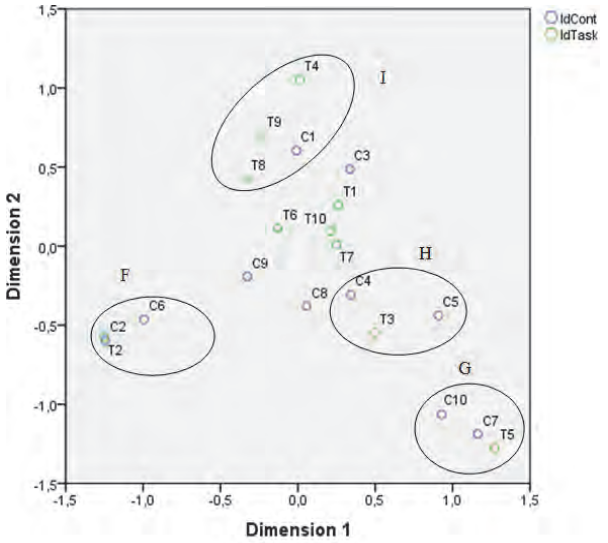

Figure 4. Plot of Task and Contact in "setting up, preparation, installation, mounting, disassembling, and dismantling". The label in each Task and Contact from Tables 1 and 2 is indicated.
Source: Elaborated by the authors.

Table 7.
The phi coefficient analysis of Task and Accident Mechanisms in "setting up, preparation, installation, mounting, disassembling, and dismantling".

Task	C1	C2	C3	C4	C5	C6	C7	C8	C9	C10	C11
T1	#		#		#						#
T2		#				#			#		
T3					#		#	#		#	#
T4	#		#								
T5				#	#		#				
T6		#									#
T7				#				#			
T8	#										
T9	#										
T10			#	#							

Source: Elaborated by the authors based on Accidents notified in the Andalusian manufacturing sector 2003-2012

2. Scenario G: "Working with hand-held tools - motorized" (T5) tasks are associated with "struck - by flying object" (C7) or "contact with a pointed material agent (nail, sharp tool etc.)" contacts (C10).
3. Scenario H: "Working with hand-held tools – manual" (T3) tasks area associated with "contact with sharp Material Agent (knife, blade etc.)" contacts (C5).
4. Scenario I: "Carrying vertically - lifting, raising, lowering an object" (T4), "movements on the spot" (T8) and "transporting a load - carried by a person" (T9) tasks are associated with "physical stress - musculoskeletal system" (C1) contacts.

The phi coefficient test identifies the following significant associations (Table 7):

4. Discussion

In this paper Multiple Correspondence Analysis is used to identify intervention areas for preventive programs. For such identification, the accident scenario concept is used.

The first of the areas is identified as an example (Scenario A), in which tasks related to "movements" (T3) are associated with accident mechanisms in terms of "slipping - stumbling and falling -fall" or with "body movement without any physical stress", which leads to "impact with or against a stationary object" (M4) and (M8). The methodology presented identifies an intervention area focused on the prevention of falls and other movements, which leads to impact with stationary objects.

Although difficult to interpret the meaning of the dimensions in MCA, each scenario consists of accidents that are similar in the transformed space, and thus the preventive activities should be effective considering the flow of events.

The method presented allowed the main association candidates for public intervention programs to be easily identified. Each can be an object of further detailed research before designing the relevant intervention program [20].

Multiple Correspondence Analysis offers an improvement on the analysis of the relative frequency of each combination of variables [7,9] because the association in the transformed space of dimensions identifies an internal relationship that is related to the structure of the accident in terms of the codification of the variables used to describe the circumstances.

Although it is difficult to name the dimensions, the explanation of the inertia in the model is a measure of how the model explains those relationships between the categories of the variables.

It should be noted that this identification of accident scenarios is only based on some variables included in the technological subsystem. Other subsystems, such as human factors and organization, are unfortunately not yet incorporated with the same level of detail in ESAW. As Jacinto et al. (2009) [21] have proposed, it is necessary to incorporate new variables, such as individual contributing factors, work place factors and organizational and management factors to future research.

New variables available, such as the worker's level of training, should be included in Multiple Correspondence Analysis for a more detailed identification of the accident scenarios.

In the phi test that was performed, not all the associations found were significant. We should highlight the differences in the methods, MLA and phi test..

4.1. Application in the design of preventive programs

The identification of scenarios should be complemented by accident analysis, with the specific accident scenario in order to identify the most frequent causes.

For example, in [19] there is an analysis of the most frequent causes of the accident mechanisms in the Andalusian manufacturing sector.

Therefore, the combination of Multiple Correspondence Analysis as presented in this paper, and the results of the analysis for the most prevalent causes of each of the accident mechanisms can be used to more effectively design public safety programs.

Note than in ESAW, some contacts relate to musculoskeletal injuries that come from physical stress, so some of the accidents reported are not the usual accidents

generally considered in other scientific research on this topic.

4.1. Application of the initial analysis of types of accidents with little research available

In this paper, there is an exploratory analysis of accidents the following activities: "setting up, preparation, installation, mounting, disassembling, and dismantling." These accidents are part of the manufacturing activities, but in most cases involve construction techniques.

This paper presents an initial identification of the most important accident scenarios, and shows the usefulness of this method to analyze accidents with almost no literature available. It also makes suggestions as to which direction the following research should be focused.

Most of the scenarios identified in "setting up, preparation, installation, mounting, disassembling, and dismantling" have been studied in the literature for other activities, such as falls, handling, loss of control and being struck by accidents.

Therefore the exploratory methodology presented could be very effective for types of accidents for which there is only a small amount of literature available.

4.2. Limitations of the method

There is a concern related to quality of the data and underreporting issues, as there is with any method using accident reports data,. As was mentioned in Molinero-Ruiz et al. (2015) [13], public authorities need to look for a better and more reliable database for ESAW in order to enable better research on this topic.

Another limitation is the lack of information about how many workers are exposed to the risk that the individual worker was exposed to when the accident occurred.

Regarding the specific accident mechanism, it must be noted that the data is based on manufacturing in Andalusia and used all accidents. Other studies [22,23] show different results depending on the countries or industries analyzed or the injuries included, for instance when limiting results to fatal and non-slight accidents.

References

[1] Khanzode, V.V., Maiti, J. and Ray, P., Occupational injury and accident research: A comprehensive review. Safety Science, 50(5), pp. 1355-1367, 2012. DOI: 10.1016/j.ssci.2011.12.015

[2] European Commission. European Statistics on Accidents at Work (ESAW) – Methodology (ed. 2001): Luxembourg, Office for Official Publications of the European Communities. 2002

[3] Rajala, H.-K. and Väyrynen, S., Constructing ''core stories" for contributing practical safety actions in industrial units. Safety Science, 48(10), pp. 1393-1401, 2010. 10.1016/j.ssci.2010.05.014

[4] Chi, C.-F. and Chen, C.-L., Reanalyzing occupational fatality injuries in Taiwan with a model free approach. Safety Science 41(8), pp. 681-700, 2003. DOI: 10.1016/S0925-7535(02)00018-8

[5] Palamara, F., Piglione, F. and Piccinini, N., Self-Organizing map and clustering algorithms for the analysis of occupational accident databases. Safety Science, 49(8-9), pp. 1215-1230, 2011. DOI: 10.1016/j.ssci.2011.04.003

[6] Carrillo-Castrillo, J.A., Rubio-Romero, J.C., Guadix, J. and Onieva, L., Risk assessment of maintenance operations: The analysis of performing task and accident mechanism. International Journal of Injury Control and Safety Promotion, 2014. DOI:10.1080/17457300.2014.939196

[7] San Miquel-Pera, L., Vintró, C. and Freijo, M. Characteristics of the 3 most common types of occupational accident in Spanish sub-surface and surface mining, from 2003–2008. DYNA, 79(172), pp. 118-125, 2012.

[8] Conte, J.C., Rubio, E., García, A.I. and Cano, F., Occupational accidents model based on risk–injury affinity groups. Safety Science, 49(2), pp. 306-314, 2011. DOI: 10.1016/j.ssci.2010.09.005

[9] Silva, J.F. and Jacinto, C., Finding occupational accident patterns in the extractive industry using a systematic data mining approach. Reliability Engineering and System Safety, 108, pp. 108-122, 2012. DOI: 10.1016/j.ress.2012.07.001

[10] Hale, A., Ale, B., Goosens, L., Heijer, T., Bellamy, L., Mud, M., Roelen, A., Baksteen, H., Post, J., Papazoglou, I., Bloemhoff, A. and Oh, J., Modeling accidents for prioritizing prevention. Reliability Engineering and System Safety, 92(12), pp. 1701-1715, 2007. DOI: 10.1016/j.ress.2006.09.025

[11] Jacinto, C., Guedes-Soares, C., Fialho, T., Antão, P. and Silva, S.A., An overview of occupational accidents notification systems within the enlarged EU. Work, 39, pp. 369-378, 2004.

[12] Benavides, F., Delclos, G., Cooper, S. and Benach, J., Comparison of fatal occupational injury surveillance systems between the European Union and the United States. American Journal of Industrial Medicine, 44(4), pp. 385-391, 2003. DOI: 10.1002/ajim.10290

[13] Molinero-Ruiz, E., Pitarque, S., Fondevila-McDonald, Y. and Martin-Bustamante, M., How reliable and valid is the coding of the variables of the European Statistics on Accidents at Work (ESAW)? A need to improve preventive public policies. Safety Science, 79, pp. 72-79, 2015.

[14] Instituto Nacional de Seguridad e Higiene en el Trabajo. Análisis de la calidad y especificidad de la cumplimentación del parte de accidente de trabajo en el sistema Delt@ periodo 2003-2008. Unpublished report, 2010.

[15] European Commission. Eurostat: Your key to european statistics. [On line]. 2012. Available at: http://epp.eurostat.ec.europa.eu/.

[16] Jacinto, C. and Aspinwall, E., A survey on occupational accidents' reporting and registration systems in the European Union. Safety Science, 42(10), pp. 933-960, 2004. DOI: 10.1016/j.ssci.2004.07.002

[17] Jacinto, C. and Guedes-Soares, C., The added value of the new ESAW/Eurostat variables in accident analysis in the mining and quarrying industry. Journal of Safety Research, 39(6), pp. 631-644, 2008. DOI: 10.1016/j.jsr.2008.10.009

[18] Pérez-Alonso J., Carreño-Ortega A. and Vázquez-Cabrera F.J., Callejón-Ferre A.J., Accidents in the greenhouse-construction industry of SE Spain. Applied Ergonomics, 43(1), pp. 69-80, 2012. DOI: 10.1016/j.apergo.2011.03.007

[19] Chi, C.-F., Chang, T.-C. and Hung, K.-H., Significant industry–source of injury–accident type for oc-cupational fatalities in Taiwan. International Journal of Industrial Ergonomics, 34(2), pp. 77-91, 2004. DOI: 10.1016/j.ergon.2004.03.002

[20] Carrillo-Castrillo, J.A., Rubio-Romero, J.C. and Onieva, L., Causation of severe and fatal accidents in the manufacturing sector. International Journal of Occupational Safety and Ergonomics, 19(3), pp. 423-434, 2013. DOI: 10.1080/10803548.2013.11076999

[21] Jacinto, C., Canoa, M. and Guedes, C., Workplace and organizational factors in accident analysis within the food industry. Safety Science, 47(5), pp. 626-635, 2009. DOI: 10.1016/j.ssci.2008.08.002

[22] Bellamy, L.J., Manuel, H.J. and Oh, J., Investigated serious occupational accidents in The Netherlands, 1998–2009. International Journal of Occupational Safety and Ergonomics, 20(1), pp. 19-32, 2014. DOI: 10.1080/10803548.2014.11077033

[23] European Commission., J. Causes and circumstances of accidents at work in the EU. Luxembourg: Office for Official Publications of the European Communities, 2009.

J.A. Carrillo-Castrillo, received his BSc. and MSc. in Industrial Engineering in 1995 from the University of Seville, Spain, his MSc. in Manufacturing Systems Engineering in 1996 from the Rensselaer Polytechnic Institute, USA, and his PhD in Industrial Organization in 2015 from the University of Seville, Spain. From 1996 to 2002, he worked for

enterprises in the manufacturing sector in Spain as a quality manager, responsible for e-commerce and reengineering. Since 2002 he has worked for the public administration in different departments such as information technologies, occupational health and safety and currently in the innovation at health department as a secondary Director. Recently he has also worked as adjunct professor. His research interests include: occupational safety, innovation management, industrial management and organizational design.
ORCID: 0000-0003-2873-1895

J.C. Rubio-Romero, (PhD, MSc, MEng), is an Industrial Engineer and an Associate Professor of "Safety at Work" in the School of Industrial Engineering of the University of Malaga, Spain. He obtained his PhD in 2000 in occupational health and safety in the industry, and is currently the Chair of Prevention and Social Corporate Responsibility at the University of Malaga as well as the director of the research group, "Operations and Sustainability: Quality, ICT and Risk Prevention at Work". Dr. Rubio has spent over 18 years undertaking research into workplace health and safety and has published a wide range of textbooks, reports, and papers, especially on management of workplace health and safety in the manufacturing industry and at construction sites.
ORCID: 0000-0002-5122-7526

J. Guadix, studied Industrial Engineering and obtained his PhD in the School of Industrial Engineering from the University of Seville, Spain, in 2004. His research interests include operations research, service industry and, health and safety. He has been a consultant for several leading services companies and Regional Government Administrations since 2000. Currently, he is Associate Professor and Vice-Rector of Technology Transfer at the University of Seville, Spain.
ORCID: 0000-0002-3221-5095

L. Onieva, received his BSc. Eng and MSc. in Industrial Engineering in 1984 and his PhD in Industrial Organization in 1986 from the University of Seville, Spain, after which he joined the Department of Industrial Organization and Enterprise Management. He has been a full professor since 1995 and he has been chairman of his department and Vice-chancellor of Innovation of the University of Seville. He has also been the Director of the Innovation Foundation of the University of Seville and President of the Association for the developing of the Organization Engineering (ADINGOR). As researcher he has been responsible of numerous R+D+R funded by public and/or private entities and he has published several books and papers in prestigious national and international journals. His research interests are industrial management, operations research and innovation.
ORCID: 0000-0002-4466-615X

UNIVERSIDAD NACIONAL DE COLOMBIA
SEDE MEDELLÍN
FACULTAD DE MINAS

Área Curricular de Ingeniería Administrativa e Ingeniería Industrial

Oferta de Posgrados

Especialización en Gestión Empresarial
Especialización en Ingeniería Financiera
Maestría en Ingeniería Administrativa
Maestría en Ingeniería Industrial
Doctorado en Ingeniería - Industria y Organizaciones

Mayor información:

E-mail: acia_med@unal.edu.co
Teléfono: (57-4) 425 52 02

UNIVERSIDAD NACIONAL DE COLOMBIA
SEDE MEDELLÍN
FACULTAD DE MINAS

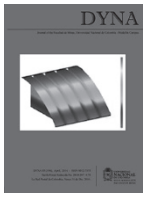

DYNA
http://dyna.medellin.unal.edu.co/

A qualitative analysis on occupational health and safety conditions at small construction projects in the Brazilian construction sector

Haroldo Pereira Gomes [a], Pedro Miguel Ferreira Martins Arezes [b] & Luiz Carlos Fadel de Vasconcellos [c]

[a] *Federal Center of Technological Education Celso Suckow da Fonseca, Rio de Janeiro, Brazil, haroldopgomes@gmail.com.*
[b] *Center Algoritmi, University of Minho, Guimarães, Portugal, parezes@dps.uminho.pt*
[c] *National Schol of Public Health-Fiocruz, Rio de Janeiro, Brazil, elfade@globo.com*

Received: December 03rd, 2015. Received in revised form: March 02nd, 2016. Accepted: March 14th, 2016.

Abstract
The main objective of this study is to analyze the perception of Occupational Health and Safety in small construction projects in the Brazilian construction industry. The adopted approach is qualitative in nature and seeks to understand the character of the current practices through interviews held with 'actors' who are directly involved in small-scale building sites, as well as with others who are involved in large-scale work sites. In Brazil, there is a weakness in supervision at small construction projects. This is due to numerous factors, such as the low visibility of these types of works and short deadlines, as well as the lack of knowledge about Occupational Health and Safety. This study reinforces and illustrates the idea of the inherent dangers involved in the occupational health of workers in small construction projects. It also indicates that there is a need to put greater emphasis on compliance with Occupational Health and Safety principles, which are covered by the current Brazilian Legislation and Regulatory Standards. This should be undertaken in order to ensure that the work in small-scale building sites is more visible and, especially, to ensure acceptable health and safety conditions for construction workers.

Keywords: Occupational; Health and Safety; construction; accident prevention; small construction projects.

Un análisis cualitativo de las condiciones de salud y seguridad en el trabajo en pequeños proyectos de construcción en el sector de la construcción brasileña

Resumen
Este estudio analiza la percepción de Salud y Seguridad Ocupacional en pequeños proyectos de construcción en la industria de la construcción brasileña. El enfoque adoptado es de naturaleza cualitativa y trata de comprender el carácter de las prácticas actuales a través de entrevistas. En Brasil, hay una debilidad en la supervisión en pequeños proyectos de construcción. Esto se debe a factores como la baja visibilidad de este tipo de obras, así como la falta de conocimiento sobre la Salud y Seguridad Ocupacional. Este estudio refuerza la idea de los peligros inherentes a la salud ocupacional de los trabajadores. Hay necesidad de poner énfasis en el cumplimiento de los principios de Seguridad y Salud Ocupacional. Esto debe asegurar que el trabajo en las obras de construcción a pequeña escala sea más visible y para garantizar las condiciones de salud y seguridad aceptables para trabajadores de la construcción.

Palabras clave: Ocupacional; salud y seguridad; construction; prevención de accidentes; pequeños proyectos de construcción.

1. Introduction

The main regulatory legislation covering safety and accident prevention in the Civil Construction Industry (CCI) in Brazil is the Regulatory Standard – NR-18. This is a legal document and it provides several guidelines to ensure a good working environment and safe working conditions in construction industry workplaces. It was established by Decree 3214 of June 8th 1978 [1]. This regulatory standard is the most important tool that focuses on measures for the prevention of accidents, as well as on Occupational Health for this business sector. Despite this, the document is only really followed by the larger companies, where contract workers are part of the formal employment market: this legally implies an employment relationship, and a formal contract.

© The author; licensee Universidad Nacional de Colombia.

The NR-18 requires that all kinds of construction projects, regardless of the size of the construction site, should follow the established rules [2].

The standard also states that companies with more than 20 employees must prepare a specific accident prevention program: the Program of Working Conditions and Environment (PCMAT). Therefore, in construction sites with fewer than 20 employees, there is no legal obligation to comply with these rules [3,4].

It is also necessary that all construction projects, regardless of their size, adopt the Environmental Risk Prevention Program (PPRA for its acronym in Portuguese). This is the initial reference to risk-prevention in all construction sites (provided by NR-9 and is established by the same Decree). In addition, the Program for Medical Control of Occupational Health (PCMSO for its acronym in Portuguese) aims to preserve and guarantee the workers' collective health, and the NR-35, of April 2014, deals with working at heights and the safety requirements to do so. However, in small construction projects, given their temporary and provisional character, such regulations are rarely considered, which results in the absence of the development or monitoring of any accident prevention program or workers' health promotion programs [4,5].

When trying to better define the concept of a small construction project, we assumed that it involves activities that include: repair, demolition, painting, cleaning and maintenance. Small house constructions, house renovations, painting facades, as well as small public works are generally included under this label, and many are artisanal endeavors, that are unplanned and with informal labor and temporary work.

Even if the rules and legal documents were to be adopted in the entire country, in the recent past in Brazil those small construction projects – houses, apartments or offices – were never inspected, and, therefore, there was no need for them to be supervised. To perform any residential construction work, the resident would only have to inform the condo board about the need to enter the building with construction materials, or about a possible shutdown of the water valve [2,6,7].

According to data from the Statistical Yearbook of Social Security [8], in 2012 there were 705,239 accidents, of which 62,874 were in the construction industry (CCI). These accidents are mostly caused by poor working conditions at building sites, especially due to falls, machine handling, sharp equipment and electrical installations [9].

In this context, the goal of this study is to demonstrate that the invisibility of small construction projects in the Brazilian construction industry makes them less secure, and that, coupled with the weakness in the application of Occupational Health and Safety Policies, this framework that makes these small construction projects increasingly prone to accidents [10-14].

2. Materials and methods

As the research developed, we decided to take a qualitative approach in order to analyze the knowledge and perspectives of professionals in various fields of training, as well as various performance levels in the construction industry in relation to Health and Safety Policies in small construction projects [15].

We undertook an analysis of the interviews, which were grouped by previously selected themes, to identify which looks that these respondents had on each of the topics [16].

This approach allowed us to establish a dynamic relationship between the real world and the subject, that is, an inseparable link between the objective world – where there are rules, laws and norms – and the subjectivity of the subject: what he thinks, how he sees his work environment and its relationship to his own work. As this was a study of a qualitative nature, a sample of professionals involved in building construction was selected, which was sufficiently representative of the area that was studied.

The research was conducted in three cities in the Rio de Janeiro Federal State. The cities, and their inhabitants' descriptions, according to IBGE data [17], are the following:

- the capital city, with the same name of the state – Rio de Janeiro, which has more than 6 million inhabitants;
- Niterói, which has around 500 thousand inhabitants;
- and Angra dos Reis, with 170 thousand inhabitants.

These diverse cities have allowed a more comprehensive view of the small construction projects taking place in medium and large cities in the State –in which there are many projects due to the growth of these cities, especially in the capital. Also, due to the authors' knowledge of construction work and people linked to this activity, there was an effort to diversify the categories of people interviewed as much as possible in order to obtain the widest range of opinions as possible, both about the construction sites and the occupational health of construction workers.

In general, it is very difficult to gain the trust of a worker in the lower level of the hierarchy in such a way that he/she can express his/her opinion about the reality of his/her labor. There is a frequent fear that if they express criticisms it could be used against them. It was also important to interview people who are in command and guide the works in order to gain a bigger picture of the group of people involved in a particular workplace. This was the case as the aim of this study was to find out the flaws that lead to the inherent dangers of occupational health and work injuries in construction. Thus, semi-structured interviews, with professionals from various categories were considered to be the best option to achieve the goals of this study. The interviews were carried out by following a script that served as a guide to better understand the professionals' perception about the characteristics of small construction projects. This script was previously prepared and underwent certain adjustments after a pilot test with a sample of some typical respondents. The interviews were not recorded and all respondents were previously informed of the survey's main content survey and had the guarantee that they would not be identified.

The central focus was to see how these respondents saw the differences between large and small construction projects, with emphasis on the knowledge they had on regulations: protection practices; the most commonly encountered failures; the differences between protection, inspection and surveillance in accordance with the size of the works; perception of the protective equipment; the understanding of the causality of the most frequent accidents on building sites and in the practices of prevention; as well as the role of the State in supervising working conditions and occupational safety.

The interviewees included people responsible for supervision, as well as professionals from several areas that operate in the sector or are directly involved in the processes of small construction projects, and the workers themselves. In order to draw comparisons, professionals from large-scale construction projects were also interviewed. A total of thirty-one people were interviewed:

- 2 auditors/labor inspectors: a doctor and an engineer;
- 2 Occupational Safety engineers;
- 6 civil engineers working on small construction projects;
- 3 civil engineers working on large-scale construction projects;
- 1 engineer from the Municipal Office of construction works;
- 1 architect of a large construction project;
- 1 occupational physician;
- 3 building technicians;
- 1 construction foreman;
- 2 people in charge of construction works;
- 2 site managers on small construction projects ;
- 2 trade union representatives;
- 2 bricklayers;
- 2 painters;
- 1 small-project employee

The interviews were carried out either on the construction sites or in their offices, as would be the case of an actual inspection by auditors/inspectors. During the description of the interviews we state that all the professionals were male, although there were women involved [2] as a further means of identity protection.

In this study, a sample of 31 Respondents was considered, which is broad enough to include different professionals who are rather directly or indirectly involved in the construction industry. The answers allowed us to outline an overview of the research in which "the assessment of the theoretical saturation from a sample is made by a continuous process of analysis of data, which began in the early process of collection [18]". We arranged a comprehensive reading of the entire material, and then the most significant content from the reports was selected, which was analyzed as being relevant issues.

3. Results

Considering the size of the group interviewed, we cannot generalize the answers, but we can certainly see that these responses revealed many insights that are common to the world of construction workers.

3.1. Different comprehensions of small work

The conceptualization or definition of what respondents consider to be a small construction project aimed objectively at focusing on what kind of specific safety measures should be adopted by this type of project. This is an extremely controversial issue, in which the most frequent distinction was made between small or large works, depending on the number of workers involved on these sites.

For a civil engineer, "a small building site has up to 8 employees". According to a person in charge of the works, a small building site has "less than 50 employees". Another engineer, from the Municipal Office of Works, said that "a small work has up to 50 employees", while an auditor engineer believed that the small construction site "has between 100 and 200 workers".

This divergence among respondents reveals an absence of a specific parameter based on a choice of classification criteria in the literature, as well as expressing a lack of knowledge of the rules.

3.2. Occupational safety and health in small construction projects

Each respondent also had a different understanding regarding safety in small construction projects, which leads to a weakness in the appreciation of the reasons for and aims of Occupational Health. In fact, most respondents expressed their understanding by making comparisons with the large-scale construction projects and gave more emphasis to the use of Personal Protective Equipment (PPE) while ignoring other forms of workplace and job safety. Either explicitly or implicitly, they stated that in a small work, there is no safety policy and attributed this deficiency to various reasons.

"The worker involved in an accident or is ill as a result of a situation in which PPE was not used, besides being at fault, is considered irresponsible, negligent etc. [19]". Thus, there are only a few times when the many factors that limit the use of PPE and other safety items are valued. Often, the safety equipment is not provided by employers and, also, workers also neglect the use of this equipment "because rarely the technicians responsible for security matters and occupational health give them due importance. [19]".

Based on his own experience as a civil engineer of a small construction project, the lack of safety in the small construction projects is because they are directed by supervisors and instructors who generally lack the necessary training in basic safety principles. This exposes the workers to heightened risks of accident frequency. "The fact is that, today, my main competitors are those in charge, and supervisors of constructions sites who gather a small team and do renovation work, facades, etc., without having professional qualifications to meet the safety standards and prevention of accidents at work in their small construction projects".

Similarly, the sample building technician also attributed the lack of prevention and safety to the small construction projects' short deadlines, while in larger projects, because they take longer to complete, health practices are applied with more vigor. "In small construction projects, the principles of prevention and safety are not accounted for". Thus, this professional was suggesting that small work on a facade or a renovation is done over a short period, which undermines monitoring and surveillance of the workers' health and safety and its basic principles and practices. Because these are projects that often last only a few days, in a country as large as Brazil, such supervision is hard to enforce, and all too often the owner of the property himself is unaware that these standards covering workers' safety should be applied. This leaves their use to the workers' discretion.

In contrast, a safety engineer thought that safety should not only be found in large-scale construction sites, because the workers' safety and health precepts should ensure everyone's mutual safety. Thus, the respondent pointed out that the application of safety standards must be present both in large and small projects: "practicing safety is just one aspect, and the target for the prevention of accidents is the human being. Thus there should not be many differences only due to the size of the work sites, since every individual should be subject to the correct (and legal) requirement of the prevention policy that is adopted at the workplace".

Another civil engineer of a small work considers that technicians and engineers must ensure accident safety and prevention, which, in his opinion, is synonymous with the use of protective equipment. According to him, "the PPE for a small or large work is the same. What differs is the equipment for collective protection. As such, in a large works, it may be necessary, for worker safety protection, to employ CPE". He then concludes that "the use of equipment is crucial for worker protection, as is the monitoring of its use by engineers and technicians, i.e. those responsible for the training and the use of safety equipment".

A trade union representative, who is also a safety technician, highlighted the crucial contribution of these professionals – the engineers and technicians. He also mentioned the need to incorporate the knowledge that comes from workers' experience as something key in creating a safety and accident prevention policy that strengthens and makes the management more efficient and resolute. According to him, "everything that may contribute to safety on the job is important, it is also important to listen to the person in charge, the workman, the bricklayer. These are all people who make a valuable contribution to safety at work". He also pointed out something else as being extremely important: "companies with fewer than 20 employees could have an environmental risk prevention program, thus the conditions of the working environment and the inherent risks could be evaluated".

In the same terms, the auditor who is a doctor pointed out that it is not about distinguishing between small or large construction sites, but about being committed to the workers' health because "it is important to have quality rather than quantity". Also, everything depends on the company's organization, and he concluded that "everything will depend on the company's focus, as for some people, safety and health are not an investment but an expense: a bureaucratic obligation".

3.3. Small construction projects versus knowledge and applicability of rules

Few respondents demonstrated a broad or even partial knowledge of the NR-18 and its applicability for small construction projects. "The implementation of the NR 18 – Working Conditions and Environment in the Construction Industry, which make it mandatory for establishments with twenty employees or more to prepare the Working Conditions and Environment in the Construction Industry – PCMAT" policy, means that even in small construction projects "it is recommended that the same concepts are applied [3]", with the obvious necessary adaptations.

However, more than half of the respondents had no knowledge of the rules in the industry, for example the architect who said he was unaware of the NR-18 and that "all I have learned was due to practice". A construction technician also claimed to have no knowledge about the rules, saying: "I never studied them it any school or course I attended. But, if it is a standard, it applies to all works". The engineer at the Municipal Office of Works similarly declared he was unaware of the NR-18 and any safety policy and prevention of accidents: "I do not know of any safety policy and accident prevention. I do not know about the NR-18".

Other interviewees said they were partially aware or had only heard of the NR. A civil engineer said: "As I am an engineer I know them, but I do not fully know their content". A construction technician pointed out: "I have heard of the NR-18, but I do not know the norms in-depth".

Among those who knew the standard there were different opinions. For example, the auditor who is a doctor pointed out that the NR-18 resulted from Convention 167 of the International Labour Organization (ILO) and highlighted its importance as a disciplinary standard in the industry, in terms of the creation of the standard: "the development of the NR-18 is key for the CCI sector, first because it is a standard that allows the company to organize, to plan the operation of the construction site and all the inherent duties". He also stated that the rules should be applied to works of any size. the auditor who is an engineer also related the norm to the ILO Convention, saying that the NR-18 was an adaptation of International Standards. However, "there is no standard applicable if the company does not have the basic principle to apply it. However, the NR -18 is very important because it 'civilized' the world of work in the CCI, giving it direction".

However, for the auditor who is a doctor the standard is intended to standardize all situations and, given its complexity, it generates difficulty of applicability in practice. This is because it only considers, for example, accidents at work as homogeneous phenomena, "creating a standard that tries to embrace everything and ends up leaving margins for errors and failures in the rules themselves and in their applicability. Each accident at work is different from another, but the fact that the NR-18 procedures were not applied is rarely noticed". This interviewee also questioned whether the standard was flawed, in the sense that it was intended to be applied to everything, but actually, there should be different parameters for each type of work.

One of the construction technicians, who works on small construction projects, also highlighted the importance of the NR-18 for all kinds of workplaces. However, according to the definition of the auditor who is an engineer, he believes that its effective application depends on the builder's willingness to do so: "for the working masses these rules often pass by unnoticed, but if the workers were aware of the rule, it would make a serious contribution to its applicability. I consider the NR-18 fundamental as a working tool, for the construction technicians' performance of and the preservation of workers' health and lives".

Four professionals in the area of safety – two auditors, one safety technician and one safety engineer – commented on the complexity of the NR-18. They identified issues such

as the fact that the rules standardize every situation as if the accidents were always the same, most being completely preventable falls. In this sense, the safety engineer commented on the excesses of wanting to standardize the small construction site: "the big projects are well supervised and, therefore, tend to comply with the rules, and the company is required to apply all the methodologies of the NR-18. However, in the small construction projects it is almost impossible to comply with everything required by the standards".

For one of the auditors (engineer), the standards contain some determinations that are difficult to put into practice at every site: "many measures can be implemented and others cannot, it depends on the work environment (...) the rules are applicable where appropriate, and these are work safety rules that establish universal safety links". He also pointed out other precautions in safety policy that need to be taken into account in small construction projects: "for small construction projects, the burden is not the rules, but other needs related to the work process and to the bureaucracy. There is a need for doctors, accurate documentation, planning and various mechanisms that the small companies cannot take care of. There should be rules, even when they are small construction projects: houses, condominiums, domestic work". The respondent concludes that, after all, there are companies that are mediocre at performing their duties; however, "since the inspection does not see them..."

It is worth mentioning the opinion working at a civil engineer of a large construction site, who said that he also knows the rules and puts them into practice with great accuracy, despite the financial burden that this might represent. However, he mentioned that it is necessary to make the requirements for small construction projects more explicit: "I believe that the standard could give greater emphasis to the smaller works, which often cannot afford to meet the demands of everything that is requested, such as changing rooms, cafeterias, etc.".

For a civil engineer, it is necessary to educate the workers, the technicians and the employers in order to ensure that the rules are applied: "there is no difference in the applicability of the standards relating to the size of the construction site or building. Therefore, the standards must be applied and, concomitantly, the awareness of both the employee and the employer must be promoted".

3.4. Workplace accidents and their causality

There are only a very few studies in academic literature about the percentage of workers in the construction sector who have suffered some kind of industrial accident (considering that the official data only refers, as a rule, to Employees with a formal contract in larger works as they are rare in small construction projects). One of these rare studies indicates that approximately 42% of construction workers suffer accidents [20]. Considering that this percentage represents almost half the workforce, it is worth contemplating if many of the accidents, such as falls, cuts, punctures and electrical shocks, could not have been avoided.

The auditor (engineer) notes that in Brazil the blame for the accident lies on the worker, when it should be attributed to the working conditions and the work process itself. The same engineer compares the different rhythms imposed in the works as one of the causalities of accidents: "in other countries, the rules have a purpose. The Government states that in a given industrial sector there should be fewer than "X" accidents, while in Brazil, the blame is on the worker, who is not alone in being guilty. The main determinant for accidents is the work process".

Thus, it is possible to state, as this respondent pointed out, that it is the job content – the pace, the production of the work – that causes the accidents. For him, "the pace of the work is different when considering small or large construction projects, and, therefore, the way of thinking is different. Serious industrial accidents usually happen in the large construction works, in which, theoretically, there is more protection". He concluded that Companies "have to keep in mind the principle that there should be no risk at the workplace" and not that the blame must lie on the worker who committed some type of error/mistake.

The auditor (doctor) also questions the blame imposed on the employee in accidents at work, and highlights the new standard on machines as a breakthrough to overcome this viewpoint, as the underlying principle is fail safe: "the issue refers not to the worker himself, but the pace of work. That is, what is required of the employee is to understand his working condition. In the new industrial safety standard for machines there is a new principle: the fail safe concept. The concept of always putting the blame on the worker is withdrawn". In addition, a safety engineer also criticized putting the blame on the worker, emphasizing the need to ensure the existence of prevention of accidents in the workplace, regardless of the size of the company: "safety is the main point, and the aim of accident prevention is the protection of the human being".

3.5. Fragility of public policies

It was found that, with respect to the public policies, three of the 31 respondents raised important issues concerning supervision; all are professionals in areas directly involved with the responsibility of preventing accidents, namely the auditor (engineer), one civil engineer and one person in charge of the works. Some of the respondents pointed out the failures of the Government and of the supervisors as the main causes of the accidents that are still happening.

For the civil engineer of a small construction project, the Government is negligent and surveillance is non-existent. According to him, the supervision is merely bureaucratic and ineffective, and he associated the absence of safety policies to the absence of government effectiveness: "in my company, we are complying with all the accident prevention and safety regulations, I am the engineer responsible for the works. I believe that the entrepreneur has to do the social part, take care of workers' safety and prevent accidents at work". In terms of the shortcomings of surveillance, the auditor initially highlighted the lack of appropriate training of the auditors themselves in being able to fulfill their function: "currently, the auditors are not prepared for the work they do. Recently, civil service examinations have allowed people with any initial training background to apply as auditors, which

increases the gap between normative evaluation and the production of technical knowledge". A union representative, besides highlighting once again the firm action of the union, hinted that the practice of surveillance is sufficient to solve the companies' safety issues: "although everything is notified, when the company no longer meets the NR-18 the union acts firmly in promoting an inspection, in order to maintain the required level of workers' health and safety".

4. Discussion

The NR-18 brought important innovations; however, it is not necessary to advance the legislation, but rather with its applicability in all of the country's building Sites. The risks must be noted, and on each site a risk map must be created, which allows all workers to observe the critical points of the building site. Thus accidents can be avoided and the fundamental rights of citizens can be improved in order to preserve their health, life, safety and ensure decent work.

However, there is a large gap between what the legislation requires or recommends and how it is applied. It is true that in the larger construction sites there is a more effective obedience to the precepts of the Occupational Safety and Health standards, whereas in small construction projects, following these criteria depends on the conscience of each worker. Often, a small renewing a facade or remodeling is done without an engineer or architect's supervision, and it is not uncommon that the bricklayer decides the criteria to carry out the work. In such cases, he may even outsource to one or two assistants, but the issues of safety and health are left aside. Situations can occur, for example hanging on railings to place frames or not even wearing a mask for sanding plaster when lowering ceilings. In addition to these risks to the safety and health of the worker, there may be structural risks in the workplace. The worker himself may or may not know whether these risks exist, depending on his level of education. Very often, however, this knowledge is only acquired through practice.

Regarding the different views on small construction projects, the divergence between what the respondents interpret by small projects is very shocking. It appears that even engineers are unaware of the NR-18 criteria (describing small construction projects as those that have fewer than 20 employees, as having more personnel would mean the rules apply). They consider that a small construction site may have from 100 to 200 employees. It has been pointed out that the lack of knowledge of what constitutes a small project is very common and, in this sense, there are only few who realize that the work of remodeling a facade is considered to be a small work [2, 4]. In this sense, other researchers have shown that the rules should apply to every type and size of work, as long as they are clearly adapted according to the size. However, the lack of knowledge and doubts were clearly reflected by the respondents' answers [3].

As for Occupational Health and Safety in small construction projects, the employee who is blamed when involved in an accident or becomes ill because of a situation in which the PPE was not used, is considered negligent. However, a safety engineer commented that, "safety is paramount, and the aim of accident prevention is the human being". In this aspect, it does not matter whether the bricklayer works at a large construction site or performs a particular service for the owner of a residence: the differences in safety levels will certainly exist, but there is a need to educate the worker and the contractor about this need. Thus, "every individual should be subject to accident prevention in the workplace [19]".

This indicates the need to recall the issue of the recent collapses of entire buildings in Rio de Janeiro, particularly the accident in Cinelândia, where three office buildings collapsed simultaneously. The cause was the lack of safety and supervision in the small task of remodeling of an office in the largest building (with more than 20 floors). This required the removal of the internal structure of its floor, which caused an accident that had a "domino effect". If the workers and users of the commercial buildings had understood the rules, and the safety of the work itself, as well as necessary supervision perhaps this accident could have been avoided. The literature showed that the nomadic nature of construction workers makes it difficult to control the works and, therefore, work at small construction projects can be a real danger [21]. Another study summarizes that the very construction process leads to a weakness in the health of the worker [5].

Regarding the relationship between small-sized construction projects and the knowledge and the applicability of the rules, the result of the interviews unveiled that more than half of those interviewed were unaware of the NR-18. If engineers and employees of a Municipal Office of Works are ignoring them, how is it possible to make an individual worker with less theoretical training (such the site manager, bricklayers, and support staff, etc.) to know and make sure they comply with its principles?

The standard should be simplified in order to be applicable to small construction projects [3]. Perhaps, in this way, a handbook for contractors and employees would be a more practical way to raise awareness.

Several Researchers consider that accidents in CCI and its causes are due to the lack of notification, that is, supervision [2]. According to one respondent, an auditor who is an engineer, the cause of the high rate of accidents lies in the size of the work: major works have a higher degree of protection, while smaller works have a different pace, and the "way of thinking is different". Therefore, it was considered that it is important to clarify to those who are self-employed or working in small construction projects the importance of equipment, safety, and protection of their own health and that of their colleagues. It is also common that many workers – regardless of the size of the work and provided there is no visible inspection – consider safety items unnecessary to prevent accidents. This is also more common in small construction projects. Therefore, promoting education, training and health are essential in this context.

Finally, concerning the fragility of the public policies, it is the Government's responsibility to ensure the Welfare of all. However, the States often fails to monitoring the construction sites and to fulfill their obligations to the construction companies [15]. Yet, for one interviewee, a civil engineer, the Government is negligent in terms of this issue and there is no effective supervision. The rules exist but are

not used, and there is a lack of supervision, creating a negative snowball effect [22].

All around the world, studies are being held on the on the health and safety of workers in the construction industry and. In the European Union– at every economic level– countries are seeking to adapt to new realities and advocating a greater protection for the workers in this important sector. Examples of EU countries would be the UK and France: countries with a strong economy and which have traditionally been pioneers in labor legislation. They are seeking to review accidents to improve prevention programs. Similarly, countries with economies that are still being consolidated in the EU, such as Poland and the countries that recently joined, such as the Czech Republic, Lithuania and Hungary, are still reviewing the causality of accidents in the construction industry to create or adapt good practices for safety and prevention.

Studies held in the UK in 2003 show that inspectors estimate that 50% of the accidents in the construction industry are the contractor's fault, and that the safety and health of the workers in the construction industry must be considered to be their highest priority. Thus, this study recommends a review of workers' safety and health policies, an accurate review of accidents, improvement of audit reports and consultation with workers, since they are the ones who deal with the risks on building sites every day [23].

Another study evaluates the importance of training for professional assistants in small companies in the construction industry, explaining that, in France, the small businesses are those with fewer than 20 employees. In addition, it highlights that 40% of artisanal enterprises are included in the construction sector (with about 250,000 companies). To avoid the risk of accidents, the *Organisme Professionel de Prévention du Bâtiment et des Travaux Publics* (OPPBTP) has developed a program with the *Fédération Française du Bâtiment* (FFB) in order to develop training and promote best practices in safety and prevention [24].

Another study shows that the construction industry is characterized by the high rate of accidents and that, in Poland, in 2012; this figure reached 9.17 people per 1,000 workers. This is the highest percentage of all EU countries. In this context, the authors present three models to analyze the causes of accidents in the construction industry: the analysis of the causes of failures, the energy transfer method, and the accidents in the workplace of the European Union (Eurostat) [25].

By analyzing the use of ergonomic equipment for injury prevention in construction, Kaminskas stated that, in 2000, 43% of construction workers in the European Union believed they were at risk in their work. Furthermore, the author states that the 12 candidate countries applying to become members of the European Union at that time (Estonia, Lithuania, Latvia, Poland, Czech Republic, Slovakia, Hungary, Slovenia, Romania, Bulgaria, Cyprus and Malta) had a percentage of 42% industrial accidents, whereas the European Union had 27%[26].

With these few examples, it is possible to see that Brazil also falls within the same international context of accident prevention and evaluation of worker safety and health in the construction industry. Admittedly, in the United States and Canada, as in many European Union countries, some problems in relation to work in the construction industry are region-specific and are not found in Brazil. For example, we can highlight the use of foreign labor, unskilled or even illegal immigrants, which is not the case in Brazil (or the problem is minimal). The international financial crisis that is affecting the construction industry worldwide is also a factor; however, this has so far not affected Brazil. What can be observed in the international literature, is that in relation to the risks of accidents at work, there is a common element, i.e., the fact that the legislation is detailed but not always observed. Good safety and prevention practices are not always applied and, finally, there is a need to review these best practices, in particular when it comes to small construction sites that are remodeling a building or perhaps repairing a facade, which worldwide, and especially in Brazil, still remain 'invisible' [23 - 26].

5. Suggestions and recommendations

The discussion, as it has been presented, had the intention to suggest the adaptation of the current standard and the creation of a specific legislation for small construction projects, emphasizing only the most important items of safety and accident prevention. The fact that the accidents are mainly falls, electrocution and perforation accidents, these three aspects should be prioritized.

It also seems clear for the authors that the Municipal Office of Works needs to have engineers and safety technicians who are responsible for certain areas of the city. These professionals would be responsible for visiting small construction projects that, under some criteria of classification and inspection, would be the responsibility of their office. Thus, simplifying does not mean diminishing the responsibility of employers, but rather helping small construction projects so that they can meet the minimum requirements regarding accident prevention

Another suggestion is the regularization of small construction projects. If these small projects, within the appropriate parameters, were officially notified, there would be a greater awareness and wider application of safety and accident prevention regulations at all building sites. It must be considered that a small project is an essential component of urban housing infrastructure. It is possible to verify by random criteria that in any block of any city in Brazil, regardless of its size, there are innumerable multitudes of small construction projects. These are both the responsibility of the Government, and of private companies, even perhaps of the ordinary citizen.

6. Conclusion

In the microcosm that is the construction site, it is evident that in large companies the safety and accident prevention regulations are practiced more regularly, either because more specialized personnel work on these projects – technicians, doctors and engineers –, or because they are more visible in terms of surveillance. This makes the company feel obliged to comply with regulations.

This situation does not occur in small construction projects when a façade is being remodeled, for example. As

several interviewees pointed out, small projects do not comply with laws, rules or knowledge about safety. And, since these projects are ephemeral, temporary and highly mobile, there is no supervision. It was also shown that the use of the seat belt, helmet, goggles, gloves and boots (all PPEs) are the maximum that most of those responsible for works actually enforce. They have little knowledge about organization, such as the work pace, requirements, training, safety devices and redundancies, and management of health and life protection.

As discussed in a recent study [2], since April 2014 it has become mandatory on a national level for interior works of any size to follow the rules of supervision and inspection that were created by the Brazilian National Standards Organization – ABNT, NBR 16280/2014 [1]. With this regulation, some preventive measures for occupational safety and health were introduced. In addition, new regulations have been implemented in some Brazilian States, for example state that was analyzed in this paper, Rio de Janeiro, the third most populous in Brazil. This state is currently going through a period of major investments in infrastructure due to previous works that were undertaken for the FIFA World Cup in 2014, as well as for the forthcoming 2016 Olympic Games. It should be noted that in this state, State Law (6,400/2013), which imposes supervision on internal or external works; and complementary State Law (126/2013), which imposes supervision every five years; as well as in the municipality of Rio de Janeiro, Decree 37426 of 2013, which establishes technical inspection, were created with a view to further supervise works. Residences with one or more families (i.e. houses or apartments), are however excluded from these regulations. This issue has become more important insofar as these laws and regulations only came into force after serious work accidents occurred in commercial or residential interiors, with the collapse of entire buildings.

However, if works with fewer employees are exempt from following safety requirements, each contractor or worker will have to consider their own safety and that of their colleagues.

In this context, it seems important to make the smaller construction projects more 'visible', in order to begin some practices that are increasingly oriented and focused on the promotion of the construction workers' health and safety. Thus, the current study aimed to identify, through the opinion of people involved in construction works, the level of their knowledge about the promotion of health and safety working conditions.

Among the various types of professional occupations that were interviewed in this study, only a few knew the specific legislation. Some accused workers of trying to systematically avoid the use of safety equipment, while some workers accused employers of not informing them about the need to use of this equipment. Regardless, their reactions denote the lack of information and the negligence of the companies or contractors who do not prioritize safety. The respondents, besides revealing that they have a worrying lack of knowledge of the health and safety rules, pointed out that accident prevention is limited to the use of a few PPE, not understanding, or knowing, that there are many other measures, both personal and collective, that could be adopted. Blaming the worker has been a constant practice, although the real cause of the accidents lies in the lack of corporate responsibility with regard to work organization.

To transform the reality of failures into safe policies and health practices for the construction worker, even in small construction projects, it is necessary to take into account some aspects, namely: awareness, learning and accumulated knowledge, motivation, supervision and surveillance, guidance, and effective accident prevention management on the construction sites. However, there is still a long way to go. There is a general recognition that the work process needs to be modified, but some important aspects are still missing, such as disseminating knowledge and good safety practices, promoting workers' health and giving more 'visibility' to small construction projects, as well as ensuring safe and healthy working conditions for workers in the small construction industry in Brazil.

Acknowledgements

The authors would like to thank to the Federal Center of Technological Education Celso Suckow da Fonseca (CEFET-RJ, Brazil), as well as the Coordination of Improvement of Higher Education Personnel (CAPES, Brazil), who have awarded this research study with a grant o: Case n. BEX 1651 /14-5.

References

[1] Brasil., Ministério do Trabalho e Emprego. Associação Brasileira de Normas Técnicas – ABNT. NBR 16.280/2014. [Online]. 2015. [Date of reference January 15th of 2015]. Available at: http://www.abntcatalogo.com.br/norma.aspx?ID=311358.

[2] Gomes, H.P., Arezes, P.M.F.M. and Vasconcellos, L.C.F., Environment, health and safety policy in small construction sites: An analysis of the situation in Brazil. Paper 108. SHO. U. Minho, pp.127-129, 2015.

[3] Fleuringer, A.T.B. e Pusch, J., A execução da obra e a excelência profissional. Programa de Excelência. Projetos, execução e manutenção. Engenharia, Arquitetura, Agronomia e Geociências. CREA-PR e Entidades de Classe. Curitiba: CREA-PR, 2010.

[4] Gomes, H.P., Construção civil e saúde do trabalhador: um olhar sobre as pequenas obras, PhD. dissertation. Escola Nacional de Saúde Pública Sergio Arouca, Fundação Oswaldo Cruz, Rio de Janeiro, Brazil, 2011.

[5] Dalcul, A.L.P.C., Estratégia de prevenção dos acidentes de trabalho na construção civil: Uma abordagem integrada construída a partir das perspectivas de diferentes atores sociais, PhD. dissertation. Universidade Federal do Rio Grande do Sul, Porto Alegre, Brazil, [Online]. 2001. [Date of reference January 15th of 2015]. Available at: http://hdl.handle.net/10183/1747.

[6] Silva, J.B.V., A falta de planejamento das pequenas empresas na construção civil. [Online]. [Date of reference January 17th of 2014]. Available at: http://www.ecivilnet.com/artigos/planejamento_pequenas_empresas_construcao_civil.htm.

[7] Santos, A.R.M., O Ministério do Trabalho e Emprego e a saúde e segurança no trabalho. In: Chagas, A.M.R., Salim, C.A. and Servo, L. M.S. (Eds.). Saúde e segurança no trabalho no Brasil: Aspectos institucionais, sistemas de informação e indicadores. Brasília: IPEA, 2011, pp. 21-76.

[8] Brasil., Ministério da Previdência Social. Anuário Estatístico da Previdência Social. [Online]. AEPS 2012. Brasília: Ministério da Previdência Social. [Date of reference January 15th of 2015]. Available at: http://www.previdencia.gov.br/wp-content/uploads/2013/05/AEPS_2012.pdf.

[9] Saurin, T.A., Famá, C.C. e Formoso, C.T., Princípios para o projeto de sistemas de medição de desempenho em segurança e saúde no trabalho: A perspectiva da engenharia de resiliência. Prod.,23(2), pp.387-401, 2013. DOI: 10.1590/S0103-65132012005000072
[10] Melo-Filho, E.C., Rabbani, E.R.K. and Barkokébas Jr, B., Avaliação da segurança do trabalho em obras de manutenção de edificações verticais. Prod.,22(4), pp.817-830, 2012. DOI: 10.1590/S0103-65132012005000024
[11] Bridi, M.E. et al., Identificação de práticas de gestão da segurança e saúde no trabalho em obras de construção civil. Ambient. constr.,13(3), pp.43-58, 2013.
[12] Costa, L.R., Subcontratação e informalidade na construção civil, no Brasil e na França. Cad. CRH, 24(62), pp.413-434, 2011. DOI: 10.1590/s0103-49792011000200012
[13] Costa, L.R. e Tomasi, A.P.N., De peão a colaborador: Racionalização e subcontratação na construção civil. Cad. CRH, 27(71), pp.347-365, 2014. DOI: 10.1590/S0103-49792014000200009
[14] Silva Jr., D.C. e Cambraia, F.B., Modelo do processo de ação fiscal de segurança e saúde do trabalho na construção de edificações. Ambient. constr., 13(3), pp.29-41, 2013.
[15] Tauil, R., O poder de polícia e a fiscalização municipal, [Online]. 2006. Consultor Municipal. [Date of reference January 25th of 2015] Available at: www.consultormunicipal.adv.br.
[16] Minayo, M.C.S., O desafio do conhecimento: Pesquisa qualitativa em saúde. São Paulo: Hucitec, 2010.
[17] Brasil. Instituto Brasileiro de Geografia e Estatística – IGBE. [Online]. [Date of reference February 07th of 2015]. Available at: www.igbe.gov.br.
[18] Fontanella, B.J.B. et al., Amostragem por saturação em pesquisas qualitativas em Saúde. Cad. Saúde Pública, Rio de Janeiro, 24(1), pp. 17-27, 2008.
[19] Vasconcellos, L.C.F., A voz do povo é a voz de deus: Provérbios da boca do povo e os riscos à saúde no trabalho. Boletim da Saúde, Porto Alegre, 20(1), pp. 159-168, 2006.
[20] Carvalho, R.J.M. et al., Condições de trabalho na construção de edificações no triângulo Crajubar – CE. In: XVIII Encontro Nacional de Engenharia de Produção. Anais. Rio de Janeiro: RJ, Brasil, 1998, 6 P.
[21] Lima, R.O., Verificação da qualidade na construção civil em um pequeno canteiro de obra de Foz do Iguaçu, uma mudança de paradigma. Foz do Iguaçu: União Dinâmica das Faculdades Cataratas. Curso de Engenharia Civil, 2008.
[22] Takahashi, M.A.B.C. et al., Precarização do trabalho e risco de acidentes na construção civil: Um estudo com base na Análise Coletiva do Trabalho (ACT). Saude Soc., 21(4), pp. 976-988, 2012. DOI: 10.1590/S0104-12902012000400015
[23] Dalton, M., An examination of dutyholder responsibilities: Fatal construction accidents 1997-2002. University of Manchester, Institute of Science and Technology/ Health and Safety Authority, Manchester, U.K. 2003.
[24] Branca, A., Prevention training for spouses and/or other assistants in very small firms (VSES) in the building industry. Safety Science Monitor, Short Communication I-2, 1(3), 2007.
[25] Hola, B. and Mariusz, S., Analysis of the development of accident situations in the construction industry. Procedia Engineering, XXIII Science Direct. R-S-P Seminar, Theoretical Foundation of Civil Engineering, 91, pp. 429-434, 2014.
[26] Kaminskas, K.A., The prevention of trauma by ergonomic equipment in the construction industry. Safety Science Monitor. Article IV-4, 1(7), 2003.

H.P. Gomes, has a PhD. in Public Health from the National School of Public Health- Oswaldo Cruz Foundation in Rio de Janeiro, Brazil. He is a visiting fellow on the Post Doctoral Program/University of Minho – Portugal. He is also a professor at the Federal Center of Technological Education Celso Suckow da Fonseca (CEFET-RJ, Brazil) and has experience in the areas of occupational health and construction industry.
ORCID: 0000-0001-9787-7383

P.M.F.M.Arezes, has a PhD. in Industrial and Systems Engineering from U. Minho, in Portugal, and he is currently a full professor of Ergonomics and Human Factors at the same university. He is also a visiting faculty member at MIT's AgeLab in the USA. He leads the Human Engineering Research Group and he is also the Coordinator of the Engineering Design and Advanced Manufacturing (EDAM) focus area of the MIT Portugal Program at U. Minho, and the chair of the steering board of the "Leaders for Technical Industries (LTI)"PhD program at U. Minho, Portugal.
ORCID: 0000-0001-9421-9123

L.C.F. Vasconcellos, has a PhD. in Public Health from the National School of Public Health - Oswaldo Cruz Foundation in Rio de Janeiro, Brazil. He is also a professor at the same school. He graduated in Medicine from the School of Medicine and Surgery. He also works as a Doctor in the Brazilian Ministry of Health at the Oswaldo Cruz Foundation. He has experience in medicine and public health, with emphasis on occupational medicine, occupational health and health policies.
ORCID: 0000-0002-7679-9870

UNIVERSIDAD NACIONAL DE COLOMBIA
SEDE MEDELLÍN
FACULTAD DE MINAS

Área Curricular de Ingeniería Administrativa e Ingeniería Industrial

Oferta de Posgrados

Especialización en Gestión Empresarial
Especialización en Ingeniería Financiera
Maestría en Ingeniería Administrativa
Maestría en Ingeniería Industrial
Doctorado en Ingeniería - Industria y Organizaciones

Mayor información:

E-mail: acia_med@unal.edu.co
Teléfono: (57-4) 425 52 02

UNIVERSIDAD NACIONAL DE COLOMBIA
SEDE MEDELLÍN
FACULTAD DE MINAS

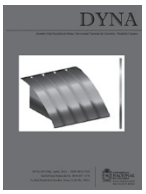

DYNA
http://dyna.medellin.unal.edu.co/

Emerging risk in the construction industry: Recommendations for managing exposure to nanomaterials

Beatriz María Díaz-Soler [a], María Dolores Martínez-Aires [b] & Mónica López-Alonso [c]

[a] *Escuela Técnica Superior de Ingeniería de la Edificación, Universidad de Granada, Granada, España. atriz@correo.ugr.es*
[b] *Escuela Técnica Superior de Ingeniería de la Edificación, Universidad de Granada, Granada, España. aires@ugr.es*
[c] *Escuela Técnica Superior de Ingeniería de Caminos, Canales y Puertos, Universidad de Granada, Granada, España. mlopeza@ugr.es*

Received: November 30th, 2015. Received in revised form: March 02nd, 2016. Accepted: March 14th, 2016.

Abstract
Nanotechnology has aroused great interest in the construction industry because new materials with outstanding properties are being designed, and the features of traditional materials can be improved. However, exposure to nanomaterials is the most recent new emerging risk in the construction industry and the current knowledge about this topic is limited. This paper aims to identify the main aspects regarding the exposure to and use of nanomaterials in the construction sector from a risk prevention perspective. This starting point allows authors to establish a set of recommendations structured in order to identify how and where to act in order to manage the risk of exposure to nanomaterial on construction sites.

Keywords: emerging risk; safety risks; health risk; engineering controls; organizational measures; personal protection equipment.

Riesgo emergente en la industria de la construcción: Recomendaciones para controlar la exposición a nanomateriales

Resumen
La nanotecnología ha despertado un gran interés en la industria de la construcción por el diseño de nuevos materiales con propiedades extraordinarias y por la mejora de las prestaciones de los materiales tradicionales. Sin embargo, la exposición a nanomateriales es un nuevo riesgo emergente en la industria de la construcción y los conocimientos actuales sobre este tema son limitados. Este documento tiene como objetivo identificar los principales aspectos relacionados con la exposición y el uso de nanomateriales en el sector de la construcción desde la perspectiva de la prevención de riesgos. Este punto de partida permite a los autores establecer una serie de recomendaciones estructuradas para identificar cómo y dónde actuar con el fin de controlar el riesgo de exposición a los nanomateriales en las obras de construcción.

Palabras clave: riesgo emergente; riesgos para la seguridad; riesgos para la salud; medidas de control técnicas; medidas de organización; equipos de protección personal.

1. Introduction

The European Commission defines a nanomaterial as: a natural, incidental or manufactured material containing particles, in an unbound state, or as an aggregate or as an agglomerate where, for 50% or more of the particles in the number size distribution, one or more external dimensions is in the size range 1 nm-100 nm [1]. This is not, however, a definitive definition; in fact it should have been revised in 2014 in the light of new scientific advances. Nanostructured materials were not considered in the previous definition, but according to the International Organization for Standardization they should have been. Even though almost all materials have surfaces that are morphologically and chemically heterogeneous at the nanoscale, if they have been intentionally modified or texturized [2] they should be catalogued as an engineered nanomaterial. From the point of view of preventing risks in the workplace, it is necessary to distinguish between those produced intentionally and with specific properties (engineered or manufactured nanomaterials), and those that are made up of ultrafine particles (incidental and natural nanomaterial).

© The author; licensee Universidad Nacional de Colombia.

1.1. Economic and technological progress

We are possibly facing a new economic and social revolution: the nano-revolution [3] or the sixth economic wave [4]. Nanotechnology has been identified as an essential facilitating technology [5] that will be the basis for innovation. New products will bring these scientific and technological developments to the market. This boom was quantified in a macroscopic study of indicators based on nanotechnological patents [6], and this positive trend has been confirmed [7]. In fact, estimates of this economic and technological growth [8] show that the volume of revenue from nanotechnology-based products will rise to 2 billion Euros in 2015 [9].

1.2. Nanoproducts in construction

Many of the nanotechnology-based products currently used in daily life can be found in on-line inventories. They are present in almost all fields, including construction, agriculture, sports, medicine, cleaning, computers and electronics, cosmetics… [10-13]. This last area is where nanotechnology has had the biggest impact [14].

The construction industry has been considered to be of the most promising fields for nanotechnology [15], but it is still in the early stages of expansion [16]. There are several reasons for this, but generally speaking there is little knowledge of nanotechnology in the industrial sector [17], in the construction business [18] and among the general public [19].

In spite of this, the potential of nanomaterials in the construction industry cannot be ignored, particularly for nanoparticles of titanium dioxide (TiO_2), zinc oxide (ZnO), aluminium oxide (Al_2O_3), silver (Ag) and silica (SiO_2) [20]; their use is only expected to increase [21]. Many reviews and reports [17,22-30] provide a detailed overview of applications available in construction materials such as ceramics, metals, wood, stone, etc. Some examples are mentioned hereafter. Photocatalytic concrete with nanoparticles of titanium dioxide (TiO_2) has antibacterial, self-cleaning and self-decontaminating properties that, at the same time, makes it last longer and helps it keep its look throughout its useful life [31]. Glass with nanosilica gel inside offers very good thermal and acoustic insulation properties while also avoiding annoying shadows and glare [32]. Nanostructured steels manage to gain up to five times more strength than traditional solutions [33]. There is also anti-graffiti paint that is water- and oil-proof, stopping the paint from sticking and making it easier to clean afterwards [34]. Finally smart developments have been reported, such as building materials containing nano-sensors, and self-healing materials mixed with nanoparticles [35,36].

2. Occupational health and safety

Exposure to nanomaterials is becoming one of the most significant risks in the workplace [37], particularly for the construction industry [38]. Despite being at risk when exposed to nanomaterials, workers have received very little attention in scientific studies [39]. Moreover, when comparing the construction business to other sectors, fewer studies have been conducted on the risks associated with harmful substances or toxic products [40].

Besides, there are no safety specific standards to work with nanomaterials. Although current standards in force can be applied to nanomaterials, these need to be adapt [41]. Work is being undertaken to standardize parameters and methodologies as well as create the appropriate terminology and definitions [42]. However, on the whole, European political activity to date [43] has been scarce in terms of guaranteeing secure nanotechnology development. Specifically, in the area of prevention, we are still waiting for the final conclusions on Occupational Health and Safety legislation [44]; these should have been finished in 2013.

It became clear that it was necessary to delve deeper into nano-safety. Initiatives have been put forward, such as the EU Nano Safety Cluster, which aims to maximize the synergies between those research projects that are looking at nanotechnology from the point of view of toxicology, ecotoxicology, exposure assessment, interaction mechanisms, risk assessment and standardization [45]. One Nano Safety Cluster´s research project is in the area of scaffolding. It deals with strategies, methods and tools to manage risks with nanomaterials in the construction industry sector [46]; the final results have still not been published. The following papers and reports address this topic [18,20,47,48].

2.1. Exposure to nanomaterials: identification and quantification

There are many scenarios during the life-cycle of nanomaterials that are used in construction, for example nanoproduct manufacturing, construction sites or disposal in the demolition field [47]. This paper focuses on construction sites.

On construction sites, the riskiest tasks involve handling dusty or liquid materials or when their application generates dust or aerosols, for example when spraying a nano-coating, or during cleaning activities. Conversely, risks of exposure to nanoparticles when handling solid prefab-nanoproducts, nano-enhanced ceramics for example, are expected to be small because the nanomaterials are embedded in a matrix; however, exposure may take place as the material wears [18].

In order to control workers' exposure to nanomaterials, industrial hygiene cannot continue without changes [49]. In fact, the usual exposure index [mass per unit of volume] is not the most appropriate because it does not take into account other crucial toxicity parameters when particles become very small [50]. Besides, the instruments, techniques and traditional measurements of aerosol sampling are not the best solution to assess exposure to a nanostructured particle aerosol [51,52]; although, work is being done to resolve these issues [53]. Moreover, it is necessary to understand the relationship between the nanomaterial parameters and their toxicological effects; however, for the time being, there is no international consensus [54]. However, there are proposals such as the nano reference values (NRV) [55] and environmental limit values, which are based on known values for the parent materials and distinguish between insoluble and soluble for derivatives of mutagenic, carcinogenic compounds, or any that alter the reproductive function of fibrous nanomaterials [56]. In addition, there are also exposure values for nanoparticles of titanium dioxide (TiO_2) [57] and for carbon nanotubes [58-60].

There are few case studies on environmental exposure that apply building nanoproducts. Their results indicate that certain levels of exposure are acceptable; for example, analysis of exposure when spraying self-cleaning coatings with nanoparticles of titanium dioxide (TiO_2). Also, three cases that deal with mortar repair using nanoparticles of silica (SiO_2) conclude that exposure was below the reference values [61,62], and it even suggested that this exposure might be lower as the nanoparticles detected may originate from the electrical equipment and the machinery used [20]. Another study evaluates exposure when making mortars with nanoparticles of zirconium dioxide (ZrO_2). It concludes that the occupational limit values were not reached, but they were greater than the values for indoor air [63].

2.2. Damage to health: toxicokinetic and health effects

The deposit and absorption of nanoparticles in the organism occurs through three main paths: by inhalation, through the skin and by digestive tract [64]. In construction workers it occurs mainly by inhalation [38]. Depending on the particles' size, shape and chemical composition, they are capable of entering the lungs and can reach the different parts of the respiratory system [65], see Figure 1.

The nanoparticles can also enter the organism through the skin [66] and by ingestion as a result of poor safety practices, as well as by swallowing materials trapped in the upper respiratory tract [67]. In relation to transport of nanomaterials through the organism, it is also necessary to consider translocation, which is a specific property of nanomaterials. Nanomaterials can cross biological barriers unaltered and appear in various other parts of the body [68]. Finally, removal processes through the body may either be entirely or partially by chemical or physical elimination [69].

Factors that influence nanoparticle toxicity depend on exposure, the organism and the nanomaterials [69]. Recent reviews summarize the results of studies that suggest nanomaterials are harmful to our health [70-73]. For example, an in vivo study concluded that of titanium dioxide (TiO_2) nanoparticles seem to induce DNA damage and genetic instability [74]. Alternatively, other in vivo studies looking at entry through the skin with different formulations concluded that negative effects on health were not expected [75]. Another example, carbon nanotubes could have an even greater capacity to cause mesotheliomas than crocidolite asbestos [76], although these findings were questioned because nanotubes are not absorbed through the lungs [77]. This shows that the current knowledge is limited and sometimes contradictory regarding the toxicology of nanomaterials.

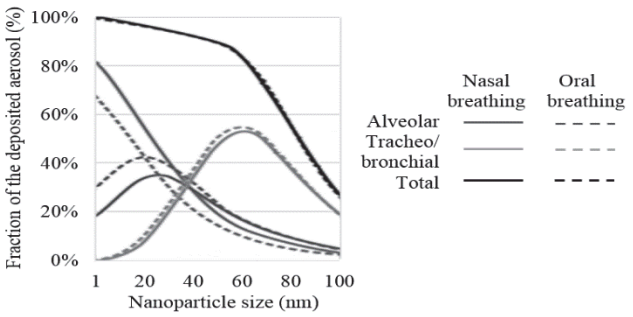

Figure 1. Total and regional deposit of nanoparticles depending on the particle diameter.
Source: Adapted from [65].

2.3. Impact on safety: risk of fire and explosion

In general, the catalytic effects and the risk of fire or explosion should be taken into account in the safety assessment when handling nanopowder [78]. However, it is also thought that the specific environmental conditions needed to pose a risk are not easily obtained [67]. In any case, it is important to consider other factors that increase the probability of ignition and the violence of the explosion such as the presence of a solvent, humidity, temperature, etc. [79,80]. In fact, these factors are important in different jobs on construction sites; they could indeed be present simultaneously and incompatibilities are possible [48].

3. Recommendation for managing exposure to nanomaterials

Faced with the difficult task of carrying out a quantitative risk assessment owing to the absence of firm toxicological and exposure information, qualitative risk assessment, control banding (CB) allows a simplified process to be used in order to determine the potential risk of exposure probability and severity of damage, as well as the corresponding risk level and their associated safety measures: general ventilation (level 1), ventilation by localized extraction or smoke hoods (level 2), confinement (level 3) and seeking external advice (level 4) [81]. Also, there are other methodologies and strategies for risk assessments, for example, taking into account the exposure route of entry, the aspect of identification and the toxicological screening; these three levels are defined with their corresponding actions [82].

In this paper a set of preventive and protective measures is presented according to the characteristics of the nanomaterial: in suspension (dispersed nanomaterials aerosol), solid form freely mobile nanomaterials (dispersed nanomaterials dust and friable solids) and fixed in a solid matrix or embedded on a surface [83]. The principal aim is to avoid entry into the body by inhalation or through the skin (and thus by ingestion). The authors choose this strategy, because the characteristics of nanomaterials determine the exposure risks [84]. In fact, it is important to note that some building nanoproducts may display different material forms during their life-cycles, and this affects potential occupational exposure. For example, this aspect is included in the Risk Assessment Document and the case of Sepiolite Clay is analyzed [85].

The recommendations presented are the result of a review of scientific literature and documentation from prestigious Institutes of Occupational Safety and Health. The vast majority of safety guidelines and protocols to manage exposure to nanomaterials, focus on laboratory research environments. Only some specific interactive examples for construction sites that have been provided by BAuA (Bundesanstalt für Arbeitsschutz und Arbeitsmedizin) [86]. Prevention criteria and measures protection oriented research in general and construction environments have been unified

Table 1.
Elimination of nanoproducts.

Characteristics of nanoproduct	Action	Recommendations
When the use of nanoproducts arises	Elimination.	If possible, it should only be considered if the specific properties of nanomaterials offset possible new risks [41].

Source: Own elaboration.

Table 2.
Substitution of nanoproduct, working equipment and working processes.

Characteristics of nanoproduct	Action	Recommendations
Solid form freely mobile nanomaterials.	Nanoproduct replaced.	The option that generates the least dust during use is always recommended. This is critical in the case of nanopowders where the option that generates the least dust during use is always recommended, for example with cement [86].
	Working equipment replaced.	Suction systems to trap dust on grinding and cutting equipment are always recommended [86]. These systems should have filters HEPA (High Efficiency Particulate Air) [67].
In suspension.	Working processes replaced.	Using other equipment that does not generate aerosols, for example for the application of paints use rollers instead of sprays.

Source: Own elaboration

Table 3.
Engineering controls.

Characteristics of nanoproduct	Action	Recommendations
Solid form freely mobile Nanomaterials & in suspension	Localized extraction.	When confinement is not possible, it local exhaust will be used [88]. Using laboratory chemical hoods on the construction site is impossible; therefore, using blower/vacuum electric portable is proposed as alternative. Ventilation by dilution can control the level of environmental pollution of nanoparticles [67]. Ventilation by dilution cannot, in any case, be a single measure of exposure control [88]. Ventilation by dilution should be complementary to the application of localized extraction or confinement. It is not recommended as a single measure, as contaminant dispersion to other areas could be aided.
Solid form freely mobile nanomaterials: only friable solids	Confinement.	The works should be carried out in closed circuit systems [41]. Use glove-bags [88]. Carrying out the tasks in a closed circuit system is impossible. However, it is possible to use glove-bags to handle small friable solids.

Source: Own elaboration.

Table 4.
Work practices.

Characteristics of nanoproduct	Action	Recommendations
Solid form freely mobile nanomaterials.	Work practices related To environment (equipment and work processes).	Take into account the operating temperature of the electrical equipment [78]. Place nonskid mats on the floor so that any material that falls on the mats can be easily cleaned by just removing them. Another advantage is that the material is not dragged elsewhere [89]. People should not move near the worker handling the nanoproducts to avoid air turbulence [90]. Section off the work area [69]. Use one of the several proposed pictograms, because for the time being there is no standard European pictogram to warn of danger from exposure to nanomaterials.
Solid form freely mobile nanomaterials & in suspension & fixed in a solid matrix or embedded on a surface.	Personal hygiene measures.	Do not store or consume food and drink in the workplace, avoid applying cosmetics, wash hands before eating or leaving the job and avoid touching your face or other exposed parts of the body with contaminated fingers [67].
	Treatment nanowastes	Nanowaste should be treated as hazardous waste [91]. Safe practices should be extended to treat nanowastes [92].
	Work practices related to PPE.	Storing clothes and protective gear with loose contamination in a closed bag or other sealable container [93]. Pay attention to possible wear of personal protection measures [94] Close attention must be paid that gloves and cuffs fit correctly [89].
In the event of solid-spills.	Spills Control.	Wet systems and vacuum cleaners equipped with HEPA filters should always be used [67].
In the event of liquid-spills.		Adsorbents should be used [67].

Source: Own elaboration.

Table 5.
Personal Protection.

Characteristics of nanoproduct	Action	Recommendations
Solid form freely mobile nanomaterials & in suspension & fixed in a solid matrix or embedded on a surface.	Gloves	Nitrile gloves are generally recommended but latex is also used [89]. However, if it is necessary to protect against others risks, the gloves will be suitable.
	Coveralls	Coverall nonwoven: Tyvek-type [89].
Solid form freely mobile nanomaterials & in suspension.	Respiratory protection	FF P3-type disposable masks have been recommended [89]. FF P2-type disposable masks have been recommended [86]. In this case, we recommend FF P3-type, for greater worker´s protection.
	Eye protection	As a minimum, close fitting safety glasses should be worn [95].

Source: Own elaboration.

and selected to be applied to construction sites. These basic key recommendations for exposure to nanomaterials in the construction workplace are described below, following the stages of the traditional Industrial Hygiene structure from a conservative and preventive outlook [87]. It is important to note that these recommendations should be in line with other risks detailed on construction sites: falls from heights, electrocution, etc.

In the tables below, the characteristics of the nanoproducts, the action and recommendations that should be taken account is presented. Table 1 presents the eliminations as the first option, despite it being the most complicated. Table 2, presents the different types of replacements for products, working equipment and processes. In this case we should take into account the risks posed by the new replacement, so the choice influences the safety conditions. The engineering controls are summarized in Table 3. In Table 4, work practice suitability is listed and finally, Table 5 shows personal protection at work using nanoproducts

Complementarily to all the above steps, workers should receive information and training and should be consulted on the planning, organization and implications for health and safety on the use of nanotechnology [96].

Regarding health surveillance, although it is not mandatory and there is no evidence of the impact of nanomaterials based on epidemiological studies [48], the current knowledge is sufficient to carry out specific protocols [97]; for example, CSIC (Centro Superior de Investigaciones Científicas) have already developed specific medical protocols in Spain [98].

4. Conclusions

The nanotechnology has a substantial impact in the construction industry. The landscape of occupational risk prevention when using nanomaterials is vague and complicated. Thus, it is necessary to conduct more research focusing on this topic in order to suitably safeguard workers.

Previous experience with hazardous materials, such as asbestos, should be used to set a precedent and move forward cautiously [48]. With this principle of precaution in mind, the most important contribution made by this work has been to identify a series of specific recommendations according to the characteristics of the nanomaterial and from a conservative point of view to manage exposure to nanomaterial in workplace construction. These recommendations should keep up with new scientific breakthroughs.

References

[1] European Commission., Recomendación de la Comisión de 18 de Octubre de 2011 relativa a la definición de nanomaterial. Diario Oficial de la Union Europea, 2011.

[2] International Organization for Standardization (ISO)., ISO TS 8004-1:2010 Nanotechnologies - Vocabulary - Part 1: Core terms, 2011.

[3] Feliz, I.O. and Pitarke, J.M., Nanotechnology: The great challenge of the little one. DYNA (Spain), 89(5), pp. 496-500, 2014. DOI: 10.6036/7120

[4] Shelley, T., Nanotecnología. Nuevas promesas, nuevos peligros. Barcelona, El Viejo Topo, 2006.

[5] European Commission., High-Level expert group on key enabling technologies, [Online]. 2013 [Date of reference August 22th of 2013]. Available at: http://ec.europa.eu/enterprise/sectors/ict/key_technologies/kets_high_level_group_en.htm.

[6] Moledo-Frojan, F.J., Macroscopic survey about nanotechnology patents. DYNA, 83(1), pp. 11-19, 2008.

[7] Organisation for Economic and Co-operation and Development (OECD). Patents by technology, [On line]. 2013 [Date of reference August 22th of 2013]. Available at: http://stats.oecd.org/Index.aspx?DatasetCode=PATS_IPC.

[8] Adlakha-Hutcheon, G., Khaydarov, R., Korenstein, R., Varma, R., Vaseashta, A., Stamm, H., et al., Nanomaterials, Nanotechnology applications, consumer products, and benefits. Nanomaterials: Risks and Benefits, pp. 195-207, 2009.

[9] Hwang, D. and Bradley, J., The Recession's Ripple Effect on Nanotech, Lux Research. Inc., 2010.

[10] ANEC/BEUC., ANEC/BEUC Inventory of products claiming to contain nanoparticles available on the EU market, [Online]. 2013. [Date of reference July 26th of 2015]. Available at: http://docshare.beuc.org/Common/GetFile.asp?ID=30511&mfd=off&LogonName=Guesten.

[11] Der Bund für Umwelt und Naturschutz Deutschland. Nanoproduktdatenbank, [Online]. 2013. [Date of reference July 26th of 2015]. Available at: http://www.bund.net/nc/themen_und_projekte/nanotechnologie/nanoproduktdatenbank/produktsuche/.

[12] Nanowerk., Nanotechnology products and applications, [Online]. 2013 [Date of reference July 26th of 2015]. Available at: http://www.nanowerk.com/products/products.php.

[13] Woodrow Wilson Centre., The Project on emerging nanotechnologies, [Online]. 2013 [Date of reference June 14th of 2013]. Available at: http://www.nanotechproject.org/iphone/.

[14] Singh, P. and Nanda, A., Nanotechnology in cosmetics: A boon or bane? Toxicol Environ Chem, 94(8), pp. 1467-1479, 2012. DOI: 10.1080/02772248.2012.723482

[15] Salamanca-Buentello, F., Persad, D.L., Court, E.B., Martin, D.K., Daar, A.S. and Singer, P.A., Nanotechnology and the developing world. PLoS Medicine, 2(5), pp. 0383-0386, 2005.

[16] Bartos, P.J.M., Nanotechnology in Construction: A roadmap for development, 2009.

[17] Mann, S., Nanotechnology and Construction, Nanoforum, 2006.

[18] Van Broekhuizen, F. and Van Broekhuizen, P., Nano-products in the European construction industry. European Federation of Building and Wood Workers and European Construction Industry Federation, 2009.

[19] European Commission., Biotechnology in Europe. Special Eurobarometer, 2010.

[20] Van Broekhuizen, P., Van Broekhuizen, F., Cornelissen, R. and Reijnders, L., Use of nanomaterials in the European construction industry and some occupational health aspects thereof. Journal of Nanoparticle Research, 13(2), pp. 447-462, 2011.

[21] Holman, M., Nanomaterial forecast: Vols and Applications. In ICON Nanomaterial environmental health and safety research needs assessment. Lux Research, 2007.

[22] Ge, Z. and Gao, Z., Applications of nanotechnology and nanomaterials in construction. First Inter. Confer. Construc. Develop. Countries, pp. 235-240, 2008.

[23] Bhuvaneshwari, B., Sasmal, S. and Iyer, N.R., Nanoscience to nanotechnology for civil engineering - Proof of concepts. Recent Res Geogr. Geol., Energy, Environ Biomed - Proc WSEAS Int Conf Int Conf EMESEG'11, pp. 230-235, 2011.

[24] Hanus, M.J. and Harris, A.T.. Nanotechnology innovations for the construction industry. Progress in Materials Science, 58(7), pp. 1056-1102, 2013. DOI: 10.1016/j.pmatsci.2013.04.001

[25] Rafsanjani, H.N. and Kadivar, M., Application of nanotechnology in civil engineering. Advances in Building Materials, 1-3(261-263), pp. 520-523, 2011.

[26] Chong, K.P., Nanotechnology in civil engineering. Adv. Struct. Eng., 8(4), pp. 325-331, 2005. DOI: 10.1260/136943305774353151

[27] Naganathan, S., Singh, C.S.J., Shen, Y.W., Kiat, P.E. and Thiruchelvam, S., Nanotechnology in civil engineering - A review, 2014.

[28] Brockmann, T., Fontana, P., Meng, B. and Müller, U., Nanotechnology in construction engineering. Beton- und Stahlbetonbau, 103(7), pp. 446-454, 2008. DOI: 10.1002/best.200800624

[29] Zhu, W., Bartos, P.J.M. and Porro, A., Application of nanotechnology in construction. Summary of a state-of-the-art report. Materials and Structures/Materiaux et Constructions, 37(273), pp. 649-658, 2004.

[30] Khitab, A. and Arshad, M.T., Nano construction materials: Review. Rev. Adv. Mater. Sci., 38(2), pp. 181-189, 2014.

[31] Italcementi Group. i.active VERTICAL Hormigón fotocatalítico, [Online]. 2014 [Date of reference June 24th of 2014]. Available at: http://es.i-nova.net/es/content?articleId=67971.

[32] Kalwall., The World's most powerful translucent daylighting system, [Online]. 2014. [Date of reference June 18th of 2014]. Available at: http://www.kalwall.com/aerogel.htm.

[33] MMFX Steel Corporation of America., Corrosion Resistant. High-Strength. Over 100-Year Service Life. [Online]. 2014. [Date of reference April 4th of 2014]. Available at: http://www.mmfx.com/advantages/.

[34] Nanopinturas., Materiales de construcción, [Online]. 2014. [Date of reference June 30th of 2014]. Available at: http://www.nanopinturas.com/pdf/protect.pdf.

[35] Koleva, D.A., Nano-materials with tailored properties for self healing of corrosion damages in reinforced concrete, IOP self healing materials. The Netherlands, SenterNovem, 2008.

[36] Yang, Y., Lepech, M.D., Yang, E. and Li, V.C., Autogenous healing of engineered cementitious composites under wet-dry cycles. Cem Concr Res, 39(5), pp. 382-390, 2009. DOI: 10.1016/j.cemconres.2009.01.013

[37] European Agency for Safety and Health at Work (EU-OSHA)., Previsiones de los expertos sobre los riesgos químicos emergentes en relación con la seguridad y la salud en el trabajo. Facts, 84, 2009.

[38] Sanz, F., Estudio sobre riesgos laborales emergentes en el sector de la construcción. Revisión bibliográfica, Madrid, Instituto Nacional de Seguridad e Higiene en el Trabajo (INSHT), 2013.

[39] International Council of Nanotechnology (ICON)., Nano-EHS Database Analysis Tool, [Online]. 2015. [Date of reference March 8th of 2015]. Available at: http://icon.rice.edu/report.cfm.

[40] Instituto Nacional de Seguridad e Higiene en el Trabajo (INSHT)., VI Encuesta Nacional de Condiciones de Trabajo, 2007.

[41] Tanarro, C. and Gálvez, V., Nanopartículas: ¿Un riesgo pequeño?, Instituto de Seguridad e Higiene en el Trabajo, 2009.

[42] International Organization for Standardization (ISO). Standars, [Online]. 2014. [Date of reference June 24th of 2014]. Available at: http://www.iso.org/iso/home/search.htm?qt=nano&sort=rel&type=simple&published=onCreated%2021-ago-2013%2017:09:46Last%20Modified%2030-mar-2014%2022:28:23.

[43] European Commission. Policies, [Online]. 2013. [Date of reference August 19th of 2012]. Available at: http://ec.europa.eu/nanotechnology/policies_en.html.

[44] European Commission. Segunda revisión de la normativa sobre los nanomateriales, Comunicación de la Comisión al Parlamento Europeo, al Consejo y al Comité Económico y social europeo, 2012.

[45] NanoSafety Cluster., About the NanoSafety Cluster, [Online]. 2013. [Date of reference June 8th of 2013]. Available at: http://www.nanosafetycluster.eu/.

[46] NanoSafety Cluster. Scaffold, [Online]. 2013. [Date of reference July 8th of 2013]. Available at: http://www.nanosafetycluster.eu/eu-nanosafety-cluster-projects/seventh-framework-programme-projects/scaffold.html.

[47] Lee, J., Mahendra, S. and Alvarez, P.J.J., Nanomaterials in the construction industry: A review of their applications and environmental health and safety considerations. ACS Nano, 4(7), pp. 3580-3590, 2010. DOI: 10.1021/nn100866w

[48] Silva, F., Arezes, P. and Swuste, P., Nanomaterials in contruction - occupational safety and health aspects. Congress of Innovation on Sustainable Construction CINCOS´14, 2014.

[49] Tanarro, C., Nota Técnica de Prevención 877: Evaluación del riesgo por exposición a nanopartículas mediante el uso de metodologías simplificadas, Instituto Nacional de Seguridad e Higiene en el Trabajo, 2010.

[50] Oberdörster, G., Oberdörster, E. and Oberdörster, J., Nanotoxicology: An emerging discipline evolving from studies of ultrafine particles. Environ Health Perspect, 113(7), pp. 823-839, 2005. DOI: 10.1289/ehp.7339

[51] Maynard, A.D., Kuempel, E.D., Airborne nanostructured particles and occupational health. Journal of Nanoparticle Research, 7, pp. 587-614, 2005. DOI: 10.1007/s11051-005-6770-9

[52] Oberdörster, G., Oberdörster, E. and Oberdörster, J., Nanotoxicology: an ermerging discipline evolving from studies of ultrafine particles. Environmental Health Perspectives, pp. 173-179, 2005. DOI: 10.1289/ehp.7339

[53] NANODEVICE. Project summary, [Online]. 2013. [Date of reference September 1st of 2013]. Available at: http://www.nano-device.eu/index.php?id=123.

[54] Savolainen, K., Alenius, H., Norppa, H., Pylkkanen, L., Tuomi, T. and Kasper, G., Risk assessment of engineered nanomaterials and nanotechnologies-A review. Toxicology, 269(2-3), pp. 92-104, 2010. DOI: 10.1016/j.tox.2010.01.013

[55] Dekkers, S. and de Heer, H., Tijdelijke nano-referentiewaarden. Bruikbaarheid van het concept en van de gepubliceerde methode. RIVM Rapport 601044001/2010, 2010.

[56] British Standards Institution (BSI)., PD 6699-2: Guide to safe handling and disposal of manufactured nanomaterials, 2007.

[57] National Institute for Occupational Safety and Health (NIOSH). Occupational exposure to titanium dioxide. Current Intelligence Bulletin, 63, 2011, 117 P.

[58] National Institute for Occupational Safety and Health (NIOSH). Occupational exposure to carbon nanotubes and nanofibers. Curr Intell Bull, 161-A, pp. 1-149, 2010.

[59] Nanocyl. Responsible care and nanomaterials case study Nanocyl. Praga, 2009.

[60] Pauluhn, J., Multi-walled carbon nanotubes (Baytubes (R)): Approach for derivation of occupational exposure limit. Regulatory Toxicology and Pharmacology, 57(1), pp. 78-89, 2010.

[61] IFA. Institut für Arbeitsschutz der Deutschen Gesetzlichen Unfallversicherung. Criteria for assessment of the effectiveness of protective measures, 2010.

[62] Schulte, P.A., Murashov, V., Zumwalde, R., Kuempel, E.D. and Geraci, C.L., Occupational exposure limits for nanomaterials: State of the art. Journal of Nanoparticle Research, 12(6), pp. 1971-1987, 2010. DOI: 10.1007/s11051-010-0008-1

[63] Sousa, S.P.B., Ribeiro, M.C.S. and Santos-Baptista, J., Potencial risks related to polymer mortars production with nano ZrO2. Internacional Symposium on Occupational Safety and Hygiene, pp. 331-334, 2015.

[64] Current knowledge about nanotechnology safety. Proceedings: Annual Reliability and Maintainability Symposium, 2006.
[65] CIPR - Commission Internationale pour la protection Radiobiologique. Publication 66: Human respiratory tract model for radiological protection, Oxford, 1994.
[66] Hoet, P.H.M., Bruske-Hohlfeld, I. and Salata, O.V., Nanoparticles: Known and unknown health risks. Journal of of Nanobiotechnology, 2004. DOI: 10.1186/1477-3155-2-12
[67] Rosell, M.G. and Pujol, L., Nota Técnica de Prevención 797: Riesgos asociados a la nanotecnología, Instituto Nacional de Seguridad e Higiene en el Trabajo, 2008.
[68] Gálvez, V. y Tanarro, C., Toxicología de las nanopartículas, Instituto Nacional de Seguridad e Higiene en el Trabajo (INSHT), 2010.
[69] Ricaud, M. et Witschger, O., Les nanomatériaux: Definitions, risques toxicologiques, caractérisation de l'exposition professionnelle et mesures de prevention, Institut National de Recherche et de Sécurité, 2012.
[70] Dusinska, M., Magdolenova, Z. and Fjellsbo, L.M., Toxicological aspects for nanomaterial in humans. Methods Mol Biol, 948, pp. 1-12, 2013. DOI: 10.1007/978-1-62703-140-0_1
[71] Castranova, V., Overview of current toxicological knowledge of engineered nanoparticles. J Occup Environ Med, 53(6), pp. S14-S17, 2011. DOI: 10.1097/JOM.0b013e31821b1e5a
[72] Zhang, M., Jin, J., Chang, Y., Chang, X. and Xing, G., Toxicological properties of nanomaterials. J Nanosci Nanotechnol, 14(1), pp. 717-729, 2014. DOI: 10.1166/jnn.2014.9198
[73] Arora, S., Rajwade, J.M. and Paknikar, K.M., Nanotoxicology and in vitro studies: The need of the hour. Toxicol Appl Pharmacol, 258(2), pp. 151-165, 2012. DOI: 10.1016/j.taap.2011.11.010
[74] Lindberg, H.K., Falck, G.C., Suhonen, S., Vippola, M., Vanhala, E., Catalán, J., et al., Genotoxicity of nanomaterials: DNA damage and micronuclei induced by carbon nanotubes and graphite nanofibres in human bronchial epithelial cells in vitro. Toxicol Lett, 186(3), pp. 166-173, 2009. DOI: 10.1016/j.toxlet.2008.11.019
[75] NANODERM., Quality of skin as a barrier to ultra-fine particles. Final Project., QLK4-CT-2002-02678 2007.
[76] Poland, C.A., Duffin, R., Kinloch, I., Maynard, A., Wallace, W.A.H., Seaton, A., et al., Carbon nanotubes introduced into the abdominal cavity of mice show asbestos-like pathogenicity in a pilot study. Nature Nanotechnology, 3(7), pp. 423-428, 2008. DOI: 10.1038/nnano.2008.111
[77] Kane, A.B. and Hurt, R.H., Nanotoxicology: The asbestos analogy revisited. Nature Nanotechnology, 3(7), pp. 378-379, 2008. DOI: 10.1038/nnano.2008.182
[78] Ostiguy, C., Lapointe, G., Ménard, L., Cloutier, Y., Trottier, M., Boutin, M., et al. Nanoparticles: Actual knowledge about occupational health and safety risks and prevention measures, Institut de recherche Robert-Sauvé en santé et en sécurité du travail (IRSST), 2006.
[79] Pritchard, D.K., Literature review. Explosion hazards associated with nanopowders, [Online]. 2013. [Date of reference June 22th of 2004]. Available at: http://www.hse.gov.uk/research/hsl_pdf/2004/hsl04-12.pdf.
[80] Beck, H., Glienke, N. and Mohlmann, C., Combustion and explosion characteristics of dusts. BIA-Report 13/97, 1997.
[81] Zalk, D.M., Paik, S.Y. and Swuste, P., Evaluating the control banding nanotool: A qualitative risk assessment method for controlling nanoparticle exposures. Journal of Nanoparticle Research, 11(7), pp. 1685-1704, 2009. DOI: 10.1007/s11051-009-9678-y
[82] Ling, M., Lin, W., Liu, C., Huang, Y., Chueh, M. and Shih, T., Risk management strategy to increase the safety of workers in the nanomaterials industry. J Hazard Mater, 229, pp. 83-93, 2012. DOI: 10.1016/j.jhazmat.2012.05.073
[83] Gerritzen, G., Huang, L., Killpack, K., Murcheva, M. and Conu, J., A review of current practices in the nanotechnology industry, International Council on Nanotechnology (ICON), 2006.
[84] European Commission. Types and uses of nanomaterials accompanying the communication from the Commission to the European Parliament, the Council and the European Economic and Social Committee on the Second Regulatory Review on Nanomaterials, 2012.
[85] Dupont. Nanomaterial risk assessment document sepiolite clay, pangel S-9, [Online]. 2015. [Date of reference March 8th of 2015]. Available at: http://www.epa.gov/opptintr/nano/dupont2.pdf.
[86] BAuA., Nanorama-Baustelle, [Online]. 2014. [Date of reference June 24th of 2014]. Available at: http://nano.dguv.de/nanorama/bgbau/.
[87] Díaz-Soler, B.M., Martínez-Aires, M.D. and López-Alonso, M., Recommendations for the control of the exposition to nanomaterials in the construction industry, Guimarães (Portugal), Sociedade Portuguesa de Segurança e Higiene Ocupacionais (SPOSHO), 2015.
[88] Gibbs, L.M., Lamba, F., Stoxkmeier, B.C. and Kojola, W., General safe practices for working with engineered nanomaterials in research laboratories, National Institute for Occupational Safety and Health (NIOSH), 2012.
[89] Occupational Safety and Health Administration (OSHA). Introduction to nanomaterials and occupational safety and health, SH-21008-10-60-F-48 2010.
[90] Johnson, A.E. and Fletcher, B., The effect of operating conditions on fume cupboard containment. Saf Sci, 24(1), pp. 51-60, 1996. DOI: 10.1016/S0925-7535(96)00068-9
[91] NEPHH'S CONSORTIUM. Guidelines for responsible management of waste nanomaterials, 2012.
[92] Díaz-Soler, B.M., Martínez-Aires, M.D. and Martín-Morales, M., Safe workplace practices for handling nanowastes an overview. Internacional Symposium on Occupational Safety and Hygiene, pp. 193-196, 2015. DOI: 10.1201/b18042-40
[93] U.S. Department of Energy., Approach to nanomaterial ES&H revision 3a-May 2008, Nanoscale Science Research Centers, 2008.
[94] Occupational Safety and Health Administration (OSHA). CFR 1910.132. General requirements: Personal protective equipment, Washington D.C 2008.
[95] European Commission., Guidance on the protection of the health and safety of workers from the potential risks related to nanomaterials at work. Employment, Social Affairs & Inclusion, 2014.
[96] Ministerio de Trabajo y Seguridad Social. Ley 31/1995, de 8 de noviembre, de Prevención de Riesgos Laborales. Boletín Oficial del Estado, 1995.
[97] Schulte, P., Geraci, C., Zumwalde, R., Hoover, M., Castranova, V., Kuempel, E., et al. Sharpening the focus on occupational safety and health in nanotechnology. Scandinavian Journal of Work Environment & Health, 34(6), pp. 471-478, 2008. DOI: 10.5271/sjweh.1292
[98] Centro Superior de Investigaciones Científicas (CSIC). Unidad de vigilancia de la Salud y Medicina del Trabajo CSIC (Madrid), [Online]. 2013. [Date of reference September 1st of 2013]. Available at: http://www.icb.csic.es/fileadmin/formacionOfertas/unidad_de_vigilancia_de_salud_laboral.pdf.

B.M. Díaz-Soler, received her BSc in Technical Architecture in 2011 and her MSc. in Management and Integrated Safety in Construction in 2013, all them from the Universidad of Granada, Spain. At present, she is a PhD student on the Doctoral programme in Civil Engineering at the University of Granada. Her research interests include Health and Safety, Nanotechnology in Construction Industry and waste management.
ORCID: orcid.org/0000-0003-4332-1456

M.D. Martínez-Aires, received her BSc. in Organization Industrial Engineering 2004 from the University of Jaén, Spain, and Technical Architecture in 1993, from the University of Granada, Spain. She received her PhD in Civil Engineering in 2009 from the University of Granada, Spain. Currently, she is a full professor in the Department of Building Construction at the University of Granada. Her research interests include: Health and Safety, Prevention through Design (PtD), Ergonomics and Bibliometric Analyses.
ORCID: orcid.org/0000-0002-9292-5048

M. López-Alonso, received her BSc. in Civil Engineering in 1995 from the University of Granada, Spain. She received her PhD degree in Civil Engineering in 2013 from the University of Granada, Spain. Currently, she is an associate professor in the Department of Construction Engineering and Projects at the University of Granada. Her research interests include: Health and Safety, Prevention costs, Ergonomics, Construction Materials and Bibliometric Analyses.
ORCID: orcid.org/0000-0002-1343-1374

UNIVERSIDAD NACIONAL DE COLOMBIA
SEDE MEDELLÍN
FACULTAD DE MINAS

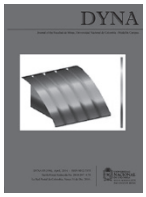

DYNA
http://dyna.medellin.unal.edu.co/

Differences in muscular activity between obese and non-obese workers during manual lifting

Ana Colim [a], Pedro Arezes [b], Paulo Flores [c] & Ana Cristina Braga [d]

[a] *Production and Systems Department, University of Minho, Guimarães, Portugal. ana.colim@dps.uminho.pt*
[b] *Production and Systems Department, University of Minho, Guimarães, Portugal. parezes@dps.uminho.pt*
[c] *Mechanical Engineering Department, University of Minho, Guimarães, Portugal. pflores@dem.uminho.pt*
[d] *Production and Systems Department, University of Minho, Guimarães, Portugal. acb@dps.uminho.pt*

Received: December 01rd, 2015. Received in revised form: February 02nd, 2016. Accepted: March 09th, 2016.

Abstract
The prevalence of obesity is increasing throughout the workforce. Manual lifting tasks are common and can produce significant muscle loading. This study compared muscular activity between obese and non-obese subjects, using surface Electromyography (EMG), during manual lifting. Six different lifting tasks (with 5, 10 and 15 kg loads in free and constrained styles) were performed by 14 participants with different obesity levels. EMG data normalization was based on the percentage of Maximum Contraction during each Task (MCT). Muscle Activation Times (AT) before each task were also evaluated. The study suggests that obesity can increase MCT and delay muscle AT. These findings reinforce the need to develop further studies focused on obesity as a risk factor for the development of musculoskeletal disorders.

Keywords: obesity; manual lifting; surface electromyography; maximum contraction during task; muscle activation time.

Diferencias en la actividad muscular entre trabajadores obesos y no obesos durante la elevación manual de cargas

Resumen
La prevalencia de la obesidad está aumentando también entre los trabajadores. Las tareas de elevación manual son comunes y pueden producir una significativa carga muscular. El actual estudio comparó la actividad muscular entre sujetos obesos y no obesos, mediante la aplicación de electromiografía de superficie (EMG) durante la elevación manual de cargas. Seis tareas de elevación muy diversas (con cargas de 5, 10 y 15 kg y con estilos de elevación libre y restringido) fueran solicitadas a los 14 sujetos con diferentes niveles de obesidad. La normalización de los datos de EMG fue basada en el porcentaje de la contracción máxima (MCT) durante cada tarea. También se ha evaluado el tiempo de la activación (AT) del músculo antes de cada tarea. El estudio sugiere que la obesidad puede aumentar el MCT y retrasar el AT del músculo. Estos resultados refuerzan la necesidad de desarrollar nuevos estudios, los cuales se deben centrar en la obesidad como un factor de riesgo para la aparición de síntomas y trastornos musculoesqueléticos.

Palabras-clave: obesidad; elevación manual; electromiografía de superficie; contracción máxima durante la tarea; tiempo de activación muscular.

1. Introduction

1.1. Effects of obesity on work performance

Improved social conditions among the population have led to an increase in the incidence of obesity in several countries, principally in the industrialized world. Global statistics confirm that obesity has more than doubled since 1980 and that, currently, more than 1.4 billion adults are overweight [1]. Obese subjects therefore represent a growing fraction of the workforce [2].

Obesity can be associated with psychological, social and physical problems, including Work-related Musculoskeletal Disorders (WRMSDs), which can negatively affect productivity [3,4]. Additionally, overweight subjects are absent from work due to illness more frequently and for longer periods than the non-obese [5]. This absenteeism is frequently related to WRMSDs [6].

© The author; licensee Universidad Nacional de Colombia.

Specific studies have analyzed different activities of daily life, comparing obese with non-obese subjects. Biomechanical studies of human walking have demonstrated that body fat mass (BFM) affects this activity [7]. For example, obese subjects reveal higher ground reaction forces [8], altered knee joint kinematics [9] and higher metabolic rates, even though the explanation for this last aspect has not been clearly established [10].

Additionally, stressful working postures are known to be related to the risk of WRMSDs. These postures can be affected by excessive BFM. However, the effects of obesity on posture maintenance during occupational tasks are rarely investigated [11]. Postural analysis tools, frequently used in workplace ergonomic interventions, seem to consider only people with normal weight. Based on this assumption, Park et al. [12] carried out psychophysical research with obese and non-obese subjects who were asked to perform static box-holding tasks in different working postures. In this study, the obese group reported higher perceived overload in all the postures considered, demonstrating that obesity increases postural stress. The findings of another study [13], also showed that the trunk posture of obese subjects was more flexed and that they experienced increased hip joint moment and greater hip-to-bench distance during a simulated standing work task.

Furthermore, it has also been demonstrated that obese subjects have more problems with work-restricting musculoskeletal pain than subjects of normal weight [14]. From the biomechanical point of view, excessive body mass can negatively affect the behavior of muscles and spine during the performance of physical activities. Different studies have correlated obesity with impairments to muscle activity, such as decreased muscle strength [7,15,16], as well as with lower back pain [17,18], although the epidemiological research literature has still not demonstrated a clear link between obesity and the latter phenomenon [19].

It is important to emphasize that lower back pain and its associated disorders continue to be the most common musculoskeletal problem in the workplace. It is associated with high costs to industry and can negatively influence the quality of life of workers. Several findings have shown that workers who perform manual materials handling, including lifting tasks, are exposed to a greater risk of back pain and/or WRMSDs than others whose jobs do not require this type of task [20,21]. However, such activities are very common in a wide variety of industrial workplaces [22]; they can have a range of additional occupational and individual WRMSD risk factors associated with them too. One of these individual risk factors is individual body composition, including excessive BFM [20].

In this context, Singh et al. [23] used a psychophysical approach and showed that obesity does not seem to reduce the maximum acceptable weight during manual lifting. However, these authors pointed out that this area requires further study, using other kinds of data, such as biomechanical information. Consequently, Xu et al. [24] analyzed lifting kinematics and kinetics in subjects with different body compositions, testing the hypothesis that heavier people lift more slowly, in order to minimize musculoskeletal load. However, obese subjects in fact registered higher values for kinematic trunk variables than their normal weight counterparts.

As mentioned above, although obesity has been intensively studied in recent years, research findings remain somewhat controversial. For example, the effect of excessive BFM on the function of the locomotor system is not yet well understood [7]. In addition, ergonomic studies are required to provide a more complete understanding of the effects of obesity on work performance [25], including during manual lifting tasks.

1.2. Assessment of obesity

Currently, obesity is assessed using different techniques, but each has several potential limitations and they should therefore be applied with caution. Among other available techniques, which include the body mass index (BMI), percentage of BFM, waist circumference (WC), WC/height ratio and WC/hip ratio, have been widely used in the assessment of obesity and to quantify the risk of obesity-related disorders [26].

It should be noted that in previous research into the effects of obesity on work performance, BMI has been the principal indicator used for obesity assessment. BMI is only based on a subject's weight and height; it does not distinguish fat-free body mass and fat mass, as it does not characterize body fat mass distribution [27]. BMI is an anthropometric measure commonly applied in epidemiological studies. However its specificity and predictive ability in identification of health problems associated with obesity have been questioned. BMI is considered to be a fallible measure for a detailed assessment of body composition and, therefore, should not be used to classify the individual level of obesity [28], implying the need to use more appropriate and comprehensive obesity assessment techniques.

For these reasons, in this study obesity levels were categorized according to subjects' BFM, determined by bioelectrical impedance analysis (BIA). This body composition assessment technique is easy to apply, non-invasive, relatively inexpensive and portable [29]. BIA allows for the quantification of body impedance by connecting electrodes to different areas of the body in order to create a circuit through which a current can pass. As the different human tissues exhibit different resistances to the passage of electric current, BIA devices determine the amount of lean body mass and body water as well as fat. Thus, the BFM can be obtained by calculating the difference between weight and lean body mass in individuals [28]. These results are obtained by way of predictive analytical expressions adjusted to individual factors such as gender, age, height and level of physical activity. These equations (which vary according to the equipment used) must be validated for the population in question, including obese individuals [30].

1.3. Muscular activity analysis during manual lifting

Obesity has been associated with impaired muscle function and reduced muscle strength [7,15,16]. These alterations to muscle activity can increase an individual's predisposition to WRMSDs [31]. Concerning occupational contexts, one of the key elements in WRMSD prevention is understanding the muscular demands of commonly performed tasks [32], such as manual lifting. In this field, surface EMG has been widely used

in ergonomic studies focused on various risk factors for MSDs, in an effort to optimize lifting tasks and so reduce the risk of such disorders developing [32-34]. In order to analyze muscular activity for each obesity level, surface EMG data was collected, as the principal role of the technique is the objective evaluation of muscle activity associated with particular manual work tasks [35].

The main purpose of the current study was to examine possible differences between the muscular contraction and activation times of obese and non-obese subjects during manual lifting. The intention was also to study some task conditions (different load weights and postural restraints) that might produce variations in muscular responses for the obese subjects.

2. Materials and Method

2.1. Subjects and experimental trials

Ten healthy males and four women, with no history of musculoskeletal disorders, volunteered to participate in the study. After signing an informed consent form, different anthropometric measures (weight, stature, shoulder height, WC) were collected. An OMRON BF306 Body Fat Monitor was used to determine the individuals' obesity levels (5 were "Normal", 4 were "High" and 5 were "Too high"). This equipment measures the BFM percentage based on electric resistance (determined by BIA) and also integrates personal data, such as the height, weight, age and gender of participants, in order to accurately define individual obesity levels [36]. The personal data used in the obesity level definition are presented in Table 1.

In the sagittal plane, 6 symmetrical trials (3 loads x 2 styles) of lifting and replacing a test box with goods handles, and with loads of 5 kg, 10 kg and 15 kg respectively, were performed in constrained and in free conditions (Table 2). During constrained lifting, the box was placed behind a 60 cm high barrier simulating one side of an industrial bin. The high barrier was constructed to measure 120% of average male and female knee heights [34]. The box loads complied with the recommended limits defined by Portuguese national legislation [37] and in some of the guidelines published by the National Institute Occupational Safety and Health (NIOSH) [38].

Table 1.
Anthropometric data, BFM percentages and obesity levels.

Participants (n = 14)	Age (years)	Gender	Body fat mass (%)	Obesity Level
1	28	Male	15.7	Normal
2	24	Male	20.5	High
3	36	Male	22.9	High
4	28	Female	18.3	Normal
5	24	Male	12.4	Normal
6	20	Male	22.3	High
7	21	Female	16.5	Normal
8	53	Male	36.0	Too high
9	46	Female	41.2	Too high
10	22	Male	39.8	Too high
11	24	Male	21.3	High
12	23	Female	28.5	Normal
13	40	Male	27.0	Too high
14	20	Male	26.1	Too high

Source: The authors.

Table 2.
Study design overview, taking into account the 6 trial conditions.

Trials	Loads			Styles	
	5 kg	10 kg	15 kg	Free	Constrained
1	●			●	
2	●				●
3		●		●	
4		●			●
5			●	●	
6			●		●

Source: The authors.

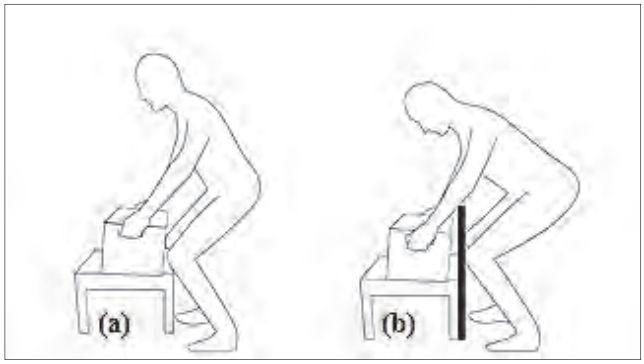

Figure 1. Schematic representation of the reaching position during (a) freestyle and (b) constrained style with barrier.
Source: The authors.

During the trials, participants stood in front of a height platform adjusted to each subject's standing knee height. They used both hands to lift the box vertically up to shoulder height and to return it to its original position in a single slow movement. In order to simulate a realistic working situation, no specific foot-placing instructions were given. The movement was subdivided into 4 phases: standing up (rest position), reaching (represented in Fig. 1), lifting, and replacing the box. However, the data analyzed in this paper relates only to the lifting phase.

2.2. EMG data collection

A portable EMG system (PLUX wireless biosignals®) was used to collect EMG data while the subjects performed the manual lifting tasks. EMG activity was collected using bipolar surface electrodes with 1 cm diameter and an inter-electrode distance of 2 cm. The EMG electrodes were affixed to the subject's body using standard placement procedures for Surface Electromyography for the Non-Invasive Assessment of Muscles [39] The zones of electrode placement were shaved, abraded and cleansed with rubbing alcohol absorbed into cotton rounds to lower the skin's electrical impedance [35].

The electrodes were located at 3 muscles recruited during this type of task: the right and left *Erector spinae* (*iliocostalis*) at L2 (RI, LI), the right and left *Erector spinae* (*longissimus*) at L1 (RL, LL) and the right and left *Deltoideus Anterior* (RD, LD) (Fig. 2).

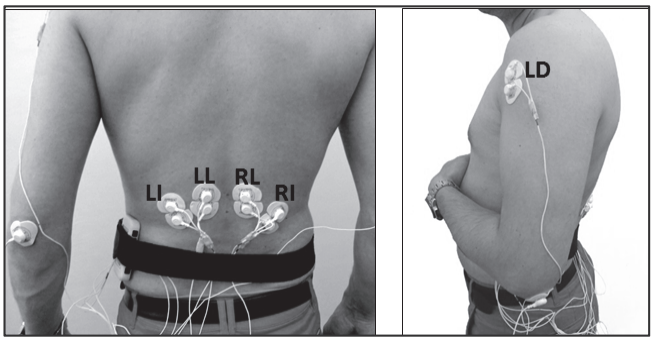

Figure 2: Sensor placement at the different muscles analyzed.
Source: The authors.

Muscle selection was based on their functionality during this type of task. The *Erector spinae* muscles are spine extensors, significantly recruited during vertical handling tasks [34]. The *Deltoideus Anterior* muscle acts during arm abduction, assists arm flexion, extension and rotation, and is also responsible for shoulder joint stability [40]. In addition, it was observed that fat mass accumulation was not high in these zones of the selected muscles, which, had it been, might have compromised EMG signal acquisition. At least one neutral reference (ground) electrode was fixed on the elbow per subject.

2.3. EMG signal processing

AcqKnowledge 3.9.0 software was used to process the EMG data. The raw EMG signals were amplified, high-pass filtered at 20 Hz and low-pass filtered at 500 Hz, rectified, and smoothed. The digital smoothing algorithm used was the root mean square (RMS), which reflects the mean power of the EMG signal [35] for each muscle and for each phase of the experimental trials. EMG data were normalized to peak value during each lifting trial, according to the following expression (1).

$$\text{MCT percentage} = \frac{Mean\ amplitude}{Peak\ value} \times 100 \qquad (1)$$

This normalization procedure has been utilized in other EMG studies with subjects presenting restrictions in their ability to perform maximum voluntary contractions, such as sufferers of musculoskeletal pathologies or obesity [41]. In addition, before each lifting trial, muscle AT was evaluated. This muscle onset quantification was based on a threshold defined by multiple SD of EMG-baseline noise [35]. In this experimental design, the independent variables were the different box loads, lifting style and obesity level. The dependent variables consisted of the MCT percentage and muscle AT.

2.4. Statistical analysis

A statistical analysis was conducted using the *IBM® SPSS® Statistics 22.0* software. For each task condition, the mean MCT percentages were compared across the subjects belonging to different obesity levels, in order to test the following hypothesis: greater mean MCT percentages are observed in individuals with higher BFM percentages. Accordingly, outcomes were compared using Pearson correlation tests, because the variables were found to behave normally (p>0.05 in the Shapiro-Wilk test).

Each muscle was then tested to see whether the task conditions (loads and barrier) produced significant effects on the mean MCT percentages in obese subjects. For this purpose a repeated measures ANOVA was applied. The assumption of normality was verified using the Shapiro-Wilk test, and the sphericity of the data was rejected by the Mauchly test (p <0.05). As the *epsilon* estimated value is greater than 0.75, the Huynh-Feldt correction was used to interpret the results for intra-subject effects.

Additionally, for each muscle considered, the following null hypothesis was also tested: i.e., that the distribution of AT is the same across different levels of obesity. To assess the normality of the AT values, the Kolmogorov test with Lilliefors correction was performed but, for most of the variables studied, this condition was not verified. Thus, the non-parametric Wilcoxon Mann-Whitney test was also applied. To reject the hypothesis, the decision rule was used to detect statistically significant evidence if p<0.05.

3. Results and Discussion

3.1. MCT percentages across obesity levels

Relative to the mean MCT percentage, a comparison of the values associated with different obesity levels showed that this variable presents higher values in the groups of "High" and "Too high" obesity. This difference was more evident in the lifting tasks involving the handling of the heavier loads, in this case, 10 and 15 kg (Fig. 3).

The Pearson correlation test demonstrated a significant linear statistical association, in that increased BFM was related to increases in MCT. This positive relation was established for the different muscles analyzed in different task conditions, as shown in Table 3.

It should be noted that the extensor muscle forces associated with these EMG values are the dominant contributor to compressive loading on the lumbar intervertebral joints [42], increasing the risk of back disorders. However, obesity is an individual risk factor commonly not included in WRMSD risk assessment. Therefore, obesity should be studied as a WRMSD risk factor during lifting.

3.2. MCT percentages of obese subjects across task conditions

During lifting tasks, the different conditions and associated risk factors do not work separately but in conjunction [43]. Accordingly, the effects of load weight and lifting style on MCT percentages of obese subjects were investigated. The summary of statistical significance for these interactions is presented in Table 4.

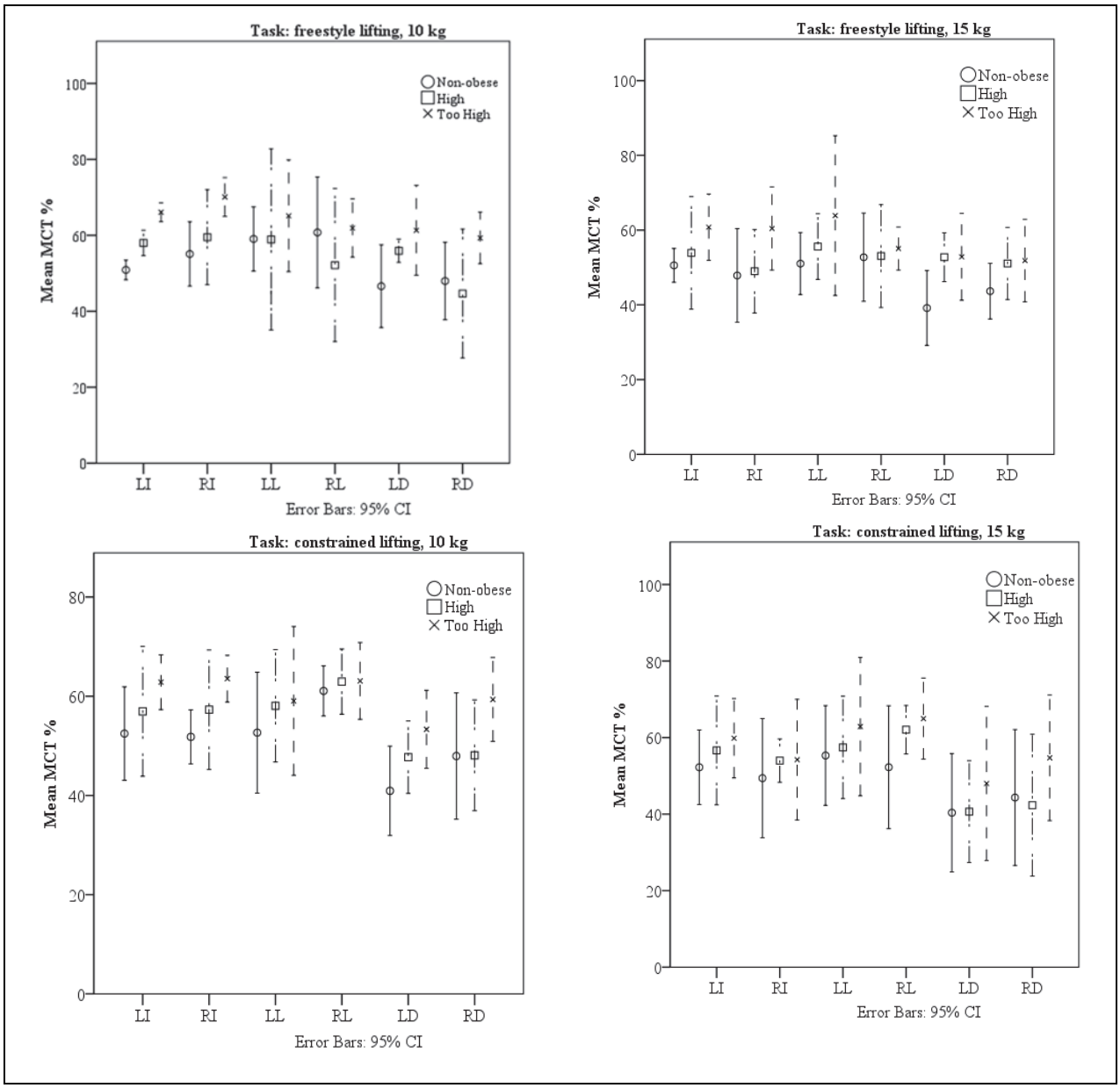

Figure 3: Representation of mean values for MCT percentage of the muscles involved across the different obesity levels and task conditions (exclusively for the handling of 10 kg and 15 kg loads). Error bars denote SD.
Source: The authors

Table 3.
Summary of statistical significance for the positive relation between individuals' BFM percentages and MCT percentages for the muscles analyzed.

Trials conditions	Muscles analyzed					
	LI	RI	LL	RL	LD	RD
5 kg Freestyle lifting	--	--	--	-	--	--
5 kg Constrained lifting	--	--	--	-	$r = 0.641$*	--
10 kg Freestyle lifting	$r = 0.792$**	$r = 0.611$*	--	-	$r = 0.572$*	--
10 kg Constrained lifting	--	$r = 0.584$*	--	-	$r = 0.742$**	$r = 0.761$**
15 kg Freestyle lifting	$r = 0.671$**	$r = 0.830$**	$r = 0.687$**	-	--	--
15 kg Constrained lifting	--	--	$r = 0.539$*	-	--	--

Legend: r coefficient of Pearson correlation; -- non-significant; * statistical significance at $p<0.05$; ** $p<0.01$.
Source: The authors.

Table 4.
Statistical significance of the influence of load and lifting style (with and without barrier) for the obese group.

	LI	RI	LL	RL	LD	RD
Obesity*Load	0.010 *	0.325	0.086	0.011 *	0.022 *	0.106
Obesity*Load*Barrier	0.461	0.696	0.531	0.771	0.083	0.105

Legend: * statistical significance at $p<0.05$.
Source: The authors.

Table 5.
Means (SD) of muscle AT across the tasks conditions for non-obese and obese subjects (including subjects with "high" and "too high" obesity levels).

			LI	RI	LL	RL	LD	RD
5 kg	Non-obese	Freestyle	-0.210 (0.358)	-0.251 (0.317)	-0.231(0.303)	-0.218 (0.286)	-0.235 (0.241)	-0.199 (0.174)
		Constrained	-0.201 (0.359)	-0.047 (0.392)	-0.253 (0.075)	-0.340 (0.079)	-0.287 (0.067)	-0.237 (0.362)
	Obese	Freestyle	0.079 (0.342)	-0.048 (0.393)	0.040 (0.389)	-0.088 (0.397)	0.031 (0.347)	0.044 (0.316)
		Constrained	-0.189 (0.276)	-0.199 (0.358)	-0.011 (0.392)	-0.115 (0.421)	-0.194 (0.257)	-0.200 (0.221)
10 kg	Non-obese	Freestyle	-0.151 (0.373)	-0.043 (0.414)	-0.330 (0.054)	-0.259 (0.083)	-0.255 (0.228)	-0.187 (0.368)
		Constrained	-0.245 (0.301)	-0.140 (0.342)	-0.427 (0.043)	-0.127 (0.452)	-0.312 (0.125)	-0.076 (0.227)
	Obese	Freestyle	-0.229 (0.115)	-0.208 (0.201)	-0.124 (0.341)	-0.152 (0.353)	-0.166 (0.255)	-0.129 (0.235)
		Constrained	-0.043 (0.342)	-0.152 (0.301)	-0.181 (0.367)	-0.061 (0.415)	-0.152 (0.232)	-0.151 (0.228)
15 kg	Non-obese	Freestyle	-0.295 (0.125)	-0.289 (0.199)	-0.313 (0.124)	-0.255 (0.201)	-0.319 (0.156)	-0.314 (0.068)
		Constrained	-0.254 (0.397)	-0.296 (0.204)	-0.314 (0.210)	-0.177 (0.262)	-0.178 (0.530)	0.006 (0.485)
	Obese	Freestyle	-0.044 (0.360)	-0.004 (0.526)	-0.169 (0.231)	-0.096 (0.388)	-0.160 (0.346)	-0.079 (0.306)
		Constrained	-0.116 (0.336)	0.048 (0.351)	-0.086 (0.344)	-0.042 (0.310)	-0.068 (0.269)	0.064 (0.203)

Source: The authors.

Significant differences mean MCT percentages of the following muscles exist for the different loads, as follows: LI [F(2; 96)= 4.863]; RL [F(2; 96)= 4.726] and LD [F(2; 96)= 3.949]. That is, significant variation exists across the different loads, in the sense that MCT values increase between 5 and 10 kg and decrease between 10 and 15 kg (being higher with 15 kg than with 5 kg loads). In these situations, the mean MCT percentages are higher in obese subjects, compared to their normal counterparts.

With increased load weight, muscle activity of the trunk extensors and the upper-extremity increases too [43]. These results from existing research are consistent with the observations of the present study, which found that MCT values increased during the lifting of 10 kg loads. However, handling of the heaviest loads can result in a load transfer to the lower body [44], which might explain the variation observed for loads of 15 kg.

In this context, many lifting tasks require workers to lift from industrial bins. The barriers formed by their sides can constrain knee flexion and increase trunk flexion during such tasks [34]. During symmetrical lifting, the trunk muscles are activated to create an extension moment, the risk of WRMSDs being broadly dependent on the resulting lumbar curvature [45]. Therefore, at the beginning of the current study, the authors predicted that excess BFM could negatively affect the posture adopted during these tasks, with the result that the constrained situation should contribute to increasing the muscular effort required at that point of the lifts. However, in obese subjects mean MCT percentages did not differ significantly under conditions of constraint caused by the high barrier, for any lifting cases.

A previous study [34] reported that in freestyle lifts the muscle activation levels were significantly lower than those for constrained situations. In the current study, this difference is not evident, perhaps because the location of muscles studied was different.

3.2. Muscle AT in obese and non-obese subjects

Concerning muscle AT, a descriptive statistical summary of these values across tasks conditions for non-obese and obese subjects is provided in Table 5.

Concerning the effect of obesity on the distribution of AT, the null hypothesis tested was rejected in the following task conditions: 10 kg constrained lifting in LL muscle (p=0.029) and 15 kg constrained lifting in RI muscle (p=0.042). Therefore, these statistically significant differences in the distribution of AT suggest that obese individuals have higher values when compared with the non-obese. These greater delays in AT registered for obese subjects suggest that increased BFM can reduce the

ability of skeletal muscle to activate rapidly before starting a movement, as also occurs in other groups with locomotor difficulties, such as the elderly or individuals with musculoskeletal disorders [31].

This poor correlation between muscle AT and increased BFM may be attributable to deficiencies in the AT quantifier currently being used.

3.3. Limitations and future work

There are several limitations that should be discussed with respect to this study. First of all, most lifting tasks in workplaces are not scaled. It is also likely that differences may exist for all obesity levels between tasks with different constraints and loads. The study was limited to the extent that only a few muscles were monitored with EMG. However, the selection of which muscles to monitor was influenced by body position, and trying to avoid regions with more accumulated adipose mass.

It is important to clarify that, since this is a pilot study in the field, the sample examined was made up of only fourteen participants. This constitutes a significant limitation. Increasing the sample size might be an important objective for future investigation.

The results of this research appear to demonstrate that increased BFM can produce some changes in muscle activity during lifting. In general, the outcomes are in line with the existing literature and emphasize the need to explore this research topic further. Excessive BFM can lead to an overreaction of the recruited muscles, causing increases in spine compressive loading and a subsequent risk of back injury. However, in order to examine this relation, further tests must be performed. Consequently, this area requires further research, which should be oriented to considering other type of data, such as information on kinematics.

4. Conclusions

The prevalence of obesity is increasing among the workforce. This research suggests that obese individuals can present changes in their muscle activity during lifting, compared to non-obese individuals. Obesity is an individual risk factor, which is very often neglected when assessing the risk of WRMSDs. Further studies are required to examine obesity as a WRMSD risk factor during lifting. Future work will involve a kinematics study, which will be carried out soon, and which it is hoped will improve our understanding of the effects of obesity on individual lifting capability.

Acknowledgments

This study was supported financially by the Portuguese Foundation for Science and Technology, under projects ID/CEC/00319/2013 and UID/EEA/04436/2013.

The authors wish also to acknowledge the commitment of the subjects who participated in this experimental study on a voluntary basis.

References

[1] World Health Organization – WHO. Obesity and overweight. Fact sheet, [Online]. 311, 2012. [Accessed: January 12th of 2012]. Available at: http://www.who.int/mediacentre/factsheets/fs311/en/index.html

[2] Flegal, K., Carroll, M., Ogden, C. and Johnson, C., Prevalence and trends in obesity among US adults, 1999-2000. JAMA, 288(14), pp. 1723-1727, 2002. DOI: 10.1001/jama.288.14.1723

[3] Lidstone, J., Ells, L., Finn, P., Whittaker, V., Wilkinson, J. and Summerbell, C., Independent associations between weight status and disability in adults: Results from the health survey for England. Public Health, 120, pp. 412-417, 2006. DOI: 10.1016/j.puhe.2005.12.003

[4] Morris, S., The impact of obesity on employment. Labour Economics. 14, pp. 413-433, 2007. DOI: 10.1016/j.labeco.2006.02.008

[5] Tsai, S., Ahmed, F., Wendt, J. Bhojani, F. and Donnelly, R., The impact of obesity on illness absence and productivity in an industrial population of petrochemical workers. AEP, 18(1), pp. 8-14, 2008. DOI: 10.1016/j.annepidem.2007.07.091

[6] Lier, H., Biringer, E., Eriksen, H. and Tangen, T., Subjective health complaints in a sample with morbid obesity and the complaints' relation with work ability. European Psychiatry. 24(S1), pp. 750, 2009. DOI: 10.1016/S0924-9338(09)70983-6

[7] Wearing, S., Henning, E., Byrne, N., Steele, J. and Hills, A., The biomechanics of restricted movement in adult obesity. Obesity Reviews, 7(1), pp. 13-24, 2006. DOI: 10.1111/j.1467-789X.2006.00215.x

[8] Browning, R. and Kram, R., Effects of obesity on the biomechanics of walking at different speeds. Medicine and Science in Sports and Exercise, 39(9), pp. 1632-1641, 2007. DOI: 10.1249/mss.0b013e318076b54b

[9] Lerner, F., Board, W. and Browning, R., Effects of obesity on lower extremity muscle function during walking at two speeds. Gait & Posture, 39, pp. 978-984, 2014. DOI: 10.1016/j.gaitpost.2013.12.020

[10] Browning, R., McGowan, C. and Kram, R., Obesity does not increase external mechanical work per kilogram body mass during walking. Journal of Biomechanics. 42, pp. 2273-2278, 2009. DOI: 10.1016/j.jbiomech.2009.06.046

[11] Blaszczyk, J., Cieslinka-Swider, J., Plewa, M., Zahorska-Markiewicz, B. and Markiewicz, A., Effects of excessive body weight on postural control. Journal of Biomechanics, 42, pp. 1295-1300, 2009. DOI: 10.1016/j.jbiomech.2009.03.006

[12] Park, W., Singh, D., Levy, M. and Jung, E., Obesity effect on perceived postural stress during static posture maintenance tasks. Ergonomics, iFirstarticle, pp. 1-14, 2009.

[13] Gilleard, W. and Smith, T., Effect of obesity on posture and hip joint moments during a standing task, and trunk forward flexion motion. International Journal of Obesity, 31(2), pp. 267-271, 2007. DOI: 10.1038/sj.ijo.0803430

[14] Peltonen, M., Lindroos, A. and Torgerson, J., Musculoskeletal pain in the obese: A comparison with a general population and long-term changes after conventional and surgical obesity treatment. Pain, 104, pp. 549-557, 2008. DOI: 10.1016/S0304-3959(03)00091-5

[15] Hulens, M., Vansant, R., Lysens, R., Claessens, A., Muls, E. and Brumagne, S., Study of differences in peripheral muscle strength of lean versus obese women: An allometric approach. International Journal of Obesity and Related Metabolic Disorders, 25(5), pp. 676-678, 2001. DOI: 10.1038/sj.ijo.0801560

[16] Maffiuletti, N., Jubeau, M, Munzinger, U., Bizzini, M, Agosti, F., De Col, A., Lafortuna, C. and Sartorio, A., Differences in quadriceps muscle strength and fatigue between lean and obese subjects. European Journal Appl. Physiol., 101, pp. 51-59, 2007. DOI: 10.1007/s00421-007-0471-2

[17] Bayramoglu, M., Akman, M., Kilinc, S., Cetin, N., Yavuz, N. and Ozker, R., Isokinetic measurement of trunk muscle strength in women with chronic low-back pain. American Journal of Physical Medicine & Rehabilitation, 80(9), pp. 650-655, 2001. DOI: 10.1097/00002060-200109000-00004

[18] Kostova, V. and Koleva, M., Back disorders (lower back pain, cervicobrachial and lumbosacral radicular syndromes) and some related risk factors. Journal Neurol. Science, 192, pp. 17-25, 2001. DOI: 10.1016/S0022-510X(01)00585-8

[19] Leboeuf-Y de, C., Body weight and low back pain: A systematic literature review of 56 journal articles reporting on 65 epidemiologic studies. Spine, 25(2), pp. 226-237, 2000. DOI: 10.1097/00007632-200001150-00015
[20] Marras, W., Occupational low back disorder causation and control. Ergonomics, 43(7), pp. 880-902, 2000. DOI: 10.1080/001401300409080
[21] Yeung, S., Genaidy, A., Huston, R., and Karwowski, W., An expert cognitive approach to evaluate physical effort and injury risk in manual lifting - A brief report of a pilot study. Human Factors and Ergonomics in Manufacturing, 12(2), pp. 227-234, 2002. DOI: 10.1002/hfm.10010
[22] Arezes, P., Miguel, S. and Colim, A., Manual materials handling: Knowledge and practices among portuguese health and safety practitioners. Work: A Journal of Prevention, 39(3), 2011.
[23] Singh, D., Park, W. and Levy, M., Obesity does not reduce maximum acceptable weights of lift. Applied Ergonomics, 40(1), pp. 1-7, 2009. DOI: 10.1016/j.apergo.2008.04.007
[24] Xu, X., Mirka, G. and Hsiang, S., The effects of obesity on lifting performance. Applied Ergonomics, 39, pp. 93-98, 2008. DOI: 10.1016/j.apergo.2007.02.001
[25] Williams, N. and Forde, M., Ergonomics and obesity. Applied Ergonomics. 40, pp. 148-149, 2009. DOI: 10.1016/j.apergo.2008.01.009
[26] Paniagua, L., Lohsoonthorn, V., Lertmaharit, S., Jiamjarasrangsi, W. and Williams, M., Comparison of waist circumference, body mass index, percent body fat and other measure of adiposity in identifying cardiovascular disease risks among Thai adults. Obesity Research & Clinical Practice, 2, pp. 215-223, 2008. DOI: 10.1016/j.orcp.2008.05.003
[27] Akpinar, E., Bashan, I., Bozdemir, N. and Saatci, E., Which is the best anthropometric technique to identify obesity: body mass index, waist circumference or waist-hip ratio?. Coll. Antropol., 31, pp. 387-393, 2007.
[28] Beechy, L., Galpern, J., Petrone, A. and Krupa-Das, S., Assessment tools in obesity — Psychological measures, diet, activity, and body composition. Physiology & Behavior, 107, pp. 154-171, 2012. DOI: 10.1016/j.physbeh.2012.04.013
[29] Kyle, U., Bosaeu, I., Lorenzo, A., Deurenberg, P., Elia, M., Gómez, J., Heitmann, B., Kent-Smith, L., Melchior, J., Pirlich, M., Scharfetter, H., Schols, A. and Pichard, C., Bioelectrical impedance analysis—part II: Utilization in clinical practice. Clinical Nutrition, 23, pp. 1430-1453, 2004. DOI: 10.1016/j.clnu.2004.09.012
[30] Horie, L., Barbosa-Silva, M., Torrinhas, R., de Mello, M., Cecconello, I. and Waitzberg, D., New body fat prediction equations for severely obese patients. Clin. Nutr., 27, pp. 350-356, 2008. DOI: 10.1016/j.clnu.2008.03.011
[31] Lewek, M., Rudolph, K. and Snyder-Mackler, L., Quadriceps femoris muscle weakness and activation failure in patients with symptomatic knee osteoarthritis. J. Orthop. Res., 22, pp. 110-115, 2004. DOI: 10.1016/S0736-0266(03)00154-2
[32] Butler, H., Hubley-Kozey, C. and Kozey, J., Electromyographic assessment of trunk muscle activation amplitudes during a simulated lifting task using pattern recognition techniques. Journal of Electromyography and Kinesiology, 19, pp. e505-e512, 2009. DOI: 10.1016/j.jelekin.2008.09.010
[33] Splittstoesser, R., Yang, G., Knapik, G., Trippany, D., Hoyle, J., Korkmaz, S., Sommerich, C., Lavender, S. and Marras, W., Spinal loading during manual materials handling in a kneeling posture. Journal of Electromyography and Kinesiology, 17, pp. 25-34, 2007. DOI: 10.1016/j.jelekin.2005.12.003
[34] McKean, C. and Potvin, J., Effects of a simulated industrial bin on lifting and lowering posture and trunk extensor muscle activity. International Journal of Industrial Ergonomics, 28, pp. 1-15, 2001. DOI: 10.1016/S0169-8141(00)00060-3
[35] Konrad, P., The ABC of EMG. USA: Noraxon INC, 2005.
[36] Deurenberg, P., Yap, M. and van Staveren, W., Body mass index and percent body fat: A meta-analysis among different ethnic groups. International Journal of Obesity, 22, pp. 1164-1171, 1998. DOI: 10.1038/sj.ijo.0800741
[37] Estado Português. Decreto-Lei nº 330/93 - Prescrições mínimas de segurança e de saúde respeitantes à movimentação manual de cargas. Diário da República, Diário da República nº 226 Série I Parte A de 25/09/1993.
[38] Waters, T., Putz-Anderson, V., Garg, A. and Fine, L., Revised NIOSH equation for the design and evaluation of manual lifting tasks. Ergonomics, 36(7), pp. 749-776, 1993. DOI: 10.1080/00140139308967940
[39] SENIAM, Surface Electromyography for the Non-Invasive Assessment of Muscles. [Online]. [Accessed: November 25th of 2012]. Available at: www.seniam.org
[40] Kothiyal, K. and Kayis, B., Workplace layout for seated manual handling tasks: An electromyography study. International Journal of Industrial Ergonomics, 27, pp. 19-32, 2001. DOI: 10.1016/S0169-8141(00)00039-1
[41] De Luca, C., The use of surface electromyography in biomechanics. Journal of Applied Biomechanics, 13, pp. 135-163, 1997.
[42] Potvin, J., McGill, S. and Norman, R., Trunk muscle and lumbar ligament contributions to dynamic lifts with varying degrees of trunk flexion. Spine, 10, pp. 1099-1107, 1991. DOI: 10.1097/00007632-199109000-00015
[43] Maiti, R. and Bagchi, T., Effect of different multipliers and their interactions during manual lifting operations. International Journal of Industrial Ergonomics, 36, pp. 991-1004, 2006. DOI: 10.1016/j.ergon.2006.08.004
[44] Frost, D., Abdoli-E, M. and Stevenson, J., PLAD (personal lift assistive device) stiffness affects the lumbar flexion/extension moment and the posterior chain EMG during symmetrical lifting tasks. Journal of Electromyography and Kinesiology, 19, pp. e403-e412, 2009. DOI: 10.1016/j.jelekin.2008.12.002
[45] McGill, S., Hughson, R. and Parks, K., Changes in lumbar lordosis modify the role of the extensor muscles. Clinical Biomechanics, 12(3), pp. 190-194, 2000. DOI: 10.1016/S0268-0033(97)00063-6

A. Colim, is a PhD. student in Industrial and Systems Engineering at the University of Minho, Portugal, where she is also an invited teaching assistant on Ergonomics and Human Factors. She holss a MSc in Human Engineering from University of Minho.
ORCID: orcid.org/0000-0003-1138-1534

P. Arezes, was awarded a PhD. in Industrial and Systems Engineering by the University of Minho, Portugal, where he is currently a Full Professor of Ergonomics and Human Factors. He is also a visiting fellow at MIT's AgeLab in the USA. He leads the Human Engineering research group and is Coordinator of the Engineering Design and Advanced Manufacturing (EDAM) area of the MIT Portugal Program at the University of Minho.
ORCID: orcid.org/0000-0001-9421-9123

P. Flores is a Full Professor in the Mechanical Engineering Department at the University of Minho, Portugal. He received his BSc. in Mechanical Engineering from the University of Minho in July 1997 and was awarded a PhD in Mechanical Engineering by the same university in February 2005. He completed Post-Doctoral studies at the ETH-Zurich, in February 2009, completing them at the University of Arizona, in August 2012. In March 2011 he concluded his professional qualification in Mechanical Engineering at the University of Minho. His current interests are: Biomechanics, Multibody Dynamics, Contact-Impact Dynamics, Engineering Education, Kinematics and the Dynamics of Mechanisms, Medical Devices and Tribology. He has published more than two hundred refereed journal and conference papers in these areas.
ORCID: orcid.org/0000-0002-7013-4202

A.C. Braga is a Chemical Engineer with an MSc. in Probability and Statistics and a PhD. in Applied Statistics. She is currently Assistant Professor at the Department of Production and Systems, School of Engineering, University of Minho, Portugal. She is responsible for curricular units in the first and 2nd cycles of studies in the area of Applied Statistics and for Quantitative and Qualitative Methods in Engineering in PhD. programs in Engineering. From 2004 to 2011 she was visiting professor in several Masters programs in Dental Medicine. She currently pursues her scientific research in Applied Statistics at the Algoritmi Centre at the University of Minho. Her area of scientific interest are: Applied Statistics in Engineering and Biostatistics.
ORCID: orcid.org/0000-0002-1991-9418

UNIVERSIDAD NACIONAL DE COLOMBIA
SEDE MEDELLÍN
FACULTAD DE MINAS

DYNA
http://dyna.medellin.unal.edu.co/

Impact of a workplace exercise program on neck and shoulder segments in office workers

Mariana Machado-Matos [a] & Pedro Miguel Arezes [b]

[a] *Healthy Generation, Lisboa, Portugal. mariana.machado.matos@gmail.com*
[b] *Centro Algoritmi, Universidad de Minho, Guimarães, Portugal. Parezes@dps.uminho.pt*

Received: November 30th, 2015. Received in revised form: March 07th, 2016. Accepted: March 11th, 2016.

Abstract
Work-related musculoskeletal disorders are a common problem among office workers. The purpose of this study is to evaluate the impact of a workplace exercise program on neck and shoulder pain and flexibility in office workers. The workstation assessment was performed using Rapid Office Strain Assessment. Workers were assessed for pain pre- and post-implementation of the workplace exercise program using the Nordic Questionnaire for Musculoskeletal Symptoms, and for flexibility. The program lasted 3 months and entailed twice weekly sessions. The sample consisted of an intervention group (n = 30) and a control group (n = 8). The results suggest improvements in pain reduction and increased flexibility. The workers had less musculoskeletal pain at the end of the evaluation. The increase in flexibility between the evaluations was significant in the intervention group, though there were slight improvements there too.

Keywords: work-related musculoskeletal disorders; workplace exercise; shoulder; neck; pain; flexibility.

Impacto de un programa de ejercicio en el trabajo en los segmentos de cuello y hombros en los trabajadores de oficina

Resumen
Trastornos musculoesqueléticos relacionados con el trabajo son un problema común entre los trabajadores de oficina. El propósito de este estudio es evaluar el impacto de un programa de gimnasia laboral en la dolor de cuello y hombro, y la flexibilidad en los trabajadores de oficina. La evaluación del puesto de trabajo se realizó a través de *Rapid Office Strain Assessment*. Los trabajadores fueron evaluados para el dolor pre y post-ejecución del programa de gimnasia utilizando el *Nordic Questionnaire for Musculoskeletal Symptoms*, y por la flexibilidad. El programa tuvo una duración de 3 meses y supuso sesiones dos veces por semana. La muestra está formada por un grupo de intervención (n = 30) y un grupo control (n = 8). Los resultados sugieren mejoras en la reducción del dolor y aumento de la flexibilidad. Los trabajadores tuvieron menos dolor musculoesquelético al final de la evaluación. El aumento de flexibilidad entre dos puntos de tiempo de la evaluación fue significativo en el grupo de intervención, aunque hubo una ligera mejora allí también.

Pal. Clave: trastornos musculoesqueléticos relacionados con el trabajo; programa de gimnasia laboral; hombro; cuello; dolor; flexibilidad

1. Introduction

Work-related musculoskeletal disorders (WRMSD) have increased among office workers in recent years, principally as a result of prolonged computer use [1,2]. Excessive use of computers has also been identified as the main reason for the increase in neck and upper limb problems [3]. About 45.5% to 63% of office workers surveyed have experienced neck pain during the previous 12 months [4,5]. Risk factors associated with computer use include prolonged sitting, fast and repetitive movements, lack of support for the upper limbs, non-neutral body position, inactivity, short or inexistent rest breaks, poor workstation ergonomics, mechanical stress concentrations (direct pressure on hard surfaces or sharp edges on soft tissues), static muscle loading, poor physical and mental condition, and others [6,7].

The relationship between sitting posture and cervical spine and shoulder changes have been extensively studied. Although it seems that there are no studies able to attest a clear relationship between posture, muscle motor activity and

© The author; licensee Universidad Nacional de Colombia.

WRMSD [2], some authors have shown that a sustained static posture for long periods of time is related to persistent muscular activity of the spine and shoulder stabilizers [8]. Others report that this muscle activity is higher in symptomatic workers compared to asymptomatic controls [9,10]. The development of upper extremity musculoskeletal disorders is associated with sustained muscle activity even at low loads[11].

Some authors suggest that there is a positive association between maintaining a sitting position for more than 95% of working time and neck pain [12]. Working in this position for long periods means the upper body must be kept in a static posture in which, anatomically, the neck supports the head, which accounts for nearly one-seventh of total body weight. In order to maintain a static posture, the muscles of the neck and shoulder overwork and become injured [13]. This condition produces a continuous static load on the neck and shoulder muscles, causing muscle tension that, in the long term, produces neck and shoulder pain and a restricted range of motion (RoM) [12]. The most frequently reported discomfort and pain among office workers is at the upper trapezius muscle [14], a problem caused by muscle tension; this pain usually radiates to the shoulder and involves muscle stiffness.

The shoulder is a complex joint that allows synchronized movement of the scapula and the humerus [15]. Simple movements such as shoulder flexion associate coordinated actions of many muscles in the neck, shoulder and trunk. Some authors have evaluated shoulder biomechanics in subjects with or without shoulder joint dysfunction [16,17]. These studies have shown that individuals with shoulder dysfunction display less tipping and upward rotation and more anterior tipping and elevation of the scapula during functional arm tasks, as well as greater activity of the upper trapezius muscle, which is associated with shoulder dysfunctions [15,17]. Studies of the interaction between posture and neck-shoulder dysfunctions also suggest that spinal misalignment allows them to occur [9,10]. Other authors have suggested that thoracic posture can affect scapula kinematics [18] because increased thoracic kyphosis, while a forward head posture can induce anterior tilt and protraction of the scapula, restricting the sub acromial space and shoulder RoM. Thus, it has been suggested that changes in shoulder biomechanics may be the cause of pain and of restricted RoM. Abnormal shoulder posture also leads to muscle imbalance and weakness, emphasizing the importance of strategies aimed at providing muscular training [19,20].

WRMSDs are a significant problem for companies in Europe, because they are a primary cause of work-related disability and loss of productivity.

In recent decades, exercise-oriented intervention has been widely used as a prevention strategy to reduce the impact of WRMSDs. Some studies have examined the benefits of exercise on work-related upper extremity disorders, but these have been based on limited evidence [21]. Certain authors have found exercise to have beneficial effects on musculoskeletal pain symptoms in several regions of the upper body, as well decreasing the number of additional pain regions, specifically in the neck. They have also concluded that neck pain is related to pain in other locations [22].

Most studies use strength exercise protocols to prevent WRMSDs [22,23]. These appear to be effective in the management of neck and shoulder pain. However, exercise with heavy loads in the presence of pain and/or of WRMSDs might be contraindicated, because overloading the neck and shoulder structures can lead to a risk of inflammation or increased pain [24].

The aim of this study was to evaluate the impact of a personalized workplace exercise program on neck and shoulder pain and flexibility in office workers.

2. Methods

2.1. Study sample

The study was conducted at the offices of an insurance brokers in Oporto, Portugal, between September and December 2013.

All workers generally perform their functions in a sitting posture and work with a range of office equipment such as computers (monitor, keyboard and mouse), telephones and documents.

The sample was intentionally composed of office workers who did and who did not participate in the workplace exercise (WEG) sessions. Participation was on a voluntary basis. There were 38 workers in the final sample, divided into two groups: the intervention group (IG) of 30, who participated in the WEG sessions, and a control group (CG) of 8 individuals who did not. The CG included workers who had undergone the entire evaluation process but who did not join the WEG sessions. An informed consent form, which briefly explained the study, its goals and the methods to be used, was distributed to all participants.

2.2. Study design

The evaluation of the workstations was carried out using Rapid Office Strain Assessment (ROSA) [25] with the goal of identifying risk factors related to discomfort at office workstations. This method allows the posture of workers and their interactions with their workstations to be examined in order to define the most appropriate exercises to be carried out during the WEG program. The method was designed to provide a rapid quantification of the risks associated with office work and was based on a set of scoring chart diagrams that included the subsections "Chair", "Monitor and Telephone" and "Keyboard and Mouse". The goal was to determine overall ROSA scores and the corresponding action level, in order to make changes to the workstations and to understand the interactions workers had with them. The workstations were not evaluated according to the group (IG or CG) to which each subject belonged, because the objective was simply to evaluate the risk associated with each workplace and not to compare the scores obtained by the two groups.

The evaluation of the workers' musculoskeletal pain symptoms was performed using an adaptation of the Portuguese version of the Nordic Questionnaire [26]. The segments evaluated were the neck and the right and left shoulders over the previous 12 months and within the previous 7 days. Each question was accompanied by a body diagram.

The measuring instrument used to gauge flexibility was the universal goniometer, model MSD EA-8161. All evaluations were carried out by the same evaluator, with the objective of improving the reliability of the measurements by

eliminating inter-measurer variability. The tests were performed in a sitting posture, as described by Clarkson [27]. The movements evaluated were lateral flexion of the neck and flexion, abduction and external rotation of the shoulder, all performed for both sides of the body. Workers were asked to bring lightweight clothing to work.

2.3. Intervention

The program lasted for 3 months, with 2 sessions per week with a duration of 15 minutes each. All the WEG sessions took place in the afternoon, with the intention of preventing fatigue, working unsolicited muscles and relaxing muscles that had been solicited for many hours at the computer.

The program was led by a physiotherapist specialized in WEG and took place in an open space near all the workers' workstations to ensure them quick access. The workers could use their normal work clothes during the sessions. The exercises performed were designed to mobilize and stretch several parts of the body, with an emphasis on the vertebral column and upper limbs, though some exercises were included for the legs because of the long hours worked in a sitting position. Sometimes, strength exercises were performed using low weights. Some sessions included playful and recreational activities such as massage, self-massage and games. The sessions were carried out with or without equipment (balloons, balls, sticks, paper) and were performed on an individual basis, as well as in pairs and in groups. All the sessions included background music to encourage wellbeing, joy and motivation. The WEG program was publicized using posters and emails sent by the Human Resources Department and which explained its objectives and raised awareness of the importance of participating.

2.4. Measurement

All participants underwent an evaluation of musculoskeletal pain symptoms and flexibility at the start of the program (M1), in order to establish a baseline, and again at the end, three months later (M2).

2.5. Statistical analysis

Data was analyzed using descriptive statistics (mean, standard deviation –SD- and percentages).

The McNemar test was used to compare differences in musculoskeletal pain symptoms between M1 and M2, while the Wilcoxon test was used to compare flexibility. The significance level was 0.05. The statistical data analysis was carried out using the SPSS program (version 22).

3. Results

3.1. Sample characterization

The study was conducted on 38 participants divided into two groups – the IG and the CG. The IG was 83.3% female and 16.7% male while the CG was 62.5% female and 37.5% male. Table 1 describes the characteristics of the sample at baseline (M1).

Table 1.
Sample characteristics at baseline.

	Intervention group	Control group
Age (years)	39.57 (7.66)	41.50 (7.75)
Weight (kg)	63.77 (10.48)	79.13 (15.29)
Height (m)	1.65 (0.06)	1.69 (0.09)
Body mass index (kg/m^2)	23.46 (3.12)	27.84 (5.23)
Smoking status	30.0%	25.0%
Physical activity status	50.0%	62.5%
Length of service (years)	8.59 (8.51)	10.43 (7.18)
Past history of illness	30.0%	50.0%

Data are expressed as mean (SD) or %
Source: The authors.

Table 2.
Pain perception in the previous 12 months. McNemar test results for difference analysis between evaluation moments.

Body region	Intervention group			Control group		
	M1	M2	*P* value	M1	M2	*P* value
Neck	60.0%	43.3%	0.180 (NS)	25.0%	37.5%	1.000 (NS)
Right shoulder	46.7%	43.3%	1.000 (NS)	12.5%	37.5%	0.500 (NS)
Left shoulder	36.7%	36.7%	1.000 (NS)	25.0%	37.5%	1.000 (NS)

Data are expressed as %. * $P < 0.05$, ** $P < 0.01$ and NS – Not significant.
Source: The authors.

3.2. Workstation evaluation

Most of the workers are seated in an open plan office environment. Their normal tasks are computer work, call answering, document-reading, writing, copy-making, and others. Of these, computer work and call answering occupy most time. The workstations are equipped with a desk, a chair, a computer (monitor, keyboard and mouse) and a telephone.

The mean final ROSA score for the 38 workstations was 3.61 (0.64) while the mean (SD) section scores were 3.45 (0.55), for the Chair, 3.11 (0.61) for the Monitor and Telephone and 2.11 (0.31) for the Mouse and Keyboard.

3.3. Musculoskeletal symptoms analysis

The workers in both groups experienced pain during their working hours. Table 2 shows worker perceptions of neck and shoulder pain, pre- and post the WEG program for the IG and for the CG during the previous 12 months.

As shown in Table 2, members of the IG experienced reduced musculoskeletal pain at M2 compared with M1, except for the left shoulder. For the CG, it was found that musculoskeletal pain increased for all body segments evaluated. However, the values of these differences are not significant.

Table 3 presents data on worker perceptions of neck and shoulder pain, pre- and post the WEG program for the IG and for the CG for the previous 7 days.

Table 3.
Pain perception in the previous 7 days. McNemar test results for difference analysis between evaluation moments.

Body region	Intervention group			Control group		
	M1	M2	*P* value	M1	M2	*P* value
Neck	33.3%	20.0%	0.125 (NS)	0.0%	12.5%	1.000 (NS)
Shoulders	26.7%	26.7%	1.000 (NS)	12.5%	37.5%	0.625 (NS)

Data are expressed as %. * $P < 0.05$, ** $P < 0.01$ and NS – Not significant.
Source: The authors.

During the previous 7 days, members of the IG perceived a reduction in musculoskeletal pain in the neck while there was no change for the shoulders. However, in the CG, pain perception increased in both segments. However, the values of these differences are not significant.

3.4 Analysis of Flexibility Levels

The results for flexibility levels are set out in Table 4. In terms of the movements analyzed, it may be observed that the RoM averages increased for the IG between the two evaluation moments. According to Table 4 these differences are significant.

Table 4.
Flexibility levels by group (in grades) and Wilcoxon test results for difference analysis between evaluation moments.

Joint	Movement	Side	Intervention group			Control group		
			M1	M2	*P* value	M1	M2	P value
Neck	Lateral Flexion	Right	35.50 (7.28)	38.97 (6.34)	<0.001**	37.75 (6.82)	38.50 (6.39)	0.098 (NS)
		Left	33.60 (7.27)	36.50 (7.53)	0.001**	38.63 (5.76)	37.50 (6.57)	0.655 (NS)
Shoulders	Flexion	Right	172.73 (9.22)	175.03 (9.15)	0.002**	177.50 (2.39)	177.88 (2.30)	0.257 (NS)
		Left	170.97 (10.78)	174.2 (9.37)	0.001**	175.75 (2.60)	176.63 (3.02)	0.038*
	Abduction	Right	172.57 (12.86)	175.97 (9.06)	0.003**	171.25 (14.26)	174.00 (8.05)	0.102 (NS)
		Left	170.67 (5.49)	174.63 (10.52)	0.002**	173.63 (8.07)	174.75 (6.45)	0.066 (NS)
	External Rotation	Right	81.30 (11.77)	85.13 (6.26)	0.007**	80.13 (14.36)	80.13 (14.36)	1.000 (NS)
		Left	79.40 (11.42)	85.20 (6.51)	<0.001**	81.63 (10.01)	81.63 (10.01)	1.000 (NS)

Data are expressed as mean (SD). * $P < 0.05$, ** $P < 0.01$ and NS – Not significant
Source: The authors.

The values remained relatively constant for the CG, while there was a slight increase in right lateral flexion of the neck and flexion and abduction of the shoulder on both sides, along with decreased left lateral flexion of the neck. Only left flexion of the shoulder presents a significant difference between the moments of evaluation.

4. Discussion

This study was intended to evaluate the effectiveness of a workplace exercise program in reducing musculoskeletal pain and improving the levels of flexibility in the neck and shoulders.

The workstation evaluation using the ROSA method found that workstations themselves can cause discomfort. Further investigation and modifications might be required here. The sitting posture adopted by workers using computers throughout the working day, as well as interactions with other elements in the workplace, can cause muscle tension in the neck and shoulder segments. Unilateral postures continue to occur too, as when workers hold their phones between the head and shoulder, causing muscle fatigue and decreased flexibility as a result of tension, which stops the muscles working at peak. The workplace exercise program was therefore planned to prioritize exercises designed to relax the musculature of the cervical spine and shoulders and decrease fatigue, reducing pain and increasing flexibility.

The first improvement observed in the IG was related to a reduction in the prevalence of worker perceptions of musculoskeletal pain at 12 months and at 7 days, although the differences between these self-evaluations were not significant. These data may indicate that the WEG program influence this change in symptoms in the neck and right shoulder. However, the fact that there was less effect on the left shoulder may indicate that a longer intervention period would be necessary in order to obtain more significant results. Although the current study took place over a period of more than 10 weeks, other authors found that this period of workplace group gymnastics had no clear effects on pain [28]. A previous study that analyzed pain perception before and after a workplace fitness program obtained different results, finding that pain reduction was not significant for the CG but was for the IG [29]. Other studies that evaluated pain perception found that it is potentially possible to reduce subjective sensations of pain in office workers [23, 30]. On the other hand, another set of studies, in this case analyzing perceptions of musculoskeletal pain in cases where workers undertook an hour of exercise a week for a year, obtained similar results to those obtained here [22]. Waling et al. compared three different protocols, focused on strength, endurance and coordination exercises for a period of ten weeks, each session lasting one hour, and achieving similar results for pain reduction to those of the current study [31]. However, it was difficult to compare the current research with these earlier studies because the duration of the sessions was very different and –furthermore- in Waling et al. the sample was exclusively female. This is an important difference, as it is known that women have a higher risk of WRMSD than males [32], a difference that can be explained by the physical and functional differences between the sexes [33]. Thus, a WEG program could have beneficial effects, decreasing muscle fatigue and, consequently, reduce the perception of pain.

The results were similar for flexibility: neck and shoulder RoM in the movements evaluated improved in the IG following the WEG program. It is known that a lack of exercise influences the levels of flexibility and that sedentary people tend to be less flexible than their active counterparts. Thus, it can be said that exercise improves flexibility [34]. Other studies focused on office workers found similar results, with improvements in the flexibility levels of the shoulder in flexion, abduction and external rotation, though the results were non-significant [35]. On the other hand, a study of metalworkers registered an increase in flexibility levels in shoulder movements [36]. Restricted RoM can also be affected by factors such as postural misalignment and muscle imbalance. The literature suggests that there is some evidence that exercise may improve posture in the upper thoracic area, helping improve mobilization of the shoulder muscles, and consequently leading to an increase in RoM [20]. An appropriate posture at the workstation, either sitting or standing, allowed subjects to reduce muscle stress and tension, as the muscles are able to work in balance and, therefore, more efficiently. The decrease in trapezius muscle tension may have influenced the increased RoM in the assessed tasks (especially in lateral neck flexion) as well as a decrease in fatigue levels in the shoulder muscles, leading, in turn, to increased external rotation RoM of the shoulder [15]. On the other hand, the exercises performed during the program were accompanied by stimuli administered by the physiotherapist with the aim of raising awareness of the importance of maintaining correct posture of the neck and upper limbs, not just during the sessions but at all times. This might be one explanation of the significant improvements in the flexibility levels in this study as compared to others, in which the workers were responsible for their own exercise routines [37].

The improvements observed in the CG may have been the result of recommendations to perform specific exercises designed for specific body parts that were formulated during assessments. These improvements may be associated with the impossibility of evaluating the IG and the CG separately. WEG sessions were held in an open space, in full view of other workers. This may have influenced CG members to engage in some of the proposed exercises.

4.1. Limitations of the study

The first recognized limitation of this study is the reduced sample size, both for the IG and the CG. Increased sample size would have permitted some sample stratification, for instance by gender, allowing analysis and comparison by group. It would also have been beneficial to have been able to exert more control over some variables, such as subject lifestyle routines, clinical history and others, in order to obtain more accurate results.

5. Conclusions

This study was designed to evaluate the effectiveness of a workplace exercise program, with the intention of reducing musculoskeletal pain and improving the levels of flexibility in neck and shoulders. The results obtained show that IG members experienced reduced musculoskeletal pain in the neck and shoulders, although the results were not statistically significant. They also demonstrated improved RoM in lateral flexion of the neck and flexion, abduction and external rotation of the shoulder, for both sides of the body. According to these results, then, the implementation of a WEG program could be beneficial to office workers.

Acknowledgments

This study received financial support from the Portuguese Foundation for Science and Technology, under project ID/CEC/00319/2013.

References

[1] Buckle, P. and Devereux, J., The nature of work-related neck and upper limb musculoskeletal disorders. Applied Ergonomics, 33, pp. 207-217, 2002. DOI: 10.1016/S0003-6870(02)00014-5

[2] Tittiranonda, P., Burastero, S., and Rempel, D., Risk factors for musculoskeletal disorders amog computer users. Occupational Medicine, 14, pp. 17-38, 1999.

[3] Punnett, L. and Wegman, D.H., Work-related musculoskeletal disorders: The epidemiologic evidence and the debate, in: J Electromyogr Kinesiol, University of Massachusetts Lowell, USA. 2004, pp. 13-23. DOI: 10.1016/j.jelekin.2003.09.015

[4] Sillanpää, J., Huikko, S., Nyberg, M., Kivi, P., Laippala, P., and Uitti, J., Effect of work with visual display units on musculo-skeletal disorders in the office environment. Occupational Medicine, 53, pp. 443-451, 2003. DOI: 10.1093/occmed/kqg120

[5] Cagnie, B., Danneels, L., Van Tiggelen, D., De Loose, V., and Cambier, D., Individual and work related risk factors for neck pain among office workers: a cross sectional study. European Spine Journal, 16, pp. 679-686, 2007. DOI: 10.1007/s00586-006-0269-7

[6] Ming, Z., Närhi, M., and Siivola, J., Neck and shoulder pain related to computer use. Pathophysiology : The Official Journal of the International Society for Pathophysiology / ISP, 11, pp. 51-56, 2004.

[7] Punnett, L. and Bergqvist, U., Visual display unit work and upper extremity musculoskeletal disorders. A Review of Epidemiological Findings. National Institute for Working Life, 16, 1997.

[8] Hägg, G.M. and Aström, A., Load pattern and pressure pain threshold in the upper trapezius muscle and psychosocial factors in medical secretaries with and without shoulder/neck disorders. International Archives of Occupational and Environmental Health, 69, pp. 423-32, 1997. DOI: 10.1007/s004200050170

[9] Szeto, G., Straker, L. and O'Sullivan, P., A comparison of symptomatic and asymptomatic office workers performing monotonous keyboard work-2: Neck and shoulder kinematics. Manual Therapy, 10, pp. 281-291, 2005. DOI: 10.1016/j.math.2005.01.004 DOI: 10.1016/j.math.2005.01.005

[10] Szeto, G., Straker, L., and O'Sullivan, P., A comparison of symptomatic and asymptomatic office workers performing monotonous keyboard work-1: Neck and shoulder muscle recruitment patterns. Manual Therapy, 10, pp. 270-280, 2005. DOI: 10.1016/j.math.2005.01.004 DOI: 10.1016/j.math.2005.01.005

[11] Visser, B. and Van Dieën, J.H., Pathophysiology of upper extremity muscle disorders. Journal of Electromyography and Kinesiology, 16, pp. 1-16, 2006. DOI: 10.1016/j.jelekin.2005.06.005

[12] Ariëns, G., Bongers, P., Douwes, M., Miedema, M., Hoogendoorn, W., van der Wal, G., et al., Are neck flexion, neck rotation, and sitting at work risk factors for neck pain? Results of a prospective cohort study. Occupational and Environmental Medicine, 58, pp. 200-207, 2001. DOI: 10.1136/oem.58.3.200

[13] Ming, Z. and Zaproudina, N., Computer use related upper limb musculoskeletal (ComRULM) disorders. Pathophysiology, 9, pp. 155-160, 2003. DOI: 10.1016/S0928-4680(03)00004-X

[14] Jensen, C., Finsen, L., Hansen, K., and Christensen, H., Upper trapezius muscle activity patterns during repetitive manual material

handling and work with a computer mouse. Journal of Electromyography and Kinesiology : Official Journal of the International Society of Electrophysiological Kinesiology, 9, pp. 317-325, 1999. DOI: 10.1016/S1050-6411(99)00007-3

[15] Ebaugh, D.D., McClure, P.W. and Karduna, A.R., Effects of shoulder muscle fatigue caused by repetitive overhead activities on scapulothoracic and glenohumeral kinematics. Journal of Electromyography and Kinesiology: Official Journal of the International Society of Electrophysiological Kinesiology, 16, pp. 224-235, 2006. DOI: 10.1016/j.jelekin.2005.06.015

[16] Klopcar, N. and Lenarcic, J., Bilateral and unilateral shoulder girdle kinematics during humeral elevation. Clinical Biomechanics Bristol, Avon, 21(Suppl 1), pp. S20-S26, 2006. DOI: 10.1016/j.clinbiomech.2005.09.009

[17] Lin, J., Hanten, W.P., Olson, S.L., Roddey, T.S., Soto-quijano, D.A, Lim, H.K., et al., Functional activity characteristics of individuals with shoulder dysfunctions. Journal of Electromyography and Kinesiology, Official Journal of the International Society of Electrophysiological Kinesiology, 15, pp. 576-586, 2005. DOI: 10.1016/j.jelekin.2005.01.006

[18] Finley, M.A. and Lee, R.Y., Effect of sitting posture on 3-dimensional scapular kinematics measured by skin-mounted electromagnetic tracking sensors. Archives of Physical Medicine and Rehabilitation, 84, pp. 563-568, 2003. DOI: 10.1053/apmr.2003.50087

[19] Kebaetse, M., McClure, P., and Pratt, N.A., Thoracic position effect on shoulder range of motion, strength, and three-dimensional scapular kinematics. Archives of Physical Medicine and Rehabilitation, 80, pp. 945-950, 1999. DOI: 10.1016/S0003-9993(99)90088-6

[20] Wang, C., Mcclure, P., Pratt, N.E. and Nobilini, R., Stretching and strengthening exercises: Their effect on three-dimensional scapular kinematics. Arch Phys Med Rehabil, 80, pp. 923-929, 1999. DOI: 10.1016/S0003-9993(99)90084-9

[21] Staal, J.B., de Bie, R.A. and Hendriks, E.J.M., Aetiology and management of work-related upper extremity disorders. Best Practice and Research: Clinical Rheumatology, 21, pp. 123-133, 2007. DOI: 10.1016/j.berh.2006.09.001

[22] Andersen, L.L., Christensen, K.B., Holtermann, A., Poulsen, O.M., Sjøgaard, G., Pedersen, M.T., et al., Effect of physical exercise interventions on musculoskeletal pain in all body regions among office workers: A one-year randomized controlled trial. Manual Therapy, 15, pp. 100-104, 2010. DOI: 10.1016/j.math.2009.08.004

[23] Sjögren, T., Nissinen, K.J., Järvenpää, S.K., Ojanen, M.T., Vanharanta, H. and Mälkiä, E.A., Effects of a workplace physical exercise intervention on the intensity of headache and neck and shoulder symptoms and upper extremity muscular strength of office workers: A cluster randomized controlled cross-over trial. Pain, 116, pp. 119-128, 2005. DOI: 10.1016/j.pain.2005.03.031

[24] Kisner, C. and Colby, L.A., Therapeutic exercise: Foundations and techniques, 5th ed., F.A. Davis Company, Philadelphia, PA, 2007.

[25] Sonne, M., Villalta, D.L. and Andrews, D.M., Development and evaluation of an office ergonomic risk checklist: ROSA-rapid office strain assessment. Appl Ergon, 43, pp. 98-108, 2012. DOI: 10.1016/j.apergo.2011.03.008

[26] Kuorinka, I., Jonsson, B., Kilbom, A., Vinterberg, H., Biering-Sorensen, F., Andersson, G., et al., Standardised Nordic questionnaires for the analysis of musculoskeletal symptoms, in: Appl Erg., Institute of Occupational Health, Department of Physiology, Helsinki, Finland., 1987: pp. 233-237. DOI: 10.1016/0003-6870(87)90010-x

[27] Clarkson, H., Musculoskeletal assessment. Joint motion and muscle testing., 3rd Ed., Lippincott Williams & Wilkins, Philadelphia, PA, 2013.

[28] Takala, E.P., Viikari-Juntura, E. and Tynkkynen, E.-M., Does group gymnastics at the workplace help in neck pain? Scand J Rehab Med, 26, pp. 17-20, 1994.

[29] Macedo, A., Trindade, C., Brito, A. and Socorro-Dantas, M., On the effects of a workplace fitness program upon pain perception: A case study encompassing office workers in a portuguese context. Journal of Occupational Rehabilitation, 21, pp. 228-233, 2011. DOI: 10.1007/s10926-010-9264-2

[30] Garganta, R., Prufer, C., Guerreiro, F., Soares, P. and Pereira, H., Effect of an exercise program in work environment on musculoskeletal disorders. Report of an experience in administrative workers., In: Proc. Int. Symp. Occup. Saf. Hyg. - SHO2012, Portuguese society of occupational safety and hygiene, Guimarães, 2012: pp. 266-267.

[31] Waling, K., Sundelin, G., Ahlgren, C. and Järvholm, B., Perceived pain before and after three exercise programs – A controlled clinical trial of women with work-related trapezius myalgia. Pain, 85, pp. 201-207, 2000. DOI: 10.1016/S0304-3959(99)00265-1

[32] Larsson, B., Søgaard, K. and Rosendal, L., Work related neck-shoulder pain: a review on magnitude, risk factors, biochemical characteristics, clinical picture and preventive interventions. Best Practice & Research. Clinical Rheumatology, 21, pp. 447-463, 2007. DOI: 10.1016/j.berh.2007.02.015

[33] Côté, J.N., A critical review on physical factors and functional characteristics that may explain a sex/gender difference in work-related neck/shoulder disorders. Ergonomics, 55, pp. 173-182, 2012. DOI: 10.1080/00140139.2011.586061

[34] Matos, M. and Arezes, P.M., Impact of an occupational gym program on flexibility in office workers, In: Occup. Saf. Hyg. SHO2015, Portuguese society of occupational safety and hygiene, Guimarães, 2015.

[35] Silveira, M., Effects of the workplace exercises in the morphologic, functional, lifestyle and absenteeism variables in workers of the pharmaceutical industry of Montes Claros - MG. Fitness & Performance Journal, 6, pp. 295-301, 2007. DOI: 10.3900/fpj.6.5.295.e

[36] Rasotto, C., Bergamin, M., Simonetti, A., Maso, S., Bartolucci, G.B., Ermolao, A., et al., Tailored exercise program reduces symptoms of upper limb work-related musculoskeletal disorders in a group of metalworkers: A randomized controlled trial. Manual Therapy, 20, pp. 56-62, 2015. DOI: 10.1016/j.math.2014.06.007

[37] Tsauo, J.-Y., Lee, H.-Y., Hsu, J.-H., Chen, C.-Y. and Chen, C.-J., Physical exercise and health education for neck and shoulder complaints among sedentary workers. Journal of Rehabilitation Medicine, 36, pp. 253-257, 2004. DOI: 10.1080/16501970410029807

M. Machado-Matos, received her BSc. in Physiotherapy in 2011 from the University Fernando Pessoa, Oporto, Portugal, and her MSc. in Human Engineering, in 2014, from the University of Minho, Portugal. She began her professional activity in 2011 in the organization Healthy Generation, since when she has been responsible, among other responsibilities, for the implementation of workplace gym programs, chair massage sessions, ergonomic evaluation and training on posture in the workplace.
ORCID: orcid.org/0000-0001-7444-9570

P.M. Arezes, was awarded in 2002 a PhD. in Industrial and Systems Engineering from the University of Minho, Portugal. He is currently a full professor of Ergonomics and Human Factors at the same university. He is a visiting fellow at MIT's AgeLab in the USA. He leads the Human Engineering Research Group at the University of Minho where he is also Director of the Engineering Design and Advanced Manufacturing (EDAM) area of the MIT Portugal Program, and Chair of the steering board of the PhD. program "Leaders for Technical Industries (LTI)" at the University of Minho.
ORCID: orcid.org/0000-0001-9421-9123

UNIVERSIDAD NACIONAL DE COLOMBIA
SEDE MEDELLÍN
FACULTAD DE MINAS

DYNA
http://dyna.medellin.unal.edu.co/

Occurrence of a skarn-type mineralogy found in Ciénaga Marbles, located in the NW foothills of the Santa Marta Massif (Colombia)

Oscar Mauricio Castellanos-Alarcón [a], Carlos Alberto Ríos-Reyes [b] & Luis Carlos Mantilla-Figueroa [b]

[a] *Programa de Geología, Universidad de Pamplona, Pamplona, Colombia, oscarmca@yahoo.es*
[b] *Escuela de Geología, Universidad Industrial de Santander, Bucaramanga, Colombia, carios@uis.edu.co*
[b] *Escuela de Geología, Universidad Industrial de Santander, Bucaramanga, Colombia, lcmantil@uis.edu.co*

Received: September 3rd, 2014.Received in revised form: August 4th, 2015.Accepted: September 20th, 2015.

Abstract
The early Cretaceous Ciénaga Marbles that crop out in the NW foothills of the Santa Marta Massif (Colombian Caribbean region) present an epigenetic mineral assemblage (skarn-type), overprinting the metamorphic mineral assemblage previously developed along the regional metamorphic history that affected this unit. The skarn-type mineralogy allows at least three paragenetic contexts to be distinguished, which are represented by the following neoformed minerals: (a) garnet, forsterite, diopside, titanite, wollastonite and calcite (early anhydrous metamorphic stage), (b) actinolite, tremolite, allanite and clinohumite (metasomatic or hydrated stage), and (c) chlorite, serpentine, sepiolite and quartz (late low temperature retrograde stage, probably due to infiltration of descending meteoric waters). The skarn-type mineralogy is observed as alteration halos developed around porphyritic granodiorites emplaced as sills between anisotropy planes related to metamorphic regional foliation of rock that are considered to be the causative bodies of the skarn-type mineralogy. Zircon U-Pb ages obtained from granodioritic bodies yielded an age of 55.5±0.7 Ma (Ypresian, Early Eocene). The formation of the skarn-type mineralogy in the Ciénaga Marbles is temporarily related to the formation and emplacement of hydrated silicate masses that were generated at the beginning of the subduction polarity change (*i.e.* when the Caribbean oceanic plate began to subduct beneath South American continental plate).

Keywords: Ciénaga Marbles; Santa Marta massif; skarn-type mineralogy; zircon U-Pb geochronology; Caribbean Plate.

Ocurrencia de una mineralogía tipo skarn reconocida en los Mármoles de Ciénaga, estribaciones NW del Macizo de Santa Marta (Colombia)

Resumen
Los Mármoles de Ciénaga del Cretácico Temprano que afloran en las estribaciones NW del Macizo de Santa Martha (región del Caribe Colombiano) presentan una asociación mineral epigenética de tipo skarn, sobreimpuesta a la asociación mineral formada previamente durante la historia de metamorfismo regional que afectó a esta unidad. La mineralogía tipo skarn permitió diferenciar al menos tres contextos paragenéticos, representados por los siguientes minerales: (a) granate, forsterita, diópsido, titanita, wollastonita y calcita (etapa metamórfica anhidra temprana), (b) actinolita, tremolita, clinonohimita y allanita (etapa metasomática o hidratada), y (c) clorita, serpentina, sepiolita y cuarzo (etapa retrógrada de baja temperatura tardía probablemente debido a infiltración descendente de aguas meteóricas). La mineralogía tipo skarn suele desarrollarse a manera de halos de alteración entorno a granodioritas porfiríticas emplazadas como *sills* entre los planos de la foliación regional de las rocas metamórficas, los cuales se consideran como los cuerpos causativos de la mineralogía tipo skarn. Dataciones U-Pb en circones de éstos cuerpos granodioríticos produjeron una edad de 55.5±0.7 Ma (Ypresiano, Eoceno Temprano). La formación de la mineralogía tipo skarn en los Mármoles de Ciénaga se relaciona temporalmente con la formación y el emplazamiento de masas silicatadas hidratadas, generadas al inicio del cambio en la polaridad de la subducción (es decir, cuando la placa oceánica del Caribe comenzó a subducir por debajo de la placa continental sudamericana).

Palabras clave: Mármoles de Ciénaga; Macizo de Santa Marta; Mineralogía tipo Skarn; Geocronología U-Pb en circones; Placa Caribe.

1. Introduction

A skarn-type mineralogy may be formed during regional or contact metamorphism and from a variety of metasomatic processes involving a great variety of fluids (magmatic, metamorphic, meteoric, and/or marine in origin). This mineral assemblage is characterized by the presence of calc-silicate minerals (e.g. garnet and pyroxene), among others

© The author; licensee Universidad Nacional de Colombia.

minerals [1-3]. The recognition of a skarn-type mineralogy is very relevant in terms of mineral exploration because of its relationship with mineral deposits formation [4-15]. The major part of skarn-type mineralogy can be related to causative igneous rocks emplaced at various tectonic settings [3]. The most economic skarn deposits are related to metasomatic processes that affect the country rocks (e.g. marbles) that are used to host hydrated silicate masses forming igneous rocks bodies. Many studies have pointed out the relationship between the skarn-type minerals (as well as the composition of the causative igneous bodies), and the mineral deposits skarn-related [10,16]. It is very useful for mineral exploration to determine a cause-effect relationship between the causative igneous bodies and the skarn-type mineralogy, and establish the mineral chemistry of garnet and pyroxene, which is very important to postulate a specific type of skarn deposit according to the skarn-type mineralogy. The aim of this paper is to report the occurrence of the skarn-type mineralogy recognized in the Ciénaga Marbles. Based on the mineralogical characteristics observed in the skarn-type mineral assemblage, we also discuss its origin, which can be associated with the magmatic-hydrothermal event forming this skarn-type epigenetic mineral assemblage. Finally, based on previous regional geology studies and zircon U-Pb geochronology data, we report some considerations to propose a link between the Caribbean oceanic plate evolution and the magmatic hydrothermal system related to the skarn-type mineralogy formation.

2. Geological background

The study area belongs to the Santa Marta Massif (SMM), which constitutes an isolated triangular-shaped range on the northern Colombian Caribbean region and represents an uplifted region (with altitudes of ca. 5800 m), located along the diffuse southern Caribbean plate boundary (Fig. 1). This was the result of an oblique convergence between the Caribbean plate and northwestern South America [17-18]. The Oca fault [19], the Santa Marta-Bucaramanga fault [20], the Cerrejón thrust sheet [21] and the Romeral suture are the major structures bounding the SMM. It is composed mainly by crystalline rocks and can be divided into three belts (Sierra Nevada, Sevilla and Santa Marta), and has a defined outboard younging pattern from east to west. The southeastern and oldest Sierra Nevada belt includes ca. 1.0-1.2 Ga high grade metamorphic rocks represented by granulites, gneisses and amphibolites that were affected during the Grenvillian orogenic event [22-24]. Jurassic plutons and volcanites intrude and cover these metamorphic rocks. Minor Carboniferous and Late Mesozoic sedimentary sequences rest in unconformity towards the southeast [25-26]. The intermediate Seville belt represents a polymetamorphic complex that includes Paleozoic gneisses and schists with Permian millonitized peraluminous granitoids [25,27-28]. The northwestern and youngest Santa Marta belt comprises an inner sub-belt of Cretaceous imbricated metamorphic rocks (greenschists and amphibolites) and an outer sub-belt of Mesozoic amphibolites, greenschists and phyllites separated by the lower to middle Cenozoic Santa Marta Batholith (SMB) [26,29-30]. The Cesar-Rancheria basin, exposed in the southeastern flank of the SMM, represents a sedimentary record that evolved from a Cretaceous passive margin to Maastrichian-Paleogene orogenic deposits linked to an accretionay and subduction event of the Caribbean plate [31]. Several quarries exploiting the Ciénaga Marbles (Santa Marta Geotectonic Province) are situated to the east of Ciénaga (Magdalena) at 11°00' North, 74°15' West, which are easily accessible from Ciénaga. Access is via the Caribbean Transverse (National Route 90) that connects with the Magdalena Trunk (National Route 45), and then turning left and continuing for 0.35 km on an unpaved road.

Metamorphic rocks from the Gaira Schists and Ciénaga Marbles, and igneous rocks are grouped into the SMB and recent deposits occur in the study area (Fig. 2). The Ciénaga Marbles host a skarn-type mineralogy, which can be associated with a magnesian-type skarn, genetically related to granitic igneous activity from the Eocene age SMB. The Gaira Schists crop out towards the northwest of the SMB. They are the result of a Middle Eocene (58.4±4.3 Ma) regional low- to middle-grade metamorphism under the greenschist and amphibolite facies [24], which have undergone retrograde metamorphism and metasomatism with abundant dykes of pegmatite, aplite and dacite [24]. The Ciénaga Marbles (early Cretaceous in age) and its surroundings are part of the Santa Marta Geotectonic Province in the SMM - a polymetamorphic complex that includes gneisses and schists of Paleozoic age with Permian mylonitic granitoids [27]. In general, they are coarse-grained white and bright marbles with granoblastic texture and sutured contacts, although they can be fine-grained dark gray marbles with a banded structure. Their spatial distribution and geometry is not very well established and their stratigraphic relationships with the surrounding rocks are difficult to establish due to numerous faults surrounding the bodies.

The relationships between marbles and schists are uncertain and not determined in the field. The Ciénaga Marbles overlies the Gaira Schists (metamorphosed to amphibolite facies before the intrusion of the SMB). They are divided into two members: (1) relatively pure and low magnesium marbles and (2) impure, in part dolomitic, sandy marbles, calcareous metasediments, metamudstones and quartzites. The SMB [25] emerges as a NE trending belt located between metamorphic rocks and is composed of

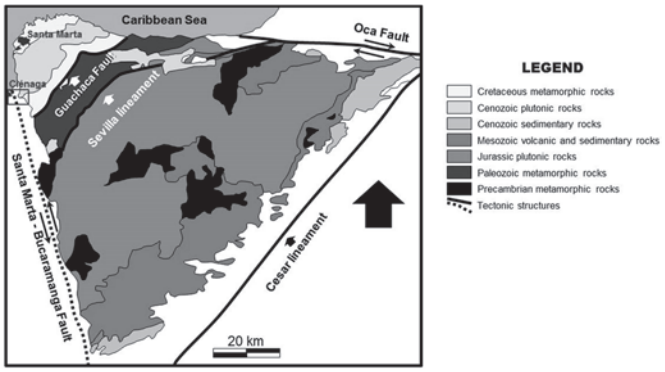

Figure 1. Generalized geological map of the SMM, showing the study area (small red line box).
Source: Adapted from Tschanz *et al*. [26].

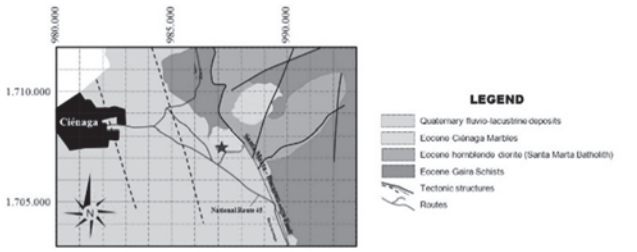

Figure 2. Geological map of the study area and distribution of the Ciénaga Marbles and sampling locality.
Source: Adapted after INGEOMINAS [34].

granodiorite to monzogranite with transitional variations and tonalite. It can show magmatic foliation similar to that reported by Gonzalez [35]. Mafic enclaves commonly occur throughout the body, with fewer pegmatitic hornblendites (cumulates of hornblende), indicating a complex magmatic history with recirculation and the mixing of materials from the lower parts of the magma chamber [36].

3. Field sampling and analytical methods

Marbles and associated rocks were collected from the mining area, taking into account their field relationships, texture and mineralogy. The petrographic analysis was performed on a trinocular NIKON LABOPHOT2-POL microscope. Mineral abbreviations are after Kretz [32]. SEM/EDS analysis was carried out by environmental scanning electron microscopy (FEI Quanta 650 FEG ESEM) under the following analytical conditions: magnification = 160-750x, HFW = 199 μm - 1.86 mm, HV = 20-30 kV, spot = 3.0, signal = SE, detector = LFD. Fractions of heavy mineral concentrates (<350 μm) were separated using traditional techniques at ZirChron LLC in Washington State University. LA-ICPMS U-Pb analyses were conducted at the GeoAnalytical Lab at the Department of Geology in Washington State University using a New Wave Nd:YAG UV 213-nm laser coupled to a ThermoFinnigan Element 2 single collector, double-focusing, and magnetic sector ICPMS. Operating procedures and parameters are discussed by Mantilla *et al*. [33].

4. Field relationships

White greyish, medium- to coarse-grained marbles of variable morphology (with sharp contacts) and thickness (from centimeter to meter scale) show a transition into carbonate-silicate rocks, which, in turn, pass into calc-silicate and carbonate-bearing silicate rocks. Finally, when carbonate tends to disappear, they are cut by porphyritic granodiorites (Fig. 3). They show a weak to strong banding (alternation of carbonate-rich and calc-silicate layers). Fig. 3a shows an excellent overview of the Bucaramanga - Santa Marta Fault. Fig. 3b shows a view of the El Futuro quarry; the actinolitic schist is at the top; and the marble is at the bottom. An intrusive contact zone between the actinolitic schist and the granodiorite is shown in Fig. 3c. Note the occurrence of part of the endoskarn (oxidation zones) and exoskarn (marble with reaction bands). Fig. 3d shows the occurrence of granodiorite with faneritic and

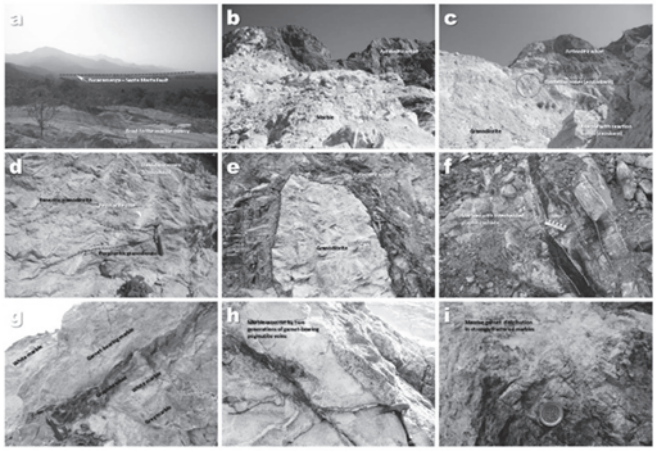

Figure 3. Field photographs of the Ciénaga Marbles and related rocks.
Source: The authors.

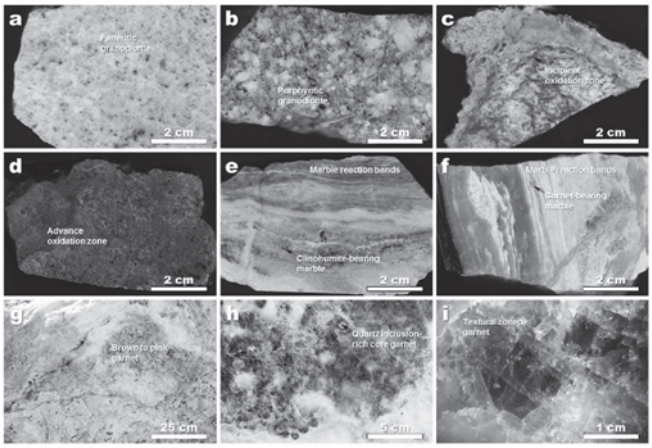

Figure 4. General macroscopic characteristics of the intrusive rocks (a)-(d) and Ciénaga Marbles (e)-(f). Photographs on several scales of the occurrence of brown to pink garnet aggregates in marble (g)-(i).
Source: The authors.

porphyritic textures, cross cut by a pegmatite, which have been affected by dextro-lateral faults; the oxidation zones (endoskarn) can be seen in the upper right part. Fig. 3e shows a well-defined intrusive contact between the granodiorite and the actinolitic schist. Note the characteristic tabular geometry of marbles interbedded with graphite schists in Fig. 3f. In Fig. 3g several marble types and interbedded graphite schists can be observed. Marble is commonly cross cut by two generations of garnet-bearing pegmatites (Fig. 3h). Fig. 3i shows the occurrence of massive brown to pink garnet in strongly fractured marbles.

General macroscopic characteristics of the Ciénaga Marbles and associated rocks are shown in Fig. 4. A granodiorite body cutting metamorphic rocks (actinolitic schists and marbles) shows a phaneritic and porphyritic texture (Figs. 4a-4b). In the endoskarn zone, incipient (Fig. 4c) to advanced (Fig. 4d) oxidation zones are developed. Figs. 4e-4f illustrates marble reaction bands. Massive brown to pink garnet aggregates commonly occur in marbles (Figs. 4g-4i).

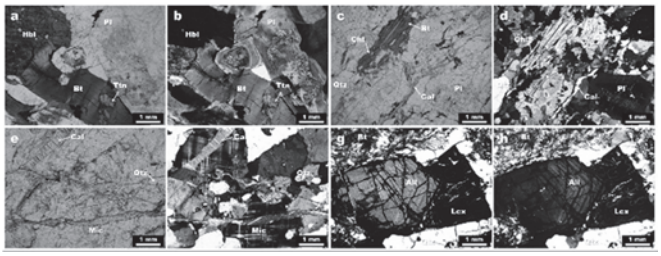

Figure 5. Endoskarn minerals in the intrusive rocks under the petrographic microscope.
Source: The authors.

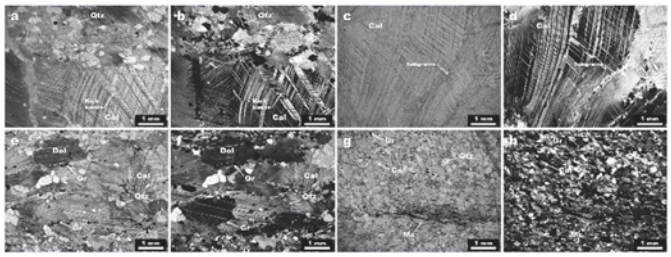

Figure 6. Petrographic features of the pure marble-forming minerals under the petrographic microscope.
Source: The authors.

5. Mineralogy and petrography

5.1. Causative rock

The emplacement of intrusive rocks belonging to the SMB (Fig. 5) affected marbles developed a skarn-type mineralogy. The main petrographic facies corresponds to a granodioritic intrusive (Figs 5a-5d), exhibits holocrystalline equigranular texture; and is mostly composed of plagioclase (well-developed albite twinning, characteristic sieve texture and alteration to sericite), quartz, biotite and hornblende, with minor zircon, titanite and apatite and chlorite as a retrograde phase. Locally, small garnet-bearing pegmatites cross cut the granodiorite (Fig. 5e-5f) and are mainly composed of quartz, plagioclase and microcline (tartan twinning), with minor epidote and muscovite, magnetite and zircon as accessory minerals, and chlorite and sericite as secondary minerals. Biotite represents a supergene mineral phase cross cut by calcite veinlets. The endoskarn zone presents a sulphide (pyrite) and oxidation (magnetite) zones, the latter with large crystals of allanite (typical textural oscillatory zoning and reaction rims of leucoxene, monacite and barite). Leucoxene can be cross cut by barite veinlets (Fig. 5g-5h). The original crystalline marbles were locally affected by a causative body (granodiorite), which gives rise to thin calc-silicate reaction bands with spotty garnet and diopside crystals near the boundary with the exoskarn zone.

5.2. Host rocks

5.2.1. Regional metamorphism (pre-skarn stage)

The regional metamorphic stage is represented by white, medium-grained, pure marbles that display a granoblastic fabric (Fig. 6). They are mostly composed of medium-grained recrystallized calcite and dolomite, and show characteristic rhombohedral cleavage and polysynthetic twinning. The associated minor minerals are quartz, muscovite and graphite. Very fine-grained zircon of high relief and extreme birrefringence occurs as inclusions in carbonates. The mineralogy of the pre-skarn stage is associated to regional metamorphism involving the recrystallization of calcite and dolomite to marbles.

5.2.2. Skarn stages

Impure marbles of the skarn stages are represented by carbonate rocks with a foliated structure and granoblastic texture. They are mainly composed by recrystallized magnesian calcite and dolomite as the dominant minerals, as well as a variety of minerals in the following petrographic classes: wollastonite-, forsterite-, diopside-, garnet-, clinohumite- and vesubianite-bearing marbles. Common minerals are graphite, quartz, diopside, garnet, wollastonite, clinohumite and forsterite. Minor minerals are tremolite, epidote-group minerals, clinochlore and muscovite. Accessory minerals are rutile, titanite, fluorapatite and pyrite. Secondary minerals are calcite and sepiolite.

Isochemical metamorphism involves recrystallization of sedimentary calcite and dolomite to coarse-grained impure marbles and changes in mineral stability without significant mass transfer. There is, thus, no injection or leaching out of new elements by magma or volatile fluids [3,37-38] involved. Previous studies of metamorphic phenomena emphasized the isochemical mineralogical changes due to metamorphic re-equilibration under differing PT regimes, although the metasomatic mass-transfer of chemical components is also recognized as an important process accompanying regional metamorphism [39-42]. Metamorphic recrystallization of carbonate and quartz and mineralogical changes affect the carbonate-bearing protolith, and circulating of high-T fluids promotes the formation of anhydrous calc-silicate minerals such as diopside, garnet (at ~400-700 °C), and probably titanite. Metasomatic metamorphism is a metamorphic process by which the chemical composition of a rock is altered in a pervasive manner and involves the introduction and/or removal of chemical components as a result of the interaction of the rock with aqueous fluids [43]. This is essentially a multistage metasomatism process, in which magma crystallizes and releases a fluid phase, producing a metasomatic skarn.

Prograde anhydrous stage. Garnet in the marble and barren skarn zones appear to show the anomalous anisotropy (which can be attributed to the presence of H_2O molecules in its chemical structure) more frequently than those in the mineralized skarn zone [44]. Fig. 7 shows the different textural morphologies of garnet under the petrographic microscope: garnet developing embayment (Figs. 7a-7b), disseminated aggregates of garnet (Figs. 7c-7d), highly tectonized garnet (Figs. 7e-7f), textural zoned garnet (Figs. 7g-7h), skeletal and idioblastic garnet (Figs. 7i-7j), garnet displaying a quartz rich inclusion-core and a poor-inclusion rim (Figs. 7k-7l).

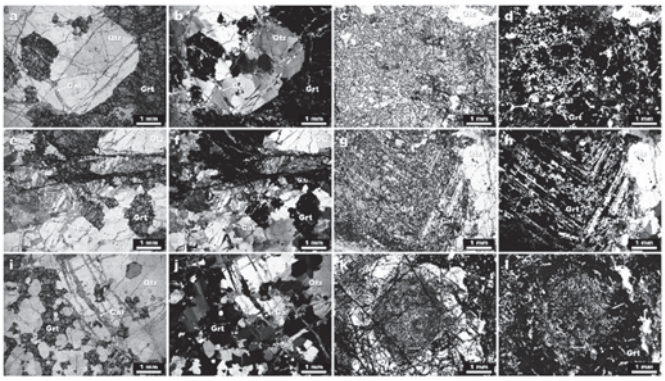

Figure 7. Skarn-type garnet of the prograde anhydrous stage displaying several textural morphologies.
Source: The authors.

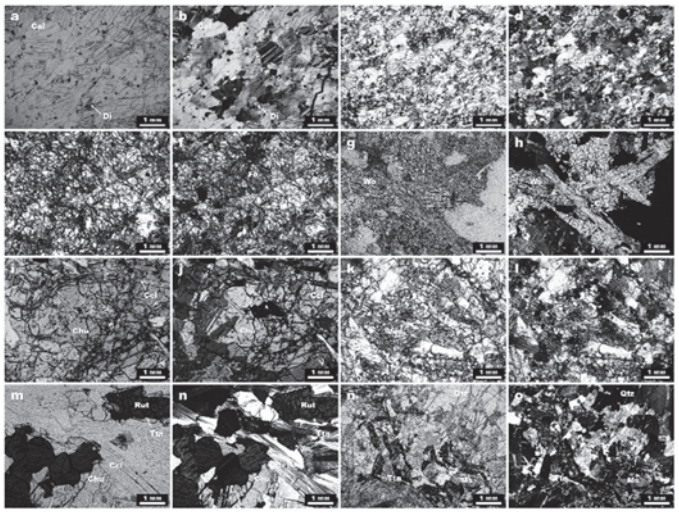

Figure 8. Skarn-type minerals of the prograde anhydrous stage.
Source: The authors.

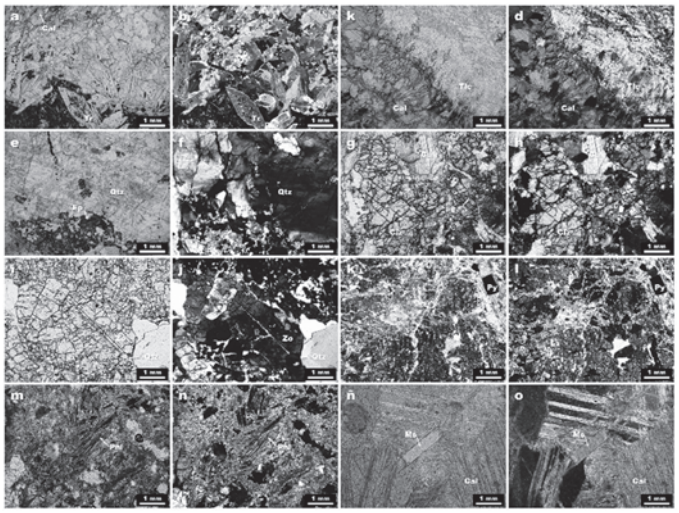

Figure 9. Skarn-type minerals from the prograde metasomatic stage.
Source: The authors.

The main petrographic aspects of the skarn-type minerals of this stage are shown in Fig. 8. Magnesian calcite occurs as very fine- to medium-grained recrystallized crystals of characteristic rhombohedral cleavage and polysynthetic twinning and is locally accompanied by dolomite. Diopside is the most abundant mineral occurring as a fine-grained granoblastic intergrowth with calcite. It has a typical short prismatic crystal or well-formed equant cross-sections, is clear to light green in color, has a high relief, near 90º cleavage angle, and interference colors that range (from blue to violet) up to mid second order (views that show two cleavages tend to be lower), and a large extinction angle. At the granodiorite-marble contact, a zone of diopside was observed. It could have been formed due to the diffusion of Ca, Mg and Si as suggested by Kenneth [45]. Occurrences of forsterite could represent the main mineral phase along with calcite and dolomite and minor phlogopite. Forsterite is largely replaced by serpentine (typical mesh texture) and comprises rounded crystals of up to 4.5 mm in size that are cut by serpentine veins. Alternating poor-wollastonite and rich-wollastonite zones can be recognized. Wollastonite is formed by the infiltration of H_2O-rich fluids close to the peak of regional metamorphism, although it can also be formed by the calcite + quartz = wollastonite + CO_2 [46] reaction. Clinohumite shows typical pleochroism from pale yellow to red-yellow and is locally intergrown with forsterite. Vesubianite occurs as scarce pleochroic (yellow to orange) crystals dispersed in the matrix. Rutile is spatially associated with dolomite marble and occurs as large grains or aggregates mimicking the occurrence of Fe-Ti oxides in the protolith. Titanite occurs in the matrix as very fine-grained aggregates with the characteristic brown color and high relief. It is in contact with calcite and diopside. Fluorapatite occurs as scattered small grains.

Prograde metasomatic stage. Fig. 9 shows the main minerals in this stage. Tremolite occurs as colorless crystals of high relief and third order interference colors, which are in contact with calcite. Very fine-grained epidote shows the typical slight pleochroism. It occurs as inclusions in calcite. Clinozoisite is colorless and shows high relief and fractures filled by quartz and calcite. Zoisite occurs as fine-grained, colorless and very high relief crystals that shows anomalous interference colors. Platy bronze brown to pale orange phlogopite shows weak pleochroism, perfect cleavage on (001) and straight extinction. Muscovite occurs as individuals of straight and serrated boundaries.

Retrograde meteoric stage. It is structurally controlled and overprints the prograde zonation sequence such as garnet and diopside. The retrograde skarn-type minerals can show vein structure. Fig. 10 shows the main minerals of the retrograde meteoric stage, which is represented by the occurrence of calcite, quartz, chlorite, serpentine, sepiolite and pyrite. Veins of quartz-calcite, which are cutting massive garnet, can be related to retrograde skarnization. In the later stage of alteration, chlorite occurs as fibrous aggregates locally replacing phlogopite. Abundant quartz occurs as fine-grained inclusions in garnet or as a matrix constituent. Coarse-grained quartz associated to skeletal garnet is cut by calcite veinlets. It sometimes occurs in complex veins, showing elongated aggregates growing over a carbonate matrix with bubbles extensions that penetrate veinlets of fibrous sepiolite aggregates. Serpentine occurs after forsterite, which implies that H_2O must have remained the dominant fluid during retrograde calc-silicate formation [47],

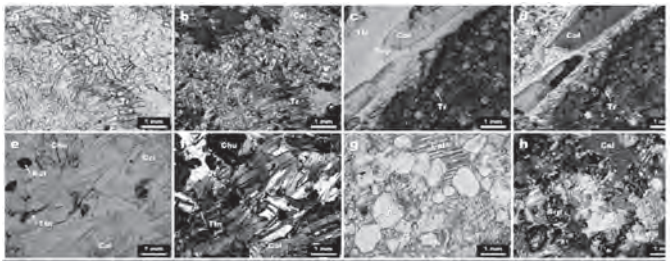

Figure 10.Retrograde minerals under the petrographic microscope.
Source: The authors.

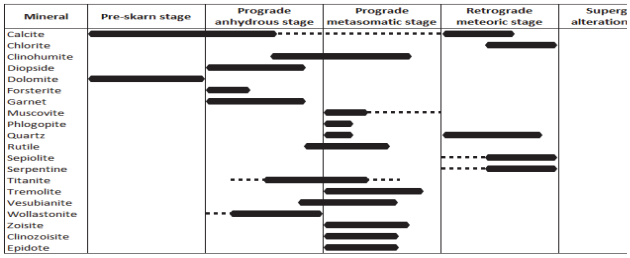

Figure 11. Paragenetic sequence of exoskarn and ore minerals from the Ciénaga Marbles.
Source: The authors.

and must be related to a low-T hydrothermal/metasomatic process [48]. It also can be formed after replacement of clinohumite and diopside. Pyrite occurs as small crystals with edges showing a bronze color and is related to calcite veinlets.

5.2.3. Supergene alteration stage

This stage is represented in the endoskarn zone and is characterized by the local occurrence of pyrite and magnetite. Moreover, in the oxidation zone, large crystals of textural zoned allanite display a strong replacement by leucoxene, although, they is also rimmed by monacite and leucoxene. Barite, occurring as a precipitated phase, rims allanite or develops veinlets cross cutting leucoxene.

Petrographic analysis of the Ciénaga Marbles, located in proximity to granitic dikes and stocks of the SMB, reveals the paragenetic sequence described above, which is shown in Fig. 11. The inexistence of ore skarn can be associated to erosion.

6. Mineral chemistry

Fig.12 shows the textural relationships observed in the skarn minerals. Figs. 12a-12c illustrate mineral relationships in the endoskarn zone. Fig. 12a shows a large garnet cross cut by quartz microveins. Fig. 12b shows a subhedral magnetite in a matrix mainly composed of quartz and chlorite with minor calcite and titanite and fluorapatite as the main accessory minerals. A large subhedral magnetite rimmed and cross cut by barite microveins can be observed in Fig. 12c. The association magnesian calcite + dolomite + clinohumite + forsterite (replaced by serpentine) is shown in Fig. 12d. Fig. 12e shows the occurrence of clinohumite along with dolomite + magnesian calcite. A replacement of forsterite by serpentine is observed in Fig. 12f; the presence of clinohumite, dolomite, magnesian calcite and clinochlore can also be noted. Fig. 12g shows fluorapatite along with magnesian calcite and clinochlore; numerous veins of magnesian calcite cross cut fluorapatite. The wollastonite + diopside + calcite association is shown in Fig. 12h. Fig. 12i shows abundant dolomite and scarce magnesian calcite that occur as matrix phases or as secondary veins cross cutting dolomite.

The retrograde stage can be documented by the occurrence of fibrous sepiolite and veinlets of barite. Similar fibrous clays have been reported by Zaaboub *et al*. [49]. According to the previous sepiolite would have precipitated directly in hydrothermal environments under alkaline conditions, high Si and Mg and low Al activity. Veinlets of barite (barium sulfate) reveals that the presence of other minerals in the precursor hydrothermal solution affected the kinetics of crystal growth of barium sulphate as has beeb reported in several studies [50-51]. In general, magnesian skarns form at temperatures 450-750 ºC and pressures of 0.5-10 kbar, they contain forsterite, diopside, clinohumite and phlogopite at the contacts between magmatic and calc-magnesian or magnesian carbonate rocks, typically host ores, and may develop in both the magmatic (prograde, in contact with magmatic fluids) and postmagmatic (retrograde) stages [42]. We suggest that the magnesian skarn-type mineralogy hosted in the Ciénaga Marbles is related to the magmatic stage of the SMB and is characterized by the occurrence of magnesian calcite and/or dolomite, forsterite and pyroxene, with the last of these occurring only due to low chemical activity of CaO. However, it can be also related to the postmagmatic stage of the SMB. A very complex skarn-type mineralogy zonation can be observed. According to Pertsev [52], magnesian skarns of both stages are commonly replaced in varying degrees by postmagmatic calc-skarns under moderate P-T conditions due to increasing CaO chemical

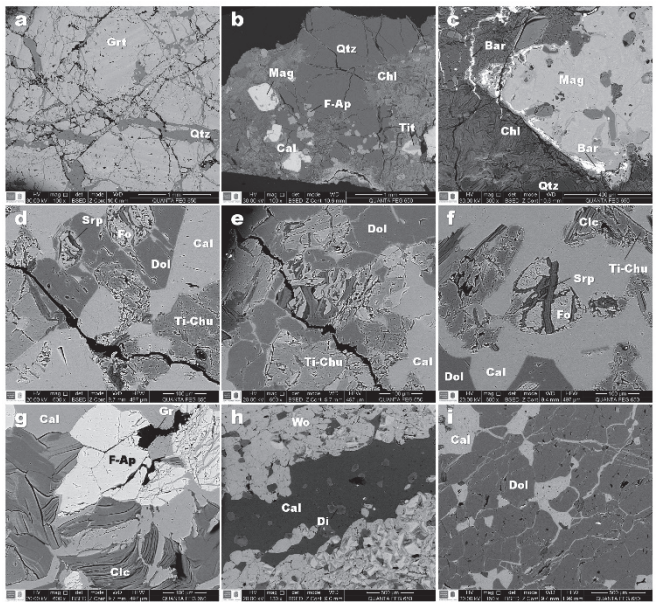

Figure 12. SEM photomicrographs of the textural relationships between skarn-type minerals.
Source: The authors.

activity with decreasing temperature and a corresponding decrease of CO_2 concentration in fluids. Therefore, low-T post-skarn alteration leads to the replacement of skarn minerals by serpentine and carbonates. Ore mineralisations accompanying the formation of magnesian skarns are magnetite and borates (ludwigite, suanite and kotoite), with a wide variety of ore mineralizations (e.g., Cu, Mo, W, Be, Sn, Pb, Zn, Au, B) that can be overprinted by low-T hydrothermal processes [42]. This the case reported in this study.

7. Skarn and ore minerals

Skarns are defined by their mineralogy, which includes a wide variety of calcium-bearing silicates and associated minerals, but is usually dominated by garnet and pyroxene [3]. Skarns can be subdivided according to several criteria. However, skarns are broken down into two broad subcategories [3,53]: exoskarns and endoskarns. In the study area, the skarn is divided into exoskarn, with subordinate endoskarn (centimeter-wide altered plutonic rocks in contact with the skarn) and skarn veins. An exoskarn can be recognized in the marbles close to the thermal source (magma or hydrothermal fluids). An endoskarn developed within the granodiorite intrusion is represented by highly sulphidation (pyrite) and oxidation (magnetite) zones, the last of these has the appearance of zoned allanite, which is rimed by monacite and cross cut by barite. Skarns may or may not host economic reserves of metals. If they do they are called skarn deposits, which are often described according to the dominant economic metal or mineral present, whether it is Cu, Fe, W, Zn-Pb, Mo, Au, etc. However, the majority of the world's economic skarn deposits occur in calcic exoskarns. The Ciénaga skarn is a magnesian type, which can explain why there is no ore zone. It can be considered as a reaction of magnesian skarn that is formed by isochemical metamorphism of thinly interlayered shales and limestones where the metasomatic transfer of components between adjacent lithologies may occur on a small scale, as suggested by some authors [2]. The previously mentioned lithological and mineralogical features (magnesian skarn-type mineralogy) may suggest a potential environment for the formation for Fe, Sn (W), Be, B, and REE deposits.

8. Skarn-type mineralogy zonation in the Ciénaga Marbles

Most skarns show a general zonation pattern of proximal garnet, distal pyroxene and vesubianite at the contact between skarn and marble. Skarn minerals may display systematic color or compositional variations within the larger zonation pattern [42]. Atkinson and Einaudi [4] describe it, with proximal garnet being commonly dark red-brown, becoming lighter brown and finally pale yellow-green near the marble front. A granodiorite of the SMB intruded into the Ciénaga Marbles. Metamorphism and metasomatism produced millimeter to centimeter scale reaction zones near the contact. The contact zone shows evidence of assimilation of the marbles by granodioritic magma. Most major skarn deposits are directly related to igneous activity and broad

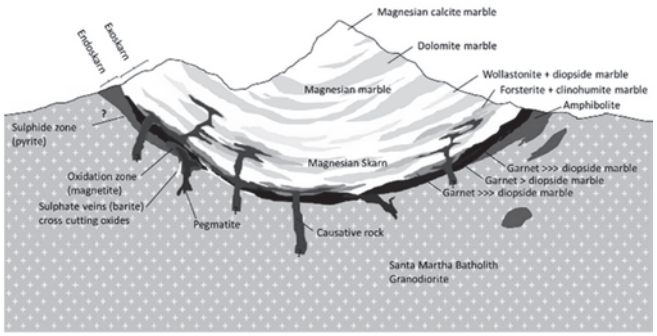

Figure 13. Idealized cross section (not to scale) through the skarn-type mineral distribution in the Ciénaga Marbles.
Source: The authors.

correlations between igneous composition and skarn type have been previously described [1,5]. We suggest a zonation pattern for the skarn-type mineralogy, which does not extend on a large area, although it can provide important evidence as exploration guides. We suggest that skarn-type minerals were formed at different stages and P-T conditions, not coexisting each other based on the general idea of chemical equilibrium. Fig. 13 shows an idealized cross section through the skarn-type mineral distribution in the Ciénaga Marbles. The following zones and mineral assemblages were identified (in order of decreasing grade): The endoskarn is developed within the granodiorite intrusion and is represented by very small sulphidation (pyrite) and oxidation (magnetite) zones; the last of them with the occurrence of zoned allanite, rimed by monacite and leucoxene and cross cutting by barite veinlets. The exoskarn is represented by the following zones: Garnet zone (next to the contact) consists of grossularite garnet, diopside, and minor calcite and quartz. We have no evidence on the occurrence of pale green garnet, then, we suggest that a proximal red-brown to brown garnet can be close to the marble. The change in pyroxene color is less pronounced but typically reflects a progressive increase in Fe and/or Mn towards the marble front [54], which has not been confirmed yet in the study area. Diopside zone mainly composed of diopside and calcite, and minor garnet. Monticellite zone contains magnesian calcite, dolomite, clinohumite, forsterite, phlogopite, with serpentine as the main retrograde mineral phase. Taking into account that these minerals are absent in most other types of skarn [42], this reveals a magnesian skarn-type mineralogy. Idocrase (vesubianite) zone consists of vesubianite in association with calcite, diopside, wollastonite and phlogopite. Inner zone consists of magnesian calcite and dolomite marble, showing little metasomatism.

9. U-Pb Geochronology

Sample SMS-2-3 (granodiorite cutting the Cienaga Marbles) was dated by U/Pb (Table 1). It was collected and dated due to its close relationship to the skarn-type mineralogy developed around its borders. Analytical data and U-Pb isotope ratios indicate the presence of at least two ages: the first one is made up of 27 of the 42 performed analysis

(~64% of all analyzes, with ages ranging from 60.7 to 54.3±0.7 Ma; and the second one is made up of 15 of the 42 performed analysis (~ 36% of all analyzes), with ages ranging from 1065.3±15 to 62.8±0.8 Ma. After considering the analytical and systematic error (Fig. 14), the first group of ages can be clearly related to the crystallization of a granitoid at 55.5±0.7 Ma. Taking into account that the skarn-type mineralogy is the result of magmatic-hydrothermal processes and is developed around granitic rocks, we suggest that the formation of the skarn-type mineralogy occurred at the same time as the granitoid crystallized. This absolute age coincides with when the onset of magmatism developed: the start of the change in polarity of the subduction of the Caribbean plate beneath of the South American plate. This is in accordance with the model proposed by Cardona *et al*. [27], and is part of a more regional scale model proposed by others [55-56]. Similar ages for this magmatism were reported by Mejía *et al*. [28]. We assume these magmas correspond to molten silicate enriched in hydrothermal fluids and, therefore, they should be considered to be of high interest for mineral exploration due to their ability to form magmatic-hydrothermal systems. The second group of ages led to the following subgroups being differentiated: (1) with 3 ages ranging from 62.8±0.8 to 79.9±1.3 Ma, (2) with 6 ages ranging from 98.6±1.4 to 143.4±1.7 Ma, (3) with 2 ages ranging from 230.3±3.3 to 235.1±3.1 Ma, (4) with 1 age of 444.8±5.0 Ma, and (5) with 2 ages ranging from 1057.8±15.3 to 1065.3±15 Ma. The SMS-2-3-14 analysis (244.9±3.2 Ma) is excluded from the above groups because it is projected to some distance from the concordia curve (Fig. 14a). It is possible to suggest that the ages ranging from 62.8±0.8 to 79.9±1.3 Ma (Late Cretaceous - Early Paleocene) may be legacies that represent mainly derived zircons of oldest igneous rocks, such as those reported by Cardona *et al*. [27]. They can also be been formed in tectonic environments of intra-oceanic magmatic arcs and in environments own of a late collisional stage.

Table 1.
U–Pb analytical results in different zones within the zircons studied in SMS-2-3 sample that correspond to ages measured by LA-ICPMS.

Points of analysis	U ppm	Th U	$^{238}U/^{206}Pb$	1 σ (%-e)	$^{207}Pb/^{206}Pb$	1 σ (%-e)	$^{206}Pb/^{238}U$ age (Ma)	1 σ (abs-e)	$^{207}Pb/^{206}Pb$ age (Ma)	1 σ (abs-e)	Best age (Ma)	1 σ (abs-e) (Ma)
SMS-2-3_42	2.188	0.27	1.144.541	1.39	0.0469	1.17	56.1	0.8	43.0	27.9	**56.1**	**0.8**
SMS-2-3_41	825	0.35	1.156.547	1.44	0.0473	1.54	55.5	0.8	65.2	36.2	**55.5**	**0.8**
SMS-2-3_40	1.060	0.41	1.080.091	1.46	0.0475	1.58	59.4	0.9	74.4	37.1	**59.4**	**0.9**
SMS-2-3_39	845	0.31	1.173.206	1.45	0.0528	1.60	54.7	0.8	321.5	36.0	**54.7**	**0.8**
SMS-2-3_38	2.666	0.11	562.595	1.39	0.0490	0.78	113.6	1.6	147.2	18.1	**113.6**	**1.6**
SMS-2-3_37	1.080	0.31	1.153.490	1.78	0.0484	2.53	55.6	1.0	119.0	58.6	**55.6**	**1.0**
SMS-2-3_36	1.554	0.26	1.174.055	1.47	0.0487	1.29	54.7	0.8	135.0	29.9	**54.7**	**0.8**
SMS-2-3_35	645	0.31	1.162.160	1.56	0.0482	2.01	55.2	0.9	108.3	46.8	**55.2**	**0.9**
SMS-2-3_34	309	0.31	445.445	1.60	0.0518	1.92	143.1	2.3	277.8	43.3	**143.1**	**2.3**
SMS-2-3_33	1.163	0.38	1.130.086	1.45	0.0480	1.53	56.8	0.8	99.1	35.8	**56.8**	**0.8**
SMS-2-3_32	1.026	0.24	1.113.687	1.42	0.0464	1.62	57.6	0.8	17.9	38.4	**57.6**	**0.8**
SMS-2-3_31	506	0.24	1.151.824	1.66	0.0473	2.74	55.7	0.9	65.7	64.0	**55.7**	**0.9**
SMS-2-3_30	1.133	0.22	1.163.056	2.26	0.0478	2.47	55.2	1.2	90.2	57.4	**55.2**	**1.2**
SMS-2-3_29	949	0.33	1.183.233	1.31	0.0475	1.63	54.3	0.7	75.4	38.3	**54.3**	**0.7**
SMS-2-3_28	932	0.40	833.424	1.76	0.0494	1.47	76.9	1.3	164.8	34.1	**76.9**	**1.3**
SMS-2-3_27	1.157	0.48	1.181.463	1.29	0.0471	1.57	54.3	0.7	55.5	37.1	**54.3**	**0.7**
SMS-2-3_26	1.759	0.03	1.021.716	1.23	0.0476	1.20	62.8	0.8	81.4	28.3	**62.8**	**0.8**
SMS-2-3_25	2.089	0.58	139.991	1.17	0.0562	0.65	444.8	5.0	461.9	14.4	**444.8**	**5.0**
SMS-2-3_24	1.194	0.34	1.175.772	1.45	0.0464	1.97	54.6	0.8	19.6	46.7	**54.6**	**0.8**
SMS-2-3_23	519	0.31	77.217	1.17	0.0749	0.75	785.0	8.7	1065.3	15.0	**1065.3**	**15.0**
SMS-2-3_22	1.224	0.51	1.163.784	1.31	0.0470	1.43	55.2	0.7	47.0	33.9	**55.2**	**0.7**
SMS-2-3_21	993	0.30	1.153.031	1.25	0.0469	1.73	55.7	0.7	46.6	40.9	**55.7**	**0.7**
SMS-2-3_20	1.652	0.33	444.559	1.19	0.0488	0.95	143.4	1.7	137.8	22.2	**143.4**	**1.7**
SMS-2-3_19	1.015	0.46	1.154.251	1.41	0.0493	1.42	55.6	0.8	160.9	32.8	**55.6**	**0.8**
SMS-2-3_18	704	0.30	1.156.202	1.48	0.0472	1.87	55.5	0.8	59.2	43.9	**55.5**	**0.8**
SMS-2-3_17	837	0.34	1.159.776	1.42	0.0488	1.47	55.3	0.8	138.5	34.1	**55.3**	**0.8**
SMS-2-3_16	760	0.34	1.156.884	1.39	0.0482	1.53	55.5	0.8	109.0	35.7	**55.5**	**0.8**
SMS-2-3_15	881	0.34	1.216.329	1.89	0.0489	2.92	52.8	1.0	144.4	67.1	**52.8**	**1.0**
SMS-2-3_14	629	0.20	258.285	1.32	0.0545	0.76	244.9	3.2	392.8	16.9	**244.9**	**3.2**
SMS-2-3_13	1.134	0.14	552.158	1.49	0.0492	1.00	115.7	1.7	158.6	23.2	**115.7**	**1.7**
SMS-2-3_12	614	0.68	649.008	1.44	0.0481	1.28	98.6	1.4	104.8	30.0	**98.6**	**1.4**
SMS-2-3_11	1.859	0.16	1.127.777	1.39	0.0473	1.36	56.9	0.8	63.1	32.0	**56.9**	**0.8**
SMS-2-3_10	638	0.15	1.152.014	2.75	0.0516	1.76	55.7	1.5	265.6	39.8	**55.7**	**1.5**
SMS-2-3_9	2.168	0.31	500.368	1.62	0.0490	0.63	127.6	2.0	145.9	14.7	**127.6**	**2.0**
SMS-2-3_8	899	0.36	1.163.266	1.43	0.0472	1.33	55.2	0.8	57.7	31.5	**55.2**	**0.8**
SMS-2-3_7	306	0.64	274.890	1.44	0.0529	1.31	230.3	3.3	323.6	29.5	**230.3**	**3.3**
SMS-2-3_6	1.165	0.56	1.057.737	1.63	0.0494	1.35	60.7	1.0	169.0	31.3	**60.7**	**1.0**
SMS-2-3_5	521	0.27	269.250	1.36	0.0509	1.11	235.1	3.1	235.9	25.5	**235.1**	**3.1**
SMS-2-3_4	720	0.34	1.157.765	1.53	0.0478	1.70	55.4	0.8	89.1	39.9	**55.4**	**0.8**
SMS-2-3_3	542	0.14	65.228	1.35	0.0746	0.77	919.5	11.6	1057.8	15.3	**1057.8**	**15.3**
SMS-2-3_2	809	0.57	867.787	1.55	0.0490	1.20	73.9	1.1	148.8	28.0	**73.9**	**1.1**
SMS-2-3_1	971	0.13	1.138.402	1.45	0.0483	1.45	56.4	0.8	112.7	33.8	**56.4**	**0.8**

Source: The authors.

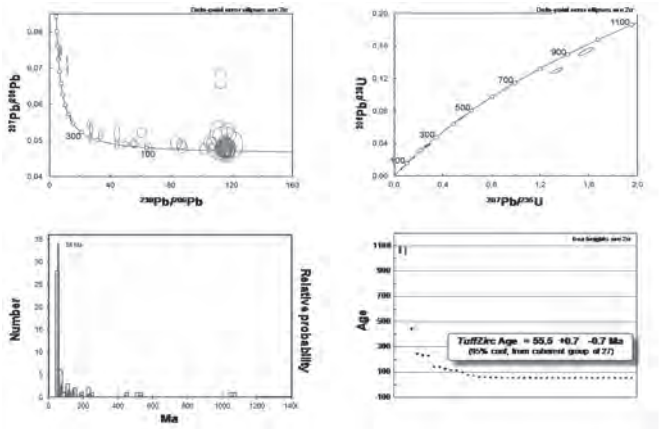

Figure 14. U-Pb ages obtained from zircon analyses in sample SMS-2-3. (a)-(b) U-Pb concordia diagrams, showing inheritance and crystallization ages of the granitic body. (c) Diagram of distribution of age ranges, showing the dominance of ages around 55 Ma. (d) Distribution diagram of all ages (error 2s).
Source: The authors.

The latter is considered to be the cause of the terminal magmatism, developed prior to the change in polarity of subduction. We also consider that some of these values represent mixed ages obtained at intermediate possible areas zoned zircons. Therefore, ages ranging from 98.6±1.4 to 143.4±1.7 Ma should be considered. However, considering that they represent older magmatic events (mainly Early Cretaceous), and not a mix of ages, these data could be very important as they may be indicating older magmatic events probably related to the geological evolution of the Caribbean's earliest stages. Ages between 230.3±3.3 and 235.1±3.1 Ma (Triassic) may be related to inherited zircons from rocks associated to the Triassic-Jurassic magmatic period documented in several studies [22,24-27,30,58]. They may also represent a mix of ages obtained at intermediate areas of zoned zircons. The age of 444.8±5.0 Ma (Ordovician Late) may be related to inherited zircons from rocks associated with the Paleozoic Early magmatic period [58]. Ages from 1057.8±15.3 to 1065.3±15 Ma can be attributed to inherited zircons from Grevillian metamorphic rocks reported in the Northern Andes, particularly in the SMM.

10. Conclusions

The Ciénaga Marbles that formed in a magmatic arc tectonic environment (emplacement of the lower to middle Cenozoic SMB), developed in a continental crust. The skarn-type mineralogy is hosted in lower Cretaceous marbles, and it is related to small granitic dikes and stocks. The Ciénaga skarn-type mineralogy is regarded to have formed by the reactions of the lower Cretaceous carbonate sedimentary sequence with the SMB, although it cannot be considered as a skarn deposit. The main general features of the skarn-type mineralogy are summarized as follows: (1) A typical exoskarn with a magnesian skarn-type mineralogy can be recognized; however, we cannot rule the existence of a calcium skarn-type mineralogy. (2) The exoskarn is composed mainly of garnet and diopside. (3) A late stage is composed of hydrous minerals such as sepiolite, chlorite and serpentine. (4) The occurrence of clinohumite confirms the occurrence of a magnesian skarn-type mineralogy at the Ciénaga Marbles. The presence of clinohumite, serpentine and Mg-chlorite would represent minerals of the retrograde stage. We also consider that the presence of forsterite, pyroxene and garnet belong to the prograde or isochemical metamorphism stage. (5) A skarn-type mineralogy was recognized and its precursor mineralogy is mainly represented by dolomitic marbles to explain the development of a magnesian skarn. (6) Taking into account that this term should be applied to a mixture of calcic and magnesian marbles, we suggest that this is not a calcic-magnesian system. (7) The obtained zircon U-Pb ages (from granodioritic bodies) yielded an age of 55.5±0.7 Ma (Ypresian, Early Eocene), which is also assumed to be the age of the formation of the skarn-type mineralogy in the Ciénaga Marbles and coincides with the beginning of the subduction polarity change (*i.e.* when the Caribbean oceanic plate began to subduct beneath South American continental plate).

Acknowledgments

We are grateful to geologist H. Cotes for the support on our visits to the marble quarry. Thanks to the Universidad Industrial de Santander and Universidad de Pamplona for providing us research facilities. Thanks to the Microscopy Laboratory in the Guatiguará Technological Park and its professional staff for assistance with SEM data acquisition. The manuscript was greatly improved based on the critical and helpful reviews and comments by anonymous reviewers. We are most grateful to the previously mentioned people and institutions for their support.

References

[1] Zharikov, V.A., Skarns. International Geology Review, 12(5-6), pp. 541-559, pp. 619-647, 1970. DOI: 10.1080/00206817009475262.

[2] Zarayskiy, G.P., Zharikov, V.A., Stoyanovskaya, F.M. and Balashov, V.N., The experimental study of bimetasomatic skarn formation. International Geology Review, 29(6), pp. 761-858, 1987. DOI: 10.1080/00206818709466181.

[3] Meinert, L.D., Dipple, G.M. and Nicolescue, S., World skarn deposits. In: Hedenquist. J.W., Thompson. J.F.H., Goldfarb. R.J., Richards. J.P., Editors, Economic Geology 100th Anniversary Volume, Society of Economic Geologists, Inc. Littleton, Colorado pp. 299-336, 2005. DOI: 10.2113/gsecongeo.77.4.745.

[4] Atkinson, W.W.,Jr. and Einaudi, M.T., Skarn formation and mineralization in the Contact Aureole at Carr Fork, Bingham, Utah. Economic Geology, 73(7), pp. 1326-1365, 1978. DOI: 10.2113/gsecongeo.73.7.1326.

[5] Einaudi, M.T., Meinert, L.D. and Newberry, R.J., Skarn deposits. Economic Geology, 75, pp. 317-391, 1981.

[6] Newberry, R.J. and Einaudi, M.T,. Tectonic and geochemical setting of tungsten skarn mineralization in the Cordillera. Arizona Geological Society Digest, 14, pp. 99-112, 1981.

[7] Einaudi, M.T. and Burt, D.M., Introduction - terminology, classification, and composition of skarn deposits. Economic Geology, 77, pp. 745-754, 1982. DOI: 10.2113/gsecongeo.77.4.745

[8] Burt, D.M., Skarn deposits - Historical bibliography through 1970. Economic Geology, 77, pp. 755-763, 1982. DOI: 10.2113/gsecongeo.77.4.745.

[9] Meinert, L.D., Gold skarn deposits - Geology and exploration criteria. Economic Geology, 6, pp. 537-552, 1989. DOI: 10.2113/gsecongeo.101.1.199.

[10] Meinert, L.D., Skarns and skarn deposits. Geoscience Canada, 19, pp. 145-162, 1992. DOI: 10.2113/gsecongeo.95.6.1183.

[11] Meinert, L.D., Compositional variation of igneous rocks associated with skarn deposits - Chemical evidence for a genetic connection between petrogenesis and mineralization: In Thompson, J.F.H., Eds., Magmas, fluids, and ore deposits, Mineralogical Association of Canada Short Course Series, 23, pp. 401-418, 1995. DOI: 10.1016/j.oregeorev.2015.08.004.

[12] Meinert, L.D., Application of skarn deposit zonation models to mineral exploration. Exploration and Mining Geology, 6, pp. 185-208, 1997.

[13] Meinert, L.D., A review of skarns that contain gold. Mineralized Intrusion - Related Skarn systems: Mineralogical Association of Canada Short Course, 26, pp. 359-414, 1998.

[14] Newberry, R.J., W. and Sn-Skarn deposits: A 1998 Status Report. Mineralized Intrusion - Related Skarn Systems: Mineralogical Association of Canada Short Course, 26, pp. 289-335, 1998.

[15] Meinert, L.D., Lentz, D.R. and Newberry, R.J., Introduction to a Special Issue Devoted to Skarn Deposits. Economic Geology, 95, pp. 1183-1184, 2000. DOI: 10.2113/95.6.1183.

[16] Swanson, S.E., Newberry, R.J., Coulter, G.A. and Dyehouse, T.M., Mineralogical variation as a guide to the petrogenesis of the tin granites and related skarns, Seward Peninsula, Alaska. Geological Society of America Special Paper, 246, pp. 143-160, 1990. DOI: 10.1130/SPE246-p143.

[17] Pindell, J.L., Higgs, R. and Dewey, J.F., Cenozoic palinspastic reconstruction, paleogeographic evolution and hydrocarbon setting of the northern margin of South America. In: Pindell, J.L. and Drake, C.L., Eds., Paleogeographic evolution and non-glacial eustasy, northern South America. Society of Economic and Petroleum Mineralogists Special Publication, 58, pp. 45-85, 1998.

[18] Moreno-Sánchez, M. and Pardo-Trujillo, A., Stratigraphical and sedimentological constraints on western Colombia: Implications on the evolution of the Caribbean plate. In: Bartolini, C., Buffler, R.T., Blickwede, J., Eds., The Circum-Gulf of Mexico and the Caribbean: Hydro-carbon habitats, basin formation and plate tectonics. AAPG Memoir, 79, pp. 891-892, 2003.

[19] Irving, E.M., Structural evolution of the northernmost Andes, Colombia. USGS Professional Paper 846, Washington DC, 27 P., 1971. DOI: 10.1017/S0016756800050780.

[20] Campbell, C.J., The Santa Marta wrench fault of Colombia and its regional setting. In: Saunders, J.B., Ed., Transactions of the Fourth Caribbean Geological Conference. Port-of-Spain, pp. 247-262, 1965.

[21] Kellogg, J., Cenozoic and tectonic history of the Sierra de Perijá, Venezuela-Colombia, and adjacent basins. GSA Memoir, 162, pp. 239-261, 1984. DOI: 10.1130/MEM162-p239.

[22] Restrepo-Pace, P.A., Ruiz, J., Gehrels, G. and Cosca, M., Geochronology and Nd isotopic data of Grenville-age rocks in the Colombian Andes: New constraints for late Proterozoic – early Paleozoic paleocontinental reconstructions of the Americas. Earth and Planetary Science Letters, 150, pp. 427-441, 1997. DOI: 10.1016/S0012-821X(97)00091-5.

[23] Ordóñez-Cardona, O., Pimentel, M.M. y De Moraes, R., Granulitas de Los Mangos: Un fragmento grenviliano en la parte SE de la Sierra Nevada de Santa Marta. Revista Academia Colombina de Ciencias, 26, pp. 169-179, 2002.

[24] Cordani, U., Cardona, A., Jiménez, D., Liu, D. and Nutman, A., Geochronology of Proterozoic basement inliers in Colombian Andes: Tectonic history of remnants of a fragmented Greenville belt. In: Vaughan, A., Leat, P., Pankhurst, R., Eds., Terrane processes at margins of Gondwana. Geological Society, London, Special Publications, 246, pp. 329-346, 2005.

[25] Tschanz, C.M., Marvin, R.F. and Cruz, B., Geology of the Sierra Nevada de Santa Marta (Colombia) - Informe 1829. INGEOMINAS, Bogotá, 1969.

[26] Tschanz, C., Marvin, R., Cruz, J., Mehnert, H. and Cebula, E., Geologic evolution of the Sierra Nevada de Santa Marta. Geological Society of America Bulletin, 85, pp. 269-276, 1974. DOI: 10.1130/0016-7606(1974)85<273:GEOTSN>2.0.CO;2.

[27] Cardona, A., Valencia, V., Bustamante, C., García-Casco, A., Ojeda, G., Ruiz, J., Saldarriaga, M. and Weber, M., Tectono-magmatic setting and provenance of the Santa Marta Schists, northern Colombia: Insights on the growth and approach of Cretaceous Caribbean oceanic terranes to the South American continent. Journal of South American Earth Sciences, 29, pp. 784-804, 2010. DOI: 10.1016/j.jsames.2009.08.012.

[28] Mejía, H.P., Santa, E.M., Ordóñez-Cardona, O. y Pimentel, M., Consideraciones petrográficas, geoquímicas y geocronológícas de la parte occidental del batolito de Santa Marta. DYNA, 75(155), pp. 223-236, 2008.

[29] Doolan, B.L., The structure and metamorphism of the Santa Marta area Colombia, South America. PhD Thesis, New York State University, New York, USA 1970, 200 P.

[30] MacDonald, W.D., Doolan, B.L. and Cordani, U.G. Cretaceous – Early Tertiary metamorphic K–Ar age values from the South Caribbean. Geological Society of America Bulletin, 82, pp. 1381-1388, 1971. DOI: 10.1130/0016-7606(1971)82[1381:CTMKAV]2.0.CO;2.

[31] Bayona, G., Lamus-Ochoa, F., Cardona, A., Jaramillo, C., Montes, C. y Tchegliakova, N., Procesos orogénicos del Paleoceno para la Cuenca Ranchería (Guajira, Colombia) y áreas adyacentes definidos por análisis de procedencia. Geología Colombiana, 32, pp. 21-46, 2007.

[32] Kretz, R., Symbols for rock-forming minerals. American Mineralogist, 68, pp. 277-279, 1983. DOI: 10.2138/am.2010.3371.

[33] Mantilla-Figueroa, L.C., Bissig, T., Valencia, V. and Craig, H., The magmatic history of the Vetas-California mining district, Santander Massif, Eastern Cordillera, Colombia. Journal of South American Earth Sciences, 45, pp. 235-249, 2013. DOI: 10.1016/j.jsames.2013.03.006.

[34] INGEOMINAS. Geología de la Plancha 18. Escala 1:100000, 2007.

[35] González, G., Mecanismo y profundidad de emplazamiento del Plutón de Cerro Cristales, Cordillera de la Costa, Antofagasta, Chile. Revista Geológica de Chile, 26, pp. 43-66, 1999. DOI: 0.4067/S0716-02081999000100003.

[36] Duque, J.F., Orozco, T., Cardona, A., Ferrari, L., Ruiz, J. y Valencia, V., El Batolito de Santa Marta, Colombia. Registro de la instalacion de una zona de subduccion Paleogena de la Placa Caribe bajo la Placa Samericana. Geos., 28(2). Sesión Regular: Geoquímica y Petrología. GEOQP-15 CARTEL, 2008.

[37] Bucher, K. and Frey, M., Petrogenesis of metamorphic rocks. 6ª ed., Complete revision of Winkler's textbook, Berlin Heidelberg, Springer-Verlag, 1994, 318 P.

[38] Bucher, K. and Grapes, R., Petrogenesis of Metamorphic Rocks. 8ª ed., Berlin Heidelberg, Springer-Verlag, 2002, 341P.

[39] Yardley, B.W.D. and Baltatzis, E., Retrogression of staurolite schists and the sources of infiltrating fluids during metamorphism. Contributions to Mineralogy and Petrology, 89, pp. 59-68, 1985. DOI: 10.1007/BF01177591.

[40] Ferry, J.M., Regional metamorphism of the Waits River formation, eastern Vermont: Delineation of a new type of giant hydrothermal system. Journal of Petrology, 33, pp. 45-94, 1992. DOI: 10.1093/petrology/33.1.45.

[41] Ague, J.J., Crustal mass transfer and index mineral growth in Barrow's garnet zone, northeast Scotland. Geology 25, pp. 73-76, 1997. DOI: 10.1130/0091-7613(1997)025<0073:CMTAIM>2.3.

[42] Oliver, N.H.S., Rubenach, M.J. and Valenta, R.K., Precambrian metamorphism, fluid flow, and metallogeny of Australia AGSO. Journal of Australian Geology & Geophysics, 17(4), pp. 31-53, 1998. DOI: 10.1016/S0024-4937(00)00021-9.

[43] Zharikov, V.A., Pertsev, N.N., Rusinov, V.L., Callegari, E. and Fettes, D.J., A systematic nomenclature for metamorphic rocks: 9. Metasomatic rocks. Recommendations by the IUGS Subcommission on the Systematics of Metamorphic Rocks. Recommendations, web version of 01.02.2007, 2007.

[44] Ardila, R., Carrascal, E.R. y Oyarzún, J., Proposición de un modelo genético para los yacimientos cupríferos tipo skarn de San Antonio y Panulcillo, Región de Coquimbo, Chile. En: VI Congreso Geológico Chileno, 1, pp. 256-260, 1991.

[45] Kenneth, Sh,. Mineralogical zoning in a Scapolite-Bearing Skarn body on San Gorgonio Mountain, California. American Mineralogist, 60, pp. 785-797, 1975.
[46] Cartwright, I. and Buick, I.S., Formation of wollastonite-bearing marbles during late regional metamorphic channelled fluid flow in the upper calcsilicate unit of the Reynolds Range group, central Australia. Journal of Metamorphic Geology, 13(3), pp. 397-417, 1995. DOI: 10.1111/j.1525-1314.1995.tb00228.x.
[47] Damman, A.H. and Kieft, C., W-Mo polymetallic mineralization and associated calcsilicate assemblages in the Gasborn area, West Bergslagen, Central Sweden. Canadian Mineralogist, 28, pp. 17-36, 1990.
[48] Del Lama, E.A., Candia, M.A.F. and Szabó, G.A.J., Petrography and metamorphism of the metasedimentary country-rocks of the Jacurici Valley Chromitite-Hosting mafic-ultramafic complexes, Bahia, Northeastern Brazil. Geologia USP. Série Científica, 1(1), pp. 1-15, 2001.
[49] Zaaboub, N., Abdeljaouad, S. and López-Galindo, A., Origin of fibrous clays in Tunisian Paleogene continental deposits. Journal of African Earth Sciences, 43(5), pp. 491-504, 2005. DOI: 10.1016/j.jafrearsci.2005.08.013.
[50] Merdhah, A.B.B. and Yassin, A.A.M., Laboratory Study on precipitation of Barium Sulphate in Malaysia sandstone cores. The Open Petroleum Engineering Journal, 2, pp. 1-11, 2009. DOI: 10.2174/1874834101002010001.
[51] Merdhah, A.B.B., Yassin, A.A.M. and Muherei, M.A., Laboratory and prediction of barium sulfate scaling at high-barium formation water. Journal of Petroleum Science and Engineering, 70, pp. 79-88, 2010. DOI: 10.1016/j.petrol.2009.10.001.
[52] Pertsev N.N., High temperature metamorphism and metasomatism of carbonate rocks. Nauka Publishing, Moscow, 1977.
[53] Grammatikopoulos, T.A. and Clarkb, A.H., A comparative study of wollastonite skarn genesis in the Central Metasedimentary Belt, southeastern Ontario, Canada. Ore Geology Reviews, 29(2), pp. 146-161, 2006. DOI: 10.1016/j.oregeorev.2005.11.007.
[54] Harris, N.B. and Einaudi, M.T., Skarn deposits in the Yerington district, Nevada: Metasomatic skarn evolution near Ludwig. Economic Geology, 77, pp. 877-898, 1982. DOI: 10.2113/gsecongeo.77.4.877.
[55] Pindell, J.L. and Barrett, S.F., Geological evolution of the Caribbean region: A plate-tectonic perspective. In: Dengo, G. and Case, J.E., Eds., The Caribbean region, The Geology of North America, H, Geological Society of America, 1990, pp. 405-432.
[56] Pindell, J.L., Regional synopsis of Gulf of Mexico and Caribbean evolution: Gulf coast section, Society for Sedimentary Geology, 13th Annual Research Conference Proceedings, 1993, pp. 251-274.
[57] Vinasco, C., Cordani, U., González, H., Weber, M. and Peláez, C., Geochronological, isotopic and geochemical data from Permo-Triassic granitic gneisses and granitoids of the Colombian Central Andes. Journal of South American Earth Sciences, 21, pp. 355-371, 2006. DOI: 10.1016/j.jsames.2006.07.007.
[58] Ayala, R.C., Bayona, G., Cardona, A., Ojeda, C., Montenegro, O.C., Montes, C., Valencia, V. and Jaramillo, C., The paleogene synorogenic succession in the northwestern Maracaibo block: Tracking intraplate uplifts and changes in sediment delivery systems. Journal of South American Earth Sciences, 39, pp. 93-111, 2012. DOI: 10.1016/j.jsames.2012.04.005.

O.M. Castellanos-Alarcón, received his BSc in Geology in 1999 from the Universidad Industrial de Santander, Colombia. He was awarded an MSc in Geology in 2001 from the Shimane University, Japan. He has been working as a full-time Lecturer on the Geology Program, Universidad de Pamplona, Colombia, since 2003. He is specialist in mineralogy, experimental mineralogy, petrology and geochemistry of metamorphic rocks.
ORCID: 0000-0003-0620-0540.

C.A. Ríos-Reyes, received his BSc in Geology in 1989 and his Post-graduate Diploma in University Teaching in 1995 from the Universidad Industrial de Santander, Colombia. He was awarded an MSc in Geology from the Shimane University, Japan, in 1999. He was awarded a PhD in Applied Sciences from the University of Wolverhampton, England, in 2008. He has been working as a full-time Lecturer of the School of Geology, Universidad Industrial de Santander, Colombia, since 1992, He is a specialist in mineralogy, experimental and environmental mineralogy, petrology and geochemistry of metamorphic rocks.
ORCID: 0000-0002-3508-0771.

L.C. Mantilla-Figueroa, received his BSc in Geology in 1987 and his MSc in Mineralogical Sciences in 1989 from the Moscow Geological Prospecting Sergo Odzhinikidze Institute, Russia. He was awarded his PhD in Petrology and Geochemistry in 1999 from the Universidad Complutense de Madrid, Spain. Recently, he has undertaken a postdoctoral research in Metallogeny at the University of British Columbia, Canada. He has been working as a full-time Lecturer in the School of Geology, Universidad Industrial de Santander, Colombia, since 1993. He is a specialist in the petrology and geochemistry of igneous and metamorphic rocks, regional geology, process fluid-rock interaction, and exploration of mineral deposits.
ORCID: 0000-0002-2112-8041.

UNIVERSIDAD NACIONAL DE COLOMBIA
SEDE MEDELLÍN
FACULTAD DE MINAS

Área Curricular de Ingeniería
Geológica e Ingeniería de Minas y Metalurgia

Oferta de Posgrados

Especialización en Materiales y Procesos
Maestría en Ingeniería - Materiales y Procesos
Maestría en Ingeniería - Recursos Minerales
Doctorado en Ingeniería - Ciencia y Tecnología de Materiales

Mayor información:

E-mail: acgeomin_med@unal.edu.co
Teléfono: (57-4) 425 53 68

UNIVERSIDAD NACIONAL DE COLOMBIA
SEDE MEDELLÍN
FACULTAD DE MINAS

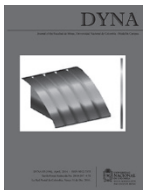

DYNA
http://dyna.medellin.unal.edu.co/

Decontamination of industrial textile wastewater using photocatalysis

José Herney Ramírez-Franco [a] & Hugo Ricardo Zea-Ramírez [b]

[a] *Departamento de Ingeniería Química y Ambiental, Universidad Nacional de Colombia, Bogotá, Colombia, jhramirezfra@unal.edu.co*
[b] *Departamento de Ingeniería Química y Ambiental, Universidad Nacional de Colombia, Bogotá, Colombia, hrzear@unal.edu.co*

Received: November 21th, 2014 Received in revised form: August 1st, 2015. Accepted: February 25th, 2016.

Abstract
Iron-doped TiO_2 catalysts were prepared by impregnation in order to study their photocatalytic activity in the treatment of wastewater from the textile industry. Characterization of the catalysts before and after reaction was performed using techniques including total surface area measurement, X-Ray diffraction and elemental analysis via X-Ray fluorescence. Varying pH conditions, H_2O_2 concentrations and catalyst quantities were evaluated during the photocatalytic reactions. Fe-TiO_2 catalysts were shown to be highly active in the reduction of chemical oxygen demand (% COD) and % color reduction in the water treated.

Keywords: Fe doped TiO_2, Photocatalysis, Color reduction, COD, Wastewater.

Descontaminación de aguas de desecho de la industria textil usando Fotocatálisis

Resumen
Catalizadores de TiO_2 dopado con hierro se prepararon por impregnación para estudiar su actividad fotocatalítica en el tratamiento de aguas residuales de la industria textil; la caracterización de los catalizadores antes y después de la reacción incluyó área superficie total, difracción de rayos X y análisis elemental por medio de fluorescencia de rayos X. Durante la reacción fotocatalitca se evaluaron varias condiciones de pH, concentración de H_2O_2 y cantidad de catalizador; los catalizadores de Fe-TiO_2 demostraron una alta actividad para la reducción de la Demanda Química de Oxigeno (% DQO) y de % Color de las aguas tratadas.

Palabras clave: TiO_2 dopado con Fe, Fotocatálisis, Reducción de Color, DQO, aguas de desecho.

1. Introduction

Processes used in the textile industry require large amounts of water and generate considerable quantities of contaminated wastewater. The effluents involved usually contain azo-dye colorants along with heavy metals, bleaches and acids which are extremely toxic. Dyes released into the environment can break down into toxic, carcinogenic or mutagenic products [1,2]. The introduction of more stringent regulations by Bogotá's Secretary of the Environment (Resolution 3957/2009) saw the establishment of permitted thresholds for pollution factors including heavy metals, tensoactives, biochemical oxygen demand (BOD), chemical oxygen demand (COD), grease and fat, pH, temperature, suspended solids and Color.

Treatment using chemical methods (e.g., reduction, oxidation) [3,4], physical methods (e.g., adsorption) [5], selective membranes [6], electrochemical processes [6] and biological methods [7,8] have been studied and applied in order to reduce dye contamination. However, these methods can be site specific, expensive and cumbersome to operate. The efficiency of biological treatment in reducing COD depends heavily on the BOD/COD ratio. The average value of this ratio in the textile industry is 0.35 [9], below the value recommended for total COD removal. The ratio should be increased to a value of not less than 0.6 if acceptable biodegradability in the effluent is to be achieved.

Advanced oxidation processes (AOPs), have attracted interest in the treatment of organic and sometimes inorganic contaminants in wastewater. AOPs are based on physico-chemical processes capable of producing profound changes in the chemical structure of pollutants. The process involves the generation of powerful transient species: the hydroxyl radical ($HO^{\bullet}$) in particular. Such radicals facilitate the oxidation of organic molecules via a reaction mechanism involving hydrogen abstraction or the electrophilic interaction with double bonds forming highly reactive organic radicals ($R^{\bullet}$), which react with oxygen to generate

© The author; licensee Universidad Nacional de Colombia.

peroxyl radicals, leading in turn to a chain of oxidative reactions that contribute to the partial or complete degradation of contaminant molecules.

Physical and chemical properties such as photoactivity, chemical stability and nontoxicity have made TiO_2 one of the commonest materials used in photocatlytical applications [10]. TiO_2 is a light sensitive semiconductor that absorbs electromagnetic radiation close to the UV region. This means it is an active photocatalyst capable of producing free radicals that promote partial and complete oxidation [11-14]. Because of its photocatalytic characteristics, TiO_2 has been extensively used in dye removal processes [15,16]. The photo-efficiency of TiO_2 is affected by its wide band-gap energy (Eg = 3.2 eV) and the high recombination rate of its photogenerated electron-hole pairs [17]. To overcome these disadvantages, TiO_2 is doped with metals in order to increase its capacity to absorb from the visible portion of the sun's spectrum [18]. Many metal ions, particularly from transition metals, have been used as dopants for TiO_2, and their effects on its performance have been variously reported [10, 19]. Iron has frequently been identified as an appropriate metal ion dopant, because of its electron configuration [20,21].

This paper presents results for the photocatalytic performance of an Fe-TiO_2 catalyst for the decontamination of textile wastewater evaluated for several pH conditions, H_2O_2 concentrations and catalyst quantities, before and after reaction.

2. Materials and Methods

2.1. Wastewater characterization

Several wastewater samples from the textile industry in Bogotá (Colombia) were characterized; the values obtained were compared with the permitted levels established by Resolution 3957/2009 (Table 1). Industrial effluent complies with most of the permitted limit values. However, COD and Color values (identified in boldface) exceeded the standard.

The results reported in Table 1 may be used to calculate the % reduction in COD (76.4%) and Color (97.5%) required to comply with Resolution 3957/2009.

Table 1.
Textile wastewater characterization.

Parameter	Units	Detected	Resolution 3957/2009
Cadmium, Cd	(mg/L)	<0.003	0,02
Nickel, Ni	(mg/L)	<0.07	0.5
Chrome, Cr	(mg/L)	0.06	1,0
Phenols	(mg/L)	<0.07	0,2
Lead, Pb	(mg/L)		0,1
SAAM, tensoactives	(mg/L)	<0.07	10
BOD	(mg/L)	2,686	800
COD	**(mg/L)**	**6,382**	**1500**
Grease and Fat	(mg/L)	69	100
TSS	(mg/L)	255	600
pH		6.42-7.99	9-May
Temperature	(°C)	16-24	<30
Sedimentable solids	(mg/L)	9.0-13	2,0
Color	**Pt-Co 1/20 units**	**2028**	**50**

Source: The authors

2.2. Catalyst synthesis and characterization

The catalysts were prepared using wet impregnation; TiO_2 (Mba8668- Industrial Grade) was impregnated with an aqueous solutions of iron nitrate, $Fe(NO_3)_3$, (Sigma-Aldrich) of proper concentrations, generating a catalyst with a weight load of 7%. The mixture was kept under constant stirring (250 rpm) for 72 hours at 50°C; the remaining paste was calcined at 450°C with a heating rate of 10°C/min. After calcination, the catalyst was ground and sieved with a mesh size of 200. The catalyst surface areas were evaluated by the Brunauer-Emmett-Teller (BET) method of liquid nitrogen adsorption isotherms at 77 K, using AUTOSORB-1 (QUANTACHROME) equipment. Previous to the N_2 adsorption the catalyst sample was degassed for 20 h at 200°C. Crushed and sieved catalyst samples were characterized by XRD using Ni-filtered Cu-Ka radiation in an X-PERT PRO PANALYTICAL diffractometer operating in continuous scan mode between 20 and 80°. JADE Software (MDI, Inc) was used to analyze the collected X-Ray diffraction (XRD) data and compared against the International Centre for Diffraction Data ICDD database. Elemental chemical analysis was performed by means of X-ray fluorescence (XRF) on a ZSX PRIMUS (Rigaku) equipped with a 4kW Rhodium anode.

2.3. Catalyst activity test

Photocatalytic activity was evaluated in a batch reactor made of quartz (250 ml), irradiated by 9 UV–A lamps (wavelength 320 to 400 nm). Reactor and lamps were located inside a temperature-controlled chamber. The reaction volume for all the experiments was 200 ml of reactive solution, adjusted to the pH selected for each experiment. At reaction time equals zero (t=0) the correct amounts of powdered catalyst and hydrogen peroxide, defined during experimental design, were added to the reaction volume, light sources being switched on simultaneously. All experiments were carried out at room temperature. COD and Color changes were determined by spectrophotometric methods, in compliance with the US EPA Standard Methods 5220-D and Standard Methods 2120 C, respectively [22].

3. Results and Discussion

3.1. Catalyst characterization

The XRD patterns of the fresh catalyst (after calcination) and following reaction are shown in Fig. 1 (profiles a and b, respectively). The XRD profiles revealed a high crystallinity with a predominantly rutile phase (characteristic peaks at 2θ angles equal to: 27.6º, 37.2º, 54.46º). In addition, weak and broad peaks at 2θ angles 56.7º and 41.2º indicated that the iron was present as small well dispersed magnetite crystals (Fe_3O_4). No major change was observed by XRD in the catalyst after it had been used several times in the reaction. This structural stability is related to the low catalyst deactivation apparent during the deactivation tests.

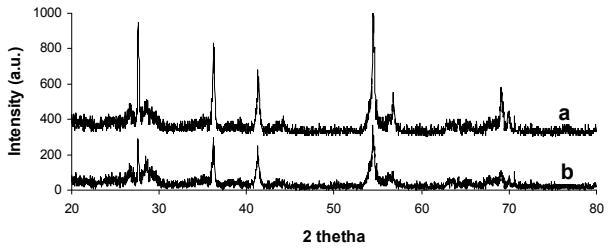

Figure 1. XRD profiles of catalyst (a) fresh and (b) after reaction.
Source: The authors.

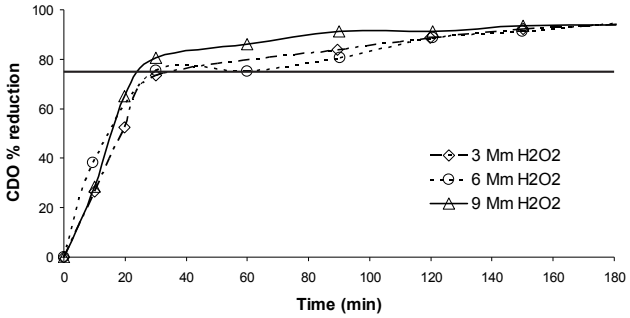

Figure 2. H_2O_2 effect on % COD reduction, $C_{catalyst}$ = 1g/L, pH = 3.
Source: The authors.

Table 2.
Experimental conditions of COD reduction experiments and % COD reduction.

Test No	pH	Fe-TiO_2 g/L	H_2O_2x10^{-3} [M]	% COD Reduction
E1	3	1.0	3	95
E2	3	1.0	6	95
E3	3	1.0	9	95
E4	3	1.5	3	89
E5	3	2.0	3	88
E6	5	1.0	3	63
E7	5	1.0	6	74
E8	5	1.0	9	77
E9	5	1.5	3	66
E10	5	2.0	3	59
E11	5	1.5	6	69
E12	5	1.5	9	79
E13	3	1.5	9	97
E14	5	2.0	6	69
E15	5	2.0	9	72
E16	3	1.5	6	95
E17	3	2.0	9	92
E18	3	2.0	6	89
E10	5	2.0	3	59

Source: The authors

The N_2 adsorption isotherm of the fresh catalyst at 77 K and after reaction shows the typical behavior of a Type III isotherm with a characteristic Type H4 hysteresis, common in low surface area materials. BET surface area values calculated for the fresh (13.22 m^2/g) and after reaction (13.35 m^2/g) catalyst show no change in surface area of the catalyst as a result of continuous exposure to reaction conditions. X-ray fluorescence (XRF) results of the synthesized catalyst confirms the expected iron loading, close to 7.17% in weight.

3.2. Catalyst activity

Table 2 summarizes experimental conditions for all the activity experiments performed and the % COD reduction achieved. These experiments cover a wide spectrum of operation conditions achieved by varying the amount of catalyst added to the reaction solution, initial pH, and H_2O_2 dosage. The concentration values used are based on previous research [23].

The % COD reduction reported in Table 2 was measured after 180 minutes of reaction. The lowest % COD reduction achieved was 59% at pH 5, using 2.0 g/L of Fe-TiO_2 and 3 mM H_2O_2. The highest % COD reduction (97%) was obtained at pH 3, using 1.5 g/L of Fe-TiO_2 and 9 mM H_2O_2.

Most of the experiments run at pH 3 (6 out of 9) saw % COD reduction above 90% and only 3 were below 90%. But even these were above 88%. By contrast, in all of the experiments run at pH 5 reduction was below the 77% COD required to comply with Resolution 3957/2009.

Figs. 2 to 4 present the profiles of the reactions corresponding to pH 3. As described previously all the reactions performed at pH 3 had reduction values above 77%, enough to comply with Resolution 3957/2009. Fig. 2 shows the % COD reduction for the experiment using 1 g/L of Fe-TiO_2 for different H_2O_2 concentrations. There is no significant difference in the profiles of each of the H_2O_2 concentrations, all of which rapidly reduced the % COD in the first 40 minutes of the experiment, reaching the reduction goal (77%, represented in the figure by the continuous horizontal line) in about 35 minutes; after 40 minutes the three profiles reached COD reduction values above 90%, while after 140 minutes a plateau of around 96% COD reduction was reached.

During experiments performed with different dosage of H_2O_2 in the reaction solutions (see Fig. 2), the Fe-TiO_2 photocatalytic activity indicated a significant increase in the formation of the OH radical, which was certainly caused by iron oxidation in a photo-Fenton reaction, as follows (1):

$$Fe^{3+} + HO^- + hv \rightarrow Fe^{2+} + HO^{\bullet} \quad (1)$$

By contrast, in the case of the % COD reduction profiles for the experiments with 1.5 g/L of Fe-TiO_2, there was a clear difference between the initial % COD reduction rate of the 3 mM of H_2O_2 that reached 77% reduction in just under 20 minutes before it slowed down d dramatically, reaching only 89% of reduction at 180 minutes and finishing below the % COD reduction achieved by the 6 and 9 mM of the H_2O_2 experiments (Fig. 3). The 6 and 9 mM of H_2O_2 % COD reduction profiles followed an almost identical tendency, starting slowly compared to the experiment run at 3 mM of H_2O_2, which reached 77% of COD reduction after 90 minutes, attaining 96 and 97% after 180 minutes, respectively. H_2O_2 can play a dual function: as a strong oxidant itself and as an electron scavenger; proper H_2O_2 concentration has been found to enhance the degradation rate of compounds, as a result of greater efficiency in the generation of hydroxyl radicals and the inhibition of electron-hole pair recombination, according to the following equation (2):

$$e^- + H_2O_2 \rightarrow HO^\bullet + HO^- \quad (2)$$

Several experiments previously performed within our research group and reported elsewhere [23], coincide in the identification of suitable H_2O_2 concentrations. At higher concentrations, scavenging of HO radicals will occur, as described by the following reaction (3):

$$H_2O_2 + HO^\bullet \rightarrow HOO^\bullet + H_2O \quad (3)$$

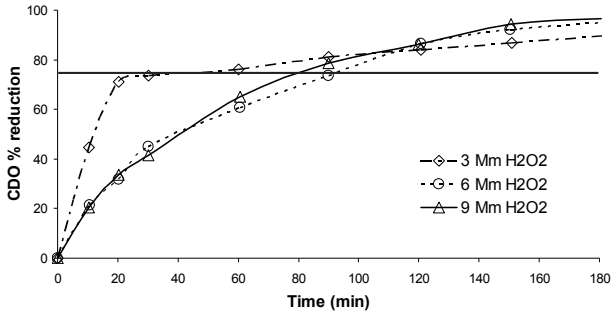

Figure 3. H_2O_2 effects on % COD reduction, $C_{catalyst}$ = 1.5g/L, pH = 3. Source: The authors.

Fig. 4 shows the % COD reduction for the experiment using 2 g/L of Fe-TiO_2 for different amounts of H_2O_2. Initially there was a difference in the rate of COD reduction, the 3 and 9 mM H_2O_2 concentrations being, respectively, the fastest and slowest. As the reaction time went beyond 100 minutes the difference grew smaller and after 180 minutes all achieved COD reductions above 90%.

The results for % COD reduction of the 3 different catalyst amounts with the fixed dosage of H_2O_2 indicated an apparent detrimental effect as the amount of catalyst increased: at 1 g/L of catalyst, 77% COD reduction was reached before 40 minutes, independently of the H_2O_2 dosage used. There was, furthermore, little difference between the rate of reduction, all of which reached % COD reduction above 90% after 160 minutes. In the experiments using 1.5 g/L and 2 g/L of catalyst (with the exception of the one using 3 mM H_2O_2 dosages with 1.5 g/L), all the % COD reduction profiles underperformed compared to the results obtained for the 1 g/L experiments. A clear trend has been identified in the literature in terms of the effects of homogeneous iron concentration in Fenton processes, suggesting that an excess of homogenous iron in the reaction consumes free radicals and organically generated free radicals ($HO^\bullet$) via parallel reaction, reducing the possibility that the radical will continue with the

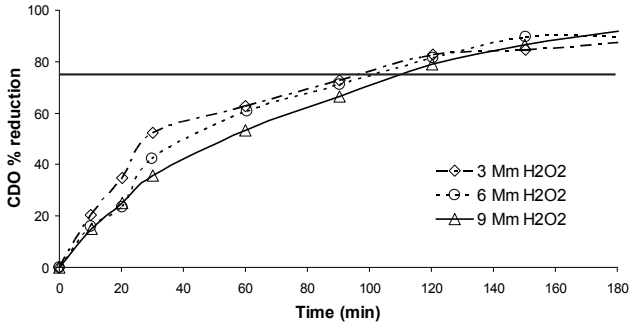

Figure 4. H_2O_2 effect on % COD reduction, $C_{catalyst}$ = 2g/L, pH = 3. Source: The authors.

Table 3.
Experimental conditions of Color reduction experiments and % COD reduction

Test No	pH	Fe-TiO_2 g/L	$H_2O_2x10^{-3}$ [M]	% Color Reduction
EC1	3	1.0	3	97
EC2	3	1.0	6	98
EC3	3	1.0	9	98
EC4	3	1.5	3	96
EC5	3	2.0	3	90
EC6	3	1.5	9	97
EC7	3	1.5	6	95
EC8	3	2	9	94
EC9	3	2	6	92

Source: The authors

oxidation (degradation) of the contaminant molecule. Some of the proposed chemical reactions through which homogeneous iron reacts are shown:

$$FeOH^+ + HO^\bullet \rightarrow Fe^{3+} + 2HO^- \quad (4)$$

$$Fe^{2+} + HO_2^\bullet \rightarrow Fe^{3+} + HO_2^- \quad (5)$$

$$Fe^{3+} + HO_2^\bullet \rightarrow Fe^{2+} + O_2 + H^+ \quad (6)$$

These % COD reduction experiments allow us to conclude that pH 3 and lower quantities of catalyst in the reaction are beneficial for the oxidation process.

Table 3 summarizes the conditions of the the Color reduction experiments performed and the % Color reduction obtained.

The % Color reduction reported in Table 3 was measured after 180 minutes of reaction. The lowest % Color reduction achieved was 90% using 2.0 g/L of Fe-TiO_2 with a concentration of 3 mM H_2O_2 and the highest (97%) using 1 g/L of Fe-TiO_2 and a dosage of 6 and 9 mM H_2O_2. It is important to highlighted that the 3 mM H_2O_2 with 1g/L of Fe-TiO_2 also achieved a high % Color reduction (97%), virtually the same value as with the 6 and 9 mM H_2O_2 dosage. The 1 g/L TiO_2 experiments outperformed all the % Color reduction experiments, independently of H_2O_2 dosage.

Figs. 5, 6 and 7 present the profiles of the reactions corresponding to catalyst amounts 1, 1.5 and 2 g/L. In the case of the 1 g/L experiments, the reaction profile followed the same trend as for the three H_2O_2 dosages, reaching 97.5% of Color reduction after 160 minutes. For the experiment run using 1.5 g/L the % Color reduction rate showed a small difference, as a function of H_2O_2 dosage: the 3 mM H_2O_2 dose being slightly more active than the 6 and 9 mM H_2O_2 doses. This small difference disappeared after 160 minutes when all three experiments achieved a % Color reduction above 90%, but barely reached the target Color reduction of 97%. None of the experiments run at 2 g/L Fe-TiO_2 reached the target Color reduction value.

Most of the experimental data collected in the photocatalytic tests showed an initial fast reduction of COD (between 0 and 20 minutes). After the initial fast reduction the degradation rate reduced considerably. Experiments performed in our research group for the same reaction, using several types of catalyst, have shown similar behavior [23], which has also been reported by independent studies [24] that

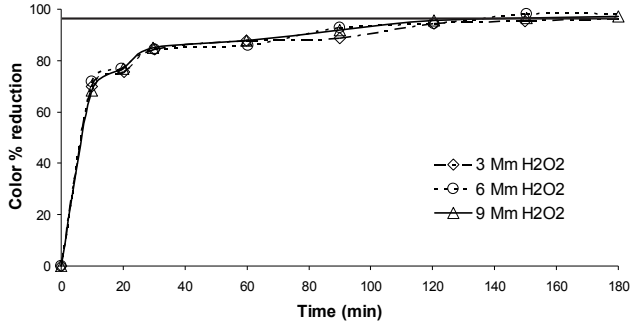

Figure 5. H_2O_2 effect on % Color reduction, $C_{catalyst}$ = 1g/L, pH = 3.
Source: The authors.

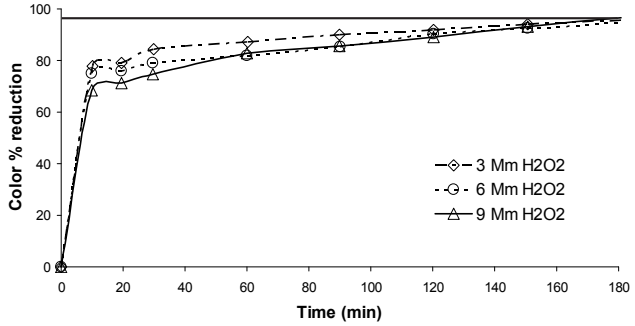

Figure 6. H_2O_2 effect on % Color reduction, $C_{catalyst}$ = 1.5g/L, pH = 3.
Source: The authors.

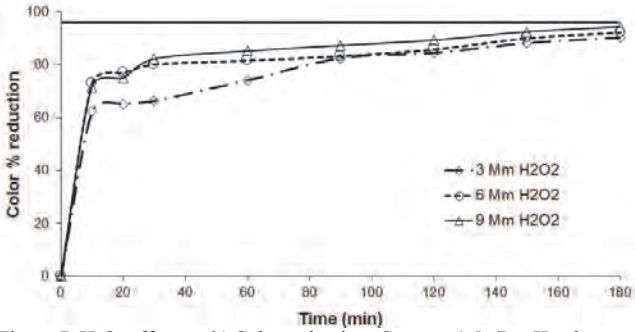

Figure 7. H_2O_2 effect on % Color reduction, $C_{catalyst}$ = 1.5g/L, pH = 3.
Source: The authors.

have related this characteristic behavior to a two stage degradation mechanism, typical in Fenton processes. In this mechanism ferrous ions react rapidly with peroxide to form hydroxyl radicals and ferric ions. The hydroxyl radicals formed degrade the contaminant molecule very actively. These ferric ions might react with peroxide to generate hydroperoxyl radicals and ferrous ions.

Textile industry dyes normally consist of molecules formed by benzene and naphthalene rings bonded by an azo linkage (N=N), all of which exhibit different absorbance peaks. The chromophore containing the azo linkage has absorption in the visible region, while the benzene and naphthalene rings absorb in the UV region. Indeed, the disappearance of the absorbance signal in the visible range corresponds to an almost complete decolorization (breakdown of the chromophore group). The rupture of the bond between the benzene and naphthalene rings generate additional contaminant molecules that must be mineralized, thus increasing the COD values the catalyst must reduce.

The mechanism of the homogeneous Fenton H_2O_2 oxidation decomposition process is not well established. Many oxidizing species have been suggested as being involved, in addition to the HO radicals. Some of the literature [25] has proposed an initial and rapid adsorption of the peroxide molecule on the catalytic specie (Fe^{3+}). However, other papers have suggested a different initial reaction step in which the organic molecule is the one adsorbed on the catalytic specie [26]. Nevertheless, the involvement of the following steps has been suggested in most of the works found in the literature, which correspond to the Fe^{3+} reduction generating moderate oxidative HO_2 radicals, followed by Fe^{3+} regeneration with formation of the hydroxyl radicals:

$$X - Fe^{3+} + H_2O_2 \rightarrow X - Fe^{2+} + HO_2^{\bullet} + H^+ \quad (7)$$

$$X - Fe^{2+} + H_2O_2 \rightarrow X - Fe^{3+} + HO^- + HO^{\bullet} \quad (8)$$

where X represents the surface of the catalyst. However, it should be remarked that the radicals can also be generated on the surface of the solid catalytic material, so that they are actually "caged" in the solid structure, subsequently reacting with the adsorbed reagent(s) without generating radicals. Obviously, in addition to the steps indicated here, many other radical reactions occur, including those involving the reaction intermediates.

TiO_2 crystallinity can greatly influence the photocatalytic activity, which is widely believed to be phase-dependent. The XRD result shows a well define rutile phase before and after reaction, eliminating any possible variance in the photocatalytic activity originated by differences in the crystal phases. Furthermore, the XRD profiles indicate that superficial iron species are present as magnetite crystals and that there is no formation of any iron-titanium solid solution. Generally the effect of the addition of a dopant element to TiO_2 is to facilitate the mechanism by which the conduction band electrons (e^-) and the valence band holes are generated at the surface by light energy values equaling or exceeding the band gap energy [27]. These holes may react with either the surface hydroxyl ions or with water to produce hydroxyl radicals ($OH^{\bullet}$). The electrons react with adsorbed molecular oxygen, to yield superoxide anion radicals [28] that act as oxidizing agents, thus providing an additional source of the hydroxyl radicals. These hydroxyl radicals are strong oxidants that can react with the dye molecules, leading to their destruction. These types of behavior have also been reported for the treatment of chemical industry wastewater using a solar photoreactor and Titanium Dioxide (Degussa P-25) [29].

4. Conclusions

The photocatalytic performance of an Fe-TiO_2 catalyst for the decontamination of textile wastewater has been evaluated in order to achieve compliance with Resolution 3957/2009 emitted by the Bogotá Secretary of the Environment. Catalyst characterization shows a low surface area non- iron-titanium solid solution of 7.17% Fe_3O_4 (magnetite) supported on a well-

defined rutile phase. Before and after reaction, characterization reveals no major changes in the crystal structure, surface area or catalyst composition as a result of catalyst exposure to reaction conditions. Characterization of wastewater from the textile industry showed deficiencies in the treatment of the COD and Color parameters. An Fe-TiO_2 catalyst prepared by impregnation showed a high % COD and % Color reduction - high enough, indeed, to comply with Resolution 3957/2009

Acknowledgements

The authors would like to thank Diana Varela for the experimental work on which this paper is based and the manager and technicians of the Electrochemistry and Catalysis Laboratory of the Chemical Engineering Department at the National University of Colombia.

References

[1] Zaharia, C. and Suteu, D., Optimization study of orange 16 dye sorption from aqueous systems using sawdust wastes. Chemical Bulletin of Politehnica University of Timisoara, 56(70), pp. 24-28, 2011.

[2] Sharma, S., et al., Toxicity assessment of textile dye wastewater using swiss albino rats. Australasian Journal of Ecotoxicology, 13, pp. 81-85, 2007.

[3] Brown, G. and JR., D., Photo reduction of methylorange sensitized by colloidal titanium dioxide. J Chem Soc Faraday Trans, 80, pp. 1631-1643, 1984. DOI: 10.1039/F19848001631.

[4] Slokar, Y. and A., Le Marechal, Methods of decoloration of textile wastewater. Dyes Pigments, 37, pp. 335-356, 1998. DOI: 10.1016/S0143-7.

[5] DeJohn, P.B. and Hutchins, R.A., Treatment of dye wastes with granular activated carbon. Journal Textile Chemist and Colorist, 8, pp. 34-38, 1976.

[6] Suarez-Parra, R., et al., Visible light-induced degradation of blue textile azo dye on TiO2/CdO-ZnO coupled nanoporous films. Solar Energy Materials and Solar Cells, 76(2), pp. 189-199, 2003. DOI: 10.1016/S0927-0248(02)00346-X.

[7] Kalyushnyi, S. and Sklyar, V., Biomineralisation of azo dyes and their breakdown products in anaerobic–aerobic hybrid and UASB reactors. Water Sci. Technol., 41, pp. 23-30, 2000.

[8] Yoo, E., Libra, J. and Wiesmann, U., Reduction of azo dyes by desulfovibrio desulfuricans. Water Science & Technology, 41(12), pp. 15-22, 2000.

[9] Andreozzi, R., et al., Advanced Oxidation Processes (AOP) for water purification and recovery. Catalysis Today, 53(1), pp. 51-59, 1999. DOI: 10.1016/S0920-5861(99)00102-9.

[10] Maji, S.K., et al., Effective photocatalytic degradation of organic pollutant by ZnS nanocrystals synthesized via thermal decomposition of single-source precursor. Polyhedron, 30(15), pp. 2493-2498, 2011. DOI: 10.1016/j.poly.2011.06.029.

[11] Davidson, A. and Che, M., Temperature-induced diffusion of probe vanadium (IV) ions into the matrix of titanium dioxide as investigated by ESR techniques. The Journal of Physical Chemistry, 96(24), pp. 9909-9915, 2002. DOI: 10.1021/j100203a061.

[12] Fujishima, A., Rao, T.N. and Tryk, D.A., Titanium dioxide photocatalysis. Journal of Photochemistry and Photobiology C: Photochemistry Reviews, 1(1), pp 1-21, 2000. DOI: 10.1016/S1389-5567(00)00002-2.

[13] Fujishima, A. and Zhang, X., Titanium dioxide photocatalysis: present situation and future approaches. Comptes Rendus Chimie, 9(5-6), pp. 750-760, 2006. DOI: 10.1016/j.crci.2005.02.055.

[14] Noh, J.H., et al., Microwave dielectric properties of nanocrystalline TiO2 prepared using spark plasma sintering. Journal of the European Ceramic Society, 27(8-9), pp. 2937-2940, 2007. DOI: 0.1016/j.jeurceramsoc.2006.11.018.

[15] Mu, Y., et al., TiO2-mediated photocatalytic degradation of Orange II with the presence of Mn2+ in solution. Journal of Photochemistry and Photobiology A: Chemistry, 163(3), pp. 311-316, 2004. DOI: 10.1016/j.jphotochem.2003.08.002.

[16] Rao, K.V.S., Lavédrine, B. and Boule, P., Influence of metallic species on TiO2 for the photocatalytic degradation of dyes and dye intermediates. Journal of Photochemistry and Photobiology A: Chemistry, 154(2-3), pp. 189-193, 2003. DOI: 10.1016/S1010-6030(02)00299-X.

[17] Franco, A., et al., Photocatalytic decolorization of methylene blue in the presence of TiO2/ZnS nanocomposites. J Hazard Mater, 161(1), pp. 545-550, 2009. DOI: 10.1016/j.jhazmat.2008.03.133.

[18] Kiwi, J. and Morrison, C., Heterogeneous photocatalysis. Dynamics of charge transfer in lithium-doped anatase-based catalyst powders with enhanced water photocleavage under ultraviolet irradiation. The Journal of Physical Chemistry, 88(25), pp. 6146-6152, 2002. DOI: 10.1021/j150669a018.

[19] Luo, Z. and Q.-H. Gao, Decrease in the photoactivity of TiO2 pigment on doping with transition metals. Journal of Photochemistry and Photobiology A: Chemistry, 63(3), pp. 367-375, 1992. DOI: 10.1016/1010-6030(92)85202-6.

[20] Adán, C., et al., Structure and activity of nanosized iron-doped anatase TiO2 catalysts for phenol photocatalytic degradation. Applied Catalysis B: Environmental, 72(1-2), pp. 11-17, 2007. DOI: 10.1016/j.apcatb.2006.09.018.

[21] Herrmann, J.-M., Heterogeneous photocatalysis: Fundamentals and applications to the removal of various types of aqueous pollutants. Catalysis Today, 53(1), pp. 115-129, 1999. DOI: 10.1016/S0920-5861(99)00107-8.

[22] APHA, A.W., Standard methods for the Examination of water and water and wastewater. 16 Ed, 1995.

[23] Ramirez, J.H., Costa, C.A. and Madeira, L.M., Experimental design to optimize the degradation of the synthetic dye Orange II using Fenton's reagent. Catalysis Today, 107(1), pp. 68-76, 2005. DOI: 10.1016/j.cattod.2005.07.060.

[24] Malik, P.K. and Saha, S.K., Oxidation of direct dyes with hydrogen peroxide using ferrous ion as catalyst. Separation and Purification Technology, 31(3), pp. 241-250, 2003. DOI: 10.1016/S1383-5866(02)00200-9.

[25] Dantas, T.L.P., et al., Treatment of textile wastewater by heterogeneous Fenton process using a new composite Fe2O3/carbon. Chemical Engineering Journal, 118(1), pp. 77-82, 2006. DOI: 10.1016/j.cej.2006.01.016.

[26] Feng, J., et al., A novel laponite clay-based Fe nanocomposite and its photo-catalytic activity in photo-assisted degradation of Orange II. Chemical Engineering Science, 58(3), pp. 679-685, 2003. DOI: 10.1016/S0009-2509(02)00595-X.

[27] Han, T., Wu, C. and Chien-Te, H., Hydrothermal synthesis and visible light photocatalysis of metal-doped titania nanoparticles. Journal of Vacuum Science, 25(2), pp. 430-435, 2009. DOI: 10.1116/1.2714959.

[28] Ya-Fang, T., et al., Preparation of Fe-doped TiO2 nanotube arrays and their photocatalytic activities under visible light. Materials Research Bulletin, 45(2), pp. 224-229, 2010. DOI: 10.1016/j.materresbull.2009.08.020.

[29] Restrepo, G., et al., Evaluation of photocatalytic treatment of industrial wastewater using solar energy. DYNA, 75(155), pp. 145-153, 2008.

H. Zea, received his BSc. Eng. in Chemical Engineering, in 1997, from the Fundación Universidad de America, Bogotá, Colombia, his MSc. in Chemical Engineering in 2000, from the Universidad Nacional de Colombia. Bogotá, Colombia and his PhD. in Chemical Engineering in 2004, from the University of New Mexico, Albuquerque, USA. Between 2005 and 2007 he worked in alternative energy research, followed by a Postdoctoral appointment from mid-2007 to 2008. Since 2008 he has been associate professor at the Chemical and Environmental Engineering Department at the Universidad Nacional de Colombia, Bogotá, Colombia. His research interests include materials, chemical reactions, separation processes and environmental remediation.
ORCID: 0000-0002-6801-1879.

J.H. Ramirez, received his BSc. Eng. in Chemical Engineering in 1998, from the Universidad Nacional de Colombia, Manizales, Colombia, his MSc. in Chemical Engineering in 2003, from the Universidade Sao Paulo, Brazil and his PhD. in Chemical Engineering in 2008, from The Universidade do Porto, Portugal. Since 2008 he has been associate professor at the Chemical and Environmental Engineering Department at Universidad Nacional de Colombia, Bogotá, Colombia. His research interests include materials, chemical reactions, environmental catalysis and environmental remediation.
ORCID: 0000-0003-1766-1174.

UNIVERSIDAD NACIONAL DE COLOMBIA
SEDE MEDELLÍN
FACULTAD DE MINAS

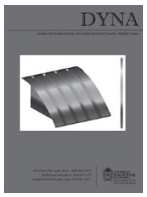

DYNA
http://dyna.medellin.unal.edu.co/

Nutritional composition of meals at work and its relationship with manufacturing workers' anthropometric profile and energy expenditure

Eliana Aparecida Queiroz Bortolozo [a], Luiz Alberto Pilatti [a], Maria Helene Canteri [a] & Pedro Arezes [b]

[a] *Department of Production Engineering. Federal Technological University of Paraná, Ponta Grossa, Brazil, bortolozo@utfpr.edu.br, lapilatti@utfpr.edu.br, canteri@utfpr.edu.br.*
[b] *Algoritmi Center de La Universidade de Minho, Guimaraes, Portugal. Parezes@dps.uminho.pt*

Received: November 30th, 2015. Received in revised form: March 10th, 2016. Accepted: March 16th, 2016.

Abstract
The objective of this study was to verify whether the energy content and nutritional composition of meals consumed at work (lunch) correlated with the energy expenditure and nutritional status of workers from different sectors (administration and production) of different industries. The sample consisted of 292 workers. Many anthropometric dimensions were assessed, such as physical activity energy expenditure, and daily energy expenditure (DEE). Food intake was measured directly for five days. The study comprised an assessment of the correlation between sectors and gender, a qualitative assessment between obesity indicators, and a principal component analysis (PCA). Overweight workers prevailed, and DEE differed by gender and work sector ($p<0.05$). PCA showed that the majority of the individuals with high energy expenditure and high energy and fats consumption levels were males.

Keywords: meals, worker, nutrition, energy expenditure.

La alimentación de los trabajadores en la industria y su relación con los datos antropométricos y el gasto energético

Resumen
Este estudio tuvo como objetivo verificar la correlación entre la composición energética y nutricional de la comida consumida en el ambiente de trabajo (almuerzo), el gasto energético y el estado nutricional de trabajadores de diferentes sectores (administración y producción) en diferentes industrias. La muestra comprendió 292 trabajadores. Han sido evaluados diversos índices antropométricos, gasto energético en la actividad física y gasto energético diario (GED). El consumo alimenticio fue mensurado por observación directa, durante cinco días. El studio consistió en una evaluación de la correlación entre los sectores y género; una evaluación cualitativa entre los indicadores de obesidad y una Análisis de componentes principales (PCA). Se encontró prevalencia de trabajadores con sobrepeso y diferencia estadística del GED en función del género y sector de trabajo ($p<0,05$). En la PCA, fue posible determinar que pertenece al sexo masculino la gran mayoría de los individuos que presentaron un mayor gasto energético, mayores tenores de consumo de energía y lípidos.

Palabras clave: alimentación; trabajador; nutrición; gasto energético.

1. Introduction

Scientific and technological progress have increased people's life expectancy; changed their behavior, for example, by encouraging them to adopt a more energy-dense diet; and reduced physical activity. Notoriously, people have developed health problems related to these changes, such as overweight and obesity, both with a high global incidence [1-3].

In the study context, obesity may be related to higher absenteeism, occupational diseases, lower productivity, and higher health care costs [4-6]. Janssen et al. [7] studied these relationships and concluded that obese workers are more likely to report occupational accidents, especially those aged 40 or over who are less physically active. Barringto et al. [8] examined the association between perceived stress, eating behavior, physical activity (PA), and body mass index (BMI) in 621 healthy workers from the construction industry. Those authors concluded that high levels of perceived stress were

© The author; licensee Universidad Nacional de Colombia.

associated with poor diets and low level of PA.

Based on the supposition that adults spend half of their waking hours at work, quality food and encouragement for more physical activity at work in order to ensure full health and benefit the workers' professional practice and life as a whole, may promote, for example, a normal weight [5,9,10].

Workers' meals must meet workers' energy and nutritional requirements in order to benefit their health, for example, by controlling weight and other risks that facilitate the development of degenerative diseases [11]. Much evidence regarding the habitual intake of unhealthy foods has been documented by studies that investigated workers' diets, especially the low intake of fruits and non-starchy vegetables, and the high intake of high-sugar and high-fat foods [12-14]. To ensure that workers have a proper diet, especially low-income workers, in 1976, Brazil implemented a food and nutrition policy called Worker's Food Program (WFP). This program aimed to ensure that workers' nutritional requirements are met at work and to promote education in nutrition-related topics. Its guidelines have been changed to adapt to the changes seen in the nutritional profile of active adults [15].

Health status and performance in daily physical activities, including work, depend, among other things, on the balance between energy requirement and the intake of energy nutrients. The balance between energy requirement and intake may be neutral, negative, or positive. A positive energy balance results in the accumulation of excess adipose tissue, leading to obesity [16]. In this context, a gap was identified in the literature regarding the nutritional composition of workers' food intake with respect to their nutritional requirements, taking into account specific characteristics, such as gender and type of work. Hence, the goal of the current study was to verify whether the energy content and nutritional composition of meals consumed at work (lunch) are correlated with the energy expenditure and nutritional status of workers from different sectors (administration and production) of different industries.

2. Materials and Methods

2.1. Design and sampling

This cross-sectional study included workers from many industries, such as logging, chemical, metal-mechanic, foundry, and food in the city of Ponta Grossa, in the central region of the state of Paraná, Brazil. Data were collected from companies from five different industries (metal-mechanic, chemical, logging, food, and casting) because of easy access. The inclusion criteria for the companies were: belonging to different industries, being of different sizes based on the number of employees, enrolled in the Workers' Food Program (WFP), and having in-house food services.

The sample size was calculated with a confidence interval of 95% (95%CI) and 0.05 error margin for estimating the mean – finite population, using Equation 1 below [17] (n=sample size; N=population size; population standard deviation (SD); E=error margin for estimating a population parameter; $Z_{\alpha/2}$ =critical value related to the degree of confidence used for normal distribution).

$$n=\frac{N.\sigma^2.(Z_{\alpha/2})^2}{(N-1)E^2+\sigma^2.(Z_{\alpha/2})^2} \quad (1)$$

The sample size was calculated based on the following data: total number of factory workers in the studied region (18.439); mean BMI SD of 4.25; and maximum error margin of 0.5 based on the results of a pilot study (n=40), totaling 274 individuals. The study effectively assessed 292 workers, 70.2% from the production sector (factory floor, laboratory, general services, and maintenance), and 30.0% from the administrative sector (administrative, management, and commercial jobs).

The data were separated into classes to stratify the results by gender (male/female), administrative sector (administrative, management, and commercial jobs), and production sector (factory floor, general services, laboratory, and maintenance). The inclusion criteria were: males and females aged 18 to 55 years, enrolled in WFP, a minimum education level of 5 years of elementary school, working during the day shift at one of the studied companies, and having lunch at the company's food service restaurant. The study was approved by the Research Ethics Committee of the Federal Technological University of Paraná (UTFPR) - CAAE 14331813.0.0000.5547 – under protocol number 361.283.

A structured questionnaire was applied to collect sociodemographic data, namely age, gender, marital status, education level, work sector, and salary.

2.2. Assessment of anthropometric data, energy expenditure, and nutritional composition

Anthropometric data, such as indicators of nutritional status, were collected individually by trained personnel in a closed room as recommended by Onis et al. [18]. The individuals were weighed barefoot with a digital electronic platform scale (W835A-Wiso) with a maximum capacity of 150 kg and accuracy of 100 g, and the weight of the uniform was subtracted. Height was measured by a portable stadiometer mounted on the wall. The individuals were measured barefoot, looking straight ahead, holding the legs together, and letting the arms hang down each side of the body. Waist circumference (WC) was measured at the smallest circumference between the iliac crest and the last rib. Hip circumference (HC) was measured at the widest point of the buttocks seen laterally. The body mass index (BMI=mass/height^2), waist-to-hip ratio (WHR=WC/HC), and waist-to-height ratio (WHeR=WC/height) were then computed. Nutritional status was classified as follows: underweight (BMI < 18.5kg/m^2); normal weight (18.5 kg/m^2 ≤ BMI ≤24.9kg/m^2); overweight (25.0kg/m^2 ≤ BMI ≤ 29.9kg/m^2), and obese (BMI ≥30.0kg/m^2) [19].

Abdominal obesity was assessed by the following indices: WC, WHR, and WHeR, and classified as follows: males with waist circumference (WC) of between 94 and 102 cm and females with WC of between 80 and 88 cm had abdominal obesity grade I; males with WC ≥ 102 cm and females with WC ≥ 88 cm had abdominal obesity grade II. Regarding WHR, males with WHR > 0.92 and females with WHR > 0.83 were considered abdominally obese. Regarding WHeR, males and females with WHeR > 0.5 were considered abdominally obese [20,21].

The daily energy expenditure (DEE) was given by a predictive equation recommended by the World Health Organization [22] taking into account the basal metabolic rate (BMR). The BMR was calculated taking gender, age, and body mass into consideration. The ideal body weight was used for calculating the BMR of underweight, overweight, or obese individuals according to BMI to avoid under- or overestimation. Formulas for predicting the BMR are a good option for clinical and epidemiological studies because of their usefulness and low cost [23]. Physical activity energy expenditure (PAEE) was monitored using a pedometer (Yamax Gigi Walker SW – 700) on five consecutive days [24].

Food intake during lunch at work was measured directly on five consecutive days when workers helped themselves, taking into account the preparations and respective standard weights or volumes in cooking units. The food was weighed three times using an electronic scale with accuracy of 0.01g. Volumes were measured using a 500mL beaker. After the meal, the leftovers on the plate were recorded and the amounts consumed were calculated in grams or milliliters. The DietWin software was used to calculate the energy content and nutrient composition (proteins, carbohydrates, total fats, saturated fats, and sodium) of the meal. The results were compared with WFP's recommendations and with the estimated energy expenditure, considering that lunch should provide 30-40% of the workers' requirements. The study considered that the following amounts [15] should be consumed during the main meal (lunch): carbohydrates: 83-268g; proteins: 15-30g; lipids: 10-27g; saturated fats: <9g; fibers: >7.5g, and sodium: <960mg.

2.3. Statistical treatment

The software used for the descriptive analysis and statistical tests was Statistica for Windows 5.0 (Statsoft®). Data normality was assessed using the Kolmogorov-Smirnov (n>100) test, rejecting the null hypothesis when $p \geq 0.05$. Pearson's test was used to assess the correlation between the two variables, work sector (administrative and production) and gender (female and male), with normal distribution, and the Spearman test was used to assess the asymmetric data.

Statistical inference (percentage of individuals) qualitatively assessed the obesity indicators (BMI, WC, WHR, and WHeR) with 95% CI and error margin of ±2%.

The Pirouette software (Infometrix®) was applied to run the principal component analysis (PCA), which correlated body weight, BMI, energy expenditure, and lipid content. The significance level was set at 5% ($p<0.05$) for all tests. Data values highly incompatible with the dataset were considered outliers and removed from the dataset. The principal component (PC) loadings and scores were graphed. A labeling system based on gender and work sector was proposed as a pattern recognition technique.

3. Results and discussion

The volunteers consisted of workers from the following industries: metal-mechanic (n=67, 22.9%); chemical (n=30, 10.3%), logging (n=30, 10.3%), food (n=83, 28.4%), and casting (n=82, 28.1%). The sample included 87 administrative workers (29.8%) and 205 production workers (70.20%). The mean ages of the males (n=224) and females (n=68) were 33.7±8.84 years and 31.5±8.84 years, respectively.

3.1. Anthropometric results

The BMI of the workers did not differ by gender or by work sector ($p>0.05$). The sample's average BMI (26.40±4.67kg/m^2) indicated a prevalence of overweight. Indeed, 16.0% and 19.0% of the females and males, respectively, were obese, and 31.0% and 42.0% of the females and males, respectively, were overweight (Fig. 1; Tables 1 and 2). Other studies with workers reported similar findings [1,13].

Regarding WC, 64.7% (n=189) of the participants were not abdominally obese, 21.2% (n=62) had abdominal obesity grade I, and 14.1% (n=41) had abdominal obesity grade II, not differing by gender ($p>0.05$). Regarding WHR, 20.2% (n=59) of the participants were abdominally obese, most of whom were males and/or production workers ($p<0.05$). Workers with low education level (less than eight years of formal education) had significantly higher WHR than those with higher education ($p<0.05$). This fact is corroborated by a study that found that type of work (as a function of education level) and gender (greater in males) influence the incidence of abdominal obesity [25,26].

Regarding WHeR, 42.1% of the participants were abdominally obese, most of whom were also males and/or production workers ($p>0.05$). According to Bauman et al. [25], being male correlates with obesity but is not a determinant of it.

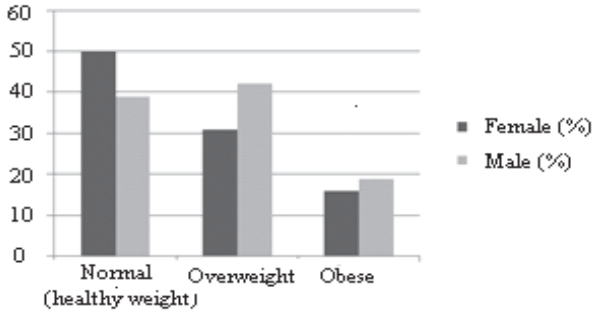

Figure 1. Prevalences of overweight and obesity (%) in a population of factory workers by gender.
Source: Bortolozo et al.

Table 1.
Anthropometric data of the manufacturing-plant workers by gender (mean ± standard deviation).

Variables	All	Women (n=68)	Men (n=224)
BMI (kg/m²)	26.40 (±4.67)	25.61 (±5.25)	26.61 (±4.85)
WC (cm)	87.110 (±12.02)	70.06 (±10.58)	89.54 (±11.50)
WHR* (cm)	0.85 (±0.08)	0.77 (±0.07)	0.88 (± 0.07)
WHeR* (cm)	0.51 (±0.07)	0.50 (± 0.06)	0.52 (±0.70)

Note: BMI: body mass index; WC: waist circumference; WHR: waist-to-hip ratio; WHeR: waist-to-height relationship; *lines with statistical differences.
Source: Bortolozo et al.

Table 2.
Anthropometric data of the manufacturing-plant workers by work sector (mean ± standard deviation).

Variables	Administrative (n=87)	Production (n=205)
BMI (kg/m²)	26.37 (±4.89)	26.45 (±4.35)
WC (cm)	83.33 (±12.26)	88.26 (±11.38)
RHR * (cm)	0.80 (±0.07)	0.86 (±0.07)
WHeR * (cm)	0.49 (±0.06)	0.52 (±0.06)

Note: BMI: body mass index; WC: waist circumference; WHR: waist-to-hip ratio; WHeR: waist-to-height relationship; *lines with statistical differences.
Source: Bortolozo et al.

Table 3.
Basal metabolic rate, physical activity energy expenditure, and daily energy expenditure of factory workers.

	BMR (Kcal)	PAEE (Kcal)	DEE (Kcal)
General (n=292)	1629.64(±155)	530.10 (±340)	2182.20 (447.00)
Women (n=68)	1483.04*(±126)	305.47* (±185)	1718.10* (±242)
Men (n=224)	1669.95*(±155)	598.98* (±347)	2331.28* (±379)
Administrative (n=87)		365.36* (±237)	1972.41* (±349)
Production (n=205)		618.02* (±354)	2302.78* (±436)

Note: BMR: basal metabolic rate; PAEE: physical activity energy expenditure; DEE: daily energy expenditure. *statistically different ($p<0.05$)
Source: Bortolozo et al.

The statistical interference test (error margin of ±2%) showed that obesity indices based on BMI were strongly correlated with WC and WHeR. On the other hand, the frequencies of obesity and overweight classified by BMI were weakly correlated with WHR. Although BMI is a widely used as an obesity indicator, alone it may not be an accurate indicator of body fat [27].

3.2. Energy expenditure

Table 3 shows the sample's BMR, PAEE, and DEE.

Taking the sample's characteristics (gender, mass, height, and age) into account, the mean BMR (kcal) was 1657.88 kcal (± 178). This value is close to that estimated by Frankenfield et al. [28] in a study of adults (1701.0 kcal). The BMR of males (1727.4) was higher than that of females (1405.0 kcal) ($p<0.05$). The mean PAEE was 530.10±340 kcal, differing significantly by gender and work sector. Males and production workers had higher PAEE than women and administrative workers, respectively.

Other studies have also found that administrative workers are more sedentary than those with supposedly more active jobs (production sector) [1,25,29]. This result was expected since PAEE is the component with more variability in energy expenditure [30].

The estimated daily energy requirement based on DEE not stratified by gender and work sector was close to the recommended value of the 2000 kcal ($p>0.05$) [15]. Therefore, the energy values differed significantly by gender and work sector (production or administrative). The significant differences in the energy requirements of workers with different characteristics have been considered by the WFP guidelines, which recommend that the menu should be adapted to the work activities undertaken [15]. According to the Dietary Reference Intakes (DRIs) guidelines, the energy requirement or Estimated Energy Requirement (EER) is defined as a mean daily amount of energy that promotes the energy balance of healthy individuals, which can vary by gender and level of physical activity [31]. However, studies about meals at work that verify menu adaptation were not found.

Regarding PAEE, it was verified that a number of other factors, namely education level and income, also showed different results ($p<0.05$). Workers with higher education levels (complete or incomplete) and higher income (more than 10 times the minimum salary) had lower PAEE than those with lower education levels and lower incomes. This result may have been influenced by the higher concentration of production workers with lower education levels, who are statistically more active. Hence, work activities may directly impact workers' daily level of physical activity, especially that of administrative workers.

3.3. Nutritional composition of lunch

Diet is an important environmental risk factor for obesity and other chronic noncommunicable diseases. The issue that requires determination is whether meals at work are promoting energy balance.

The menus of the study's in-house food services contain the following preparations on a daily basis: rice, beans, high-protein preparation (meat or meat-based product), side dish (pasta or legumes), salad (three or more options), dessert (fruit or sweet), juice (natural or artificial), and bread. Salt soybean oil, and other condiments for the salads are readily available. The amount of main dish or animal-protein preparation available for each worker is limited and distributed by the food service employees. The workers may eat as much of the other preparations as they please.

Fig. 2 shows the energy values recommended by the WFP, as well as the daily energy requirement of all workers, workers by gender, and workers by work sector. The energy requirement at lunch was based on the recommendation that 30-40% of the daily energy requirement (DER) should be provided by the main meal (lunch or supper) [15]. The mean energy content of this meal corresponded to 654.66-872.88 kcal, 515.40-687.20 kcal for females, 699.30-932.40 kcal for males, 591.72-788.96 kcal for administrative workers, and 690.83-921.11 kcal for production workers. The maximum recommended energy values (800 kcal) differed by gender and work sector. This is probably because the values recommended by the WFP for the main meal are based on a daily energy requirement of 2000 kcal, while the DEE of males and production workers was close to 2400 kcal/day, and of women and administrative workers, it was less than 2000 kcal/day.

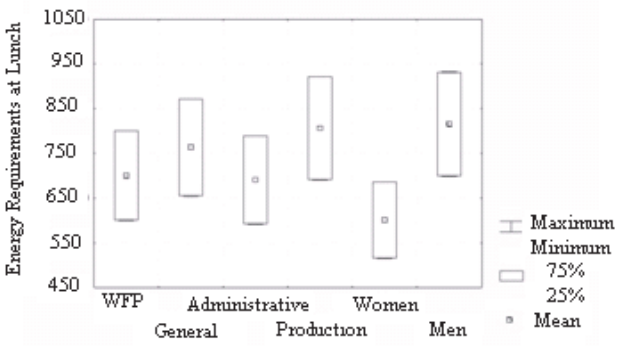

Figure 2. Energy content of lunch recommended by the Worker Food Program estimated by a study with factory workers.
Note: energy requirement in kcal; WFP: Worker Food Program [15].
Source: Bortolozo et al.

These differences can be considered in menu planning or by the educational approach directed at workers. Bauce [29] studied Venezuelan workers and established daily energy values for the main meal (lunch) by gender: 863.5 kcal for females and 1239.2 kcal for males. An energy intake that is in balance with one's energy requirement is a factor that promotes health and improves workers' performance in daily activities [16].

Table 4 presents the nutritional composition of lunch, taking into account the individual intake of the study sample.

Energy, protein, carbohydrate, and fiber intakes differed by gender and work sector ($p<0.05$), and were higher in males and production workers who had higher energy and lipid intakes. These differences may demonstrate some food intake adaptation based on individual requirements, even when the food services do not adapt the menus or the workers do not receive counseling.

Table 4.
Mean (standard deviation) food intake during lunch by a sample of factory workers.

Nutrients	Total	Women (n=68)	Men (n=224)	Adm. (n=87)	Prod. (n=205)
Energy (kcal)	776.13 (± 201)	644.02[a] (±164)	816.24[a] (±194)	672.36[b] (±191)	831.00[b] (±170)
Protein (g)	50.58 (±11)	45.08[a] (±13)	52.25[a] (±10)	47.32[b] (±11)	52.29[b] (±11)
Carbohydrate (g)	108.92 (±40)	85.51[a] (±27)	116.32[a] (±40)	87.89[b](±31)	120.03[b] (±39)
Total fat (g)	16.98 (±5.8)	16.51 (±6.3)	17.13 (±5.6)	16.97 (±6.2)	16.99 (±5.49)
Saturated fat (g)	5.37 (±2.3)	5.26 (±2.4)	5.41 (±2.2)	5.37 (±2.4)	5.38 (±2.14)
Fiber (g)	14.06 (±5.6)	10.76[a] (±4.9)	15.05[a] (±5.4)	11.27[b] (±5.2)	15.53[b] (±5.3)
Sodium (mg)	1689 (±540)	1625.73 (±606)	1707.83 (±531)	1670.54 (±570)	1698.32 (±536)

Note: Adm.: administrative workers; Prod.: production workers; [a] differed significantly by gender and [b] by work sector ($p<0.05$). Recommended values [15]: protein: 15-30g; total fat; 10-27g; saturated fat < 9g; fiber > 7.5g; sodium < 960mg.
Source: Bortolozo et al.

Likewise, the National Health and Nutrition Examination Survey (NHANES) found that adult male Americans have a higher energy intake, compared to females [32]. Other studies of adults reported similar findings [33,34].

Regarding nutrients, the carbohydrate, lipid, and saturated fat contents are within the WFP recommendations. However, the protein, fiber, and sodium contents exceed the recommended values. A positive fact about the food consumed at work was its high fiber content mainly due to the availability of three types of salad and fruit-based desserts at least three times a week. It is very important to ensure the intake of fruits and non-starchy vegetables at work, since adults usually consume few servings of these food groups in their regular diets [34]. In the case of proteins, the estimated values differed ($p<0.05$) from the values recommended for the main meal (15-20g) [15]. The main dish (meat), legumes, and dairy desserts contributed to a high protein intake.

The mean sodium intake was much higher than the recommended levels (<960 mg), especially because table salt was available for seasoning the salads. Excessive sodium intake is an important risk factor for chronic noncommunicable diseases (NCDs), especially high blood pressure [36]. Mishra & Mohanty [12] assessed the foods consumed at work by Asian Indian factory workers and found that their intakes of energy, protein, fat, some minerals, and some vitamins were too high.

Significant correlations ($p<0.01$) were found between body weight and BMI ($r = 0.84$), weight and DEE ($r = 0.52$), BMI and DEE ($r = 0.27$), energy and DEE ($r = 0.38$), and energy and fats ($r = 0.50$). All correlations were positive, indicating that an increase in one variable promotes an increase in the other variable.

Principal component analysis (PCA) was used on the data of 288 workers after outlier exclusion.

In PCA, two groups or relationships between the variables already contain much of the statistical information of the dataset. The first principal component (PC1) explained 44.96% of the total data variance, and PC2 explained 30.93%, totaling 75.89%. The results obtained from the loadings showed that the following factors contributed most to the separation in decreasing order of variance: for PC1, the differences observed in LPA (0.6372) and DEE (0.6826); for PC2, age (0.6395) and BMI (0.6688).

PCA showed that most individuals with high energy expenditure and high energy and fat intakes were males, many of whom were production workers. Hence, the influence of gender and type of work on energy intake and expenditure is confirmed, a finding also corroborated by Allman-Farinelli et al. [26]. Moreover, males also had the highest BMI and weights, regardless of their work sectors.

It is also important to acknowledge some limitations of the current study, which included, for example, the lack of control over some variables as exclusion criteria, such as body weight or nutritional status, because they were precisely the objects of analysis. Other variables such as race, age limit, different work shifts, and differences between companies were also ignored.

4. Conclusions

The current study investigated the energy content and nutrient composition of the main meal (lunch) consumed at

work, by associating these variables with the energy expenditure and anthropometric data of industrial workers.

The study results show a prevalence of overweight, especially in males regarding abdominal obesity, and that energy intake varies by gender and type of work.

The mean energy values of the meals provided by the studied companies met the estimated requirements. However, the energy content estimated for gender and work sector differ from the energy content recommended by the WFP.

The nutritional composition of the lunch consumed at work complies with the recommended values for carbohydrates, fats, and saturated fats. However, protein and sodium contents were high. Sodium intake was the main problem found for this meal as it far exceeded the recommended levels. The high availability of salads resulted in a high fiber content.

The study results provide valuable information for professionals who work in the workers' health field and intend to implement nutrition and physical activity programs that will not only impact the work environment but quality of life as a whole. For the food service managers, it was possible to confirm the importance of assessing the specific characteristics of the workers involved, taking into account the different energy requirements and nutritional statuses.

Other risk factors for chronic noncommunicable diseases, such as hypertension, should be investigated, considering the high sodium content of the meals provided by the studied companies. Analyzing the worker's behavior away from work to better understand free-time activities could better clarify the high incidence of overweight workers, including production workers. Investigation of the same variables in workers working night shifts and in companies not enrolled in the WFP could also constitute an important study focus.

Acknowledgments

The authors wish to thank to CAPES for the scholarship granted to one of the authors, in the scope of the Program *Doutorado Sanduiche* (Capes grantees – Protocol: 4284/14-3).

References

[1] Chau, J.Y., Van der Ploeg, H.P., Merom, D., Chey, T. and Bauman, A.E., Cross-sectional associations between occupational and leisure-time sitting, physical activity and obesity in working adults. Preventive medicine, 54(3), pp. 195-200, 2012.

[2] Cocker, K.A., De Bourdeaudhuij, I.M. and Cardon, G.M., The effect of a multi strategy workplace physical activity intervention promoting pedometer use and step count increase. Health Education Research, 25(4), pp. 608-619, 2010.

[3] Byers, T. and Sedjo, R.L., Does intentional weight loss reduce cancer risk? Diabetes, Obesity and Metabolism, 13(12), pp. 1063-1072, 2011.

[4] Thompson, D.L., The costs of obesity: What occupational health nurses need to know. AAOHN Journal: Official Journal of the American Association of Occupational Health Nurses, 55(7), pp. 265-270, 2007.

[5] Christensen, J., Faber, A., Ekner, D., Overgaard, K., Holtermann, A. and Sogaard, K., Diet, physical exercise and cognitive behavioral training as a combined workplace based intervention to reduce body weight and increase physical capacity in health care workers—A randomized controlled trial. BMC Public Health, 11(1), pp. 671-672, 2011.

[6] Linde, J.A., Nygaard, K.E., Mitchell, N.R., Maclehose, R.F., Harnack, L.J., Cousins, J.M. and Jeffery, R.W., Health Works: Results of a multi-component group-randomized worksite environmental intervention trial for weight gain prevention. International. Journal of Behavioral Nutrition and Physical Activity, 9(1), pp. 14-15, 2012.

[7] Janssen, I., Bacon, E. and Pickett, W., Obesity and its relationship with occupational injury in the canadian workforce. Journal of Obesity, 2011, pp. 1-6, 2011.

[8] Barringto, W.E., Ceballos, R.M.; Bishop, S.K., McGregor, B.A. and Beresford, S.A., Perceived stress, behavior, and body mass index among adults participating in a worksite obesity prevention program, Seattle, 2005–2007. Preventing Chronic Disease, 9, pp. 1-9, 2012.

[9] Maruyama, C., Kimura, M., Okumura, H., Hayashi, K. and Arao, T., Effect of a worksite-based intervention program on metabolic parameters in middle-aged male white-collar workers: a randomized controlled trial. Preventive Medicine, 51(1), pp. 11-17, 2010.

[10] Quinn, M.M., Occupational health, public health, worker health. American Journal of Public Health, 93(4), pp. 256, 2003.

[11] Kim, H.J., Hong, J.I., Mok, H.J. and Lee, K.M., Effect of workplace-visiting nutrition education on anthropometric and clinical measures in male workers. Clinical Nutrition Researches, 1, pp. 49-57, 2012.

[12] Mishra, B.K. and Mohanty, S., Dietary intake and nutritional anthropometry of the workers of INDAL, Hirakud. Anthropologist, 11(2), pp. 99-107, 2009.

[13] Tamers, S.L., Beresford, A.S., Cheadle, A.D., Zheng, Y., Bishop, S.K. and Thompson, B., The association between worksite social support, diet, physical activity and body mass index. Preventive Medicine, 53(1-2), pp. 53-56, 2011.

[14] Del Duca, G.F., Silva, K.S., Garcia, L.M.T., de Oliveira, E.S.A. and Hanhas, M.V., Clustering of unhealthy behaviors in a Brazilian population of industrial workers. Preventive Medicine, 54(3), pp. 254-258, 2012.

[15] Brasil. Portaria Interministerial [Online]. n. 66. 2006. Diário Oficial da República Federativa do Brasil. [date of reference November 20th, of 2013]. Available at: http://portal.mte.gov.br/data/files/FF8080812BCB2790012BD4ABD1F559C0/p_20060825_66.pdf

[16] Goris, A.H.C. and Westerter, K.R., Physical activity, fat intake and body fat. Physiology & Behavior, 94(23), pp. 164-168, 2008.

[17] Triola, M.F: Introdução à Estatística, Rio de Janeiro: LTC; 2008.

[18] Onis, M., Onyango, A.W., Van den Broeck, J., Chumlea, W.C. and Martorell, R., Growth reference study group measurement and standardization protocols for anthropometry used in the construction of a new international growth reference. Food Nutrition Bulletin, 25(1), s27-s36, 2000.

[19] World Health Organization. Obesity: Preventing and managing the global epidemic WHO Technical Report, [Online]. 2000. [date of reference November 20th of 2013]. Available at: http://www.who.int/nutrition/publications/obesity/WHO_TRS_894/en/.

[20] World Health Organization. Preventing chronic diseases: a vital investment Geneva, Ottawa: Public Health Agency of Canada, [Online]. 2005. [date of reference October 10th of 2012]. Available at: <http://www.who.int/chp/chronic_disease_report/en/.

[21] Koning, L., Merchant, A.T., Pogue, J. and Anand, S.S., Waist circumference and waist-to-hip ratio as predictors of cardiovascular events: meta-regression analysis of prospective studies. European Heart Journal, 28(7), pp. 850-856, 2007.

[22] World Health Organization. Human Energy requirements Food and Nutrition Technical Series. Report of a Joint, [Online]. 2001. [date of reference November 20th of 2013]. Available at: http://http://www.who.int/nutrition/publications/nutrientrequirements/9251052123/en/index.html.

[23] Volp, A.P., de Oliveira, F.E., Alves, R.D.M., Esteves, E.A. and Bressan, J., Energy expenditure: Components and evaluation methods. Nutrición Hospitalaria, 26(3), pp. 430-440, 2011.

[24] Tudor-Loke, C., Giles-Corti, B., Knuiman, M. and McCormack, G., Tracking of pedometer – determined physical activity - In adults WHO Relocate: Results from reside. International Journal of Behavioral Nutrition and Physical Activity, 5(1), pp. 5-39, 2008.

[25] Bauman, A., Bull, .F, Chey, T., Craig, C., Ainsworth, B.E., Sallis, J.F. and Pratt, M., The International prevalence study on physical activity: results from 20 countries. International Journal of Behavioral Nutrition and Physical Activity, *6*(21), pp. 1-11, 2009.

[26] Allman-Farinelli, M.A., Chey, T., Merom, D., and Bauman, A.E. Research occupational risk of overweight and obesity: an analysis of the

Australian Health Survey. Journal of Occupational Medicine Toxicology, 5(14), pp. 1-9, 2010.
[27] Snijder, M.B., Nicolaou, M., Valkengoed, I.G., Brewster, L.M. and Stronks, K., Newly proposed body adiposity index (bai) by Bergman et al. is not strongly related to cardiovascular health risk. Obesity, 20(6), pp. 1138-1139, 2012.
[28] Frankenfield, D.C, Rowe, W.A., Smith, J.S., Cooney, R.N., Validation of several established equations for resting metabolic rate in obese and nonobese people. Journal American Dietetic Association, 103(9), pp. 1152-1159, 2003.
[29] Bauce, G.J., Fórmula dietética institucional para trabajadores amparados por la Ley de Alimentación del Trabajador. Revista do Instituto Nacional de Higiene, 41(2), pp. 37-45, 2010.
[30] Escott-Stump, S., Mahan, K. and Raymond, J., Krause Alimentos, Nutrição e Dietoterapia. Rio de Janeiro: Elsevier, 2013.
[31] Dietary Reference Intakes for Energy, Carbohydrate, Fiber, Fat, Fatty Acids,Cholesterol, Protein, and Amino Acids [Online]. 2002. [Date of reference October 20th of 2013]. Available at: http//www.nap.edu.
[32] Ford, E.S. and Dietz, W.H., Trends in energy intake among adults in the United States: findings from NHANES. The American Journal of Clinical Nutrition, 97(4), pp. 848-853, 2013.
[33] Castetbon, K., Vernay, M., Malon, A., Salanave, B., Deschamps, V., Roudier, C. and Herceberg, S., Dietary intake, physical activity and nutritional status in adults: the French nutrition and health survey (ENNS, 2006–2007). British Journal of Nutrition, 102(5), pp. 733-743, 2009.
[34] Bortolozo, E., Pilatti, L.A., Canteri, M.H. and Arezes, P., Nutritional status and food intake at workplace as health indicators for industrial workers, Proceedings book of the International Symposium on Occupational and Hygiene – SHO2015, pp. 38-40, 2015.
[35] Artinian, N.T., Fletcher, G.F., Mozajjarian, D., Kris-Etherton, P., Van Horn, L., Lichtenstein, A.H., and Meininger, J.C., Interventions to promote physical activity and dietary lifestyle changes for cardiovascular risk factor reduction in adults: a scientific statement from the American Heart Association. Circulation, 122(4), pp. 406-441, 2010.
[36] Taylor, R.S., Ashton, K. ., Moxham, T., Hooper, L. and Ebrahim, S., Reduced dietary salt for the prevention of cardiovascular disease a meta-analysis of randomized controlled trials (Cochrane review). American Journal of Hypertension, 24(8), 2011.

E.Q. Bortolozo, is Dr. in Production Engineering at the Federal Technological University of Paraná, Brazil. She is a grantee of the Program Doutorado Sanduiche / University of Minho – Portugal. She is also a professor at the Federal Technological University of Paraná and has experience in the areas of food science and technology, health, and quality of life.
ORCDI: 0000-0002-6926-8852.

L.A. Pilatti, - is Dr. in Physical Education completed at the State University of Campinas (UNICAMP), Brazil. He is full professor at the Federal Technological University of Paraná (UTFPR), Brasil. He is involved with the graduate programs in production engineering (PPGEP) and teaching of science and technology (PPGECT) at the Campus Ponta Grossa.
ORCDI: 0000-0003-2679-9191.

M.H. Canteri, is Dr. in Food Technology at the Federal University of Paraná, and in Agricultural Sciences at the University of Avignon et Pays de Vaucluse. She is a professor at the Federal Technological University of Paraná, Brazil. She collaborates with the master's program in food science and technology and is a tenured professor of the graduate program in production engineering (Quality of Life and Agroindustrial Innovation).
ORCDI: 0000-0003-2800-4006.

P. Arezes, has a PhD. in Industrial and Systems Engineering completed at UMinho, in Portugal, and he is currently a full professor in Ergonomics and Human Factors at the same university. He is also a visiting fellow at MIT's AgeLab in the USA. He leads the Human Engineering research group and he is the coordinator at UMinho of the Engineering Design and Advanced Manufacturing (EDAM) area of the MIT Portugal Program, and the chair of the steering board of the PhD program "Leaders for Technical Industries (LTI)" at UMinho.
ORCDI: 0000-0001-9421-9123.

UNIVERSIDAD NACIONAL DE COLOMBIA
SEDE MEDELLÍN
FACULTAD DE MINAS

Área Curricular de Ingeniería Administrativa e Ingeniería Industrial

Oferta de Posgrados

Especialización en Gestión Empresarial
Especialización en Ingeniería Financiera
Maestría en Ingeniería Administrativa
Maestría en Ingeniería Industrial
Doctorado en Ingeniería - Industria y Organizaciones

Mayor información:

E-mail: acia_med@unal.edu.co
Teléfono: (57-4) 425 52 02

UNIVERSIDAD NACIONAL DE COLOMBIA
SEDE MEDELLÍN
FACULTAD DE MINAS

DYNA
http://dyna.medellin.unal.edu.co/

Study of a repair technique in carbonated blended mortars: Electrochemical re-alkalization

Ana María Aguirre [a] Ruby Mejía-de Gutiérrez [b] Jean Paul Restucci [c] & Alexander Alvarado [d]

[a] *Escuela Ingeniería de Materiales, Universidad del Valle, Cali, Colombia. ana.aguirre@correounivalle.edu.co*
[b] *Escuela Ingeniería de Materiales, Universidad del Valle, Cali, Colombia. ruby.mejía@correounivalle.edu.co*
[c] *Escuela Ingeniería de Materiales, Universidad del Valle, Cali, Colombia. jeanpaulrestucci@gmail.com*
[d] *Escuela Ingeniería de Materiales, Universidad del Valle, Cali, Colombia. alexalvarbueno@gmail.com*

Received: February 18th, 2015. Received in revised form: December 15th, 2015. Accepted: February 10th, 2016.

Abstract
The present article studies the influence of two pozzolanic additions, metakaolin (MK) and silica fume (SF), and the water/binder ratio (w/b) on the electrochemical re-alkalization (ER) of reinforced mortars as a technique to prevent reinforcement corrosion in carbonated concrete. Mixtures with a 10% (by weight) addition as a replacement for cement at w/b ratios of 0.45 and 0.65 were prepared. Test specimens were exposed to carbonation in a chamber under controlled conditions (1% CO_2, 65%RH, and 25°C), until reaching two levels of carbonation (50% and 100%). ER was applied for a period of 15 days using sodium carbonate as the electrolyte and a current density of 1 A/m^2. From the evaluated additions, MK is highlighted, which generated a resistance increase of 53.51% relative to that of the reference mixture and contributes to improvements of durability properties. Regarding the ER technique, the specimens with greater w/b ratios and partial carbonation were more effective.

Keywords: Carbonation, Electrochemical Re-alkalization, Blended Mortars, Silica Fume, Metakaolin

Estudio de una técnica de reparación aplicada a morteros adicionados carbonatados: Realcalinización electroquímica

Resumen
En este artículo se estudia la influencia de dos adiciones puzolánicas, metacaolin (MK) y humo de sílice (HS), y la relación agua/cementante (a/C) en el proceso de realcalinización electroquímica (RE) de morteros reforzados como método de prevención de la corrosión en concretos carbonatados. Especímenes con un 10% en peso como reemplazo del cemento de MK o HS y relaciones a/C de 0.45 y 0.65 se expusieron a condiciones climáticas controladas (1% CO2, 65%HR y 25°C), hasta alcanzar dos niveles diferentes de carbonatación (50% y 100%). Se aplicó RE por 15 días con una densidad de corriente de 1 A/m2 utilizando como electrolito carbonato de sodio. Los especímenes adicionados con MK y relación a/c 0.45 presentaron un incremento notable en la resistencia a compresión (53.51%) y mejores propiedades de durabilidad. Respecto a la técnica RE, los especímenes con mayores relaciones a/c y carbonatación parcial presentan una mayor efectividad.

Palabras clave: Carbonatación, Realcalinización Electroquímica, Morteros adicionados, Humo de sílice, Metacaolín

1. Introduction

Since the last decade, concrete has become the most important material in the construction field worldwide, reaching a production of approximately 1.5 to 3 tons per capita per year in the industrialized world [1]. Concrete is a ceramic material that can withstand a wide range of compressive stress. However, concrete is susceptible to cracking against other types of mechanical stresses, such as bending, traction, shear, etc. To improve its mechanical properties, reinforced concrete can be used, which is a composite material obtained from combining concrete and reinforcing steel. Reinforced concrete is widely used in the construction of buildings, bridges, tunnels, and skyscrapers [2].

Although this material is considered durable, after a certain period of time, it suffers from deterioration primarily

© The author; licensee Universidad Nacional de Colombia.

caused by environmental agents and service conditions, which in addition to the loss of concrete durability, contribute to the corrosion of the reinforcing steel [2,3].

Concrete is an alkaline material with a pH between 12.6 and 13.6. Under these pH conditions, steel spontaneously forms a protective passive layer. However, the latter can be destroyed by aggressive agents (chloride ions and/or carbon dioxide), thus causing its depassivation. Specifically, carbonation is a process where atmospheric CO_2 enters into the concrete and decreases its alkalinity by reducing the pH to approximately 9, and consequently, the passive layer is destabilized, which allows corrosion of the reinforcing steel to occur [2-4]. The CO_2 penetration rate depends on environmental factors and on factors related to the concrete itself; therefore, it can occur in urban and industrial environments. Relative humidity is an important environmental factor, which ranges between 50 and 70% because the diffusion of CO_2 does not occur in completely dry concretes nor in fully saturated concretes. A temperature increase can also accelerate this phenomenon. Another crucial parameter is the CO_2 concentration, which in urban environments, can reach values of approximately 0.1%. Factors associated with concrete that contribute to CO_2 propagation include an inadequate curing process, poor compaction, and high w/b ratios that generate more permeable concretes [2].

The concretes durability standards [5-7] specify the types of exposures under which a structure can be affected by carbonation-induced corrosion during its service life. These standards specify the conditions of high humidity, medium humidity, or wetting-drying cycles. There are a variety of ways to prevent concrete deterioration, such as the design of the material and control of the construction process. The incorporation of additions (pozzolanic or steel related) into concrete, such as metakaolin (MK) and silica fume (SF), which modify porosity and reduce permeability, have been studied to evaluate the resistance to CO_2 diffusion; however, the results have been controversial because in general, blended concretes are more susceptible to carbonation than non-blended concretes, and therefore, a more demanding curing process is required for the pozzolanic reactions to reach their development [2,8-12].

Other alternative methods include rehabilitation electrochemical techniques, such as electrochemical re-alkalization (ER) and cathodic protection, which can be applied to in-service concretes. These two techniques are based on the application of a cathodic current; for re-alkalization, the current is temporary, whereas for cathodic protection, it is permanent [13]. During the electrochemical re-alkalization process, a direct current of 1-2 A/m^2 is applied with respect to the steel surface (cathode), and an electrochemical cell is formed with an auxiliary anode; sodium carbonate is generally used as an alkaline electrolyte, and its duration lasts between 3 to 21 days [13,14]. During the treatment process, electrochemical reactions are generated on the cathode surface, producing hydroxyl ions, and therefore, the pH in the surroundings of the reinforcing steel increases. Simultaneously, the alkaline electrolyte enters into the concrete interior, which increases the pH from the surface towards the interior and acts as a collector of the carbon dioxide present in the cementitious matrix [15]. This technique was developed at the end of the 1980s by John Miller in Norway, was patented by NORCURE ® and is primarily used in Northern Europe [14,16]. Regarding the technique efficiency, Yeih & Chang [15] reported that this treatment increases the pH values around the reinforcing steel (to approximately 11) despite the compressive resistance, elastic modulus, and adherence to the concrete decreasing linearly as the passing current and time increase. Ribeiro et al. [17] performed studies with pozzolanic cements, from where it was concluded that these cements require a greater passing charge density and longer treatment time to re-alkalize the entire structure. Corrêa de Araújo [18] evaluated the use of different electrolytes, such as calcium hydroxide, potassium hydroxide, and sodium carbonate, which determined that the latter two are efficient in both the structure repassivation and its re-alkalization. González et al. [19] proposed the use of potassium carbonate to maintain a more alkaline medium in the anodic region, which takes advantage of the conductive and mobility character of K+ to allow for a lower applied voltage necessary for current circulation. Tong et al. [20] demonstrated the increase of the pH around the rods after one year of application and corroborated the decrease of the corrosion activity, though the authors could not verify the repassivation of the steel rods. Bertolini et al. [16] mentioned that the application of the technique presents several potential secondary effects, such as hydrogen embrittlement, alkali-aggregate reaction, and loss of adherence, and claim that an extremely elevated current density can affect the concrete microstructure.

As shown by different published studies, ER is an effective method to solve the problem of carbonated concretes aimed at extending their useful life [15,17,19-23]. However, several authors claim that steel repassivation is not achieved, and thus, it is suggested that the technique should be used as a prevention method, i.e., before corrosion reaches the reinforcing steel [20,24].

The present research determines the susceptibility to carbonation of Portland cement mortars with and without the addition of MK and SF at a 10% proportion and evaluates the application of the electrochemical re-alkalization (ER) technique as a method to prevent corrosion of the steel embedded in specimens carbonated at different CO_2 penetration levels.

2. Experimental Procedure

2.1. Materials

Ordinary Portland cement (OPC) and two pozzolanic additions, MK and SF, were used to produce the mortars. A cement replacement percentage of 10% was chosen for each of the additions, which accounts for the results of previous investigations [2,25-27]. The chemical characterization of these materials, which was determined by X-ray fluorescence (XRF), is presented in Table 1. It should be noted that the OPC corresponds to commercial cement blended with limestone.

Table 1.
Chemical composition of the MK,SF, and cement (OPC) used.

Material	LOI[a]	SiO_2 (%)	Fe_2O_3 (%)	Al_2O_3 (%)	CaO (%)	MgO (%)	SO_3 (%)
OPC	8.57	21.26	4.43	5.52	54.38	4.46	1.85
MK	1.10	49.55	0.39	47.14	0.17	1.21	0.0
SF	1.95	93.85	1.32	2.40	0.0	0.0	0.0

[a]LOI: Loss on ignition at 1000 °C.
Source: The authors

2.2. Specimen Preparation

In the present work, mortars of Portland cement (OPC) were prepared using a cement:sand proportion of 1:2.75 with two different water/binder (w/b) ratios of 0.45 and 0.65. Six different mixtures were produced: two reference OPC specimens (OPC45 and OPC65) and four specimens corresponding to the specimens with a replacement of 10% for each addition and their respective w/b ratios (MK45, MK65, SF45, and SF65). A corrugated steel rod with a diameter of 6 mm was placed in the center of several specimens. The first specimens without steel were used to evaluate the mechanical properties and durability and to monitor the carbonation process, and the specimens with steel were used for electrochemical monitoring (Fig. 1).

2.3. Testing techniques

The following properties were tested in the simple mortars: compressive strength, capillary suction [28], and electrical resistivity [29]. Tests were performed on the specimens after 28 days of curing. The carbonation test was performed on specimens with and without reinforcing steel at a curing age of 28 days inside a climatic chamber under controlled conditions of CO_2 concentration (1%), relative humidity (65%), and temperature (25°C). The carbonation front was monitored through the cross-sections of the mortars removed from the chamber at different ages and the subsequent spraying of the surface with a 1% phenolphthalein aqueous solution using the pH as the developer. Based on the results, the exposure time in the chamber was determined to obtain the carbonation levels in the reinforced specimens, a partial level (50%) and a complete level (100%). Subsequently, the rehabilitation technique was applied (re-alkalization) to each of the specimens. For the steel corrosion study, the linear polarization resistance technique was applied, Rp [30]; this test was performed using Potentiostat/Galvanostat GAMRY PC14 equipment at 0.167 mV/s with applied overpotentials of -20 to +20 mV; Ag/AgCl was used as the reference electrode material. The calculation of the corrosion current was performed by the Stern-Geary equation (1).

$$Icorr = \frac{B}{Rp} \quad (1)$$

where B is a constant that depends on the Tafel slopes, whose estimated value is 26 mV or 52 mV depending on the active or passive state of the steel, respectively. In this study, the value of B used was 0.026 V, which stimulates the corrosion active condition [31,32].

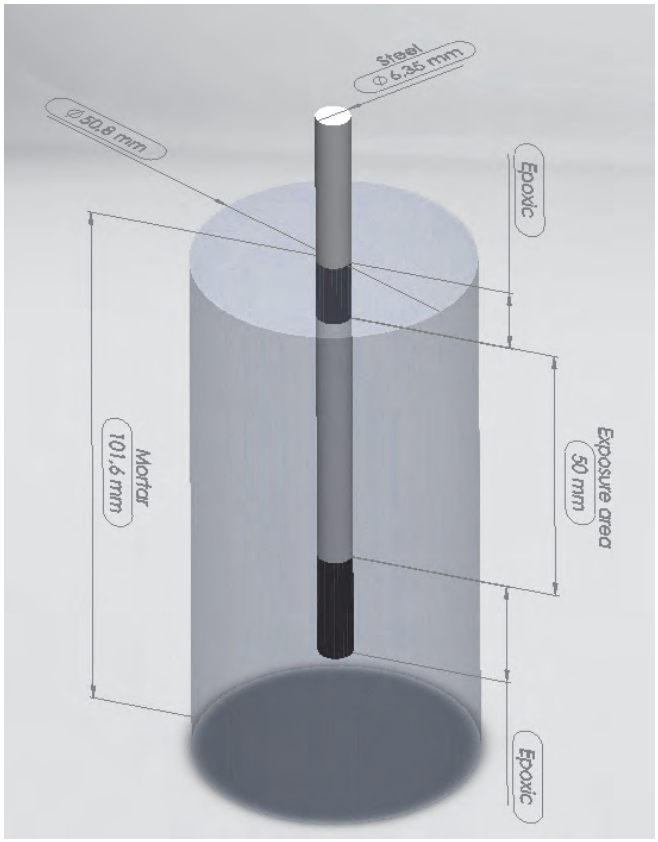

Figure 1. Design of the test sample.
Source: The authors

2.4. Electrochemical Re-alkalization (ER)

The ER process was implemented according to the NACE *Standard Practice SP0107-2007* [33], for which the following components were used: external anode, galvanized steel mesh; alkaline electrolyte, sodium carbonate Na_2CO_3 at 1 M; cellulose pulp placed between the external anode and the concrete surface; and current source. For this study, a current density of 1 A/m^2 was applied for 15 days, which corresponds to the current density used by different researchers [15,19,21,23]. Regarding the assembly, the external anode is fixed on the concrete surface, which is embedded in the alkaline electrolyte and is connected to the positive pole of the source, and the reinforcing steel is connected to the negative pole of the source. For this study, several specimens were connected to a single source; therefore, a parallel connection was set for each of them. To ensure the passage of the selected current density, a variable resistance of 1 kΩ was used to adjust the current passing through each specimen, and a resistance of 1 Ω was used to monitor the potential difference between the anode and the cathode. Therefore, the current can be verified by means of Ohm's law (Figs. 2 and 3).

Once the ER process ended, the verification of the re-alkalized front in the concrete was performed by applying the phenolphthalein indicator, and the electrochemical monitoring of the corrosion state in the steel was performed using Rp.

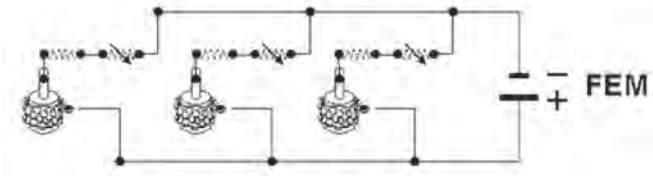

Figure 2. Schematic assembly of the experiment.
Source: The authors

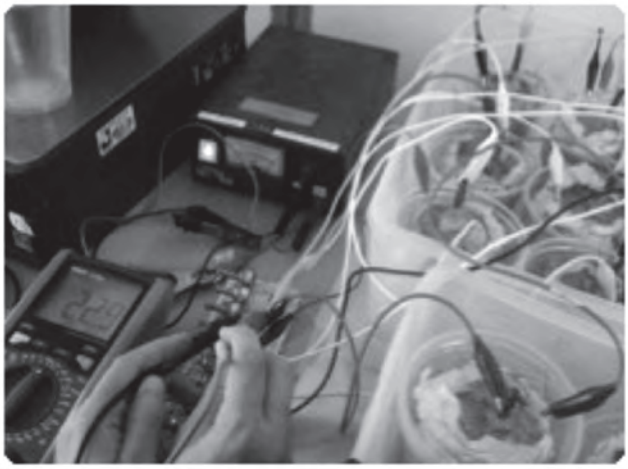

Figure 3. Monitoring during the re-alkalization
Source: The authors

3. Results and discussion

3.1. Mechanical properties

Fig. 4 shows the compressive strength of the specimens at a curing age of 28 days for the two tested w/b ratios (0.45 and 0.65). The figure shows that the increment in the w/b ratio affects the mortar mechanical properties [34] as expected. In general terms, it is also observed that the blended mortars exhibited a greater resistance. It should be noted that in the specimens with an addition of SF at a w/b ratio of 0.65, the SF particles agglomerated, a phenomenon to which the lower resistance is attributed. The resistance reported by the test samples blended with MK after 28 days of curing should be highlighted, which represents a 53.51% difference with respect to the reported value of OPC at the same w/b ratio of 0.45.

3.2. Capillary absorption

Table 2 shows the capillary absorption coefficients K ($Kg/m^2s^{1/2}$) and the resistance to water penetration m (s/m^2). The values show that the addition of pozzolanic materials reduces the capillary absorption coefficient (K_{SUC}) and increases the resistance to water penetration (m). The w/b ratio behaves in the opposite manner. The greatest increase of m is observed with the addition of MK, which is a 32.5% and 125% difference with respect to OPC for w/b ratios of 0.45 and 0.65, respectively. These results agree with what has been found by different researchers and with reported compressive strengths [25,35,36].

3.3. Electrical Resistivity

The electrical resistivity of the specimens was determined using the four-point method, also called the Wenner method, for which the resistivity meter, *Resipod Proceq*, was used with a distance of 38 mm between the points. Specimens with dimensions of 7.65 cm × 15.24 cm were used. Fig. 5 shows the electrical resistivity values, which indicate that the blended specimens presented a greater electrical resistivity with respect to OPC. Noticeably, this property is increased as the w/b ratio decreases. The greatest resistivity is reported for the OPC+MK specimens with a resistivity increase of 1.93 and 2.00 times that of OPC for w/b ratios of 0.45 and 0.65, respectively. This behavior has been reported in previous investigations by a variety of authors [37-39].

3.4. Carbonation front

Fig. 6 shows the carbonation depth temporal behavior for the different concrete specimens during the exposure period of accelerated carbonation. According to the dimensions of the test samples, partial carbonation (50%) is reached at a carbonation front of 12.7 mm, whereas total carbonation is reached at 25.4 mm. From the figure, it is observed that, in general, the mixtures with a w/b content of 0.65 reach the carbonation level in less time; the effect of the w/b ratio increase was more critical for the non-blended mixture. From the evaluated additions, the better performance of MK is highlighted. In this case, under the test conditions (CO_2 1%, RH 65%, 25°C), a carbonation depth of 50% was obtained

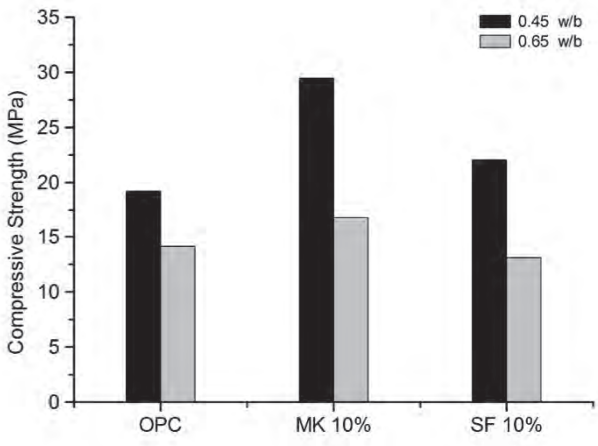

Figure 4. Compressive strength of the specimens
Source: The authors.

Table 2.
Parameters of capillary absorption.

Specimen	w/b ratio	K_{SUC} ($Kg/m^2s^{1/2}$)	m (10^7 s/m^2)
OPC	0.45	0.053	3.20
	0.65	0.210	0.39
MK 10%	0.45	0.044	4.24
	0.65	0.135	0.88
SF 10%	0.45	0.046	3.58
	0.65	0.143	0.80

Source: The authors

after 77 and 93 hours for the mixtures with w/b ratios of 0.65 and 0.45, respectively, and a complete carbonation of the specimen occurred after approximately 235 hours with values that exceeded up to 80% more than those that were obtained with SF. For the mixtures blended with SF, an increment in the carbonation depth is observed with respect to OPC.

3.5. Electrochemical Re-alkalization

As was previously mentioned, the ER technique was applied to specimens with two carbonation levels, partial (50%) and complete (100%). The exposure times in the climatic chamber were obtained from the data in Fig. 6. The re-alkalization process efficiency was evaluated by the phenolphthalein test and the determined linear polarization resistance.

Fig. 7 shows the specimens before and after ER. A magenta coloration can be observed after the ER treatment, which is indicative of non-carbonated regions in regions that were previously colorless and is where the pH increase is deduced

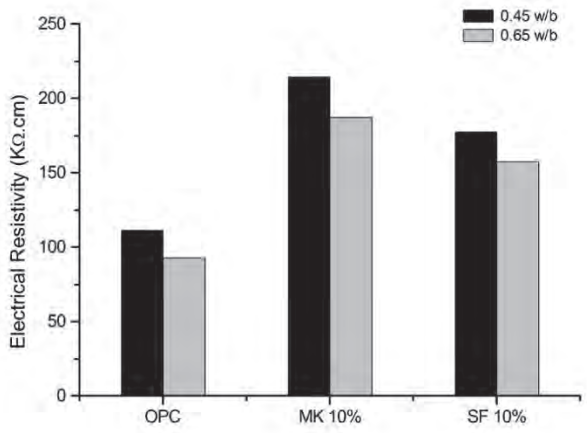

Figure 5. Electrical resistivity of the mortars
Source: The authors

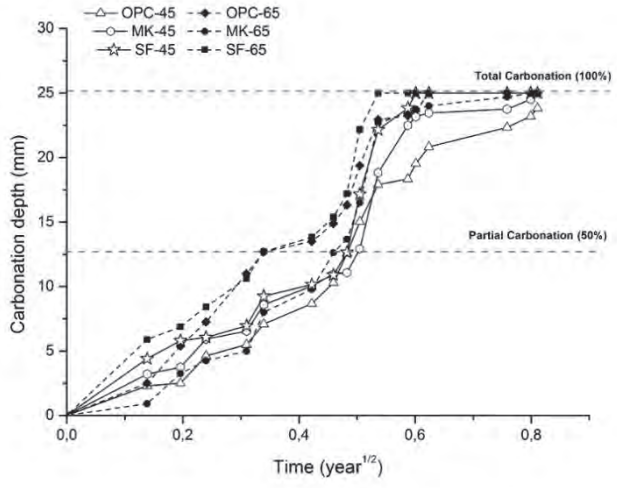

Figure 6. Carbonation depth of the specimens exposed to accelerated carbonation (1% CO2, 65% RH, 25°C)
Source: The authors

in the specimens for both carbonation levels (50 and 100%). It should be noted that the violet coloration occurs more in the central part of the specimen surrounding the reinforcing steel, which coincides with the results presented by Redaelli & Bertolini [23]. It is also observed that in the case of partial carbonation, the re-alkalization front is superior compared to that of the complete carbonation level.

The corrosion current (Icorr) was determined by the linear polarization technique, Rp, in the carbonated specimens after reaching the proposed carbonation levels (partial and complete) and in the specimens after applying ER using a depolarization time (TP) of 15 days. The corresponding results are shown in Fig. 7. Abdelaziz, Abdelalim and Fawzy [40] suggested that to obtain reliable electrochemical measurements after applying the rehabilitation electrochemical methods, it is important to give a TP because immediately after the system is disconnected, the reinforcing steel is polarized due to the electrical field generated by the treatment. In general, it is observed that the corrosion rate decreases after applying ER; however, the efficiency is superior at a greater w/b ratio. Thus, for partial carbonation, the reduction in the corrosion rate of the MK0.65 mixture is 82.5%, followed by OPC0.65 with 42.6%, and finally by SF with 16.6%. This effect is attributed to the decrease in the ohmic resistance with an increasing w/b ratio [17]. Notably, the specimens blended with MK decreased until reaching a low corrosion level after ER (Fig. 8). The specimens with the addition of SF did not present satisfactory results, which may indicate the need to increase the treatment time [17].

For complete carbonation, a greater percentage decrease of *Icorr* was observed for OPC0.65 at 59%, followed by MK0.65 at 47%, and finally SF0.65 at 27.6%. However, none of the specimens reached a low corrosion level. This result coincides with that mentioned by Miranda et al. [24], who suggested that at elevated carbonation levels, the application of ER may not be efficient; therefore, the authors recommended using this technique as a prevention method, i.e., before corrosion reaches the reinforcing steel.

4. Conclusions

According to the results obtained in the present study, the following can be concluded:

- Amongst the used additions, MK significantly influenced concrete performance when used as a cement replacement at an addition of 10% by weight. MK positively contributes to the resistance increment in orders of up to 53.5% at a w/b ratio of 0.45. Likewise, positive effects were observed when the absorption greatly decreases and the resistivity of the mixture increases.
- The mixtures blended with MK and exposed to equal conditions of CO2, RH%, and temperature require more time to carbonate compared with the mixtures with SF and OPC. Increases in the w/b ratio accelerate the process.
- Based on the electrochemical results obtained by the linear polarization resistance technique, it became evident that the application of ER generates a positive variation in the measurements of icorr. Thus, the test samples are partially carbonated with values of icorr in the range of 0.72–1.59 μA/cm2; after ER is applied, the values range from 0.2–1.02

μA/cm2. In the specimens with complete carbonation, the icorr decreased from 1.03-2.63 μA/cm2 to 0.7–1.66 μA/cm2; however, even though these values are reduced, most of the values are within the moderate corrosion region.

- The electrochemical re-alkalization (ER) processes were more effective for the partially carbonated specimens, and among these, the specimens blended with MK and with greater contents of the w/b ratio reached low corrosion levels by the end of the process.
- ER is a prevention technique more than a rehabilitation technique, as evidenced in its greater efficiency for test samples with a partial carbonation level. The application of ER increases the useful life of steel in the presence of carbonated mortars.

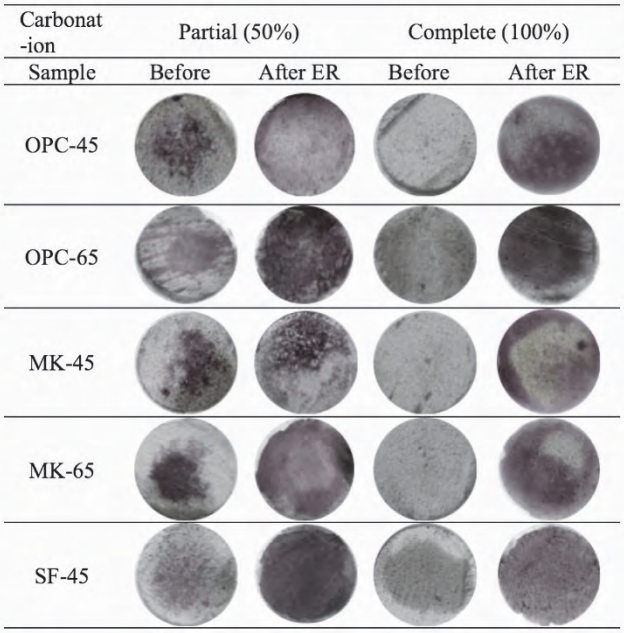

Figure 7. Evolution of the partial/complete carbonation front before and after ER.
Source: The authors

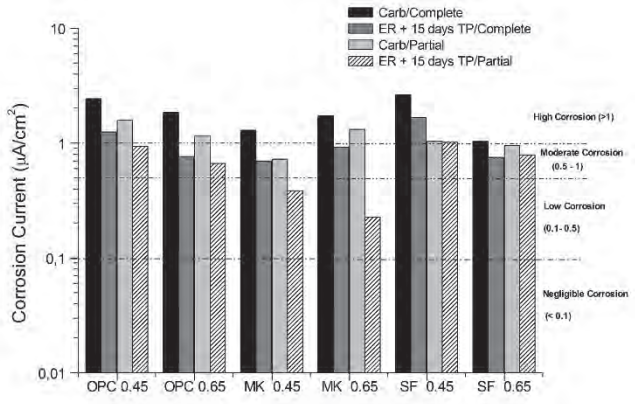

Figure 8. Corrosion current of the mortars subjected to complete carbonation (Carb/Complete), partial carbonation (Carb/Partial) after the ER treatment plus 15 days of TP for the partial and complete levels (ER + 15 days TP/Complete, ER + 15 days TP/Partial).
Source: The authors

Acknowledgements

The authors wish to thank the Universidad del Valle (Cali, Colombia), the Center of Excellence in New Materials (CENM), and Colciencias for providing their support for the development of the present study.

References

[1] Glavind, M., Sustainability of cement, concrete and cement replacement materials in construction, in Sustainability of Construction Materials, Woodhead Publishing, Cambridge, UK, 2009. DOI: 10.1533/9781845695842.120

[2] Aguirre, A.M. and Mejía-de Gutiérrez, R., Durability of reinforced concrete exposed to aggressive conditions. Materiales de Construcción, 63(309), pp. 7-38, 2013. DOI: 10.3989/mc.2013.00313

[3] Baccay, M.A., Otsuki, N., Nishida, T. and Maruyama, S., Influence of cement type and temperature on the rate of corrosion of steel in concrete exposed to carbonation. Corrosion, 62(9), pp. 811-821, 2006. DOI: 10.5006/1.3278306

[4] Han, S.-H., Park, W.-S. and Yang, E.-I., Evaluation of concrete durability due to carbonation in harbor concrete structures. Construction and Building Materials, 48(0), pp. 1045-1049, 2013. DOI: 10.1016/j.conbuildmat.2013.07.057

[5] ACI201 Guide to Durable Concrete. 2001.

[6] EN206-1 Hormigón - Parte 1: Especificación, comportamiento, fabricación y conformidad. 2008.

[7] NTC5551 Durabilidad de Estructuras de Concreto. 2007.

[8] Kim, H.-S., Lee, S.-H. and Moon, H.-Y., Strength properties and durability aspects of high strength concrete using Korean metakaolin. Construction and Building Materials, 21(6), pp. 1229-1237, 2007. DOI: 10.1016/j.conbuildmat.2006.05.007

[9] Kulakowski, M.P., Pereira, F.M. and Molin, D.C.C.D., Carbonation-induced reinforcement corrosion in silica fume concrete. Construction and Building Materials, 23(3), pp. 1189-1195, 2009. DOI: 10.1016/j.conbuildmat.2008.08.005

[10] San Nicolas, R., Cyr, M. and Escadeillas, G., Performance-based approach to durability of concrete containing flash-calcined metakaolin as cement replacement. Construction and Building Materials, 55(0), pp. 313-322, 2014. DOI: 10.1016/j.conbuildmat.2014.01.063

[11] Lizarazo-Marriaga, J. and López-Yépez, L., Effect of silica fume addition on the chloride-related transport properties of high-performance concrete. DYNA, 79(171), pp. 105-110, 2012.

[12] Restrepo, J.C., Restrepo, O.J. y Tobón, J.I., Efectos de la adición de metacaolín en el cemento. DYNA, 73(150), pp. 131-141, 2006.

[13] Bertolini, L., Elsener, B., Pedeferri, P. and Polder, P., Corrosion of steel in concrete: Prevention, diagnosis, repair. Weinheim:Wiley-VCH Verlag GmbH & Co. KGaA, 2004.

[14] Mietz, J., Electrochemical realkalisation for rehabilitation of reinforced concrete structures. Materials and Corrosion, 46(9), pp. 527-533, 1995. DOI: 10.1002/maco.19950460904

[15] Yeih, W. and Chang, J.J., A study on the efficiency of electrochemical realkalisation of carbonated concrete. Construction and Building Materials, 19(7), pp. 516-524, 2005. DOI: 10.1016/j.conbuildmat.2005.01.006

[16] Bertolini, L., Bolzoni, F., Elsener, B., Pedeferri, P. y Andrade, C., La realcalinización y la extracción electroquímica de los cloruros en las construcciones de hormigón armado. Materiales de Construcción, 46(244), pp. 45-55, 1996.

[17] Ribeiro, P.H.L.C., Meira, G.R., Ferreira, P.R.R. and Perazzo, N., Electrochemical realkalisation of carbonated concretes – Influence of material characteristics and thickness of concrete reinforcement cover. Construction and Building Materials, 40(0), pp. 280-290, 2013.

[18] Corrêa-de Araújo, W., Estudo da repassivação da armadura em concretos carbonatados através da técnica de realcalinização química, PhD Thesis, Universidade de São Paulo, São Paulo, Brazil, 2009.

[19] González, F., Fajardo, G., Arliguie, G., Juárez, C.A. and Escadeillas, G., Electrochemical realkalisation of carbonated concrete: An alternative approach to prevention of reinforcing steel corrosion.

International Journal of Electrochemical Science, 6, pp. 6332-6349, 2011.
[20] Tong, Y., Bouteiller, V., Marie-Victoire, E. and Joiret, S., Efficiency investigations of electrochemical realkalisation treatment applied to carbonated reinforced concrete — Part 1: Sacrificial anode process. Cement and Concrete Research, 42(1), pp. 84-94, 2012.
[21] Bertolini, L., Carsana, M. and Redaelli, E., Conservation of historical reinforced concrete structures damaged by carbonation induced corrosion by means of electrochemical realkalisation. Journal of Cultural Heritage, 9(4), pp. 376-385, 2008.
[22] Carvajal, A M., Acuña, A., Acuña, F., Herrera, A. y Vera, R., Estudio sobre un método de recuperación de hormigones carbonatados: proceso de realcalinización. Revista de la Construcción, 4(1), pp. 35-40, 2005.
[23] Redaelli, E. and Bertolini, L., Electrochemical repair techniques in carbonated concrete. Part I: Electrochemical realkalisation. Journal of Applied Electrochemistry, 41(7), pp. 817-827, 2011.
[24] Miranda, J.M., González, J.A., Cobo, A. and Otero, E., Several questions about electrochemical rehabilitation methods for reinforced concrete structures. Corrosion Science, 48(8), pp. 2172-2188, 2006.
[25] Mejía-de Gutiérrez, R., Rodríguez, C., Rodríguez, E., Torres, J. y Delvasto, S., Concreto adicionado con metacaolín: Comportamiento a carbonatación y cloruros. Revista Facultad de Ingeniería Universidad de Antioquia, 48(pp. 55-64, 2009.
[26] Siddique, R. and Klaus, J., Influence of metakaolin on the properties of mortar and concrete: A review. Applied Clay Science, 43(3-4), pp. 392-400, 2009.
[27] Valipour, M., Pargar, F., Shekarchi, M. and Khani, S., Comparing a natural pozzolan, zeolite, to metakaolin and silica fume in terms of their effect on the durability characteristics of concrete: A laboratory study. Construction and Building Materials, 41(0), pp. 879-888, 2013.
[28] ASTMC1585-13 Standard Test Method for Measurement of Rate of Absorption of water by Hydraulic-Cement Concretes. 2013.
[29] UNE83988-2 Determinación de la resistividad eléctrica. Parte 2: Método de las cuatro puntas o de Wenner. España, pp. 2008.
[30] ASTMG59-97 Standard Test Method for Conducting Potentiodynamic Polarization Resistance Measurements. 2014.
[31] Andrade, C. and González, J.A., Quantitative measurements of corrosion measurements. Werkstoffe und Korrosion, 29, pp. 515-519, 1978.
[32] Andrade, C. and Alonso, C., Corrosion rate monitoring in the laboratory and on-site. Construction and Building Materials, 10(5), pp. 315-328, 1996.
[33] NACESP0107-2007 Standard Practice Electrochemical Realkalization and Chloride Extraction for Reinforced Concrete. 2007.
[34] Poon, C.S., Kou, S.C. and Lam, L., Compressive strength, chloride diffusivity and pore structure of high performance metakaolin and silica fume concrete. Construction and Building Materials, 20(10), pp. 858-865, 2006.
[35] Torres-Agredo, J., Mejía-de-Gutiérrez, R. y Delvasto-Arjona, S., Efecto del porcentaje de adición de metacaolín en las propiedades finales del concreto adicionado. Ing. Univ., 15(1), pp. 77-90, 2010.
[36] Torres-Agredo, J. y Mejía-de-Gutiérrez, R. Influencia de la composición mineralógica de los caolines sobre el desempeño de morteros adicionados con MK. DYNA, 74(153), pp. 61-67, 2007.
[37] Ramezanianpour, A.A., Pilvar, A., Mahdikhani, M. and Moodi, F., Practical evaluation of relationship between concrete resistivity, water penetration, rapid chloride penetration and compressive strength. Construction and Building Materials, 25(5), pp. 2472-2479, 2011.
[38] Ramezanianpour, A.A. and Bahrami-Jovein, H., Influence of metakaolin as supplementary cementing material on strength and durability of concretes. Construction and Building Materials, 30(0), pp. 470-479, 2012.
[39] Parande, A.K., Ramesh-Babu, B., Aswin-Karthik, M., Deepak-Kumaar, K.K. and Palaniswamy, N., Study on strength and corrosion performance for steel embedded in metakaolin blended concrete/mortar. Construction and Building Materials, 22(3), pp. 127-134, 2008. DOI: 10.1016/j.conbuildmat.2006.10.003
[40] Abdelaziz, G.E., Abdelalim, A.M.K. and Fawzy, Y.A., Evaluation of the short and long-term efficiencies of electro-chemical chloride extraction. Cement and Concrete Research, 39(8), pp. 727-732, 2009.

A.M. Aguirre, received a BSc degree in Electronic Engineering in 2007, from Pontificia Universidad Javeriana Cali, Colombia, she is currently a PhD student at Universidad del Valle, Colombia. Her research interests include corrosion protection of concrete structures, mineral additions, coatings, geopolymers and alkaline activation of by-products and minerals.
ORCID: 0000-0001-9986-6557

R. Mejia-de Gutiérrez, received a BSc. in Chemistry in 1972and MSc in 1986 from Universidad del Valle, Colombia, and her PhD degree was obtained in 1997 from Universidad Complutense, Madrid, Spain. Currently, she is a professor in the Engineering Materials School, Universidad del Valle, Cali, Colombia. She is coordinator of the Master's and Doctoral programs focus area of Materials Engineering. Senior researcher and director of the research group Composite Materials – GMC (CENM). Her research interests include: industrial waste valorization, geopolymers, alkaline activation, alternative cementitious binders, durability, corrosion of concrete structures and composites materials.
ORCID: 0000-0002-5404-2738

J.P. Restucci, received a BSc degree in Materials Engineering in 2014 from Universidad del Valle, Cali, Colombia.

A. Alvarado, received a BSc degree in Materials Engineering in 2014 from Universidad del Valle, Cali, Colombia. He is currently a Young Researcher at Universidad del Valle.

UNIVERSIDAD NACIONAL DE COLOMBIA
SEDE MEDELLÍN
FACULTAD DE MINAS

Área Curricular de Ingeniería
Geológica e Ingeniería de Minas y Metalurgia

Oferta de Posgrados

Especialización en Materiales y Procesos
Maestría en Ingeniería - Materiales y Procesos
Maestría en Ingeniería - Recursos Minerales
Doctorado en Ingeniería - Ciencia y Tecnología de Materiales

Mayor información:

E-mail: acgeomin_med@unal.edu.co
Teléfono: (57-4) 425 53 68

UNIVERSIDAD NACIONAL DE COLOMBIA
SEDE MEDELLÍN
FACULTAD DE MINAS

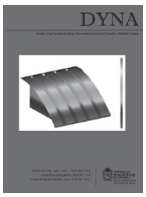

DYNA
http://dyna.medellin.unal.edu.co/

The manufacture of a maxillofacial prosthesis from an axial tomography using simulation technologies with a virtual machine tool and four-axis machining

Jorge Andrés García-Barbosa [a] José Manuel Arroyo-Osorio [b] & Ernesto Córdoba-Nieto [c]

[a] *Facultad de Ingeniería Mecánica, Universidad Santo Tomás, Bogotá, Colombia. jorgegarcia@usantotomas.edu.co*
[b] *Departamento de Ingeniería Mecánica y Mecatrónica,, Universidad Nacional de Colombia, Bogotá, Colombia. jmarroyoo@unal.edu.co*
[c] *Departamento de Ingeniería Mecánica y Mecatrónica,, Universidad Nacional de Colombia, Bogotá, Colombia. ecordoban@unal.edu.co*

Received: March 16th, 2015. Received in revised form: November 19th, 2015. Accepted: February 10th, 2016.

Abstract
The surfaces of a personalized maxillofacial prosthesis were manufactured in a relatively short period of time and at a moderate cost. The surface topography was generated with a Computer-Aided Design system from the Computerized Axial Tomography of a maxillofacial area. The design of the machining manufacturing process, its simulation and verification, were facilitated by the use of a virtual machine tool equivalent to the real machine tool available. Finally, the manufacturing process was successfully achieved by using a conventional 3-axis vertical machining center equipped with a fourth external rotational axis. Using a 3-axis machine tool with an additional axis is less expensive than using a 5-axis machine. There is abundant literature on machining of free-form surfaces using a 5-axis machine tool, but there are few precedents for the manufacturing of this kind of surface using a 4-axis machine.

Keywords: process planning; simulation and verification of processes; multi-axis machining; free-form surface machining; prosthesis manufacturing.

Manufactura de una prótesis maxilofacial, a partir de una tomografía axial, usando tecnologías de simulación en una máquina herramienta virtual y maquinado de cuatro ejes

Resumen
Se fabricaron las superficies de una prótesis maxilofacial personalizada en un lapso de tiempo relativamente corto y con un costo moderado. La topografía de la superficie de la prótesis se recreó en un sistema CAD a partir de una tomografía axial computarizada. El diseño, la simulación y la verificación del proceso de fabricación por maquinado se facilitó gracias al uso de una máquina herramienta virtual equivalente a la máquina real disponible. El proceso de fabricación se ejecutó exitosamente en un centro de maquinado de tres ejes dotado de un cuarto eje de rotación externo. Una máquina herramienta de tres ejes con un eje adicional es menos costosa de operar que una máquina de cinco ejes. Es abundante la literatura sobre maquinado de superficies de forma libre usando máquinas herramienta de cinco ejes, pero hay pocos antecedentes sobre la fabricación de una superficie de este tipo utilizando cuatro ejes de movimiento.

Palabras clave: planificación de procesos; simulación y verificación de procesos; maquinado multiejes; maquinado de superficies complejas; manufactura de prótesis.

1. Introduction

A prosthesis is an artificial implant which replaces or substitutes a part of the human body while maintaining its functionality and aesthetic appearance [1,2]. Commands to generate surfaces, which are available in CAD systems, are insufficient to generate the complex geometry of an anatomically-shaped implant with precision. Nevertheless, it is possible to obtain complete geometric information on facial morphology with developments achieved in the automatic

© The author; licensee Universidad Nacional de Colombia.

processing of three-dimensional (3D) data [3]. A custom-made implant that fits the patient´s anatomy exactly can be designed with precision because of the notable evolution of production technologies [4,5]. However, the efficacy of computer-aided technologies in the design and manufacturing of maxillofacial prostheses has not been completely tested [6].

Reverse engineering is a process that makes it possible to obtain a 3D virtual CAD model from an actual physical object [7]. Recent advances in reverse-engineering technologies are relevant in the manufacturing process of personalized prostheses. These advances make it possible to obtain a CAD model of the prosthesis by using the results of standard diagnostic tools like computerized tomography or magnetic resonance [4,8]. The surfaces of a maxillofacial prosthesis can be classified as free-form surfaces, and they are frequently fabricated by precision-casting of titanium alloys [4]. An alternative, in order to simplify the manufacturing process and reduce manufacturing time is to fabricate them by machining [1].

The definition of a free-form surface is more intuitive than formal. It can be defined as a surface that contains one or more regions with curvatures different from zero, that are non-quadratic and can be represented parametrically or discretized. Free-form surfaces are widely used in the automotive, aerospace and medical industries, and multi-axis machining is mainly used to produce them [9]. Nevertheless, milling by using a 5-axis machine requires considerable investment in equipment, specialized software to generate the cutting-path trajectories and a highly skilled programmer [10]. An alternative way to produce components with free-form surfaces is by using traditional 3-axis machine tools (low speed and low cost) equipped with a fourth external rotational axis [11].

In addition, modelling and simulation of manufacturing systems and their technological operations have been developed to emulate the physics of the process, thus reducing the cost of production tests [12]. Many contemporary systems for computer-aided machining (CAM) include software to implement virtual models of machine tools with a high degree of realism. It is possible to simulate the machining process accurately with a virtual machine tool because this makes it possible to verify the kinematics of cutting-tool trajectory as well as to check for collisions, servomechanism dynamics, and tool-changing and work-material clamp devices [13-15]. These simulation characteristics are especially useful in the planning of manufacturing processes involving machine tools with more than three axes.

This study shows the process carried out in order to obtain the geometry of a maxillofacial prosthesis and its manufacturing in which a 4-axis milling machine was used instead of precision casting. The topography of the surface was generated with a CAD-CAM system from a computerized axial tomography. The design, simulation and verification of the manufacturing process was made in a virtual machine tool equivalent to the real three-axis machining center with an external rotational fourth-axis. The manufacturing process was achieved as planned and the surfaces of the prosthesis were obtained successfully. The operation of the machine tool used is less expensive than that of a 5-axis machine tool. Interestingly, no precedent was found in the literature regarding the manufacturing of free-form surfaces using a 4-axis machine tool.

2. Materials and Methods

2.1. CAD model of the surface

A file in STL (Standard Tessellation Language) format was obtained from the computerized axial tomography of a human maxillofacial area. This STL file approximates the surface to a set of discrete plane triangles, but this format does not represent a solid model with information about volume, center of mass and moments of inertia [16]. In order to obtain the solid model of the prosthesis, the CAD module of the NX-Siemens-PLM software was used, which has the capacity to generate continuous surfaces using the B-REP (Boundary Representation) method. Based on control points that were obtained from the STL file and using the B-REP tool, it was possible to generate a set of patches of interconnected surfaces and, finally, a compound surface which enclosed the STL model.

In order to guarantee surface smoothness and homogeneity, the first condition that must be met is contact or coincidence in position (G0) on the borders of the surface patches. To ensure geometric continuity or smoothness, the direction of the tangents (G1) [17] must also coincide. Fig. 1 illustrates the analysis of position and tangency (geometric continuity) on one of the borders between some of the surface patches. The condition of tangency can be assessed by reflection analysis; continuity exists if there is a smooth transition between two adjacent patches of geometric patterns. A complete 3D-model was generated after verifying the conditions of position and tangency on the borders of the set of surface patches in which the geometry of the STL file was enclosed.

2.2. Surface manufacturability analysis

Fig. 2 shows how the workpiece orientation was defined relative to the CAD reference system. The center of mass and the axes of the main moments of inertia of the workpiece were aligned with the axes of the Work Coordinate System (WCS). For a surface generated by a machining operation, the specifications of geometrical and dimensional tolerances, as well as the absence of interferences between the cutting tool and the surface [9] must be ensured.

During the machining of a free-form surface, global or local interferences can appear as shown in Fig. 3a, 3b. A draft analysis of the concave surface was undertaken, placed in the previously defined orientation and taking into account a vertical machining center with three degrees of freedom. Several zones of interference were found and identified with dark gray as shown in Fig. 3c. The conditions of interference detected demonstrated the need to use a machine tool with more than three degrees of freedom.

A curvature analysis was carried out on the model surfaces to determine the maximum admissible radius for the cutting tools. Fig. 4 illustrates that the smallest radius begins at 2.0 mm. Based on this information, the ball-nose cutting tools to be used in the roughing process (diameter 8.0 mm), in the semi-finishing process (diameter 6.0 mm), and in the finishing process (diameter 4.0 mm) were chosen.

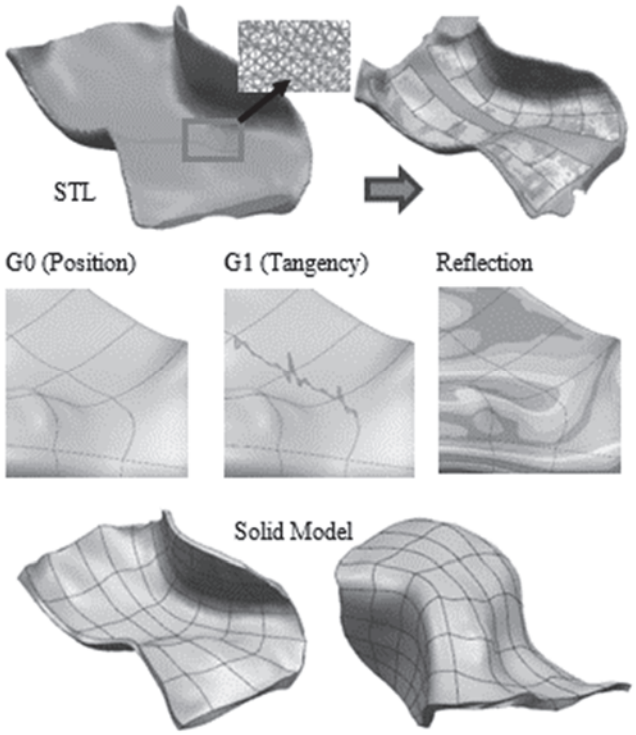

Figure 1. Prosthesis CAD model generation from STL file using the B-REP method.
Source: The authors.

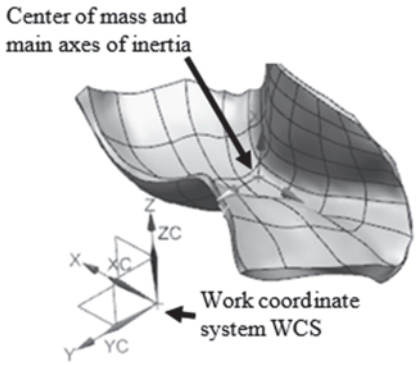

Figure 2. Workpiece orientation relative to the work coordinate system
Source: The authors.

2.3. Work material, machine tool and process parameters

The work material selected was a bar of 12L14 steel. Functional materials such as titanium alloys, cobalt-chromium-molybdenum alloys or stainless steel were not used due to the fact that the main objective of this study was to verify whether it was possible to make the prosthesis with the available technology.

The machine tool used was a Leadwell V-20 vertical machining center with three axes, with a maximum rotational frequency of the spindle of 8000 min^{-1}, and power of 5.5 kW. The machining center was equipped with a fourth rotational axis (Golden Sun CNC-151R) with maximum rotational frequency of 22 min^{-1}, maximum torque of 225 Nm and angular

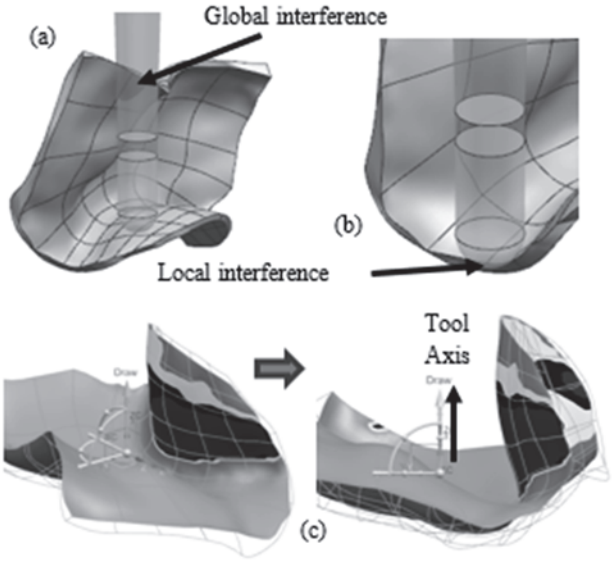

Figure 3. Global (a) and local (b) interferences; draft analysis of the prosthesis (c).
Source: The authors.

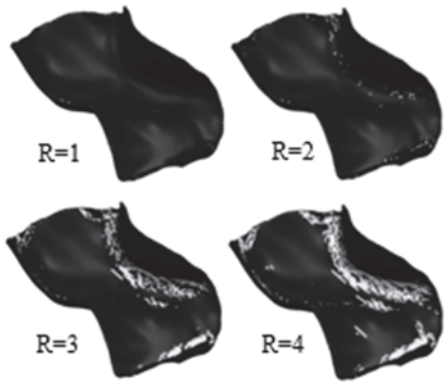

Figure 4. Curvature analysis for minimal tool radius [mm].
Source: The authors.

precision of 0.001º. The Fanuc 0MD machine-tool controller controls all four axes simultaneously, so the prototype was manufactured with a machine tool with four degrees of freedom (CMV-4DOF).

2.4. Verification and simulation of the manufacturing process

The Integrated Simulation and Verification (ISV) module of NX-Siemens-PLM software was used to make a virtual model of the vertical machining center and its accessories as shown in Fig. 5. The assembly made it possible to simulate the manufacturing process with a high degree of realism and to verify the correct generation of the programmed toolpaths, as well as to detect any conflicts in numerical control programming and collisions between setup accessories [18].

It is possible to define pairs of technological components with the ISV module, the main purpose of which is to detect possible interferences between them in the simulation process.

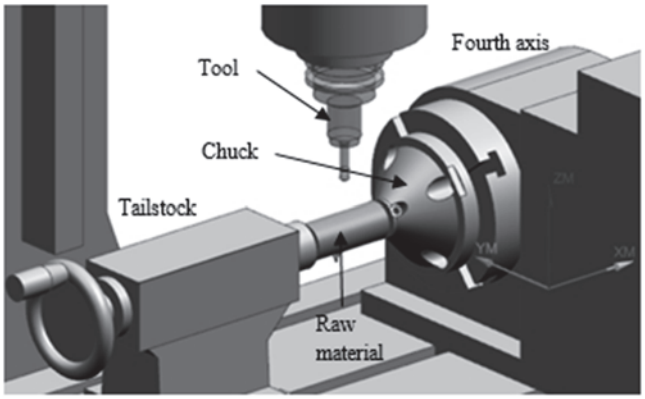

Figure 5. Virtual machine tool setup
Source: The authors.

It is essential to make sure there are no collisions between components such as the chuck, the tailstock, the tool holder, the work material, the spindle and the fourth external axis. The pairs are indispensable not only for detecting any possible collisions between technological agents but also for evaluating any possible in-process collisions between the workpiece and the cutting-tool body. This is in fact the most critical situation to be detected in a multi-axis machining process.

Following the preliminary planning process, the setup of work material, cutting tools and clamping devices was mounted in the virtual machining center. The cylindrical work material was aligned with the 'x' axis of the machining center and fixed between the chuck and the tailstock (Fig. 5).

A first roughing process with an end milling cutter was done taking account of the material removal shape element volume criteria (MRSEV) [19] that resulted in volumes V1, V2 and V3 shown in Fig. 6a. After that, a second roughing process was performed using a cavity-mill strategy, which took into account a constant depth cut in z-axis (Fig. 6b). For semi-finishing and finishing of the convex surface, ball-nose

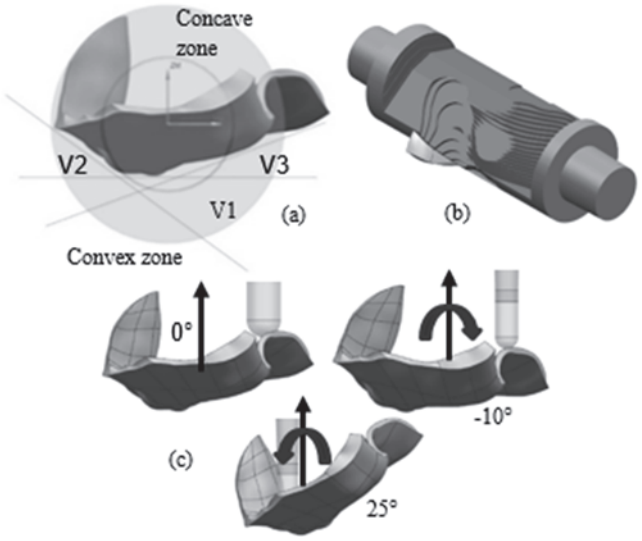

Figure 6. (a) and (b), roughing process. (c) 3+1 strategy for machining of concave surface.
Source: The authors.

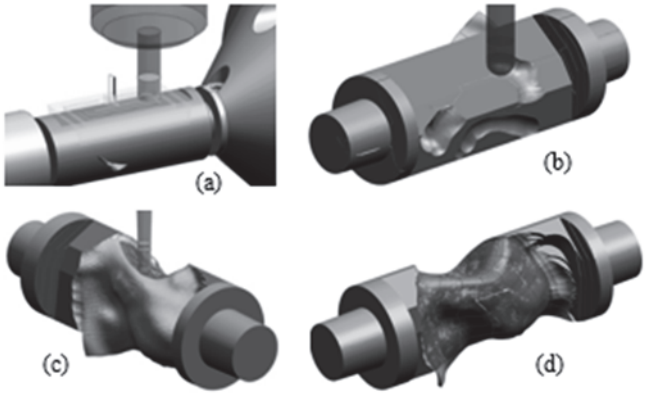

Figure 7. (a) Roughing trajectories verification, (b) Collision detection, (c) Surface finish verification, (d) final convex surface.
Source: The authors.

milling cutters and variable contour cutting strategies were used based on the normal vector to the surface. These strategies were made possible by using the fourth external rotational axis; i.e. four simultaneous axes were employed. Fixed-contour cutting strategies with three axes were applied for the concave surface; the work-piece was oriented in such a way as to permit the access of the cutter (strategy 3+1 axis), with position angles of 0º, -10º and 25º (Fig. 6c).

3. Results

The simulation of cutting-tool path trajectories and material removal were completed according to the process plan. The absence of interferences between the cutting tool with the devices and with the work and machined surfaces (Fig. 7a) was also verified. An example of virtual collision between the in-process workpiece and the cutting tool is illustrated in Fig. 7b. Fig. 7c, 7d show the simulation of the finishing process and the final convex surface obtained. Fig. 8 summarizes the methodology applied in designing and planning the process.

The manufacturing process was executed in the actual machine tool after having been designed, simulated and verified in the virtual machine tool, including verification of the trajectories of each cutting tool and verification of the absence of collisions between the setup components.

The manufacturing program was carried out without any problems, in accordance with the strategies and results established in the designing process. Fig. 9 shows the concave and convex surfaces obtained and verified in the virtual machine tool, and the same surfaces obtained in the actual setup. The manufacturing time estimated in the virtual process was 18 hours and 52 minutes; the real time spent was 15% higher. The main reasons for this difference were a feed adjustment during the machining process and programmed stops after each tool-change to verify the correct performance of the process.

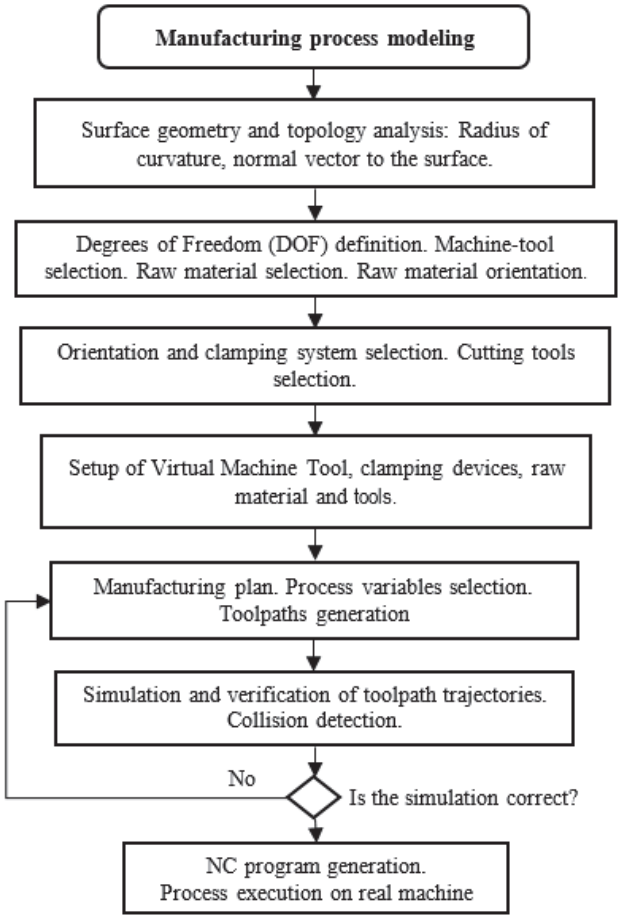

Figure 8. Manufacturing process workflow.
Source: The authors.

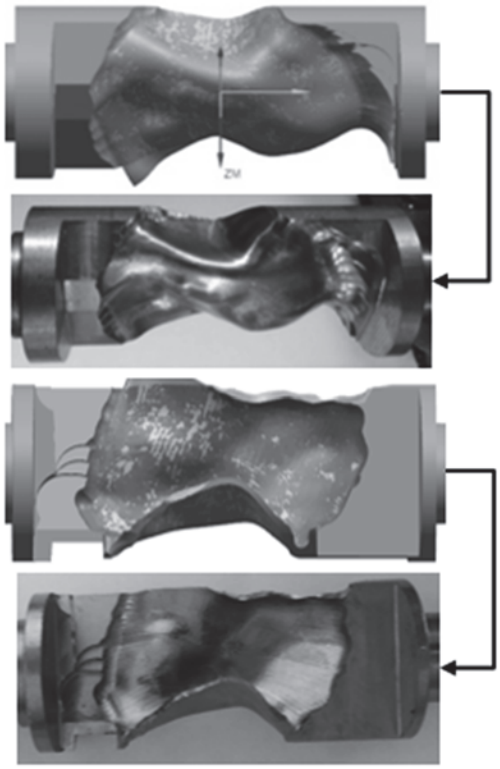

Figure 9. Virtual and actual convex surfaces (Top). Virtual and actual concave surfaces (Bottom).
Source: The authors.

4. Discussion

Multi-axis machining of free-form surfaces is a complex task which requires the latest tools developed for product modelling, process planning and machine-tool emulation.

Given that the efficacy of computer-aided technologies in the design and manufacturing of maxillofacial prostheses has not been completely tested [6]; we explored the integration of several technologies to achieve the engineering design and the manufacturing of the complex geometry, typical of prosthesis parts, as have other authors [8,17].

Most previous research in multi-axis machining have been concerned with tool path computation for 5-axis CNC machines, and very little research has been done for 4-axis [9,11]. Several works on prosthesis machining have been written on the use of 5-axis machining [1,8,17], but no research was found regarding the manufacturing of prosthesis surfaces using a 4-axis machine tool as we did in this work. As the operation of a 4-axis machine tool is less expensive than that of a 5-axis machine tool; the cost of the prosthesis could also be reduced.

5. Conclusions

The geometry of the free-form surfaces of a customized maxillofacial prosthesis and its subsequent manufacturing process were achieved in a relatively short time with moderate costs through the integration of an axial tomography using simulation technologies in a virtual machine tool and four-axis machining.

The topography of the surfaces was obtained with the NX-Siemens CAD software system from a STL file obtained with a computerized axial tomography. The tools for verifying surface quality, especially in terms of continuity and tangency, were essential in this process.

A virtual machine-tool equivalent to the actual machining center equipped with a fourth external axis made the design, simulation and verification of the machining process easier. Said virtual machine made it possible to undertake a realistic simulation and to detect some setup mistakes. A digital simulated process contributes to reducing the wasted time in manufacturing and to calculating the process time.

The manufacturing process was carried out in a 3-axis machining center equipped with a fourth external axis. The operational cost of this machine is less than that of a 5-axis machine. According to the results of this work, 4-axis machining technology is a viable way to produce free-form surfaces like those found in maxillofacial prostheses.

Acknowledgments

The authors wish to acknowledge the funding received from Colciencias (contract RC723-2011) and from the División de Investigación of the Universidad Nacional de Colombia (DIB2030100). The physical assembly was

implemented in the Laboratorio Fabrica Experimental – LabFabEx. The digital setup was done in the Laboratorio de Manufactura Multieje of Universidad Santo Tomás. Special acknowledgments go to Industrias Médicas Sampedro, which proposed and provided the information about the geometry of the surface; to Ingeniería Predictiva IDCAE for their technical support with the Siemens NX PLM software, and, finally, to RACSI S.A. for providing the cutting tools.

References

[1] Ferreira, P., Relvas, C. and Simões, F., Analysis of machining operations of a femoral prosthesis using CAM applications. Key Engineering Materials, (554-557), pp. 2029-2037, 2013. DOI: 10.4028/www.scientific.net/KEM.554-557.2029.

[2] Plazas, C.E. and Perilla, J.E., The past, present and near future of materials for use in biodegradable orthopaedic implants. Ingeniería e Invetigación [Online], 31(2), pp. 124-133, 2011. [date of reference November 29th of 2015]. Available at: http://www.revistas.unal.edu.co/index.php/ingeinv/article/view/23471/24323

[3] Tsuji, M., Noguchi, N., Ihara, K., Yamashita, Y., Shikimori, M. and Goto, M., Fabrication of a maxillofacial prosthesis using a computer-aided design and manufacturing system. Journal of Prosthodontics, 13(3), pp. 179-183, 2004. DOI: 10.1111/j.1532-849X.2004.04029.x.

[4] Singare, S., Liu, Y., Li, D., Lu, B., Wang, J. and He, S., Individually prefabricated prosthesis for maxilla reconstruction. Journal of Prosthontics, XX, pp. 1-6, 2007. DOI: 10.1111/j.1532-849X.2007.00266.x.

[5] Sánchez, J., Hernandez R.J. and Torres, J.E., The mechanical design of a transfemoral prosthesis using computational tools and design methodology. Ingeniería e Investigación [Online], 32(3), pp. 14-18, 2012. [date of reference November 29th of 2015]. Available at: http://www.revistas.unal.edu.co/index.php/ingeinv/article/view/35934/37227

[6] Eggbeer, D., Bibb, R., Evans, P. and Ji, L., Evaluation of direct and indirect additive manufacture of maxillofacial prostheses. Proceedings of the Institution of Mechanical Engineers, Part H : Journal of Engineering in Medicine, 226(9), pp. 718-728, 2012. DOI: 10.1177/0954411912451826.

[7] Kiatpanichgij, S., Afzulpurkar, N. and Kim, T., Three-Dimensional model reconstruction from industrial computed tomography-scanned data for reverse engineering. Virtual and Physical Prototyping, 9(2), pp. 97-114, 2014. DOI: 10.1080/17452759.2014.883475.

[8] Chang, C.C., Lee, M.Y. and Wang, S.H., Digital denture manufacturing - An integrated technologies of abrasive computer tomography, CNC machining and rapid prototyping. International Journal of Advanced Manufacturing Technology, (31), pp. 41-49, 2006. DOI: 10.1007/s00170-005-0181-z.

[9] Lasemi, A., Xue, D. and Gu, P., Recent development in CNC machining of freeform surfaces : A state-of-the-art review. Computer-Aided Design, 42(7), pp. 641-654, 2010. DOI: 10.1016/j.cad.2010.04.002.

[10] Suh, S.H., Lee, J.J. and Kim, S.K., Multiaxis machining with additional-axis NC System: Theory and development. International Journal of Advanced Manufacturing Technology, [Online]. (14), pp. 865-875, 1998. [date of reference November 29th of 2015] Available at: http://link.springer.com/article/10.1007%2FBF01179075

[11] Shan, C., Chen, X., Duan, W., Wang, W. and Liu, W., Four-axis tool orientation smoothing for spiral machining of blades based on step length. Proccedings of international conference on innovative and manufacturing, 2014, pp. 245-250.

[12] Altintas, Y., Kersting, P., Biermann, D., Budak, E., Denkena, B. and Lazoglu, I., Virtual process systems for part machining operations. CIRP Annals - Manufacturing Technology, 63(2), pp. 585-605, 2014. DOI: 10.1016/j.cirp.2014.05.007.

[13] Kadir, A.A., Xu, X. and Hämmerle, E., Virtual machine tools and virtual machining—A technological review. Robotics and Computer-Integrated Manufacturing, 27(3), pp. 494-508, 2011. DOI: 10.1016/j.rcim.2010.10.003.

[14] Altintas, Y., Brecher, C., Weck, M. and Witt, S., Virtual machine tool. CIRP Annals - Manufacturing Technology, [Online]. 54(2), pp. 115-138, 2005. [date of reference November 29th of 2015] Available at: http://www.sciencedirect.com.ezproxy.unal.edu.co/science/article/pii/S0007850607600225

[15] Abdul-Kadir, A. and Xu, X., Towards high-fidelity machining simulation. Journal of Manufacturing Systems, 30(3), pp. 175-186, 2011. DOI: 10.1016/j.jmsy.2011.04.004.

[16] Bianconi, F., Bridging the gap between CAD and CAE using STL files. International Journal of CAD/CAM, [Online]. 2(1), pp. 55-67, 2002. [date of reference November 29th of 2015] Available at: http://www.ijcc.org/on-line(pdf)/2(1)55-67.pdf

[17] Chaves-Jacob, J., Linares J.M. and Sprauel, J.M., Increasing of surface quality in friction free-form surfaces of knee prosthesis. CIRP Annals - Manufacturing Technology, 60 pp. 531-534, 2011. DOI: 10.1016/j.cirp.2011.03.059.

[18] García-Barbosa, J.A., Arroyo-Osorio, J.M. and Córdoba-Nieto, E., Simulation and verification of parametric numerical control programs using a virtual machine tool. Production Engineering, 8(3), pp. 1-7, 2014. DOI: 10.1007/s11740-014-0534-2.

[19] Gupta, S., Kramer, T., Nau, D., Regli, W. and Zhang, G., Building MRSEV models for CAM applications. Advances in Engineering Software, 20(2-3), pp. 121-139, 1994. DOI: 10.1016/0965-9978(94)90054-X.

J.A. García-Barbosa, received a BSc. in Mechanical Engineering in 1996 from the Universidad de América, Bogotá, Colombia. He has a MSc. degree in Materials and Processes since 2006, and he is a PhD Candidate in Science and Technology of Materials at the Universidad Nacional de Colombia. Bogotá, Colombia. He works in the Mechanical Engineering Faculty at Universidad Santo Tomás, Bogotá, Colombia. His research interests are about technologies related with multiaxis-machining and micro-machining and their influence on surface integrity.
ORCID: 0000-0002-7020-4688

J.M. Arroyo-Osorio, is currently associate professor of the Mechanical and Mechatronics Department at Universidad Nacional de Colombia, sede Bogotá, Colombia. He has worked in research and teaching in manufacturing systems engineering, machining processes, soft computing applications and laser surface treatments. He served as manufacturing engineer in the automotive assembly company CCA-Colombia (1995-1999). He has a BSc. in Mechanical Engineering (1995), a MSc. in Computer Systems Engineering (2003) and a PhD. in Materials and Manufacturing (2009).
ORCID: 0000-0003-3636-8029

E. Córdoba-Nieto, is currently full professor at Universidad Nacional de Colombia. His main research topics are manufacturing, machining theory, CNC manufacturing and industrial automation. He has written several books and articles about machining, cutting tools, clamping devices and industrial automation. He has led projects with Colciencias, SENA, Fedemetal and others. He is the director of the Laboratory LabFabEx (Laboratorio Fábrica Experimental) and founder of Mechatronics Engineering Program at Universidad Nacional de Colombia, sede Bogotá, Colombia. He has a BSc. in Mechanical Engineering (1973) and a MSc. in Manufacture and Machine Design (1974) both of them from the Peoples' Friendship University of Russia.
ORCID: 0000-0002-6527-1069

UNIVERSIDAD NACIONAL DE COLOMBIA
SEDE MEDELLÍN
FACULTAD DE MINAS

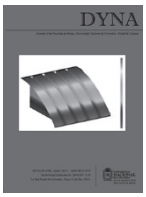

DYNA
http://dyna.medellin.unal.edu.co/

The influence of design methodology on a designer's emotional parameters and on design results

Vicente Chulvi [a] & Mª Carmen González-Cruz [b]

[a] *Departamento de Ingeniería Mecánica y Construcción, Universitat Jaume I., Castellón, Spain. chulvi@emc.uji.es*
[b] *Dep. de Projectes d'Enginyeria, Universitat Politècnica de València, Valencia, Spain. mcgonzal@dpi.upv.es*

Received: March 24th, 2015. Received in revised form: August 15th, 2015. Accepted: January 15th, 2016.

Abstract
This paper presents the results of an experiment carried out on 21 subjects, all of whom had an engineering background, with the aim of determining the influence of the designer's attitude on the design process and on the finished design. The participants were asked to solve a range of design problems by employing different methods while their emotional response parameters were being registered by a non-invasive neuroheadset. The recorded data was used firstly to compare the different reactions of the subjects when using different design methods. A second analysis was carried out to determine whether the variations in the emotional parameters bore any direct relation to the creativity of the outcomes. The results obtained indicate a relation between emotional parameters, individuals and the design method used. However, there does not appear to be any direct association between emotional parameters and the creativity of the results.

Keywords: Conceptual design; creativity; emotional response; design methodology.

Influencia de la metodología de diseño en los parámetros emocionales del diseñador y en los resultados del diseño

Resumen
El presente artículo presenta el resultado de un experimento llevado a cabo sobre 21 individuos, todos ellos con perfil de ingeniería, con el objeto de determinar la influencia de la actitud del diseñador sobre el proceso de diseño y sobre los resultados finales. A los participantes se les pidió que resolvieran una serie de problemas de diseño utilizando diferentes métodos, mientras que su respuesta emocional fue registrada a través de un casco encefalográfico no invasivo. Los datos registrados fueron utilizados, en primer lugar, para comparar las diferentes reacciones de los individuos al utilizar diferentes metodologías de diseño. Un segundo análisis se he llevado a cabo para determinar si las variaciones en los parámetros emocionales tienen una relación directa con los resultados de creatividad. Los resultados obtenidos apuntan a una relación entreindividuo, parámetros emocionales y método de diseño utilizado. Sin embargo, no parece apreciarse una asociación directa entre parámetros emocionales y creatividad de los resultados.

Palabras clave: Diseño conceptual; creatividad; respuesta emocional; metodología de diseño.

1. Introduction

Designers are directly influenced by many different factors, all of which affect the designs they produce [1]; these include: the environment [2, 3], level of education [4- 6], age [7], personal and cultural values [8], perceptions [9] and even the emotions experienced during the design phase [10] and the way in which these emotions, also known as emotional intelligence [11], are dealt with. It can therefore be inferred that all these variables imply that designers experience different mental processes and have different emotional responses to each design problem, which can affect individual designs.

Creativity is one of the most sought-after results when designing products. Many different definitions of creativity exist in the literature and many of these share common elements [12-15]. One of the most generally accepted definitions maintains that: "Creativity happens through a process by which a subject uses his skills to generate ideas, solutions and products that turn out to be novel and useful". This implies that the creativity of a product is closely tied to the individual and to the design process.

© The author; licensee Universidad Nacional de Colombia.

Therefore, on the one hand we can find a large number of studies that focus on defining the individual's creative potential, or creative intelligence, such as those found in [16-20], among others. On the other hand, many authors focus on developing techniques, tools or methods aimed at increasing creativity and innovation in the design process itself [21-23]. Lastly, there are those who prefer to evaluate creativity by its outcomes [15,24,25].

In spite of the fact that responsibility for the results has been divided up between the individual and the process employed, it is not difficult to envisage that a number of individuals will achieve very different results while using the same process or design method, as has been found in previous studies [26,27]. This leads us to accept that different individuals will react in different ways to the stimuli produced by a certain design method. In fact, there are studies that defend different styles of thinking and different reactions during the design process, such as classifying thinking into convergent or divergent, as in [28], or grouping individuals as adaptive or innovative, as in [29], among others.

This paper presents the results of an experiment carried out on 21 individuals who had been asked to find a solution to a variety of design problems by employing different methods while their emotional response parameters were recorded by a non-invasive neuroheadset. The data thus obtained was then used to compare the different individual reactions when using different design methods. A second analysis was also carried out to determine whether the variations in the emotional parameters had a direct relationship with the creativity of the solutions. The aim of the study is to find out if the method used to design affects emotions in the designer, and if the emotions of the designer in his work affect the creativity of the results. As a result, the methods that are more conducive to developing creative solutions could be identified.

2. Tools and Methods

2.1. Methodology

Twenty-one students taking a master's degree in different branches of engineering took part in the experiment. A preliminary session was held to brief them collectively on the design methods they would be asked to use in the tests. Each of the participants was then asked individually to find a creative solution to three design problems, one from each of the design methods used in the tests (Table 1). The third problem was specially selected for its limitations as regards its potential for innovation. This was done in order to determine whether the fact of facing a difficult problem with hidden challenges would also cause variations in the subjects' emotional parameters. The problems, methods and work order were varied to include all the possible combinations (as will be shown in Table 4).

During the entire problem-solving process the subjects wore an EmotivEpoc headset that recorded their emotional parameters. They were allowed 30 minutes to solve each of the problems, after which they were advised that they had to hand in their solution in the form of a sketch, scheme or notes, for which they were allowed an additional 5 minutes.

Table 1.
Statements of the problems to be solved

Problem 1: Design an office desk that can be easily raised or lowered to allow people to work either seated or standing.
Problem 2: Design a suitcase whose size can be altered according to the volume of luggage it contains. The case should be light and easy to use and carry.
Problem 3: Design a rectangular table for use in a practice laboratory including electric plugs for different types of apparatus. Remember that wires must be kept wound up and out of sight so as not to interfere with the work area.

Source: The authors

2.2. Design methods

Three different types of method were chosen for use in solving the design problems, in accordance with the classification proposed in Shah et al. [13]: one was logical, one intuitive and in one they were given carte blanche. The Su-Fields tool from TRIZ [30] was selected for use in the logical method, and SCAMPER [31] for the intuitive method. In one of the exercises the subjects were not given any instructions and were allowed to solve the problem any way they chose.

2.2.1. TRIZ (Su-Fields)

This tool consists of a functional analysis of the problem, which is schematized into substances (physical elements) and fields (function-executing modes), as shown in Fig. 1. The idea is to find all the aspects that can be improved and then act on each aspect individually. Five rules are proposed which are to be applied to each problem:

S2 being a substance that acts on S1 via field F1:

Rule 1 says that substance S2 must be replaced by a new substance S3, which generates a new field F2 over S1.

Rule 2 says that a new substance S3 must be added to act over S2 via a new field F2.

Rule 3 says that that a new substance S3 must be added to act over S1 via a new field F2.

Rule 4 says that that a new substance S3, between S1 and S2, must be added to act over S1 and S2 via a new field F2.

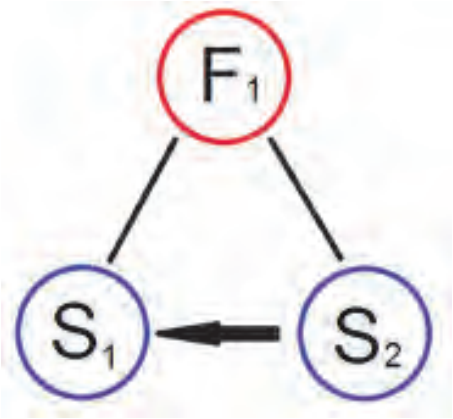

Figure 1. Basic scheme of Su-Field modelling.
Source: The authors

Figure 2. Emotiv EPOC neuroheadset.
Source: The authors

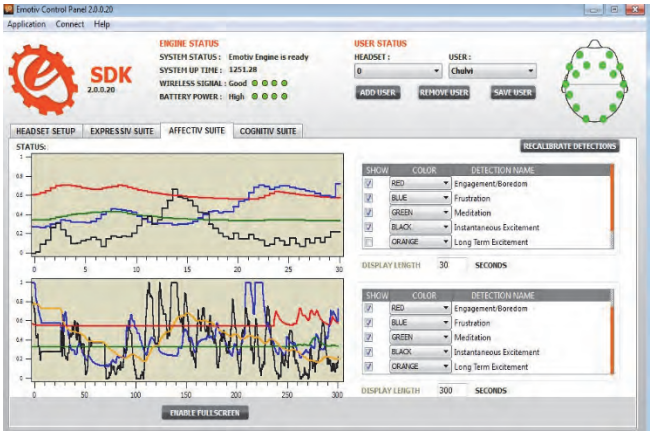

Figure 3. Interface of the affective suite of the Emotiv EPOC Software Development Kit.
Source: The authors

Rule 5 says that that a substance S3, not related to S1 and S2, must be added in such a way that the newly generated field F2 acts over S1 and S2.

2.2.2. SCAMPER

This method consists of applying the following questions to the design problem:

- What can I Substitute?
- What can I Combine?
- What can I Adapt?
- What can I Magnify?
- Can I Propose other uses?
- What can I Eliminate?
- Can I Reorder or invert any part?

2.3. Emotive Epoc

Throughout the tests, participants wore the Emotiv Epoc non-invasive neuroheadset (Fig.2), which can measure cerebral electrical activity through the scalp. Four emotional variables were directly recorded by the software provided by the manufacturer, consisting of: frustration, meditation, interest and excitement (Fig.3).

2.4. Creativity assessment

Creativity was assessed by a consensus of two specialists in the field (the authors of this work) using the metric developed by J. Moss [24], which estimates creativity by a combination of two parameters: a product's usefulness and unusualness. The former is determined by assessing the degree to which the product satisfies the requirements of a good standard (or teacher's) solution. Creativity is assessed on a scale of zero to three; zero being a design that does not achieve the set requirements, and three being considered better than the teacher's solution

The degree of unusualness is determined by the inverse probability of the idea arising within a homogeneous group of solutions, i.e. by comparing the product with the other products created as solutions to the same problem. This parameter is also assessed on a scale of zero to three; zero for a commonplace solution and three for showing exceptional originality. The overall creativity of the product is then scored by multiplying the above two parameters. The application of Moss's metric can be seen in Table 2.

Table 2.
Moss's scale

		The solution does not satisfy the functional requirements	**The solution barely satisfies the requirements**	**The solution is as good as the standard solution**	**The solution is better than the standard solution**
		0	1	2	3
>10% of similar ideas	0	0	0	0	0
6-10% of similar ideas	1	0	1	2	3
1-5% of similar ideas	2	0	2	4	6
<1% of similar ideas	3	0	3	6	9

Source: [24]

Table 3.
Extract from the compilation of brain parameters

P 1				
Time(s)	**Frustration**	**Meditation**	**Excitement**	**Interest**
781.12	70	33	45	56
782.38	67	33	44	55
783.25	65	33	46	55
784.38	63	33	38	55
785.13	62	33	48	55
786.25	61	33	52	55
787.13	60	33	55	57
788.13	59	34	58	62
788.63	59	35	56	67
789.76	58	36	53	72
790.63	56	36	48	79
792.22	53	36	44	82
793.25	51	37	34	81
794.25	49	38	24	79
795.25	47	38	24	79
796.13	46	39	22	79
797.38	45	38	21	81
798.13	44	39	26	81
799.38	43	38	27	78
800.38	43	37	27	74

Source: The authors

3. Results

A total of 21 solutions were obtained for each of the three design problems. Some examples are given in Fig. 4 together with data on the brain parameters of the participants. Table 3 contains an extract of the parameters of one of the subjects, where frustration, meditation, excitement and interest are judged on a scale of 1-100 where 100 is the max level of an emotion. Unfortunately, data on the parameters from five participants had to be left out of the analysis due to defective contacts and interference. The results and the analysis given below were therefore carried out on the valid data from 16 participants. As it can be observed in Table 3, the values of the parameters show a variation over time tracked. Statistical means are used for data analysis in order to compare the design methods.

As has been described in Section 2.4, the designs were judged by consensus between two specialists using Moss's metric (1966) to obtain values for usefulness, unusualness and creativity. Table 4 gives a summary of the results obtained, the emotion averages over time obtained by direct measurement during the tests, and the values awarded by the judges for usefulness, unusualness and creativity.

Table 4.
Summary of the results obtained

Sub.	Prob.	Method	Frustration	Meditation	Excitement	Interest	Unusualness	Utility	Creativity
	1	SCAMPER	52.06	37.54	32.35	59.55	1	2	2
1	2	TRIZ	67.65	33.28	64.08	56.23	2	1	2
	3	No method	67.66	35.02	41.93	70.27	0	2	0
	1	SCAMPER	49.32	36.77	67.73	63.37	0	2	0
2	2	TRIZ	60.12	34.52	19.48	58.25	0	2	0
	3	No method	59.53	29.80	69.19	50.63	0	2	0
	1	SCAMPER	44.72	36.92	28.00	65.34	0	2	0
3	2	TRIZ	46.96	35.61	35.61	59.77	3	2	6
	3	No method	42.42	27.76	35.41	51.09	0	2	0
	1	SCAMPER	21.68	33.00	20.32	55.00	0	2	0
4	2	TRIZ	78.56	32.95	54.14	55.15	2	1	2
	3	No method	33.72	23.64	42.89	46.09	0	2	0
	1	SCAMPER	54.60	33.10	33.99	61.28	1	1	1
5	2	TRIZ	5.10	34.28	29.76	56.16	2	1	2
	3	No method	5.67	31.47	37.71	68.87	0	2	0
	1	SCAMPER	60.60	38.24	29.29	59.62	1	0	0
6	2	TRIZ	66.52	33.49	37.86	54.21	1	1	1
	3	No method	59.10	30.29	32.89	64.13	0	2	0
	1	SCAMPER	62.52	39.31	33.58	62.54	1	0	0
7	2	TRIZ	66.40	33.14	36.13	56.61	1	2	2
	3	No method	62.70	33.86	25.21	69.95	0	2	0
	1	TRIZ	44.67	35.53	33.12	67.65	0	2	0
8	2	No method	41.61	36.22	27.74	66.48	0	2	0
	3	SCAMPER	39.11	38.70	23.10	65.83	0	2	0
	1	TRIZ	61.20	36.68	38.60	62.89	0	2	0
9	2	No method	49.48	38.23	39.80	70.97	1	2	2
	3	SCAMPER	47.53	40.72	79.86	64.84	0	2	0
	1	TRIZ	48.47	35.29	42.90	67.18	3	2	6
10	2	No method	39.14	33.22	33.33	69.28	0	2	0
	3	SCAMPER	36.23	37.48	49.88	68.52	0	2	0
	1	TRIZ	47.06	34.11	68.53	64.43	0	2	0
11	2	No method	42.87	37.18	39.80	61.47	0	2	0
	3	SCAMPER	45.24	40.24	52.51	68.11	0	2	0
	1	TRIZ	52.29	36.25	34.67	64.22	0	2	0
12	2	No method	31.93	34.27	32.37	64.20	0	2	0
	3	SCAMPER	21.06	36.37	39.74	61.84	2	2	4
	1	No method	46.22	33.82	33.83	71.52	0	1	0
13	2	SCAMPER	50.70	30.17	38.33	55.04	0	2	0
	3	TRIZ	35.25	32.61	27.05	53.11	0	2	0
	1	No method	41.86	34.32	35.53	68.35	0	1	0
14	2	SCAMPER	46.92	32.08	16.67	57.59	0	2	0
	3	TRIZ	47.88	35.92	37.95	54.01	2	2	4
	1	No method	38.49	33.91	26.70	72.07	0	1	0
15	2	SCAMPER	46.43	32.03	33.30	57.04	2	1	2
	3	TRIZ	47.71	35…05	28.18	53.29	0	2	0
	1	No method	47.34	33.58	37.89	69.32	2	1	2
16	2	SCAMPER	47.23	33.36	30.79	54.49	2	1	2
	3	TRIZ	39.69	32.62	30.32	52.75	0	2	0

Source: The authors

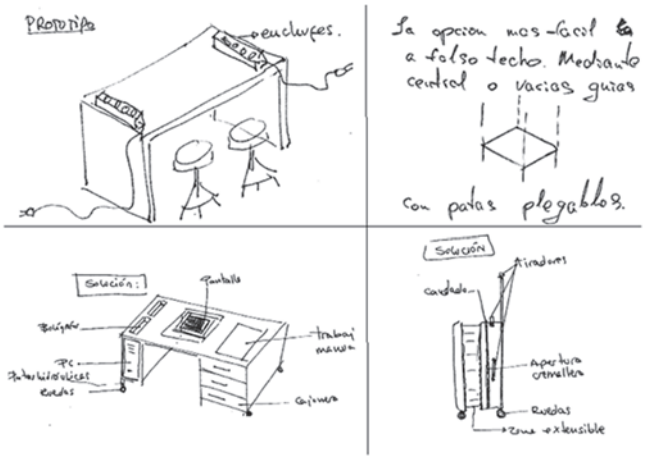

Figure 4. Some of the solutions provided by the students.
Source: The authors

3.1. Influence of design method on the emotive response

ANOVA was utilized in the first analysis to discover whether the emotional variables (frustration, meditation, excitement and interest) were influenced by the method used and the problem to be solved, or whether the variations in these variables could be attributed to individual subjects, regardless of the problem to be solved or the method employed to solve it. The results of this analysis are given in Tables 5, 6 and 7. In Table 5 it can be seen that method appears to have an influence on meditation and interest, while the variations in frustration and excitement are non-significant. Table 6 shows that the type of problem to be solved does not affect any of the emotional parameters and in Table 7 it can be seen that the individual seems to bear a certain relationship with frustration, but has no significant effect on the other variables.

However, as both method and individual do seem to influence the emotional response, a joint statistical analysis was performed using Tukey's proof [32] to find out whether there was any interaction between these elements. The results are given in Table 8, where it can be seen that there does not appear to be a significant difference between method and subject. However, after eliminating the noise that a significant factor can cause on another, certain aspects showed a significance that was not previously apparent. In this case, method was seen to significantly affect the emotional responses of frustration, meditation and interest, while the individual had an effect on frustration and meditation.

Table 5.
Influence of method on emotional response.

Emotional Response	F-critic = 3.20
Frustration	F(2, 45)=2.69, p=0.079
Meditation	F(2, 45)=**4.45**, p=0.017
Excitement	F(2, 45)=0.06, p=0.943
Interest	F(2, 45)=**3.97**, p=0.025

Source: The authors

Table 6.
Influence of problem on emotional response.

Emotional Response	F-critic = 3.20
Frustration	F(2, 45)=1.18, p=0.317
Meditation	F(2, 45)=1.42, p=0.252
Excitement	F(2, 45)=0.64, p=0.534
Interest	F(2, 45)=3.07, p=0.056

Source: The authors

Table 7.
Influence of the individual on emotional response

Emotional Response	F-critic = 1.99
Frustration	F(15, 32)=**2.36**, p=0.020
Meditation	F(15, 32)=1.60, p=0.130
Excitement	F(15, 32)=1.45, p=0.182
Interest	F(15, 32)=1.18, p=0.333

Source: The authors

Table 8.
Effect of interaction between method and individual on emotional response

Emotional Response			F-critic
Frustration	Method	F(2,29)=**4.29**, p=0.023	3.33
	Subject	F(15,29)=**2.82**, p=0.008	2.03
	Interaction	F(1,29)=0.57, p=0.455	4.18
Meditation	Method	F(2,29)=**5.94**, p=0.007	3.33
	Subject	F(15,29)=**2.06**, p=0.047	2.03
	Interaction	F(1,29)=0.27, p=0.609	4.18
Excitement	Method	F(2,29)=0.06, p=0.938	3.33
	Subject	F(15,29)=1.32, p=0.250	2.03
	Interaction	F(1,29)=0.02, p=0.898	4.18
Interest	Method	F(2,29)=**4.49**, p=0.020	3.33
	Subject	F(15,29)=1.42, p=0.202	2.03
	Interaction	F(1,29)=0.50, p=0.485	4.18

Source: The authors

3.2. Influence of emotive response on the creativity of the outcomes

As seen in Table 4, we now had the values of unusualness, usefulness and creativity for each of the designs obtained. As in the preceding section, here it was advisable to check whether the method used, the problem to be solved or the individual subjects had influenced these results. Tables 9, 10 and 11 present the results of the ANOVA analysis of these three factors on the unusualness, usefulness and creativity of the solutions. From these tables it can be seen that the method used to solve the problem does have an influence on unusualness and creativity, that the problem to be solved influences usefulness, and that the individual has no influence on any of these three aspects.

Table 9.
Influence of method on unusualness, usefulness and creativity

	F-critic = 3.20
Unusualness	F(2, 45)=**3.48**, p=0.039
Usefulness	F(2, 45)=0.61, p=0.550
Creativity	F(2, 45)=**3.40**, p=0.042

Source: The authors

Table 10.
Influence of problem on unusualness, usefulness and creativity

	F-critic = 3.20
Unusualness	F(2, 45)=2.93, p=0.064
Usefulness	F(2, 45)=**5.05**, p=0.010
Creativity	F(2, 45)=1.27, p=0.292

Source: The authors

Table 11.
Influence of individual on unusualness, usefulness and creativity

	F-critic = 1.99
Unusualness	F(15, 32)=0.56, p=0.887
Usefulness	F(15, 32)=1.14, p=0.365
Creativity	F(15, 32)=0.50, p=0.922

Source: The authors

Table 12.
Pearson coefficients of the interaction of emotional response with creative factors

	Unusualness
Frustration	r=0.205, n=47, p=5.05e-32
Meditation	r=0.074, n=47, p=2.14e-50
Excitement	r=0.059, n=47, p=2.72e-24
Interest	r=-0.171, n=47, p=5.03e-47
	Usefulness
Frustration	r=-0.339, n=47, p=5.25e-31
Meditation	r=-0.078, n=47, p=1.40e-49
Excitement	r=0.072, n=47, p=9.15e-24
Interest	r=0.011, n=47, p=2.89e-47
	Creativity
Frustration	r=0.039, n=47, p=1.30e-31
Meditation	r=0.087, n=47, p=2.92e-49
Excitement	r=0.056, n=47, p=3.80e-24
Interest	r=-0.100, n=47, p=1.21e-46

Source: The authors

Pearson's correlation coefficient was used to determine whether emotional response had any influence on the creativity of the results. The values of the coefficients thus obtained are given in Table 12, in which it can be seen that all the values are quite low, except in the case of frustration, which only showed low values for unusualness and usefulness. This would seem to indicate that a direct correlation cannot be established between the designer's emotional response during the design process and the creativity of the results obtained.

4. Discussion

This paper deals primarily with an analysis of aspects of the design process that could somehow influence the subject's emotional response. One of the aspects considered was the problem to be solved, which was found to be non-significant (see Table 6) in spite of the fact that a purposely difficult design problem with little room for innovation was included in the experimental design.

Another aspect considered was the method used by the subjects to develop their designs; in this case, significant variations were found in the emotional parameters meditation and interest (see Table 5). In other words, the method selected affects the way in which the designer approaches the problem and, according to its difficulty, requires varying amounts of interest and meditation, or concentration.

The third factor considered was the individual subject (as regards level of education, culture and personal characteristics) and his special reaction to the design process. Here we found that the subject causes significant variations as regards frustration level (Table 7). This means his ability to find the right solution while working under pressure will largely depend on his personal characteristics and not on the method used or the problem to be solved.

None of the factors considered in the study was found to significantly affect the emotional parameter excitement.

We also studied whether the subject's emotional variables during the design process had any influence on the creativity of the results. First, we looked at the effect of the three factors mentioned above on creativity. As expected, we found method to be significant, in agreement with previous studies in this field that have shown that the design method affects creativity and its associated parameters [26, 27, 33]. However, we were somewhat surprised to find that the problem had a significant effect on the usefulness parameter; this may possibly have been due to including Problem 3 (which gave little room for innovation) in the tests, forcing the subjects to resort to standard, well proven solutions. As can be seen in Table 4, all the solutions to Problem 3 were given a usefulness score of 2 by the judges. Dunnett's post hoc analysis subsequently revealed that Problem 3 showed significant deviation (see Table 13).

As regards the relationship between emotional parameters and the creativity of the design, the Pearson's coefficients obtained were low enough to rule out this possibility. The only one of these parameters that proved to be a little higher than the rest was frustration in relation to unusualness and usefulness, with coefficients of 0.205 and -0.339, which, even though comparatively low, still indicate that the frustration level during design may have a slight positive influence on unusualness and a slight negative influence on usefulness.

5. Conclusions

From the results of the tests carried out in the course of this work it can be concluded firstly, that both the individual and the method used have a significant effect on emotional response during the design phase. However, both these factors affect the emotional response in different ways; or, in other words, they each affect different emotional parameters. Firstly, the subject's individual personality appears to influence his frustration level, regardless of the problem to be solved or method used. Secondly, method appears to significantly influence meditation and interest. Also, even though no significant relationship was found between the individual subject and method, the joint analysis of these factors shows that the individual also affects the meditation and frustration levels, and that method seems to affect frustration, meditation and interest.

Therefore, even though the analysis showed no direct relationship between individual and method as regards emotional response, a rather more complex underlying reality can be perceived that will require further studies on a larger scale and on a greater number of emotional and personal variables in order to identify the factors to be considered when analysing the relationship between individual and method.

Since it has been shown that the design method does have an effect on the designer's emotional response, the next step will be to

Table 13.
Result of Dunnett's post hoc test using Problem 1 as control.

	Mean (Mi)	Control mean (Mc)	Mean square error (MSe)	n	t'	t
P 2	1.65	1.44	0.26	16	1.04	2.32
P 3	2.00			16	3.12	2.32

Source: The authors

determine the methods that positively and negatively affect this response, the design process and its outcomes. One of these outcomes, the creativity of the solutions, was analyzed in the present study and its conclusions indicate that the subject's emotional response during the design phase has no effect on the creative aspect of the results. This has important implications for design methods that promote creativity, since it helps to confirm their validity and utility regardless of whoever uses them. However, our intention is not to isolate the designer from the final results, as there are additional factors that impinge on creativity, including: creative intelligence, training, experience, tools available, surroundings, and a long list of other factors currently under in-depth study or scheduled for future studies [2-10, 19, 34, 35].

Future work will examine the whole range of variables that influence creativity in design, with the aim of optimizing all possible aspects of the design process and to rule out the factors that play no part in the outcome of the creative process.

References

[1] Lidwell, W., Holden, K. and Butler, J., Universal principles of design: 125 ways to enhance usability, influence perception, increase appeal, make better design decisions, and teach through design. Rockport Pub, 2010.

[2] Gerard, R.M., Differential effects of colored lights on psychophysiological functions, PhD Thesis. University of California, USA, 1958.

[3] Soler, L.C.T., Creativity in computer systems. Ingeniería e Investigación, 23(2), pp. 25-30, 2003. DOI: 25-30 2248-8723 0120-5609

[4] Sheppard, S. and Jenison, R., Examples of freshman design education. International Journal of Engineering Education.13(4), pp. 248-261, 1997.

[5] Chulvi, V., Rivera, J. and Vidal, R., Creative experience in engineering design: The island exercise. DYNA, 81(185), pp. 86-93, 2014. DOI: 10.15446/dyna.v81n185.36570

[6] Aizpun, M., Sandino, D. and Merideno, I., Developing students' aptitudes through University-Industry collaboration. Ingeniería e Investigación, 35(3), pp. 121-128, 2015. DOI: 10.15446/ing.investig.v35n3.48188

[7] Atman, C.-J., Cardella, M.-E. and Turns, J., Comparing freshman and senior engineering design processes: An in-depth follow-up study. Design Studies 26(4), pp. 325-357, 2005. DOI: 10.1016/j.destud.2004.09.005

[8] Kumar. K. and Bjorn-Andersen, N., A cross-cultural comparison of is designer values. Communications of the ACM. 33(5), pp. 528-538, 1990. DOI: 10.1145/78607.78613

[9] Manchado-Pérez, E. and Berges-Muro, L., Sistemas de retículas: Un método para diseñar nuevos conceptos de producto hacia el usuario. DYNA 80(181), pp. 16-24, 2013.

[10] Norman, D., Emotion & Design: Attractive things work better. Interactions. 9(4), pp. 36-42, 2002. DOI: 10.1145/543434.543435

[11] Salovey, PP. and Mayer, J.-D., Emotional intelligence. Imagination, Cognition and Personality. 9(3), pp. 185-211, 1989. DOI: 10.2190/DUGG-P24E-52WK-6CDG

[12] Sternberg, R.-J. and Lubart, T.-I., The concept of creativity: Prospects and paradigms. Handbook of Creativity. 1, pp. 3-15, 1999.

[13] Shah, J.-J., Smith, S.-M. and Vargas-Hernandez, N., Metrics for measuring ideation effectiveness. Design Studies. 24(2), pp. 111-134, 2003. DOI: 10.1016/S0142-694X(02)00034-0

[14] Sarkar, PP. and Chakrabarti, A., Development of a method for assessing design creativity. International conference on engineering design, ICED'07 28 - 31 august 2007, cite des sciences et de l'industrie, Paris, France 2007.

[15] Sarkar, PP. and Chakrabarti, A., Studying engineering design creativity-developing a common definition and associated measures. In: Gero J., (Ed.). Invited paper in the Proceedings of the NSF Workshop on Studying Design Creativity. 2008.

[16] Hocevar, D. and Bachelor, PP., Handbook of Creativity. Springer, 1989, pp. 53-75.

[17] Corbalán, F., Martínez, F. and Donolo, D., CREA. Inteligencia Creativa. Una medida cognitiva de la creatividad. Madrid: TEA eds, 2003.

[18] Guilford, J., Personality. McGraw-Hill, New York, 1959.

[19] Torrance, E.-P., Reynolds, C.-R. and Riegel, T., Your style of learning and thinking, forms A and B preliminary norms, Abbreviated technical notes, scoring keys, and selected references. Gifted Child Quarterly. 21(4), pp. 563-573, 1977.

[20] Otis, A., Otis-Lennon School ability test-(OLSAT 8). The Psychological Corporation, San Antonio, TX, USA, 2006.

[21] Altshuller, G., Creativity as an exact science: The theory of the solution of inventive problems. Gordon and Breach Science Publishers, 1984.

[22] Kwak, Y.-H. and Anbari, F.-T., Benefits, obstacles, and future of six sigma approach. Technovation, 26(5-6), pp. 708-715, 2006. DOI: 10.1016/j.technovation.2004.10.003

[23] Thompson, G. and Lordan, M., A review of creativity principles applied to engineering design. Proceedings of the Institution of Mechanical Engineers, Part E: Journal of Process Mechanical Engineering. 213(1), pp. 17-31, 1999. DOI: 10.1243/0954408991529960

[24] Moss, J., Measuring creative abilities in junior high school industrial arts. American Council on Industrial Arts Teacher Education, 1966.

[25] O'Quin, K. and Besemer, S.-PP., The development, reliability, and validity of the revised creative product semantic scale. Creativity Research Journal. 2(4), pp. 267-278, 1989. DOI: 10.1080/10400418909534323

[26] Chulvi, V., González-Cruz, M. and Mulet, E., Influence of the type of idea-generation method on the creativity of solutions. Research in Engineering Design. 24(1), pp. 33-41, 2013. DOI: 10.1007/s00163-012-0134-0

[27] Chulvi, V., Mulet, E. and Chakrabarti, A., Comparison of the degree of creativity in the design outcomes using different design methods. Journal of Engineering Design. 23(4), pp. 241-269, 2012. DOI: 10.1080/09544828.2011.624501

[28] Guilford, J., Cognitive styles: What are they? Educational and Psychological Measurement. 40(3), pp. 715-735, 1980. DOI: 10.1177/001316448004000315

[29] Kirton, M., Adaptors and innovators: A description and measure. Journal of Applied Psychology. 61(5), pp. 622-629, 1976. DOI: 10.1037/0021-9010.61.5.622

[30] Belski, I., Improve your thinking: substance-field analysis. TRIZ4U, 2007.

[31] Eberle, B., Scamper on: More creative games and activities for imagination development. Prufrock Pr, 1996.

[32] Tukey, J.-W., One degree of freedom for non-additivity. Biometrics. 5(3), pp. 232-242, 1949. DOI: 10.2307/3001938

[33] Chulvi, V., Sonseca, Á. and Mulet, E., Assessment of the relationships among design methods, design activities, and creativity. Journal of Mechanical Design. 134(11), pp. 111004-111004.11, 2012. DOI: 10.1115/1.4007362

[34] Kim, M., Kim, Y. and Lee, H., An underlying cognitive aspect of design creativity: Limited commitment mode control strategy. Design Studies. 28(6), pp. 585-604, 2007. DOI: 10.1016/j.destud.2007.04.006

[35] Artola-González, T., PIC-A: Prueba de imaginación creativa para adultos. Manual. Madrid, 2012.

V. Chulvi, is professor at the Department of Mechanical Engineering and Construction at the Universitat Jaume I of Castellón, Spain. Chulvi earned a BSc in Mechanical Engineering (2001), an MSc in Mechanical Engineering (2007) and a PhD in Engineering (2010). His main research focuses on design and creativity within the research group DACTIC of the Universitat Jaume I of Castellón, Spain. ORCID: orcid.org/0000-0002-0708-3852

M.C. González-Cruz, holds a PhD in Industrial Engineering from the Universitat Politècnica de València, Spain. After working in several engineering companies, she now works as an associate professor/senior lecturer in Project Engineering (undergraduate), and Project Management (graduate). She is currently the Head of the Department of Project Engineering and she is also in charge of the MSc in Project Management at Universitat Politècnica de València, Spain. She has conducted research on the use of design methodology in industry, creativity and innovation management, and currently, she works in analysis and development of forecasting and bid models on procurement.
ORCID: orcid.org/0000-0002-6987-5732

UNIVERSIDAD NACIONAL DE COLOMBIA
SEDE MEDELLÍN
FACULTAD DE MINAS

DYNA
http://dyna.medellin.unal.edu.co/

Computational simulation of laminar heat convection of nanofluids in a circular tube and squared duct

Diego Andrés Vasco-Calle [a], Daming Chen [b] & Jorge Acevedo-Cabello [c]

[a] *Facultad de Ingeniería, Departamento de Ingeniería Mecánica, Universidad de Santiago de Chile, Santiago de Chile, Chile. diego.vascoc@usach.cl*
[b] *Facultad de Ingeniería, Departamento de Ingeniería Mecánica, Universidad de Santiago de Chile, Santiago de Chile, Chile. daming.chen@usach.cl*
[c] *Facultad de Ingeniería, Departamento de Ingeniería Mecánica, Universidad de Santiago de Chile, Santiago de Chile, Chile. jorge.acevedo.c@usach.cl*

Received: March 30th, 2015. Received in revised form: October 1rd, 2015. Accepted: January 30th, 2016.

Abstract
Nanofluids are colloidal suspensions of nanometer-sized particles (metals, metallic oxides or carbon nanotubes) in a base fluid (polar or non-polar). Nanofluids have interesting properties that make them useful especially in the design of compact heat transfer equipment. Laminar convective heat transfer of nanofluids (water, Al_2O_3) in a square and circular ducts has been studied numerically using the software ANSYS/FLUENT 12.1. Results for the Nusselt number, skin coefficient friction, temperature and velocity profiles are presented for four nanoparticle volume fractions (φ = 0 − 20%) and Reynolds numbers (Re = 800, 1300 and 2000). For the studied Re numbers, Nu is decreased by 12% and 10%, when φ is increased from 0% to 10% and from 10% to 20%, respectively. Regard to the skin friction factor, the obtained value is increased around a 30% when φ is increased 10%.

Keywords: nanofluids; CFD; laminar-forced convection

Simulación computacional de convección de calor laminar de nanofluidos en tubo circular y ducto cuadrado

Resumen
Los nanofluidos son soluciones coloidales de partículas de tamaño nanométrico (metales, óxidos metálicos o nanotubos de carbono) en un fluido base (polar o apolar). Los nanofluidos poseen propiedades interesantes que los hacen útiles especialmente en el diseño de equipos de transferencia de calor más compactos. En el presente trabajo se estudia el proceso de convección laminar de un nanofluido (agua, Al_2O_3) al interior de un ducto cuadrado y un tubo circular mediante el software ANSYS/FLUENT 12.1. Se presentan resultados para el número de Nusselt, el factor de fricción, perfiles de temperatura y velocidad para cuatro concentraciones volumétricas de nanopartículas (φ = 0 - 20%) y números de Reynolds (Re=800, 1300 y 2000). Para los Re estudiados, Nu disminuye un 12% y 10% cuando φ aumenta de 0% a 10% y de 10% a 20%, respectivamente. En el caso del coeficiente de fricción, el valor obtenido aumenta alrededor de un 30% cuando φ es aumentado un 10%.

Palabras clave: nanofluidos; CFD; convección forzada laminar

1. Introducción

Los nanofluidos son soluciones coloidales de partículas de tamaño nanométrico (metales, óxidos metálicos o nanotubos de carbono) en un fluido base como agua, etilenglicol, oleofinas y parafinas. Los nanofluidos poseen propiedades térmicas interesantes que los hacen útiles en varias aplicaciones de transferencia de calor, tales como enfriamiento de motores automotrices, refrigeración doméstica, equipos HVAC, intercambiadores de calor y almacenamiento de energía térmica. Hoy, los estudios con nanofluidos se enfocan principalmente al diseño de intercambiadores más compactos y eficientes.

Existen principalmente dos técnicas para sintetizar nanofluidos; el método de dos pasos [1] y el método de un solo paso, descrito por Zhu et al. [2]. La dispersión de una pequeña cantidad de nanopartículas en un fluido base incrementa notablemente su conductividad térmica. Masuda

© The author; licensee Universidad Nacional de Colombia.

et al. [3] han demostrado que nanofluidos con nanoparticulas de CuO y Al_2O_3 aumentan su conductividad térmica en un 20% y un 30%, respectivamente. Wu et al. [4], realizaron pruebas para verificar el aumento de la tasa de transferencia de calor en nanofluidos con varios tipos de nanopartículas (Cu, Al, C/Cu) en un material de cambio de fase (parafina). Los experimentos realizados arrojaron mejores resultados con nanopartículas de cobre (1 wt%), estabilizadas con en el fluido base mediante un dispersante. En esta investigación, se observó que los tiempos de calentamiento y enfriamiento son reducidos en un 30.3% y 28.2%, respectivamente.

La densidad efectiva y la capacidad calorífica efectiva de un nanofluido pueden calcularse mediante el principio físico de la regla de mezclado [5]. Sin embargo, no hay una teoría general para predecir la conductividad térmica de nanofluidos, la cual depende de las conductividades térmicas del fluido base y las nanopartículas, la concentración volumétrica, el área superficial y la forma de las nanopartículas [6]. Sin embargo, se han propuesto varias correlaciones empíricas para el cálculo la conductividad térmica aparente de mezclas bifásicas [7]. La información experimental para la viscosidad efectiva de nanofluidos es limitada [8 , 9] cuando las propiedades reolólogicas de algunos fluidos son modificadas al adicionarse nanopartículas.

Las simulaciones numéricas de transferencia de calor con nanofluidos son realizadas mediante dos métodos [10]. El primer método considera que la suposición de un medio continuo es válida para fluidos con partículas nanométricas suspendidas [11]. La otra alternativa implementa un modelo bifásico para la descripción de las fases líquida y sólida [12].

En el presente trabajo se realiza una simulación computacional de flujo de calor convectivo en un ducto cuadrado y un tubo circular de un nanofluido (agua, Al_2O_3), considerado un medio continuo, mediante el software ANSYS/FLUENT 12.1. El modelo físico corresponde al montaje experimental estudiado por Zeinali Heris et al. [13], Wang y Mujumdar [10], considerando temperaturas diferentes para la pared (T = 10ºC) y el fluido a la entrada (T = 0ºC), intervalo de temperatura en el cual las propiedades del agua se suponen variables con la temperatura de acuerdo a las ecuaciones constitutivas propuestas por Zografos et al. [14]. Se analiza el efecto del número de Reynolds (Re = 800, 1300 y 2000) y la concentración de nanoparticulas (0%, 5%, 10% y 20%) en el número de Nusselt, el coeficiente de fricción y la distribución de temperaturas a lo largo del ducto y el tubo.

2. Modelo físico y matemático

El modelo físico simulado computacionalmente corresponde a un plano longitudinal de un ducto de sección de cuadrada y un plano axisimétrico de un tubo circular del mismo diámetro hidráulico (D_H = 1 cm) y 1 m de longitud. Estas dimensiones corresponden al estudio experimental realizado por Zeinali Heris et al. [13], para el caso de transferencia de calor del mismo nanofluido estudiado en el presente trabajo, pero a un intervalo de concentraciones volumétricas más bajo (φ = 0% − 2.5%). Las paredes de la superficie del ducto se consideran isotérmicas y el agua ingresa a una temperatura constante.

El cálculo del número de Reynolds está basado en el diámetro hidráulico, la velocidad de entrada y las propiedades del nanofluido obtenidas a la temperatura pelicular. El modelo matemático para el flujo, considerado incompresible y Newtoniano, está comprendido por las ecuaciones de continuidad, eq. (1), Navier-Stokes, eq. (2) y energía, eq. (3), complementado por condiciones de borde de primera clase para la temperatura en la pared y a la entrada, (T_w = 10ºC) y (T_{in} = 0ºC), respectivamente; y condiciones de no deslizamiento en las paredes del ducto (V_w = 0), además de condición de simetría en el plano medio y axisimetría en el caso del ducto circular.

$$\nabla \cdot \mathrm{v} = 0 \tag{1}$$

$$-\nabla\mu_{nf}\nabla\,\mathrm{v} + (\mathrm{v}\cdot\rho_{nf}\nabla)\mathrm{v} + \nabla\mathrm{p} = 0 \tag{2}$$

$$\nabla k_{nf}\nabla T + (\mathrm{v}\cdot\rho_{nf}Cp_{nf}\nabla)T = 0 \tag{3}$$

Las propiedades termofísicas del agua (viscosidad, densidad, conductividad térmica y capacidad calorífica) se consideran variables con la temperatura en el intervalo de 0ºC a 10ºC. Las ecuaciones constitutivas implementadas están disponibles en el estudio experimental realizado por Zografos et al. [14]. La viscosidad es descrita por el modelo:

$$\mu(\mathrm{T}) = \frac{0.03828}{\mathrm{T} - 253.33} \tag{4}$$

mientras la densidad, conductividad térmica y capacidad calorífica son descritas por polinomios de tercer orden:

$$\rho(\mathrm{T}) = 1022.4 - 0.1105\mathrm{T} + 9.63\mathrm{x}10^{-4}\mathrm{T}^2 - 3.011x10^{-6}\mathrm{T}^3 \tag{5}$$

$$\mathrm{k}(\mathrm{T}) = -0.633 + 0.0072\mathrm{T} - 1.14\mathrm{x}10^{-5}\mathrm{T}^2 + 4.24\mathrm{x}10^{-9}\mathrm{T}^3 \tag{6}$$

$$\mathrm{Cp}(\mathrm{T}) = -3755.9 + 67.95\mathrm{T} - 0.1915\mathrm{T}^2 + 0.0001785\mathrm{T}^3 \tag{7}$$

Las propiedades termofísicas del fluido base son modificadas por la adición de nanopartículas de Al_2O_3. La viscosidad es calculada a partir del modelo propuesto por Brinkman [15]:

$$\mu_{nf} = \frac{\mu(\mathrm{T})}{(1-\varphi)^{2.51}} \tag{8}$$

la conductividad térmica del nanofluido es descrita mediante el modelo de Maxwell [16]:

$$k_{nf} = \frac{k_s + 2k(\mathrm{T}) - 2\varphi(k(\mathrm{T}) - k_s)}{k_s + 2k(\mathrm{T}) + \varphi(k(\mathrm{T}) - k_s)}k(\mathrm{T}) \tag{9}$$

mientras la densidad y la capacidad calorífica se obtienen mediante las ecuaciones (10) y (11), respectivamente:

$$\rho_{nf} = (1-\varphi)\rho(T) + \varphi\rho_s \quad (10)$$

$$Cp_{nf} = \frac{\varphi\rho_s Cp_s + (1-\varphi)\rho(T)Cp(T)}{\varphi\rho_s + (1-\varphi)\rho(T)} \quad (11)$$

donde las propiedades de las nanopartículas de Al_2O_3 están denotadas con el subíndice s y están dadas por:

$$\rho_s = 8954.0\,\frac{kg}{m^3};\ k_s = 400\,\frac{W}{mK};\ Cp_s = 383.0\,\frac{J}{kgK} \quad (12)$$

La conductividad térmica y la capacitancia térmica del nanofluido en función de la concentración de nanopartículas y la temperatura están representadas esquemáticamente en las Figs 1 y 2, respectivamente. La conductividad térmica del fluido aumenta aproximadamente un 35% al aumentar en un 10% la concentración de nanopartículas.

La capacitancia térmica, definida como el producto de la densidad con la capacidad calorífica, disminuye al aumentar la concentración de nanopartículas (aproximadamente un 2%), lo que es explicado por la disminución de la capacidad calorífica producto de la adición de las nanopartículas de Al_2O_3.

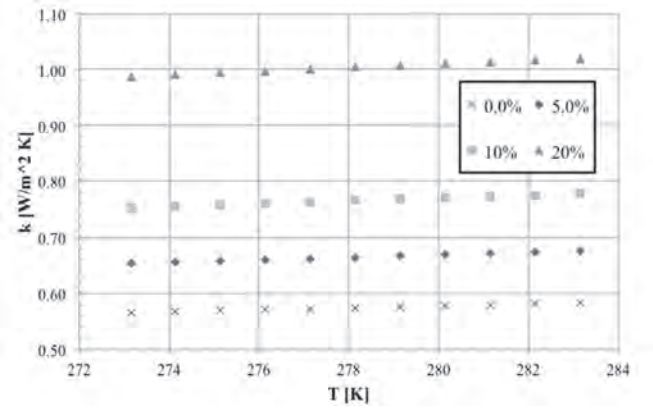

Figura 1. Conductividad térmica del nanofluido (agua y Al_2O_3) en función de la temperatura y concentración volumétrica de partículas como parámetros.
Fuente: Propia

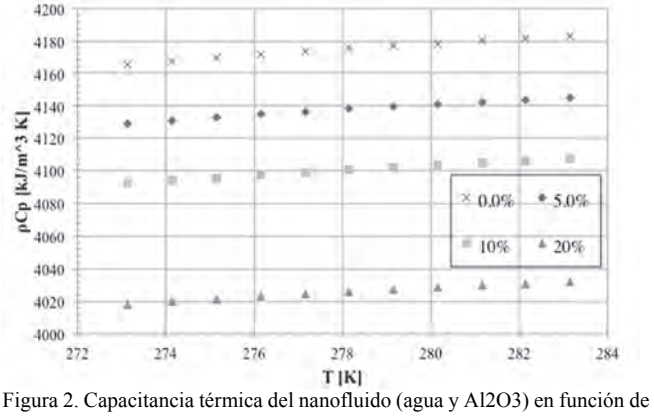

Figura 2. Capacitancia térmica del nanofluido (agua y Al2O3) en función de la temperatura y concentración volumétrica de partículas como parámetros.
Fuente: Propia.

3. Implementación computacional

Las simulaciones han sido realizadas mediante el software comercial basado en el método de los volúmenes finitos ANSYS/FLUENT 12.1. Todos los parámetros computacionales implementados son los disponibles por defecto en el software, excepto los criterios de convergencia para la velocidad (1×10^{-4}) y la temperatura (1×10^{-7}). Las mallas utilizadas en las simulaciones son estructuradas, de volúmenes finitos rectangulares, más concentrados cerca a las paredes isotérmicas del ducto.

3.1. Validación

La implementación del software, los modelos físicos y matemáticos son validados mediante comparación de los números de Nusselt obtenidos numéricamente con valores predichos usando el modelo empírico de Sieder y Tate [17].

$$\overline{Nu}_{nf} = 1.86\left(Re_{nf}Pr_{nf}\frac{D_h}{L}\right)^{1/3}\left(\frac{\mu_{nf}}{\mu_{wnf}}\right)^{0.14} \quad (13)$$

donde el subíndice *nf* se refiere a propiedades evaluadas a la temperatura de entrada (T=0ºC), mientras que *wnf* se refiere a la viscosidad del nanofluido a la temperatura de la pared (T=10ºC). En la Tabla 1 se presentan los resultados de la validación, observándose porcentajes de error menores al 7%. De acuerdo a los menores porcentajes de errores obtenidos en la validación, se seleccionaron los números de Reynolds de 800, 1300 y 2000 para realizar las simulaciones respectivas.

3.2. Análisis del tamaño de malla

La selección del número de volúmenes de control apropiado para garantizar que los resultados son independientes del tamaño de la malla, se basa en el estudio especificado en la Tabla 2, donde los valores entre paréntesis representan los errores relativos al tamaño de malla anterior. De acuerdo a los errores relativos consecutivos entre los resultados obtenidos para el número de Nusselt y el coeficiente de fricción, se selecciona una malla con 256,000 volúmenes finitos para realizar todas las simulaciones.

Tabla 1.
Comparación de los números de Nusselt obtenidos numéricamente y calculado a partir del modelo de Sieder y Tate [17].

$Pe^{1/3}$	Nu (numérico)	Nu (Sieder & Tate)	Error %
15	6.24	6.68	6.56
17	7.25	7.55	3.97
18	7.76	7.98	2.76
20	8.79	8.83	0.45
23	10.34	10.09	2.48

Fuente: Propia.

Tabla 2.
Estudio del tamaño de malla realizado para el caso con Re=2000 y φ = 10%.

Malla	Nu (Error %)	C_f (Error %)
160k	8.46	0.0006140
192k	8.64 (2.12)	0.0006692 (8.99)
256k	8.80 (1.93)	0.0007756 (15.90)
288k	8.85 (0.48)	0.0007915 (2.05)

Fuente: Propia.

4. Resultados y Análisis

En la situación física planteada, se estudia el efecto del número de Reynolds (Re = 800, 1300, 200) y el efecto de la concentración volumétrica de las nanopartículas (φ = 0%, 5%, 10%, 20%) en la transferencia de calor (número de Nusselt y perfiles de temperatura) y mecánica de fluidos (coeficientes de fricción). En las Figs. 3 y 4, se presentan los perfiles de temperatura obtenidos en varias posiciones a lo largo del ducto y el tubo, respectivamente, para cada concentración volumétrica de nanopartículas analizada y un número de Reynolds de 800. Las figuras se presentan solo la sección de los ductos donde se observa un mayor efecto de la concentración de nanopartículas y la posición longitudinal en la distribución de temperaturas. En ambas situaciones se observa como un aumento en la concentración de nanopartículas mejora la transferencia de calor entre las paredes del ducto y el nanofluido, lo que se evidencia en la tendencia del perfil de temperatura a un perfil parabólico desarrollado.

Otra característica común en las Figs 3 y 4 es el efecto más importante sobre la forma del perfil de temperaturas al aumentar la concentración de nanopartículas hasta una concentración del 20%.

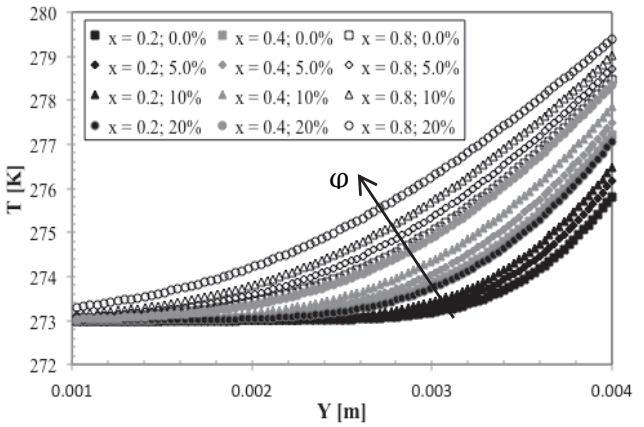

Figura 3. Perfil de temperatura para un flujo laminar (Re=800) a lo largo de un ducto de un nanofluido con diferentes concentraciones de nanopartículas φ.
Fuente: Propia.

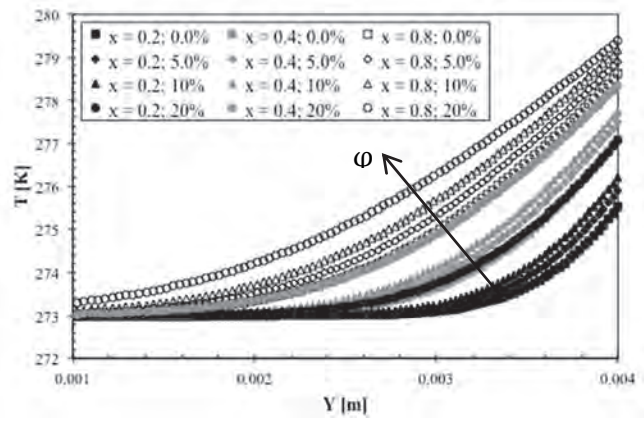

Figura 4. Perfil de temperatura para un flujo laminar (Re=800) a lo largo de un tubo de un nanofluido con diferentes concentraciones de nanopartículas φ.
Fuente: Propia.

En las Figs. 5 y 6, se observan los perfiles de temperatura obtenidos en varias posiciones a lo largo del ducto, para cada concentración volumétrica de nanopartículas analizada y números de Reynolds de 1300 y 2000. Al aumentar el número de Reynolds aumenta la longitud (Le) que le toma al flujo alcanzar la condición de fluido-dinámicamente desarrollado (Re =1300: $L_e \approx 0.65$m y Re = 2000: $L_e \approx 1.0$m). La condición de flujo térmicamente desarrollado se alcanza en una posición mayor. Por este motivo, el efecto de la concentración de nanopartículas en la distribución de temperaturas es menos evidente que para el caso estudiado de Re=800.

El número de Nusselt calculado numéricamente se relaciona el coeficiente convectivo y la conductividad térmica del nanofluido de acuerdo a la ecuación:

$$\overline{Nu}_{nf} = \frac{\bar{h} D_h}{k_{nf}} \qquad (14)$$

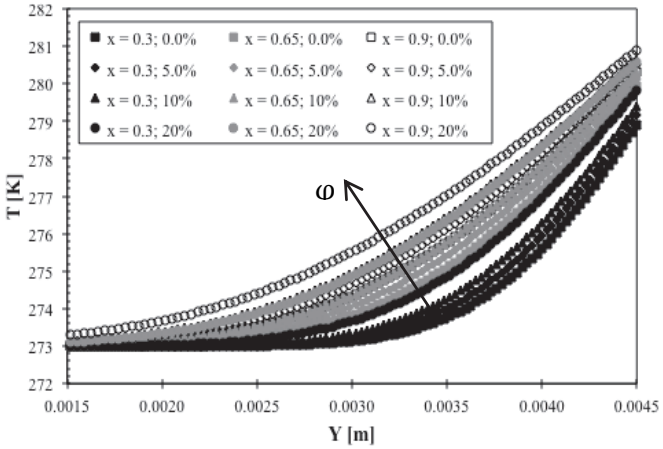

Figura 5. Perfil de temperatura para un flujo laminar (Re=1300) a lo largo de un ducto de un nanofluido con diferentes concentraciones de nanopartículas φ.
Fuente: Propia.

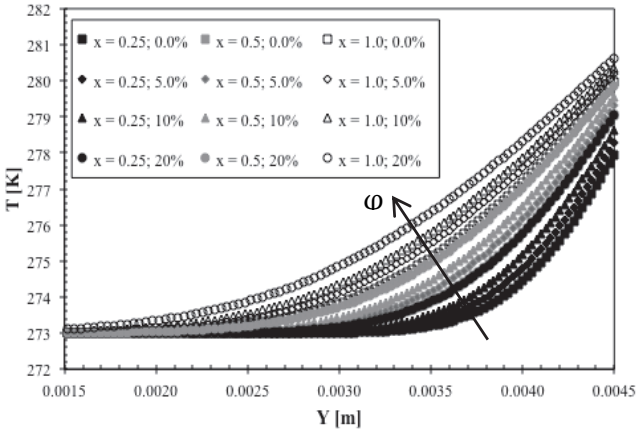

Figura 6. Perfil de temperatura para un flujo laminar (Re=2000) a lo largo de un ducto de un nanofluido con diferentes concentraciones de nanopartículas φ.
Fuente: Propia.

En las Tablas 3 a 5, para cada número de Reynolds, se observa que el número de Nusselt disminuye alrededor del 12% y un 10% cuando la concentración de nanopartículas aumenta de 0% a 10% y de 10% a 20%, respectivamente. Esto se explica por la preponderancia que adquiere la conducción de calor por efecto del aumento de la conductividad térmica del fluido. Sin embargo, el efecto convectivo también aumenta, como lo muestran los valores obtenidos para el coeficiente de transferencia de calor, por efecto del aumento de la concentración de nanopartículas.

Para cada número de Reynolds analizado, un aumento de un 5% y un 10% en la concentración de nanopartículas implica un incremento del coeficiente convectivo de un 8.5% y 17.5%, respectivamente.

Respecto al coeficiente de fricción, los resultados reportados en las Tablas 3 a 5 muestran que existe un aumento diferenciado en cada caso cuando la concentración de nanopartículas aumenta un 10%. Para Re=800, un incremento de φ del 0% al 10% y del 10% al 20% implica un aumento del coeficiente de fricción, y por lo tanto del esfuerzo del corte en la pared, del 23% y el 35%, respectivamente. En los otros dos casos, Re=1300 y Re=2000, estos aumentos diferenciados son del 25% y 32% y del 20% y el 38%, respectivamente.

5. Conclusiones

En el presente trabajo fue analizado computacionalmente el efecto de la concentración de nanopartículas (φ = 0−20%) y el número de Reynolds (Re=800; 1300; 2000), en la transferencia de calor de un flujo laminar de un nanofluido (agua, Al_2O_3) al interior de un tubo y un ducto de sección cuadrada.

Tabla 3.
Número de Nusselt, coeficientes de transferencia y de fricción para Re=800. En paréntesis, los valores obtenidos para un tubo circular.

φ (%)	Nu	$\bar{h}\left[\frac{W}{m^2K}\right]$	C_f
0.0	7.08	407.13 (519.86)	0.00025391
0.5	6.65	442.52 (564.77)	0.00028400
10.0	6.23	477.10 (613.04)	0.00031358
20.0	5.60	562.25 (705.88)	0.00042573

Fuente: Propia.

Tabla 4.
Número de Nusselt, coeficientes de transferencia y de fricción para Re=1300. En paréntesis, los valores obtenidos para un tubo circular.

φ (%)	Nu	$\bar{h}\left[\frac{W}{m^2K}\right]$	C_f
0.0	8.55	491.67 (640.53)	0.00041709
0.5	8.04	535.01 (696.99)	0.00046550
10.0	7.56	578.96 (755.21)	0.00052115
20.0	6.75	677.72 (878.66)	0.00068729

Fuente: Propia.

Tabla 5.
Número de Nusselt, coeficientes de transferencia y de fricción para Re=2000.

φ (%)	Nu	$\bar{h}\left[\frac{W}{m^2K}\right]$	C_f
0.0	10.08	579.65	0.00064641
0.5	9.44	628.17	0.00071073
10.0	8.80	673.92	0.00077565
20.0	7.98	801.21	0.000107081

Fuente: Propia.

Para cada número de Reynolds estudiado se observa una disminución del número de Nusselt al aumentar la concentración de nanopartículas. Este resultado indica la importancia que adquiere la conducción de calor por efecto del aumento de la conductividad térmica del fluido.

Por efecto de la adición de nanopartículas, la convección también se incrementa. Para cada número de Reynolds analizado, un aumento de un 5% y un 10% en la concentración de nanopartículas implica un incremento del coeficiente convectivo de un 8.5% y 17.5%, respectivamente.

El coeficiente de fricción aumenta de forma diferencial cuando la concentración de nanopartículas aumenta un 10%. En el caso Re=800, un incremento de φ del 0% al 10% y del 10% al 20% implica un aumento del coeficiente de fricción del 23% y el 35%, respectivamente. Mientras para Re=1300 y Re=2000, estos aumentos diferenciados son del 25% y 32% y del 20% y el 38%, respectivamente. El coeficiente de fricción aumenta de forma diferencial cuando la concentración de nanopartículas aumenta un 10%. En el caso Re=800, un incremento de φ del 0% al 10% y del 10% al 20% implica un aumento del coeficiente de fricción del 23% y el 35%, respectivamente.

Agradecimientos

D.A. Vasco y D. Chen agradecen el apoyo suministrado por el proyecto FONDECYT 11130168.

D.A. Vasco y J. Acevedo agradecen a la Vicerrectoría de Investigación y Desarrollo de la Universidad de Santiago de Chile.

Powered@NLHPC: Esta investigación fue parcialmente apoyada por la infraestructura de supercómputo del NLHPC (ECM-02).

Bibliografía

[1] Teng, T.-P., Thermal conductivity and phase-change properties of aqueous alumina nanofluid. Energy Conversion and Management, 67(1), pp. 369-375, 2013. DOI: 10.1016/j.enconman.2012.12.004

[2] Zhu, H.T., Lin, Y.S. and Yin, Y.S., A novel one-step chemical method for preparation of copper nanofluids. Journal of Colloid and Interface Science, 277(1), pp. 100-103, 2004. DOI: 10.1016/j.jcis.2004.04.026

[3] Masuda, H., Ebata, A. and Teramae, K., Alteration of thermal conductivity and viscosity of liquid by dispersing ultra-fine particles. Dispersion of Al2O3, SiO2 and TiO2 ultra-fine particles. Netsu Bussei, 7(4), pp. 227-133, 1993.

[4] Wu, S., Zhu, D., Zhang, X. and Huang, J., Preparation and melting / freezing characteristics of Cu / paraffin nanofluids as phase-change material (PCM). Energy Fuels, 24(17), pp. 1894-1898, 2010. DOI: 10.1021/ef9013967

[5] Ding, Y., Alias, H., Wen, D. and Williams, R.A., Heat transfer of aqueous suspensions of carbon nanotubes (CNT nanofluids). International Journal of Heat and Mass Transfer, 49(1-2), pp. 240-250, 2006. DOI: 10.1016/j.ijheatmasstransfer.2005.07.009

[6] Wang, X.Q. and Mujumdar, A.S., A review on nanofluids - Part II: Experiments and applications. Brazilian Journal of Chemical Engineering, 25(4), pp. 631-648, 2008b. DOI: 10.1590/S0104-66322008000400002

[7] Corsione, M., Empirical correlating equations for predicting the effective thermal conductivity and dynamic viscosity of nanofluids. Energy Conversion and Management, 52(1), pp. 789-793, 2011. DOI: 10.1016/j.enconman.2010.06.072

[8] Abu-Nada, E., Masoud, Z. and Hijazi, A., Natural convection heat transfer enhancement in horizontal concentric annuli using nanofluids. International Communications in Heat and Mass Transfer,

35(5), pp. 657-665, 2008. DOI: 10.1016/j.icheatmasstransfer.2007.11.004
[9] Xuan, Y. and Li, Q., Heat transfer enhancement of nanofluids. International Journal of Heat and Fluid Flow, 21(1), pp. 58-64, 2000. DOI: 10.1016/S0142-727X(99)00067-3
[10] Wang, X.Q. and Mujumdar, A.S., A review on nanofluids - Part I: theoretical and numerical investigations. Brazilian Journal of Chemical Engineering, 25(4), pp. 613-630, 2008a. DOI: 10.1590/S0104-66322008000400001
[11] Khanafer, K. and Vafai, K., A critical synthesis of thermophysical characteristics of nanofluids. International Journal of Heat and Mass Transfer, 54(19-20), pp. 4410-4428, 2011. DOI: 10.1016/j.ijheatmasstransfer.2011.04.048
[12] Murshed, S.M.S., Leong, K.C. and Yang, C., Thermophysical and electrokinetic properties of nanofluids - A critical review. Applied Thermal Engineering, 28(17-18), pp. 2109-2125, 2008. DOI: 10.1016/j.applthermaleng.2008.01.005
[13] Zeinali-Heris, S., Nassan, T.H., Noie, S., Sardarabadi, H. and Sardarabadi, M., Laminar convective heat transfer of Al2O3 / water nanofluid through square cross-sectional duct. International Journal of Heat and Fluid Flow, 44(1), pp. 375-382, 2013. DOI: 10.1016/j.ijheatfluidflow.2013.07.006
[14] Zografos, A.I., Martin, W.A. and Sunderland, J., Equations of properties as a function of temperature for seven fluids. Computer Methods in Applied Mechanics and Engineering, 61(2), pp. 177-187, 1987. DOI: 10.1016/0045-7825(87)90003-X
[15] Brinkman, H.C. The viscosity of concentrated suspensions and solutions. The Journal of Chemical Physics, 20(4), pp. 571-571, 1952. DOI: 10.1063/1.1700493
[16] Maxwell, J., A treatise on electricity and magnetism. Third Edition. Oxford: Clarendon Press, 1891.
[17] Sieder, E.N. and Tate, G.E., Heat transfer and pressure drop of liquids in tubes. Industrial & Engineering Chemistry, 12(28), pp. 1429-1435, 1936. DOI: 10.1021/ie50324a027

D.A. Vasco-Calle, recibió el título de Ing. Químico en 2004, el título de MSc. en Ciencias Químicas en 2007 y el grado de Dr. en Ingeniería de Procesos en 2013. Actualmente es profesor del área de termofluidos del Departamento de Ingeniería Mecánica de la Universidad de Santiago de Chile. Sus intereses en investigación incluyen: materiales de cambio de fase, nanofluidos, CFD y computación de alto rendimiento.
ORCID: 0000-0001-7456-4683

D. Chen, recibió el título de Ing. y MSc. en Ingeniería Civil Mecánica en 2014. Actualmente es instructor de laboratorio y profesor de cátedra de en la Facultad de Ingeniería de la Universidad de Santiago de Chile, Chile. Sus intereses en investigación incluyen: CFD, microfluidos y nanofluidos y modelamiento de materiales hiperelásticos en aplicaciones biológicas.
ORCID: 0000-0001-9008-5412

J.L. Acevedo-Cabello, recibió el título de Ing. Civil en Mecánica en 2004 y el grado de Dr. en Ciencia e Ingeniería de los Materiales en 2013. Actualmente es profesor del área de sólidos del Departamento de Ingeniería Mecánica de la Universidad de Santiago de Chile, Chile. Las líneas de investigación que actualmente desarrolla son: transferencia de calor con cambio de fase, optimización de procesos y vida útil de los materiales.
ORCID: 0000-0003-0106-3794

UNIVERSIDAD NACIONAL DE COLOMBIA
SEDE MEDELLÍN
FACULTAD DE MINAS

Área Curricular de Ingeniería
Geológica e Ingeniería de Minas y Metalurgia

Oferta de Posgrados

Especialización en Materiales y Procesos
Maestría en Ingeniería - Materiales y Procesos
Maestría en Ingeniería - Recursos Minerales
Doctorado en Ingeniería - Ciencia y Tecnología de Materiales

Mayor información:

E-mail: acgeomin_med@unal.edu.co
Teléfono: (57-4) 425 53 68

UNIVERSIDAD NACIONAL DE COLOMBIA
SEDE MEDELLÍN
FACULTAD DE MINAS

DYNA
http://dyna.medellin.unal.edu.co/

Viscoelastic behavior of yellow pitahaya treated with 1-MCP

Laura Sofía Torres-Valenzuela [a], Alfredo Adolfo Ayala-Aponte [b] & Liliana Serna-Cock [c]

[a] *Facultad de Ingeniería, Universidad La Gran Colombia Seccional Armenia, Armenia, Colombia. torresvallaura@miugca.edu.co*
[b] *Escuela de Ingeniería de Alimentos, Universidad del Valle, Cali, Colombia. alfredo.ayala@correounivalle.edu.co*
[c] *Facultad de Ingeniería y Administración. Universidad Nacional de Colombia. Palmira, Colombia. lserna@unal.edu.co*

Received: May 4th, 2015. Received in revised form: November 1rd, 2015. Accepted: January 18th, 2016.

Abstract
Foods may have both solid and liquid properties, and are described as viscoelastic products. Knowledge on such viscoelastic features is very useful for quality control and/or food stability. The purpose of this work was to evaluate the effect of the application of 1-MCP on the viscoelastic properties of minimally processed yellow pitahaya during refrigeration storage, by using a stress relaxation test. Viscoelastic parameters were determined through Generalized Maxwell and Peleg's rheologic models. Both rheological models proved suitable to predict viscoelastic behavior; however, Peleg's model better described this behavior. Samples of treated and non-treated pitahaya with 1-MCP decreased their elastic behavior (firmness decrease) during storage. Fruit treated with 1-MCP showed a greater elastic component than non-treated samples during storage. These two rheological models were suitable for predicting the viscoelastic behavior, however

Keywords: Stress relaxation; Generalized Maxwell; Peleg; *Selenicereus megalanthus.*

Comportamiento viscoelástico de pitahaya amarilla tratada con 1-MCP

Resumen
Los alimentos pueden exhibir características de sólido y de líquido y se describen como productos viscoelásticos. El conocimiento de las propiedades viscoelasticas es muy útil para el control de la calidad y/o estabilidad de los alimentos. El objetivo de este trabajo fue evaluar el efecto de la aplicación de 1-MCP sobre propiedades viscoelásticas de muestras de pitahaya amarilla mínimamente procesada durante el almacenamiento en refrigeración, empleando la prueba de esfuerzo de relajación. Los parámetros viscoelásticos se determinaron mediante los modelos reológicos de Maxwell Generalizado y Peleg. Estos dos modelos reológicos fueron apropiados para predecir el comportamiento viscoelástico, sin embargo, el modelo de Peleg describió mejor este comportamiento. Las muestras de pitahaya tratada y no tratadas con 1-MCP disminuyeron su comportamiento elástico (disminución de firmeza) durante el almacenamiento. La fruta tratada con 1-MCP presentó mayor componente elástico que las muestras no tratadas durante el almacenamiento.

Palabras clave: Esfuerzo de relajación; Maxwell generalizado; Peleg, *Selenicereus megalanthus*.

1. Introduction

Yellow pitahaya is a cactus from tropical and sub-tropical America, that belongs to the group of promising fruit for plantation [1]. It is included in the ten most promising fruits for exportation from Colombia [2,3].

Before 1989, Japan was the main destination of yellow pitahaya; exports were suspended due to the presence of Mediterranean fruit fly (*Ceratitis capitata*) larva, resulting in a reduction in production [4]. In order to mitigate the impact of this suspension, Protocol T106 was signed in January 2008, this protocol allows for the importation of minimally processed pitahaya into the United States, taking into account that this process removes the risk of the presence of Mediterranean fruit fly in the fruit.

Minimally processed products are one of the fastest growing areas in the food industry. However, cutting fruit results in a decrease in shelf life [5], changes to texture and a reduced firmness of the cell wall[6,7]. These changes set limits to storage time resulting in a shorter shelf life [8].

The mechanical and / or textural properties of foods are important for quality control and consumer acceptance [9-11]; these properties are one of the four main quality features of foods [12]. Foods, which exhibit both liquid and solid properties, are described as viscoelastic products [13]. Most foods behave as a viscoelastic material under given levels of applied stress and

© The author; licensee Universidad Nacional de Colombia.

within certain time scales [14]. In order to study the viscoelastic behavior of foods it is important to learn about rheological properties, which study the science of flow and deformation of matter [15]. Various rheologic models are used to represent materials and predict their viscoelastic behavior [16]. Such models include various combinations of Hookean solid elements (springs), and elements of Newtonian flow (dashpot) [17]. One of the tests used to establish a foods viscoelastic behavior is stress relaxation [16,18]. This test consists of subjecting a piece of food to a constant load for a determined period of time, in which such stress significantly decreases [19,20]. In addition, it allows for the definition of parameters such as relaxation time, elasticity and viscosity modules [21]. Results of stress relaxation analysis are important because they provide information on firmness, acceptation and processing of fruit [12], and predict changes of material during manipulation [16]. This test is widely used to establish foods viscoelastic properties, and their experimental values are mainly adjusted by Maxwell and Peleg's models [13,16,20].

1-Methylcyclopropene (1-MCP) is a compound that inhibits ethylene action both on whole fruit and cut fruit; it has been demonstrated to have the potential to reduce the softening of minimally processed products such as pineapple [22], melon 'Galia' [23], kiwi fruit [24,25], mango 'Kent' and 'Keitt', marmalade fruit 'Fuyu' [24], and pear 'Blanquilla' [25]. Application of 1-MCP on minimally-processed yellow pitahaya, may represent an alternative to reduce changes to texture during storage [25].

The purpose of this work is to evaluate the effect of applying 200 µgL-1 of 1-MCP on the viscoelastic properties of minimally-processed yellow pitahaya samples during refrigerated storage, by using a stress relaxation test.

2. Methodology

2.1. Raw Material

Yellow pitahaya at ripeness stage 3 [26], from the municipality of Roldanillo, Valle del Cauca, Colombia was used. Harvested fruit pieces were classified, washed with current water, hygenized with chlorated water (200 μgL^{-1}), washed with distillate water and dried at room air.

2.2. Preparation and application of 1-MCP

A powder formulation of 1-MCP (3.8% w / w) supplied by Rohm and Haas Chemical Ltd. (Philadelphia, Pennsylvania) was used. Solutions of 40 L of 1-MCP at a concentration of 200 μgL^{-1} were prepared using distillate water. Selected fruit pieces were submerged for 10 min into the solution, then they were washed in distillate water for 5 min (to remove excess of 1-MCP), and dried at room air.

2.3. Minimal processing, packaging and storage

Previously 1-MCP treated and non-treated (control) fruit pieces were transversely cut at a thickness of 1.0 ± 0.1 and a diameter of 6 cm, using a mechanical cutting machine Javar (model GE 250, Cali, Colombia). They were vacuum packed, in a low density polyamide and polyethylene coextruded flexible packaging, 70-micra thick and permeability at O_2 39 cm^3 m^{-2} day-1 Atm-1 at 23°C permeability at CO2 of 107 cm3 m-2 day^{-1} Atm^{-1} at 23°C and permeability at water vapor of 10.2 g cm^3 m^{-2} day^{-1} Atm^{-1} at 38°C. Bags were sealed using a sealing strength of 1.5 Kg cm^{-1} at 160°C per 3 s. The packed fruits were stored for 16 days in an environmental chamber (1000 L Dies, Colombia) at 10 ± 1°C and 85% relative humidity.

2.4. Stress relaxation

At each storage period of time, samples were removed from the climate chamber. Disks 4 cm in diameter were then cut out from the slices by using a cork borer. Such slices were tested for stress-relaxation by using a texturemeter (EZ-Test, Shimadzu, USA), adapted to a 6-cm cylindrical plate. The samples were placed on an aluminum base lubricated with liquid paraffin to prevent effects from friction[20], and compressed at 0.8 mm (8% initial height), at a compression velocity of 10 mm/min. This stress compression was kept constant for 600 s.

2.5. Relaxation modeling

Stress-relaxation experimental values (stress-time) were adjusted to generalized Maxwell (Ec. 1) and Peleg (Ec.2) models. For Ec. 1 three elements were used, where ε_i is the elastic module of element i, θ_i is the time relaxation of element i and $\sigma(t)$ is the stress for one time t.

$$\sigma(t) = \varepsilon_0 + \varepsilon_1 * e^{\left(\frac{-t}{\theta 1}\right)} + \varepsilon_2 * e^{\left(\frac{-t}{\theta 2}\right)} \quad (1)$$

The model is composed of two Maxwell elements and a spring in parallel. Each Maxwell element consists of a Newtonian dashpot in series with a Hookean spring [13]. Constants of a generalized Maxwell model were obtained by non-linear regression (Levenberg-Marquard), using an SPSS 11.5 program for Windows (SPSS Inc, Chicago, 2002).

Peleg and Normand proposed Ec 2, which may be adjusted through linear regression, were σ_0 is the initial stress, σ the stress of each time t during relaxation process, k1 is the reciprocal of initial decrease of velocity and k2 is an hypothetic value of normalized asymptotic force [15] [16].

$$\frac{\sigma_0 t}{\sigma_0 - \sigma} = k1 + k2t \quad (2)$$

These non-dimension constants are related to the elasticity of material subject to stress relaxation, and were obtained through linear regression with Microsoft® Office Excel 2007.

2.6. Experimental design

A completely randomized factorial design 2x4 was used, with two factors: Concentration of 1-MCP solution with two levels: 0 and 200 μgL^{-1}, where 0 is the control treatment (without 1-MCP application), and storage time with 4 levels

0, 4, 12, and 16 days. The effect of 1-MCP concentration and storage time was determined by analyzing the variance (ANOVA) at 5% probability using the Statgraphics software version Demo (Minitab Inc., State College, PA, 2007). All determinations were performed in triplicate.

3. Results

3.1. Analysis of relaxation

Fig. 1 shows typical curves of stress relaxation of pitahaya samples at various days of storage. In all treatments the relaxation curve decreased in function of storage time.

3.2. Relaxation modeling

Maxwell model constants for treated and non-treated samples during storage are shown in Table 1.

A good adjustment of experimental values is seen, showing an R^2 variation between 0.989 and 0.996, which shows that the Maxwell model is suitable for predicting experimental results. Elasticity constants of module ε_o, $\varepsilon 1$ and ε_2 associated to the 3 springs of Maxwell, did not show any pattern of trend in the viscoelastic analysis of pitahaya samples during storage. On day 4 treated samples showed lower values in elastic models compared to the control, indicating minor elastic behavior, or minor firmness, but on day 12 it was inverse showing more elastic component than the control. On day 16 only the elastic module ε_2 showed a higher value in samples treated with 1-MCP. Significant differences between the control and 200 $\mu g.L^{-1}$ 1-MCP application were observed in all the elastic module (ε_i) and the first time relaxation (θ_1) ($p < 0.05$); the second time relaxation was not affected ($p > 0.05$).

In terms of relaxation time constants, (θ_1 and θ_2), associated to viscous behavior or liquid phase of foods [13], it was observed that control treatment showed minor values (except for $\theta 1$ on day 4). This fact means that at less relaxation time, the material dissipates faster due to the imposed load, indicating a behavior more similar to liquid (less firmness) than to solid [27]. Therefore, according to these relaxation times, samples treated with 1-MCP showed higher values of solidity, perhaps due to minor degradation of pectins and hemicellulose by the effect of decreasing enzymatic activity [28].

This behavior is the same as behavior reported in uniaxial compression tests of yellow pitahaya treated with 200 μgL^{-1} of 1-MCP during storage [29,30].

Table 1.
Maxwell generalized model constants for samples treated with 200 μgL^{-1} of 1-MCP and control during storage

Treatment	ε_0 (Pa)	ε_1 (Pa)	$\theta 1$ (s)	ε_2 (Pa)	$\theta 2$ (s)	R^2
Day 0 200	2988.74	1280.10	11.62	789.10	220.85	0.995
Control	2988.74	1280.10	11.62	789.10	220.85	0.995
Day 4 200	2782.78	1566.15	9.68	912.39	230.10	0.996
Control	4428.79	2180.89	10.88	1295.50	214.97	0.995
Day 12 200	2737.15	1578.93	10.01	923.59	219.34	0.995
Control	2425.97	1357.80	9.64	597.35	189.73	0.993
Day 16 200	2087.04	1177.47	11.37	699.51	588.61	0.989
Control	2425.97	1357.72	9.65	597.34	189.74	0.993

Source: The authors.

Table 2.
Constants of Peleg's model for fruit treated with 200 μgL^{-1} of 1-MCP and control during storage

Time	Control			200 $\mu g\ L^{-1}$		
(Days)	k_1	k_2	R_2	k_1	k_2	R2
0	68,8	2,27	0,999	68,8	2,27	0,999
4	68,8	2,16	0,999	70,2	2,07	0,999
12	54,7	2,16	0,999	62,6	2,06	0,999
16	53,9	2,16	0,999	72,9	2,08	0,997

Source: The authors.

According to the above results relaxation time parameter is more suitable than elasticity modules εo, ε1 and ε2 to describe viscoelastic behavior of pitahaya samples treated and non-treated with 1-MCP during storage. Table 2 shows rheological constants (k1 and k2) of Peleg's model. Correlation coefficients (R_2) for control samples varied between 0,9987 and 0,9993 and for treated samples between 0,9984 and 0,9993. These values show that Peleg´s model fits the experimental values better than Maxwell´s model.

It can be seen that k1 parameter decreases in control treatment from 68.8 to 53.9 during storage, while in the samples treated with 1-MCP no trend is seen. The reciprocal of K1 constant of Peleg's model depicts the initial decay rate during relaxation time [13]; therefore a decrease of this parameter is an indication of stress relaxation decline, associated with minor firmness. This table shows that the application of 1-MCP

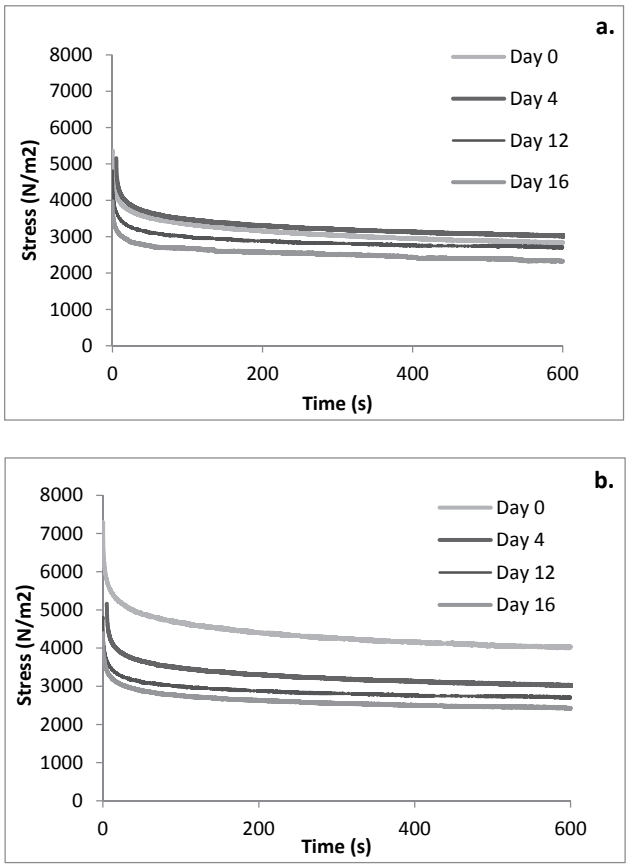

Figure 1. Relaxation curve of pitahaya slices (a) treated with 1-MCP and (b) control in function of storage time.
Source: The authors.

increased k1 values compared to the control during storage ($p<0.05$), which means that the application of 1-MCP decreased stress relaxation reduction, associated with a more elastic or solid material. This behavior may be attributed to the fact that 1-MCP impacted enzymatic activity decrease, and consequently a lower degradation of fruit pectins and hemicelluloses is achieved [28].

Parameter k2 represents material solidity degree when $k_2 \rightarrow \infty$ is considered an ideal elastic solid [16]. A slight decrease of this parameter during storage may be seen in both treatments, associated with a mild loss of solidity or firm,ess of samples. This result may be due to a low weight loss because of dehydration of the fruit [31]. However, the ANOVA did not show any significant difference ($p>0.05$). No significant difference was observed, ($p>0.05$) when comparing control treatment and samples with an application of 1-MCP, with values relatively close varying between 2.06 and 2.27. This result indicates that parameter k2 was not suitable to describe fruit viscoelastic properties.

The results demonstrate that during storage of slices of yellow pitahaya, the viscoelastic properties were more sensitive to the viscous component (relaxation times and K1), than to the elastic component (elastic modules and K2). This behavior may be explained by using minimally processed fruit with the characteristics of fresh fruit, therefore its viscous component was predominant.

4. Conclusion

Yellow pitahaya samples treated and non-treated by applying 200 µgL-1 of 1-MCP decreased their elastic behavior (firmness decrease), due to the effect of storage time in refrigeration, perhaps due to natural and irreversible degradation of pectins and hemicelluloses. The application of 200 µgL-1 of 1-MCP positively impacted fruit elastic behavior, showing more elasticity or solidity than non-treated samples (control) during storage, in relation to increasing relaxation time in the Maxwell model, and higher k1 values in the Peleg model. It was shown that Maxwell's and Peleg's rheologic models are suitable to predict the viscoelastic behavior of minimally processed yellow pitahaya samples; however, Peleg's model showed the best adjustments of experimental values. The stress relaxation test may become a useful tool to evaluate the viscoelastic behavior of yellow pitahaya samples during storage in refrigeration.

Acknowledgments

The authors of this work wish to thank the Ministerio de Agricultura y Desarrollo Rural de Colombia, and the Asociación de productores de pitahaya amarilla – Asoppitaya for funding this project.

References

[1] Braga-Marques, V., Amato-Moreira, R., Ramos, J.D., Arcanjo-de Araujo, N. and Reis-Silva, F.O.D., Fenologia reprodutiva de pitaia vermelha no município de Lavras, MG, Ciência Rural, 41(6), pp. 984-7, 2011.

[2] Ayala-Aponte, A.A., Giraldo-Cuartas, C.J. y Serna-Cock, L., Cinéticas de deshidración osmótica de pitahaya amarilla (*Selenicereus megalanthus*), Interciencia, 35(7), pp. 539-544, 2010.

[3] Ayala-Aponte, A.A., Serna-Cock, L. y Giraldo-Cuartas, C.J., Efecto de la agitación sobre la deshidratación osmótica de pitahaya amarilla (*Selenicereus megalanthus s.*) empleando soluciones de sacarosa, Interciencia, 34(7), pp. 492-496, 2009.

[4] Ortiz, X., Acevedo, X. and Martínez, H., Características y estructura de los frutales de exportación en Colombia. En: Agrocadenas O, Ed. Ministerio de Agricultura y Desarrollo Rural, Bogotá, 2002.

[5] Soliva-Fortuny, R.C. and Martín-Belloso, O., New advances in extending the shelf-life of fresh-cut fruits: A review, Trends in Food Science & Technology, 14(9), pp. 341-53, 2003. DOI: 10.1016/s0924-2244(03)00054-2

[6] Rico, D., Martín-Diana, A.B., Barat, J.M. and Barry-Ryan, C., Extending and measuring the quality of fresh-cut fruit and vegetables: A review, Trends in Food Science & Technology, 18(7), pp. 373-386, 2007. DOI: 10.1016/j.tifs.2007.03.011

[7] Salvador, A., Varela, P. and Fiszman, S.M., Consumer acceptability and shelf life of "Flor de invierno" pears (*Pyrus communis L.*) under different storage conditions, Journal of Sensory Studies, 22, pp. 243-255, 2007.

[8] Taherian, A.R. and Ramaswamy, H.S., Kinetic considerations of texture softening in heat treated root vegetables, International Journal of Food Properties, 12(1), pp. 114-128, 2008. DOI: 10.1080/10942910802312207

[9] Mayor, L., Cunha, R. and Sereno, A., Relation between mechanical properties and structural changes during osmotic dehydration of pumpkin, Food Research International, 40(4), pp. 448-460, 2007. DOI: 10.1016/j.foodres.2007.02.004

[10] Sauvant, P., Cansell, M., Hadj-Sassi, A. and Atgié, C., Vitamin A enrichment: Caution with encapsulation strategies used for food applications, Food Research International, 46(2), pp. 469-479, 2012. DOI: 10.1016/j.foodres.2011.09.025

[11] Muliawan, E.B. and Hatzikiriakos, S.G., The effect of refrigerated storage on the rheological properties of three commercial mozzarella cheeses, International Journal of Food Engineering, 4(4), pp. 1-19, 2008.

[12] Bourne, M., Food texture and viscosity concept and measurement. California, USA: Academic Press an Elsevier Science Imprint, 2002.

[13] Hassan, B., Alhamdan, A.M. and Elansari, A.M., Stress relaxation of dates at khalal and rutab stages of madurity, Journal of Food Engineering, 66, pp. 439-445, 2005.

[14] Pereira, P.A.P., de Souza, V.R., Teixeira, T.R., Queiroz, F., Borges, S. V. and Carneiro, J.d.D.S., Rheological behavior of functional sugar-free guava preserves: Effect of the addition of salts, Food Hydrocolloids, 31(2), pp. 404-412, 2013. DOI: 10.1016/j.foodhyd.2012.11.014

[15] Steffe, J.F., Rheological methods in food process engineering. Segunda ed: East Lansing, MI: Freeman Press, East Lansing, USA, 1996.

[16] Moghimi, A., Saiedirad, M.H. and Moghadam, E.G., Interpretation of viscoelastic behaviour of sweet cherries using rheological models, International Journal of Food Science & Technology, 46(4), pp. 855-861, 2011. DOI: 10.1111/j.1365-2621.2011.02563.x

[17] Sahin, S. and Gülüm-Sumnu, S., Physical properties of foods. Springer Science+Businessm Media, Ankara, Turkey, 2006.

[18] Peleg, M., Characterization of the stress relaxation curves of solid foods, Journal of Food Science, 44(1), pp. 277-281, 1979.

[19] Rodrigues, A.C.C., Cunha, R.L. and Hubinger, M.r.D., Rheological properties and colour evaluation of papaya during osmotic dehydration processing, Journal of Food Engineering, 59(2-3), pp. 129-135, 2003. DOI: 10.1016/s0260-8774(02)00442-9

[20] Rodríguez-Sandoval, E., Fernández-Quintero, A. and Cuvelier, G., Stress relaxation of reconstituted cassava dough, LWT - Food Science and Technology, 42(1), pp. 202-206, 2009. DOI: 10.1016/j.lwt.2008.03.007

[21] Danalache, F., Beirão-da-Costa, S., Mata, P., Alves, V.D. and Moldão-Martins, M., Texture, microstructure and consumer preference of mango bars jellified with gellan gum, LWT - Food Science and Technology, 62(1), pp. 584-591, 2015. DOI: 10.1016/j.lwt.2014.12.040

[22] Rocculi, P., Cocci, E., Romani, S., Sacchetti, G. and Rosa, M., Effect of 1-MCP treatment and N2O MAP on physiological and quality changes of fresh-cut pineapple, Postharvest Biology and Technology, 51(3), pp. 371-377, 2009. DOI: 10.1016/j.postharvbio.2008.07.010
[23] Ergun, M., Jeong, J., Huber, D.J. and Cantliffe, D.J., Physiology of fresh-cut 'Galia' (*Cucumis melo var. reticulatus*) from ripe fruit treated with 1-methylcyclopropene, Postharvest Biology and Technology, 44(3), pp. 286-292, 2007. DOI: 10.1016/j.postharvbio.2006.08.019
[24] Vilasboas, E. and Kader, A., Effect of 1-methylcyclopropene (1-MCP) on softening of fresh-cut kiwifruit, mango and persimmon slices, Postharvest Biology and Technology, 43(2), pp. 238-244, 2007. DOI: 10.1016/j.postharvbio.2006.09.010
[25] Arias, E., López-Buesa, P. and Oria, R., Extension of fresh-cut "Blanquilla" pear (*Pyrus communis L.*) shelf-life by 1-MCP treatment after harvest, Postharvest Biology and Technology, 54(1), pp. 53-58, 2009. DOI: 10.1016/j.postharvbio.2009.04.009
[26] ICONTEC. NTC 3554. Frutas frescas: Pitahaya. Colombia: Federación Nacional de Cafeteros de Colombia, 1996.
[27] Supavititpatana, T. and Apichartsrangkoon, A., Combination effects of ultra-high pressure and temperature on the physical and thermal properties of ostrich meat sausage (yor), Meat Science, 76(3), pp. 555-560, 2007. DOI: 10.1016/j.meatsci.2007.01.007
[28] Blankenship, S.M. and Dole, J.M., 1-Methylcyclopropene: A review, Postharvest Biology and Technology, 28(1), pp. 1-25, 2003. DOI: 10.1016/s0925-5214(02)00246-6
[29] Serna, L., Torres, L.S. and Ayala, A.A., Effect of pre- and postharvest application of 1-methylcyclopropene on the maturation of yellow pitahaya (*Selenicerus megalanthus Haw*), Vitae, 19, pp. 49-59, 2012.
[30] Serna-Cock, L., Torres-Valenzuela, L.S .and Ayala-Aponte, A., Changes in mechanical properties of minimally-processed yellow pitahaya treated with 1-MCP, DYNA, 79(174), pp. 71-78, 2012.
[31] Manganaris, G., Crisosto, C., Bremer, V. and Holcroft, D., Novel 1-methylcyclopropene immersion formulation extends shelf life of advanced maturity 'Joanna Red' plums (Prunus salicina Lindell), Postharvest Biology and Technology, 47(3), pp. 429-433, 2008. DOI: 10.1016/j.postharvbio.2007.07.006

L.S. Torres-Valenzuela, received a BSc. in Agricultural Engineering in 2007 from the Universidad del Valle, Cali, Colombia, and an MSc. degree in Food Engineering from the Universidad del Valle, Cali, Colombia. She is a professor in the area of Biotechnology and Food Technology in the Universidad La Gran Colombia, Armenia, Colombia. Her research interests include: preservation, food processing and biotechnology.
ORCID: 0000-0001-8032-1901

A.A. Ayala-Aponte, received a BSc. in Agricultural Engineering in 1993 from the Universidad del Valle, Cali, Colombia and a PhD. degree in Science and Food Technology in 2011 from the Universidad Politécnica de Valencia, Spain. He is a professor in the area of Food Technology and Engineering, in the Universidad del Valle, Cali, Colombia. His research interests include: preservation and food processing.
ORCID: 0000-0003-0310-3577

L. Serna-Cock, received a BSc. in Bacteriology from the Universidad Católica de Manizales, Colombia in 1987, and a PhD degree in Food Engineering from the Universidad del Valle, Cali, Colombia. She is a professor in the area of Biotechnology in the Universidad Nacional de Colombia, Palmira, Colombia. Her research interests include: preservation, food processing and biotechnology.
ORCID: 0000-0003-2911-0871

UNIVERSIDAD NACIONAL DE COLOMBIA
SEDE MEDELLÍN
FACULTAD DE MINAS

Área Curricular de Medio Ambiente

Oferta de Posgrados

Especialización en Aprovechamiento de Recursos Hidráulicos
Especialización en Gestión Ambiental
Maestría en Ingeniería Recursos Hidráulicos
Maestría en Medio Ambiente y Desarrollo
Doctorado en Ingeniería - Recursos Hidráulicos
Doctorado Interinstitucional en Ciencias del Mar

Mayor información:

E-mail: acia_med@unal.edu.co
Teléfono: (57-4) 425 5105

UNIVERSIDAD NACIONAL DE COLOMBIA
SEDE MEDELLÍN
FACULTAD DE MINAS

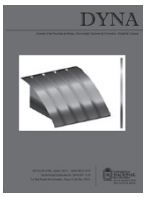

DYNA
http://dyna.medellin.unal.edu.co/

Adopting Ecodesign Management Systems in the construction sector. Analysis from the perspective of stakeholders

Beñat Landeta-Manzano [a], Germán Arana-Landín [b], Patxi Ruiz de Arbulo-López [a] & Pablo Díaz de Basurto-Uraga [a]

[a] *E. Técnica Superior de Ingeniería de Bilbao, Universidad del País Vasco (UPV/EHU), Bilbao, España. benat.landeta@ehu.eus*
[b] *E.U. Politécnica de Donostia- San Sebastián, Universidad del País Vasco (UPV/EHU), San Sebastián, España. g.arana@ehu.eus*

Received: May 14th, 2015. Received in revised form: November 18th, 2015 Accepted: February 17th, 2016.

Abstract
In order to analyze the main reasons, the adoption process, outcomes and satisfaction obtained by the architecture firms and other actors involved in the process of adopting the ISO 14006 eco-design standard, we developed a qualitative research using a Delphi type methodology, based on the results of a previous multiple case study research conducted with nine architecture firms. Among the main results, it should be highlighted the difficulties faced by architecture firms to obtain environmental information of raw materials, the poor recognition given by the client to environmental aspects compared with costs and the limited role of government supporting eco-design adoption, increasing the level of requirements of environmental legislation, and taking into account environmental issues in public tenders. It is also noteworthy the main stakeholders involved in the adoption and certification process of the ISO 14006 have demonstrated a medium or medium-high level of satisfaction.

Keywords: Sustainability; Eco-design; Standardization; Environmental Impact; Life cycle; Green building.

Adopción de Sistemas de Gestión de Ecodiseño en el sector de la construcción. Análisis de la perspectiva de los diferentes agentes involucrados

Resumen
Partiendo de los resultados de un estudio de casos previo realizado con 9 estudios de arquitectura, hemos desarrollado una investigación cualitativa mediante un grupo de expertos tipo Delphi con objeto de analizar de las principales motivaciones, el proceso de adopción, los resultados y el grado de satisfacción obtenidos por los estudios de arquitectura y el resto de agentes que participan en el proceso de adopción del estándar ISO 14006. Entre los principales resultados, destacan las dificultades que tienen los estudios para obtener información medioambiental de las materias primas, el escaso reconocimiento medioambiental en relación al coste que otorga el cliente y el papel que tiene la administración pública impulsando programas de promoción, aumentando el nivel de exigencia de la legislación medioambiental y valorando aspectos medioambientales en los concursos públicos. Asimismo, es destacable que los principales agentes que intervienen en el proceso han mostrado un nivel de satisfacción medio o medio-alto.

Palabras clave: Sostenibilidad; Ecodiseño; Normalización; Impacto Ambiental; Ciclo de vida; Edificación sostenible.

1. Introducción

Las numerosas consecuencias negativas de tipo ambiental que está generando el desarrollo económico en los últimos años, han creado la necesidad de generar herramientas de gestión con objeto de minimizar los impactos ambientales [1-5]. En esta línea, en la literatura encontramos numerosos artículos que señalan, tanto en el sector de la construcción como a nivel industrial, que la integración de criterios medioambientales en el diseño y fabricación de productos puede conseguir una importante reducción de los impactos que podrían tener esos productos a lo largo de todo su ciclo de vida, desde la extracción de las materias primas para su fabricación, hasta su depósito en un vertedero [3-5].

Concretamente, en el sector de la construcción la función de los estudios de arquitectura resulta clave en todo lo concerniente

© The author; licensee Universidad Nacional de Colombia.

al ecodiseno, debido a que desarrollan su trabajo en las fases incipientes del proceso de creación del producto en un sector caracterizado por el elevado impacto medioambiental de los productos que se construyen [6-7]. Por estos motivos, con objeto de gestionar adecuadamente el proceso de ecodiseño se han desarrollado numerosas herramientas y estrategias sectoriales [8-11], entre las que los estándares de ecodiseno se pueden considerar como una de las herramientas genéricas más reseñables [12]. En relación a los estándares más específicos del sector, ISO y CEN han desarrollado una serie de estándares destinados a controlar la sostenibilidad medioambiental del sector de la construcción que se resumen en la Tabla 1.

Sin embargo, también se observa que, como sucede en otros sectores de actividad económica, los estándares no específicos del sector de la construcción están teniendo una fuerte influencia [13]. Entre ellos cabe destacar la norma ISO 14006 [14], cuyo objetivo es servir de guía para aquellas organizaciones que deseen incorporar la variable medioambiental en el proceso de diseño y desarrollo del producto, en la medida en que la organización pueda tener control o influencia, y quieran integrar dicho proceso en su Sistema de Gestión Ambiental (SGA) [14].

En principio, el estándar ISO 14006 no se creó con fines de certificación, sin embargo, la entidad nacional de acreditación de cada país puede decidir si en ese país es certificable o no. Concretamente, en España este estándar es certificable y, según información proporcionada por las empresas auditoras, de las 236 empresas certificadas en España a finales de 2014, 174 (74%) eran empresas pertenecientes al sector de la construcción. Concretamente, 171 de estas empresas eran estudios de arquitectura que si bien tenían una dimensión significativamente mayor que los estudios no certificados, más del 90% de ellos contaban con menos de 20 trabajadores.

Teniendo en cuenta estos aspectos y que en la literatura existe una escasez de estudios en relación a la adopción de estándares de ecodiseño en el sector de la construcción, el objetivo de este artículo es analizar las motivaciones, el proceso de adopción y certificación, los resultados y el grado de satisfacción obtenidos por los agentes que participan en el proceso de adopción y certificación del estándar ISO 14006. Con este objetivo, a continuación se expone el análisis de la literatura que nos ha servido de base para el desarrollo de un estudio empírico tipo Delphi cuya metodología se expone en el apartado tres. Seguidamente, se hace una descripción de los principales resultados obtenidos en este estudio, que nos han permitido obtener unas conclusiones que consideramos de interés para los principales agentes que intervienen en el proceso. En el último apartado, se describe la bibliografía utilizada en esta investigación.

Tabla 1.
Normas medioambientales elaboradas por ISO y CEN orientadas al sector de la construcción.

Reference	Standard and/or project title
ISO/TS 12720:2014 [15]	Sustainability in buildings and civil engineering works. Guidelines on the application of the general principles in ISO 15392.
ISO 15392:2008 [16]	Sustainability in building construction. General principles.
ISO 16745:2015 [17]	Environmental performance of buildings. Carbon metric of a building. Use stage.
ISO 21929-1:2011 [18]	Sustainability in building construction. Sustainability indicators. Part 1: Framework for the development of indicators and a core set of indicators for buildings.
ISO/TS 21929-2:2015 [19]	Sustainability in building construction. Sustainability indicators. Part 2: Framework for the development of indicators for civil engineering works.
ISO/CD 21930:2015 [20]	Sustainability in buildings and civil engineering works. Environmental declaration of building products.
ISO 21930:2007 [21]	Sustainability in building construction. Environmental declaration of building products
ISO 21931-1:2010 [22]	Sustainability in building construction. Framework for methods of assessment of the environmental performance of construction works. Part 1: Buildings.
ISO/NP 21931-2 [23]	Sustainability in building construction. Framework for methods of assessment of the environmental performance of construction works. Part 2: Civil engineering works.
ISO/TR 21932:2013 [24]	Sustainability in buildings and civil engineering works. A review of terminology.
ISO 12655:2013 [25]	Energy performance of buildings. Presentation of measured energy use of buildings.
ISO 16343:2013 [26]	Energy performance of buildings. Methods for expressing energy performance and for energy certification of buildings.
ISO 16346:2013 [27]	Energy performance of buildings. Assessment of overall energy performance.
ISO/TR 16344:2012 [28]	Energy performance of buildings. Common terms, definitions and symbols for the overall energy performance rating and certification.
ISO 13153:2012 [29]	Framework of the design process for energy-saving single-family residential and small commercial buildings.
ISO/DTR 16822 [30]	Building environment design. List of test procedures for heating, ventilating, air-conditioning and domestic hot water equipment related to energy efficiency.
ISO/NP 19454 [31]	Building environment design. Indoor environment. Daylight opening design process in order to ensure sustainability principles in visual environment.
ISO 16818:2008 [32]	Building environment design. Energy efficiency. Terminology.
ISO 23045:2008 [33]	Building environment design. Guidelines to assess energy efficiency of new buildings.
ISO/TR 21932:2013 [34]	Sustainability in buildings and civil engineering works. A review of terminology.
ISO/TS 12720:2014 [35]	Sustainability in buildings and civil engineering works. Guidelines on the application of the general principles in ISO 15392.
EN 15978:2011 [36]	Sustainability of construction works. Assessment of environmental performance of buildings. Calculation method.
EN 16309:2014+A1:2014 [37]	Sustainability of construction works - Assessment of social performance of buildings - Calculation methodology.
EN 15643-2:2011 [38]	Sustainability of construction works. Assessment of buildings - Framework for the assessment of environmental performance.
EN 15978:2011 [39]	Sustainability of construction works. Assessment of environmental performance of buildings. Calculation method.
EN 15643-1:2010 [40]	Sustainability of construction works. Sustainability assessment of buildings - General framework.
prEN 15643-5 [41]	Sustainability of construction works - Sustainability assessment of buildings and civil engineering works - part 5: framework on specific principles and requirement for civil engineering works.

Fuente: Elaboración propia a partir de información obtenida por ISO y CEN.

2. Análisis de la literatura

En la literatura existen numerosos estudios que analizan los resultados de distintas metodologías orientadas a mejorar la sostenibilidad en el sector de la construcción, como la metodología verde, los modelos energéticos, o las declaraciones medioambientales de producto basadas en Análisis del Ciclo de Vida (LCA) entre otras [6].

Sin embargo, en la literatura no se encuentran muchos estudios que analicen la adopción de sistemas de gestión de ecodiseño en el sector de la construcción. Existen estudios de casos que analizan las motivaciones, el proceso de adopción y los resultados obtenidos por las empresas [12,42,43]. Éstos coinciden en señalar que las principales motivaciones están en relación a la cultura de la organización y la valoración del certificado en licitaciones públicas. En relación al proceso de adopción consideran que ha sido más complicado que el de otros sistemas de gestión ambientales como la ISO 14001, pero que tiene más sentido, ya que el impacto medioambiental que produce un estudio es muchos menor que el que tienen sus diseños. Además, en la mayoría de los casos la experiencia previa en el trabajo con otros sistemas de gestión, principalmente ISO 9001, les ha ayudado mucho. En relación a los resultados, los estudios de arquitectura se encuentran bastante satisfechos con la adopción del estándar. En general, los estudios coinciden en señalar que la adopción del estándar ISO 14006 ha contribuido a mejorar su imagen y su posición en las licitaciones. Asimismo, señalan que el proceso de mejora continua les ha permitido reducir el impacto medioambiental y los costes, principalmente, a través de la optimización del consumo de agua y energía.

Por otra parte debido a que la difusión del estándar no es muy importante existe una escasez de estudios cuantitativos. Tan sólo hemos encontrado un estudio que analiza la influencia de la adopción de estándares de ecodiseño en la rentabilidad [44]. En dicho trabajo de investigación se concluye que los estudios que han adoptado el estándar de ecodiseño son más rentables. Sin embargo, no se demuestra que la causa del aumento de la rentabilidad esté en relación con la adopción del estándar, sino que se concluye que existe un efecto selección, es decir, los estudios que se certifican son los más rentables.

Sin embargo, en todos los trabajos de investigación identificados y analizados solamente se tiene en cuenta la perspectiva de las empresas, y no hemos encontrado en la literatura trabajos que tengan en cuenta la opinión del resto de grupos de interés que participan en el proceso de adopción y certificación de estándares de ecodiseño. Y sin embargo, como afirma Heras [45], en la adopción de un sistema de gestión los diferentes agentes básicos involucrados en el proceso de implantación son: las propias empresas que implantan y certifican el modelo; en segundo lugar, los organismos certificadores; en tercer lugar, las empresas que ofrecen servicios de consultoría o asesoría en la implantación; y, en cuarto lugar, también se podría implicar a la propia administración, que mediante los programas de apoyo a la implantación, pueden influir también, de alguna forma, en el proceso. A fin de cuentas, son partícipes y observadores, y el propio investigador nunca estará más cerca del objeto de la investigación que lo están ellos [46]. Además, pueden actuar como jueces en la evaluación de los principales resultados de un estudio [47].

Por ello, consideramos que es necesario contar con la opinión de los demás agentes involucrados en el proceso de adopción, además de la de las propias empresas. Por estos motivos, hemos planteando un estudio analizando las opiniones de los directivos y responsables de diseño de los estudios de arquitectura, empresas auditoras, empresas consultoras, expertos académicos, instituciones públicas y asociaciones o clústeres para analizar y contrastar de forma lo más objetiva posible la perspectiva de los distintos agentes que intervienen en el proceso.

3. Metodología

En esta investigación se ha empleado una metodología tipo Delphi basada en la opinión de un grupo de expertos, combinada con un conjunto de entrevistas en profundidad desarrolladas en tres fases sucesivas.

Aunque no ha sido una técnica profusamente empleada para tratar de analizar la influencia de los modelos de gestión basados en estándares en el desempeño de las empresas [48], existen numerosos estudios en otros campos de conocimiento en los que se emplea la metodología Delphi como herramienta para llevar a cabo estudios de carácter cualitativo [49].

Este tipo de metodologías surge del reconocimiento de la superioridad del juicio de grupo sobre el juicio individual, gracias a la generación de conocimiento de un grupo de individuos a través de la estructuración del proceso de comunicación humana enfocada en el análisis de cuestiones particulares [50].

Tal como se refleja en la Figura 1, definido el objetivo de la investigación, antes de comenzar el estudio Delphi, a modo de pre-test se formó un grupo de expertos, compuesto por profesionales y especialistas de distintos ámbitos (consultorías, organismos certificadores, organismos públicos y especialistas académicos). El pre-test consistió en la realización de entrevistas en profundidad semi-estructuradas a 11 expertos, 3 miembros de empresas certificadas, 2 de consultoras, 3 de auditoras, 2 especialistas académicos y un miembro del Comité ISO/TC 207 encargado de elaborar la norma, siguiendo un guión, basado en el empleado en un estudio de casos con 9 estudios de arquitectura llevado a cabo en una investigación anterior. Posteriormente y para finalizar el trabajo de campo, al objeto de reforzar las conclusiones extraídas del estudio mediante grupo expertos (triangulación teórica) [51], se optó por crear un panel de expertos suficientemente equilibrado, con una combinación de expertos participantes en el estudio Delphi y otros nuevos, a los que se les mostraron los resultados de la fase anterior, con el objeto de obtener una opinión grupal fidedigna que redujera el grado subjetividad en la valoración de las conclusiones del análisis de los resultados, un elemento ciertamente innovador en esta área de conocimiento, pero que es señalado como una de las posibles técnicas que proporciona validez constructiva a una investigación cualitativa [52]. Al efecto, el autor señala que es necesario contar con expertos de diferentes disciplinas, pero también es posible la participación de expertos de una misma área de conocimiento, pero de diferentes ámbitos, como es el

presente caso. De cualquier forma los expertos deben aportar diferentes perspectivas. Por lo tanto, si cada experto o evaluador interpreta la información proporcionada de la misma manera, entonces es posible hablar de validez constructiva [53]. Además, la triangulación permite a los investigadores profundizar en la comprensión de los problemas y maximizar su confianza en los resultados de estudios cualitativos [54,55].

Una vez concluido el pre-test y, a tenor de los buenos resultados, se comenzó el estudio Delphi propiamente dicho. Se elaboró un cuestionario general, dirigido a 20 expertos de distintos ámbitos: 5 pertenecientes a empresas certificadas, 5 a empresas auditoras, 4 a empresas consultoras, 2 a expertos académicos, 3 a instituciones públicas y un miembro del cluster de la construcción (Eraikune). Las preguntas fueron abiertas basadas en la experiencia del estudio de casos y las aportaciones recogidas en la literatura [51]. La versión piloto de los cuestionarios fue revisada y corregida por un grupo de evaluación formado por un directivo de una empresa totalmente ajena a la investigación, un consultor empresarial y dos académicos con amplia experiencia en el uso de metodologías cualitativas.

Con objeto de cumplir los objetivos del estudio se formularon cuestiones tratando de adecuarse a la fuente de evidencia. En la primera fase, se realizaron una serie de preguntas abiertas cuyos resultados fueron la base para la elaboración del segundo cuestionario que constaba de preguntas cerradas que pudieran ser valoradas. En él, se les dio a conocer a los mismos expertos que respondieron el primer cuestionario, aquellas cuatro respuestas que con más asiduidad se repitieron por cada aspecto y se les pidió que valoraran su grado de conformidad del 1 al 7 (1, nada de acuerdo; 7, completamente de acuerdo) con las afirmaciones realizadas en el cuestionario inicial. Se planteó este sistema de valoración para todas las cuestiones planteadas en el segundo cuestionario. Asimismo, con la intención de enriquecer el estudio, al final de cada cuestionario se facilitó un espacio reservado para que los expertos realizasen las aportaciones que considerasen oportunas.

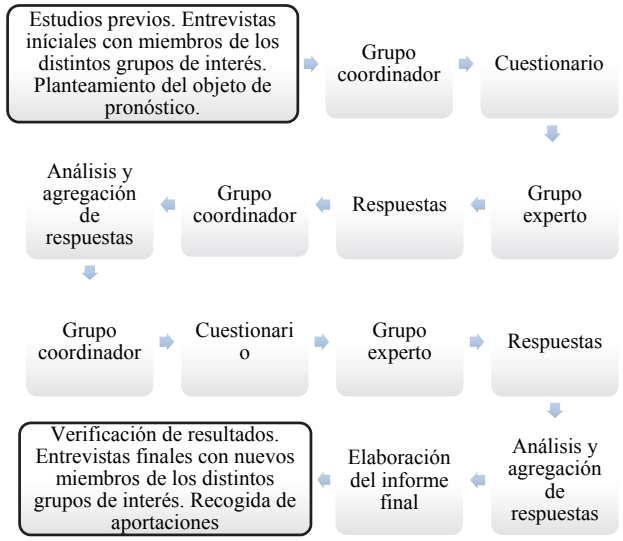

Figura 1. Esquema del proceso de investigación en el estudio mediante grupo de expertos
Fuente: Elaboración propia a partir de Landeta [49].

Por último, los resultados del estudio fueron presentados y analizados en nuevas entrevistas en profundidad, 4 realizadas a expertos participantes en la fase anterior (un miembro de una empresa certificada, un consultor, un auditor y un especialista académico) y 4 realizadas a nuevos expertos pertenecientes a cada uno de estos grupos.

4. Desarrollo del estudio

El estudio fue desarrollado entre febrero de 2013 y febrero de 2015. Posteriormente, los resultados obtenidos fueron clasificados en relación a los objetivos principales en cuatro apartados: motivaciones, proceso, resultados y grado de satisfacción que se desarrollan a continuación.

4.1. Motivaciones

Teniendo en cuenta que el sector de la construcción aglutina el 74% de los certificados emitidos en España, el primer objetivo que nos marcamos fue conocer las razones que explicaban la fuerte incidencia que ha tenido la ISO 14006 en el sector.

En este sentido, los expertos señalan como principal factor el hecho de que se trata de un sector con gran potencial de mejora ambiental. Este hecho ha llevado a las instituciones públicas a impulsar programas de ayuda para adoptar y certificar el estándar que ha favorecido la actitud de las empresas. Otros aspectos destacados son la imagen de marca como aspecto diferenciador por parte de los estudios de arquitectura y que facilita la obtención de certificados relacionados con la sostenibilidad y la eficiencia energética de edificios.

Por otro lado, preguntados sobre aquellos factores que pueden limitar la difusión futura del estándar, los expertos creen que no valorar la certificación siquiera en las licitaciones públicas tendría un efecto negativo en la difusión del estándar, aún más teniendo en cuenta que la tendencia en el sector es la certificación medioambiental de edificios. En el momento actual también preocupa la escasa sensibilidad medioambiental de los promotores, principalmente privados, según se concluye del estudio de casos, y la creencia de que aumentan los costes operativos de las empresas y la propia ejecución del proyecto.

En relación a la decisión de adoptar un Sistema de Gestión de Ecodiseño conforme al estándar ISO 14006, los expertos del sector de la construcción destacan, entre los principales factores, la mejora de la imagen de marca y la diferenciación con respecto de la competencia. Los estudios también se certifican porque su competencia también lo hace, y quieren evitar encontrarse en una posición de desventaja en las licitaciones públicas. En este sentido, la integración y adecuada gestión de la variable medioambiental en el diseño y desarrollo de futuros proyectos arquitectónicos será clave para poder ofrecer un servicio en línea con la tendencia actual de la legislación europea en la materia.

En las empresas parece que los principales agentes interesados en adoptar el estándar sean los directivos, cuya mayor motivación es mejorar la imagen de empresa, y las personas de la oficina técnica, donde se gestan los proyectos, que generalmente son los que muestran una mayor concienciación medioambiental (ver Tabla 2).

Tabla 2.
Nivel de motivación y valoración de la motivación principal de los grupos de interés para apoyar la adopción del estándar por parte de las empresas.

Grupo de interés	Valoración	Motivación principal grupo	Valoración
Directivos	●●●●●●○	Imagen de la empresa	●●●●●●●
Oficina Tecnica	●●●●●●○	Concienciación ambiental	●●●●●●●
Comerciales	●●●●●○○	Herramienta de marketing	●●●●●○○
Subcontratas técn	●●●●○○○	Concienciación ambiental	●●●●●○○
Constructoras	●●●○○○○	Beneficiarse de las mejoras	●●●●○○○
Promotores	●●●●○○○	Beneficiarse de las mejoras	●●●●○○○
AA.PP.	●●●●●○○	Cumplir objetivos ambientales	●●●●●○○
Clientes	●●●●○○○	Reducción de costes en uso	●●●●○○○

Fuente: Elaboración propia.

Tabla 3.
Grado de apoyo a la adopción del estándar por parte de los grupos de interés y nivel de importancia de la dificultad principal.

Grupo de interés	Valoración	Dificultad principal grupo	Valoración
Directivos	●●●●●●○	Miedo a lo desconocido, a nuevos retos y exigencias.	●●●●●●○
Oficina Técnica	●●●●●○○	Falta de información ambiental de materiales.	●●●●●●○
Comerciales	●●●●●○○	Mayor coste proyecto, aunque se reduzca el coste en uso.	●●●●●○○
Subcontratas técnicas	●●●●●○○	Mayor complejidad del trabajo (cambios en procesos)	●●●●●●○
Constructoras	●●●●○○○	Falta de conocimiento sobre ecodiseño.	●●●●●○○
Promotores	●●●●●○○	Escasa valoración del estándar ISO 14006 en el mercado.	●●●●○○○
AA.PP.	●●●●●○○	Falta de recursos económicos y herramientas para comparar las alternativas en los concursos.	●●●●●○○
Clientes	●●●●●●○	Falta de conocimiento sobre ecodiseño.	●●●●●●○

Fuente: Elaboración propia.

Promotoras y clientes, en general, y constructoras, en especial, parecen no mostrar una actitud positiva, de apoyo y colaboración a los estudios. De hecho, éstos se encuentran con dificultades a la hora de implementar soluciones arquitectónicas ambientalmente más sostenibles en cada nuevo proyecto. Desde luego, parece que el nivel de concienciación medioambiental de promotores, clientes, subcontratas de servicios y constructoras es inferior al personal de las empresas certificadas y, sobre todo, de la oficina técnica.

Con respecto a las subcontratas de servicios técnicos —ingenierías especialistas en su mayoría—, los estudios de arquitectura afirman haber logrado su colaboración en mayor o menor medida. Es posible que su motivación se deba a la necesidad de seguir manteniendo las relaciones comerciales y vean además una oportunidad para adaptarse a la tendencia en el sector e incluso acceder a nuevos mercados.

Por otro lado, los grupos de interés también pueden mostrarse reacios a apoyar el proceso de adopción y certificación, lo que puede llegar a entorpecer e incluso impedir la consecución de los objetivos del proceso. De acuerdo con las valoraciones de la Tabla 3, los directivos y los clientes especialmente son los grupos que mayores dificultades plantean. Aunque el resto de actores o grupos de interés también pueden mostrar serias dificultades.

4.2. Proceso de adopción

En relación al proceso de adopción, la investigación confirma los resultados obtenidos en el estudio de casos (ver Tabla 3). Las empresas en general no consideran que el proceso de adopción y certificación haya sido complicado, aspecto que reafirman el panel de expertos de la tercera fase.

En general, los grupos de interés destacan distintos aspectos que dificultan o impiden incluso el inicio del proceso. Los directivos, en general, no ven claro el retorno económico, ni los costes totales del proceso. Inicialmente existe un desconocimiento de las exigencias a cumplir y las herramientas disponibles. El personal de la oficina técnica tiene dificultades para obtener la información medioambiental de los materiales, el departamento comercial teme la subida del coste de venta, las constructoras y las subcontratas tienen miedo al cambio y esperan un aumento de la complejidad de los trabajos y, por último, los clientes desconocen qué es el ecodiseño, lo cual les genera desconfianza y en muchos casos les lleva a realizar valoraciones erróneas acerca del producto.

Con el fin de saber más acerca de los obstáculos durante el proceso de adopción del estándar ISO 14006, se les preguntó a los expertos sobre aquellos que entendían que podían ser los más difíciles de superar para las empresas. Desde luego no parecen existir limitaciones impuestas por la normativa técnica y urbanística existente, ni una falta de concienciación medioambiental de los empleados que puedan suponer un obstáculo en el proceso. Por el contrario, existe una necesidad de implantar nuevas herramientas y metodologías en la rutina de trabajo, y de obtener apoyo externo que guíe a las empresas en el proceso de adopción y certificación del estándar. Las empresas destacan como obstáculo fundamental las dificultades para lograr información medioambiental necesaria sobre materiales, componentes y sistemas constructivos. Esto concuerda totalmente con las opiniones recogidas en las entrevistas en el estudio de casos. Para todos los estudios de arquitectura, obtener datos medioambientales de materiales, substancias o componentes, había supuesto inicialmente un quebradero de cabeza. Cabe decir que en su mayoría se trata de microempresas, con problemas para encontrar carga de trabajo debido a la crisis que vive el sector.

Entre los elementos facilitadores, todos señalaron la importante ventaja de la experiencia de tener un sistema de gestión implantado. Estar certificados conforme a la ISO 9001 y/o la ISO 14001, permite reducir el miedo al papeleo y centrarse prácticamente en los aspectos técnicos del proceso de elaboración de los proyectos. En este punto cabe señalar que los estudios de arquitectura al contrario que con la ISO 9001 no valoran mucho la adopción de la ISO 14001, afirman que les aporta muy poco, ya que el impacto medioambiental de su actividad en sus instalaciones es muy poco significativo.

Tabla 4.
Nivel de aportación de los grupos de interés externos a las empresas y valoración de la aportación principal.

Grupo de interés	Valoración	Principal aportación	Valoración
Consultoras	●●●●●○○	Formación inicial y elección de herramientas	●●●●●○○
Certificadoras	●●●●●●○	Experiencia acumulada en certificación	●●●●○○○
Asociaciones o clústeres	●●●●●●○	Tractores de proyectos sectoriales	●●●●●○○
Organismos públicos	●●●●○○○	Programas de ayudas y subvenciones	●●●●●●●
Universidades	●●●○○○○	Fuente de ideas, herramientas, información	●●●○○○○
Centros tecnológicos	●●●○○○○	Implementación mejoras técnicas ecodiseño	●●●●○○○

Fuente: Elaboración propia.

Siguiendo las indagaciones sobre los elementos facilitadores del proceso de adopción y certificación, a los expertos se les preguntó sobre las herramientas de ecodiseño más empleadas entre las empresas, y parece que éstas siguen mayormente las recomendaciones de los sistemas de certificación de sostenibilidad de edificios (tipo LEED, BREEAM…).

En cuanto a otros elementos que facilitan el desarrollo y éxito del proceso de adopción y certificación conforme a la ISO 14006 son las ayudas externas, ver Tabla 4. Concretamente, las ayudas proporcionadas por asociaciones o clúster y certificadoras son las más valoradas. La principal aportación de los primeros es el efecto tracción que realizan a través de programas sectoriales y, de los segundos, la experiencia en el proceso de adopción y certificación que aportan. El trabajo de las consultoras también está bien valorado y destaca como principal aportación la formación para principiantes que imparten, así como la ayuda en la selección adecuada de herramientas de ecodiseño (gestión, evaluación de impactos medioambientales…). Por último, también son muy valorados los programas de ayudas y subvenciones desarrollados por las administraciones públicas (AA.PP).

A los expertos también se les preguntó sobre los criterios que emplean las empresas en la selección de los proyectos que ecodiseñan inicialmente. Parece que las empresas prefieren apostar por proyectos no demasiado complejos, similares a otros de los que se tenga referencia, y en los que el cliente se muestre sensible con respecto al comportamiento medioambiental del edificio, así como, por los proyectos destinados a participar en concursos públicos en los que se valora el ecodiseño.

Con respecto a la extensión del ecodiseño a otros proyectos, hay diversos elementos facilitadores. Entre ellos está la legislación ambiental, cada vez más exigente, lo que obliga a establecer en las empresas un sistema de alerta legislativa. Además, la adopción del estándar de ecodiseño implica tener que mejorar el comportamiento medioambiental del edificio proyectado, lo que implícitamente puede suponer adelantarse incluso a futuras obligaciones medioambientales. En cualquier caso, existe cierto desacuerdo entre los expertos con respecto al tema.

Por otro lado, las empresas también deben hacer frente a obstáculos que limitan la extensión del ecodiseño al resto de sus proyectos. La principal, según los expertos, es la falta de reconocimiento por parte del cliente del comportamiento o desempeño medioambiental de sus proyectos. Tampoco ayuda la limitación de recursos propios, la crisis de demanda en el sector, ni el incremento de costes de ejecución del proyecto debido a la implementación de soluciones técnicas ambientalmente más sostenibles.

4.3. Principales resultados

En cuanto a los resultados obtenidos, tal como se muestra en la Tabla 5, a nivel general, los expertos creen que las empresas valoran la mejora del comportamiento medioambiental de sus proyectos. Asimismo, consideran que les sirve para dinamizar el nivel de innovación de los estudios, les lleva a adquirir un mayor conocimiento sobre nuevas tecnologías, componentes y materiales. Otros resultados importantes son la apertura de nuevos mercados, la mejora del posicionamiento en concursos públicos, y el aumento de la motivación en el personal de la oficina técnica, si bien, sobre este último aspecto hay cierta falta de consenso. Por otro lado, resulta reseñable que los expertos señalen que el certificado ayuda a las empresas a mejorar su imagen y credibilidad, pero no tanto la de sus proyectos, ya que el hecho de que el producto sea ecodiseñado, en general, no es valorado positivamente por el cliente. El mercado aún no valora la mejora medioambiental del producto y entiende que "el ecodiseño suena a caro". En todo caso importa el ahorro de costes en la fase de uso, habida cuenta del creciente coste de la energía, el agua y otros gastos.

Respecto al aspecto económico de los resultados del proceso de adopción y certificación, los expertos parecen compartir la opinión de que la adopción del estándar de ecodiseño implica un incremento de los costes muy bajo en las fases de elaboración del proyecto, obtención de materiales y componentes, y ejecución de obra. No obstante, en las fases de uso y fin de vida, existe un efecto de ahorro de los costes que pretende compensar el incremento en la inversión inicial. Esto concuerda con las afirmaciones de los entrevistados en el estudio de casos.

Según los expertos, el incremento de coste de compra debe estar justificado con el ahorro económico en la fase de uso. Este hecho contribuye a mejorar ligeramente el cumplimiento de las expectativas del cliente. Sin embargo, existe bastante consenso a la hora de señalar que los resultados empresariales no se ven afectados de forma importante ya que no se han observado efectos ni sobre las ventas, ni sobre el margen comercial, pero si señalan que la productividad y la rentabilidad se reducen ligeramente. Este hecho concuerda con los resultados obtenidos en el estudio de casos en donde los entrevistados afirmaban, en general, que la adopción del estándar había supuesto añadir más tareas a las habituales, de ahí el incremento de los costes operativos, aún a pesar de la mejora de los métodos de trabajo en la elaboración de los proyectos. No obstante, en ningún caso se obtuvieron datos cuantitativos fehacientes del impacto económico en las empresas.

Sin embargo, otros aspectos importantes que se han visto influenciados positivamente son: la comunicación ambiental, y el cumplimiento de las necesidades de los clientes y la legislación medioambiental futura.

Tabla 5.
Principales resultados obtenidos por las empresas con la adopción y certificación del estándar ISO 14006.

Resultados	Valoración[1]
Conocimiento de tecnologías, componentes, materiales, etc.	●●●●●●○
Impactos ambientales de los edificios en su ciclo de vida.	●○○○○○○
Apertura de nuevos mercados.	●●●●●○○
Posicionamiento en concursos públicos.	●●●●●●○
Motivación del personal técnico de proyectos.	●●●●●○○
Imagen y credibilidad de la organización.	●●●●●●○
Crecimiento de las ventas	●●●●○○○
Margen comercial	●●●●○○○
Productividad	●●●○○○○
Rentabilidad económica	●●●○○○○
Cuota de mercado	●●●●○○○
Internacionalización	●●●●○○○
Cumplir necesidades cliente	●●●●●○○
Comunicación medioambiental	●●●●●○○
Legislación medioambiental futura	●●●●●○○

Fuente: Elaboración propia.

Tabla 6.
Principales efectos medioambientales que produce la adopción del estándar en cada fase del ciclo de vida.

Fase	Efectos	Valoración
Obtención materiales	Reducción del agotamiento de materias primas y de emisiones.	●●●●●●○
	Mejora del impacto medioambiental de los materiales empleados.	●●●●●●○
Redacción proyecto	Introducción de nuevos conceptos y soluciones constructivas.	●●●●●○○
	Mejora global del desempeño medioambiental de la construcción.	●●●●●○○
Ejecución de obra	Identificación y evaluación de los impactos medioambientales	●●●●●●○
	Reducción de las materias primas, emisiones y residuos.	●●●●●○○
Uso	Reducción de emisiones.	●●●●●●○
	Reducción de la demanda energética.	●●●●●●●
Fin de vida	Mejora en la gestión de residuos.	●●●●●○○
	Información disponible para la deconstrucción.	●●●●●○○

Fuente: Elaboración propia.

Por otro lado, dado el creciente interés del sector por las certificaciones de evaluación de la sostenibilidad de la edificación (LEED, BREEAM…), se les preguntó a los expertos sobre las ventajas y desventajas que comparativamente proporciona el estándar ISO 14006. En su opinión, se trata de dos conceptos distintos con objetivos distintos, pero incluso con la certificación conforme a la ISO 14006 se busca también el reconocimiento del mercado, y al fin y al cabo, mejorar las ventas. De todas formas, la principal ventaja del estándar ISO 14006 parece ser, sin lugar a dudas, la adopción de una sistemática de trabajo en las empresas basada en la mejora continua de proyectos ambientalmente más sostenibles.

Con respecto a los proyectos que realizan los estudios de arquitectura, los expertos aseguran que la adopción y certificación ha supuesto la búsqueda de conceptos y soluciones innovadoras que han permitido alcanzar mejoras medioambientales en todas las fases del ciclo de vida. En la Tabla 6 se muestran los principales efectos medioambientales señalados por los expertos, entre los que destacan los relacionados con la reducción de la demanda energética en la fase de uso, la reducción de emisiones en varias fases, la utilización de materiales de menor impacto y un mayor control en relación a la identificación y evaluación de impactos medioambientales.

4.4. Grado de satisfacción

En cuanto al grado de satisfacción que obtienen los distintos grupos de interés, en la Tabla 7 se observa que la empresa y los departamentos que directamente pertenecen a ésta, muestran un grado de satisfacción ligeramente positivo, ya que entre otros aspectos consideran que les ayuda a mejorar su posición en el mercado gracias al refuerzo de la imagen de marca y mejora del posicionamiento en concursos públicos, y además, la mejora del comportamiento medioambiental ayuda a dar un nuevo enfoque a sus proyectos e incrementa el valor añadido de su trabajo.

Tabla 7.
Nivel de satisfacción de los grupos e interés y valoración de las principales aportaciones de la adopción y certificación del estándar ISO 14006 que les ha supuesto.

Grupo de interés	Valoración Satisfacción	Aportaciones	Valoración aportación
Empresa	●●●●●○○	Las organizaciones apuestan por una decisión que mejora su posición en el mercado.	●●●●●○○
		Los proyectos están mejor concebidos y tienen mejor comportamiento ambiental.	●●●●●○○
Directivos	●●●●●○○	Diferenciación e imagen de marca.	●●●●●●○
		Competitividad.	●●●●●●○
		Acceso a concursos públicos.	●●●●●●○
Oficina Técnica	●●●●●○○	Nuevo enfoque a los proyectos.	●●●●●○○
		Incrementar el valor añadido de su trabajo.	●●●●●○○
		Contribución a la sociedad.	●●●●○○○
Comercial	●●●●●○○	Argumento de venta adicional.	●●●●○○○
		Acceso a nuevos mercados.	●●●●○○○
Subcontratas Servicios técnicos	●●●●○○○	Ofertar nuevas líneas de trabajo.	●●●●○○○
		Riesgo de garantizar resultado y funcionamiento.	●●●●○○○
Constructoras	●●●●○○○	Apertura de nuevas oportunidades de negocio.	●●●●●○○
		Ampliar la gama de soluciones constructivas.	●●●●○○○
		Apoyar el compromiso cliente en mejora continua.	●●●○○○○
Promotores	●●●●○○○	Acceso a nuevos mercados.	●●●●○○○
		Diferenciación con respecto a competidores.	●●●●○○○
AA.PP.	●●●●○○○	Contribución a la estrategia medioambiental del territorio.	●●●●○○○
		Mejora de la competitividad de las empresas.	●●●●●○○
Clientes	●●●●○○○	Información medioambiental verificable.	●●●○○○○
		Mayor valor añadido de los proyectos.	●●●●○○○
		Ahorro económico en ciertos casos.	●●●●●○○

Fuente: Elaboración propia.

1 *1* significa que los resultados han disminuido significativamente y *7* que han aumentado significativamente.

Sin embargo, el resto de agentes no se muestran satisfechos pero tampoco insatisfechos. En general, observan aspectos positivos que vienen a compensar los riesgos y las incertidumbres. Entre estos aspectos, las constructoras destacan la apertura de nuevas oportunidades de negocio, las Administraciones Publicas la mejora de la competitividad de las empresas y los clientes el ahorro económico en la fase de uso en ciertos casos, principalmente, ligado a la mayor eficiencia que pueden obtener en la utilización de la energía y el agua.

5. Discusión y conclusiones

En España, el estándar ISO 14006 no ha tenido la difusión esperada en el sector industrial. Sin embargo, entre los agentes que desarrollan las funciones de diseño en el sector de la construcción, los estudios de arquitectura, la difusión ha sido notablemente superior. La especial incidencia que ha tenido la crisis económica en el sector y la necesidad que han tenido los estudios de arquitectura de apostar por elementos diferenciadores que les supongan un mejor posicionamiento en las licitaciones públicas han sido decisivos. Por otra parte, el fuerte impacto medioambiental que tienen las actividades de la construcción ha creado entre los estudios de arquitectura una concienciación medioambiental, que a su vez ha impulsado a muchos de estos estudios a adoptar el estándar, un aspecto también recogido en la literatura [56].

En cuanto al proceso de adopción y certificación, los distintos agentes coinciden en señalar que éste no ha sido especialmente complicado. En general, los estudios trabajaban con un sistema de gestión basado en los estándares ISO 9001 e ISO 14001, si bien este último había muchos estudios que no lo habían adoptado. Se considera que en el proceso de adopción y certificación las consultoras han aportado principalmente una formación inicial básica a empresas, y han colaborado en la elección y desarrollo de herramientas de ecodiseño. Por su parte, las certificadoras han tenido un papel importante transmitiendo entre otros aspectos su experiencia, las asociaciones o clústeres han tenido especial relevancia ya que han impulsado proyectos sectoriales que han obtenido gran adhesión y, por último, las AAPP pese a tener un papel menos valorado, han desarrollado programas de ayudas y subvenciones que han sido decisivos en la difusión del estándar.

En general, las empresas muestran un grado de satisfacción medio-alto. Principalmente, les ha aportado conocimientos en nuevos desarrollos de tecnologías, componentes y materiales que contribuyen a reducir los impactos medioambientales de los proyectos que llevan a cabo, les ha permitido ganar credibilidad frente al resto de agentes, y mejorar su imagen y su posición en las licitaciones públicas. Sobre este último aspecto, un miembro de una asociación del sector de la construcción señalaba que las empresas certificadas conforme a la ISO 14006 son empresas que, en general, tienen mejor imagen, pero antes de certificarse también la tenían, puesto que las empresas que entran en procesos de licitación habitualmente tienen un sistema de gestión más desarrollado y una capacidad de innovación mucho mayor. Este comentario ha sido compartido por prácticamente la totalidad de los miembros del panel de expertos de la tercera y última fase de la investigación que ha servido para reafirmar las conclusiones obtenidas en estudios anteriores, en donde se apreciaba la existencia de un efecto de selección [44].

En relación al impacto medioambiental de los diseños, los estudios de arquitectura los han conseguido reducir de forma significativa. En este sentido, es destacable la reducción de la demanda energética del edificio y, en menor medida, la utilización de materiales de menor impacto ambiental y la reducción de emisiones, especialmente, en la fase de uso. En relación a la valoración que hace el cliente de estos resultados, el único aspecto que valora es el relativo a la demanda energética del edificio. Este aspecto es cada vez más valorado por los clientes, principalmente por dos motivos: la exigencia de los certificados medioambientales de edificios y la espectacular subida que ha tenido el coste energético, precisamente uno de los componentes de mayor peso en la factura de la fase de uso de los edificios.

Por último, en relación a las limitaciones de esta investigación, señalar que pese a que la metodología empleada no nos permita obtener resultados significativos a través de análisis cuantitativos, éstos sirven para recoger las perspectivas de los distintos grupos que intervienen en el proceso de adopción y certificación de estos sistemas, y confrontarlas. Este hecho nos ha permitido obtener una opinión global de grupo y unas conclusiones de interés para especialistas académicos y los distintos profesionales que trabajan en la gestión de sistemas de ecodiseño. Además, esta investigación puede servir de base para el desarrollo de nuevos estudios de carácter cuantitativo en los que se analicen la influencia de las distintas variables que intervienen en el proceso.

Agradecimientos

El presente artículo se ha realizado en el marco del Grupo de Investigación GIC12/158 - IT763/13 del Sistema Universitario Vasco financiado por el Gobierno Vasco.

Referencias

[1] Vega, L., Ordoñez, J.I., and Pinilla, G., Towards a systemic assessment of environmental impact (SAEI) regarding alternative hydrosedimentological management practice in the Canal del Dique, Colombia. Ingeniería e Investigación, 33(3), pp. 41-48, 2013

[2] Barreto, A.E.H., Correa, M.M.J., Muñoz, A.O. and de Correa, C.M., Tecnologías para la reducción de emisiones de gases contaminantes en plantas cementeras. Ingeniería e Investigación, 28(3), pp. 41-46, 2008

[3] Brutland, G.H., Our common future. Report of the World Commission on Environment and Development, New York, 1987.

[4] Arana, G. and Heras, I. Adopción de la Norma UNE 150301 de ecodiseño. Un estudio de casos. DYNA Bilbao, 85(8), pp. 652-661, 2010. DOI: 10.6036/3736

[5] Berardi, U., Sustainability assessment in the construction sector: rating systems and rated buildings. Sustainable Development, 20(6), pp. 411-424, 2012. DOI:10.1002/sd.532

[6] Hamza, N. and Horne, M., Educating the designer: An operational model for visualizing low-energy architecture. Building and Environment, 42(11), pp. 3841-3847, 2007. DOI: 10.1016/J.BUILDENV.2006.11.003

[7] Arana, G., Cilleruelo, E. and Aldasoro, J.C., ISO 14006. Experiencias previas de estudios de arquitectura que han adoptado el estándar de

ecodiseño UNE 150301: 2003. Informes de la Construcción, 64(527), pp. 319-330, 2012. DOI: 10.3989/ic.11.010
[8] Bunz, K.R., Henze, G.P. and Tiller, D.K., Survey of sustainable building design practices in North America, Europe and Asia. Journal of Architectural Engineering, 12(1), pp. 33-62, 2006. DOI: 10.1061/(ASCE)1076-0431(2006)12:1(33)
[9] Ding, G.K., Sustainable construction—The role of environmental assessment tools. Journal of Environmental Management, 86(3), pp. 451-464, 2008. DOI: 10.1016/j.jenvman.2006.12.025
[10] Brandon, P.S. and Lombardi, P., Evaluating sustainable development in the built environment. John Wiley and Sons, 2010.
[11] Tsai, C.Y. and Chang, A.S., Framework for developing construction sustainability items: the example of highway design. Journal of Cleaner Production, 20(1), pp. 127-136, 2012. DOI: 10.1016/J.JCLEPRO.2011.08.009
[12] Arana, G. and Heras, I., Paving the way for the ISO 14006 ecodesign standard: An exploratory study in Spanish companies. Journal of Cleaner Production, 19(9), pp. 1007-1015, 2011. DOI: 10.1016/J.JCLEPRO.2011.01.013
[13] Landeta, B., Arana, G., Ruíz de Arbulo, P. and Díaz de Basurto, P., The standard ISO14006: A helpful tool to improve the competitiveness of the architecture firms. Revista Ingeniería de Construcción, 28(2), pp. 155-171, 2013. DOI: 10.4067/S0718-50732013000200004
[14] ISO 14006:2011, Environmental management systems. Guidelines for incorporating eco-design, Geneva, 2011.
[15] ISO/TS 12720:2014, Sustainability in buildings and civil engineering works. Guidelines on the application of the general principles in ISO 15392, International Organization for Standardization, International Organization for Standardization, Geneva, 2014.
[16] ISO 15392:2008, Sustainability in building construction. General principles, International Organization for Standardization, Geneva, 2008.
[17] ISO 16745:2015, Environmental performance of buildings. Carbon metric of a building. Use stage, International Organization for Standardization, Geneva, 2015.
[18] ISO 21929-1:2011, Sustainability in building construction. Sustainability indicators. Part 1: Framework for the development of indicators and a core set of indicators for buildings, International Organization for Standardization, Geneva, 2011.
[19] ISO/TS 21929-2:2015, Sustainability in building construction. Sustainability indicators. Part 2: Framework for the development of indicators for civil engineering works, International Organization for Standardization, Geneva, 2015.
[20] ISO/CD 21930, Sustainability in buildings and civil engineering works. Environmental declaration of building products, International Organization for Standardization, Geneva, 2015.
[21] ISO 21930:2007, Sustainability in building construction. Environmental declaration of building products, International Organization for Standardization, Geneva, 2007.
[22] ISO ISO 21931-1:2010, Sustainability in building construction. Framework for methods of assessment of the environmental performance of construction works. Part 1: Buildings, International Organization for Standardization, Geneva, 2010.
[23] ISO/NP 21931-2, Sustainability in building construction. Framework for methods of assessment of the environmental performance of construction works. Part 2: Civil engineering works, International Organization for Standardization, Geneva, 2015.
[24] ISO/TR 21932:2013, Sustainability in buildings and civil engineering works. A review of terminology, International Organization for Standardization, Geneva, 2013.
[25] ISO 12655:2013, Energy performance of buildings. Presentation of measured energy use of buildings, International Organization for Standardization, Geneva, 2013.
[26] ISO 16343:2013, Energy performance of buildings. Methods for expressing energy performance and for energy certification of buildings, International Organization for Standardization, Geneva, 2013.
[27] ISO 16346:2013, Energy performance of buildings. Assessment of overall energy performance, International Organization for Standardization, Geneva, 2013.
[28] ISO/TR 16344:2012, Energy performance of buildings. Common terms, definitions and symbols for the overall energy performance rating and certification, International Organization for Standardization, Geneva, 2012.
[29] ISO 13153:2012, Framework of the design process for energy-saving single-family residential and small commercial buildings, International Organization for Standardization, Geneva, 2012.
[30] ISO/DTR 16822, Building environment design. List of test procedures for heating, ventilating, air-conditioning and domestic hot water equipment related to energy efficiency, International Organization for Standardization, Geneva, 2015.
[31] ISO/NP 19454, Building environment design. Indoor environment. Daylight opening design process in order to ensure sustainability principles in visual environment, International Organization for Standardization, Geneva, 2015.
[32] ISO 16818:2008, Building environment design. Energy efficiency. Terminology, International Organization for Standardization, Geneva, 2008.
[33] ISO 23045:2008, Building environment design. Guidelines to assess energy efficiency of new buildings, International Organization for Standardization, Geneva, 2008.
[34] ISO/TR 21932:2013, Sustainability in buildings and civil engineering works. A review of terminology, International Organization for Standardization, Geneva, 2013.
[35] ISO/TS 12720:2014, Sustainability in buildings and civil engineering works. Guidelines on the application of the general principles in ISO 15392, International Organization for Standardization, Geneva, 2014.
[36] EN 15978:2011, Sustainability of construction works. Assessment of environmental performance of buildings. Calculation method, Comité Européen de Normalisation, Brussels, 2011.
[37] EN 16309:2014+A1:2014, Sustainability of construction works - Assessment of social performance of buildings - Calculation methodology, Comité Européen de Normalisation, Brussels, 2014.
[38] EN 15643-2:2011, Sustainability of construction works. Assessment of buildings - Framework for the assessment of environmental performance, Comité Européen de Normalisation, Brussels, 2011.
[39] EN 15978:2011, Sustainability of construction works. Assessment of environmental performance of buildings. Calculation method, Comité Européen de Normalisation, Brussels, 2011.
[40] EN 15643-1:2010, Sustainability of construction works. Sustainability assessment of buildings - General framework, Comité Européen de Normalisation, Brussels, 2010.
[41] prEN 15643-5, Sustainability of construction works - Sustainability assessment of buildings and civil engineering works - part 5: framework on specific principles and requirement for civil engineering works, Comité Européen de Normalisation, Brussels, 2015.
[42] Trigo, A.D.P., Ramila, F.C. and Colindres, J.I.M., Aulas de ecodiseño: análisis de ciclo de vida y ecodiseño en la industria. DYNA Ingeniería e Industria, 86(1), pp. 74-79, 2011. DOI: 10.6036/3848
[43] Arana, G., Landeta, B., Ruiz de Arbulo, P. and Díaz de Basurto, P., Analysis of the effects of the adoption of eco-design standards on business performance in the architecture firms. DYNA, 80(181), 201-209, 2013.
[44] Landeta, B., Arana, G., Ruiz de Arbulo, P. and Díaz de Basurto, P., Sustainability through Eco-Design: Shedding light on the adoption of the ISO 14006 Standard. En Sustainable Operations Management. Springer International Publishing, 2015. pp. 163-181. DOI: 10.1007/978-3-319-14002-5_8
[45] Heras, I., La gestión de la calidad en las empresas vascas: Estudio de la aplicación de la ISO 9000 en las empresas de la CAPV, Tesis Dr., Departamento de Organización de Empresas, Universidad del País Vasco (UPV/EHU), España, 2000.
[46] Blumer, H., What is wrong with social theory. Qualitative methodology: Firsthand involvement with the social world, Chicago: Markham, pp. 52-62, 1970. DOI: 10.1093/sf/50.2.265
[47] Denzin, N.K. and Lincoln, Y.S. (Eds.). Collecting and interpreting qualitative materials (Vol. 3), Sage, 2008.
[48] Heras, I., How quality management models influence company results–conclusions of an empirical study based on the Delphi

method. Total Quality Management and Business Excellence, 17(6), pp. 775-794, 2006. DOI: 10.1080/09593960600597768
[49] Landeta, J., El método Delphi: Una técnica de previsión para la incertidumbre, Ariel, 1999.
[50] Sahal, D. and Yee, K., Delphi: An investigation from a Bayesian viewpoint. Technological Forecasting and Social Change, 7(2), pp. 165-178, 1975. DOI: 10.1016/0040-1625(75)90056-6
[51] Castells, M., Toward a sociology of the network society. Contemporary sociology, pp. 693-699, 2000.
[52] Yin, R., Case study research: Design and methods, fifth edition, Thousand Oaks, CA: Sage Publications, 2013.
[53] Françoise, O., Bourgault, M. and Pellerin, R., ERP implementation through critical success factors' management. Business Process Management Journal, 15(3), pp. 371-394, 2009. DOI: 10.1108/14637150910960620
[54] Loo, R., The Delphi method: A powerful tool for strategic management. Policing: An International Journal of Police Strategies and Management, 25(4), pp. 762-769, 2002. DOI: 10.1108/13639510210450677
[55] Dootson, S., An in-depth study of triangulation. Journal of Advanced Nursing, 22(1), pp. 183-187, 1995. DOI: 10.1046/j.1365-2648.1995.22010183.x
[56] Häkkinen, T. and Belloni, K., Barriers and drivers for sustainable building. Building Research and Information, 39(3), pp. 239-255, 2011. DOI: 10.1080/09613218.2011.561948

B. Landeta-Manzano, es Dr. Ing. Industrial y MSc. en Gestión de Proyectos EURO MPM, todos por la Universidad del País Vasco (UPV/EHU), España. Ha desempeñado labores como técnico especialista en sistemas de generación de frío/calor, gestor de proyectos en ingeniería, y gerente de una empresa de instalaciones industriales. Desde el año 2008 es profesor en la Universidad del País Vasco (UPV/EHU), España. Actualmente, trabaja líneas de investigación relacionadas con la gestión de la innovación, el ecodiseño y la competitividad de las empresas.
ORCID: 0000-0003-4496-3792

G. Arana-Landín, es Ing. de Organización por la Universidad de Navarra, España y Dr. por la Universidad del País Vasco (UPV/EHU), España. Actualmente, trabaja para la Universidad del País Vasco (UPV/EHU) como profesor titular de Universidad del Departamento de Organización de Empresas. Ha participado en numerosos proyectos de investigación y ha publicado numerosos artículos de investigación en revistas internacionales de primer nivel, principalmente relativos a la adopción de sistemas de gestión por parte de las empresas.
ORCID: 0000-0003-2027-7157

P. Ruiz de Arbulo-López, es licenciado en CCEE y Empresariales por la "Comercial" de la Universidad de Deusto, España, MSc. en Gestión de Empresas por la UPV/EHU, España, MSc. en Organización e Ingeniería de la Producción por la Universidad Politécnica de Cataluña, España, y Dr. por la Universidad del País Vasco (UPV/EHU), España. Actualmente, es profesor del Departamento de Organización de Empresas de la Universidad del País Vasco (UPV/EHU), España. Ha publicado diversos artículos en revistas académicas y profesionales, y es secretario académico del departamento de Organización de Empresas desde el año 2009.
ORCID: 0000-0003-4881-0304

P. Díaz de Basurto-Uraga, es Dr. Ing. Industrial por la Escuela Técnica Superior de Ingeniería de Bilbao (UPV/EHU), España. Trabaja como Catedrático de Universidad y Director del Departamento de Organización de Empresas en la Universidad del País Vasco (UPV/EHU), España. Ha participado en numerosos proyectos de investigación y ha publicado numerosos artículos de investigación en revistas internacionales de primer nivel, relacionadas con el área de Organización de empresas.
Orcid: 0000-0003-3364-7698

UNIVERSIDAD NACIONAL DE COLOMBIA
SEDE MEDELLÍN
FACULTAD DE MINAS

Área Curricular de Ingeniería Administrativa e Ingeniería Industrial

Oferta de Posgrados

Especialización en Gestión Empresarial
Especialización en Ingeniería Financiera
Maestría en Ingeniería Administrativa
Maestría en Ingeniería Industrial
Doctorado en Ingeniería - Industria y Organizaciones

Mayor información:

E-mail: acia_med@unal.edu.co
Teléfono: (57-4) 425 52 02

UNIVERSIDAD NACIONAL DE COLOMBIA
SEDE MEDELLÍN
FACULTAD DE MINAS

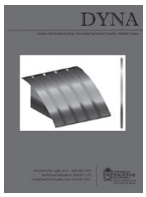

DYNA
http://dyna.medellin.unal.edu.co/

Numerical experimentation for the optimal design of reinforced rectangular concrete beams for singly reinforced sections

Arnulfo Luevanos-Rojas

Juarez University of the State of Durango, Gómez Palacio, Durango, Mexico. arnulfol_2007@hotmail.com

Received: December 26th, 2014. Received in revised form: August 1rd, 2015. Accepted: March 10th, 2016.

Abstract
This paper presents a model for the optimal design of reinforced rectangular concrete beams for singly reinforced sections. It develops an analytical approach to the problem, based on a criterion of minimum cost and minimum weight design with a reduced number of design variables. Representative examples are presented to illustrate the applicability of the formulation in accordance with building code requirements for structural concrete (ACI 318S-13), including the comments on the standards. A comparison is made between the optimal design solution and current design practice for reinforced rectangular concrete beams. The optimal solution for the design of reinforced rectangular concrete beams shows clearly that significant savings can be made in the costs of the construction materials used – i.e. reinforcement steel and concrete. In addition, the problem formulation can be applied using a nonlinear mathematical programming format.

Keywords: optimal design; minimum cost design; minimum weight design; reinforced rectangular concrete beams; singly reinforced sections.

Experimentación numérica para el diseño óptimo de vigas rectangulares de concreto reforzado para secciones simplemente reforzadas

Resumen
En este trabajo se presenta un modelo para el diseño óptimo de vigas rectangulares de concreto armado para secciones simplemente reforzadas. Un enfoque analítico del problema basado en un criterio de diseño de costo mínimo y diseño de peso mínimo con un número reducido de variables de diseño se desarrollan. Ejemplos típicos se presentan para ilustrar la aplicabilidad de la formulación de acuerdo con los códigos de construcción de concreto estructural (ACI 318S-13) y los comentarios. Una comparación se hace entre la solución del diseño óptimo y la práctica del diseño actual de vigas rectangulares de concreto armado. La solución óptima para el diseño de vigas rectangulares de concreto armado muestra claramente que los ahorros significativos se pueden hacer en los costos de los materiales de construcción utilizados para la fabricación de vigas como son el acero de refuerzo y concreto. Además, la formulación del problema se puede aplicar en un formato de programación matemática no lineal.

Palabras clave: diseño optimo; diseño de costo mínimo; diseño de peso mínimo; vigas rectangulares de concreto reforzado; secciones simplemente reforzadas.

1. Introduction

Structural design requires judgment, intuition and experience, in addition to the ability to design structures that are safe, serviceable and economical. Design codes do not necessarily produce designs that satisfy all of these conditions [1].

Structural design is an iterative process. The initial design is the first step in the process. Though the various aspects of structural design are controlled by many codes and regulations, structural engineers must exercise caution and use their judgment, as well as getting their calculations right, if they are to interpret the various provisions of the code in a manner that produces efficient and economically rational designs [2].

The optimum design of structures has been the topic of a large number of studies in the field of structural design. A designer's goal is to develop an "optimal solution" for the structural design under consideration. This normally implies the most economic structure that does not impair the functional purposes the structure is intended to satisfy [3].

© The author; licensee Universidad Nacional de Colombia.

Objective Statement	Objective Function
Select the least cost member	minimize (cost)
Select the least weight member	minimize (weight)

Source: The author

An optimum design is generally considered to be the one design that best satisfies the criteria for the project. Typically there is some kind of objective function that can be computed from the variables that define a design. The value of the objective function is used to compare feasible designs and to determine the "best" or "optimum" design [4].

In structural engineering, the objective statement can also be put in the form of an objective function. Some typical objective statements, and their associated objective functions are:

In structural design, design constraints are frequently referred to as LIMIT STATES. Limit States are conditions of potential failure, where failure is defined as any state that makes the design infeasible (i.e., it will not work for its intended purpose) [4,5].

Limit states take the general form of:

$$\text{Demand} < \text{Capacity}$$

Structural limit states tend to fall into two major categories: strength and serviceability [4,5].

1) Strength Limit States

Strength-based limit states are potential modes of structural failure. For steel members, the failure may mean either yielding (permanent deformation) or rupture (actual fracture). The strength-based limit state may be written in the general form:

$$\text{Required Strength} < \text{Nominal Strength}$$

Required strength is the internal force derived from the analysis of the structure being designed. For example, when designing a beam, required strength is the maximum moment, M, computed for the beam. Nominal strength is the predicted capacity of the beam, for example in bending; it is the maximum moment, M_n, that the beam is capable of supporting (a function of the stress capacity of the material and the section properties of the member) [4,5].

Typically, structural design specifications use the following variables to denote the different strengths:

P = Axial Force
M = Bending Moment
V = Shear Force
R = Reaction Force

2) Serviceability Limit States

Serviceability limit states are conditions that are not strength-based but may still make a structure unsuitable for its intended use. The most common serviceability limit states in structural design are deflection, vibration, slenderness and clearance. Serviceability limit states may be written in the general form:

$$\text{Actual Behavior} < \text{Allowable Behavior}$$

An example is deflection. A loaded cantilever beam will display deflection at the free end (actual behavior) that must be kept lower than allowable deflection (allowable behavior) [4,5].

Serviceability limit states tend to be less rigid requirements than strength-based limit states, as the safety of the structure is not in question. Serviceability limit states don't tend to put people's lives at risk nor do they risk property damage [4,5].

It is worth noting that some engineers find it useful to divide the left side of limit state inequalities by the right, as follows:

$$(\text{Required Strength}/\text{Nominal Strength}) < 1.00$$
$$(\text{Actual Behavior})/(\text{Allowable Behavior}) < 1.00$$

This is useful for two reasons. It makes comparison easier (the resulting value must be < 1.00) and the resulting number provides information on the percentage of capacity used. Knowing the percentage of capacity makes it easier to decide which limit states are critical as work progresses on optimizing a complex design problem.

The best solution is the one that returns the section with the best objective function value [4,5].

The titles of some papers that discuss the use of optimization methods are: "Validación de soluciones obtenidas para el problema del despacho hidrotérmico de mínimo costo empleando la programación lineal binaria mixta" [6]; "Route optimization of urban public transportation" [7]; "Methodology for distribution centers location through multicriteria analysis and optimization" [8]; and "Multiobjective optimization of the reactive power compensation in electric distribution systems" [9].

The optimization of building structures is a prime goal of designers and has been investigated by many researchers in the past, in papers such as: "Optimum Design of Unstiffened Built-up Girders" [10]; "Shape Optimization of RC Flexural Members" [11]; "Sensitivity Analysis and Optimum Design Curves for the Minimum Cost Design of Singly and Doubly Reinforced Concrete Beams" [12]; "Optimal Design of a Welded I-Section Frame Using Four Conceptually Different Optimization Algorithms" [13]; "New Approach to Optimization of Reinforced Concrete Beams, Computer and Structures" [14]; "Cost Optimization of Singly and Doubly Reinforced Concrete Beams with EC2-2001" [15]; "Cost Optimization of Reinforced Concrete Flat Slab Buildings" [16]; "Multi Objective Optimization for Performance-Based Design of Reinforced Concrete Frames" [17]; "Design of Optimally Reinforced RC Beam, Column, and Wall Sections" [18]; "Cost Optimization Of Doubly Reinforced Rectangular Beam Section" [3].

Artificial Neural Networks (ANNs) have been used in the field design of concrete structure , the most important results being achieved in the structural design process and structural analysis. Relevant papers here are: "Modelling Confinement Efficiency of Reinforced Concrete Columns with Rectilinear Transverse Steel using Artificial Neural Network" [19]; "Simulating Size Effect on Shear Strength of RC Beams

without Stirrups using Neural Networks" [20]; "Neural Network Evaluation of Steel Beam Patch Load Capacity" [21]; "Damage Assessment in Structure From Changes in Static Parameter using Neural Networks" [22]; "Genetically optimized artificial neural network based optimum design of singly and doubly reinforced concrete beams" [1]; "Optimum Design of Singly and Doubly Reinforced Concrete Rectangular Beam Sections: Artificial Neural Networks Application" [2]. The ANN models built by these researchers basically establish the structural parameters of the inputs to the ANN model, such as material properties, boundary conditions and the size of the structure in question, in order to predict its ability to resist the load for which it is designed [2,23].

Optimization is highly linked to the selection of the most suitable structural system, sized to ensure the least overall cost. In structural design, many parameters are incremental in nature, rendering a continuous approach almost impossible to implement in any given practical optimization exercise [2,24].

This paper presents a model for achieving optimal design of reinforced rectangular concrete beams for singly reinforced sections. It develops an analytical approach to the problem, based on a criterion of minimum cost and minimum weight design with a reduced number of design variables. Representative examples are presented to illustrate the applicability of the formulation in according with building code requirements for structural concrete (ACI 318-13), including the comments on the standards. A comparison is made between the optimal design solution and current design practice for reinforced rectangular concrete beams. The optimal solution for design of reinforced rectangular concrete beams clearly shows that significant savings can be made in the costs of the materials used for their fabrication, that is, reinforcement steel and concrete.

2. Methodology

2.1. Optimization technique

With optimization problems the goal is to minimize the weight, volume or cost of the structure under certain deterministic behavioral constraints. The mathematical formulation of a typical structural optimization problem with respect to the design variables and objective and constraint functions can be expressed in standard mathematical terms as a nonlinear programming problem as follows [6-9,25-28]:

$$Min\ F(x_1, x_2 \dots x_n) \tag{1}$$

subject to

$$\begin{gathered} h_j(x) \leq 0, j = 1 \dots m \\ x_i^k \leq x_i \leq x_i^s, i = 1 \dots n \end{gathered} \tag{2}$$

where: x is the vector of design variables, $F(x_1, x_2 \dots x_n)$ is the objective function to be minimized, $h_j(x)$ is the behavioral constraint, and x_i^k and x_i^s are the lower and the upper bounds of typical design variable x_i.

2.2. Problem formulation

The goal of optimization is to find the best solution amongst a set of candidate solutions, using efficient quantitative methods. In beam design, the decision variables represent the quantities to be determined, and a set of decision variable values constitutes a candidate solution. An objective function, which is either maximized or minimized, expresses the goal, or performance criterion, in terms of decision variables. The set of allowable solutions and, hence, the objective function value, is constrained by factors that govern the beam design.

Fig. 1 shows the geometry of a typical single reinforced rectangular section with a simplified rectangular stress block, as provided in the ACI Code [29-31].

The following factors are defined for a given problem:

$$h = d + r \tag{3}$$

where: h is total depth, d is effective depth, and r is coating.

In eq. (2), h (the geometric property) is a function of the effective depth, d is variable, and the coating r is constant.

When a rectangular beam section is designed, the nominal bending moment M_n, with a cross section width b or effective depth d, and material properties f'_c and f_y are generally given.

The equations given in the ACI Code [29-31] are:

$$M_u = \emptyset_f b d^2 \rho f_y \left(1 - \frac{0.59 \rho f_y}{f'_c}\right) \tag{4}$$

$$\rho = \frac{A_s}{bd} \tag{5}$$

$$\rho_b = \frac{0.85 \beta_1 f'_c}{f_y}\left(\frac{600}{600 + f_y}\right) \tag{6}$$

$$0.65 \leq \beta_1 = \left(1.05 - \frac{f'_c}{140}\right) \leq 0.85 \tag{7}$$

$$\rho_{max} = 0.75 \rho_b \tag{8}$$

$$\rho_{min} = \begin{cases} \dfrac{0.25\sqrt{f'_c}}{f_y} \\ \dfrac{1.4}{f_y} \end{cases} \tag{9}$$

$$M_u = \emptyset_f M_n \tag{10}$$

where: M_u is the factored maximum moment, $\emptyset_f$ is the strength reduction factor by bending, with value 0.90, ρ is ratio of A_s to bd, β_1 is the factor relating the depth of the equivalent rectangular compressive stress block to neutral axis depth, f_y is the specified yield strength of reinforcement of steel, f'_c is the specified compressive strength of concrete at 28 days, and M_n is the nominal bending moment.

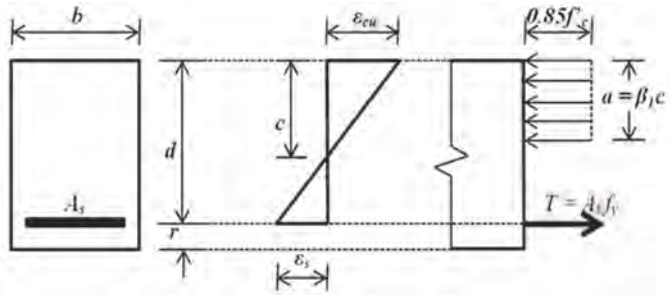

Figure 1. Singly reinforced rectangular beams.
Source: The author, adapted from ACI 318S-13.

2.2.1.1. Objective function: cost minimization

A cost function is defined as the total cost C_t, which is equal to the cost of flexural reinforcement C_s, plus the cost of concrete, C_c. These costs involve material and fabrication costs, respectively. The costs refer to the unit costs of reinforcement steel and concrete for a given unit volume. The cost of the beam of a unit length is:

$$C_t = C_s V_s + C_c V_c \tag{11}$$

where: V_s is volume of reinforcement steel and V_c is volume of concrete per unit length of beam. These equations are:

$$V_s = A_s \tag{12}$$

$$V_c = b(d + r) - A_s \tag{13}$$

Substituting eq. (12) and (13) into eq. (11) produces the following equation:

$$C_t = C_s A_s + C_c[b(d + r) - A_s] \tag{14}$$

If we consider $\alpha = C_s / C_c$ and this is substituted into eq. (14) produces the following equation:

$$C_t = C_c[b(d + r) + (\alpha - 1)A_s] \tag{15}$$

2.2.1. Case 1

Assuming that the constant parameters are: M_u, b, f'_c and f_y then the design variables are: ρ, A_s and d.
The objective function to minimize is:

$$C_t = C_c[bd + br + (\alpha - 1)A_s] \tag{16}$$

subject to:

$$\frac{M_u}{\emptyset_f f_y} = dA_s\left(1 - \frac{0.59A_s f_y}{bdf'_c}\right) \tag{17}$$

$$\rho \leq 0.75\left[\frac{0.85\beta_1 f'_c}{f_y}\left(\frac{600}{600 + f_y}\right)\right] \tag{18}$$

$$\rho \geq \begin{cases} \dfrac{0.25\sqrt{f'_c}}{f_y} \\ \dfrac{1.4}{f_y} \end{cases} \tag{19}$$

$$A_s = \rho bd \tag{20}$$

2.2.1.2. Case 2

Now assume that the constant parameters are: M_u, d, f'_c and f_y.
The design variables are: ρ, A_s and b.
The objective function to minimize is:

$$C_t = C_c[b(d + r) + (\alpha - 1)A_s] \tag{21}$$

subject to:

$$\frac{M_u}{\emptyset_f d^2 f_y} = \rho b\left(1 - \frac{0.59\rho f_y}{f'_c}\right) \tag{22}$$

$$\rho \leq 0.75\left[\frac{0.85\beta_1 f'_c}{f_y}\left(\frac{600}{600 + f_y}\right)\right] \tag{23}$$

$$\rho \geq \begin{cases} \dfrac{0.25\sqrt{f'_c}}{f_y} \\ \dfrac{1.4}{f_y} \end{cases} \tag{24}$$

$$A_s = \rho bd \tag{25}$$

2.2.2. Objective: function to minimize the weight

A weight function is defined as total weight, W_t, which is equal to the weight of flexural reinforcement, W_s, plus the weight of concrete, W_c. These weights record only the weight of materials; they refer to the unit weights of reinforcement steel and concrete for a given unit volume. The weight of the beam of a unit length is:

$$W_t = W_s V_s + W_c V_c \tag{26}$$

Substituting eq. (12) and (13) into eq. (26) produces:

$$W_t = W_s A_s + W_c[b(d + r) - A_s] \tag{27}$$

If we consider $\gamma = W_s / W_c$ and it is substituted into eq. (27) the result is as follows:

$$W_t = W_c[b(d + r) + (\gamma - 1)A_s] \tag{28}$$

2.2.2.1. Case 3

Now assume that the constant parameters are: M_u, b, f'_c and f_y.
The design variables are: ρ, A_s and d.
The objective function to minimize is:

$$W_t = W_c[bd + br + (\gamma - 1)A_s] \quad (29)$$

subject to:

$$\frac{M_u}{\emptyset_f f_y} = dA_s\left(1 - \frac{0.59A_s f_y}{bdf'_c}\right) \quad (30)$$

$$\rho \leq 0.75\left[\frac{0.85\beta_1 f'_c}{f_y}\left(\frac{600}{600 + f_y}\right)\right] \quad (31)$$

$$\rho \geq \begin{cases} \dfrac{0.25\sqrt{f'_c}}{f_y} \\ \dfrac{1.4}{f_y} \end{cases} \quad (32)$$

$$A_s = \rho bd \quad (33)$$

2.2.2.2. Case 4

Now assume that the constant parameters are: M_u, d, f'_c and f_y.
The design variables are: ρ, A_s and b.
The objective function to minimize is:

$$W_t = W_c[b(d + r) + (\gamma - 1)\rho bd] \quad (34)$$

subject to:

$$\frac{M_u}{\emptyset_f d^2 f_y} = \rho b\left(1 - \frac{0.59\rho f_y}{f'_c}\right) \quad (35)$$

$$\rho \leq 0.75\left[\frac{0.85\beta_1 f'_c}{f_y}\left(\frac{600}{600 + f_y}\right)\right] \quad (36)$$

$$\rho \geq \begin{cases} \dfrac{0.25\sqrt{f'_c}}{f_y} \\ \dfrac{1.4}{f_y} \end{cases} \quad (37)$$

$$A_s = \rho bd \quad (38)$$

MAPLE 14 software, designed to solve the optimization problem, was used to assess the optimal design with respect to minimum cost and minimum weight of reinforced rectangular concrete beams for singly reinforced sections.

3. Numerical Problems

3.1. Case Example 1

A rectangular beam section with b = 30 *cm* is given. Values must be determined for the optimum ratio of the reinforcement steel, ρ, its optimum area, A_s, and the optimum effective depth, d, for M_u = 700 *kN-m*, f'_c = 28 *MPa* and f_y = 420 *MPa*. It is assumed that r = 4 *cm*, and the ratio of reinforcement steel cost to concrete cost is: α = 90.

Substituting the corresponding values into eq. (16) in order to obtain the objective function, and into eq. (17)-(20) to find the constraints, produces:

Minimize:

$$C_t = C_c(0.3d + 0.012 + 89A_s) \quad (39)$$

subject to:

$$\frac{1}{540} = dA_s\left(1 - \frac{29.5A_s}{d}\right) \quad (40)$$

$$\rho \leq 0.02125 \quad (41)$$

$$\rho \geq \begin{cases} 0.00315 \\ 0.00333 \end{cases} \quad (42)$$

$$A_s = 0.3\rho d \quad (43)$$

The optimal solution is:
$C_t = 0.47831C_c$
$A_s = 0.0023763\ m^2 = 23.763\ cm^2$
$d = 0.84941\ m = 84.941\ cm$
$\rho = 0.00933$

Fig. 2 presents the plot of the objective function and the constraint functions.

Example 1 is developed by employing the standard design method, using eq.s (4)-(10). The results are presented in Table 1. It may be seen from this table that the derived optimum design formulae for singly reinforced sections give an accurate estimate of the minimum material cost.

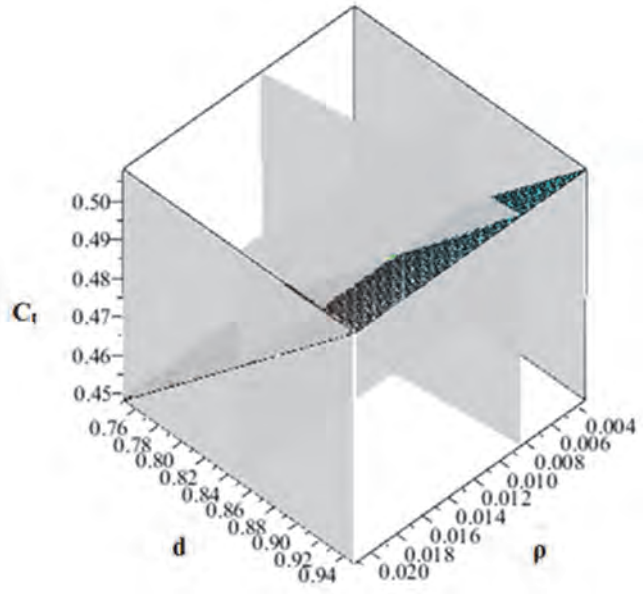

Figure 2. Functions for Example 1.
Source: The author.

3.2. Case Example 2

A rectangular beam section, effective depth d = 26 *cm*, giving a total depth of h = 30 *cm* is given. Values must be determined for the optimum ratio of reinforcement steel ρ, its optimum area, A_s, and its optimum width b, for M_u = 700 *kN-m*, f'_c = 28 *MPa* and f_y = 420 *MPa*. It is assumed that r = 4 *cm*, and the ratio of reinforcement steel cost to concrete cost is: α = 90.

Substituting the corresponding values into eq. (21) in order to obtain the objective function and into eq.s (22)-(25) to find the constraints results in the following:

Minimize:

$$C_t = C_c(0.3b + 89A_s) \tag{44}$$

subject to:

$$\frac{125}{4563} = \rho b(1 - 8.85\rho) \tag{45}$$

$$\rho \leq 0.02125 \tag{46}$$

$$\rho \geq \begin{cases} 0.00315 \\ 0.00333 \end{cases} \tag{47}$$

$$A_s = 0.26\rho b \tag{48}$$

The optimal solution is:

$$C_t = 1.25705C_c$$
$$A_s = 0.00877\ m^2 = 87.7\ cm^2$$
$$b = 1.58773\ m = 158.773\ cm$$
$$\rho = 0.02125$$

Fig. 3 plots the objective function and the constraint functions.

Example 2 is developed by employing the standard design method, using eq. (4)-(10). The results are presented in Table 2. This table also shows the derived optimum design formulae for singly reinforced sections, giving an accurate estimate of the minimum material cost.

Table 1.
Results by standard design method for Example 1.

Effective depth (cm)	Reinforcement steel ratio	Reinforcement steel area (cm^2)	Total material cost ($/m)
59.814	0.02125	38.1314	$0.53081C_c$
60.000	0.02108	37.9440	$0.52970C_c$
70.000	0.01444	30.3240	$0.49188C_c$
80.000	0.01065	25.5600	$0.47948C_c$
84.941	**0.00933**	**23.7630**	**$0.47831C_c$**
90.000	0.00822	22.1940	$0.47953C_c$
100.000	0.00655	19.6500	$0.48688C_c$
110.000	0.00536	17.6880	$0.49942C_c$
120.000	0.00446	16.0560	$0.51490C_c$
130.000	0.00378	14.7420	$0.53320C_c$
138.203	0.00333	13.8065	$0.54949C_c$

Source: The author.

3.3. Case Example 3

A rectangular beam section with b = 30 *cm* is given. Values must be determined for the optimum ratio of reinforcement steel ρ, its optimum area, A_s, and the optimum effective depth, d, for M_u = 700 *kN-m*, f'_c = 28 *MPa* and f_y = 420 *MPa*. It is assumed that r = 4 *cm*, and the ratio of reinforcement steel weight to concrete weight is: γ = 3.

Substituting the corresponding values into eq. (29) in order to obtain the objective function and also into eq.s (30)-(33) to find the constraints results in the following:

Minimize:

$$W_t = W_c(0.3d + 0.012 + 2A_s) \tag{49}$$

subject to:

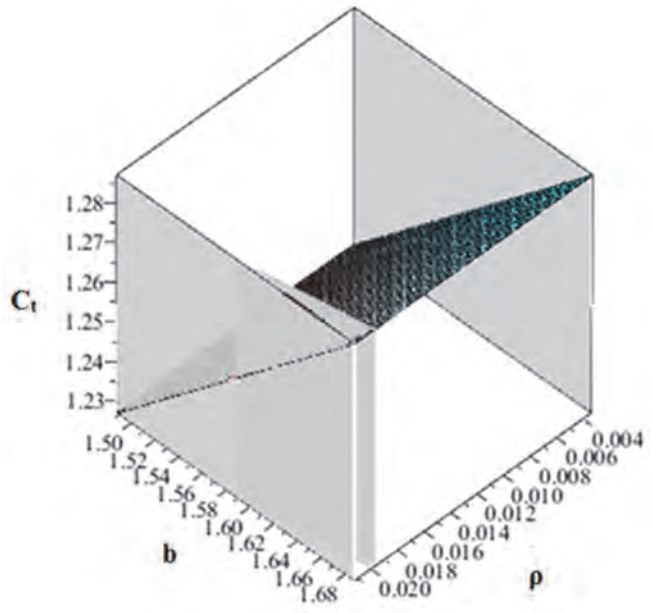

Figure 3. Functions, Example 2.
Source: The author.

Table 2.
Results by standard design method for Example 2

Width (cm)	Reinforcement steel ratio	Reinforcement steel area (cm^2)	Total material cost ($/m)
158.773	**0.02125**	**87.7221**	**$1.25705C_c$**
160.000	0.02104	87.5264	$1.25898C_c$
180.000	0.01813	84.8484	$1.29515C_c$
200.000	0.01595	82.9400	$1.33817C_c$
250.000	0.01230	79.9500	$1.46156C_c$
300.000	0.01002	78.1560	$1.59559C_c$
350.000	0.00846	76.9860	$1.73518C_c$
400.000	0.00732	76.1280	$1.87754C_c$
500.000	0.00577	75.0100	$2.16759C_c$
600.000	0.00477	74.4120	$2.46227C_c$
700.000	0.00406	73.8920	$2.75764C_c$
800.000	0.00353	73.4240	$3.05347C_c$
847.630	0.00333	73.3878	$3.19604C_c$

Source: The author.

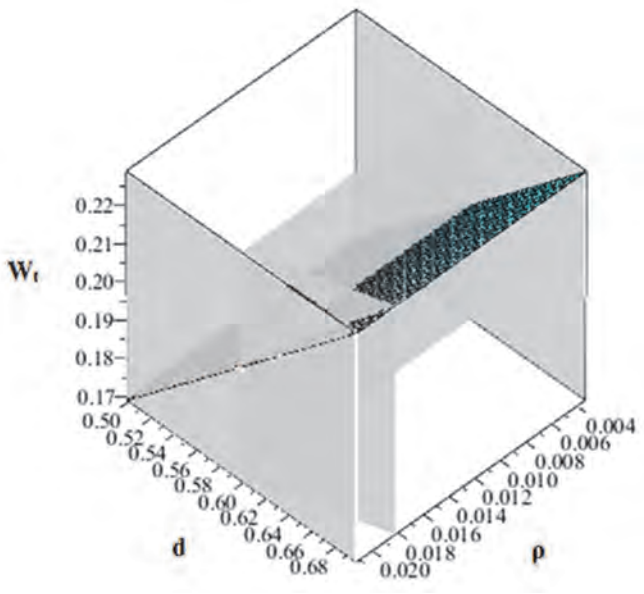

Figure 4. Functions, Example 3.
Source: The author.

$$\frac{1}{540} = dA_s\left(1 - \frac{29.5A_s}{d}\right) \tag{50}$$

$$\rho \leq 0.02125 \tag{51}$$

$$\rho \geq \begin{cases} 0.00315 \\ 0.00333 \end{cases} \tag{52}$$

$$A_s = 0.3\rho d \tag{53}$$

The optimal solution is:
$W_t = 0.19907W_c$
$A_s = 0.00381\ m^2 = 38.1\ cm^2$
$d = 0.59814\ m = 59.814\ cm$
$\rho = 0.02125$

Fig. 4 presents the plot of the objective function and the constraint functions.

Example 3 employs the standard design method using eq.s (4)-(10). The results are presented in Table 3. It is apparent from this table that the derived optimum design formulae for singly reinforced sections give an accurate estimate of minimum material weight.

Table 3.
Results by standard design method for the Example 3

Effective depth (cm)	Reinforcement steel ratio	Reinforcement steel area (cm^2)	Total material weight (kN/m)
59.814	**0.02125**	**38.1314**	**$0.19907W_c$**
60.000	0.02108	37.9440	$0.19959W_c$
70.000	0.01444	30.3240	$0.22806W_c$
80.000	0.01065	25.5600	$0.25711W_c$
84.941	0.00933	23.7750	$0.27158W_c$
90.000	0.00822	22.1940	$0.28644W_c$
100.000	0.00655	19.6500	$0.31593W_c$
110.000	0.00536	17.6880	$0.34554W_c$
120.000	0.00446	16.0560	$0.37521W_c$
130.000	0.00378	14.7420	$0.40495W_c$
138.203	0.00333	13.8065	$0.42937W_c$

Source: The author.

3.4. Case Example 4

A rectangular beam section of effective depth $d = 26\ cm$ is given. Values must be determined for the optimum ratio of reinforcement steel ρ and its optimum width b, for $M_u = 700\ kN\text{-}m$, $f'_c = 28\ MPa$ and $f_y = 420\ MPa$. It is assumed that $r = 4\ cm$, and the ratio of reinforcement steel weight to concrete weight is: $\gamma = 3$.

Substituting the corresponding values into eq. (34) in order to obtain the objective function and also into eq.s (35)-(38) to find the constraints results in the following:

Minimize:

$$W_t = W_c(0.3b + 2A_s) \tag{54}$$

subject to:

$$\frac{125}{4563} = \rho b(1 - 8.85\rho) \tag{55}$$

$$\rho \leq 0.02125 \tag{56}$$

$$\rho \geq \begin{cases} 0.00315 \\ 0.00333 \end{cases} \tag{57}$$

$$A_s = 0.26\rho b \tag{58}$$

The optimal solution is:
$W_t = 0.49386W_c$
$A_s = 0.00877\ m^2 = 87.7\ cm^2$
$b = 1.58773\ m = 158.773\ cm$
$\rho = 0.02125$

Fig. 5 displays the plot of the objective function and the constraint functions.

Example 4 employs the standard design method using eq.s (4)-(10). The results are presented in Table 4. It is apparent from this table that the derived optimum design formulae for singly reinforced sections give an accurate estimate of minimum material weight.

4. Results

Table 1 presents the results, using the standard design method for Case Example 1. The constant parameters are: M_u, b, f'_c and f_y. The design variables are: ρ, A_s and d. The ranges considered vary from the minimum ratio of reinforcement steel, ρ_{min}, and the maximum ratio, ρ_{max}, allowing the variation of the effective depth, d, reinforcement steel area, A_s, and the total material cost, C_t, to be observed. The corresponding total material cost, C_t, of the beam per unit length is then obtained from eq. (39), its minimum value being $0.47842C_c$ \$/m (in terms of the concrete cost per unit volume). Consequently, the results obtained by employing the standard design method and optimal design are equal.

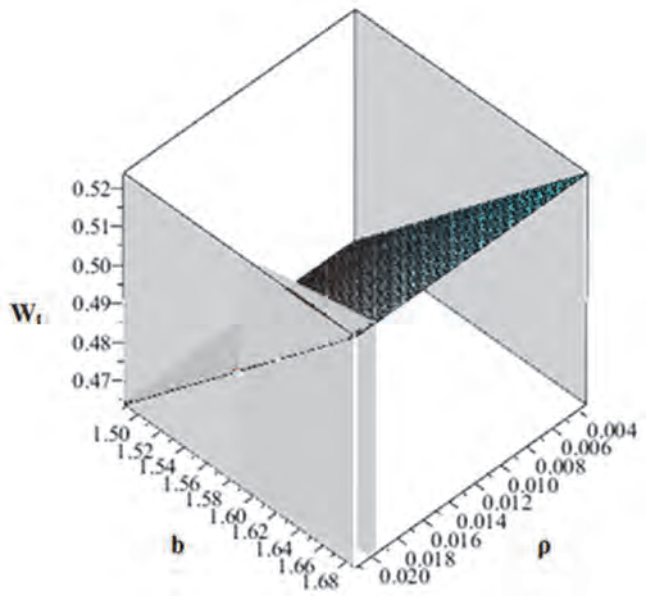

Figure 5. Functions, Example 4.
Source: The author.

Table 4.
Results by standard design method for the Example 4

Width (cm)	Reinforcement steel ratio	Reinforcement steel area (cm^2)	Total material weight (kN/m)
158.773	**0.02125**	**87.7221**	**0.49386W_c**
160.000	0.02104	87.5264	0.49751W_c
180.000	0.01813	84.8484	0.55697W_c
200.000	0.01595	82.9400	0.61659W_c
250.000	0.01230	79.9500	0.76599W_c
300.000	0.01002	78.1560	0.91563W_c
350.000	0.00846	76.9860	1.06540W_c
400.000	0.00732	76.1280	1.21523W_c
500.000	0.00577	75.0100	1.51500W_c
600.000	0.00477	74.4120	1.81488W_c
700.000	0.00406	73.8920	2.11478W_c
800.000	0.00353	73.4240	2.41468W_c
847.630	0.00333	73.3878	2.55757W_c

Source: The author.

Table 2 presents the results using the standard design method for Case Example 2. The constant parameters are: M_u, d, f'_c and f_y. The design variables are: ρ, A_s and b. The ranges considered vary between the minimum ratio of reinforcement steel, ρ_{min}, and the maximum ratio, ρ_{max}, allowing the variation of the effective depth, d, reinforcement steel area, A_s, and the total material cost, C_t, to be observed. The corresponding total material cost of the beam per unit length, Ct, is then obtained from eq. (44) and found to be 1.25705C_c \$/m as its minimum value (in terms of the concrete cost per unit volume). This value corresponds to the maximum ratio of reinforcement steel ρ_{max}. Thus, the results presented by employing the standard design method and optimal design are equal.

Table 3 shows the results using the standard design method for case Example 3. The constant parameters are: M_u, b, f'_c and f_y. The design variables are: ρ, A_s and d. The ranges considered vary between the minimum ratio of reinforcement steel, ρ_{min}, and the maximum ratio, ρ_{max}, allowing the variation of the effective depth, d, reinforcement steel area, A_s, and the total material weight, W_t, to be observed. The corresponding total material weight W_t of the beam per unit length is then obtained from eq. (49) and found to be 0.19907W_c kN/m as its minimum value (in terms of the concrete weight per unit volume). This value corresponds to the maximum ratio of reinforcement steel ρ_{max}. Thus, the results presented by employing the standard design method and optimal design are equal.

Table 4 presents the results using the standard design method for case Example 4. The constant parameters are: M_u, d, f'_c and f_y. The design variables are: ρ, A_s and b. The ranges considered vary between the minimum ratio of reinforcement steel, ρ_{min}, and the maximum ratio, ρ_{max}, allowing the variation of the effective depth, d, reinforcement steel area, A_s, and the total material weight W_t. The corresponding total material weight W_t of the beam per unit length is then obtained from eq. (54) and found to be 0.49386W_c kN/m as its minimum value (in terms of the concrete weight per unit volume). This value corresponds to the maximum ratio of reinforcement steel ρ_{max}. Thus, the results presented by employing the standard design method and optimal design are equal.

Therefore, the derived optimum design formulae for singly reinforced sections give a very accurate estimate of the minimum cost and minimum weight for the four Representative examples.

5. Conclusions

This study dealt with the design of minimum cost (Cases 1 and 2) and minimum weight (Cases 3 and 4) reinforced rectangular concrete beams for singly reinforced sections. An analytical approach to the problem, based on a criterion of minimum cost and minimum weight design, plus a set of constraints that comply with building code requirements for structural concrete (ACI 318S-13), including the comments on the standards, was formulated. Cases 1 and 3 assume that the constant parameters are: M_u, b, f'_c and f_y, and that the design variables are ρ, A_s and d. Cases 2 and 4 imply that the constant parameters are: M_u, d, f'_c and f_y, and that the design variables are ρ, A_s and b.

The standard design method (classical method) generally uses the maximum ratio of reinforcement steel to obtain the cross-section of the beam.

The research reported in this paper concludes as follows:

- Case 1: The optimum steel ratio is usually smaller than maximum ratio, ρ_{max}, and greater than minimum ratio, ρ_{min}.
- Cases 2, 3 and 4: The optimum steel ratio is equal to the maximum ratio ρ_{max}.
- According to Case 1 the optimum section is very economical compared to other sections that may be obtained using the standard design method.
- The procedure developed as a result of this research can serve as the basis for designing reinforced concrete beams, while a structure designed using the optimum section will not necessarily provide an optimum design for the entire structure in terms of material costs.

Using the optimal design for Case 1, this paper successfully developed a model to predict the reinforcement

steel ratio and lowest cost of reinforced rectangular concrete beams for singly reinforced sections

Suggested future research includes: 1) Optimal design of other types of structural members for reinforced concrete and structural steel; 2) Optimum design for whole structures.

References

[1] Saini, B., Sehgala, V.K. and Gambhir, M.L., Genetically optimized artificial neural network based optimum design of singly and doubly reinforced concrete beams, Asian Journal of Civil Engineering (Building and Housing), [Online]. 7(6), pp. 603-619, 2006. Available at: http://citeseerx.ist.psu.edu/viewdoc/download?doi=10.1.1.133.2193&rep=rep1&type=pdf

[2] Yousif, S.T., ALsaffar, I.S. and Ahmed, S.M., Optimum design of singly and doubly reinforced concrete rectangular beam sections: Artificial neural networks application, Iraqi Journal of Civil Engineering, [Online]. 6(3), pp. 1-19, 2010. Available at: http://www.iasj.net/iasj?func=fulltext&aId=14126

[3] Bhalchandra, S.A. and Adsul, P.K., Cost optimization of doubly reinforced rectangular beam section, International Journal of Modern Engineering Research, [Online]. 2(5), pp. 3939-3942, 2012. Available at: http://www.ijmer.com/papers/Vol2_Issue5/FJ2539393942.pdf

[4] Quimby, T.B., A Beginner's guide to the structural engineering, Quimby & Associates Consulting Engineers, [Online]. 2012. Available at: http://www.bgstructuralengineering.com/BGSCM13_Sample.pdf

[5] Manual of Steel Construction LRFD (Load Resistance Factor Design), Structural Members Specifications & Codes, 3td Edition, AISC (American Institute Steel Construction), 2009.

[6] Ortiz-Pimiento, N.R. y Díaz-Serna, F.J., Validación de soluciones obtenidas para el problema del despacho hidrotérmico de mínimo costo empleando la programación lineal binaria mixta, DYNA, [Online]. 75(156), pp. 43-54, 2008. Available at: http://www.redalyc.org/articulo.oa?id=49612071005

[7] Jaramillo-Alvarez, P., Gonzalez-Calderon, C.A. and Gonzalez-Calderon, G., Route optimization of urban public transportation, DYNA, [Online]. 80(180), pp. 41-49, 2013. Available at: http://www.redalyc.org/articulo.oa?id=49627455007

[8] Soto-de la Vega, D., Vidal-Vieira, J.G. and Vitor-Toso, E.A., Methodology for distribution centers location through multicriteria analysis and optimization, DYNA, 81(184), pp. 28-35, 2014. DOI: 10.15446/dyna.v81n184.39654

[9] Santos-Azevedo, M.S., Pérez-Abril, I., León-Benítez, C., Cabral-Leite, J. and Holanda-Bezerra, U., Multiobjective optimization of the reactive power compensation in electric distribution systems, DYNA, 81(187), pp. 175-183, 2014. DOI: 10.15446/dyna.v81n187.40979

[10] Ha, T., Optimum design of unstiffened built-up girders, Journal of Structural Engineering, 119(9), pp. 2784-2792, 1993. DOI: 10.1061/(ASCE)0733-9445(1993)119:9(2784)

[11] Rath, D.P., Ahlawat, A.S. and Ramaswamy, A., Shape optimization of rc flexural members, Journal of Structural Engineering, 125(2), pp. 1439-1445, 1999. DOI: 10.1061/(ASCE)0733-9445(1999)125:12(1439)

[12] Ceranic, B. and Fryer, C., Sensitivity analysis and optimum design curves for the minimum cost design of singly and doubly reinforced concrete beams, Structural and Multidisciplinary Optimization, 20, pp. 260- 268, 2000. DOI: 10.1007/s001580050156

[13] Jarmai, K., Snyman, J.A., Farkas, J. and Gondos, G., Optimal design of a welded I-section frame using four conceptually different optimization algorithms, Structural and Multidisciplinary Optimization, 25, pp. 54- 61, 2003. DOI: 10.1007/s00158-002-0272-5

[14] Leps, M. and Sejnoha, M., New approach to optimization of reinforced concrete beams, Computer and Structures, 81, pp. 1957-1966, 2003. DOI: 10.1016/S0045-7949(03)00215-3

[15] Barros, M.H.F.M., Martins, R.A.F. and Barros, A.F.M., Cost optimization of singly and doubly reinforced concrete beams with EC2-2001, Structural and Multidisciplinary Optimization, 30, pp. 236- 242, 2005. DOI: 10.1007/s00158-005-0516-2

[16] Sahab, M.G., Ashour, AF. and Toropov, V.V., Cost optimization of reinforced concrete flat slab buildings, Engineering Structures, 27, pp. 313-322, 2005. DOI: 10.1016/j.engstruct.2004.10.002

[17] Zou, X., Chan, C., Li, G. and Wang, Q., Multi objective optimization for performance-based design of reinforced concrete frames, Journal of Structural Engineering, 133(10), pp. 1462-1474, 2007. DOI: 10.1061/(ASCE)0733-9445(2007)133:10(1462)

[18] Aschheim, M., Hernández-Montes, E. and Gil-Martin, L., Design of optimally reinforced RC beam, column, and wall sections, Journal of Structural Engineering, 134(2), pp. 231-239, 2008. DOI: 10.1061/(ASCE)0733-9445(2008)134:2(231)

[19] Tang, C., Chen, H. and Yen, T., Modelling confinement efficiency of reinforced concrete columns with rectilinear transverse steel using artificial neural network, Journal of Structural Engineering, 129(6), pp. 775-783, 2003. DOI: 10.1061/(ASCE)0733-9445(2003)129:6(775)

[20] Oreta, A.W.C., Simulating size effect on shear strength of RC beams without stirrups using neural networks, Engineering Structures, 26, pp. 681-691, 2004. DOI: 10.1016/j.engstruct.2004.01.009

[21] Fonseca, E.T., Vellasco, P.C.G da, de Andrade, S.L. and Vellasco M.M.B.R., Neural network evaluation of steel beam patch load capacity, Advanced in Engineering Software, 34, pp. 763-772, 2003. DOI: 10.1016/S0965-9978(03)00104-2

[22] Maity, D. and Saha, A., Damage assessment in structure from changes in static parameter using neural networks, Sadhana, 29, Part 3, pp. 315-327, 2004. DOI: 10.1007/BF02703781

[23] Zhou, G., Deng, P., Xun, X. and Yaqub, R., Innovative ANN technique for predicting failure / cracking load of masonry wall panel under lateral load, Journal of Computing in Civil Engineering, 24(4), pp. 377-387, 2010. DOI: 10.1061/(ASCE)CP.1943-5487.0000040)

[24] Al-Assaf, A. and Saffarini, H.F., Optimization of slabs using object oriented programming, Computers and Structures, 82(9-10), pp. 741-752, 2004. DOI: 10.1016/j.compstruc.2004.02.009

[25] The MathWorks, Maple User Manual, The MathWorks, Inc. United States, 2010.

[26] Kalashnikov, V.V., Some problems of lexicographic minimization, Optimizatsia, 21(38), pp. 109-120, 1978.

[27] Kalashnikov, V.V., Separate step method for minimization of Ill-conditioned functions, Optimizatsia, 25(42), pp. 70-85, 1980.

[28] Kalashnikov, V.V., Method for minimization of Ill-conditioned functions by selecting singular directions, Optimizatsia, 30(47), pp. 35-49, 1982.

[29] ACI 318S-13 (American Concrete Institute), Building code requirements for structural concrete, including the comments on the standards, Committee 318, 2013.

[30] González-Cuevas, O.M. y Robles-Fernández-Villegas, F., Aspectos fundamentales del concreto reforzado, Limusa, México, 2005.

[31] McCormac, J.C. and Brown, R.H., Design of reinforced concrete, John Wiley & Sons, New York, 2013.

A. Luévanos-Rojas, received a BSc. Eng. in Civil Engineering in 1981, an MSc. in Planning and Construction in 1996, and a PhD. Eng. in Planning and Construction in 2009, all from the Faculty of Engineering, Science and Architecture at the Juarez University of the State of Durango, Mexico. He was awarded an MSc. in Structures by the Higher School of Engineering and Architecture at the National Polytechnic Institute, Mexico City, in 1983 and an MSc. in Administration by the Faculty of Accounting and Administration at the Autonomous University of Coahuila, Mexico in 2004. From 1983 to 2009, he was a full time professor and -from 2009 to 2014- professor and researcher at the Faculty of Engineering, Science and Architecture at the Juarez University. His research interests include: mathematical models applied to structures, methods of structural analysis, design of concrete and steel members, and analysis of non-prismatic members. In addition, he is an Advisor and Collaborator of the "Revista de Arquitectura e Ingeniería" and Associate Editor of the journal "ICIC Express Letters Part B: Applications". He is a member of the National System of Researchers of Mexico.
ORCID: 0000-0002-0198-3614.

UNIVERSIDAD NACIONAL DE COLOMBIA
SEDE MEDELLÍN
FACULTAD DE MINAS

DYNA
http://dyna.medellin.unal.edu.co/

A study of co-movements between U.S. and Latin American stock markets: A cross-bicorrelations perspective

Semei Coronado [a], Omar Rojas [b], Rafael Romero-Meza [c] & Francisco Venegas-Martínez [d]

[a] *Department of Quantitative Methods, Universidad de Guadalajara, Zapopan, México, semeic@cucea.udg.mx*
[b] *School of Business and Economics, Universidad Panamericana, Guadalajara, México. orojas@up.edu.mx*
[c] *Facultad de Administración y Negocios, Universidad Autónoma de Chile, Región Metropolitana, Chile, rafael.romero@uautonoma.cl*
[d] *Superior School of Economics, Instituto Politécnico Nacional, Ciudad de México, México. fvenegas1111@yahoo.com.mx*

Received: March 20th, 2015. Received in revised form: November 24th, 2015. Accepted: December 10th, 2015

Abstract
This work applies a test that detects dependence between pairs of variables. The kind of dependence is a non-linear one, and the test is known as cross-bicorrelation, which is associated with Brooks and Hinich [1]. We study dependence periods between U.S. Standard and Poor's 500 (SP500), used as a benchmark, and six Latin American stock market indexes: Mexico (BMV), Brazil (BOVESPA), Chile (IPSA), Colombia (COLCAP), Peru (IGBVL) and Argentina (MERVAL). We have found windows of nonlinear dependence and co-movement between the SP500 and the Latin American stock markets, some of which coincide with periods of crisis, leading to an interpretation of a possible contagion or interdependence.

Keywords: Financial crisis; cross-bicorrelations; nonlinear dependence; co-movement; financial markets.

Un estudio de comovimientos entre las bolsas de valores de Estados Unidos de Norteamérica y América Latina: Una perspectiva de la bicorrelación cruzada

Resumen
Este trabajo aplica una prueba para detectar dependencia entre pares de variables. Este tipo de dependencia es no linear, y la prueba es conocida como bicorrelación cruzada, la cual es asociada a Brooks y Hinich [1]. Estudiamos periodos de dependencia no-lineal entre el índice Standard and Poor's 500 (SP500) de EUA y seis índices de mercados accionarios latinoamericanos: México (BMV), Brasil (BOVESPA), Chile (IPSA), Colombia (COLCAP), Perú (IGBVL) and Argentina (MERVAL). Hemos encontrado ventanas de dependencia no-lineal y de co-movimiento entre el SP500 y los mercados accionarios latinoamericanos, algunas de las cuales coinciden con períodos de crisis, lo cual da paso a posibles interpretaciones de contagio o interdependencia.

Palabras clave: Crisis financiera; bicorrelaciones cruzadas; dependencia no lineal; co-movimiento; mercados financieros.

1. Introduction

The study of the transmission of shocks from one country to another and the correlations between several countries and co-movements that cannot be explained by strong economic arguments has attracted the attention of researchers in economics and finance, as well as of practitioners. Research on this topic has significant effects, on both asset pricing, allocation and forecasting, as well as on other elements cf. [2-4].

Recently, co-movements between financial markets have been studied, with emphasis on the return on stock market indexes, through econometric or time series models that allow for a better understanding of the behavior of markets, especially through periods of crisis. A lot of this research has studied interdependencies and co-movements from the point of view of contagion, cf. [5-10]. Several approaches are adopted to analyze the co-movements between financial markets, some of which use quantitative tools borrowed

© The author; licensee Universidad Nacional de Colombia.

mostly from physics and computational sciences, cf. [11-13].

According to [6], if two markets are highly correlated, and the correlation does not increase in one of the markets after a financial crisis, but on the contrary, there is a continuous variation in its co-movement, then both markets are highly interdependent and contagion cannot be considered as the cause of the relationship between the two markets. Thus, for these authors the privileged dimension is a linear dependency. However, there is an important line of research that emphasizes the need for an empirical verification of nonlinear univariate and multivariate dependencies. Several arguments have been put forward in favor of this route of investigation, according to [14]. On the one hand, if after running a regression there is an indication of nonlinear dependence in the error terms of a standard model, the most common being the linear one, it can be argued that the standard model does not represent the data sufficiently well. On the other hand, if the evidence of nonlinear behavior is found in the first moment, the conditional mean, the formulation of a trading scheme built on this finding would be conceivable. This would ensure that benefits greater than a passive trading plan are obtained.

In order to explore these –less known and less obvious– nonlinear relationships between financial markets and how they co-move, in this work we use the Brooks and Hinich [1] nonlinearity test, that uses a measure of the dependence between pairs of variables called the cross-bicorrelations between time series, using bivariate autoregressive vectors in high frequency data. According to [15] these tests can be viewed as natural multivariate extensions of Hinich's portmanteau bicorrelation and whiteness statistics, but in this case the test examines nonlinear characteristics for pairs of variables. The advantage in using the cross-bicorrelation test is that it addresses the specific window frames in which the nonlinear dependence is present and also signals the direction of the nonlinear dependence, which is not provided by the Granger causality test

Both univariate [16-24] and multivariate [25-27] tests have been successfully applied to analyze the nonlinear behavior of different financial and economic time series. However, to the best of our knowledge, this is the first time that such a multivariate nonlinear test is used to uncover how stock markets co-move.

Seminal works analyzing Latin American stock markets as [24] and [22] use the univariate test, as is the case of the bicorrelation. In our case, we implement a bivariate test, the cross-bicorrelation that allows us to study co-movement between pairs of variables. Thus, the cross-bicorrelation is a multivariate extension of the bicorrelation, and the cross-bicorrelation can capture most types of dependence between pairs of series of the third-order statistics.

In this paper, we use the non-linearity test proposed by [1] in order to uncover the cross-covariances and cross-correlations between U.S. Standard and Poor's 500 (SP500), used as a benchmark, and six Latin American stock market indexes: Mexico (BMV), Brazil (BOVESPA), Chile (IPSA), Colombia (COLCAP), Peru (IGBVL) and Argentina (MERVAL). We found windows of nonlinear dependence between the SP500 and the Latin American stock markets, some of which coincide with periods of crisis, leading to an interpretation of possible contagion or interdependence.

Table 1.
Summary statistics for the returns

	Mean	Min	Max	Std-Dev	Skew-ness	Kurtosis	JB
SP500	0.03	-9.47	10.96	1.23	-0.32	14.15	15727
BMV	0.06	-7.27	10.44	1.27	0.06	9.24	4905
BOVESPA	0.06	-12.10	13.68	1.79	-0.07	7.94	3073
IPSA	0.05	-7.17	11.80	1.03	-0.03	13.19	13100
COLCAP	0.08	-13.25	18.13	1.36	-0.12	23.85	54822
IGBVL	0.07	-13.29	12.82	1.54	-0.52	13.18	13191
MERVAL	0.10	-12.95	10.43	1.99	-0.57	7.03	2216

Source: The authors used data from *Bloomberg*.

The organization of the document is the following: Section 2 presents the information collected. Section 3 describes the methodology used. Section 4 reports the empirical results. Finally, the main conclusions are presented in Section 5.

2. The data

For this study we consider daily returns of seven stock market indexes, namely the U.S. Standard and Poor's 500 (SP500) is taken as a baseline market for comparison against six Latin American stock market indexes: Mexico (BMV), Brazil (BOVESPA), Chile (IPSA), Colombia (COLCAP), Peru (IGBVL) and Argentina (MERVAL). Daily closing prices from January 2nd, 2003 to January 8th, 2015, for a total of 3025 observations of each index were obtained from *Bloomberg*. The data was sampled for this period of time in order to capture the effects that the U.S. might have had on the Latin American equity markets during the sub-prime financial crunch and to have a broad view of other possible cross-bicorrelation phenomena. Prices were converted into a continuous rate of returns, taking natural log differences between consecutive daily closing prices of equity markets. Table 1 presents summary statistics for these returns. The statistics are consistent, as expected, with some of the characteristic particularities of financial variables [28,29]. In particular, the kurtosis indicates that return distributions are leptokurtic. Furthermore, the Jarque-Bera statistic (JB) confirms returns not normally distributed. Although the results of the KPSS test for seasonality are not listed, it does not reject the null hypothesis of seasonality or the results of the ADF and PP tests, under the null hypothesis of a unit root. Both tests with a 5% significance level are available upon request.

3. Methodology

Brooks and Hinich [1] claim that the cross-bicorrelation test would allow a researcher identify any existence of nonlinear dependence between two pairs of variables. The size of the sample series is N, with two stationary variables $x(t_k)$ and $y(t_k)$. As we are working with the first percentual logged differences and small sub-samples of the total series, to assume stationarity is more than reasonable. Each series is separated into equal length non-overlapping moving time windows or frames, where t is an integer and k represents the k-th window and, both series are jointly

covariance stationary, which have been standardized. The test's null hypotheses states that the two variables $x(t_k)$ and $y(t_k)$ have no dependence and in fact are pure white noise. The alternative hypothesis states that the series have cross-covariances, $C_{xy}(r)$ defined as $E[x(t_k)y(t_k+r)]$ or any of the cross-bicovariances, $C_{xxy}(r,s)$ defined as $E[x(t_k)x(t_k+r)y(t_k+s)]$, different from zero.

Under the null hypothesis, $C_{xy}(r)$ and $C_{xxy}(r,s)$ are zero for every r,s except when $r=s=0$. According to the test, there is dependence between a pair of variables if $C_{xy}(r) \neq 0$ or $C_{xxy}(r,s) \neq 0$ for at least one value of r or a pair of values of r and$s$, respectively. Next, we present the statistics that give the r sample xy cross-correlation and the r,s sample xxy cross-bicorrelation, respectively

$$C_{xy}(r) = (N-r)^{-1}\sum_{t=1}^{N-r} x(t_k)y(t_k+r), \quad (1)$$

for $r \neq 0$, and

$$C_{xxy}(r,s) = (N-m)^{-1}\sum_{t=1}^{N-m} x(t_k)x(t_k+r)y(t_k+s) \quad (2)$$

where $m = \max(r,s)$.

We can interpret the cross-bicorrelations as the degree of relation of the value of one variable with the value of the cross-correlation of the two variables. The second-order test does not include current elements, and is executed on the errors terms of an $AR(2)$ fit to clean out the univariate autocorrelation arrangement. Thus current correlations will not be reason for rejecting the null hypothesis. To perform the third-order test, we apply the test on the errors terms of a $VAR(2)$ model having a current term in one of the equations (the order p of the $AR(p)$ and $VAR(p)$ models is chosen to optimize the Schwartz (BIC) criterion). The pre-whitening step is grounded on the elimination of any presence of linear correlation or cross-correlation. Therefore any outstanding dependence between the variables should be classified as nonlinear. Let $L = N^c$ where $0 < c < 0.5$ (for our case of study we use $c = 0.4$, $N = 3025$, and thus we have 121 non-overlapped windows of length 25 days). The corresponding test statistics for non-zero cross-correlations and cross-bicorrelations are

$$H_{xy}(N) = \sum_{r=0}^{L}(N-r)C_{xy}^2(r) \quad (3)$$

And

$$H_{xxy}(N) = \sum_{s=-L}^{L}\sum_{r=1}^{L}(N-m)C_{xxy}^2(r,s), \quad (4)$$

Table 2.
Number and percentage of significant (at the 5% level) cross-bicorrelation windows and correlations between *xxy* and *yyx*, and values of most significant bicorrelations. All cross-correlations and correlations are against SP500.

Series	Significant cross-bicorrelation windows	Correlations (*xxy, yyx*) for all windows	Correlation (*xxy, xy*) for largest window
BMV	20 (16.5%)	0.79	0.19
BOVESPA	34 (28.1%)	0.70	0.12
IPSA	18 (14.9%)	0.75	0.08
COLCAP	17 (14.0%)	0.73	0.10
IGBVL	29 (24.0%)	0.74	-0.01
MERVAL	31 (25.6%)	0.55	0.50

Source: The authors.

for $-s \neq -1,1,0$, respectively. In these statistics L is the number of times that the correlations are verified and $L(2L-1)$ is the number times that the cross-bicorrelations are probed. Following [15], we state that H_{xy} and H_{xxy} are asymptotically χ^2 with L and $L(2L-1)$ degrees of freedom, respectively, as $N \to \infty$.

4. Empirical results

In Table 2, we report the results for the cross-bicorrelation test. All tests are run taking SP500 as the benchmark for comparison, since the effects of the U.S. on Latin America are the ones we wanted to test. We present the number and percentage of significant (at the 5% level) cross-bicorrelation windows, correlation for all windows and the correlation for the largest window. As can be seen, the countries with the most significant cross-bicorrelation windows are Brazil (BOVESPA), Argentina (MERVAL) and Peru (IGBVL), with 28.1%, 25.6% and 24.0% of significant windows, respectively. On the other hand, Colombia (COLCAP), Chile (IPSA) and Mexico (BMV) are the countries with less significant windows (14.0%, 14.9% and 16.5%, respectively). As for the correlations for all windows, most countries present a correlation between 0.70 and 0.79, with the exception of Argentina (0.55). Furthermore, the country with an episode of largest correlation (0.50) was Argentina, whereas the one with the lowest correlation for a single episode was Peru (-0.01). These results shed light on the degree of dependence and co-movement between economies.

In Table 3 we present the dates of significant cross-bicorrelation windows between the SP500 benchmark and the six Latin American stock market indexes, labeled in the following way: BMV (A), BOVESPA (B), IPSA (C), COLCAP (D), IGBVL (E) and MERVAL (F). All windows are of 25 labor days of length, for a total of 121 windows. During 2003, Brazil and Argentina showed significant cross-bicorrelation windows with the U.S. For the years of 2004 to April 2007, the markets do not co-move, with the exception of a significant window from 6/26 to 7/31 between SP500 and BMV. In the middle of 2007 the effects of the U.S. are visible on some Latin American countries: Mexico, Brazil and Peru are affected earlier than Chile, Colombia and Argentina. However, the effects of the sub-prime financial

Table 3.
Dates of significant cross-bicorrelation windows between SP500 and the corresponding Latin American stock market, labeled as follows: BMV (A), BOVESPA (B), IPSA (C), COLCAP (D), IGBVL (E) and MERVAL (F). All windows are of 25 labor days of length, for a total of 121 windows. The numbers in the A-F columns represent the corresponding window that is significant.

Year	Starting date	Finishing date	A	B	C	D	E	F
2003	1/3	2/7		1			1	1
2003	2/10	3/17		2				2
2003	3/18	4/22		3				3
2003	5/29	7/2						5
2003	7/3	8/7						6
2003	9/15	10/17						8
2006	6/26	7/31	36					
2007	1/31	3/7						
2007	3/8	4/12						
2007	5/18	6/22					45	
2007	7/31	9/4	47	47		47	47	
2007	10/10	11/13		49				49
2007	11/14	12/19	50	50	50		50	50
2008	12/20	1/28	51	51	51		51	
2008	1/29	3/4		52	52		52	
2008	3/5	4/9	53	53	53	53	53	53
2008	4/10	5/14		54		54		
2008	5/15	6/19		55				55
2008	6/20	7/25		56		56	56	56
2008	7/28	8/29		57			57	
2008	9/2	10/6	58	58	58	58	58	58
2008	10/7	11/10	59	59	59	59	59	59
2008	11/11	12/17	60	60	60	60	60	60
2009	12/17	1/23	61	61	61	61	61	61
2009	1/26	3/2	62	62	62	62	62	62
2009	3/3	4/6	63	63	63	63	63	63
2009	4/7	5/12	64	64	64	64	64	64
2009	5/13	6/17	65	65	65		65	65
2009	6/18	7/24	66		66	66	66	66
2009	7/24	8/27		67				67
2009	10/5	11/6	69	69				
2010	1/22	2/26					72	
2010	4/6	5/10					74	
2010	5/11	6/15	75	75	75		75	75
2010	6/16	7/21		76				76
2010	8/26	9/30					78	
2011	2/24	3/30					83	
2011	5/6	6/10					85	
2011	7/19	8/22	87	87	87	87	87	87
2011	8/23	9/27	88	88	88	88	88	88
2011	9/28	11/1	89	89	89	89	89	89
2011	11/2	12/7	90	90	90	90	90	90
2012	12/8	1/13		91				91
2012	1/17	2/21		96				
2013	3/28	5/2					104	
2013	6/10	7/15		106				
2014	1/13	2/18		112				112
2014	9/23	10/27		119				119
2015	12/3	1/8				121		121

Source: The authors.

crisis were felt on all countries from September 2008 lasting till July 2009 (Table 3 (cont.)). From August 2009 to June 2011, there was not much co-movement, Peru being the exception with significant cross-bicorrelation windows during these years. Another block of co-movement was visible from July to December 2011, which might have happened due to the European sovereign debt crisis and some of the concerns over the U.S.'s slow economic growth and its credit rating being downgraded. From 2012 to January 2015, the countries that continued to show significant cross-bicorrelations with the U.S. were Brazil and Argentina.

In Fig. 1 and Fig. 2, we plot the $(1-p)$-values of the significant cross-bicorrelation windows between SP500 and Mexico, Brazil and Colombia (Fig. 1), and Chile, Peru and Argentina (Fig. 2). These windows correspond to the ones reported in Table 2 and 3. It is clear how there are two main periods of nonlinear dependence between U.S. and Latin American stock markets: 2008-2009 and 2011. Brazil and Argentina showed cross-bicorrelations with the U.S. in 2003.

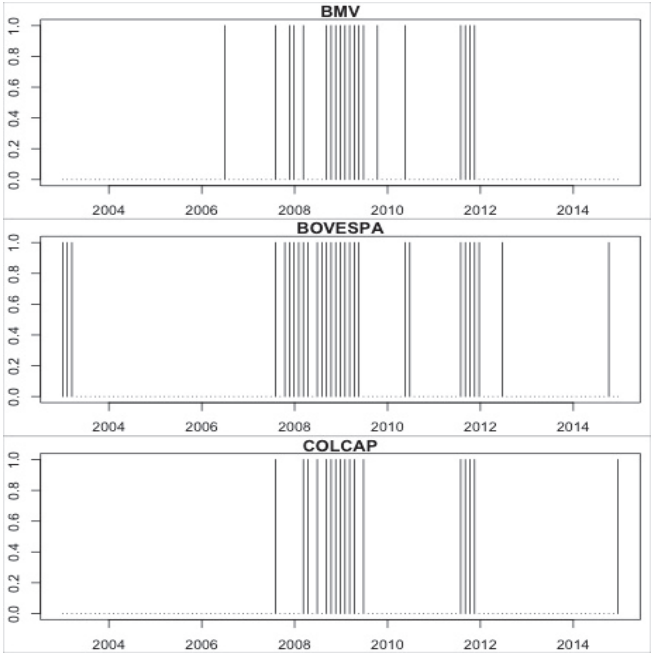

Figure 1. $(1-p)$-values of the significant cross-bicorrelation windows between SP500 and Mexico, Brazil and Colombia, respectively.
Source: The authors.

In Fig. 3 we plot the normalized prices for the SP500, BOVESPA and COLCAP indexes. The SP500 is the benchmark and it is compared with BOVESPA that presents the most significant cross-bicorrelation windows (28.1%) and COLCAP that presents the least significant percentage of windows (14.0%). We also plot the returns and the $(1-p)$-values of the significant cross-bicorrelation windows. As can be seen in the prices and returns plots, it is clear how for the year 2008 and the year 2011, the SP500 falls in prices and has a higher volatility before the other indexes.

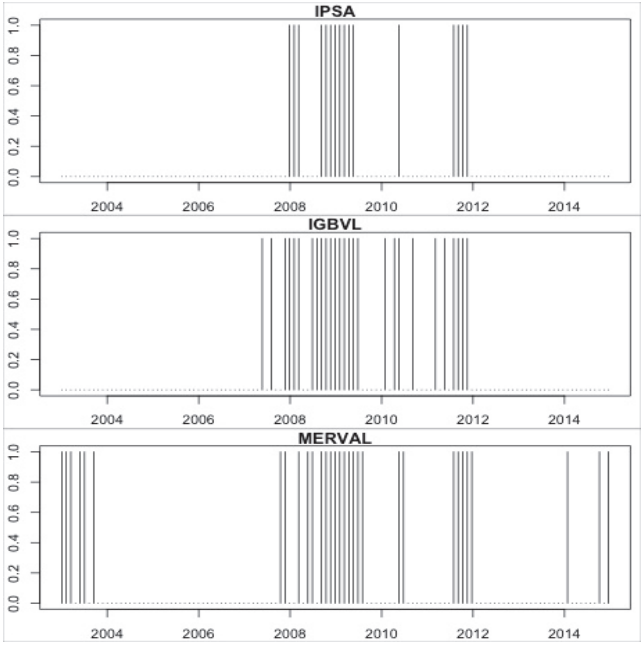

Figure 2. $(1-p)$-values of the significant cross-bicorrelation windows between SP500 and Chile, Peru and Argentina, respectively.
Source: The authors.

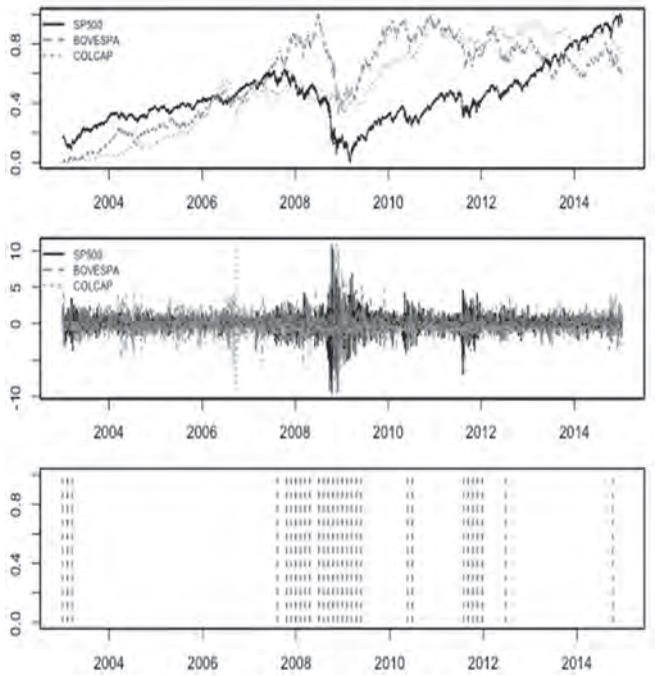

Figure 3. Plot of normalized prices, returns and $(1-p)$-values of the significant cross-bicorrelation windows (top, middle, bottom, respectively) for SP500, BOVESPA and COLCAP.
Source: The authors.

5. Conclusions

In this document we have successfully applied the Brooks and Hinich [1] cross-bicorrelation test to uncover the cross-covariances and cross-correlations between U.S. Standard and Poor's 500 (SP500), used as a benchmark, and six Latin American stock markets indexes: Mexico (BMV), Brazil (BOVESPA), Chile (IPSA), Colombia (COLCAP), Peru (IGBVL) and Argentina (MERVAL). We found windows of nonlinear dependence between SP500 and the Latin American stock markets, some of which coincide with periods of crisis, giving way to an interpretation of possible contagion or interdependence. Using a different but related methodology, [23] found that there are several periods where there were international financial crises that present strong univariate nonlinearity for several Latin American financial markets.

This nonlinearity test presents several advantages, since it would be capable of detecting any form of nonlinear dependence of the third-order statistics between two pairs of variables. Furthermore, it offers a helpful tool for academics to study the functional form of the nonlinear association between the pairs of variables by defining in which direction the cross-bicorrelations flow and which of the lags are important. Given that this test allows the researcher to determine the third-order nonlinear dependency forms between pairs of series, it can be used as a supplementary instrument to the Granger causality test.

We have identified some moments of cross-bicorrelations that might be interesting to explore from a deeper economic point of view and it is left as a work in progress. Furthermore, following [23], it would be interesting to run a test including overlapped windows in a rolling scheme. Thus, like [23] it would be possible to identify the start, the end, the intensity and persistence of the cross-bicorrelation instead of just the bicorrelation.

Acknowledgements

The authors would like to acknowledge Jorge Ahumada García (MSc in Economics student, ITAM) for his help providing some of the data used in this paper and Itzel Cano (Universidad Panamericana) for her help formatting some of the tables. All errors remain the sole responsibility of the authors.

The authors are grateful for the support of FONDECYT (Project 1111034).

References

[1] Brooks, C., and Hinich, M.J., Cross-correlations and cross-bicorrelations in sterling exchange rates, Journal of Empirical Finance. 6(4), pp. 385-404, 1999. DOI: 10.1016/S0927-5398(99)00007-9

[2] Velásquez, J.D., Franco, C.J. and Camacho, P., Nonlinear time series forecasting using MARS, DYNA. 81(184), pp. 11-19, 2014. DOI; 10.15446/dyna.v81n184.39699

[3] Velásquez, J.D., Zambrano, C. and Franco, C.J., A comparison of exponential smoothing and neural networks in time series prediction, DYNA. [Online]. 80(182), pp. 66-73, 2013. [date of reference December 1rd of 2015]. Available at: http://revistas.unal.edu.co/index.php/dyna/article/view/41564/43245

[4] Velásquez, J.D., Morales, Y.O. and Franco, C.J., Time series analysis and forecasting in energy markets using the R language, DYNA. [Online]. 78(165), pp. 287-296, 2011. [date of reference December 1rd of 2015]. Available at: http://revistas.unal.edu.co/index.php/dyna/article/view/25670

[5] Aloui, R., Ben Aïssa, M.S. and Nguyen,D.K., Global financial crisis, extreme interdependences, and contagion effects: The role of economic structure?, Journal of Banking & Finance. 35(1), pp. 130-141, 2011. DOI: 10.1016/j.jbankfin.2010.07.021.

[6] Forbes, K.J. and Rigobon, R., No contagion, only interdependence: measuring stock market comovements, The Journal of Finance. 57(5), pp. 2223-2261, 2002. DOI: 10.1111/0022-1082.00494.
[7] Kenourgios, D., Samitas, A. and Paltalidis, N., Financial crises and stock market contagion in a multivariate time-varying asymmetric framework, Journal of International Financial Markets, Institutions and Money 21(1), pp. 92-106, 2011. DOI: 10.1016/j.intfin.2010.08.005.
[8] Caramazza, F., Ricci, L. and Salgado, R., International financial contagion in currency crises, Journal of International Money and Finance. 23(1), pp. 51-70, 2004. DOI: 10.1016/j.jimonfin.2003.10.001
[9] Corsetti, G., Pericoli, M. and Sbracia, M., Some contagion, some interdependence: More pitfalls in tests of financial contagion, Journal of International Money and Finance. 24(8), pp. 1177-1199, 2005. DOI: 10.1016/j.jimonfin.2005.08.012
[10] Chiang, T.C., Jeon, B.N. and Li, H., Dynamic correlation analysis of financial contagion: Evidence from Asian markets, Journal of International Money and Finance. 26(7), pp. 1206-1228, 2007. DOI: 10.1016/j.jimonfin.2007.06.005
[11] Laloux, L., Cizeau, P., Bouchaud, J.P. and Potters, M., Noise dressing of financial correlation matrices, Physical Review Letters. 83(7) pp. 1467-1470, 1999. DOI: 10.1103/PhysRevLett.83.1467.
[12] Plerou, V., Gopikrishnan, P., Rosenow, B., Amaral, L.A.N., Guhr, T. and Stanley, H.E., Random matrix approach to cross correlations in financial data, Phys. Rev. E. 65(6), pp. 66126-66144, 2002. DOI: 10.1103/PhysRevE.65.066126
[13] Evans, T. and McMillan, D.G., Financial co-movement and correlation: evidence from 33 international stock market indices, International Journal of Banking, Accounting and Finance. 1(3), pp. 215-241, 2009. DOI: 10.1504/IJBAAF.2009.022711
[14] Czamanski, D., Dormaar, P., Hinich, M.J. and Serletis, A., Episodic nonlinearity and nonstationarity in Alberta's power and natural gas markets, Energy Economics. 29(1), pp. 94-104, 2007. DOI: 10.1016/j.eneco.2006.08.002
[15] Hinich, M.J., Testing for dependence in the input to a linear time series model, Journal of Nonparametric. Statistics. 6(2-3), pp. 205-221, 1996. DOI: 10.1080/10485259608832672
[16] Coronado-Ramírez, S., Celso-Arellano, P.L.,and Rojas,O., Adaptive market efficiency of agricultural commodity futures contracts, Contaduria y Administración. 60(2), pp. 389-401, 2015. DOI: 10.1016/S0186-1042(15)30006-1
[17] Romero-Meza, R., Bonilla, C.A. and Hinich, M.J., Nonlinear event detection in the Chilean stock market, Applied Economics Letters. 14(13), pp. 987-991, 2007. DOI:10.1080/13504850600706024
[18] Hinich, M.J. and Serletis, A., Episodic nonlinear event detection in the Canadian exchange rate, Journal of the American Statistical Association. 102(477), pp. 68-74, 2007. DOI: 10.1198/016214506000001004
[19] Bonilla, C.A., Maquieira, C.P. and Romero-Meza, R., Nonlinear behaviour of emerging market bonds spreads: The Latin American case, Applied Economics. 40(2), pp. 2697-2702, 2008. DOI: 10.1080/00036840600970245
[20] Lim, K.P.R., Brooks, D. and Hinich, M.J., Nonlinear serial dependence and the weak-form efficiency of Asian emerging stock markets, Journal of International Financial Markets, Institutions and Money. 8(5), pp. 527-544, 2008. DOI: 10.1016/j.intfin.2007.08.001
[21] Coronado-Ramírez, S., Ramírez-Grajeda, M. and Celso-Arellano, P.L. Inefficiency in the international coffee market: The case of Colombian arabica, African J. Agric. Res. 9(5), pp. 556-561, 2014. DOI: 10.5897/AJAR11.2228
[22] Bonilla, C.A., Romero-Meza, R. and Maquieira, C., Nonlinearities and garch inadequacy for modeling stock market returns: Empirical evidence from Latin America, Macroeconomics Dynamics. 15(5), pp. 713-724, 2011. DOI: 10.1017/S1365100510000295
[23] Romero-Meza, R., Bonilla, C., Benedetti, H. and Serletis, A., Nonlinearities and financial contagion in Latin American stock markets. Economic Modelling, 51, pp. 653-656, 2015. DOI: 10.1016/j.econmod.2015.09.012
[24] Bonilla, C.A., Romero-Meza, R. and Hinich, M.J., Episodic nonlinearity in Latin American stock market indices. Applied Economics Letters, 13(3), 195-199, 2006. DOI: 10.1080/13504850500392750
[25] Brooks, C. and Hinich, M.J., Bicorrelations and cross-bicorrelations as non-linearity tests and tools for exchange rate forecasting, Journal of Forecasting. 20(3), pp. 181-196, 2001. DOI: 10.1002/1099131X(200104)20:3<181::AIDFOR781>3.0.CO;2-R
[26] Serletis, A., Malliaris, A.G., Hinich, M.J. and Gogas, P., Episodic nonlinearity in leading global currencies, Open Economics. Review. 23(2), pp. 337-357, 2012. DOI: 10.1007/s11079-010-9194-9
[27] Romero-Meza, R., Coronado, S. and Serletis, A., Oil and the economy: A cross bicorrelation perspective, The Journal of Economics Asymmetrics. 11, pp. 91-95, 2014. DOI: 10.1016/j.jeca.2014.08.003
[28] Cont, R., Empirical properties of asset returns: Stylized facts and statistical issues, Quantitative. Finance. 1, pp. 223-236, 2001. DOI: 10.1080/713665670
[29] Rojas, O. and Trejo-Pech, C., Financial time series: Stylized facts for the Mexican stock exchange index compared to developed markets, in Nonlinear Time Series and Finance, Coronado-Ramírez, S., Celso-Arellano, P.L. and Trejo-Pech, C., Eds. Universidad de Guadalajara, Mexico, 2014, pp. 228-245.

S. Coronado, obtained a PhD. degree in Business and Economics from the University of Guadalajara, in Guadalajara, Mexico. He is a research professor in the Department of Quantitative Methods at the University of Guadalajara. He is currently a member of the Mexican National System of Researchers (Level I, CONACYT) where his research areas of interest are time series, emerging market finance and applied statistics.
ORCID: 0000-0002-7945-7155

O. Rojas, received his PhD in Mathematics from La Trobe University, Melbourne, Australia. He is associate professor and research Director at the School of Business and Economics at Universidad Panamericana, Guadalajara, Mexico. His research areas of interest are: nonlinear time series and multivariate statistical methods applied to business. He is a member of Mexican National System of Researchers (Level C, CONACYT).
ORCID: 0000-0002-0681-3833

R. Romero-Meza, received a Dr. of Business Administration (DBA) from Boston University. He is research professor at Facultad de Administración y Negocios at Universidad Autónoma de Chile, and he is also Director of Global Council of PKF International Finance. Dr. Romero-Meza has over twenty academic articles in applied economics, applied economics letters, macroeconomic dynamics, economic modelling, the Journal of Economic Asymmetries among others. He participates as referee in several journals: Energy Economics, Economics Letters, INNOVAR, Emerging Markets. His research and teaching interests are in emerging markets, efficient markets, nonlinear time series, and corporative finance.
ORCID: 0000-0001-5108-2681

F. Venegas-Martinez, was a PhD. researcher in Finance at Oxford University. He received his PhD in Mathematics and a second PhD in economics from Washington State University. He is a professor in Instituto Politécnico Nacional, Mexico. Dr. Vengas-Martínez is a member of the Mexican National System of Researchers (Level III, CONACYT). He participates in more than 20 editorial boards and scientific research journals, in Mexico and internationally. Dr Venegas-Martínez has over a hundred academic articles in The Brazilian Journal of Probability, Journal of the Inter-American Statistics and Econometrics, Journal of Economic Dynamics and Control, International Journal of Theoretical and Applied Finance, Journal of Economic Modeling, Journal of Development Economics, among others. His research areas of interest are stochastic process, econometrics, time series, and economic development.
ORCID: 0000-0002-1528-5593

UNIVERSIDAD NACIONAL DE COLOMBIA
SEDE MEDELLÍN
FACULTAD DE MINAS

DYNA

DYNA
http://dyna.medellin.unal.edu.co/

A comparative study for the design of rectangular and circular isolated footings using new models

Arnulfo Luévanos-Rojas

Juarez University of Durango State, Gómez Palacio, Durango, México. arnulfol_2007@hotmail.com

Received: June 4th, 2015. Received in revised form: January 18th, 2016. Accepted: January 22th, 2016.

Abstract
This paper presents a comparative study for the design of reinforced concrete isolated footings that are rectangular or circular in shape and subjected to axial load and moments in two directions using new models to obtain the most economical footing. The new models take into account the real soil pressure acting on contact surface of the footing and this pressure is different in all the contact area, with a linear variation, this pressure is presented in terms of the axial load, the larger moment around the "X" axis and the smaller moment around the "Y" axis, where the centroidal axes are "X" and "Y" of the footing. The main part of this research is to show the differences between the two models. Results show that the circular footings are more economical compared to the rectangular footings. Therefore, the new model for the design of circular isolated footings should be used, and complies with real conditions.

Keywords: rectangular footings design; circular footings design; bending moments; bending shear; punching shear.

Un estudio comparativo para diseño de zapatas aisladas de forma rectangular y circular usando nuevos modelos

Resumen
Este trabajo presenta un estudio comparativo para diseño de zapatas aisladas de concreto reforzado de forma rectangular y circular sometidas a carga axial y momentos en dos direcciones usando nuevos modelos para obtener la zapata más económica. Los nuevos modelos consideran la presión real del suelo actuando sobre la superficie de contacto de la zapata y esta presión es diferente en toda el área de contacto, con una variación lineal, esta presión se presenta en términos de la carga axial, el momento mayor alrededor del eje "X" y el momento menor alrededor del eje "Y", donde los ejes centroidales son "X" e "Y" de la zapata. La parte principal de esta investigación es mostrar las diferencias de los dos modelos. Los resultados muestran que las zapatas circulares son más económicas con respecto a las zapatas rectangulares. Por lo tanto, el nuevo modelo para diseño de zapatas aisladas circulares se debe utilizar, y cumple con las condiciones reales.

Palabras clave: diseño de zapatas rectangulares; diseño de zapatas circulares; momentos flexionantes; cortante por flexión; cortante por penetración.

1. Introduction

A foundation is a part of the structure which transfers the loads to the soil. Foundations are classified into superficial and deep foundations. There are important differences between the two: depending on geometry, type of soil, and structural functionality, and its constructive systems [1-11].

A superficial foundation is a structural member where the dimensions of the cross section are large in comparison to the height. The function of this type of foundation is to transfer the loads of a building to the soil at relatively shallow depths, less than 4 m approximately in relation to the level of the natural ground surface [1-12].

The distribution of soil pressure under a footing is a function of the type of soil, the relative rigidity of the soil and the footing, and the depth of foundation at the level of contact between the footing and the soil. A concrete footing on sand under concentric loading will have a pressure distribution similar to Fig. 1a. When a rigid footing is resting on sandy soil, the sand near the edges of the footing tends to displace laterally when the footing is loaded. This tends to decrease in soil pressure near the edges, whereas soil at a distance from

© The author; licensee Universidad Nacional de Colombia.

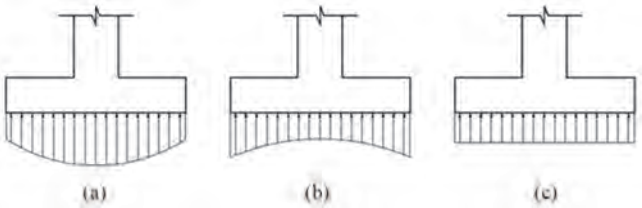

Figure 1. Pressure distribution under footing: (a) footing on sand; (b) footing on clay; (c) equivalent uniform distribution.
Source: [9-12].

the edges of a footing is relatively confined. On the other hand, the pressure distribution under a footing on clay is similar to Fig. 1b. As the footing is loaded, the soil under the footing deflects in a bowl-shaped depression, relieving the pressure under the middle of the footing. For design purposes, it is common to assume the soil pressures are linearly distributed. The pressure distribution will be uniform if the line of action of the resultant force passes though the centroid of the footing (see Fig. 1c) [9-12].

In the design of superficial foundations, specifically in the case of isolated footings there are three types of the application of loads: 1) Concentric axial load, 2) Axial load and moment in one direction (uniaxial bending), 3) Axial load and moment in two directions (biaxial bending) [1-14].

The hypothesis used in the classical model is to take into account the uniform pressure for the design, i.e., the same pressure at all points of contact of the foundation with the soil; this design pressure is the maximum value that occurs in an isolated footing [1-14].

The classical model for the dimensioning of footings is developed by trial and error, i.e., a dimension is proposed and using the expression of the bidirectional bending one obtains the stresses acting on the contact surface, which must meet the following conditions: 1) The minimum stress should be equal to or greater than zero, because the soil is not capable of withstanding tensile stresses, 2) The maximum stress must be equal to or less than the allowable capacity that the soil can withstand [1-14].

Some papers present the use of load testing on foundations: Non-destructive load test in pilots [15]; Evaluation of the integrity of deep foundations: analysis and in situ verification [16]; Others, show the use of static load tests in the geotechnical design of foundations [17]; Stability of slender columns on an elastic foundation with generalised end conditions [18]; A novel finite element method for designing floor slabs on grade and pavements with loads at edges.

Mathematical models that calculate the dimensions of rectangular, square and circular isolated footings subjected to axial load and moments in two directions (biaxial bending) were developed [1,3,6], and also a comparative study between the rectangular, square and circular footings with respect to the contact surface on soil was presented [8].

Mathematical models for the design of isolated footings of rectangular and circular shape using a new model were presented [7,9].

This paper presents a comparative study for the design of reinforced concrete isolated footings that are rectangular or circular in shape and that support a rectangular column subjected to axial load and moments in two directions to obtain the most economical footing. The new models take into account the real soil pressure acting on contact surface of the footing and this pressure is different in all of the contact area, with a linear variation, this pressure is presented in terms of the axial load, the larger moment around the "X" axis and the smaller moment around the "Y" axis, where the centroidal axes are "X" and "Y" of the footing. The comparison is presented between the two new models in terms of: 1) Moment around a *a'-a'* axis that is parallel to the "*X-X*" axis and moment around a *b'-b'* axis that is parallel to the "*Y-Y*" axis; 2) Bending shear (unidirectional shear force) is localized on a *c'-c'* axis that is parallel to the "*X-X*"; 3) Punching shear (bidirectional shear force); 4) Materials used (reinforcement steel and concrete). This study shows the differences between the two models to propose the most economical footing.

2. Methodology

2.1. General conditions

According to Building Code Requirements for Structural Concrete (ACI 318-13) and Commentary the critical sections are: 1) The maximum moment is located on the face of the column, pedestal, or wall, for footings supporting a concrete column, pedestal, or wall; 2) Bending shear is presented at a distance "*d*" (distance from extreme compression fiber to centroid of longitudinal tension reinforcement) shall be measured from face of column, pedestal, or wall for footings supporting a column, pedestal, or wall; 3) Punching shear is localized so that its perimeter "b_o" is a minimum but need not approach closer than "*d/2*" to: (a) Edges or corners of columns, concentrated loads, or reaction areas; and (b) Changes in slab thickness such as edges of capitals, drop panels, or shear caps [7,9,10,20].

The general equation for any type of footings subjected to bidirectional bending is [1-14, 21]:

$$\sigma = \frac{P}{A} \pm \frac{M_x C_y}{I_x} \pm \frac{M_y C_x}{I_y} \quad (1)$$

where: σ is the stress exerted by the soil on the footing (soil pressure), A is the contact area of the footing, P is the axial load applied at the center of gravity of the footing, M_x is the moment around the axis "X", M_y is the moment around the axis "Y", C_x is the distance in the direction "X" measured from the axis "Y" up the farthest end, C_y is the distance in direction "*Y*" measured from the axis "X" up the farthest end, I_y is the moment of inertia around the axis "Y" and I_x is the moment of inertia around the axis "X" [1-14, 21].

2.2. A new model for rectangular footings

Fig. 2 shows the pressures diagram for a rectangular footing subjected to axial load and moment in two directions (biaxial bending), where there are different pressures in the four corners and these vary linearly along the contact surface [7].

The stresses anywhere on a rectangular footing subjected to biaxial bending by equation (1) are found [7]:

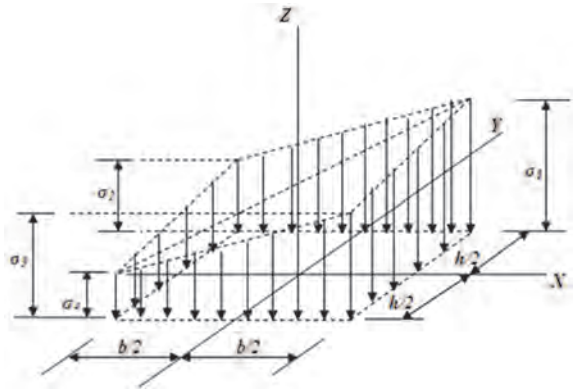

Figure 2. Soil pressures on the rectangular footings.
Source: [7].

$$\sigma(x,y)=\frac{P}{bh}+\frac{12M_x y}{bh^3}+\frac{12M_y x}{hb^3} \tag{2}$$

where: h is the side of the parallel footing the axis "Y", b is the side of the parallel footing the axis "X", $A = bh$, $I_x = bh^3/12$, $I_y = hb^3/12$, $C_x = x$, $C_y = y$ [7].

2.2.1. Moments

Critical sections for moments are presented in section *a'-a'* and *b'-b'*, as shown in Fig. 3 [7].

2.2.1.1. Moment around the a'-a' axis

The resultant force "F_{R1}" is obtained through the volume of pressure on the area formed by the axis a'-a' and the corners 1 and 2 of the footing, this is as follows [7]:

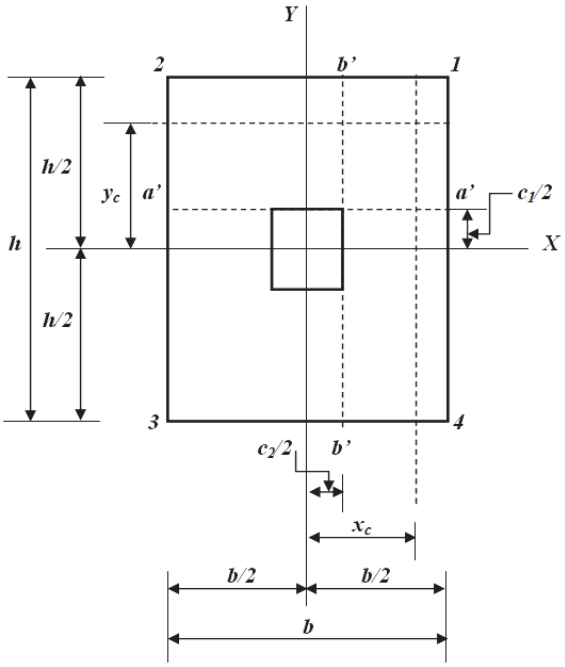

Figure 3. Critical sections for moments.
Source: [7].

$$F_{R1}=\frac{P(h-c_1)}{2h}+\frac{3M_x(h^2-{c_1}^2)}{2h^3} \tag{3}$$

where: c_1 is the dimension of the parallel column to the axis "Y", c_2 is the dimension of the parallel column to the axis "X" [7].

Now, the gravity center "y_c" of the soil pressure is [7]:

$$y_c=\frac{Ph^2(h^2-{c_1}^2)+4M_x(h^3-{c_1}^3)}{4Ph^2(h-c_1)+12M_x(h^2-{c_1}^2)} \tag{4}$$

Moment around the axis *a'-a'* is [7]:

$$M_{a'-a'}=\frac{[Ph^2+2M_x(2h+c_1)](h-c_1)^2}{8h^3} \tag{5}$$

2.2.1.2. Moment around the b'-b' axis

The resultant force "F_{R2}" is obtained through the volume of pressure on the area formed by the axis *b'-b'* and corners 1 and 4 of the footing, this is [7]:

$$F_{R2}=\frac{P(b-c_2)}{2b}+\frac{3M_y(b^2-{c_2}^2)}{2b^3} \tag{6}$$

Now, the gravity center "xc" of the soil pressure is [7]:

$$x_c=\frac{Pb^2(b^2-{c_2}^2)+4M_y(b^3-{c_2}^3)}{4Pb^2(b-c_2)+12M_y(b^2-{c_2}^2)} \tag{7}$$

Moment around the axis *b'-b'* is [7]:

$$M_{b'-b'}=\frac{[Pb^2+2M_y(2b+c_2)](b-c_2)^2}{8b^3} \tag{8}$$

2.2.2. Bending shear (unidirectional shear force)

Critical section for the bending shear is obtained at a distance "d" to from the junction of the column with the footing is presented in section c'- c' as seen in Fig. 4 [7].

The bending shear "V_f" is obtained through the volume of pressure on the area formed by the axis c'-c' and corners 1 and 2 of the footing [7].

Now, the bending shear "V_f" is [7]:

$$V_f=\frac{[Ph^2+3M_x(h+c_1+2d)](h-c_1-2d)}{2h^3} \tag{9}$$

2.2.3. Punching shear (bidirectional shear force)

Critical section for punching shear appears at a distance "*d/2*" to from the junction of the column with the footing in the two directions occurs in the rectangular section formed by the points 5, 6, 7 and 8, as shown in Fig. 5 [7].

The punching shear acting on the footing "V_p" is obtained through the volume of pressure on the total area minus the rectangular area formed by points 5, 6, 7 and 8 [7].

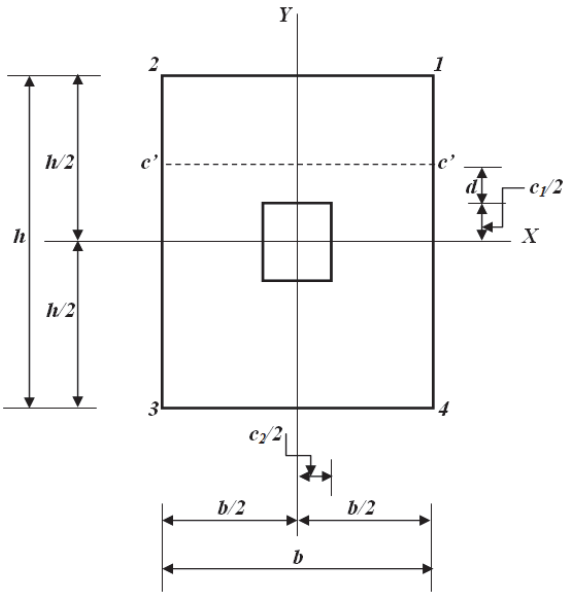

Figure 4. Critical sections for the bending shear.
Source: [7].

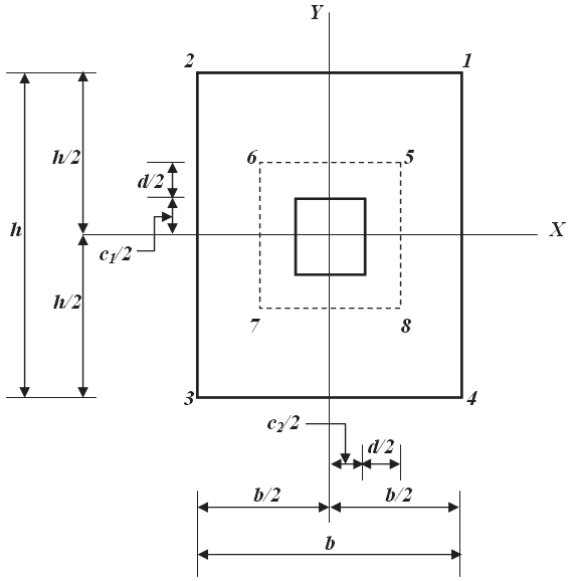

Figure 5. Critical sections for the punching shear supporting a rectangular column.
Source: [7].

Now, the punching shear "V_p" is as follows [7]:

$$V_P = \frac{P[bh - (c_1 + d)(c_2 + d)]}{bh} \tag{10}$$

2.3. A new model for circular footings

Fig. 6 shows the pressures diagram for a circular footing subjected to axial load and moment in two directions (biaxial bending), where pressures are presented differently and varying linearly along the contact surface [9].

The stresses anywhere on a circular footing subjected to bidirectional bending by the equation (1) are found [9]:

$$\sigma(x,y) = \frac{P}{\pi R^2} + \frac{4M_x y}{\pi R^4} + \frac{4M_y x}{\pi R^4} \tag{11}$$

where: R is the radius of the footing, $A = \pi R^2$, $I_x = \pi R^4/4$, $I_y = \pi R^4/4$, $C_x = x$, $C_y = y$ [9].

2.3.1. Moments

Critical sections for moments are presented in section *a'-a'* and *b'-b'*, as shown in Fig. 7 [9].

2.3.1.1. Moment around the axis a'-a'

The resultant force "F_{R1}" is obtained through the volume of pressure on the area formed by the semicircle that is above the axis *a'-a'* of the footing, this is presented as follows [9]:

$$F_{R1} = \frac{P\left[2\pi R^2 - c_1\sqrt{4R^2 - {c_1}^2} - 4R^2\, Asin\left(\frac{c_1}{2R}\right)\right]}{4\pi R^2} + \frac{M_x(4R^2 - {c_1}^2)^{3/2}}{3\pi R^4} \tag{12}$$

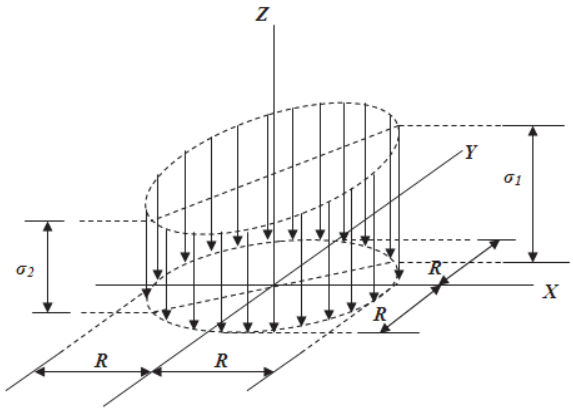

Figure 6. Soil pressures on the circular footings.
Source: [9].

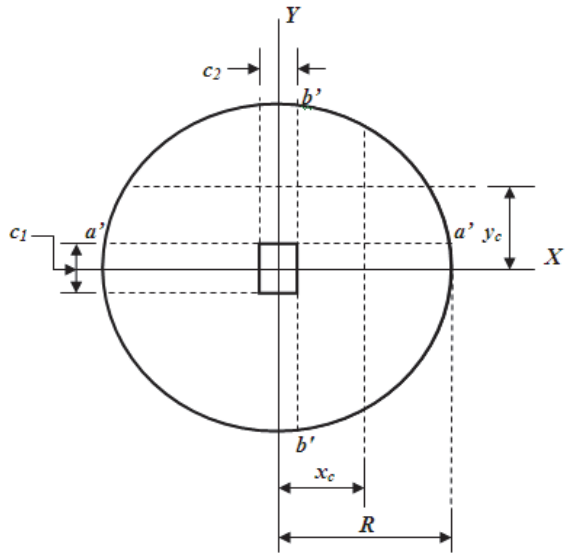

Figure 7. Critical sections for bending moments.
Source: [9].

Now, the gravity center "y_c" of the soil pressure is [9]:

$$y_c = \{2PR^2(4R^2 - {c_1}^2)^{3/2} + 3M_x[4\pi R^4 + c_1(2R^2 - {c_1}^2)\sqrt{4R^2 - {c_1}^2} - 8R^4\, Asin(c_1/2R)]\} / 2\{3PR^2[2\pi R^2 - c_1\sqrt{4R^2 - {c_1}^2} - 4R^2\, Asin(c_1/2R)] + 4M_x(4R^2 - {c_1}^2)^{3/2}\} \quad (13)$$

Moment around the axis *a'-a'* is [9]:

$$M_{a'-a'} = \{6\pi R^4(2M_x - Pc_1) + [PR^2({c_1}^2 + 8R^2) + M_x c_1({c_1}^2 - 10R^2)]\sqrt{4R^2 - {c_1}^2} + 12R^4(Pc_1 - 2M_x)\, Asin\left(\frac{c_1}{2R}\right)\} / 24\pi R^4 \quad (14)$$

2.3.1.2. Moment around the axis b'-b'

The resultant force "F_{R2}" is obtained through the volume of pressure on the area formed by the semicircle that is on the right side of the axis *b'-b'* of the footing, this is [9]:

$$F_{R2} = \frac{P\left[2\pi R^2 - c_2\sqrt{4R^2 - {c_2}^2} - 4R^2\, Asin\left(\frac{c_2}{2R}\right)\right]}{4\pi R^2} + \frac{M_y(4R^2 - {c_2}^2)^{3/2}}{3\pi R^4} \quad (15)$$

Now, the gravity center "x_c" of soil pressure is [9]:

$$x_c = \{2PR^2(4R^2 - {c_2}^2)^{3/2} + 3M_y[4\pi R^4 + c_2(2R^2 - {c_2}^2)\sqrt{4R^2 - {c_2}^2} - 8R^4\, Asin(c_2/2R)]\} / 2\{3PR^2[2\pi R^2 - c_2\sqrt{4R^2 - {c_2}^2} - 4R^2\, Asin(c_2/2R)] + 4M_y(4R^2 - {c_2}^2)^{3/2}\} \quad (16)$$

Moment around the axis *b'-b'* is [9]:

$$M_{b'-b'} = \{6\pi R^4(2M_y - Pc_2) + [PR^2({c_2}^2 + 8R^2) + M_y c_2({c_2}^2 - 10R^2)]\sqrt{4R^2 - {c_2}^2} + 12R^4(Pc_2 - 2M_y)\, Asin\left(\frac{c_2}{2R}\right)\} / 24\pi R^4 \quad (17)$$

2.3.2. Bending shear (unidirectional shear force)

Critical section for bending shear is obtained at a distance "*d*" to from the junction of the column with the footing, this is presented in section *c'- c'* (see Fig. 8) [9].

The bending shear "V_f" is obtained through the volume of pressure on the area formed by the circle that is above the axis *c'-c'* of the footing [9].

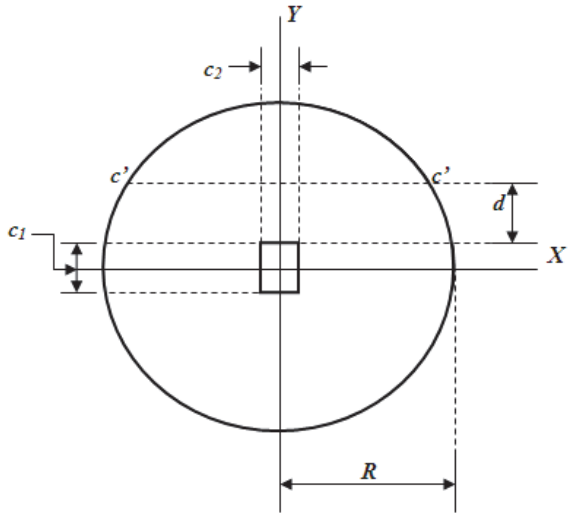

Figure 8. Critical sections for the bending shear.
Source: [9].

Now, the bending shear "V_f" is [9]:

$$V_f = \frac{P}{2\pi R^2}\left[\pi R^2 - \left(\frac{c_1 + 2d}{2}\right)\sqrt{4R^2 - (c_1 + 2d)^2} - 2R^2\, Asin\left(\frac{c_1 + 2d}{2R}\right)\right] + \frac{M_x[4R^2 - (c_1 + 2d)^2]^{3/2}}{3\pi R^4} \quad (18)$$

2.3.3. Punching shear (bidirectional shear force)

Critical section for punching shear appears at a distance "*d/2*" to from the junction of the column with the footing in the two directions occurs in the rectangular section formed by the points 5, 6, 7 and 8, as seen in Fig. 9 [9].

The punching shear acting on the footing "V_p" is obtained through the volume of pressure on the total area minus the rectangular area formed by points 5, 6, 7 and 8 [9].

Now, the punching shear "V_p" is as follows [9]:

$$V_P = P - \frac{P(c_1 + d)(c_2 + d)}{\pi R^2} \quad (19)$$

2.4. Procedure of design

Step 1: The mechanical elements (P, M_x, M_y) acting on the footing is obtained by the sum of: the dead loads, live loads and accidental loads (wind or earthquake) from each of these effects [7,9,10,22-27].

Step 2: The available load capacity of the soil "σ_{max}" is [7,9,10,22-27]:

$$\sigma_{max} = q_a - \gamma_{ppz} - \gamma_{pps} \quad (20)$$

where: q_a is the allowable load capacity of the soil, γ_{ppz} is the self-weight of the footing, γ_{pps} is the self-weight of the soil fill [7,9,10,22-27].

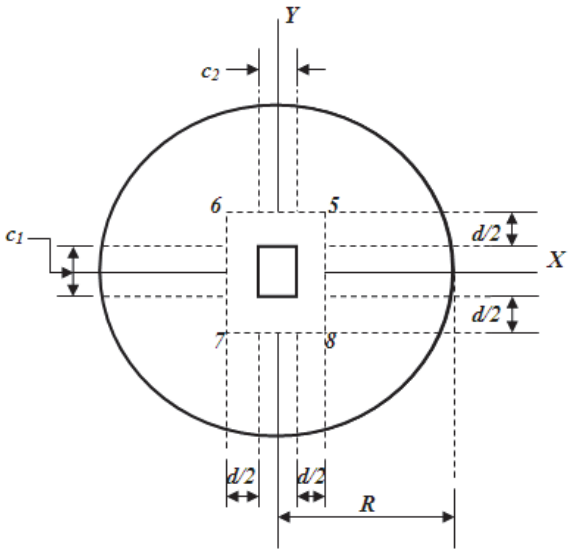

Figure 9. Critical sections for the bending shear.
Source: [9].

Step 3:

Rectangular footings

The value of "*h*" is selected according to the following equations [6,7]:

$$h = \frac{12M_x}{P} \tag{21}$$

$$\sigma_{max} M_y h^3 - P M_x h - 12 M_x^2 = 0 \tag{22}$$

where: the value of "*h*" obtained from the equation (21) is when the soil pressure is zero, and the value of "*h*" found in equation (22) is when the soil pressure is available load capacity "σ_{max}", the greater of these two values is taken to meet the two conditions, because the pressure generated by the footing must be greater than zero and less than the available load capacity of the soil [7].

The value of "*b*" is found by equation [6,7]:

$$b = \frac{M_y h}{M_x} \tag{23}$$

Circular footings

The value of "*R*" is selected according to the following equations [3,9]:

$$R = \frac{4\sqrt{{M_x}^2 + {M_y}^2}}{P} \tag{24}$$

$$\sigma_{max} \pi R^3 - PR - 4\sqrt{{M_x}^2 + {M_y}^2} = 0 \tag{25}$$

where: the value of "*R*" obtained from the equation (24) is when the soil pressure is zero and the value of "*R*" found in equation (25) is when the soil pressure is available load capacity "σ_{max}", the greater of these two values is taken to meet the two conditions, because the pressure generated by the footing must be greater than zero and less than the load capacity available the soil [9].

Note: if the wind and/or an earthquake are included in the combinations the load capacity of the soil can be increased by 33% [7,9,10,19].

Step 4: The mechanical elements (P, M_x, M_y) acting on the footing is factored [7,9,10,20].

Step 5: The maximum moment acting on the rectangular footings are obtained by equations (5) and (8) [7], and for circular footings are found by equations (14) and (17) [9], the critical section is located in the junction of the column with the footing as shown in Fig. 3 and 7, respectively.

Step 6: The effective depth "*d*" for the maximum moment is found by the following expression [7,9,10,20]:

$$d = \sqrt{\frac{M_u}{\emptyset_f b_w \rho f_y \left[1 - \frac{0.59 \rho f_y}{f'_c}\right]}} \tag{26}$$

where: M_u is the factored maximum moment at section acting on the footing, $\emptyset_f$ is the strength reduction factor by bending and its value is 0.90, b_w is width of analysis in structural member, ρ is ratio of "*As*" to "$b_w d$", f_y is the specified yield strength of reinforcement of steel, f'_c is the specified compressive strength of concrete at 28 days [7,9,10,20].

where: b_w of circular footings for moment is obtained [9]:

$$b_w = \sqrt{4R^2 - {c_1}^2} \tag{27}$$

Step 7: Bending shear (unidirectional shear force) resisted by the concrete "V_{cf}" is given [7,9,10,20]:

$$\emptyset_v V_{cf} = 0.17 \emptyset_v \sqrt{f'_c} b_w d \tag{28}$$

where: b_w of circular footings for the bending shear is found [7,9,10,20]:

$$b_w = \sqrt{4R^2 - (c_1 + 2d)^2} \tag{29}$$

Bending shear acting on the footing "V_f" is compared to bending shear resistance of concrete "V_{cf}" and must comply with the following expression [7,9,10,20]:

$$V_f \leq \emptyset_v V_{cf} \tag{30}$$

where: $\emptyset_v$ is the strength reduction factor by shear is 0.85.

Step 8: Punching shear (shear force bidirectional) resisted by the concrete "V_{cp}" is given [7,9,10,20]:

$$\emptyset_v V_{cp} = 0.17 \emptyset_v \left(1 + \frac{2}{\beta_c}\right) \sqrt{f'_c} b_0 d \tag{31a}$$

where: β_c is the ratio of long side to short side of the column and b_0 is the perimeter of the critical section [7,9,10,20].

$$\emptyset_v V_{cp} = 0.083 \emptyset_v \left(\frac{\alpha_s d}{b_0} + 2\right) \sqrt{f'_c} b_0 d \tag{31b}$$

where: α_s is 40 for interior columns, 30 for edge columns, and 20 for corner columns [7,9,10,20].

$$\emptyset_v V_{cp} = 0.33\emptyset_v\sqrt{f'_c}b_0 d \quad (31c)$$

where: $\emptyset_v V_{cp}$ must be the smallest value of equations (31a)-(31b)-(31c) [7,9,10,20].

Punching shear acting on the footing "V_p" is compared to punching shear resistance of concrete "V_{cp}" and must comply with the following expression [7,9,10,20]:

$$V_p \leq \emptyset_v V_{cp} \quad (32)$$

Step 9: The main reinforcement steel (parallel reinforcement steel to the direction of the axis "*Y*" of the footing) "A_{sp}" is calculated with the following expression [7,9,10,20]:

$$A_{sp} = wb_w d - \sqrt{(wb_w d)^2 - \frac{2M_u w b_w}{\emptyset_f f_y}} \quad (33)$$

where: w is $0.85f'_c/f_y$ [7,9,10,20].

Minimum steel "A_{smin}" by rule is [7,9,10,20]:

$$A_{smin} = \rho_{min} b_w d \quad (34)$$

where: ρ_{min} is the minimum percentage whereby the reinforcement steel is obtained [7,9,10,20]:

$$\rho_{min} = \frac{1.4}{f_y} \quad (35)$$

The parallel reinforcement steel in the direction of the axis "*X*" is used in equation (33) substituting $M_u = M_{b'\text{-}b'}$ [7,9,10,20].

The parallel reinforcement steel in the short direction portion of the total reinforcement steel, "$\gamma_s A_s$", is distributed uniformly on a band (centered with respect to the axis of the column or pedestal) where the width is equal to the length of the short side of the footing. The rest of the reinforcement steel in the short direction required, "$(1-\gamma_s)A_s$", should be uniformly distributed in the areas which are outside the central band of the footing, where "γ_s" is obtained [7,20]:

$$\gamma_s = \frac{2}{\beta + 1} \quad (36)$$

where: β is ratio of long side to short side of the footing [7,20].

After, the space of the bars "s" is obtained [7,9,10,20]:

$$s = \frac{b_w a_s}{A_s} \quad (37)$$

where: a_s is the rod area used [7,9,10,19].

And the rods length for circular footings "L_1" is found [9]:

$$L_1 = 2\sqrt{R^2 - e^2} \quad (38)$$

where: e is the distance in the direction "*Y*" measured from the axis "*X*" up where the rod is found [9].

Step 10: The development length for deformed bars "l_d" is expressed by [7,9,10,20]:

$$l_d = \frac{f_y \psi_t \psi_e}{6.6\sqrt{f'_c}} d_b \quad (39)$$

where: l_d is the minimum length that should have a deformed bar to prevent slippage, ψ_t is the traditional factor of location of the reinforcing steel which reflects the adverse effects of the position of the bars of the upper part of the section with respect to the height of fresh concrete located beneath them, ψ_e is a coating factor which reflects the effects of the epoxy coating, d_b is the diameter of the bars [7,9,10,20].

The development length for deformed bars "l_d" is compared vs. the available length of the footing "l_a" and must comply with the following expression [7,9,10,20]:

$$l_d \leq l_a \quad (40)$$

3. Numerical Problems

The design of an isolated footing that supports a square column is presented, with the basic information following: c_1 = *40 cm;* c_2 = *40 cm;* H = *1.5 m;* f'_c = *21 MPa;* f_y = *420 MPa;* q_a = *220 kN/m²;* γ_{ppz} = *24 kN/m³;* γ_{pps} = *15 kN/m³.* To case 1: P_D = *700 kN;* P_L = *500 kN;* M_{Dx} =*120 kN-m;* M_{Lx} = *80 kN-m;* M_{Dy} = *120 kN-m;* M_{Ly} = *80 kN-m.* To case 2: P_D = *700 kN;* P_L = *500 kN;* M_{Dx} =*140 kN-m;* M_{Lx} = *100 kN-m;* M_{Dy} = *120 kN-m;* M_{Ly} = *80 kN-m.* To case 3: P_D = *700 kN;* P_L = *500 kN;* M_{Dx} =*160 kN-m;* M_{Lx} = *120 kN-m;* M_{Dy} = *120 kN-m;* M_{Ly} = *80 kN-m.*

Where: H is depth of the footing, P_D is dead load, P_L is live load, M_{Dx} is moment around the axis "*X-X*" of dead load, M_{Lx} is moment around the axis "*X-X*" of live load, M_{Dy} is moment around the axis "*Y-Y*" of dead load, M_{Ly} is moment around the axis "*Y-Y*" of live load [7,9,10].

Table 1, 2 and 3 show the results to case 1, 2 and 3, respectively, and Fig. 10 presents the concrete dimensions and reinforcement steel in a general way for the two types of isolated footings.

4. Results

Effects that govern the design for isolated footings are the moments, bending shear, and punching shear.

For case 1:

a) For the maximum moment acting around the axes *a'-a'* and *b'-b'* is the same, the rectangular footing is 1.08 times that of the circular footing.

b) For the bending shear acting on the footing, there is an increase of 8% in the rectangular footing with respect to the circular footing.

c) For the punching shear, it is virtually identical for the two models of the isolated footings.

In case 2:

a) For the maximum moment acting around the axis *a'-a'*, the rectangular footing is 1.19 times the circular footing, and in the maximum moment acting around the axis *b'-b'*, the rectangular footing is 0.93 times the circular footing.

Table 1.
Comparison of results of case 1

Concept	Rectangular footing RF	Circular footing CF	RF/CF
Measures of the footings (m)	$h=3.20$ $b=3.20$	$R=1.75$	
Resultant force F_{R1} (kN)	843.01	830.30	1.02
Gravity center y_c (m)	0.927	0.883	1.05
Maximum moment acting $M_{a'-a'}$ (kN-m)	612.88	566.74	1.08
Resultant force F_{R2} (kN)	843.01	830.30	1.02
Gravity center x_c (m)	0.927	0.883	1.05
Maximum moment acting $M_{b'-b'}$ (kN-m)	612.88	566.74	1.08
Effective depth d (cm)	42	42	1.00
Total thickness t (cm)	50	50	1.00
Volume of concrete V_C (m^3)	5.12	4.81	1.06
Bending shear acting V_f (kN)	610.61	565.89	1.08
Punching shear acting V_p (kN)	1532.31	1525.38	1.00
Parallel reinforcement steel in direction of axis "Y" of the footing: Cross sectional area of steel A_s (cm^2)	44.76	48.67	0.92
Parallel reinforcement steel in direction of axis "Y" of the footing: Steel volume V_S (cm^3)	14592	14354	1.02
Parallel reinforcement steel in direction of axis "X" of the footing: Cross sectional area of steel A_s (cm^2)	44.76	48.67	0.92
Parallel reinforcement steel in direction of axis "X" of the footing: Steel volume V_S (m^3)	14592	14354	1.02

Source: Prepared by the author.

Table 2.
Comparison of results of case 2

Concept	Rectangular footing RF	Circular footing CF	RF/CF
Measures of the footings (m)	$h=3.60$ $b=3.00$	$R=1.80$	
Resultant force F_{R1} (kN)	863.87	856.05	1.01
Gravity center y_c (m)	1.033	0.909	1.14
Maximum moment acting $M_{a'-a'}$ (kN-m)	719.89	607.28	1.19
Resultant force F_{R2} (kN)	844.25	830.13	1.02
Gravity center x_c (m)	0.876	0.904	0.97
Maximum moment acting $M_{b'-b'}$ (kN-m)	570.89	584.53	0.93
Effective depth d (cm)	42	42	1.00
Total thickness t (cm)	50	50	1.00
Volume of concrete V_C (m^3)	5.4	5.09	1.06
Bending shear acting V_f (kN)	658.01	595.61	1.10
Punching shear acting V_p (kN)	1537.89	1531.66	1.00
Parallel reinforcement steel in direction of axis "Y" of the footing: Cross sectional area of steel A_s (cm^2)	47.45	50.07	0.95
Parallel reinforcement steel in direction of axis "Y" of the footing: Steel volume V_S (cm^3)	17442	15430	1.13
Parallel reinforcement steel in direction of axis "X" of the footing: Cross sectional area of steel A_s (cm^2)	50.35	50.07	1.01
Parallel reinforcement steel in direction of axis "X" of the footing: Steel volume V_S (m^3)	16245	15430	1.05

Source: Prepared by the author.

b) For the bending shear acting on the footing, there is an increase of 10% in the rectangular footing with respect to the circular footing.

c) For the punching shear it is virtually identical for the two models of the isolated footings.

In case 3:

a) For the maximum moment acting around the axis *a'-a'*, the rectangular footing is 1.28 times the circular footing, and the maximum moment acting around the axis *b'-b'*, the rectangular footing is 0.90 times the circular footing.

b) For the bending shear acting on the footing, there is an increase of 12% in the rectangular footing with respect to the circular footing.

c) For the punching shear the two models of the isolated footings are virtually identical.

Materials used for the construction of the isolated footings are the reinforcement steel and concrete.

In case 1:

a) For the concrete, there is a saving of 6% in the circular footing with respect to the rectangular footing.

b) For reinforcement steel whether it is in the direction of the axis "*Y*" or the axis "*X*" of the footing , there is a saving of 2% in the circular footing with respect to the rectangular footing and with respect to the volume of reinforcement steel.

In case 2:

a) For the concrete, there is a saving of 6% in the circular footing with respect to the rectangular footing.

b) For reinforcement steel in the direction of axis "*Y*" of the footing, there is a saving of 13% in the circular footing with respect to the rectangular footing, and in the direction of axis "*X*" of the footing, there is also a saving of 5% in the circular footing with respect to the rectangular footing and with respect to the volume of reinforcement steel.

In case 3:

a) For the concrete, there is a saving of 7% in the circular footing with respect to the rectangular footing.

Table 3.
Comparison of the results of case 3

Concept		Rectangular footing RF	Circular footing CF	RF/CF
Measures of the footings (m)		$h=3.90$ $b=2.80$	$R=1.80$	
Resultant force F_{R1} (kN)		882.04	881.97	1.00
Gravity center y_c (m)		1.114	0.914	1.22
Maximum moment acting $M_{a'\text{-}a'}$ (kN-m)		806.60	630.03	1.28
Resultant force F_{R2} (kN)		845.60	830.13	1.02
Gravity center x_c (m)		0.825	0.904	0.91
Maximum moment acting $M_{b'\text{-}b'}$ (kN-m)		528.77	584.53	0.90
Effective depth d (cm)		42	42	1.00
Total thickness t (cm)		50	50	1.00
Volume of concrete V_C (m^3)		5.46	5.09	1.07
Bending shear acting V_f (kN)		692.04	617.46	1.12
Punching shear acting V_p (kN)		1539.02	1531.66	1.00
Parallel reinforcement steel in direction of axis "Y" of the footing	Cross sectional area of steel A_s (cm^2)	53.68	50.07	1.07
	Steel volume V_S (cm^3)	21119	15430	1.37
Parallel reinforcement steel in direction of axis "X" of the footing	Cross sectional area of steel A_s (cm^2)	54.55	50.07	1.09
	Steel volume V_S (m^3)	15960	15430	1.03

Source: Prepared by the author.

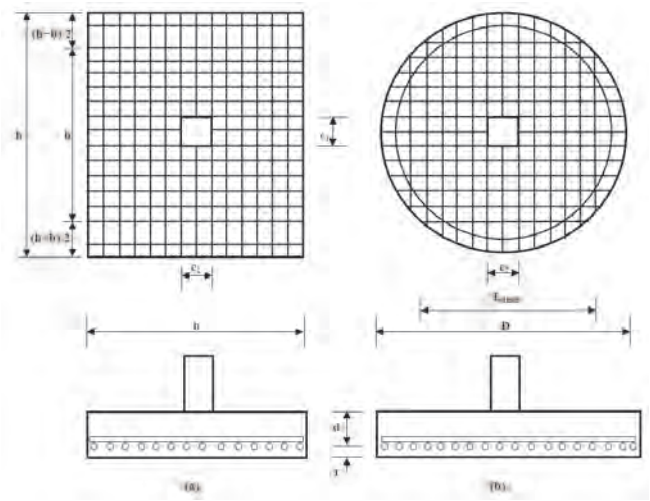

Figure 10. Typical isolated footings: (a) Rectangular, (b) Circular.
Source: Prepared by the author.

b) For reinforcement steel in the direction of axis "*Y*" of the footing, there is a saving of 37% in the circular footing with respect to the rectangular footing, and in the direction of axis "*X*" of the footing, there is also a saving of 3% in the circular footing with respect to the rectangular footing and with respect to volume of reinforcement steel.

5. Conclusions

Research reported in this paper shows the following conclusions:

- The maximum moments acting on the isolated footings are greater for the rectangular footings in comparison to circular footings in the three cases.
- When M_x is increased: The moments acting on axis *a*'-*a*' are greater for the two footings, and the difference increases, the rectangular footings being greater. The moments acting on axis *b*'-*b*' are reduced in the rectangular footings, and in the circular footings they are increased. The bending shear acting on the footings are increased for the two footings, the difference increases, the rectangular footings being greater. The punching shear is greater for the two footings, but there is not a great difference, they are virtually identical.
- The dimensions of the two footings show that the concrete volume is greater for the rectangular footings with respect to the circular footings, but the total thickness "*t*", the effective depth "*d*" and the coating "r_1" of the footings are equal in the two models.
- The reinforcement steel is greater in the rectangular footing and the greater increase is in direction "Y".

Thus the circular isolated footings satisfy the conditions of safety and economy.

The advantages of the circular isolated footings are:

1) The circular design showed a decrease in the amount of reinforcement steel and concrete required compared to the rectangular design that resulted in a more economical lesser volume.

2) In the filling produced by the excavation of the pit in the soil to place the foundations, the structural analysis as a load is taken into account, i.e., the circular footings need a lesser volume of reinforced concrete for stability of the foundations structure.

The models presented can be used in other cases, such as: 1) The footings under a concentric axial load, 2) The footings under an axial load and moment in one direction (uniaxial bending). However, the model for the circular isolated footings under an axial load and moments in two directions (biaxial bending) is proposed, because it is the most appropriate, since it is more economical and also is adjusted to real soil conditions [7,9].

The models presented in this paper apply only in the case of foundation design, where the footings must be rigid and the supporting soil layers elastic, which satisfy the equation of the biaxial bending, i.e., the variation of pressure is linear. As a suggestion for future research, in a situation where the soil type differs to the soil type in this study, for example in totally cohesive soils and totally granular soils, the pressures diagram is not linear and should be treated differently [7,9,10].

References

[1] Luévanos-Rojas, A., A mathematical model for dimensioning of footings square, International Review Civil Engineering (IRECE), [Online]. 3(4), pp. 346-350, 2012. Available at: http://www.praiseworthyprize.com/IRECE-latest/IRECE_vol_3_n_4.html#A_Mathematical_Model_for_Dimensioning_of_Footings_Square

[2] Luévanos-Rojas, A., A mathematical model for soil pressures acting on circular footings, for obtaining the moments of design, Far East Journal of Mathematical Sciences, [Online]. 69(2), pp. 219-232, 2012. Available at: http://www.pphmj.com/abstract/7000.htm

[3] Luévanos-Rojas, A., A mathematical model for the dimensioning of circular footings, Far East Journal of Mathematical Sciences, [Online]. 71(2), 357-367, 2012. Available at: http://www.pphmj.com/abstract/7251.htm

[4] Luévanos-Rojas, A., A mathematical model for soil pressures acting on circular footings, for obtaining the moments and shear forces unidirectional in direction of axes "X" and "Y", Far East Journal of Mathematical Sciences, [Online]. 71(2), pp. 369-389, 2012. Available at: http://www.pphmj.com/abstract/7252.htm

[5] Luévanos-Rojas, A., A mathematical model for pressures of ground acting on footings rectangular, ICIC Express Letters Part B: Applications, [Online]. 4(1), pp. 19-24, 2013. Available at: http://www.ijicic.org/elb-4(1).htm

[6] Luévanos-Rojas, A., A mathematical model for dimensioning of footings rectangular, ICIC Express Letters Part B: Applications, [Online]. 4(2), pp. 269-274, 2013. Available at: http://www.ijicic.org/elb-4(2).htm

[7] Luévanos-Rojas, A., Faudoa-Herrera, J.G., Andrade-Vallejo, R.A. and Cano-Alvarez M.A., Design of isolated footings of rectangular form using a new model, International Journal of Innovative Computing, Information and Control, [Online]. 9(10), pp. 4001-4022, 2013. Available at: http://www.ijicic.org/ijicic-12-10031.pdf

[8] Luévanos-Rojas, A., A comparative study for dimensioning of footings with respect to the contact surface on soil, International Journal of Innovative Computing, Information and Control, [Online]. 10(4), pp. 1313-1326, 2014. Available at: http://www.ijicic.org/ijicic-13-08003.pdf

[9] Luévanos-Rojas, A., Design of isolated footings of circular form using a new model, Structural Engineering and Mechanics, [Online]. 52(4), pp. 767-786, 2014. Available at: http://technopress.kaist.ac.kr/?page=container&journal=sem&volume=52&num=4#

[10] Luévanos-Rojas, A., Design of boundary combined footings of rectangular shape using a new model, DYNA, [Online]. 81(188), pp. 199-208, 2014. Available at: http://dyna.unalmed.edu.co/en/ediciones/188/articulos/v81n188a25/v81n188a25.pdf

[11] Das, B.M., Sordo-Zabay, E. and Arrioja-Juarez, R., Principios de ingeniería de cimentaciones, Cengage Learning Latín América, México, 2006.

[12] Bowles, J.E., Foundation analysis and design, McGraw-Hill, New York, 1996.

[13] Calabera-Ruiz, J., Calculo de Estructuras de Cimentación, Intemac Ediciones, México, 2000.

[14] Tomlinson, M.J., Cimentaciones, Diseño y Construcción, Trillas, México, 2008.

[15] Ibañez-Mora, L., Pruebas de carga no destructivas en pilotes, DYNA, [Online]. 75 (155), pp. 57-61, 2008. Available at: http://www.revistas.unal.edu.co/index.php/dyna/article/view/1740/11578

[16] Gaviria, C.A., Gómez, D. and Thomson, P., Evaluación de la integridad de cimentaciones profundas: Análisis y verificación in situ, DYNA, [Online]. 76 (159), pp. 23-33, 2009. Available at: http://www.revistas.unal.edu.co/index.php/dyna/article/view/13037

[17] Valencia, Y., Camapum, J. and Lara, L., Aplicaciones adicionales de los resultados de pruebas de carga estáticas en el diseño geotécnico de cimentaciones, DYNA, [Online]. 79 (175), pp. 182-190, 2012. Available at: http://www.revistas.unal.edu.co/index.php/dyna/article/view/28167/43527

[18] Aristizabal-Ochoa, J.D., Stability of slender columns on an elastic foundation with generalised end conditions, Ingeniería e Investigación, [Online]. 33 (3), pp. 34-40, 2013. Available at: http://revistas.unal.edu.co/index.php/ingeinv/article/view/41041

[19] Camero, H.E., A novel finite element method for designing floor slabs on grade and pavements with loads at edges, Ingeniería e Investigación, 35(2), pp. 15-22, 2015. DOI: 10.15446/ing.investig.v35n2.45603

[20] ACI 318-13 (American Concrete Institute), Building Code Requirements for Structural Concrete and Commentary, Committee 318, 2013.

[21] Gere, J.M. and Goodno, B.J., Mecánica de Materiales, Cengage Learning, México, 2009.

[22] Gambhir, M.L., Fundamentals of Reinforced Concrete Design, Prentice-Hall, of India Private Limited, 2008.

[23] González-Cuevas, O.M. and Robles-Fernández-Villegas, F., Aspectos fundamentales del concreto reforzado, Limusa, México, 2005.

[24] McCormac, J.C. and Brown, R.H., Design of Reinforced Concrete, John Wiley & Sons, New York, 2013.

[25] Mosley, W.H., Bungey, J.H. and Hulse, R., Reinforced Concrete Design, Palgrave Macmillan, New York, 1999. DOI: 10.1007/978-1-349-14911-7Parker, A., Diseño Simplificado de Concreto Reforzado, Limusa, México, 1996.

[26] Punmia, B.C., Kumar Jain, Ashok and Kumar Jain, Arun., Limit State Design of Reinforced Concrete, Laxmi Publications (P) Limited, New Delhi, India, 2007.

A. Luévanos-Rojas, received his BSc. Eng in Civil Engineering in 1981, his MSc. degree in Planning and Construction in 1996, and a PhD. Engineering degree in Planning and Construction in 2009, all of them from the Facultad de Ingeniería, Ciencias y Arquitectura of the Universidad Juárez del Estado de Durango, Gómez Palacio, Durango, México. He received an MSc degree in Structures in 1983, from the Escuela Superior de Ingeniería y Arquitectura the Instituto Politécnico Nacional, Distrito Federal, México and an MSc degree in Administration in 2004, from the Facultad de Contaduría y Administración of the Universidad Autónoma de Coahuila, Torreón, Coahuila, México. He was a full time professor between 1983 to 2009 and from 2009 to 2014, he was professor and researcher for the Facultad de Ingeniería, Ciencias y Arquitectura of the Universidad Juárez del Estado de Durango. His research interests include: mathematical models applied to structures: methods of structural analysis, members design of concrete and steel, and analysis of non-prismatic members. He is also a member of the Advisory Committee and contributor to the "Revista de Arquitectura e Ingeniería", and Associate Editor of the journal "ICIC Express Letters Part B: Applications". He is a member of the National System of Researchers of Mexico.
ORCID: 0000-0002-0198-3614.

UNIVERSIDAD NACIONAL DE COLOMBIA
SEDE MEDELLÍN
FACULTAD DE MINAS

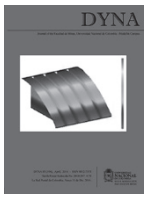

DYNA
http://dyna.medellin.unal.edu.co/

Developing a self-regulating soldering iron based on induction heating

Cuauhtémoc Mazón-Valadez, Luis Héctor Quintero-Hernández, Ernesto Edgar Mazón-Valadez, Alfonso Hernández-Sámano, José Ávila-Paz & Mario Eduardo Cano-González*

Centro Universitario de la Ciénega, Universidad de Guadalajara, México. mazon2065@hotmail.com, hectorquintero@yahoo.com, mazon_valadez@hotmail.com, h.s.alfonso@gmail.com, jocmos@hotmail.com, meduardo2001@hotmail.com.*

Received: June 11th, 2015. Received in revised form: January 18th, 2016. Accepted: January 26th, 2016.

Abstract
This work focused on the design, development and construction of a new low cost soldering iron that works by means of induction heating. The amount of electronic components has been minimized in order to reduce production costs. Additional tests were undertaken to determine the ideal tips for soldering, and the adaptations necessary to guarantee self-regulation using a nickel foil shield (due to its low curie temperature) are suggested. The new device contains a resonant inverter able to generate alternating magnetic fields of 100 *kHz* at the center of an 18-turn coil; the inverter is controlled only using an astable oscillator circuit. The paper examines criteria to select suitable soldering-tips by experimentally determining their equivalent resistance heating it within the resonant inverter or well, another one by using a rapid magnetic test. The system represents a good tool, suitable for the manufacture of development boards or electronic tasks.

Keywords: Electromagnetic induction; Heating; Resonant inverter; Soldering iron.

Desarrollo de un cautín autorregulable basado en calentamiento por inducción

Resumen
Este trabajo se enfocó en diseñar y construir un novedoso cautín económico que funciona mediante inducción magnética. Se han minimizado la cantidad de componentes electrónicos que lo conforman para disminuir su costo de producción y también se realizaron pruebas para determinar las puntas óptimas para soldar, proponiendo las adaptaciones necesarias para lograr la autorregulación empleando una cubierta de lámina de níquel por su baja temperatura de Curie. El nuevo dispositivo se compone de un inversor resonante capaz de generar campos magnéticos alternos de 100 *kHz* en el centro de una bobina de 18 espiras y éste se controla solamente con un circuito oscilador astable. Se discute un criterio para seleccionar las puntas reemplazables, basado en la resistencia equivalente obtenida experimentalmente del inversor resonante o bien otro criterio haciendo un rápido ensayo magnético. El nuevo dispositivo representa una herramienta adecuada para realizar tarjetas impresas de circuitos o tareas de electrónica.

Palabras clave: Inducción Electromagnética; Calentamiento; Inversor Resonante; Soldador.

1. Introduction

Currently, the majority of the devices specially designed to heat by using resistance or any natural fuel have been replaced by their equivalent that work via induction heating. In most cases, the pieces to be heated are composed of ferromagnetic materials, which can be heated with electromagnetic waves of frequencies in the range of tens of *kHz* due to their high magnetic permeability [1], for example induction cookers [2], that use $f \approx 30$ *kHz*. These new devices success is thanks to a non-invasive heating procedure, representing a cleaner method than the conventional ones [3]. Nevertheless, professional induction heating devices rely on more complex electronics technology and higher manufacturing costs.

Additionally, induction heaters are used in industrial applications for metallic pieces, such as dilatation, furnace welding [4] and sealing plastic bags [5]. Other new

© The author; licensee Universidad Nacional de Colombia.

applications are focused on the development of biomedical therapies like magnetic hyperthermia for the treatment of tumors [6,7].

Recently, we made a pencil-style soldering iron characterized by the fact that no cord is used in the handle [8] and that it is designed to work intermittently, unlike other commercial high frequency soldering irons [9]. With this device, it is possible to comfortably solder electronic components onto printed circuit boards (PCB), mostly by melting lead/tin wire or ecologic solder paste. The system is enhanced by a specially constructed resonant inverter that can achieve efficiencies up to 95 %.

The main aim of this work is to develop a new induction heating soldering iron for continuous use, keeping costs low to make it viable for reproduction on an industrial scale. The principal idea is to simplify the electronic stages in the control of its high power electronic circuit. Moreover, by introducing a low Curie temperature material, the need to use control electronics to limit temperature is reduced. Also, some other considerations are taken into account so the system is capable of heating a set of inexpensive commercial tips, which are typically used in resistance soldering irons.

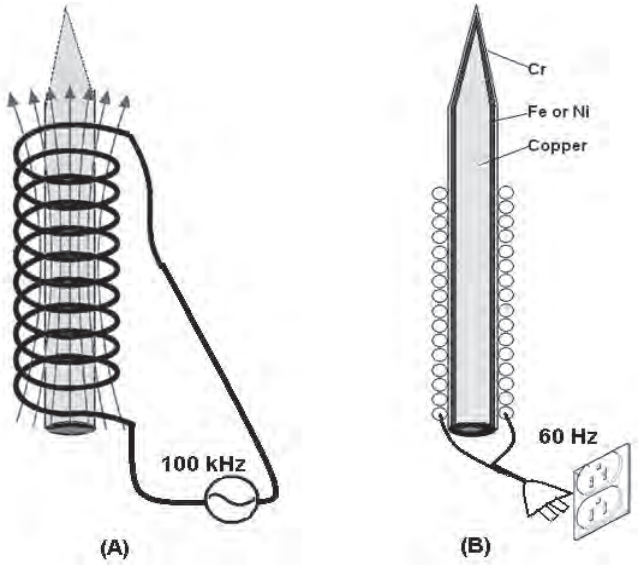

Figure 1. A cylindrical ferromagnetic rod heated with an AC magnetic field of high frequency (A) and 60 Hz.
Source: own

2. Theoretical background

2.1. Induction heating

The heating process of a soldering tip using an electromagnetic wave through an induction coil, can be reduced to the problem of an AC current flowing in a cylindrical conductor rod with radius *a*, where a current flow known as Eddy currents is induced [10]. Indeed, if the tip is ferromagnetic it could be heated using frequencies in the range of tens or hundreds of *kHz*; Fig. 1(A) shows the procedure where the ferromagnetic piece is placed inside the region of magnetic flux. The magnetic field is generated using a coil with *N* loops, length *l* and inductance *L*, which is powered with an AC power supply of high frequency. Since the magnetic permeability μ of the metal depends on the temperature, its ferromagnetic behavior could vanish at the Curie point (Curie temperature T_C), where it becomes a paramagnetic material [11,12] and the inductance of the work coil tends to *L*, because the material reaches the permeability of an empty space μ_0.

A complete analysis of the heating of several types of materials with radiofrequencies was undertaken by Brown [13], here it is observed that the magnitude of the magnetic field intensity *H* in the rod satisfies the eq. (1).

$$\frac{d^2H}{dr^2}+\frac{1}{r}\frac{dH}{dr}-H(j2\pi f\mu\sigma)=0, \qquad (1)$$

where *f* is the frequency of the wave, μ is the magnetic permeability and σ is the conductivity of the material. The solutions to this equation are the typical Bessel functions of first class and order zero, expressed in eq. (2) [13].

$$H = AJ_0(\sqrt{-2j}\,\frac{r}{s}), \qquad (2)$$

where the constant *A* depends on the initial conditions and on the skin thickness in the material *s* [14]; which is given by eq. (3). Physically, this value represents the effective surface of the material with resistivity $\rho=\frac{1}{\sigma}$, where the electric current crosses.

$$s=1\Big/\sqrt{\frac{\pi f\mu}{\rho}}. \qquad (3)$$

Following the Maxwell-Ampere law [15] and neglecting the dielectric constant of the material, it is possible to obtain a relationship between the electric field due to the induced currents on the material and the external magnetic field intensity; this is given by eq. (4).

$$\frac{1}{\sigma}\frac{dH}{dr}=E. \qquad (4)$$

Then, using the solutions of eq. (2) on eq. (4) it is possible to determine the superficial power dissipated ($p=\sigma E^2$) for the ferromagnetic rod in watts per unit length, as expressed in eq. (5) [15].

$$P=\int_{r=0}^{r=a}2\pi r\sigma E^2 dr. \qquad (5)$$

With a further analysis of the Bessel polynomials the solution for *H* is obtained, assuming uniform magnetic field intensity H_0, parallel to the flux direction in all the metal [13], to apply boundary conditions. Thus, the value of *P* is obtained as shown in eq. (6).

$$P = 8\pi H_0^2 a \frac{\rho}{s}; \qquad \frac{a}{s} > 5. \qquad (6)$$

The ratio $R_s = \frac{\rho}{s}$ is known as the superficial resistance and it can be clearly observed that by diminishing the value *s and* maintaining the same electric current, the power dissipated in the material *P* is increased. Nevertheless, the value of *s* depends on the electromagnetic properties of the material and the applied frequency.

Regarding soldering iron tips, the first point to be noted is that they are composed of at least three layers as displayed in Fig. 1(B), where the most superficial is made of Chrome (Cr) which is used to reduce corrosion and has a thickness of approximately 10 μm [16]. The next layer could be composed of a hard ferromagnetic material such as iron or nickel to increase the duration of the tip, with a thickness of 200 μm [17]. Finally these layers are covered by a thicker solid piece of copper, to increase the thermal diffusivity of the tip and therefore the eq. (6) takes different values in each of its layers.

2.2. Electromagnetic field generator

Usually, the generation of electromagnetic fields employed in induction heating is carried out with power electronic circuits known as resonant inverters. These circuits are composed of an array of semiconductors to switch the current and feed a resonant circuit. TTL technology is used in the human audible interval of frequencies; IGBT can be used up to 200 *kHz* and MOSFET technology up to 1*MHz*. They can be configured as "H-bridge" (half or whole) or "push pull", to feed a series or parallel LC circuit or "resonant tank" [18]. In general the tank resonates when the difference between its capacitive and the inductive reactance is null. The commutation of the transistors is controlled using a driver circuit to adjust the duty cycle and dead time of the transistors, which include a pre-amplification stage connected to another electronic circuit in order to isolate the driver of the switching stage [19,20]. Also, in some applications, current sensors to complement a phase lock loop stage (PLL) or a frequency compensation circuit, connected between the tank and the driver circuit [21,22] are used. All these electronic components and the engineering involved, in some devices force an increase in production costs, making it unviable to be manufactured on an industrial scale. In contrast with devices that work with fuel or resistances, where the engineering work is less complex and involves lower costs. Nevertheless as the Eddy currents produced for induction heaters are focused mainly on the heated metal piece, this technology could be more energy saving.

With a view to simplifying the resonant inverter, in this research the circuit displayed in Fig. 2 is built. It is a class D voltage-switching inverter with half H-bridge topology, with the resonant capacitor divided into two halves [23-25]. Also, a pair of mosfets transistors Q1 and Q2 (N-channel and P-channel respectively) are used to switch the current to a L_RC_R series resonant circuit ($C_R = C_{R1}+C_{R2}$), each transistor gate is

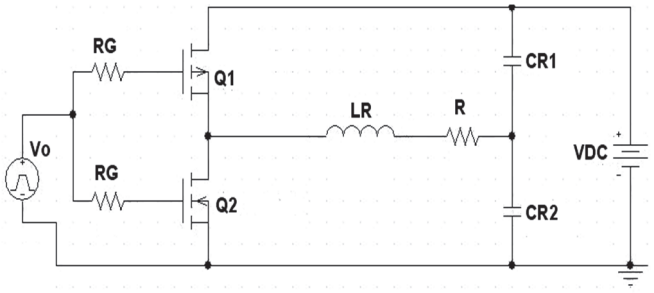

Figure 2. Diagram of the resonant inverter circuit.
Source: own

driven directly (through a simple resistance RG) with a cheap astable oscillator. While the high value of the rectangular signal activates the N-channel mosfet and closes the P-channel, the low side has the opposite effect. The whole circuit is powered with an AC to DC adapter with a tension VDC.

It is important to note that the ideal resonant frequency of this circuit satisfies eqs. (7), where L_R and C_R are the resonant inductance and capacitance respectively.

$$f_R = \frac{1}{2\pi\sqrt{L_R(C_{R1}+C_{R2})}} \qquad (7)$$

Meanwhile, the power delivered to the ferromagnetic tip by this circuit when the inverter is supplied with V_I is given by the eq. (8).

$$P_{out} = I_R V_I \cos\theta, \qquad (8)$$

where I_R is the resonant current through L_R and θ the phase shift angle with respect to V_I. From another point of view, the power dissipated on the surface of the ferromagnetic piece with resistance R_F, due to the Eddy currents I_F, also obeys the Joule law and then the eq. (8) is equivalent to the eq. (9).

$$P_{out} = I_F^2 R_F. \qquad (9)$$

Analysing eq. (8) and taking into account that the magnetic field H_0 is related with I_R in a coarse approximation and the properties of the induction coil L_R, through the eq. (10).

$$H_0 = \frac{NI_R}{l}. \qquad (10)$$

Thus the eq. (6) is rewritten as the eq. (11) and regarding the shape of eq. (9) it is possible to find an expression for the equivalent resistance of the resonant inverter *R* as the eq. (12), including the total static resistance of all the electronics components R_{dc}.

$$P = 8\pi a R_s \frac{N^2}{l^2} I_R^2; \qquad \frac{a}{s} > 5. \qquad (11)$$

$$R = \frac{8\pi a N^s}{l^2} R_s + R_{dc}. \qquad (12)$$

3. Materials and Methods

3.1. Industrial design of the new soldering iron

As a starting point, the handle of a commercial soldering iron with a pencil design based on a resistance is used; thus, a new set of pieces was adapted to work via magnetic induction. Fig. 3(A) shows the design of the new soldering iron, which contains a thermal insulating plastic handle (1), a cylindrical cavity of nonmagnetic stainless steel (2) to cover the new set of components and attach them to the handle, a cylindrical cavity of solid Teflon (3) to hold an end of the tip (8), which is inserted in a cylindrical nickel foil cavity of 200 μm thickness (7), both pieces cross through the coil center (4), isolating it from the tip and form the external shield (2) using a cylindrical cavity of silicone (5), able to resist up to 350°C, but maintaining a vacuum space to reduce the risk of the coil being heated by the tip. Finally the conical edge of the tip is clamped to a small cylindrical cavity of Teflon (6).

The final presentation of the new pencil soldering iron is displayed in Fig. 3(B), with a shape similar to the original resistance soldering iron. Fig. 3(C) also shows the cabinet with the circuit explained in Fig. 2, excluding the resonant coil (4). Moreover, the AC/DC adapter to power the circuit, a station to place the pencil and a set of 3 models of soldering tips, which are selected following the criterion explained in the next section, can also be seen in the same Fig. 3(C).

As is observed in Fig. 1, the soldering tip (6) and its nickel cavity (7) are heated directly by the resonant coil taking advantage of their ferromagnetic properties and without physical contact, with the aim of transmitting all the dissipated power on the tip, to the solder wire.

3.2. Selecting the soldering tips

As illustrated in Fig. 1(B) the soldering tips are composed mainly of Cu (diamagnetic material), they are also coated with a ferromagnetic material (Ni or Fe) and in the external surface the shield is Cr (paramagnetic material). We obtained three inexpensive soldering tips (brand Steren), Cu, cone shaped and with the following specifications: CAU-118 with 67 *mm* length and major diameter 3.6 *mm*; CAU-192 with 58 *mm* length and major diameter 4.5 *mm*; and CAU-151 with 70 *mm* length and major diameter 3.6 *mm*. However, the provider does not provide clear information about the materials involved in the coating of the tips. Table 1 displays the electromagnetic properties and the thermal diffusivity of the materials that characterize the soldering tips.

Since Cu and Cr have a small magnetic permeability μr, higher frequencies (near to MHz) are necessary to reach a small s value, as is required in the eq. (6) to dissipate a major P value. So, there is more benefit to heating the tip with a high frequency f constraining the current to a small s value in the ferromagnetic coating, which offers a quite large resistivity ρ. Additionally, as the thermal diffusivity of Cu is almost one magnitude order higher than for Ni of Fe, it is more practical to transmit the temperature faster to the solder wire through this means.

Regarding the cylindrical piece (7) detailed in Fig. 3(A) and developed to cover the welding tips; it was made with a pure Ni foil and has a 0.2 *mm* thickness. This is used to increase the effective diameter of the tips CAU-118 and CAU-151. Indeed this piece is used intentionally in order to achieve self-regulation of the tips, due to its low Curie temperature Tc = 325 °C. In this sense, when this piece and the whole tip reach this temperature, the relative permeability of Ni falls very close to μ_r = 1, then the value of *s* in all the

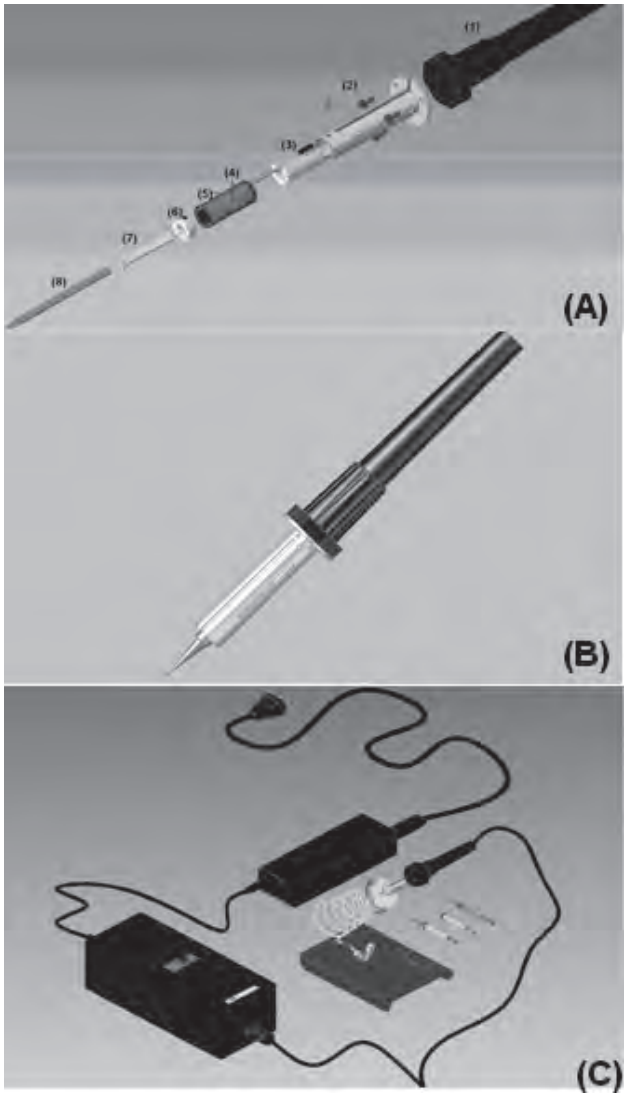

Figure 3. (A) An itemized view of all pieces of the pencil soldering iron, (B) final presentation of the pencil and (C) all the accessories of the soldering iron including its RF generator, AC/DC adapter, station and a lot of tips. Source: own

Table 1.
Electromagnetic and thermal properties of the materials composing the soldering tips.

Material	α (m²/s) $\times 10^{-6}$	ρ (Ω*m) $\times 10^{-8}$	μ_r (1)
Cu	111.2	1.7	1
Ni	12.9	6.4	600
Fe	19.3	9.7	5000
Cr	29.1	12.5	1

Source: own

layers of the tip are increased and the value of *P* diminish dramatically and the heating rate collapses. After the temperature of the tip decreases bellow Tc, the value of *s* diminishes in the Ni shield and therefore the *P* value increases and begins heating faster again.

In order to find the best frequencies to heat the tips, we conducted an exhaustive experimental assessment by using an alternative experimental setup, suitable to cover a wide range of radiofrequencies to heat them and measure their temperature simultaneously with an infrared sensor [8], finding a value approximately of f = 100 *kHz*. In addition, a characterization of their magnetic properties was made by using a vibrating sample magnetometer (VSM) [26].

3.3. Electronic features of the soldering iron

A rectangular signal of f = 100 *kHz* (in accordance with the last part of the previous section), with 15 V of amplitude and 50 % duty cycle is generated with a commercial astable multivibrator of CMOS technology. The integrated circuit CD4047 is configured using a resistance R1 = 22 *k*Ω and a capacitor C1 = 100 *pF*, powered with VCC = 15 V. Fig. 4 shows the diagram of the electronic circuit that was developed.

This rectangular voltage of the oscillator directly feeds both gate terminals of the FQA12P20 and IRFP450 mosfets, through a resistance R_G = 10 Ω at the same time. Both transistors form the voltage inverter (see Fig. 2). When the mosfet Q1 sends current through the work coil (N = 18 turns and 5 *cm* length *l*, resulting on a L_R = 1.3 μH), the current crosses in one sense closing the circuit at the capacitors bank node C_{R2} =1010 *nF*, the other capacitors bank C_{R1} = C_{R2}, works as a parallel capacitor connected by short circuit to the AC voltage source and blocking the DC components to L_R. A similar behaviour happens when the mosfet Q2 provides the current to L_R in the opposite direction. This commutation at 100 *kHz* allows the resonance of the L_RC_R circuit due to the established values in the eq. (7), generating a sinusoidal waveform.

4. Experimental Results and Discussions

After the electronic design, a main board with all the electronic components is engraved to weld; Fig. 5(A) shows the simulation in the PSPICE platform, in order to analyze the behavior between the driver signal and the resonant current. The simulation suggests a small deformation of the sinusoidal waveform due to the absence of a dead time in the ON and cut-Off state of both mosfets. Moreover Fig. 5(B) is obtained experimentally using an oscilloscope with a USB port and through flash memory; in this experiment the L_R has no soldering tip. Two overlapped waveforms, the mosfets driver signal (the rectangular shape) and the quasi-sinusoidal waveform of the resonant current are displayed here. Additionally, a good concordance between the resonant currents amplitudes obtained in these two ways was observed, with relative differences of 8 %.

Continuing with the characterization of the device, the resonant current (gray line) and voltage (dark line) signals are obtained using the PSPICE and the waveforms are shown in Fig. 6(A). As is expected, the sinusoidal current is a little deformed and also, the voltage rectangular shape is strongly modified due to counter electromotive force induced by L_R. The results of the corresponding experiment are displayed in Fig. 6(B). In this figure a set of four signals measured simultaneously is exhibited, where the uppermost corresponds to VDC which clearly is not the initial constant

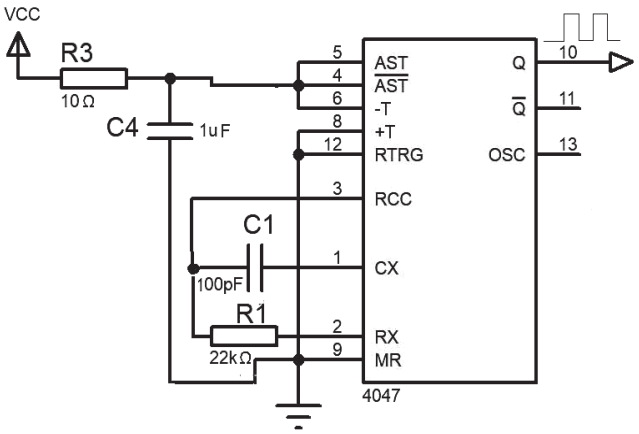

Figure 4. Oscillator circuit of f = *100* kHz using the IC CD4047.
Source: own

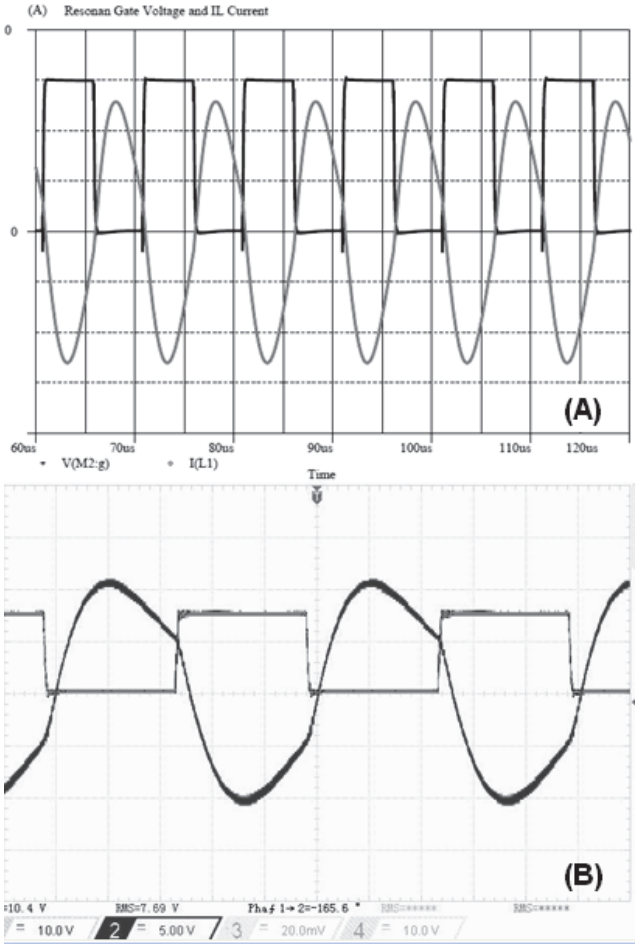

Figure 5. (A) Driver signal (rectangular shape) and resonant current (sinusoidal shape) simulated in PSPICE and (B) the same signals obtained experimentally.
Source: own.

signal, this behavior is also observed in the signal placed immediately below. These two observations highlight the interference of the power supply with the resonant circuit and a simple calculus of their RMS values gives a power consumption of 67.4 *W*. The next two signals displayed below in the same figure are the resonant voltage and current respectively, the rectangular waveform of the voltage is strongly deformed in agreement with the simulation, but in this experiment a phase shift of 19.6° between both waveforms is observed and the output total power (eq. (8)) is approximately 59.0 *W*, indicating an efficiency of $\eta = 88$ %. The value used of $R = 0.99\ \Omega$ is due to the total sum of the resistances of Q1 and Q2 (0.47 Ω each), plus the resistance of the coil of 0.05 Ω and neglecting the resistance R_C which is very short to be determined.

On the other hand, in Figs. 7(A-C) the corresponding four signals obtained from the resonant coil are displayed, in a time instant when the tips CAU-118, CAU-151 and CAU-192 are heated, respectively. A quick analysis of these measurements indicates that the counterelectromotive forces are weakened when the CAU-192 is heated, because the amplitude of the ripple induced in the waveform of the power current ADC, is less than each other measurements. Furthermore, the voltage difference between the resonant coil terminals has a trend to a more rectangular signal than each other. This phenomenon is due to the marked difference of the magnetic properties observed for CAU-192 in comparison with the other tips [26]; this implies a major equivalent resistance R in the resonant inverter. Table 2 summarizes the efficiency values determined and equivalent resistance of this RF generator, in a time instant when each soldering tips is heated. The system responds with a major efficiency with the CAU-192.

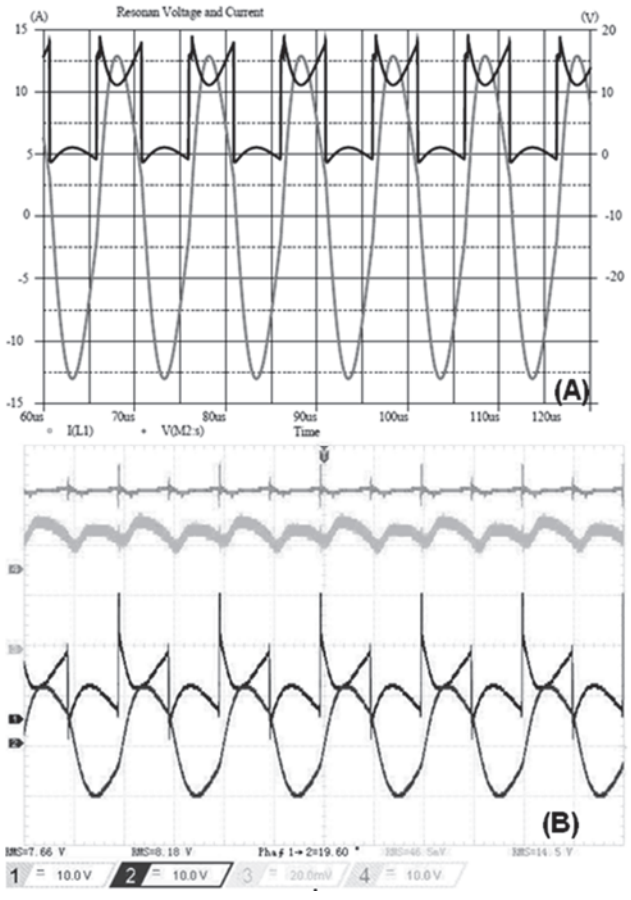

Figure 6. (A) Simulated signals of the voltage (dark) and current (gray) resonant and (B) experimental signals of the supplied DC voltage (upper), current (immediately above), in addition the corresponding resonant signals of the simulated voltage and current.
Source: own.

Table 2. Efficiency of the resonant inverter heating each tip and their equivalent resistances.

TIP	η (AU)	R (Ω)
Empty	88	0.99
CAU-118	89	1.6
CAU-151	90	1.9
CAU192	93	2.32

Source: own

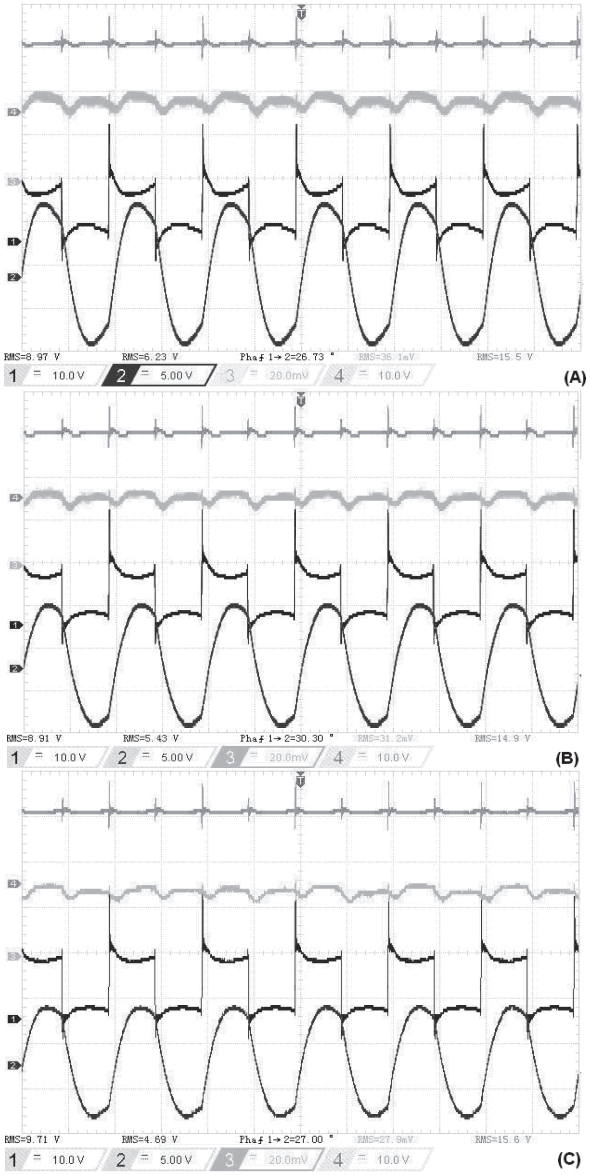

Figure 7. Experimental signals of the DC supplied voltage and current. Also, the waveforms of the resonant voltage and current at the resonant coil with the tip inside (A) CAU-118, (B) CAU-152 and (C) CAU-192.
Source: own.

After the analysis of the efficiency and equivalent resistance of the resonant inverter including the soldering tips, a last experiment is conducted to explore the self-regulation of the new soldering iron. With the aim of not overloading the thermal capability of the isolating pieces explained in Fig. 3(A), an AC/DC adapter of 12 V and 35 W maximum is used to avoid a possible overheating of the tips. In this experiment the heating curves of the tips (T vs t) are obtained connecting the output of an infrared sensor to one analogical channel of a National Instruments acquisition card in the platform of Lab-view DAQ-USB-6008. Fig. 8 shows these curves and an asymptotic behaviour in the heating of the curves CAU-118 and the CAU-151 is clearly observed. The temperature remains constant after three minutes of operation with a value near to 305 °C and 315 °C, due to the Curie temperature of the nickel-shield on these soldering tips. Although a maximum temperature of 325 °C is expected, this indicates the existence of a temperature gradient of 20 °C and 10 °C between the section of the tips submitted to the magnetic field (here the magnetic field is higher and then the heating is concentrated in this segment) and the conic extreme, respectively. Indeed, the curve of the CAU-192 never manifests an asymptotic behaviour in the temperature, indicating the absence of nickel in this tip and therefore its inner coating is based on iron. In other words, although the electromagnetic field generator has a higher efficiency when using CAU-192, it is not recommended to be used with our new self-regulated soldering iron. Furthermore, to extend its life time any other soldering tip of iron with equivalent resistance greater than R = 1.9 Ω is not recommended, nevertheless further experiments with a lot of different models of welding tips are needed to support this statement.

On the other hand, if we observe the heating during the first 60 *s* in Fig. 8, an increment above 150 ºC is recorded. This is not observed in similar measurements under the same conditions with CAU-118 and CAU-115 when the Ni cover is removed. As is displayed in Fig. 9, the increase in their temperatures does not exceed 20 ºC and 40 ºC respectively, and then their faster heating of Fig. 8 is principally due to the Ni cover, which is not necessary for CAU-192.

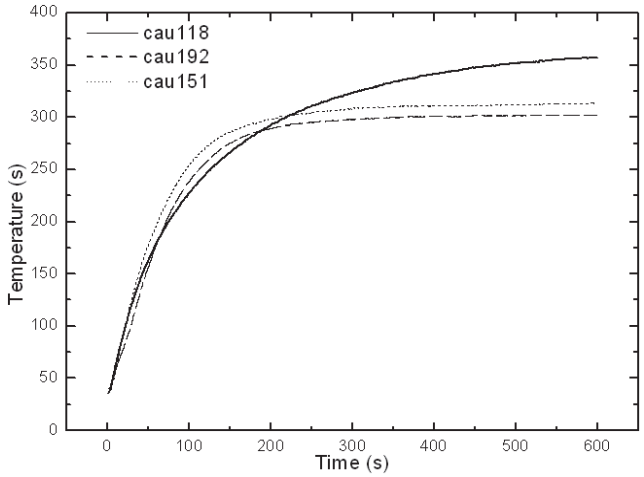

Figure 8. Heating curves of the soldering tips using the new self-regulating soldering iron, the CAU-118 and CAU-151 are covered with a cylindrical foil of Ni.
Source: own.

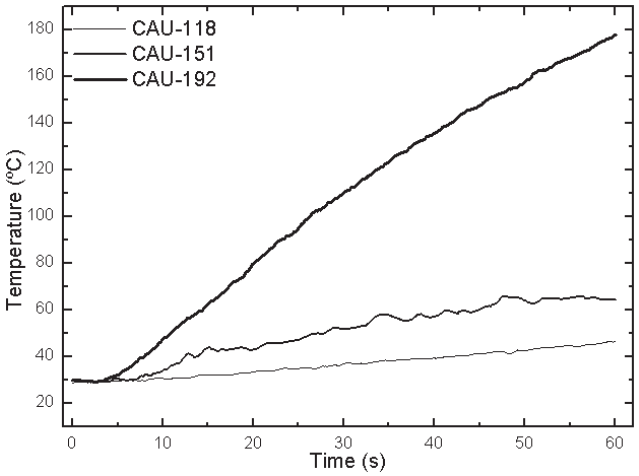

Figure 9. Heating curves of the soldering tips CAU-192 (coarse line), CAU-151 (middle line) and CAU-118 (fine line)
Source: own.

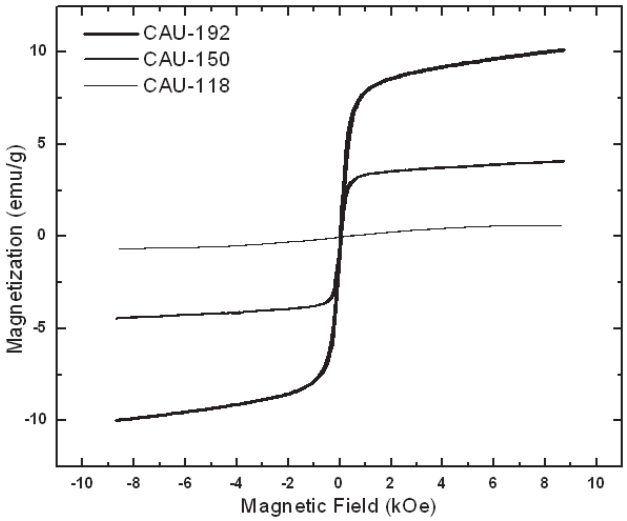

Figure 10. Magnetization curves of the soldering tips CAU-192 (coarse line), CAU-151 (middle line) and CAU-118 (fine line)
Source: own.

With the aim of establishing a criterion to select the most suitable soldering tips from those available on the electronics market, the magnetization curves of each tip are determined using a vibrating sample magnetometer Lakeshore 7300 and a cylindrical piece of 5 *mm* length extracted from each tip. The applied magnetic field ranges between ± 9 *kOe* and Fig. 10 shows the measurements.

Analysing the trends of magnetic saturation in each curve, for example to 8 kOe, the next values are observed (in emu/g): 10, 5.1 and 0.6 to the CAU-192, CAU-151 and CAU-118 respectively. Therefore, CAU-192 is the most magnetic tip as can be expected due to its composition of Fe as previously observed in Fig. 8, thus it is strongly attracted by a small magnet of NdFeB in comparison with CAU-118, which is hardly attracted by the same magnet. With this magnetic behavior, CAU-118 becomes a suitable candidate

to be covered by the cylinder of Ni, following a sure and rapid criterion to ensure its self-regulation. For its part CAU-151 is also moderately attracted by the magnet and is more difficult to define a fast criterion to select it, one possibility is undertaking a quick test in the system to confirm the behavior exhibited in Fig 9.

5. Conclusions

The design and build of an inexpensive soldering iron, characterized because it works via induction heating is presented in this paper. The magnetic field generator of this device is a very simplified resonant inverter which excludes a lot of electronic stages, trying to diminish the production costs on an industrial scale. Indeed, the device is controlled just with a commercial oscillator circuit of CMOS technology. The final presentation of the device is like the traditional pencil-shape resistance soldering irons. Moreover, a set of three different soldering tips of Cu covered with ferromagnetic materials have been analysed to accompany the new device and it is possible to define a criterion to select them based on the equivalent resistance, determined by using the resonant inverter (under the value of R_{dc} = 0.99 Ω), i.e. 0.61 Ω < R ≤ 0.91 Ω. A tip of Cu coated in Fe with a major resistance could not achieve self-regulation even when covered with Ni. Therefore, we do not recommend using these tips with this device. If the equivalent resistance is approximated to 0.61 Ω, a cover of pure Ni with a thickness of 200 μm on the tip is recommended to ensure self-regulation at a temperature near to 325 °C. Another criterion to select a replacement soldering tip based on Cu, that is covered with a piece of Ni and is self-regulating, is by means of a fast and qualitative method using a small magnet to confirm its weak magnetic interaction or attraction, indicating a very small presence of ferromagnetic material in the coating (because the Cu and Cr are diamagnetic and paramagnetic respectively), in comparison with another piece with abundant Fe which again is not recommended for this system.

The estimated production cost of the device is approximately US$ 25. This calculation only takes into account the price of all the pieces and includes all the components and accessories displayed in Fig. 3(A) and Fig. 3(C). Finally, this device is a very useful tool in any electrical workshop or instrumentation laboratory, to perform technical repair works or electronics.

Acknowledgments

All the authors are grateful to the Mexican institution CONACYT for its valuable support.

References

[1] Field, A.B., Eddy currents in large slot-wound conductors. American Institute of Electrical Engineers, Transactions 26, pp. 761-788, 1905. DOI: 10.1109/PAIEE.1905.6742159.

[2] Burdío, M., Monterde, F., Garcia, J.R., Barragan, L.A. and Martinez, A., A two-output series-resonant inverter for induction-heating cooking appliances. Power Electronics, IEEE Transactions on, 20(4), pp. 815-822, 2005. DOI: 10.1109/TPEL.2005.850925.

[3] Boadi, A., Tsuchida,Y., Todaka,T. and Enokizono, M., Designing of suitable construction of high-frequency induction heating coil by using finite-element method. Magnetics, IEEE Transactions, 41(10), pp. 4048-4050, 2005. DOI: 10.1109/TMAG.2005.854993.

[4] Bayındır, N.S., Kükrer, O. and Yakup, M., DSP-based PLL-controlled 50–100 kHz 20 kW high frequency induction heating system for surface hardening and welding applications. IEE Proceedings - Electric Power Applications, 150(3), pp. 365-371, 2003. DOI: 10.1049/ip-epa:20030096.

[5] Grooms, J.P. and Mattson, L.J., Method for induction sealing an inner bag to an outer container, US 5416303A, [Online]. 16 May 1995. http://www.google.st/patents/US5416303.

[6] Jordan, A., Scholz, R., Maier-Hauff, K., Johannsen, Wust, M., Nadobny, P.J., Schirra, H., Schmidt, H., Deger, S., Loening, S., Lanksch, W. and Felix, R., Presentation of a new magnetic field therapy system for the treatment of human solid tumors with magnetic fluid hyperthermia. Journal of Magnetism and. Magnetic. Materials, 225(1–2), pp. 118-126, 2001. DOI: 10.1016/S0304-8853(00)01239-7.

[7] Cano, M.E., Barrera, A., Estrada, J.C., Hernandez, A. and Córdova, T., An induction heater device for studies of magnetic hyperthermia and specific absorption ratio measurements. Review of Scientific Instruments, 82(11), pp. 114904-114904-6, 2011. DOI: 10.1063/1.3658818.

[8] Mazón-Valadez, Ernesto Edgar, et al. Developing a fast cordless soldering iron via induction heating. DYNA 81(188), pp. 166-172, 2014. DOI: 10.15446/dyna.v81n188.41635.

[9] Miyazaki, M., System and method for induction heating of a soldering iron, US/2010/0258554 A1, October 14 of 2010.

[10] Snown C., Alternating current distribution in cylindrical conductors, en Scientific Papers of the Bureau of Standards, USA, Washington, [Online]. 1925. 277. http://www.google.com/patents/US20100258554.

[11] Buschow, K.H.J., Encyclopedia of Materials: Science and Technology. Michigan: University of Michigan, 8, Elsevier, 2001.

[12] Kittel, C., Introduction to Solid State Physics, New York: John Wiley & Sons, 6th Ed, 1986.

[13] Brown, G.H., Hoyler, C.N. and Bierwirth, R.A., Theory and applications of the radiofrequency heating, New York: D. Van Nostrand Company, 1947.

[14] Dwight, H.B, A precise method of calculation of skin effect in isolated tubes. Journal of the American Institute of Electrical Engineers, 42(8), pp. 827-831, 1923. DOI: 10.1109/JoAIEE.1923.6593471.

[15] Jackson J.D., Classical Electrodynamics, New York: Wiley, 3rd Ed. 1998.

[16] Yoshimura, K., et al. Soldering iron with replaceable tip. U.S.

[17] Patent No. 8,569,657. [Online]. 29 Oct. 2013. Available at: http://www.google.ms/patents/WO2005115670A2?cl=en.

[18] Kent, G.M., Method of manufacturing replaceable soldering iron tips. U.S. Patent No. 3,315,350. [Online]. 25 Apr. 1967. Available at: https://www.google.com/patents/US3315350.

[19] Llorente, S., Monterde, F., Burdio, J.M. and Acero, J., A comparative study of resonant inverter topologies used in induction cookers, Applied Power Electronics Conference and Exposition, 7th. Annual IEEE, pp.1168-1174, 2002. DOI: 10.1109/APEC.2002.989392.

[20] Ye, Z., Jain, P.K. and Sen, P.C., Full-bridge resonant inverter with modified phase-shift modulation for high-frequency AC power distribution systems, IEEE Transactions on Industrial Electronics, 54(1), pp. 2831-2845, 2007. DOI: 10.1109/TIE.2007.896030.

[21] Goya, G.F., Cassinelli, N. and Ibarra-García, M.R., Magnetic hiperthermia application device, PCT/ES2009/000235, [Online]. November 12 of 2009. Available at: https://www.google.com/patents/EP2283895A1?cl=en&dq=Magnetic+Hyperthermia+Application+Device&hl=es-419&sa=X&ved=0ahUKEwitspiKq8bKAhXCRCYKHW90DaYQ6AEIIDAA.

[22] Calleja, H., Fast response control circuit for resonant inverters, International Journal of Electronics, 89(3), pp. 233-244, 2002. DOI: 10.1080/00207210210122550.

[23] Kamli, M., Yamamoto, S. and Abe, M., A 50-150 kHz half-bridge inverter for induction heating applications. IEEE Transactions on Industrial Electronics, 43(1), pp. 163-172, 1996. DOI: 10.1109/41.481422.

[24] Tai, Ch.-Ch. and Chen, M.K., The design of a half-bridge series-resonant type heating system for magnetic nanoparticle thermotherapy. PIERS [Online] 4 (2) pp. 276-280, 2007. DOI: 10.2529/PIERS070907021847.
[25] Hincapié, J.N. et al. Electrónica de potencia para el calentamiento por inducción doméstico: Revisión del estado del arte, Ingeniería y Ciencia, [Online] 9(18), pp. 237-262, 2013. Available at: http://www.scielo.org.co/pdf/ince/v9n18/v9n18a14.pdf.
[26] Tai Ch.-Ch. and Cheng, M.-K., Anti-interference design of quasi-resonant tank for magnetic induction heating system. PIERS, [Online]. 4(2) pp. 417-420, 2008. DOI: 10.2529/PIERS070907021437.
[27] Mazón-Valadez, E.E. et al., Comparison between the heating rates of a magnetic induction soldering iron and another one composed of resistance, Soldagem & Inspeção 20(2), pp. 228-237, 2015. DOI: 10.1590/0104-9224/SI2002.10.

C. Mazón-Valadez, received his BSc. degree in 2015 from the Universidad of Guadalajara, México in the Centro Universitario de la Ciénega of the Universidad de Guadalajara. His research interests include: Administration Technology.
ORCID: 0000-0001-7989-6935.

L.H. Quintero-Hernández, received his PhD in Administration in the Centro Universitario de Ciencias Económico-Administrativas. His research interests include: Small and Medium Enterprises, also design and development of technological innovation.
ORCID: 0000-0002-9222-927X.

E.E. Mazón-Valadez, received his MSc. degree in Exact Sciences and Engineering in the Centro Universitario de la Ciénega of the Universidad de Guadalajara, México. His research interests include: Magnetic Hyperthermia, Resonant Inverters and SAR.
ORCID: 0000-0002-0553-5325.

A.Hernández-Sámano, received his MSc. Phys degree in 2013 from the University of Guanajuato, México, he is a PhD. student in Physics in the Centro Universitario de la Ciénega of the Universidad de Guadalajara, México. His research interests include: Magnetic Hyperthermia, Resonant Inverters and Magnetism.
ORCID: 0000-0003-2684-313X.

J. Ávila-Paz, received his PhD. in 2015 from the Centro Universitario de la Ciénega of the Universidad de Guadalajara, México. He is currently professor in the Department of Technologic Sciences at the same university. His research interests include: magnetic hyperthermia, automation and control, and embedded systems.
ORCID: 0000-0002-4358-1090.

M.E. Cano-González, received his PhD. degree in Physics in 2007 from the University of Guanajuato, México. He is Full professor in the Basic Sciences department in the Centro Universitario de la Ciénega of the Universidad de Guadalajara, México. His research interests include: magnetic hyperthermia, resonant inverters and Monte Carlo simulations.
ORCID: 0000-0002-3334-0082.

Área Curricular de Ingeniería
Eléctrica e Ingeniería de Control

Oferta de Posgrados

Maestría en Ingeniería - Ingeniería Eléctrica

Mayor información:

E-mail: ingelcontro_med@unal.edu.co
Teléfono: (57-4) 425 52 64

UNIVERSIDAD NACIONAL DE COLOMBIA
SEDE MEDELLÍN
FACULTAD DE MINAS

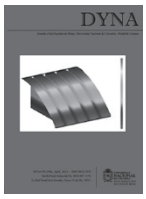

DYNA
http://dyna.medellin.unal.edu.co/

Microstructure and electrical properties of solid electrolytes of fully stabilized zirconia with rare earth mixed oxides

Rodrigo Arbey Muñoz-Meneses [a]; Paola Cristina Cajas-Daza [b]; Jose Luis Narvaez-Semanate [c] & Cosme Roberto Moreira-da Silva [d]

[a] *Facultad GAMA, Universidad de Brasília, Brasília, Brasil. ramunoz@unb.br*
[b] *Facultad de Tecnología, Universidad de Brasília, Brasília, Brasil. patolacajas@gmail.com*
[c] *Corporación Universitária Comfacauca – Popayán, Colombia. joselitopop@hotmail.com*
[d] *Facultad de Tecnología, Universidad de Brasília, Brasília, Brasil. cosmeroberto@gmail.com*

Received: July 17th, 2015. Received in revised form: January 18th, 2016. Accepted: February 02th, 2016

Abstract
In this work was obtained solid electrolytes of fully stabilized zircônia with doped of 10 and 12 mol% of Re2O3 (mixed oxides rare earth), for use in oxygen sensors and or fuel cells. The specimens were prepared by uniaxial pressing and sintered using two heating schedules, S1 and S2. Impedance diagrams show that the crystalline phases and the grain size change the electrical behavior of the ceramics. The sample with the best electrical performance was obtained with 10 mol% doped and was sintered with the curve S1. The value of the total conductivity of this sample was 2,85x10-3 Ω-1.cm-1 (taken at 600 ° C). When making a comparison between this values of conductivity with the reported in the literature is identified similarity with or traditional system zirconia-yttria the most widely used commercially as electrolyte oxygen sensors and fuel cells, confirming the potential use of the oxides mixed rare earth for these specific applications.

Keywords: Oxygen sensor, Grain growth; Grain boundaries; Solid oxide fuel cells; Sintering temperature; Electrical impedance

Microestructura y propiedades eléctricas de electrólitos sólidos de circonia totalmente estabilizada con óxidos mixtos de tierras raras

Resumen
En este trabajo fueron obtenidos electrólitos sólidos de circonia totalmente estabilizada, para uso en sensores de oxigeno y/o celdas combustibles, con dopado de 10 e 12 % mol de Re_2O_3 (óxidos mixtos de tierras raras). Los cuerpos de prueba fueron confeccionados por prensado uniaxial y sinterizados usando dos cronogramas de calentamiento, *S1* y *S2*. Diagramas de impedancia revelan que tanto las fases cristalinas presentes cuanto el tamaño de grano tienen influencia sobre el comportamiento eléctrico de las cerámicas. La muestra más conductora fue obtenida con 10% mol de dopado y sinterizada con la curva *S1*. El valor de conductividad total de esta muestra fue de $2{,}85x10^{-3}$ $\Omega^{-1}.cm^{-1}$ (tomada en 600°C). Al realizar una comparación directa de estos valores de conductividad con los reportados en la literatura, se identifica semejanza con el sistema tradicional circonia-ítria, el sistema más usado comercialmente como electrólito en sensores de oxígeno y celdas combustibles, confirmando el potencial uso de los óxidos mixtos de tierras raras para estas aplicaciones específicas

Palabras clave: sensores de oxígeno, crecimiento de grano; contornos de grano; celdas combustibles; sinterización; espectroscopia de impedancia

1. Introducción

Electrólitos sólidos a base de circonia totalmente estabilizada han sido ampliamente estudiados en las últimas décadas por su elevada conducción iónica en un amplio rango de temperatura y presiones parciales de oxígeno [1,2]. Las aplicaciones más destacadas de estos materiales son como sensores de oxígeno y celdas combustibles las cuales ganaron destaque a nivel científico por el impacto ambiental, al ayudar en el control de la contaminación atmosférica y en la generación de energía limpia, respectivamente.

© The author; licensee Universidad Nacional de Colombia.

Una celda combustible, por ejemplo, presenta ventajas en la generación de energía pues en algunos casos puede convertir más del 90% de la energía contenida en un combustible en energía eléctrica y calor, además por no poseer partes móviles, las celdas combustibles presentan más confianza cuando comparadas con los motores de combustión interna. Otra de las múltiples ventajas que se pueden citar es que al substituir las centrales termoeléctricas convencionales que producen electricidad a través de combustibles fósiles se mejorará la calidad de aire y se reducirá el consumo de agua, como también se reducirá el descarte de agua residual. Uno de los aspectos que merece principal atención son las emisiones de gases contaminantes que estos dispositivos presentan, pues se ha determinado que son diez veces menores de lo que estipulan las normativas ambientales además de producir niveles inferiores de dióxido de carbono [3].

Con un sensor de oxígeno, por su vez, se cambió de forma radical la forma como era suministrado el combustible en los vehículos, que hasta la época lo hacían con el llamado carburador, con la imposibilidad de modificar la entrega de la cantidad de combustible cuando el motor estaba encendido en diferentes situaciones de tráfico ocasionando problemas de rendimiento en los motores y emisiones de gases contaminantes debido a la quema, de forma inadecuada, del combustible. La función del sensor de oxígeno es la de monitorear la cantidad de oxígeno existente en los gases de escape, justo después de la combustión, y emitir un voltaje proporcional a esta cantidad, el cual es recibido e interpretado por la unidad de control electrónico la cual regula la cantidad de combustible entregado al motor, variando el tiempo que se tienen abiertos los inyectores [4].

Para estas dos aplicaciones el electrólito sólido es el encargado de:

1. Separar dos regiones expuestas a diferentes gases: gas de escape y gas atmosférico en el caso del sensor de oxígeno y, del mismo modo, separa el gas oxidante y el gas combustible para las celdas combustibles,
2. Permitir alta movilidad del ion oxígeno entre las dos regiones anteriormente citadas [5].

Motivado por estas aplicaciones, por el impacto científico y ambiental, en este trabajo se utilizó un aditivo para la estabilización de la circonia diferente del utilizado convencionalmente, denominado *óxidos mixtos de tierras raras*, el cual contiene como óxido mayoritario el óxido de itrio con 76 % en peso, con el objetivo principal de obtener circonia totalmente estabilizada. Se utilizó el método de los precursores poliméricos "Pechini" para la obtención de la materia prima.

2. Materiales y Métodos

Fueron usados los siguientes materiales para el desarrollo de este trabajo:

- ZrO2:10% mol Re_2O_3 (Z10-Pch), material compuesto por 11% de circonia tetragonal y 89% de circonia cúbica [6].
- ZrO2:12% mol Re_2O_3 (Z12-Pch), material compuesto por 100% de circonia cúbica [6].
- Alcohol isopropílico, grado analítico.

Antes de confeccionar los cuerpos de prueba, una molienda mecánica en molino de atricción fue realizada a la materia prima con el objetivo de romper los aglomerados presentes. La molienda fue realizada en alcohol isopropílico, y agitadas por 1 hora. Fueron utilizadas bolas de circonia (2 mm de diámetro) como material moledor en una relación 1:4. Después de la molienda, la materia prima fue secada, desagregada y tamizada en tamiz de 0,045 mm de abertura de malla. Utilizando la técnica de prensado uniaxial, fueron compactados cuerpos de prueba en troquel cilíndrico de aproximadamente 10 mm de diámetro. La presión usada fue de 187 MPa por 30s, con prensa Marcon MPH-10, en el laboratorio de ingeniería mecánica de la universidad de Brasília. Los cuerpos de prueba compactados fueron sinterizados en horno resistivo Nabertherm LHT407GN6 en temperatura de 1400 °C, por 2h, sin control de atmosfera, utilizando dos cronogramas de calentamiento a seguir:

Cronograma *S1*: El cronograma de sinterización *S1* fue usado para producir cuerpos de prueba densos, con porosidad aislada y promoviendo el crecimiento de grano. Estas características son favorecidas en temperaturas altas, pues dependen de mecanismos de sinterización térmicamente activados como la difusión por el contorno de grano y la difusión volumétrica. En este trabajo fue usada la temperatura de 1650 °C por cinco minutos, para activar estos mecanismos de sinterización.

Cronograma *S2*: El cronograma de sinterización *S2* consiste en la forma "tradicional" de sinterización usada en trabajos anteriores [7]. Caracterizada por tener una rampa de calentamiento rápida, 10 °C/min, hasta la temperatura de 1000 °C, con estancia de cinco minutos. Posteriormente la velocidad de calentamiento es disminuida a 3 °C/min, hasta alcanzar la temperatura de sinterización, manteniéndose a esta temperatura por dos horas y, finalmente, una rampa de enfriamiento a una velocidad de 5 °C/min. Estos cronogramas de sinterización pueden ser observados en la Fig. 1.

La respuesta eléctrica de los electrólitos sólidos sinterizados fue estudiada a través de la espectroscopia de impedancia. Electrodos de platina *Pt- paste Demetron 308-A* fueron depositados en sus caras paralelas y posteriormente curados a 1100 °C por 20 minutos. La impedancia de las muestras en estudio fue colectada en un rango de frecuencia de 1 MHz hasta 1 Hz, una tensión de 1000 mV fue usada, utilizando un equipo *Solartron* 1260 del laboratorio de materiales vítreos (*LAMAV*) de la Universidad Federal de San Carlos-Brasil. El rango de temperatura usada fue de 250-600 °C. A partir de los espectros de impedancia fue posible cuantificar el aporte resistivo/capacitivo de las diferentes regiones de la muestra, grano y contorno de grano además de la resistencia total.

3. Resultados y Discusión

La distribución y forma de las partículas que componen la materia prima debe estar libre de aglomerados, pues su presencia promueve la formación de cuerpos de prueba con baja densidad, comprometiendo sus propiedades mecánicas y eléctricas, entre otras [8]. Observación por microscopia electrónica de barrido (*MEB*) fue realizada en la materia

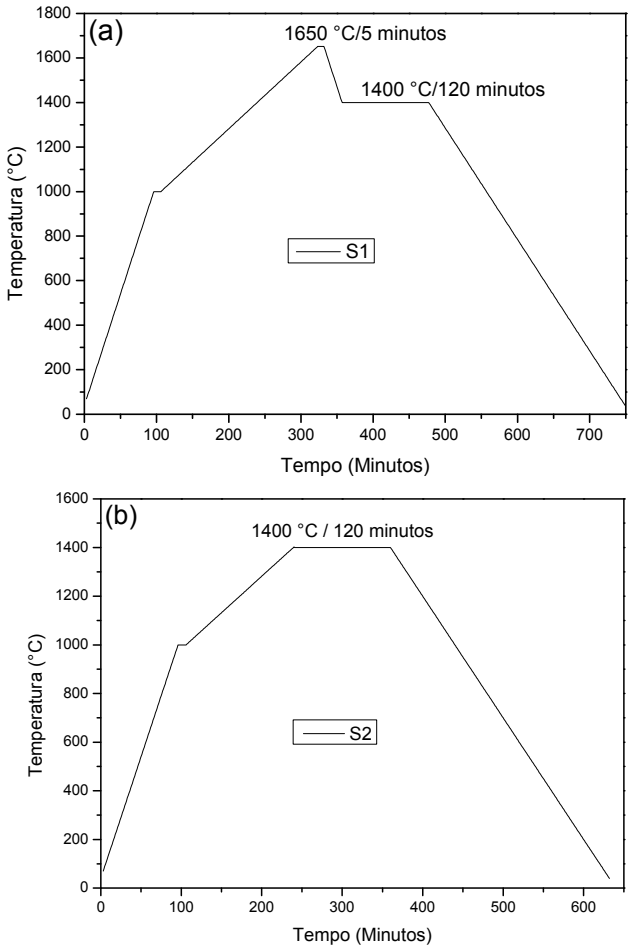

Figura 1. Cronogramas de sinterización utilizados en este trabajo, (a) S1 e (b) S2
Fuente: Los autores

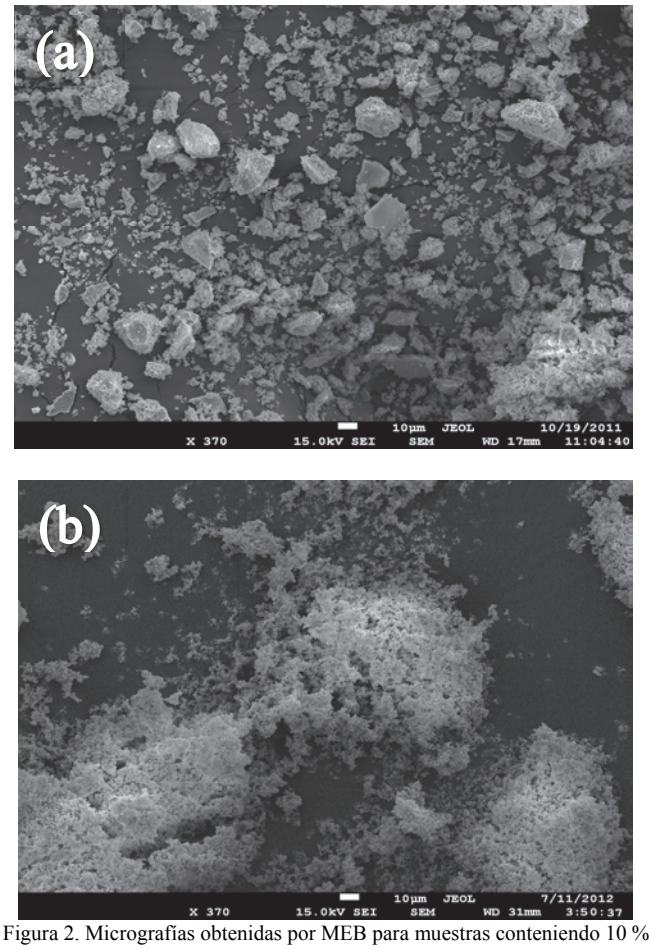

Figura 2. Micrografías obtenidas por MEB para muestras conteniendo 10 % mol de dopado, (a) antes de la molienda y (b) después de la molienda, ampliación 370X.
Fuente: Los autores

prima antes y después de la molienda, como se puede observar en la Fig. 2. En esta figura son presentadas micrografias representativas de las muestras en estudio. Es posible observar dos (2) tipos de aglomerados, fuertes y partículas con ligaciones débiles, Fig. 1 (a), se puede destacar también de esta figura el tamaño acentuado dos aglomerados, siendo en algunos casos, mayores que 10 µm. La Fig. 1 (b) presenta micrografias obtenidas por *MEB* después de la molienda, evidenciando que los aglomerados fuertes fueron desagregados en este proceso. Con la materia prima en este formato se procedió a la compactación y sinterización de los cuerpos de prueba conforme descrito en el procedimiento experimental.

Se sabe que la densidad obtenida después de la sinterización tiene influencia directa en las propiedades mecánicas, térmicas, ópticas y eléctricas finales de los materiales [9], por tal motivo, en este trabajo, se considera importante obtener cuerpos de prueba densos, con porosidad aislada, a fin de viabilizar las propiedades eléctricas de la circonia, ya que este tipo de defecto, la porosidad, es considerada una fase que bloquea los portadores de carga. La densidad aparente de los cuerpos de prueba fue calculada, usando el método de Arquímedes con inmersión de cuerpos de prueba en agua destilada, y comparada con la densidad teórica del material. Valores de densidad relativa fueron calculados e indexados en una tabla para mejor interpretación, Tabla 1. Para efectos de comparación también fueron conformados cuerpos de prueba sin molienda de la materia prima y sinterizados solamente con la curva de sinterización S1, estando estos valores también presentes en la Tabla 1. Es posible observar de la Tabla 1 una considerable diferencia en la densidad de los cuerpos de prueba que fueron sometidos al proceso de molienda, tornando esta etapa del procesamiento cerámico fundamental para la obtención de cuerpos de prueba densos, con densidades superiores a los 92% de la densidad teórica, conforme previsto para aplicaciones en sensores de oxígeno y celdas combustibles [10].

Se puede notar también de la Tabla 1 que la densidad de los cuerpos de prueba fue favorecida por el cronograma de sinterización utilizado, siendo mayor para cuerpos de prueba sinterizados con el cronograma de sinterización *S1*. Este resultado fue el esperado, pues los cuerpos de prueba que estuvieron sometidos a temperaturas altas (1650 °C), mismo que por corto periodo de tempo (5 minutos), presentaron crecimiento de grano y reducción acentuada de porosidad, como puede ser apreciado en las imágenes de la Fig. 3, obtenidas por microscopia electrónica de barrido.

Tabla 1
Densidad relativa y densidad teórica para los diferentes cuerpos de prueba sinterizados.

Muestra	Densidad relativa (%)			Densidad Teórica (g/cm³) [11]
	Cronograma de sinterización S1		Cronograma de sinterización S2.	
	Sin molienda	Con molienda		
Z10-Pch	85,85	92,84	91,35	6,01
Z12-Pch	80,13	94,65	93,65	5,99

Fuente: Los autores

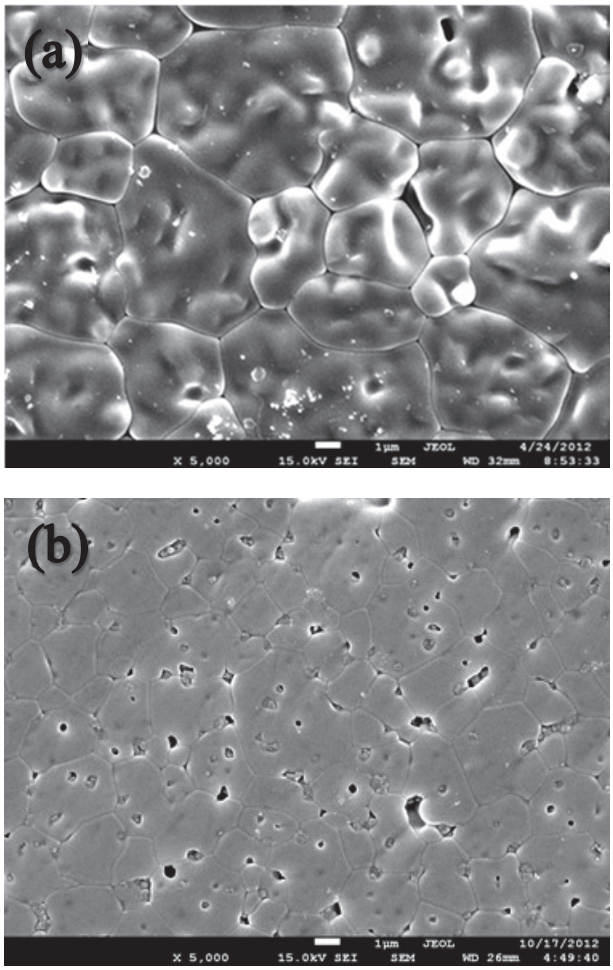

Figura 3. Micrografías obtenidas por MEB de la superficie de los cuerpos de prueba sinterizados: (a) Z10-Pch S1, (b) Z10-Pch S2, ampliación 5000X. Fuente: Los autores

Se puede notar de las Figs. 3 y 4, cuando se compara las micrografías de una misma composición y diferente cronograma de sinterización, por ejemplo, *Z12-Pch* (Fig. 4 c y d), los aspectos microestructurales, tales como tamaño medio de grano y la porosidad, están completamente ligados a el cronograma de sinterización utilizado. Esta muestra en particular, cuando sinterizada con el cronograma *S2*, presenta un tamaño medio de grano de aproximadamente 3,03 µm y porosidad con formatos irregulares localizados en los pontos triplos y poros esféricos localizados en el interior de los granos. Los aspectos microestructurales de la misma muestra sinterizada con el cronograma *S1* cambian considerablemente. El tamaño medio de grano aumento para 7,97 µm y el formato de los poros es esférico y localizado preferencialmente en el interior de los granos. Estos resultados indican que los mecanismos de sinterización que densificam, tales como difusión por el contorno de grano y la difusión por el volumen, actuaron de forma efectiva en estas muestras. Además, el aspecto visual de las muestras sinterizadas con el cronograma *S1* demuestra que el proceso de sinterización alcanzo la etapa final, caracterizada de forma general para materiales cerámicos, como microestructuras con porosidad reducida o ausente, acompañada de crecimiento del tamaño de grano. Se puede inferir entonces, que el cronograma de sinterización *S1* promueve satisfactoriamente los mecanismos de transporte de masa como a difusión de contornos de grano y la difusión volumétrica. Estos resultados son considerados de interés por dos motivos:

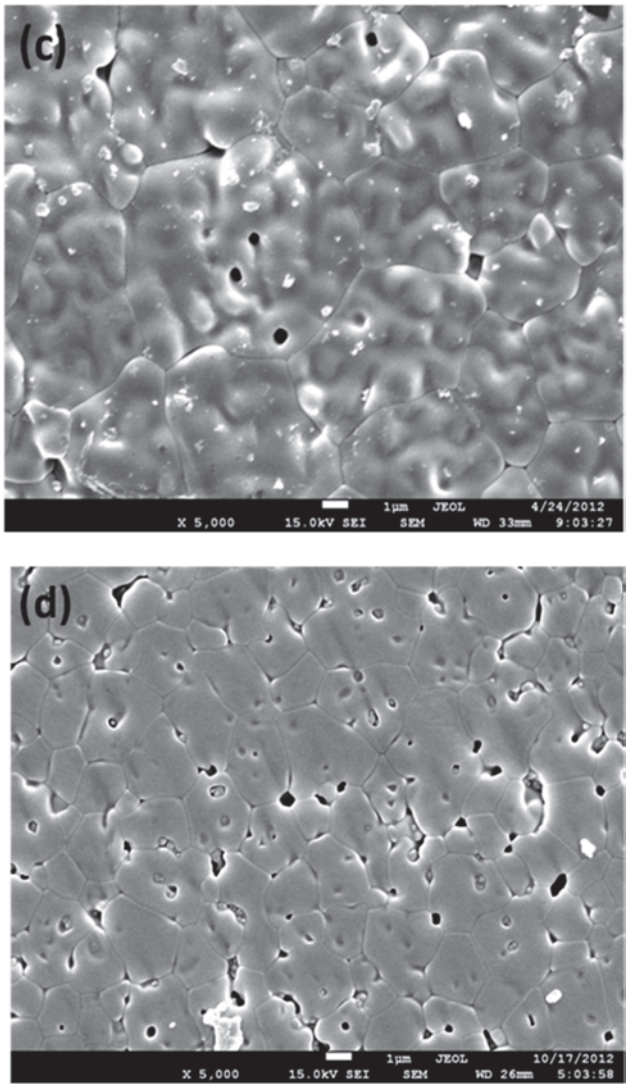

Figura 4. Micrografías obtenidas por MEB de la superficie de los cuerpos de prueba sinterizados: (c) Z12-Pch S1, (d) Z12-Pch S2, ampliación 5000X. Fuente: Los autores

Tabla 1
Tamaño medio de grano para los diferentes cuerpos de prueba sinterizados.

Muestra	Tamaño medio de grano (μm)	
	Cronograma de sinterización S1	Cronograma de sinterización. S2
Z10-Pch	6,52 ± 0,24	2,96 ± 0,31
Z12-Pch	7,97 ± 0,23	3,03 ± 0,41

Fuente: Los autores

- En términos de propiedades eléctricas, cuanto menor cantidad de contornos de grano en la muestra, menor será resistividad atribuida a este parámetro físico, promoviendo aumento de la conductividad total del material.
- La porosidad, intragranular e intergranular, son consideradas elementos o fases que se oponen al flujo de carga. La disminución de estas porosidades resulta en la mejoría de las propiedades erétricas.

Utilizando micrografías con menor aumento, en este estudio 1500X, fue efectuada la medición del tamaño medio de grano por medio de contaje del número de intersecciones existentes entre el contorno de grano y líneas rectas con longitud conocida. Estos resultados fueron indexados en la Tabla 2.

El análisis cuantitativo de la diferencia en el tamaño de grano obtenido fue atribuido al cronograma de sinterización, ya que los dos tipos de muestras fueron procesados de forma idéntica. Este resultado fue el esperado, pues la temperatura alta (1650 °C) en el cronograma de sinterización *S1*, por un tiempo de cinco minutos, favoreció la velocidad de sinterización, obteniendo cuerpos de prueba densos con dos horas de sinterización. Otros aspectos microestructurales son identificados de las micrografías: poros en los contornos de grano y en el interior de los granos y lo más importante, uniformidad en el tamaño y forma de los granos.

Finalmente, la respuesta eléctrica de las cerámicas sinterizadas fue estudiada a través de la espectroscopia de impedancia, pues esta técnica de caracterización permite establecer la dependencia en el comportamiento eléctrico de las diferentes regiones de la cerámica, grano y contorno de grano, con la temperatura. La Fig. 5 presenta diagramas típicos de impedancia para las muestras en estudio en la temperatura de 300 °C y son diferenciados claramente dos semicírculos que, en el estudio de materiales cerámicos, son atribuidos a las contribuciones resistivo capacitivas del grano (altas frecuencias) y las contribuciones resistivo capacitivas de los contornos de grano (bajas frecuencias) [10]. A partir de los diámetros de estos semicírculos sus respectivas resistividades fueron obtenidas. Cabe resaltar que estos diagramas de impedancia ya fueron corregidos por el factor geométrico de los cuerpos de prueba y que la información que está ilustrada en la figura se encuentra en parámetros de resistividad.

Se observa de la Fig. 5 (a), para la cerámica que contiene10% mol de dopante, que esta muestra presenta resistividad en el interior del grano de 437 KΩ.cm cuando sinterizada con el cronograma *S2*. Entretanto, este valor es disminuido para 290 KΩ.cm cuando utilizado el cronograma *S1*. Este comportamiento es justificado debido a la completa estabilización de la circonia, ya que la circonia totalmente estabilizada es más conductora que la parcialmente estabilizada, resultado que fue evidenciado con *DRX* usando el cronograma *S1*, [11].

Analizando la resistividad atribuida a los contornos de grano, Fig. 5, es posible observar una reducción en su valor. A Z10-Pch disminuyo en 61 KΩ.cm e Z12-Pch disminuyo en 228 KΩ.cm, comportamiento esperado debido a su modificación microestructural que fue confirmada por *MEB*. De esta forma queda claro que a disminución de la densidad de contornos de grano afecta, de forma benéfica, el comportamiento eléctrico de las cerámicas en estudio.

Con los valores de resistividad obtenidos para cada temperatura de ensayo, fue posible calcular la conductividad y, además, observar el comportamiento térmicamente activado de la conductividad total de las cerámicas. Esta dependencia de la conductividad con la temperatura es interpretada como un aumento en la movilidad del ion oxígeno.

Observando la Fig. 6(a) queda más evidente que el aumento de la conductividad de las cerámicas es dependiente de la temperatura de ensayo. También es evidente que, para una misma muestra, esta grandeza es favorecida debido al cronograma de sinterización utilizado. Este comportamiento pode ser atribuido a dos factores principales:

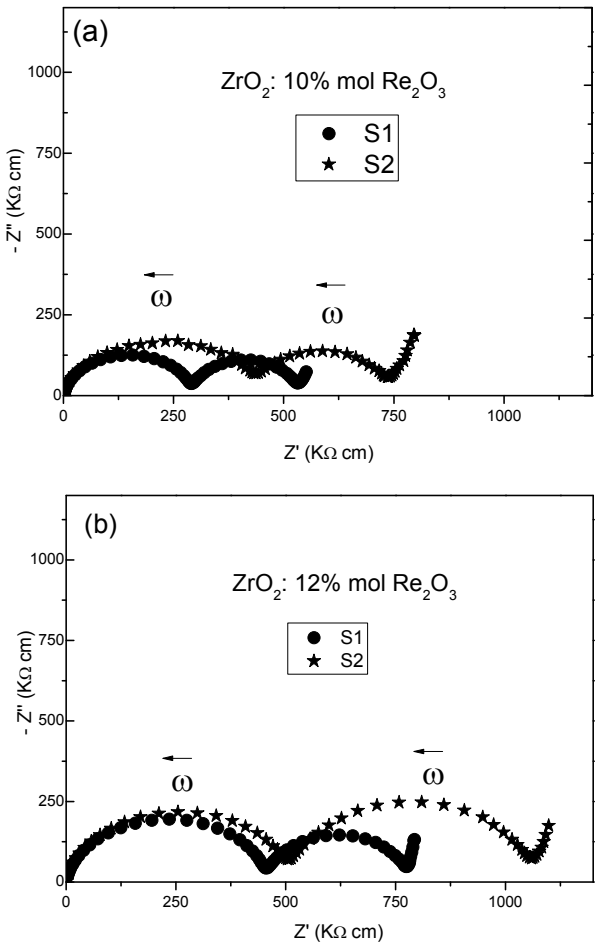

Figura 5. Diagramas típicos de impedancia de las muestras en estudio tomados en la temperatura de 300 °C: (a) Z10-Pch, (b) Z12-Pch
Fuente: Los autores

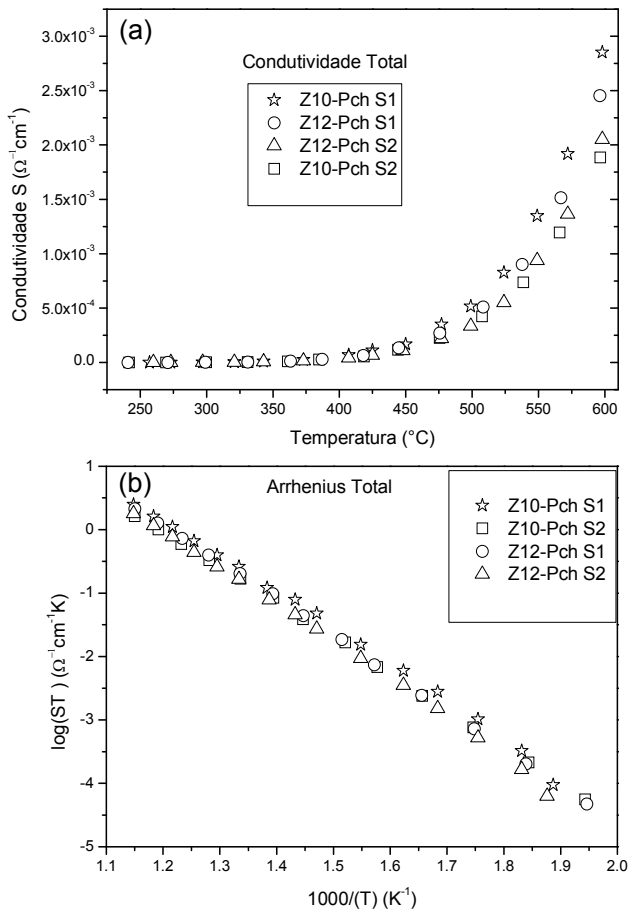

Figura 6. (a) Dependencia de la conductividad con la temperatura para la conductividad total de las cerámicas en estudio y (b) Gráficos de Arrhenius de la conductividad (log (σ TVs 1/T)) de las cerámicas referente al proceso conductivo total.
Fuente: Los autores

(i) Aumento en el tamaño de grano: físicamente para todas las muestras el aumento en el tamaño de grano implica disminución de la densidad de contornos de grano, hecho que facilita a migración de los iones oxígeno [12],
(ii) Transformaciones de fase: aumento en la conductividad favorecida con la utilización del cronograma de sinterización S1 para muestras con 10 e 12% mol de dopado, por la completa estabilización de la circonia.

Para completar los análisis eléctricos fueron construidos los gráficos de Arrhenius (Log σT Vs. 1000/T) de los cuales fue posible obtener la energía de activación para el proceso de conducción, Fig. 6(b). La energía de activación representa la energía mínima necesaria para iniciar el proceso de conducción [13].

Fue observada para cada muestra en estudio una única inclinación de la recta en el intervalo de temperatura estudiado, consecuentemente ellas no presentan desvíos en el comportamiento del tipo Arrhenius. Esta apreciación fue posible al linealizar cada reta e calcular los coeficientes de correlación (R^2), los cuales están indexados en la Tabla 3. En este caso el coeficiente de correlación está próximo de la unidad para todos los ajustes, indicando que el grado de dispersión de los puntos experimentales está alrededor de una recta hipotética. De la inclinación de estas retas hipotéticas fueron obtenidas las energías de activación total para las muestras sinterizadas con los cronogramas S1 y S2 y expuestas en la Tabla 3, presentando valores similares a los encontrados en trabajos anteriores, para conductores de oxígeno basados en óxido de circonio que están en el rango de 1 a 1.2 eV [14], [15].

Tabla 3.
Energía de activación (Ea) calculada a partir das curvas de Arrhenius para el sistema obtenido pelo método Pechini.

Muestra	Ea Total (eV)	R^2
Z10-Pch-S1	1,06	0,997
Z12-Pch-S1	1,11	0,999
Z10-Pch-S2	1,09	0,999
Z12-Pch-S2	1,12	0,998

Fuente: Los autores

Finalmente y considerando que uno de los objetivos de este trabajo era comprobar el uso del carbonato de tierras raras como aditivo de estabilización de la circonia, para posible uso en sensores de oxígeno en celdas combustibles, se comparo el resultado de las caracterizaciones eléctricas de la mejor muestra obtenida en este trabajo con valores de conductividad reportados en la literatura para sistemas de circonia, los cuales usan aditivos de estabilización de elevada pureza. Estos valores de conductividad se encuentran en la Tabla 4, donde se puede observar que los resultados obtenidos en este trabajo se encuentran en el mismo orden de grandeza en el rango de temperatura de 400 a 600 °C. Considerando linealidad en un rango de temperatura mayor en los gráficos de Arrhenius, por ejemplo hasta 800 °C, temperatura de operación de los sensores de oxígeno y celdas combustibles, se extrapoló esta gráfica para obtener el valor de conductividad en esta temperatura. Estos valores extrapolados constan también en la Tabla 4 siendo diferenciados por una estrella (*), presentando comportamiento eléctrico del orden dos 10^{-2} $\Omega^{-1}cm^{-1}$, el cual se encuentra en el orden de grandeza de los conductores de iones de oxígeno.

4. Conclusiones

En este trabajo fue usado el método de los precursores poliméricos (Pechini) con la intención de preparar sistemas basados en circonia/óxidos mixtos de tierras raras. Como ventajas de este método se puede destacar: utilización de materia prima de bajo costo, simplicidad de producción, homogeneidad química y reproductibilidad del proceso. Adicionalmente, se destaca la incorporación de una materia prima poco beneficiada, específicamente el carbonato de tierras raras, en la producción de dispositivos de alta tecnología, concretamente en la fabricación de electrólitos sólidos para aplicaciones en sensores de oxígeno y/o celdas combustibles.

Tabla 4.
Comparación de la conductividad total de las cerámicas obtenidas en este trabajo con muestras reportadas en la literatura, obtenidos en la temperatura de 400, 600 e 800 °C.

Muestra	Densidad aparente (%)	Conductividad Total (400 °C) ($10^{-5}\Omega^{-1}cm^{-1}$)	Conductividad Total (600 °C) ($10^{-3}\Omega^{-1}cm^{-1}$)	Conductividad Total (800 °C) ($10^{-2}\Omega^{-1}cm^{-1}$)
Z10-Pch-S1	92,84	7,00	2,85	4,89*
8 mol% Y_2O_3	92	-	0,59 [16]	-
8 mol% Y_2O_3	94	-	-	3,0 [17]
8 mol% Y2O3	99	-	-	6,7 [18]
8 mol% Y2O3	-	7,30 [19]		
7,75 mol% Sc2O3	94	-	-	5,88 [20]
12 mol % Y2O3	5,90	2,6 [21]	-	-

Fuente: Los autores

En las condiciones de molienda impuestas, una hora en molino de atrito, se observó cualitativamente la reducción de los aglomerados presentes en el polvo cerámico. Este resultado favoreció la acomodación de las partículas en la compactación y favoreció una alta densidad (superior a los 92 % de la teórica) en los CPS después de la sinterización.

El tamaño de grano de los cuerpos de prueba, sinterizados a 1400 °C por dos horas fue dependiente del cronograma de sinterización utilizado: muestras sinterizadas con el cronograma S2 tienen tamaños medios de grano de 2,96 µm, con un aumento a 6,52 µm cuando usado el cronograma de sinterización S1. Estos resultados indican, conforme relatado en la literatura, que los mecanismos de sinterización, difusión por el contorno de grano y difusión por el volumen operaran de forma efectiva en estas muestras, indicando que el proceso de sinterización llego a su etapa final, con microestructura homogénea y porosidad reducida, acompañada de crecimiento de grano.

La conductividad atribuida al contorno de grano fue dependiente del tamaño de grano, para muestras con la misma composición y sinterizadas con los cronogramas de sinterización S1 y S2. Una posible explicación para este fenómeno está relacionada al hecho de que muestras con tamaños de grano mayor, presentan menor cantidad de contornos de grano por unidad de volumen, consecuentemente la resistividad atribuida a los contornos de grano va a ser reducida, ocasionando un incremento de la conductividad total de las cerámicas.

Finalmente, la conductividad de la mejor muestra, Z10-Pch, fue de $2.85x10^{-3}\ \Omega^{-1}\ cm^{-1}$ tomada a 600 °C. Para saber su posible conductividad en temperaturas próximas a 800 °C, se hizo una extrapolación de la curva de Arrhenius hasta esta región. Se encontró en este caso un valor de conductividad de $4,89\ x10^{-2}\ \Omega^{-1}\ cm^{-1}$, cuyo orden de magnitud es similar al reportado en la literatura para materiales conductores de iones oxígeno.

Bibliografía

[1] Huijsmans, J., Ceramics in solid oxide fuel cells, Current Opinion in Solid State and Materials Science, 5(4), pp. 317-323, 2001. DOI: 10.1016/S1359-0286(00)00034-6

[2] Murray, E.P., Tsai, T. and Barnett, S.A., Oxygen transfer processes in (La, Sr) MnO_3/Y_2O_3 -stabilized ZrO_2 cathodes : an impedance spectroscopy study, Solid State Ionics, 110, pp. 235-243, 1998. DOI: 10.1016/S0167-2738(98)00142-8.

[3] Portal Energia: Vantagens e desvantagens das células de combustível. [Online]. [Consulta: 28 Enero 2016]. Mensaje archivado en: http://www.portal-energia.com/celulas-de-combustivel-vantagens-e-desvantagens/

[4] Mecánica básica: Función del sensor de oxígeno. [Online]. [Consulta: 28 Enero 2016]. Mensaje archivado en: http://www.mecanicabasicacr.com/auto/funcion-del-sensor-de-oxigeno.html

[5] Lopez, F.J. Desarrollo de sensores ópticos para gases y diseño de instrumentación portátil., Tesis Doctoral. Departamento de Química Analítica, Universidad de Granada, España, 365 P, 2005.

[6] Muñoz, R.A., Rodriguez, J.E. and Silva, C.R.M. Study of polymorphs of zirconia in the system ZrO2: η wt% Re2O3 Obtained by polymeric precursor method, Materials Science Forum, 727–728, pp. 1340-1344, 2012. DOI: 10.4028/www.scientific.net/MSF.727-728.1340.

[7] Muñoz, R.A., Rodrigues, A.C.M., Santos, C. and Silva, C.R.M., Effect of rare earth addition on electrical properties of zirconia based ceramics, Materials Science Forum, 660–661, pp. 652-657, 2010. DOI: 10.4028/www.scientific.net/MSF.660-661.652.

[8] Ferreira, L.F., Efeito das inclusões nanométricas de zircônia na obtenção de nanocompósitos de alumina-zircônia, Dissertação de MSc., Programa de posgraduaçao en Stricto Sensu em Engenharia e Ciência dos Materiais. Universidade de São Francisco, Brasil, 80 P, 2006.

[9] Galmarini, S, Ceramics: Sintering and microstructure, Work Practices Ceramics Process: TP3 Sintering, pp. 1–15, 2011.

[10] Caproni, E., Eletrólitos sólidos cerâmicos à base de óxido de zircônio para a detecção de oxigênio, Tese de Doutorado, 88 P., 2007.

[11] Muñoz, R.A., Microestrutura e propriedades elétricas da zircônia dopada com óxidos mistos de terras raras para aplicação como eletrólito sólido em sensores de oxigênio., Tese de Dr. .Programa de pós-Graduação em Sistemas Mecatrônicos. Departamento de Engenharia Mecânica. Universidade de Brasília-UnB, Brasil., 151 P, 2013.

[12] Irvine, J.T.S., Sinclair, D.C. and West, A.R., Electroceramics: characterization by impedance spectroscopy, Advanced Materials, 2(3), pp. 132-138, 1990. DOI: 10.1002/adma.19900020304

[13] Peters, A., Korte, C., Hesse, D., Zakharov, N. and Janek, J., Ionic conductivity and activation energy for oxygen ion transport in superlattices — The multilayer system CSZ (ZrO_2+CaO)/Al_2O_3, Solid State Ionics, 178(1–2), pp. 67-76, 2007. DOI: 10.1016/j.ssi.2006.12.004

[14] Muccillo, E.N.S., Condutores de íons oxigênio - uma breve revisão (Oxygen-ion conductors - a brief review), Cerâmica, 54, pp. 129-144, 2008. DOI: 0.1590/S03666913200800020002

[15] Abélard, P. and Baumard, J., The electrical conductivity of cubic stabilized zirconia the results of an IUPAC collaborative study, Pure and Applied Chemistry, 67(11), pp. 1891-1904, 1995.
[16] Zhang, C., Li, C.-J., Zhang, G., Ning, X.-J., Li, C.-X., Liao, H. and Coddet, C., Ionic conductivity and its temperature dependence of atmospheric plasma-sprayed yttria stabilized zirconia electrolyte, Materials Science and Engineering: B, 137(1–3), pp. 24-30, 2007. DOI: 10.1016/j.mseb.2006.10.005
[17] Li, G. and Ren, R., Preparation of YSZ-TZP solid electrolytes by gel-casting technology, Journal of Environmental Sciences, 23, pp. S170-S172, 2011. DOI: 10.1016/S1001-0742(11)61105-4
[18] Yao, H.-C., Wang, X.-W., Dong, H., Pei, R.-R., Wang, J.-S. and Li, Z.-J., Synthesis and characteristics of nanocrystalline YSZ powder by polyethylene glycol assisted coprecipitation combined with azeotropic-distillation process and its electrical conductivity, Ceramics International, 37(8), pp. 3153-3160, 2011. DOI: 10.1016/j.ceramint.2011.05.055
[19] Pimenov, A., Ullrich, J., Lunkenheimer, P., Loidl, A. and Ruscher, C. H., Ionic conductivity and relaxations in ZrO_2–Y_2O_3 solid solutions, 109, pp. 111-118, 1998. DOI: 10.1016/S0167-2738(98)00082-4
[20] Badwal, S.P.S., Electrical conductivity of Sc_20_3-ZrO_2 compositions by 4-probe d . c . and 2-probe complex impedance techniques, Journal of Materials Science, 18, pp. 3117-3127, 1983.
[21] Badwal, S.P.S. and Swain, M.V., ZrO_2-Y_2O_3 : Electrical conductivity of some fully and partially stabilized single grains, Journal of Materials Science Letters, 4, pp. 487-489, 1985.

R. Muñoz-Meneses, posee el título de Ingeniero Físico por la Universidad del Cauca, Colombia, con estudios de MSc. y Dr. en la Universidad de Brasília, Brasil. Actualmente, es profesor adjunto en la Universidad de Brasília, Brasil. Sus intereses de investigación incluyen las celdas combustibles, sensores de oxígeno y los materiales compuestos.
ORCID: 0000-0003-4634-8910

P. Cajas-Daza, posee el título de Ingeniera Física por la Universidad del Cauca, Colombia, con estudios de MSc. en la Universidad de Brasília, Brasil. Actualmente, es estudiante de doctorado en la Universidad de Brasília. Sus intereses de investigación incluyen las celdas combustibles, sensores de gas y los materiales cerámicos en general.
ORCID: 0000-0001-5008-7886

J. Narvaez-Semanate, posee el título de Ingeniero Físico por la Universidad del Cauca, Colombia, con estudios de MSc. y Dr. en la Universidad Federal de San Carlos, Brasil. Actualmente, es profesor en la Universidad del Cauca. Sus intereses de investigación incluyen las vitrocerámicas, sensores de gases y caracterización de materiales cerámicos.
ORCID: 0000-0002-4937-1414

C. Moreira da Silva, es profesor en el Departamento de Ingeniería Mecánica de la Universidad de Brasília, Brasil. Es PhD. en Materials Science por la UMIST - University of Manchester Institute of Science and Technology). Actúa en el área de materiales, en propiedades mecánicas, fluencia, celdas combustibles, metalurgia do polvos, fatiga y desgaste abrasivo.
ORCID: 0000-0001-6301-6446

UNIVERSIDAD NACIONAL DE COLOMBIA
SEDE MEDELLÍN
FACULTAD DE MINAS

Área Curricular de Ingeniería
Geológica e Ingeniería de Minas y Metalurgia

Oferta de Posgrados

Especialización en Materiales y Procesos
Maestría en Ingeniería - Materiales y Procesos
Maestría en Ingeniería - Recursos Minerales
Doctorado en Ingeniería - Ciencia y Tecnología de Materiales

Mayor información:

E-mail: acgeomin_med@unal.edu.co
Teléfono: (57-4) 425 53 68

UNIVERSIDAD NACIONAL DE COLOMBIA
SEDE MEDELLÍN
FACULTAD DE MINAS

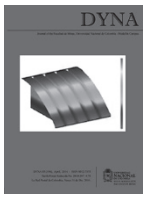

DYNA
http://dyna.medellin.unal.edu.co/

Analysis of working nanofluids for a refrigeration system

Diana C. Hernández [a], César Nieto-Londoño [b] & Zulamita Zapata-Benabithe [c]

[a] *Grupo de Energía y Termodinámica, Universidad Pontificia Bolivariana. Medellín, Colombia. dianacarolina.hernandez@upb.edu.co*
[b] *Grupo de Investigación en Ingeniería Aeroespacial, Facultad de Ingeniería Aeronáutica, Universidad Pontificia Bolivariana, Medellín, Colombia. cesar.nieto@upb.edu.co*
[c] *Grupo de Energía y Termodinámica, Facultad de Ingeniería Química, Universidad Pontificia Bolivariana, Medellín, Colombia. zulamita.zapata@upb.edu.co*

Received: May 28th, de 2015. Received in revised form: November 19th, 2015. Accepted: December 22th, 2015

Abstract
This paper presents the analysis of nanorefrigerant fluids to improve the thermal efficiency of a refrigeration system. Simulations in ANSYS FLUENT 15.0 were performed with mixtures of refrigerants R113, R123 and R134a, with Al_2O_3 nanoparticles at 1 vf% and 5 vf% (vf%, fraction volume concentration), flowing through a horizontal tube with a constant wall temperature. A mixture and the *k-e* turbulent models were employed to obtain results of heat transfer coefficient, temperature and pressure drop for each case. Results show an increment in thermal characteristics by adding 1 vf% and 5 vf% of Al_2O_3 nanoparticles to the three refrigerants selected. However, the size of the nanoparticle does not affect the thermal properties of nanofluid and the pressure drop does not show a specific pattern of behavior at different concentrations of nanoparticles. Finally, the mixture of R134a with 30 nm of mean diameter size Al_2O_3 at 1 vf% was selected because of its higher thermal efficiency and its favorable properties as a refrigerant.

Keywords: Nanofluids; Refrigeration system; Thermal efficiency; Heat transfer coefficient.

Análisis de nanofluidos para un sistema de refrigeración

Resumen
Este trabajo presenta el análisis de nanofluidos para mejorar la eficiencia térmica de un sistema de refrigeración. Se realizaron simulaciones en ANSYS FLUENT 15.0 de la mezcla de refrigerantes R113, R123 y R134a, con nanopartículas de Al_2O_3 al 1 vf% y 5 vf% de concentración, fluyendo a través de un tubo horizontal con temperatura de pared constante. Se empleó el modelo de mezcla Mixture, y el modelo de turbulencia k-e para obtener resultados del coeficiente de transferencia de calor, temperatura y caída de presión para cada uno de los casos. Los resultados muestran un aumento en las características térmicas de los tres refrigerantes utilizados. Sin embargo el tamaño de las nanopartículas no afecta las características del nanofluido, y no se presenta una tendencia en el comportamiento de la caída de la presión a diferentes concentraciones de nanopartículas. Finalmente se seleccionó la mezcla de R134a y partículas de 30 nm de diámetro de Al_2O_3 al 1vf% debido a su mayor eficiencia térmica y a sus mejores características como refrigerante.

Palabras clave: nanofluidos; sistema de refrigeración; eficiencia térmica; coeficiente de transferencia de calor.

1. Introduction

1.1. Refrigeration Systems

Refrigeration is a thermal process in which heat transfer is promoted between a system and a refrigerating fluid to remove heat and maintain a low temperature. Refrigeration systems are used for domestic, commercial and industrial applications. Additionally, they are used for food preservation, air conditioners and in the transportation industry. Refrigerants are those kinds of fluids that have the ability to absorb heat at low temperatures and pressures, and yield to higher temperatures and pressures. They can be classified into five groups [1]:

- Halocarbon: CFC-11 or R-11, CFC-12 or R-12, CFC-113 or R-113, CFC-114 or R-114 and CFC-115 or R-115.
- Hydrocarbons (HC): Methane (R-50), ethane (R.170), propane (R-290), n-butane (R-600), and isobutane (R-600a).
- Inorganic compounds: ammonia (R-717), water (H_2O), air (R-729), carbon dioxide (R-744) and sulfur dioxide (SO_2).

© The author; licensee Universidad Nacional de Colombia.

- Azeotropic mixtures: R-502 (48.8% R-22 and R-115 51.2%), R-500 (73.8% R-12 and R-152a 26.2%), R-503 (59.95% R-13 and R-23 40.1%), and R-504 (48.2% R-32 and R-115 51.8%).
- Zeotropic Mixtures: R-401A and R-401B.

Several authors have studied and identified the optimal parameters for optimal performance of the compression refrigeration cycle [1-5]. No fluid is ideal in all aspects; each refrigerant can have negative properties such as toxicity, chemical instability, flammability, high operating pressures or poor thermodynamic properties. Currently, the most widely used fluid in refrigeration and air conditioners is limited to HFCs refrigerants R134a, R32, R125, R143a and mixtures of these, as well as some hydrocarbons (propane and isobutane), ammonia and dioxide carbon [2].

Historically inorganic natural refrigerants such as R717, R744, R764, R11 or R12 have been used as CFCs and HCFCs such as R22, and R502 mixture [3]. Currently HFCs like R32 and R134a are used as replacement refrigerants, as well as zeotropic as mixtures of HFCs R404A, R407C, R410A, R507 azeotropic mixtures of HFCs and natural hydrocarbons such as R600a and R290. The CFC refrigerants R11 and R12 have been substituted by R123 (HCHC) and R134a (HFC) refrigerants with a reduction in impact on the deterioration of the ozone layer [3]. R134a is still a greenhouse gas, so in the future must be replaced. R152a, CO_2 and R1234yf have been considered as possible replacements of this. However, R152a is a flammable fluid, making it difficult to use and CO_2 requires higher working pressure than R134a, which is not practical for a refrigeration system.

Many studies have been undertaken on the impact of refrigerants in the deterioration of the ozone layer and global warming**.** Efforts have focused on finding an alternative fluid as an ideal substitute. However, the probability of finding an ideal refrigerant is practically zero, due to the number of factors that are involved in the performance of refrigeration systems [6]**.** R123 has replaced R11 in centrifugal chillers. It is a low pressure, high efficiency refrigerant, and miscible with mineral lubricants. R123 is safer than R11, but a long-term alternative to replace it (R245fa or R245ca) must be found. HCHC are less reactive than CFCs, because of their hydrogen content. R123 has a lifetime in the atmosphere and a lower ODP (Ozone Depletion Potential) than CFCs. However, the Montreal Protocol has limited its use since January 1, 1996 and is expected to gradually decrease its use until 2030 [7].

HFCs have better environmental characteristics than the CFCs because they contain no chlorine atoms and zero ODP. In [7] the authors present the R134a as an attractive option and a long-term alternative to replace R12 and R22. According to the information reported in the literature, R123 and R134a refrigerants were selected. Zeotropic and azeotropic mixtures were not chosen because their properties and characteristics are more complex for computational analysis to be undertaken. However, these mixtures are not discarded for further analysis. Additionally, testing with refrigerant R113, which has been extensively studied in experimental and computational evidence, was performed in order to have a point of comparison and validation of results.

1.2. Nanofluids

Nanofluids are a suspension of particles between 0 and 100 nm in a base fluid. They have thermophysical properties different to the base fluid due to the addition of metal or metal oxide particles to increase the coefficients of thermal conduction and convection [8,9]. The main characteristic of nanofluids is the ability to enhance heat transfer without altering the base fluid Newtonian behavior with the addition of small concentrations of solid particles [10].

Experimental and numeric tests have been performed in order to better understand the behavior of these fluids and their characteristics. Studies have focused on thermal conductivity, convective heat transfer coefficient, viscosity, evaporation phenomenon, the influence of particle size and optimal concentration of particles. Some of the advantages to using nanofluids proposed by Choi in [11] are:

- High specific surface area and therefore greater heat transfer surface between particles and fluid.
- High stability of the dispersion where the Brownian motion of particles dominates.
- Reduction of the pumping power in comparison with the base liquid, to achieve an equivalent heat transfer.
- Reduced clogging particles compared to conventional suspensions, promoting miniaturization of the system.
- Adjustable properties by varying the concentration of particles.

In [12], the authors describe the challenges faced in studying nanofluids and its characteristics such as thermal conductivity, the Brownian motion of particles, migration of these and the variation of thermophysical properties with change in temperature [8]. The long-term stability of the dispersion of nanoparticles is a technical challenge to prevent the accumulation and sedimentation of particles. The pressure drop and higher pumping power should also be considered to determine the efficiency of nanofluids. Other challenges include an increase in viscosity with greater concentration of particles, low specific heat compared to the base fluid, the prediction of thermal conductivity, high costs and production processes.

1.3. Nanorefrigerants

Recently nanoparticles have been used to enhance the thermophysical properties of refrigerants in order to achieve greater efficiency and profitability in refrigeration and air conditioning. In the literature, studies have reported rheological and heat transfer mechanisms to different concentrations of CuO nanoparticles, Al_2O_3, SiO_2, diamond, CNT (carbon nanotube), TiO_2 as refrigerants R11, R113, R123, R134a and R141b [12]. The effect of the size of the nanoparticles on heat transfer in mixtures of refrigerant, oil and nanoparticles is investigated experimentally with R113, VG68 oil and Cu particles with diameters of 20, 50 and 80 nm [13]. The results show a maximum increase of 23.8 % in the heat transfer coefficient in a pool nucleate boiling with reduced diameter from 80 to 20 nm.

One of the main factors in the efficiency of a refrigeration system with nanorefrigerants is the heat transfer in the phase change of the heat exchangers (evaporator and condenser). Heat transfer by flow boiling of a nanorefrigerant was studied by Peng et al. [14] using a mixture of R113 and CuO

particles. Experimental tests show a 29.7 % increase in the heat transfer coefficient due to the addition of CuO nanoparticles. Peng et al. [14] also proposed a correlation for heat transfer in nanorefrigerants and obtained a deviation of ± 20 % with the experimental results.

Peng et al. [14] propose using the impact factor of the nanoparticle to correct the coefficient of heat transfer of the pure refrigerant. The impact factor of the F_{HT} nanoparticle is shown in eq. (1).

$$F_{HT} = exp\left\{\varphi\left[0.8\frac{k_n}{k_{r,L}} - 39.94\frac{(\rho C_P)_n}{(\rho C_p)_{r,L}} - 0.028G - 733.26x(1-x)\right]\right\}, \quad (1)$$

where the subscript "n" and "r, L" represent the properties of nanoparticles and pure refrigerant, respectively. k is the thermal conductivity, ρ is the density, C_P is the isobaric specific heat, φ is the volume fraction of the nanoparticles, G is the mass flux and x is vapor quality. To find the heat transfer coefficient, Peng, et al. used eq. (2) [14].

$$h_{r,n} = F_{HT}h_r, \quad (2)$$

where h represents the heat transfer coefficient for both, refrigerant and the nanoparticle suspension.

Various combinations of nanoparticles have been studied to analyze the boiling heat transfer by flow boiling of a refrigerant in a horizontal pipe [15]. The nanorefrigerants they used were Cu-Al-R141b, Al_2O_3-R141b, and CuO-R141b. They did some experimental tests where the heat transfer coefficient increased by varying the mass fraction of nanoparticles. Cu particles have a better effect on improving the performance of heat transfer of nanorefrigerants due to their high thermal conductivity. Other factors influencing the performance of nanorefrigerants are mass flux and vapor quality.

The research reported in the literature focuses on the analysis of heat transfer single phase nanofluids, and some reference pool nucleate boiling. However, the research on phase change in flow boiling of nanofluids, which are very common in refrigeration systems, heat exchangers and air conditioners, is very limited. Boiling characteristics and nanofluids flow in two phases dependent on properties such as specific heat, latent heat, density, surface tension, to name but a few [16]. Further research is needed to enable a better understanding of the properties of nanofluids and how to measure them in evaporation and condensation systems for application in a refrigeration cycle.

Mahbubul et al. [17] conducted a study of the characteristics of heat transfer and pressure drop to a mixture of Al_2O_3-R141b for different concentrations and phase change due to flow boiling. The analysis was performed in a pipe of 6 mm of diameter and 1000 mm of length. The analysis was undertaken with an inlet temperature of 298 K, a pressure of 78,535 kPa, a mass flux of 100 kg/m^2.s and an input speed of 5 m/s, resulting in a turbulent flow through the pipe. The wall was subjected to a uniform heat flux of 5000 W/m^2. They used a correlation given by [14] to calculate the heat transfer coefficient. They found that both heat transfer and pressure drop increase with increasing volume concentration of nanoparticles, which can improve the performance of cooling systems by increasing energy efficiency and cooling capacity.

In a subsequent study, Mahbubul et al. [18] investigated the thermophysical properties, pressure drop and heat transfer of 30 nm Al_2O_3 nanoparticles suspended in the R-134a refrigerant. Nanoparticle concentration varied from 1 vf% to 5 vf% [17]. The pipe used for analysis was 8.12 mm of diameter and 1500 mm of length. Entry conditions were 706 kPa, 300 K, uniform mass flux of 100 kg/m^{2}s, 5 m/s of velocity and a uniform wall heat flow rate of 5000 W/m^2. In the research presented in this paper, these data were taken as a reference for the analysis of different nanorefrigerants, but using a constant wall temperature of 330 K and a temperature of 298.15 K at the inlet of the pipe.

Simulations were carried out in ANSYS FLUENT 15.0 varying the working fluid (R113, R123 and R134a), with 0 vf.%, 1 vf.% and 5 vf.% of Al_2O_3 nanoparticle concentration. Two cases were studied, at 0.5 m/s and 5 m/s (Reynolds number for R134a of 24239.40 and 242394.0 respectively) inlet velocity in a horizontal tube with a constant wall temperature. Results were compared taking into account the change in pressure drop, temperature through the tube, heat transfer coefficient and thermal conductivity between the base fluid and the nanofluid. The properties of the nanoparticles and refrigerants are shown in Table 1 and 2 respectively, these are considered constant for the study.

In [19] and [20] the properties of the nanofluid were obtained before the simulation because it was taken as a single phase model. For this reason, the Brownian effects were taken into account in order to calculate the effective thermal conductivity. In the present study, the nanofluid has a change of phase from liquid to vapor, and it is considered to be a multiphase model where particles and fluid were solved using a mixture model. "The mixture model solves the continuity equation for the mixture, the momentum equation for the mixture, the energy equation for the mixture, and the volume fraction equation for the secondary phases, as well as algebraic expressions for the relative velocities (if the phases are moving at different velocities)" [21]. The effective thermal conductivity is calculated by Fluent as a summatory of the thermal conductivity of each phase plus the turbulent thermal conductivity given by the turbulent model used.

2. Mathematical models

Two approaches have been reported in the literature to model dynamic phenomena and heat transfer of nanofluids [10]. The first approach treats nanofluids as a single phase fluid, assuming that the solid particles are in thermal equilibrium with the fluid phase and the relative velocity between them is zero. The second approach found in the literature adopted a two-phase flow, where the moving speed between the particles and the fluid is not necessarily zero. Authors argue that simulations that treat the solid phase and liquid separately have more accurate results when seen as a single phase. The most appropriate used model to simulate the flow of the two phases in CFD is the mixture model.

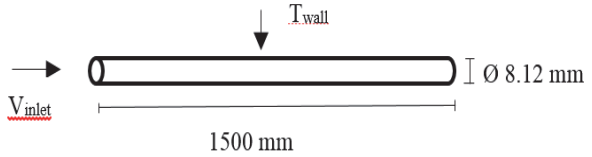

Figure 1. Model diagram
Source: The authors.

Table 1.
Properties of Al_2O_3 nanoparticles

Properties	Al_2O_3
Density, kg/m3	3880
Heat Capacity, kJ/kgK	0,729
Thermal conductivity, W/mK	40

Source: The authors.

Table 2.
Properties of Refrigerants

Properties	R134a	R123	R113
Chemical Formula	CH_2FCF_3	$CHCl_2CF_3$	CCl_2FCClF_2
Molecular weight	102,03	152,93	187,35
Boiling Point at 1 atm, K	247,01	301,11	320,85
Liquid density at 298.15 K (25°C), kg/m^3	1206	1463	1563,05
Density (Saturated vapour) at boiling point, kg/m^3	5,25	6,47	3,467
Heat Capacity (liquid) at 298.15 K (25°C) and 1 atm, kJ/kgK	1,44	0,965	0,94
Heat Capacity (saturated vapour) at 298.15 K (25°C) and 1 atm, kJ/kgK	0,852	0,721	0,939
Thermal conductivity (liquid) at 298.15 K (25°C), W/mK	0,0824	0,081	0,068248
Thermal conductivity (vapour at 1 atm) at 298.15 K (25°C), W/mK	0,0145	0,0112	0,00849
Viscosity (liquid) at 298.15 K (25°C), mPa.s	0,202	0,456	0,653
Viscosity (vapour at 1 atm) at 298.15 K (25°C), mPa.s	0,012	0,011	0,0096

Source: The authors.

Akbari et al. in [22] developed a computational study of convection with a mixture of water and Al_2O_3 nanoparticles in a horizontal pipe. The analysis was carried out with uniform heat flow to compare the single-phase model, and the three CFD models for multiphase flow (Volume of Fluid, Mixture and Eulerian). The authors found very similar results for the hydrodynamic behavior of nanofluid. However, the thermodynamic results differ in the different models used; the two-phase model being more accurate. For successful results with the single phase model it is necessary to use complex correlations to effectively characterize the properties of the nanofluid.

There are two approaches for using the two phase model. The Lagrangian-Eulerian approach, which is used when the volume fraction of the secondary phase is less than 10 vf.% and the Eulerian-Eulerian approach for higher volume fractions. Generally the amount of nanoparticles used in nanofluids is very large even for very small volume fractions; therefore, it is not advisable to use the Lagrangian-Eulerian approach due to the high computational cost that this implies [22]. Moraveji et al. in [23] made a comparison between CFD models of one and two-phases to study heat transfer by flow boiling Al_2O_3-water with 100 nm nanoparticles, in a pipe with constant heat flux on the wall. Heat transfer is enhanced by increasing the concentration of nanoparticles and the Reynolds number. Numerical data were obtained using a correlation for the Nusselt number in a horizontal line based on the Reynolds (Re) and Prandtl (Pr) numbers and the volume fraction (φ) [23].

$$Nu = 0.716Re^{0.314}Pr^{0.6}\varphi^{0.3}. \quad (3)$$

The subcooled flow boiling of Al_2O_3-water with 30 nm nanoparticles was investigated numerically by Abedini et al. in [24]. The nanoparticles have a large effect on the thermophysical properties of the base fluid, such as viscosity, specific heat and density. In this case it is assumed that a nanofluid behaves as a homogeneous liquid due to the low volume fraction of vapor during subcooled boiling, so the system is solved by a two-phase model, the phase of nanofluid and the vapor phase [24]. A Mixture Eulerian model is used for the computational solution because it represents a simple way to solve the problem by obtaining a coefficient of heat transfer consistent with experimental data. The results show that increasing the concentration of nanoparticles increases the heat transfer. However, low concentrations of particles (1 – 2 vf.%) are more effective in heat transfer coefficient.

ANSYS Fluent has the ability to solve problems with multiphase flows, which are grouped into four categories: gas-liquid or liquid-liquid flow; gas-solid flow; liquid-solid flow; and three-phase flows [21].

The Mixture Model treats phases as interpenetrating continuous phases [25]. It solves the momentum, continuity, and energy equations for the mixture, and solves the equation of volume fraction for the secondary phases and prescribes relative velocities to describe the dispersed phases through algebraic expressions.

The Mixture Model selects granular phases and calculates their properties for application in liquid-solid flows. It also allows the phases move at different velocities using the concept of sliding velocities. The Mixture and the *k-e* turbulent models were employed to obtain results for the heat transfer coefficient and temperature, and the Coupled algorithm was chosen for the pressure–velocity coupling, which solves all equations for phase velocity corrections and shared pressure correction simultaneously [21].

The continuity equation for the mixture is:

$$\frac{\partial}{\partial t}(\rho_m) + \nabla(\rho_m \vec{v}_m) = 0, \quad (4)$$

where ρ_m is the density of the mixture and $\vec{v}_m$ is the averaged flow velocity:

$$\vec{v}_m = \frac{\sum_{k=1}^{n} \varphi_k \rho_k \vec{v}_k}{\rho_m}, \quad (5)$$

where the subindex k represents the phases of the mixture.

The mixture density is defined by:

$$\rho_m = \sum_{k=1}^{n} \varphi_k \rho_k. \tag{6}$$

The momentum equation for the mixture is obtained by adding momentum equations for each phase

$$\frac{\partial}{\partial t}(\rho_m \vec{v}_m) + \nabla(\rho_m \vec{v}_m \vec{v}_m) = -\nabla p + \nabla\left[\mu_m\left(\nabla\vec{v}_m + \nabla\vec{v}_m^T\right)\right] + \rho_m \vec{g} + \vec{F} + \nabla\left(\sum_{k=1}^{n} \varphi_k \rho_k \vec{v}_{dr,k}\vec{v}_{dr,k}\right), \tag{7}$$

where $\vec{g}$ is the acceleration of gravity, n is the number of phases, μ_m is the viscosity of the mixture and is defined by:

$$\mu_m = \sum_{k=1}^{n} \varphi_k \mu_k. \tag{8}$$

The drift velocity of the second phase $\vec{v}_{dr,k}$ is defined by:

$$\vec{v}_{dr,k} = \vec{v}_k - \vec{v}_m, \tag{9}$$

The energy equation is applied as follows:

$$\frac{\partial}{\partial t}\sum_{k=1}^{n}(\varphi_k \rho_k E_k) + \nabla \sum_{k=1}^{n}\left(\varphi_k \vec{v}_k(\rho_k E_k + p)\right) = \nabla(k_{eff}\nabla T) + S_E, \tag{10}$$

where E_k is the energy of each phase, T is the temperature, S_E includes others volumetric heat sources, and k_{eff} is the effective thermal conductivity, expressed as follows:

$$k_{eff} = \sum \varphi_k (k_k + k_t) \tag{11}$$

where $k_k$represents the thermal conductivity of each phase of the mixture and k_t is the turbulent thermal conductivity defined by the turbulent model used.

From the continuity equation for phase p, it can be can obtained the volume fraction equation of the secondary phase:

$$\frac{\partial}{\partial t}\left(\varphi_p \rho_p\right) + \nabla\left(\varphi_p \rho_p \vec{v}_p\right) = -\nabla\left(\varphi_p \rho_p \vec{v}_{dr,p}\right) + \sum_{q=1}^{n} \dot{m}_{qp} - \dot{m}_{pq}, \tag{12}$$

where $\vec{v}_p$ is the velocity of phase p and $\dot{m}_{pq}$ characterizes the mass transfer from the p_{th} to q_{th} phase.

3 Results and discussion

For the simulations, different meshes were used to validate the accuracy and consistency of the results, refining the mesh and comparing the heat transfer coefficient for each case. After a mesh independence study a mesh of 1'072.768 elements was selected because the results of the heat transfer coefficient do not change significantly with the mesh.

The results cannot determine the influence of the concentration of particles in the pressure drop of the pipe since the behavior is different in each case as shown in Fig. 2 and 3, where the pressure drop is presented for the three nanorefrigerants analyzed at different concentrations of nanoparticles with a mean size diameter of 30 nm, and a different Reynolds number.

The pressure drop for simulations with an initial velocity of 0.5 m/s does not show a pattern that determines the influence of the size and concentration of nanoparticles. In this case, pressure drop for nanorefrigerant R134a and 30nm Al_2O_3 at 1vf% is 4022.5 Pa. By increasing the initial velocity at 5m/s, the pressure drop increases significantly, but is not affected by the size or by the concentration of particles. For nanorefrigerant R134a and 30nm Al2O3 at 1vf% at v=5m/s, the pressure drop is 47071.14 Pa.

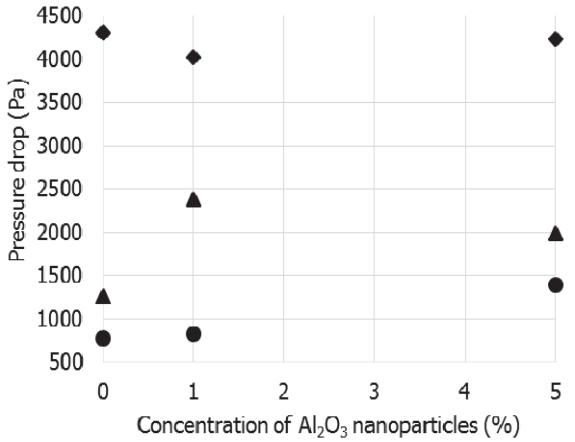

Figure 2. Pressure drop at 0.5 m/s velocity for Al2O3-R113 Re = 9718.19 (●), Al2O3-R123 Re = 13025.83 (▲) and Al2O3-R134a Re = 24239.40(♦), with 30 nm mean size diameter particles of Al2O3.
Source: The authors.

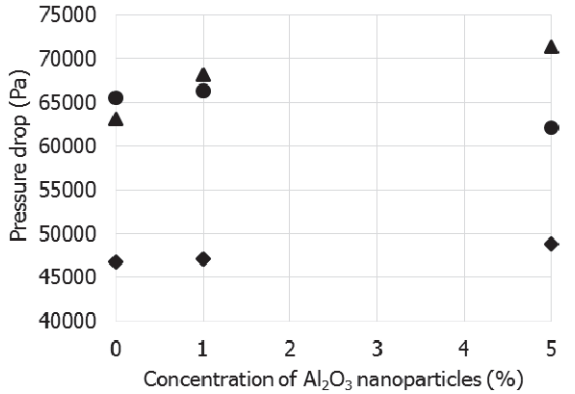

Figure 3. Pressure drop at 5 m/s velocity for Al_2O_3-R113 Re = 97181.9 (●), Al_2O_3-R123 Re = 130258.3 (▲) and Al_2O_3-R134a Re = 242394.0 (♦), with 30 nm mean size diameter particles of Al_2O_3.
Source: The authors.

An increase in the temperature of the fluid along the pipe is observed by adding nanoparticles and the improvement is greater by increasing nanoparticle concentration as shown in Fig.4. At the beginning of the pipe, the temperature of the three fluids is very similar, until 0.2 m when it starts to increase. The maximum values are obtained with a 5vf% nanoparticles concentration.

In Fig. 5a. the temperature contour in the upper half of the pipe and the velocity contour in the lower half, from the inlet through 0.2 m of length are shown, in order to compare the thermal and the hydrodynamic boundary layers. This is possible because of the symmetry of the problem. It can be observed that the thermal boundary layer develops more slowly than the hydrodynamic layer, which is why there is not a significant change in temperature in the first 0.2 m of length.

The temperature contour in the upper half of the pipe and the velocity contour in the lower half, from 0.2 m through 0.4 m of the pipe is shown in Fig. 5b., where the temperature starts to increase while the hydrodynamic boundary layer is nearly fully developed.

In addition, the influence of particle size on temperature and pressure drop was evaluated throughout the pipeline. It was observed that where the mean size of particle is 20 and 50 nm the temperature had the same behavior as in Fig. 4 where the particle size is 30 nm. Therefore, particle size does not have a significant impact on the temperature of the nanorefrigerant.

The heat transfer coefficient is presented in Fig.6. where a comparison of the three different nanorefrigerants is made at a 0.5 m/s velocity inlet with a 30 nm mean size diameter at 1 vf.% and 5 vf%. R134a has the greatest heat transfer coefficient at these conditions. Al_2O_3-R134a with 1 vf.% show a 24.60 % increase in the heat transfer coefficient in relation to the pure refrigerant, but only 11.73 % more with a concentration of 5 vf.% of particles. Al_2O_3-R113 shows an increase of 54.05 % of the heat transfer coefficient by adding 1 vf.% of nanoparticles to the pure refrigerant, and an increase of 21.16 % with 5 vf.% of nanoparticles. And Al_2O_3-R123 has a more linear behavior with a 9.87 % increase for 1 vf.% of nanoparticles in relation to the pure refrigerant and an increase of 31.62 % of the heat transfer coefficient with 5 vf.% of Al_2O_3.

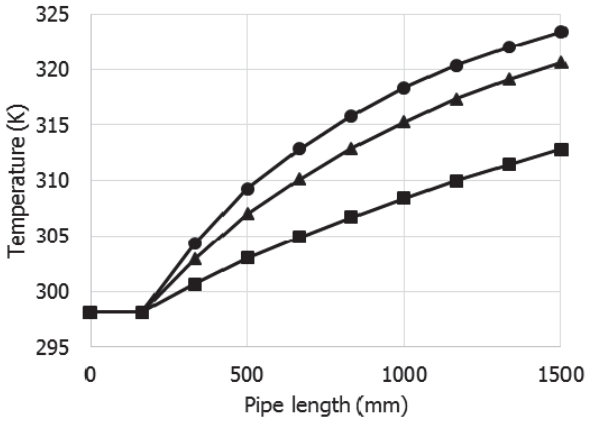

Figure 4. Temperature profiles of Al_2O_3-R134a at 0 vf.% (■), 1 vf.% (▲) and 5 vf.% (•) with 30 nm mean size diameter particles of Al_2O_3 through pipeline with 1.6 m of length.
Source: The authors.

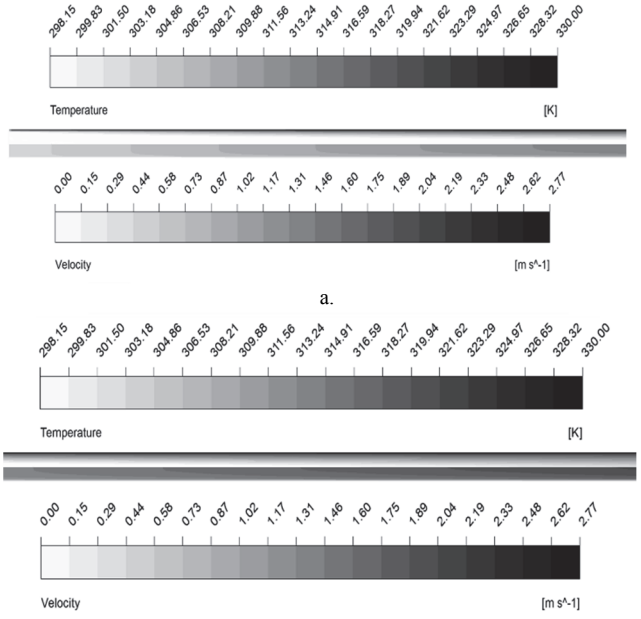

Figure 5. Temperature contour in the upper half of the pipe and velocity contour in the lower half at 0.5 m/s for Al2O3-R134a at 1 vf.% with 30 nm mean size diameter particles of Al2O3, a. from the inlet of the pipeline through 0.2 m of length. b, from 0.2 m of the pipeline through 0.4 m of length.
Source: The authors.

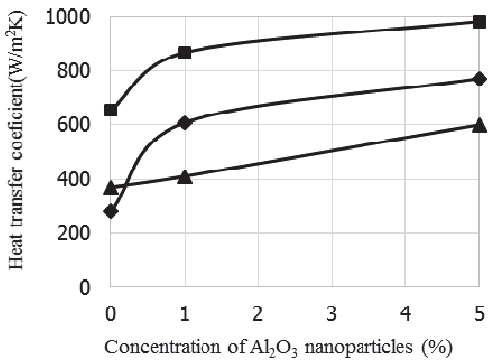

Figure 6. Heat transfer coefficient at 0.5 m/s velocity inlet for Al_2O_3-R113 (♦), Al_2O_3-R123 (▲) and Al_2O_3-R134a (■), with 30 nm mean size diameter particles of Al_2O_3
Source: The authors.

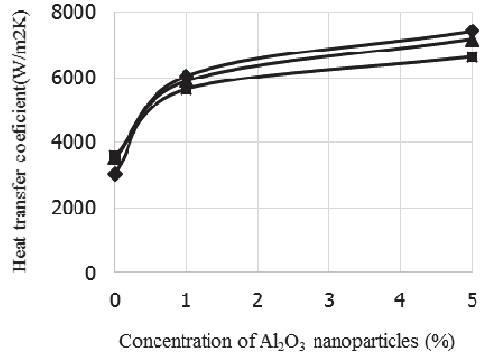

Figure 7. Heat transfer coefficient at 5 m/s velocity inlet for Al2O3-R113 (♦), Al2O3-R123 (▲) and Al2O3-R134a (■),with 30 nm mean size diameter particles of Al2O3.
Source: The authors.

Increasing the velocity inlet up to 5 m/s causes higher values of heat transfer coefficient, 3000 W/m^{2}K approximately, for base refrigerants. Fig. 7. shows a similar behavior of the heat transfer coefficient for 1 vf.% and 5 vf.% of nanoparticles. Adding 1 vf.% of Al_2O_3 to any of the studied refrigerants increases the heat transfer coefficient to 41 % approximately, and 17 % more by adding 5 % of nanoparticles, for a total of 58 % in relation to the pure refrigerant. The heat transfer coefficient was improved by increasing the nanoparticle concentration. However, the improvement with 5 vf.% of nanoparticles is not significant enough, and 1 vf.% of Al_2O_3 is adequate for further calculations.

Thermal conductivity in relation to the concentration of nanoparticles is presented in Fig. 8 and Fig. 9 at 0.5 m/s and 5 m/s respectively. These graphics show an increase in thermal conductivity by adding nanoparticles at different concentrations. Al_2O_3 nanoparticles has a great impact on R113 thermal conductivity at 0.5 m/s, while R123 and R134a have a lower thermal conductivity and a very similar tendency to increase. At 5 m/s the thermal conductivity of nanorefrigerants can have a very similar increase by adding more particles. In this example, particle size has no influence on thermal conductivity behavior.

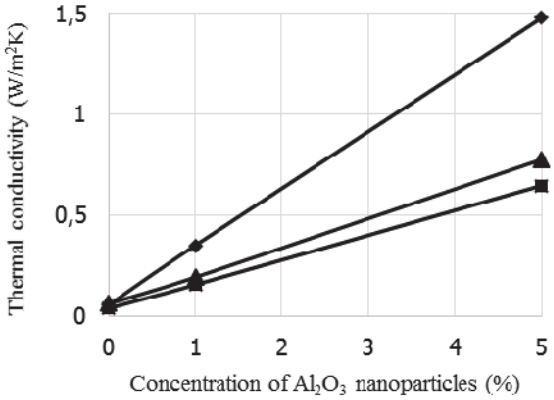

Figure 8. Thermal conductivity at 0.5 m/s velocity inlet for Al_2O_3-R113 (♦), Al_2O_3-R123 (▲) and Al_2O_3-R134a (■), with 30 nm mean size diameter particles of Al_2O_3.
Source: The authors.

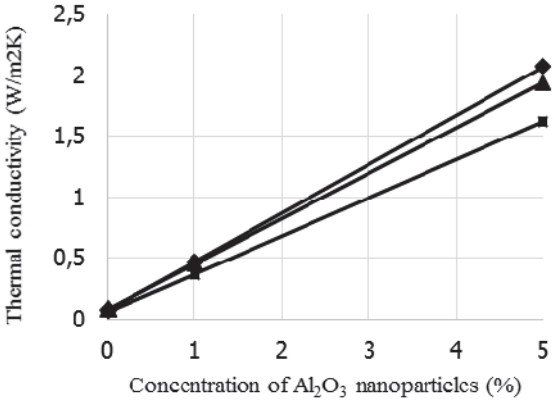

Figure 9. Thermal conductivity at 5 m/s velocity inlet for Al_2O_3-R113 (♦), Al_2O_3-R123 (▲) and Al_2O_3-R134a (■), with 30 nm mean size diameter particles of Al_2O_3.
Source: The authors.

4. Conclusions

Results show that adding nanoparticles to refrigerant fluids improves the thermal characteristics such as thermal conductivity and the heat transfer coefficient, which could mean enhancing the performance of refrigeration systems. The pressure drop of nanofluids studied does not show a particular relation with respect to the nano particles concentration, not allowing to conclude about the effect of that variable on the pressure drop, that is why further research efforts should analyze this feature as well as the migration of particles due to phase change since the mixture model is unable to predict it correctly.

It was observed that nanoparticle size does not affect the thermal characteristics of nanofluids. On the other hand, a concentration of nanoparticles results in an improvement to those characteristics, 1 vf.% being the best concentration because it has a significant impact on thermal conductivity and the heat transfer coefficient with less particles than 5 vf.% concentration.

Results show an improvement in thermal characteristics by increasing inlet velocity for each of the refrigerants, however this means a significant increase in pressure drop. At a higher inlet velocity, the difference in thermal conductivity and in heat transfer coefficient is not appreciable between the three studied nanorefrigerants.

R134a with 30 nm Al_2O_3 at 1 vf.% is a excellent option because it has a lower environmental impact and it has an exceptional thermal performance which is convenient in refrigerant systems.

Acknowledges

This work was funded by Colciencias through the Young Research Program under grant 617-2013.

References

[1] Dinçer, I. and Kanoglu, M., Refrigeration systems and applications, Second Ed., United Kingdom: John Wiley & Sons, Ltd, 2010.

[2] McLinden, M.O., Kazakov, A.F., Brown J.S. and Domanski, P.A., A thermodynamic analysis of refrigerants: Possibilities and tradeoffs for Low-GWP refrigerants. International Journal of Refrigeration, 38, pp. 80-92, 2014. DOI: 10.1016/j.ijrefrig.2013.09.032.

[3] Sarbu, I., A review on substitution strategy of non-ecological refrigerants from vapour compression-based refrigeration, air-conditioning and heat pump systems. International Journal of Refrigeration, 46, pp. 124-141, 2014. DOI: 10.1016/j.ijrefrig.2014.04.023.

[4] Domanski, P.A., Brown, J., Heo, S.J., Wojtusiak, J. and McLinden, M.O., A thermodynamic analysis of refrigerants: Performance limits of the vapor compression cycle. Int Journal of Refrigeration, 38, pp. 71-79, 2014. DOI: 10.1016/j.ijrefrig.2013.09.036.

[5] Vélez, F., Selecting working fluids in an organic rankine cycle for power generation from low temperature heat sources, DYNA, 81(188), pp. 173-180, 2014. DOI: 10.15446/dyna.v81n188.41666.

[6] Calm, J.M. and Didion, D.A., Trade-offs in refrigerant selections: Past, present, and future, International Journal of Refrigeration, 21(4), pp. 308-321, 1998.

[7] Basaran, A. and Ozgener, L., Investigation of the effect of different refrigerants on performances of binary geothermal power plants. Energy Conversion and Management, 76, pp. 483-498, 2013. DOI: 10.1016/j.enconman.2013.07.058.

[8] Saidur, R., Leong, K. and Mohammad, H., A review on applications and challenges of nanofluids, Renewable and Sustainable Energy Reviews, 15, pp. 1646-1668, 2011. DOI: 10.1016/j.rser.2010.11.035.

[9] Wong, K.V. and De León, O., Applications of nanofluids: current and future. Advances in Mechanical Engineering, 2010. DOI: 10.1155/2010/519659.
[10] Kamyar, A., Saidur, R. and Hasanuzzaman, M. Application of Computational Fluid Dynamics (CFD) for nanofluids," International Journal of Heat and Mass Transfer, 55, pp. 4104-4115, 2012. DOI: 10.1016/j.ijheatmasstransfer.2012.03.052.
[11] Choi, S.U.S.D.W.H.e., Development and application of non-Newtonian flows, First ed., 231, in: Wang, D.A.S.a.H.P. Ed., ASME Press, New York, 1995, pp. 99-105.
[12] Saidur, R., Kazi, S., Hossain, M., Rahman, M. and Mohammed, H., A review on the performance of nanoparticles suspended with refrigerants and lubricating oils in refrigeration systems, Renewable and Sustainable Energy Reviews, 15, pp. 310-323, 2011. DOI: 10.1016/j.rser.2010.08.018.
[13] Peng, H., Ding, G., Hu, H. and Jiang, W., Effect of nanoparticle size on nucleate pool boiling heat transfer of refrigerant/oil mixture with nanoparticles. International Journal of Heat and Mass Transfer, 54, pp. 1839-1850, 2011. DOI. 10.1016/j.ijheatmasstransfer.2010.12.035.
[14] Peng, H., Ding, G., Jiang, W., Hu., H. and Gao, Y., Heat transfer characteristics of refrigerant-based nanofluid flow boiling inside a horizontal smooth tube. International Journal of Refrigerant, 32, pp. 1259-1270, 2009. DOI: 10.1016/j.ijrefrig.2009.01.025.
[15] Sun, B. and Yang, D., Flow boiling heat transfer characteristics of nano-refrigerants in a horizontal tube, 38, 2014. DOI: 10.1016/j.ijrefrig.2013.08.020, pp. 206-214.
[16] Cheng, L. and Liu, L., Boiling and two-phase phenomena of refrigerant-based nanofluids: Fundamentals, applications and challenges, International Journal of Refrigeration, 36, pp. 421-446, 2013. DOI: 10.1016/j.ijrefrig.2012.11.010.
[17] Mahbubul, I., Saidur, R. and Amalina, M., Heat transfer and pressure drop characteristics of Al2O3-R141b nanorefrigerant in horizontal smooth circular tube, Procedia Engineering, 56, pp. 323-329, 2013. DOI: 10.1016/j.proeng.2013.03.126.
[18] Mahbubul, I., Fadhilah, S., Saidur, R., Leong, K. and Amalina, M., Thermophysical properties and heat transfer performace of Al2O3/R-134a nanorefrigerants. International Journal of Heat and Mass Transfer, 57, pp. 100-108, 2013. DOI: 10.1016/j.ijheatmasstransfer.2012.10.007.
[19] Togun, H. Ahmadi, G., Abdulrazzaq, T., Shkarah J.A., Kazi, S.N., Badarudin, A. and Safaei, M.R., Thermal performance of nanofluid in ducts with double, Journal of the Taiwan Institute of Chemical Engineers, vol. 47, pp. 28-42, 2015. DOI: 10.1016/j.jtice.2014.10.009.
[20] Yarmand, H., Gharehkhani, S., Newaz-Kazi, S., Sadeghinezhad E. and Reza-Safaei, M., Numerical investigation of heat transfer enhancement. The Scientific World Journal, 2014, Article ID 369593, 9 P., 2014. DOI: 10.1155/2014/369593.
[21] ANSYS, Inc, Ansys fluent 12.0 Theory Guide, ANSYS, Inc, 2009.
[22] Akbari, M., Galanis, N. and Behzadmehr, A., Comparative analysis of single and two-phase models for CFD studies of nanofluid heat transfer, International Journal of Thermal Sciences, 50(8), pp. 1343-1354, 2011. DOI: 10.1016/j.ijthermalsci.2011.03.008.
[23] Moraveji, M.K. and Esmaeili, E., Comparison between single-phase and two-phase CFD modeling of laminar forced convection flow of nanofluids in a circular tube under constant heat flux. International Communications in Heat and Mass Transfer, 39(8), pp. 1297-1302, 2012. DOI: 10.1016/j.icheatmasstransfer.2012.07.012.
[24] Abedini, E., Behzadmehr, A., Sarvari, S. and Mansouri, S., Numerical investigation of subcooled flow boiling of a nanofluid. International Journal of Thermal Sciences, 64, pp. 232-239, 2013. DOI: 10.1016/j.ijthermalsci.2012.08.008.
[25] Davarnejad, R. and Jamshidzadeh, M., CFD modeling of heat transfer performance of MgO-water nanofluid under turbulent flow, Engineering Science and Technology, International Journal, 18(4), pp. 536-542, 2015. DOI: 10.1016/j.jestch.2015.03.011.
[26] Betancur-Márquez, S., Alzate-Espinosa, G.A. and Cortés-Correa, F.B., Mejoramiento de los fluidos de perforación usando nanopartículas funcionalizadas. Boletín Ciencias de la Tierra, 35, pp. 5-14, 2014. DOI: 10.15446/rbct.n35.43179.

D.C. Hernández, received her BSc. Eng in Aeronautical Engineering in 2014, from the Universidad Pontificia Bolivariana. Medellin, Colombia. Currently, she is a young researcher at the Research group on Energy and Thermodynamic of Universidad Pontificia Bolivariana. Her research interests include: computer simulation, modeling and forecasting in heat transfer, and fluid dynamics.
ORCID: 0000-0002-0252-687X

C. Nieto-Londoño, received his BSc. Eng in Mechanical Engineering in 2003, his MSc. degree in Energy in 2006, and a Dr. degree in Engineering – Energy Area in 2012. He works on projects of numerical simulation applied to the solution, evaluation and design of several applications, including micro and nano fludis, renewable energy, micro combustion, catalytic fluid and porous media, for the Universidad Pontificia Bolivariana, Medellín, Colombia. He is currently coordinator of the Doctorate in Engineering and a researcher on the Energy and Thermodynamic Group and the Engineering Aerospace Research Group, at the Universidad Pontificia Bolivariana.
ORCID: 0000-0001-6516-9630

Z. Zapata-Benabithe, received her BSc. Eng in Chemical Engineering in 2003, her MSc. degree in Energetic Systems in 2008, and a Dr. degree in Engineering – Energy Area in 2014. She works on projects of gasification, pyrolysis and carbon materials for electrochemical energy storage, for the Universidad Pontificia Bolivariana, Medellín, Colombia. She is currently coordinator of the Thermofluids and Energy Conversion Seedbed of the Energy and Thermodynamic Group, at the Universidad Pontificia Bolivariana.
ORCID: 0000-0002-4497-4865.

UNIVERSIDAD NACIONAL DE COLOMBIA
SEDE MEDELLÍN
FACULTAD DE MINAS

Área Curricular de Ingeniería
Geológica e Ingeniería de Minas y Metalurgia

Oferta de Posgrados

Especialización en Materiales y Procesos
Maestría en Ingeniería - Materiales y Procesos
Maestría en Ingeniería - Recursos Minerales
Doctorado en Ingeniería - Ciencia y Tecnología de Materiales

Mayor información:

E-mail: acgeomin_med@unal.edu.co
Teléfono: (57-4) 425 53 68

UNIVERSIDAD NACIONAL DE COLOMBIA
SEDE MEDELLÍN
FACULTAD DE MINAS

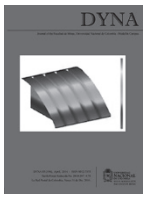

DYNA
http://dyna.medellin.unal.edu.co/

Synthesis and modification of beta zeolite for use in toluene disproportionation reaction

Santiago Mesa [a], Johana Arboleda [b] & Adriana Echavarría [c]

[a] *Instituto de Química, Universidad de Antioquia, Medellín, Colombia. santiago.mesa@udea.edu.co*
[b] *Instituto de Química, Universidad de Antioquia, Medellín, Colombia. johana.arboleda@udea.edu.co*
[b] *Instituto de Química, Universidad de Antioquia, Medellín, Colombia. adriana.echavarria@udea.edu.co*

Received: July 17th, 2015. Received in revised form: February 24th, 2016. Accepted: March 7th, 2016

Abstract:
In this paper zeolite Beta was synthesized and characterized by XRD, ATG, ATD, XRF and SEM. Subsequently various modifications were made using a surface passivation process in liquid phase with tetraethylorthosilicate (TEOS), using two loads of TEOS and three passivation cycles, in order to obtain six catalysts. These materials were characterized by NH3-TPD and tested in tolune disproportionation reaction, under different conditions of pressure and temperature. As modification cycles were increased for each catalyst, there was a change in the acidity of the solids, mainly due to deposition of an inert layer of silica on the external surface. These results were confirmed with the improvement in para-selectivity and decreasing in conversion. Despite zeolite Beta is a large pore zeolite, an improvement of the para-selectivity was obtained, achieving almost stable values for the entire range of temperature and pressure conditions.

Keywords: Beta zeolita, Surface Passivation, Catalysis, Toluene Disproportionation, Para-selectivity.

Síntesis y modificación de la zeolita beta para su uso en la reacción de desproporción de tolueno

Resumen:
En este trabajo se sintetizó la zeolita Beta y se caracterizó por las técnicas de DRX, ATG, ATD, FRX y MEB. Posteriormente se realizaron diversas modificaciones mediante un proceso de pasivación superficial en fase líquida, usando tetraetilortosilicato (TEOS), utilizando dos cargas de TEOS y tres ciclos de pasivación, dando lugar a 6 catalizadores. Dichos materiales fueron caracterizados por medio de NH_3-DTP y probados en la reacción de desproporción de tolueno, bajo diferentes condiciones de presión y temperatura. A medida que se incrementaron los ciclos de modificación para cada catalizador, se generó un cambio en la acidez de los sólidos debido principalmente a la deposición de una capa inerte de sílica sobre la superficie externa, corroborado con el mejoramiento en la para-selectividad y la disminución de la conversión de los sólidos modificados. A pesar que la zeolita Beta es una zeolita de poro grande, se logró un mejoramiento de la para-selectividad, logrando valores casi estables para todo el rango de condiciones evaluadas.

Palabras clave: Zeolita Beta, Pasivación Superficial, Catálisis, Desproporción de Tolueno, Para-selectividad

1. Introducción

Desde la década de 1950, la investigación en síntesis de zeolitas ha crecido significativamente, debido a sus amplias propiedades y al sinnúmero de aplicaciones que poseen estos materiales [1], dentro de las que se destacan los procesos de craqueo catalítico [2] y esterificación [3]. Dentro de sus propiedades se destaca la selectividad de forma. Esta característica permite la diferenciación, de acuerdo al tamaño, entre reactivos, productos e intermediarios de una reacción. Las moléculas que tengan las dimensiones adecuadas para entrar a los poros de las zeolitas, pueden ingresar y reaccionar allí. Por otro lado, las moléculas que puedan salir de los poros de las zeolitas, aparecerán como los productos finales. En este sentido, hay tres tipos de selectividad de forma [4]: i) Selectividad hacia reactivos: algunas moléculas que hacen parte de los reactivos iniciales son muy grandes y no se pueden difundir a través de los poros; ii) Selectividad hacia productos: algunos de los productos

© The author; licensee Universidad Nacional de Colombia.

formados dentro de los poros de la zeolita son muy grandes y no se pueden difundir fuera de ellos; iii) Selectividad hacia el estado de transición: algunas reacciones no ocurren debido a que su correspondiente estado de transición requiere más espacio del que hay disponible dentro de las cavidades y poros de la zeolita. Las reacciones que pueden ocurrir sin impedimento son aquellas que requieren estados de transición pequeños.

A pesar de que una de las características principales de las zeolitas es su sistema de canales (por lo que posee una alta área superficial) y la mencionada selectividad de forma, la superficie externa está disponible para que cualquier molécula, independientemente de su tamaño, pueda reaccionar allí. Esto da lugar a un comportamiento catalítico no selectivo, por lo que el interés se ha volcado hacia la pasivación de los posibles sitios activos de la superficie externa.

La pasivación superficial externa de las zeolitas se ha investigado desde hace aproximadamente dos décadas, y generalmente se han usado técnicas en fase líquida, gaseosa e incluso reacción en fase sólida, usando habitualmente alcóxidos de silicio [5-9]. No solamente se ha apuntado hacia la pasivación superficial, sino también al mejoramiento de las propiedades catalíticas mediante el uso de algunos compuestos que puedan reaccionar sobre los sitios ácidos externos y generar capas activas. H. L. Janardhan y colaboradores [10] usaron la técnica de impregnación húmeda, y usando $NH_4H_2PO_4$ lograron la deposición de una capa activa de fosfato, generando un nuevo tipo de sitios ácidos sobre la superficie del material. Dicho proceso de modificación ha tenido una amplia aplicación en reacciones que requieren selectividades considerables hacia cierto producto, por ejemplo la reacción de desproporción de tolueno selectiva [11]. Esta reacción es catalizada por zeolitas ácidas y usa tolueno como materia prima para transformarlo en benceno y xilenos [12]. La desactivación superficial de los sitios activos de la zeolita conduce a la formación selectiva de para-xileno dentro de la mezcla de xilenos formada en la reacción, y como bien es sabido, el isómero "para" es el más apetecido dentro de la mezcla de isómeros [13].

En este trabajo se sintetizó y caracterizó la zeolita Beta. Adicionalmente se le aplicó un proceso post-síntesis de pasivación superficial en fase líquida usando tetraetilortosilicato (TEOS). Se estudió la influencia del número de ciclos de modificación y la cantidad de TEOS sobre las propiedades catalíticas de los materiales en la reacción de desproporción de tolueno.

2. Metodología

2.1. Síntesis de la zeolita Beta

La síntesis de la zeolita Beta se realizó usando la composición molar Al_2O_3:947.2H_2O:2Na_2O:1K_2O:52.9SiO_2:26.2TEAOH. Inicialmente se prepararon dos soluciones, la primera (Solución 1) mezclando Hidróxido de Tetraetilamonio (35% w/w en H_2O, Alfa Aesar), NaCl (99.8%, Sigma-Aldrich), KCl (99.5%, Sigma-Aldrich) y Ludox (30% w/w en H_2O, Aldrich); mientras que la segunda (Solución 2) se preparó mezclando el agua, NaOH (98%, Sigma-Aldrich) y aluminato de sodio (grado técnico, Sigma-Aldrich). Posteriormente la solución 2 se agregó lentamente a la solución 1, para dar lugar a la formación de un gel altamente viscoso. Dicho gel se dejó en agitación durante una hora a temperatura ambiente. Finalmente el gel se dispuso en reactores que fueron llevados a la estufa a 135ºC durante 48 horas.

Con el fin de remover el agente estructurante, el material obtenido fue calcinado a 600ºC (con una rampa de 5ºC/min) durante 2 horas. Luego para la obtención de la zeolita Beta ácida, se adicionó 1 g de sólido en 50 ml de solución 0.2 M de NH_4NO_3 (Merck, 99%). La suspensión formada se dejó en agitación durante 3 horas a una temperatura entre 55 y 60ºC. Pasado este tiempo, el sólido se recuperó por filtración. Dicho proceso de intercambio se repitió 3 veces. Finalmente el material fue calcinado a 600ºC durante 6 horas para dar lugar a la zeolita Beta ácida (H-Beta).

2.2. Pasivación superficial

La modificación de la zeolita H-Beta se realizó siguiendo el proceso reportado por Shourong Zheng [14], modificando algunos parámetros. El proceso se describe a continuación: el material en polvo se dispuso en un balón de fondo redondo y se le agregó la cantidad de tetraetilortosilicato (TEOS, 98%, Merck) correspondiente, además de ciclohexano (99.5%, Sigma-Aldrich) con una relación de 20 ml/gramo de sólido. La mezcla se sometió a calentamiento en un baño de aceite, bajo condiciones de reflujo (70-80ºC) durante 3 horas. Pasado este tiempo, se removió el reflujo y el sólido se recuperó por evaporación del solvente. Finalmente, el material se sometió a calcinación a 550ºC, con una rampa de 5ºC/min durante 2 horas para remover completamente el ciclohexano y dar lugar a la deposición de una capa inerte de sílica. Este proceso se repitió dependiendo del número de ciclos de modificación deseados.

En la Tabla 1 se describen las condiciones usadas para la modificación de los sólidos, al igual que el nombre asignados para la identificación de cada uno de ellos. Los materiales fueron nombrados teniendo en cuenta la carga de TEOS usada y el número de ciclos a los que fueron sometidos. Por ejemplo, la zeolita H-Beta que se trató con 0.35 ml TEOS/g de sólido y fue sometida a un solo ciclo de pasivación fue nombrada H-Beta 0.35-1.

2.3. Caracterización

El análisis de difracción de rayos X (DRX) se llevó a cabo a temperatura ambiente en un difractómetro PANalytical Empyrean, usando una fuente de radiación de cobre (longitud de onda λ=1,5418 Å), con un goniómetro Omega/2Theta, en un rango 2θ de 5-50, a un paso de 0.02º en un modo de escaneo continuo.

Tabla 1.
Identificación de los sólidos modificados.

Identificación	ml TEOS/ g zeolita	%Carga SiO_2 teórica	Ciclos
H-Beta 0.35-1	**0.35**	**9.40**	**1**
H-Beta 0.75-1	**0.75**	**20.14**	**1**
H-Beta 0.35-2	**0.35**	**9.40**	**2**
H-Beta 0.75-2	**0.75**	**20.14**	**2**
H-Beta 0.35-3	**0.35**	**9.40**	**3**
H-Beta 0.75-3	**0.75**	**20.14**	**3**

Fuente: Los autores.

La técnica de espectroscopia de absorción atómica se usó para el seguimiento del proceso de intercambio iónico en un espectrómetro Thermo Scientific iCE Series 3000.

Además, se realizaron análisis de fluorescencia de rayos X (FRX) para determinar la composición de los materiales sintetizados, usando un equipo Axios MAX (PANalytical), de longitud de onda dispersiva con fuente de Rodio.

El análisis térmico diferencial (ATD) se realizó en un equipo TA Instruments DSC 2920, en atmosfera de aire a 30 ml/min y un rango de barrido de 30 °C a 800 °C a una velocidad de calentamiento de 10 °C/min. El análisis termogravimetrico (ATG) se llevó a cabo con un termoanalizador TA Instruments Hi-Res TGA 2950 en atmosfera de aire a 40 ml/min, en un intervalo de temperatura de 30- 800°C y a una velocidad de 10 °C/min.

Las mediciones de adsorción de nitrógeno se llevaron a cabo en un equipo ASAP 2020 (Micromeritics) a una temperatura de nitrógeno líquido de -196.69ºC y a presiones relativas entre 0.01 y 0.99.

La acidez de los sólidos fue medida mediante la técnica de desorción de amoníaco a temperatura programada (NH_3-DTP). Para ello se usó un reactor de cuarzo en forma de U, en el cual se dispone el catalizador, ubicado en un horno calentado por resistencias programables. El registro de las señales de adsorción y desorción de amoníaco se realizó mediante un detector de conductividad térmica dispuesto a 80ºC. Cada muestra fue pretratada a 150ºC bajo flujo de nitrógeno con el fin de eliminar agua e impurezas. Posteriormente la adsorción de amoníaco se llevó a cabo a 100ºC, hasta una completa saturación de la superficie del sólido. Finalmente la desorción se completó desde 40ºC hasta 500ºC a una velocidad de calentamiento de 10º/min, período en el cual se registraron las señales del detector.

Las medidas de ^{27}Al RMN se realizaron en un equipo Bruker FOURIER de 300 MHz, referenciando los desplazamientos relativos al nitrato de aluminio.

2.4. Ensayos catalíticos

Para la reacción se utilizó hidrógeno como gas de arrastre, y tolueno líquido. El tolueno y el hidrógeno son conducidos hacia un reactor tubular de acero inoxidable el cual es calentado por un horno cilíndrico con control de temperatura. Allí se ponen en contacto con un gramo de catalizador con tamaño de partícula entre 425 y 600 µm. Los productos derivados de la reacción son conducidos hacia el cromatógrafo por una línea precalentada para evitar condensación. La reacción fue trabajada a 375 y 425ºC y desde presión atmosférica hasta 400 psi, con flujo de hidrógeno de 50 ml/min y de 0.1 ml/min de tolueno; dando lugar a una velocidad espacial (*WHSV*) de 5.2 h^{-1}.

Con el fin de conocer el comportamiento catalítico de la reacción se estableció la siguiente metodología: como primera instancia, el catalizador se dejó activando una hora dentro del reactor bajo atmósfera de hidrógeno a 80 ml/min y a 375ºC. Luego de pasado este tiempo, se comenzó a inyectar tolueno a un flujo de 0.1 ml/min e hidrógeno a 50 ml/min; dejando estabilizar el sistema durante 30 minutos. Después de este lapso de tiempo, se realizó la primera inyección de los productos de reacción hacia el cromatógrafo.

Con el fin de conocer el comportamiento catalítico de los materiales a diferentes condiciones se realizó un barrido de presión y temperatura de reacción, partiendo desde presión atmosférica hasta 400 psi y desde 375 hasta 425ºC, realizando dos inyecciones cromatograficas por cada condición de presión y temperatura establecida. De esta forma se probaron 3 presiones (14.7, 100 y 400 psi) por cada temperatura (375 y 425ºC), de acuerdo a lo que se presenta en la Fig 1.

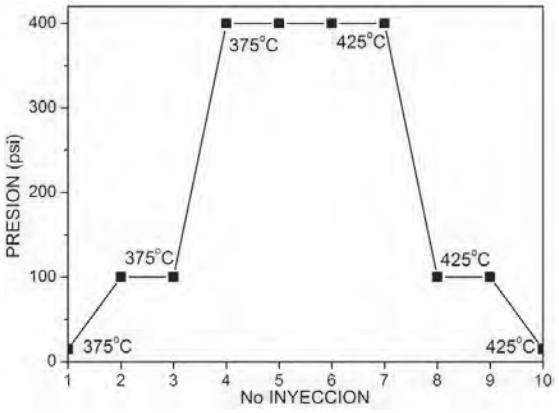

Figura 1. Esquema de las condiciones de reacción a las cuales fueron realizadas las inyecciones de productos en el cromatógrafo.
Fuente: Los autores.

Los productos de reacción fueron analizados en un cromatógrafo Agilent 7820. Los compuestos de la reacción fueron separados usando una columna HP-PONA, determinados usando un detector FID y usando flujos de 400 ml/min de aire, 40 ml/min de hidrógeno y 30 ml/min de nitrógeno.

Los porcentajes de conversión (%X), rendimiento (%R) y para-selectividad (%p-S) fueron calculados usando las siguientes ecuaciones:

$$\%X = \frac{moles\ Tolueno\ que\ reaccionaron}{moles\ totales\ productos + moles\ tolueno\ sin\ \ reaccionar} * 100 \qquad (1)$$

$$\%R_{xilenos} = \frac{moles\ mezcla\ de\ xilenos\ (meta-orto-para)}{moles\ totales\ productos + moles\ tolueno\ \text{sin}\ \ \ reaccionar} * 100 \quad (2)$$

$$\%R_{benceno} = \frac{moles\ benceno}{moles\ totales\ productos + moles\ tolueno\ \text{sin}\ \ \ reaccionar} * 100 \quad (3)$$

$$\%p - S = \frac{moles_{p-Xileno}}{moles\ mezcla\ de\ xilenos\ (meta-orto-para)} * 100 \qquad (4)$$

3. Resultados y discusión

3.1. Síntesis y Caracterización

Según los resultados de difracción de rayos X (Fig 2), se pudo establecer que la zeolita Beta sintetizada efectivamente corresponde con el patrón estándar reportado para dicho sólido [15]. La estructura de la zeolita Beta posee una serie de señales a 7.6, 13.4, 14.4, 21.2 y 22.2 [16], que pudieron ser observadas en el patrón de difracción de la zeolita obtenida.

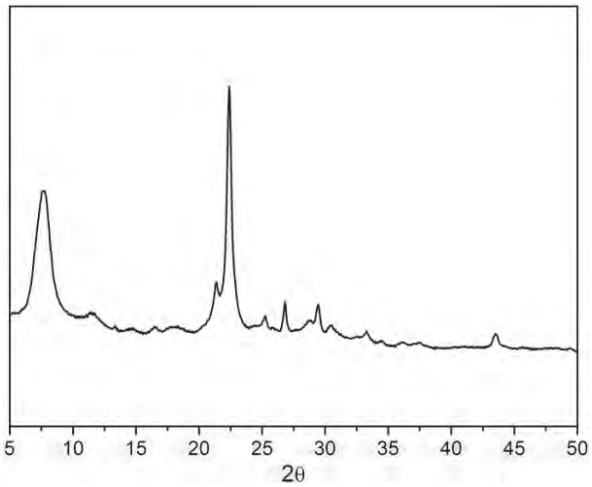

Figura 2. Patrón de difracción obtenido para la zeolita Beta.
Fuente: Los autores.

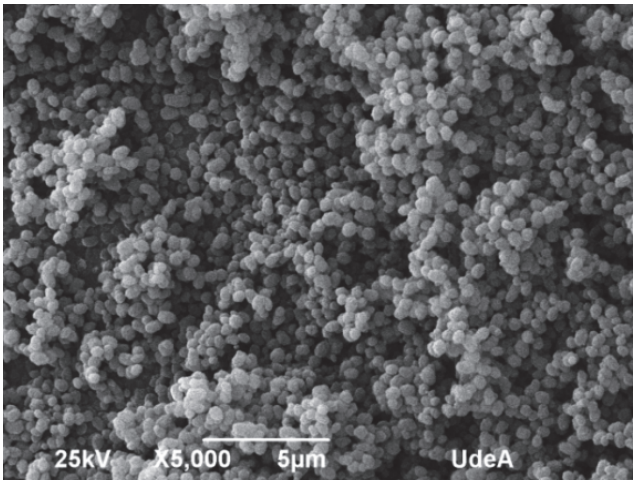

Figura 3. Microscopía electrónica de barrido para la zeolita Beta obtenida.
Fuente: Los autores.

Tabla 2.
Resultados de los análisis químicos por FRX para silicio y aluminio.

	%Si	%Al	Rel Si/Al_{Teo}	Rel Si/Al_{Exp}
BETA	**44.07**	**3.04**	**26.4**	**13.88**

Fuente: Los autores.

De acuerdo con los resultados de fluorescencia de rayos X, mostrados en la Tabla 2, se observa que efectivamente hubo una incorporación del silicio y el aluminio en la zeolita sintetizada. Sin embargo cabe resaltar que el rendimiento de la reacción de síntesis fue relativamente bajo, dado que la relación Si/Al experimental es menor que la calculada teóricamente a partir de la relación molar del gel, y por ende el silicio y el aluminio no se incorporaron totalmente a la red zeolítica.

La relación entre los parámetros de síntesis, las características estructurales y rendimientos del proceso de zeolitización no está del todo clara. Dicho proceso es térmicamente activado y usualmente se da a elevadas temperaturas, para producir cristales en un período de tiempo aceptable. Sin embargo, al parecer la nucleación está controlada más por aspectos cinéticos que por los termodinámicos [17]. Esto conduce a resaltar que los mecanismos de formación de zeolitas son complejos debido a la conjugación de reacciones, equilibrios y variaciones en las solubilidades que ocurren en la mezcla de reacción [1]. Adicionalmente, en *Verified Synthesis of Zeolitic Materials* [17] se pueden encontrar valores elevados de rendimientos, como ocurre para la zeolita Y, con un 98% basado en Al_2O_3; en contraste con otros rendimientos más bajos como el de la ZSM-35, perteneciente a la familia FER, que alcanza un 60% basado en SiO_2.

En la microscopía electrónica de barrido (Fig 3) se puede observar que la zeolita Beta obtenida presenta una morfología esférica, con formaciones de grandes conglomerados, la cual es una morfología comúnmente observada para la zeolita Beta [17,18]. Dichas agrupaciones no presentan fases crecientes parásitas o contaminaciones, según la micrografía. El tamaño de partícula aproximado es de 540 nm.

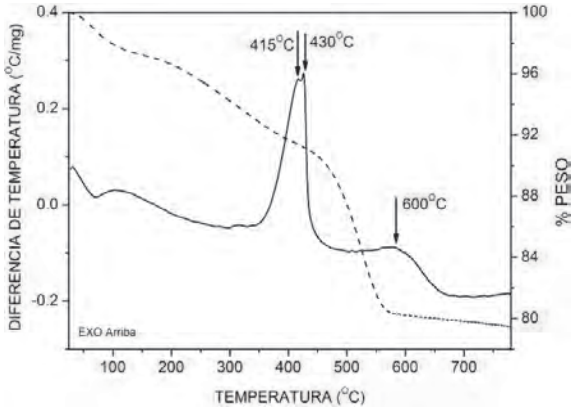

Figura 4. Análisis termogravimetrico (--) y térmico diferencial (-) de la zeolita Beta obtenida.
Fuente: Los autores.

Los análisis térmicos del la zeolita Beta obtenida se presentan en las Fig 4. En el análisis termogravimétrico se observó un primer evento térmico debido a la pérdida de humedad y agua ocluída en los poros de la zeolita. La segunda pérdida se puede dividir en dos etapas: a baja temperatura (250-400ºC), la cual es el resultado de la evolución de los cationes TEA^+ (dando lugar a trietilamonio y etileno) que no están asociadas a la estructura zeolítica como tal y que pueden hacer parte de los defectos estructurales de la red [19]. La otra etapa (a alta temperatura, >400ºC) se le asigna la pérdida de los cationes TEA^+ que balancean las especies $Al(SiO)^{4-}$ de la red, ya que dichos cationes están más fuertemente enlazados a la estructura [19]. Ambos eventos exotérmicos son diferenciables en el ATD (Entre 415-430ºC y a 600ºC aproximadamente) presentado en la Fig 5. La pérdida total en peso alcanzó un valor de 20.5%.

3.2. Zeolita Beta ácida (H-Beta) y Caracterización

Una vez el sólido fue sintetizado y calcinado, se sometió al proceso de intercambio iónico para dar lugar a su forma ácida (H-Beta). En la Tabla 3 se presentan los resultados para sodio y potasio antes y después del intercambio, obtenidos mediante absorción atómica.

Tabla 3.
Resultados de los análisis químicos por absorción atómica para sodio y potasio de la zeolita beta obtenida.

	% Antes de intercambio		% Después de intercambio		%Intercambio	
	Na	K	Na	K	Na	K
BETA	**0.23**	**0.40**	**0.01**	**0.007**	**93.1**	**98.18**

Fuente: Los autores.

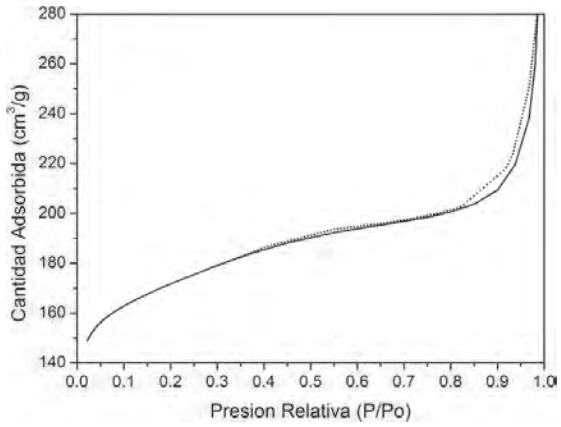

Figura 5. Isoterma de adsorción-desorción para la zeolita H-Beta.
Fuente: Los autores.

Se puede observar que el porcentaje de intercambio alcanzado fue mayor al 90%, llegando a un valor cercano al 100% para el caso del potasio. Ello da cuenta de un proceso de intercambio exitoso, que combinado con la etapa de calcinación posterior dio lugar a una activación ácida casi completa del sólido. Adicionalmente, el patrón de difracción de rayos X de la zeolita Beta ácida no presentó cambios significativos en comparación con el sólido sintetizado.

El análisis de adsorción de nitrógeno de la zeolita beta ácida se muestra en la Fig 5, presentando una isoterma de adsorción del tipo I según la clasificación de la IUPAC [20]. Las sustancias microporosas con tamaños de poros por debajo de los 20 Å exhiben este tipo de isotermas. La curva de adsorción pronunciada que se presenta a bajas presiones es debido a la condensación capilar del nitrógeno en los microporos del material. Después del llenado de los microporos, la adsorción solo puede ocurrir en la superficie externa y por ende la curva se estabiliza [21]. El área superficial del material fue de 629.36 m^2/g, con un área externa 193.85 m^2/g, lo cual está en concordancia con lo encontrado en la literatura [18,22].

3.3. Sólidos pasivados y caracterización

Los análisis químicos por fluorescencia de rayos X (FRX) de los sólidos pasivados se presentan en la Tabla 4. Se observa que en general ocurrió una disminución constante en la cantidad de aluminio a medida que se incrementa el número de ciclos y la carga de TEOS, dando como resultado un incremento en la relación Si/Al obtenida por FRX para los materiales modificados, en comparación con la zeolita sin modificar. Adicionalmente se depositaron pequeñas cantidades de silicio sobre los sólidos, de tal forma que el material con mayor modificación (H-Beta 0.75-3) tuvo el mayor incremento en la cantidad de SiO_2 con respecto al material sintetizado. Por otro lado se presentó una particularidad para los materiales H-Beta 0.75-1, H-Beta 0.35-2 y H-Beta 0.75-2: a medida que se incrementó la cantidad de TEOS, disminuyó el porcentaje de silicio en los sólidos (especialmente para los sólidos tratados con 2 ciclos). En este sentido, se cree que no hay lugar a una desilicación de la zeolita tratada, debido a que para ello se necesitan pH altamente básicos y un tratamiento diferente al que se plantea en este trabajo [23]. Es por ello que se infiere que la disminución en los porcentajes de silicio puede deberse a la relación en peso de los sólidos pasivados en comparación con el sólido ácido.

Igualmente, para los pequeños incrementos en la cantidad de sílica depositada (en comparación con la carga teórica), podría explicarse de dos maneras: 1) el agua residual presente en el TEOS o en la misma zeolita generó una hidrólisis prematura de la molécula orgánica [6], y 2) reacción del TEOS con el aluminio extra-estructural, resultando en una baja adsorción de la molécula orgánica sobre la superficie de la zeolita. Al respecto, Hui Teng [11] sugiere un tratamiento ácido antes del proceso de pasivación. Los ácidos orgánicos poseen un tamaño mayor que el poro de la zeolita, y pueden ser usados para remover selectivamente aluminio extra-estructural, dando lugar a una superficie rica en silicio, lo que puede beneficiar el proceso de deposición de la capa inerte de sílica [11].

En la Fig. 6 se muestran los análisis de desorción de amoníaco a temperatura programada de los catalizadores probados. De manera general, se observa que todos los materiales analizados presentan dos picos de desorción, uno a baja temperatura (150-250ºC) y otro a alta temperatura (350-450ºC), correspondientes a los sitios ácidos débiles y fuertes, respectivamente [24]. Los catalizadores modificados presentaron menor acidez que la zeolita ácida sin modificar. Aunque el efecto no es muy notorio para un solo ciclo de modificación, se observa que el primer pico de desorción para el material H-Beta 0.35-1 ocurre a una temperatura un poco menor (178ºC aproximadamente) que el del material sin modificar (210ºC); esto daría cuenta de una menor fuerza ácida del material modificado.

Adicionalmente, el pico de desorción de alta temperatura del catalizador H-Beta 0.35-1 es mayor que el del catalizador sin modificar, ello podría deberse al fenómeno conocido "Next-Nearest Neighbours", en el cual se expone que mientras más alejados entre sí estén los sitios ácidos, mayor fuerza ácida van a presentar, aunque la acidez total del sólido se ve disminuida [25].

Por otro lado, el pico de desorción correspondiente a los sitios ácidos débiles del catalizador H-Beta 0.75-1 es más amplio que el del sólido sin modificar, indicando una generación de sitios ácidos débiles debido posiblemente a la dealuminización causada por el proceso de modificación.

Tabla 4.
Análisis químicos por FRX para los materiales pasivados.

MUESTRA	$\%SiO_2$	$\%Al_2O_3$	%Si	%Al	Si/Al
Beta	**94.23**	**5.76**	**44.07**	**3.04**	**13.88**
HBeta 0.35-1	**94.76**	**5.19**	**44.32**	**2.74**	**15.49**
HBeta 0.75-1	**93.38**	**4.61**	**43.67**	**2.44**	**17.19**
HBeta 0.35-2	**93.76**	**4.18**	**43.85**	**2.21**	**19.04**
HBeta 0.75-2	**92.46**	**3.85**	**43.24**	**2.03**	**20.38**
HBeta 0.35-3	**95.85**	**4.09**	**44.82**	**2.16**	**19.89**
HBeta 0.75-3	**96.8**	**3.18**	**45.27**	**1.68**	**25.83**

Fuente: Los autores.

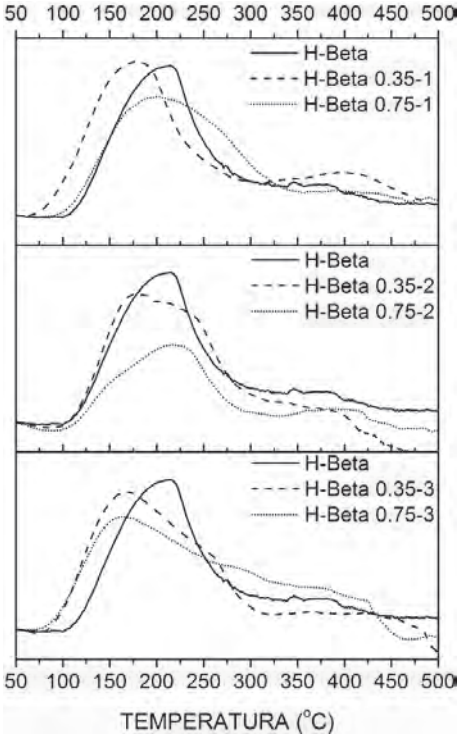

Figura 6. NH_3-DTP de los catalizadores modificados con un ciclo. Fuente: Los autores.

El catalizador H-Beta 0.35-2 presenta menor acidez que el sólido sin modificar, confirmando que efectivamente la pasivación genera una desactivación de los sitios ácidos. El efecto más notorio se da en los sitios ácidos débiles, siendo el catalizador H-Beta 0.75-2 el que presenta mayor disminución. No es posible afirmar algo concluyente sobre los sitios ácidos fuertes dado que la línea base de algunos catalizadores probados fueron inestables y oscilantes.

Un efecto interesante se observó con los sólidos pasivados con tres ciclos de modificación: a medida que se incrementó la carga de TEOS, el pico de desorción asociado a los sitios ácidos débiles se vuelve más ancho, indicando que las moléculas de amoníaco son desorbidas más lentamente. Este fenómeno tiene explicación en base a la dealuminización causada por el proceso de modificación, lo que resultó en una deposición de aluminio extra-estructural, y una generación de mayor densidad de sitios ácidos débiles [24].

El catalizador menos modificado (H-Beta 0.35-1) presentó una acidez total de 764.1 μmol/g, mientras que el más modificado (H-Beta 0.75-3) obtuvo un valor de 459.9 μmol/g; presentándose una disminución de la acidez de 39%, lo que indica que los ciclos de modificación afectan fuertemente el grado de pasivación superficial. Sin embargo no fue posible garantizar la pasivación superficial sin que ocurriera dealuminización. Los análisis de ^{27}Al RMN que se realizaron a los catalizadores H-Beta 0.35-1 y H-Beta 0.75-3 (Figuras no presentadas), mostraron dos bandas: una a 50 ppm correspondiente a los aluminios tetraedrales que hacen parte de la red zeolítica, mientras que la banda en aproximadamente -10 ppm está ligada al aluminio octaédrico, correspondiente al aluminio generado por dealuminización [18]. La relación de aluminios tetraédricos/octaédricos para el material H-Beta 0.35-1 es de 2.5/1; mientras que la relación para el sólido H-Beta 0.75-3 es de 2/1, lo que indica que efectivamente hubo una dealuminización a medida que se incrementaron los ciclos de modificación.

3.4. Catálisis

Inicialmente, en la Fig. 7 se observa que el catalizador sólido no pasivado H-Beta presenta grandes valores de conversión en todo el rango de temperatura y presión evaluadas. Los poros grandes y el carácter tridimensional de los canales de la zeolita Beta hacen que sea muy activa en la reacción, lo que genera que el tolueno llegue más fácilmente al interior del sólido, disminuyendo las limitaciones difusionales, y logrando valores de conversión de tolueno cercanos al 60% a 400 psi y 425ºC. Sin embargo, es de notar que los catalizadores modificados con un ciclo (H-Beta 0.35-1 y H-Beta 0-75-1), tuvieron conversiones mayores que el sólido sin pasivar, lo que confirma el comportamiento observado en los análisis de acidez, donde se observó una generación de sitios ácidos débiles, que posiblemente promovieron la conversión de tolueno. En este sentido, por medio del análisis de desorción de amoníaco no es posible confirmar si dichos sitios ácidos débiles son sitios ácidos del tipo Brønsted o Lewis, sin embargo se sabe que la reacción de desproporción de tolueno es catalizada por sitios ácidos del tipo Brønsted.

Por otra parte, dos y tres ciclos de modificación fueron suficientes para lograr una disminución significativa de la conversión, logrando que se depositara una capa inerte de sílica. De esta forma, el sólido sometido a más ciclos de pasivación y más carga de TEOS (H-Beta 0.75-3) fue el que obtuvo la menor conversión de tolueno.

Como era de esperarse el incremento en la presión y la temperatura generaron mayor conversión de tolueno por parte de los catalizadores. Un aumento en la presión ocasiona que el tolueno sea forzado a ingresar a los poros de la zeolita y por ende se mejore la adsorción sobre los sitios activos del catalizador [26]. En este sentido se puede observar que el incremento en la presión genera pequeños aumentos en la conversión a 375ºC, mientras que un incremento en la temperatura (de 375 a 425ºC) genera grandes cambios en la conversión, debido al carácter endotérmico de la reacción.

Así mismo, no se observó una desactivación de los sólidos por coquización, debido a la presencia de hidrógeno como gas de arrastre [26]. Los catalizadores siguieron presentando actividad a condiciones de 425ºC y presión atmosférica (condiciones de reacción de la última inyección de productos).

En la Fig 8 se muestran los rendimientos hacia xilenos de cada uno de los catalizadores ácidos. La zeolita H-Beta presentó un rendimiento de aproximadamente 25% a condiciones de 400 psi y 425ºC. También se observó que los sólidos modificados presentaron menores valores de rendimiento, siendo el catalizador con más ciclos de pasivación (H-Beta 0.75-3) con el menor rendimiento, confirmando la reducción en su actividad catalítica por cuenta de los procesos de pasivación. Sin embargo, es de notar que los valores de rendimiento de los sólidos pasivados

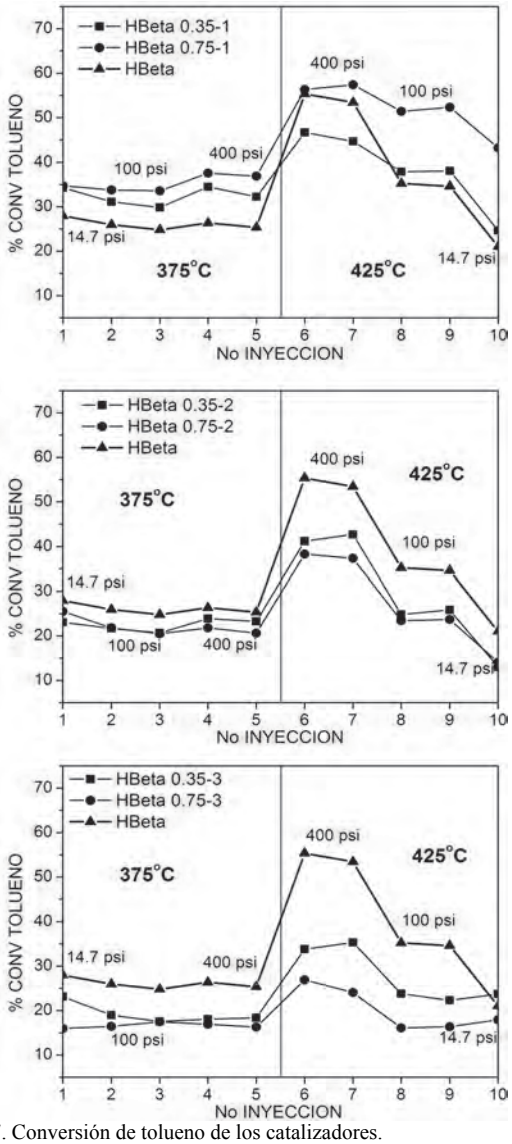

Figura 7. Conversión de tolueno de los catalizadores.
Fuente: Los autores.

con un solo ciclo, no difieren considerablemente del sólido ácido sin modificar, lo que sugiere la alta actividad que sigue presentando el sólido después de solo un ciclo de pasivación. A este respecto, Paul J. Kunkeler y colaboradores [8] indican que la superficie externa de la zeolita Beta puede ser extremadamente activa, y por ende es necesario la aplicación de procesos de modificación post-síntesis para reducir la actividad superficial, con el fin de obtener materiales catalíticos con la acidez apropiada. En este sentido, las disminuciones más fuertes en los valores de rendimiento se presentaron para los catalizadores modificados con dos y tres ciclos, bien sea usando cargas de 0.35 ó 0.75 ml/g de zeolita.

El rendimiento hacia benceno se presenta en la Fig. 9. Se observa una misma tendencia que el rendimiento hacia xilenos: el efecto más pronunciado sobre dicho rendimiento se da por cuenta de la temperatura. Sin embargo, el incremento en la presión a 375ºC generó una ligera disminución en el rendimiento del catalizador sin modificación. Al respecto, S. Al Khataff y colaboradores [26] afirman que a pesar que el incremento en la presión genera un aumento en la cantidad de benceno debido a las reacciones laterales, la presencia de hidrógeno tiende a prevenir dichas reacciones, e incluso llegando a obtenerse valores menores de selectividad y rendimiento hacia benceno al incrementar la presión.

Las selectividades hacia para-xileno en la mezcla de xilenos se muestran en la Fig 10. La para-selectividad de los catalizadores aumentó a medida que se aumentó el número de ciclos de modificación como se observa en la Fig 11. Al incrementar la presión (de 100 a 400 psi) a 375ºC no hay un cambio significativo en los valores de para-selectividad, y el efecto de la presión sobre dichos valores es más notorio a 425ºC. Sin embargo, al incrementar la temperatura de 375 a 425ºC a 400 psi, hay una disminución sustancial en los valores de para-selectividad, debido al incremento de productos derivados de reacciones laterales [26]. No obstante, el efecto de la temperatura es menos notorio a medida que se incrementan los ciclos de modificación, sin importar la carga de TEOS usada (0.35 ó 0.75 ml/g), logrando valores casi estables para el catalizador H-Beta 0.75-3. Esto podría atribuirse no solo a la pasivación de los sitios activos externos, sino también a un estrechamiento de la entrada del canal por acción de las moléculas de TEOS. El diámetro cinético del TEOS es mayor que la entrada de los poros de la zeolita, y algunos grupos hidroxilo que están cerca a la entrada de los canales pueden reaccionar, para dar lugar a enlaces Si-O-Al ó Si-O-Si [11].
Además, la zeolita Beta es clasificada como una zeolita de poro grande, y para este caso, se depositaría una capa de sílica inerte en la entrada de los canales lo que generaría un estrechamiento, dando lugar a que los productos intermediarios "grandes" no puedan salir de los canales. De hecho el rendimiento hacia productos C9+ a condiciones de 425ºC y 400 psi disminuyó desde 15% para el catalizador H-Beta, hasta un 3.5% para el catalizador H-Beta 0.75-3.

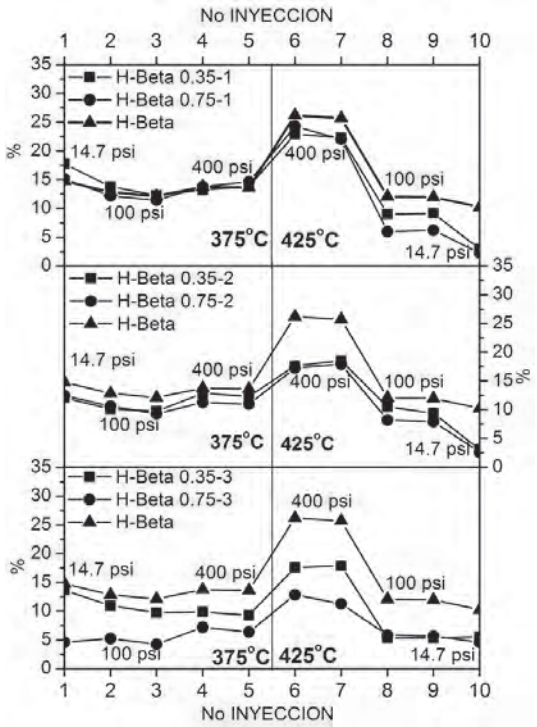

Figura 8. Rendimiento hacia xilenos.
Fuente: Los autores.

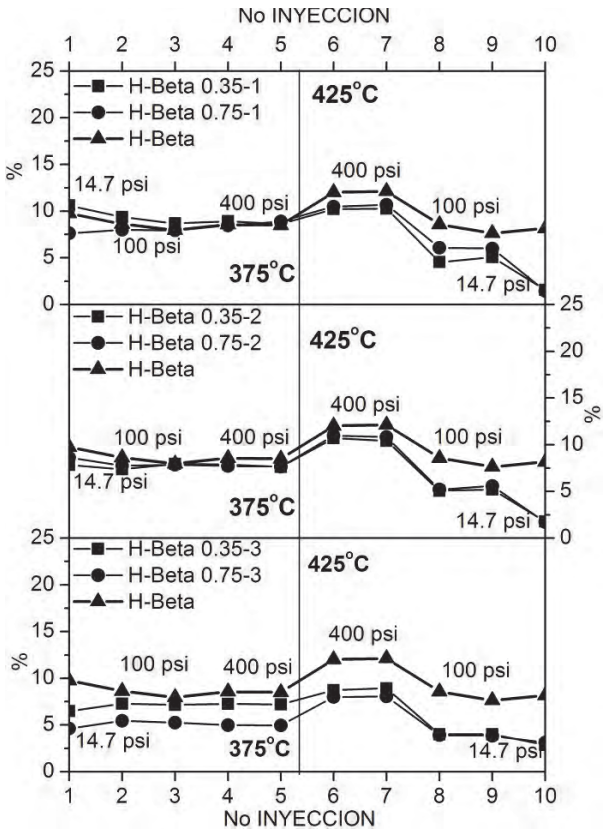

Figura 9. Rendimiento hacia benceno.
Fuente: Los autores.

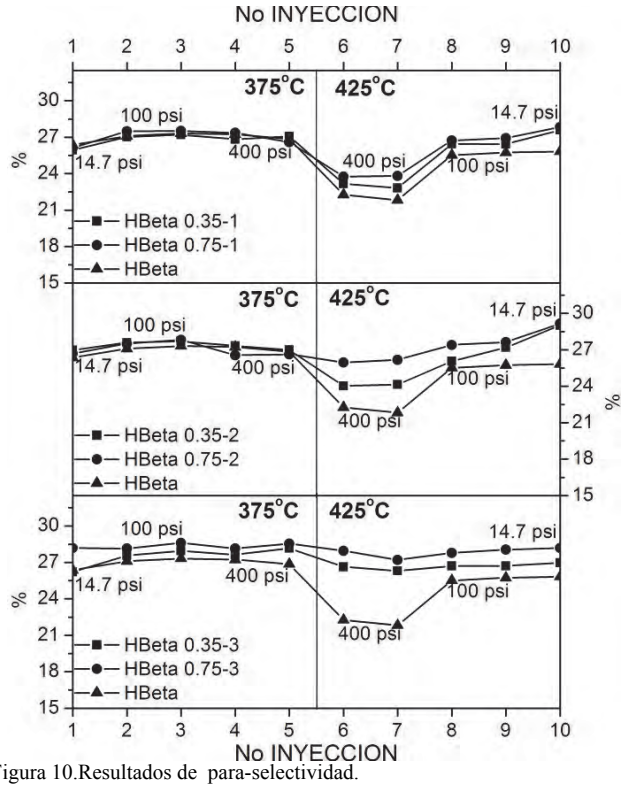

Figura 10.Resultados de para-selectividad.
Fuente: Los autores.

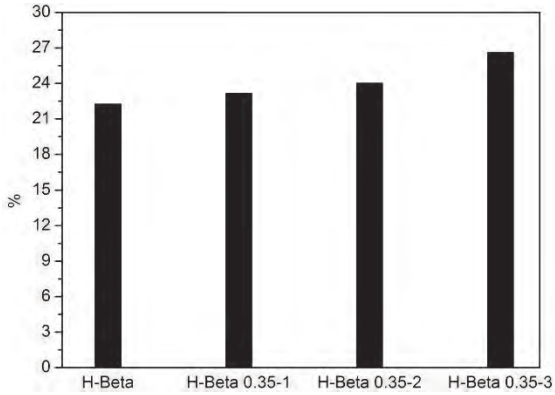

Figura 11. Resultados de para-selectividad para los catalizadores tratados con 0.35 ml de TEOS/g, a condiciones de 425ºC y 400 psi.
Fuente: Los autores.

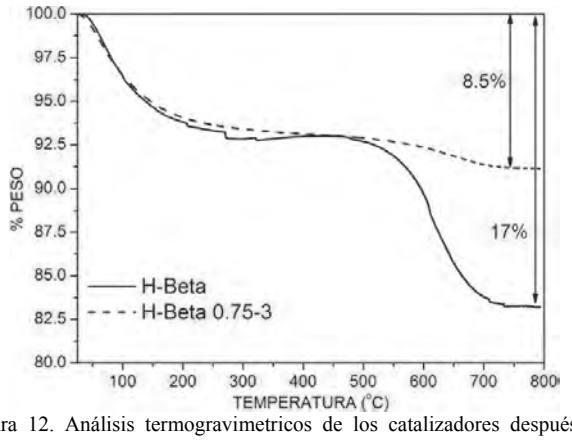

Figura 12. Análisis termogravimetricos de los catalizadores después de reacción.
Fuente: Los autores.

Con el fin de de medir la cantidad de coque depositada en los catalizadores luego de la reacción, los sólidos H-Beta y H-Beta 0.75-3 fueron sometidos a un programa de análisis termogravimétrico. Los resultados se observan en la Fig 12. Fue evidente que el sólido modificado presentó menor cantidad de coque depositado luego de la reacción, en comparación con el sólido sin pasivación.

Este hecho, combinado con el mejoramiento de la para-selectividad, indica que el sólido pasivado inhibió la formación de compuestos grandes, como etiltolueno y trimetilbenceno, que pueden formarse fuera de los poros del catalizador para dar lugar a la formación de coque.

4. Conclusiones

El método hidrotérmico es un método viable para la obtención de la zeolita Beta; esto se corroboró mediante difracción de rayos X, donde se pudo evidenciar que el difractograma obtenido experimentalmente era congruente con su homólogo simulado. Igualmente se pudo corroborar mediante absorción atómica que el intercambio iónico combinado con la etapa de calcinación posterior dio lugar a una activación ácida casi completa del sólido.

Por otro lado, fue posible realizar modificaciones a la

zeolita Beta ácida, mediante un método de pasivación superficial, usando varias cargas de TEOS y varios ciclos de modificación, dando lugar a materiales con diferentes características fisicoquímicas. Precisamente, se evidenció mediante ^{27}Al RMN que las modificaciones generaron una pequeña dealuminización debido posiblemente a las condiciones de modificación. Sin embargo, el cambio en la acidez de los sólidos es debido principalmente a la deposición de una capa inerte de sílica sobre la superficie externa, corroborado con el mejoramiento en la para-selectividad de los sólidos modificados y la disminución en la cantidad de coque depositada sobre el catalizador H-Beta 0.75-3. Además, a medida que se incrementaban los ciclos de modificación para cada catalizador, se incrementó la para-selectividad (especialmente para dos y tres ciclos) a la vez que se disminuía la conversión de tolueno, lo que indica que efectivamente los procesos de modificación lograron el bloqueo de los sitios activos externos del catalizador.

A este respecto es de notar que la zeolita Beta es una zeolita de poro grande, y por ende lograr conversiones selectivas hacia para-xileno se hace complicado. Sin embargo, mediante el proceso de pasivación se logró un mejoramiento de la para-selectividad, logrando valores casi estables para todo el rango de condiciones evaluadas.

Un ciclo de modificación no fue suficiente para lograr una pasivación notable de los sólidos. Incluso se notó que se generó mayor fuerza ácida de lo sólidos, gracias al efecto conocido como "Next-Nearest Neighbours". Por cuenta de ello, los valores de conversión de tolueno para los sólidos modificados con solo un ciclo de modificación, fueron ligeramente mayores que para el sólido sin modificación. Además, los incrementos de temperatura y presión de la reacción, generó aumentos en la conversión de tolueno. Dicho fenómeno se presenta por el incremento de reacciones laterales y por el carácter endotérmico de la reacción.

Agradecimientos

Los autores agradecen el apoyo financiero recibido por parte del Instituto Colombiano del Petróleo y al Programa de Sostenibilidad 2014-2015 de la Universidad de Antioquia.

Referencias

[1] Byrappa, K. and Yoshimura, M., Handbook of Hydrothermal Technology. New York. William Andrew Publishing/Noyes, 2001. DOI: 0.1016/B978-081551445-9.50001-5.

[2] Nancy, T.R. and Janneth. T.A., Using spent fluid catalytic cracking (FCC) catalyst as pozzolanic addition — A review. Ingeniería e Investigación, 30(2), pp. 35-42, 2010.

[3] Sanchez F.J. and Niño C.J., Influence of the aluminium impregnation [$Al(NO_3)_3$] in the beta zeolite over its acidity. Ingeniería e Investigación, 24(2). pp. 51-61, 2010.

[4] Ernst, S., Advances in nanoporous materials. 1, Elsevier, 2009. DOI: 10.1016/S1878-7959(09)00107-8.

[5] O'Connor, C.T., Moller, K.P. and Manstein, H., The effect of silanisation on the catalytic and sorption properties of zeolites. KONA, 25, pp. 230-236. 2007. DOI: 10.14356/kona.2007020.

[6] Weber, R.W., Moller, K.P. and O'Connor, C.T., The chemical vapour and liquid deposition of tetraethoxysilane on ZSM-5, mordenite and beta. Microporous and Mesoporous Materials, 35-36, pp. 533-543. 2000. DOI: 10.1016/S1387-1811(99)00248-6.

[7] Ren, X., Liang, J. and Wang, J., H-MCM-22 zeolitic catalysts modified by chemical liquid deposition for shape-selective disproportionation of toluene. Journal of Porous Materials, 13, pp. 353-357, 2006. DOI: 10.1007/s10934-006-8030-5%I

[8] Kunkeler, P.J., Moeskops, D. and van Bekkum, H., Zeolite Beta: Characterization and passivation of the external surface acidity. Microporous Materials, 11(5-6), pp. 313-323. 1997. DOI: 10.1016/S0927-6513(97)00053-9.

[9] Zheng S., Jentys, A. and Lercher, J.A., On the enhanced para-selectivity of HZSM-5 modified by antimony oxide. Journal of Catalysis, 219, pp. 310-319, 2003. DOI: 10.1016/S0021-9517(03)00234-3.

[10] Janardhan, H.L., Shanbhag, G.V. and Halgeri, A.B., Shape-selective catalysis by phosphate modified ZSM-5: Generationof new acid sites with pore narrowing. Applied Catalysys A: General, 471, pp. 12-18, 2014. DOI: 10.1016/j.apcata.2013.11.029.

[11] Teng H., Wang J., Ren X. and Chen D., Disproportionation of toluene by modified ZSM-5 zeolites catalysts with high shape-selectivity prepared using chemical liquid deposition with tetraethyl orthosilicate. Chinese Journal of Chemical Engineering, 19(2), pp. 292-298, 2011. DOI: 10.1016/S1004-9541(11)60168-7.

[12] Tsai, T-Ch., Liu, S-B. and Wang, I., Disproportionation and transalkylation of alkylbenzenes over zeolite catalysts. Applied Catalysis A: General, 181(2), pp. 355-398, 1999. DOI: 10.1016/S0926-860X(98)00396-2.

[13] Wiley, Petroleum Technology. Vol. 2.John Wiley & Sons. New York. 2007.

[14] Zheng, S., Surface modification of HZSM-5 zeolites. Tesis de Dr. der Naturwissenschaften. Institut fur Teschnische Chemie Il der Teschnischen Universitat Munchen. Munich, Germany, 2002.

[15] Wei, H., Liu, K., Xie, S., Xin,W., Li, X., Liu, S. and Xu, L., Determination of different acid sites in Beta zeolite for anisole acylation with acetic anhydride. Journal of Catalysis, 307, pp. 103-110, 2014. DOI: 10.1016/j.jcat.2013.07.010.

[16] Talebi, G., Amrollahi, M. and Fathizadeh, M., Adsorption of benzene from benzene/n-C6 and n-C7 mixture by nano Beta zeolite with different Si/Al ratios. Arabian Journal of Chemistry, In-Press. 2014. DOI: 10.1016/j.arabjc.2014.08.015.

[17] Robson, H. and Lillerud, K.P., Verified Synthesis of Zeolitic Materials. Elsevier. New York. 2001.

[18] Zarama-Pazos, M.C., Contribución a la sintesis hidrotérmica de zeolita Beta y sus posibles modificaciones con Galio. Tesis MSc.en Ciencias Químicas. Universidad Nacional de Colombia, Bogotá, Colombia, 2004.

[19] Clambor, M.A., Corma, A. and Valencia, S., Characterization of nanocrystalline zeolite Beta, Microporous and Mesoporous Materials, 25(1-3), pp. 59-74, 1998. DOI: 10.1016/S1387-1811(98)00172-3.

[20] Gregg, S.J. and Sing, K.S.W., Adsorption, surface area and porosity. Academic Press. Michigan. 1991.

[21] Abrevaya, H., Unique aspects of mechanisms and requirements for Zeolite catalysis in refining and petrochemical, In: Kulprathipanja, S. Catalysis Zeolites in Industrial Separation, Glasgow, John Wiley & Sons, 2010, pp. 406-581.

[22] Muller, M., Harvey, G. and Prins, R.,Quantitative multinuclear MAS NMR studies of zeolites. Microporous and Mesoporous materials, 34(3), pp. 281-290, 2000. DOI: 10.1016/S1387-1811(99)00180-8.

[23] Groen, J.C., Abelló, S., Villaescusa, L.A. and Pérez-Ramírez, J., Mesoporous beta zeolite obtained by desilication. Microporous and mesoporous materials, 114(1-3), pp. 93-102, 2008. DOI: 10.1016/j.micromeso.2007.12.025.

[24] Damjanovic, L. and Auroux, A., Determination of Acid/Base properties by temperature programmed desorption (TPD) and adsorption calorimetry, In: Derouane, E.G. and Chester, A.W. Eds. Zeolite Characterization and Catalysis: A Tutorial. Elsevier, pp. 107-167, 2009. DOI: 10.1007/978-1-4020-9678-5_3.

[25] Scherzer, J., Correlation between catalyst formulation and catalytic properties, In: Magee, J.S. and Mitchell, M.M., Eds. Fluid catalytic cracking: Science and Technology. Elsevier, pp. 145-182. 1993. DOI: 10.1016/S0167-2991(08)63828-8.

[26] Al-Khattaf, S., Ali, M.A. and Al-Amer, A., Effect of reaction pressure and carrier gas on toluene disproportionation over molybdenum-ZSM-5 catalyst. Energy & Fuels, 22(1), pp. 243-249, DOI: 10.1021/ef700582b. 2008.

S. Mesa, es Ingeniero de Materiales desde el 2011, recibió su grado de MSc. en Ciencias Químicas en el año 2015, ambos de la Universidad de Antioquia, Colombia. Desde el año 2012 hasta el año 2015 trabajó en investigación en catálisis usando mallas moleculares en procesos de la industria petroquímica. Sus áreas de investigación son: zeolitas y mallas moleculares, síntesis inorgánica, catálisis, petroquímica y energía.
ORCID: 0000-0002-0058-7193

J. Arboleda, recibió grado de Ingeniera Química en 2006 y de Dra. en Ciencias Químicas en 2010, de la Universidad de Antioquia, Colombia. Se ha desempeñado como docente en el área de química analítica e intrumental y como investigadora en las áreas de caracterización de nuevos materiales, aplicaciones de nuevos materiales en procesos catalíticos y microscopía electrónica. Sus áreas de investigación son: síntesis inorgánica, catálisis, petroquímica y energía, microscopia electrónica.
ORCID: 0000-0003-0588-6093

A.Echavarría-Isaza, obtuvo su grado de Ingeniera Química en el año 1993, su título de MSc. en Ciencias Quimicas en 1997 y el de Dra. en Ciencias Químicas en 2001, de la Universidad de Antioquia, Colombia. Se ha desempeñado como docente titular de la Universidad de Antioquia en las áreas de catálisis, química inorgánica y química analítica. Sus investigaciones han estado enfocadas en las áreas de zeolitas y su uso en la industria petroquímica, caracterización de materiales y catálisis heterogénea.
ORCID: 0000-0002-1733-9583

UNIVERSIDAD NACIONAL DE COLOMBIA
SEDE MEDELLÍN
FACULTAD DE MINAS

Área Curricular de Ingeniería
Geológica e Ingeniería de Minas y Metalurgia

Oferta de Posgrados

Especialización en Materiales y Procesos
Maestría en Ingeniería - Materiales y Procesos
Maestría en Ingeniería - Recursos Minerales
Doctorado en Ingeniería - Ciencia y Tecnología de Materiales

Mayor información:

E-mail: acgeomin_med@unal.edu.co
Teléfono: (57-4) 425 53 68

UNIVERSIDAD NACIONAL DE COLOMBIA
SEDE MEDELLÍN
FACULTAD DE MINAS

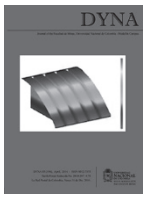

DYNA
http://dyna.medellin.unal.edu.co/

Effect of a dual tire pressure on the design parameters of thick asphalt pavements using finite element freeware

Myriam Rocío Pallares-Muñoz [a] & Julián Andrés Pulecio-Díaz [b]

[a] *Programa de Ingeniería Civil, Universidad Surcolombiana, Neiva, Colombia. myriam.pallares@usco.edu.co*
[b] *Programa de Ingeniería Civil, Universidad Surcolombiana, Neiva, Colombia. julpul7@hotmail.com*

Received: July 29th, 2015. Received in revised form: March 08th, 2016. Accepted: March 17th, 2016.

Abstract
The effect of a dual tire pressure on the design parameters of thick asphalt pavements using finite element freeware EverStressFE©1.0 is evaluated. This is trying to represent more adjusted the footprint shape and intensity of stress generated by the tires of vehicles. To validate the elastic multilayer EverStress©5.0 software was used. The results of the deformations can be concluded that the asphalt pavement designs made with analytical methods may be slightly oversized and consequently increase the cost of construction of pavements. This study marks a route to analyze the sensitivity of various factors that may affect the design of asphalt pavements. Future research is expected to integrate dynamic conditions by introducing results of field tests to full scale.

Keywords: EverStressFE©1.0, EverStress©5.0, three-dimensional modeling of pavements, contact area, tire tread, tire-footprint-pressure-distribution, free-software pavement modeling.

Efecto de la presión de contacto de una carga dual sobre los parámetros de diseño de pavimentos asfalticos gruesos usando software libre de elementos finitos

Resumen
Se evalúa el efecto de la presión de contacto de una carga dual sobre los parámetros de diseño de pavimentos asfalticos gruesos por medio del modelador libre de elementos finitos EverStressFE©1.0 intentando reproducir de una manera más ajustada la forma de la huella y la intensidad de esfuerzo generados por las llantas de los vehículos. Para la validación se empleó el software multicapa elástico EverStress©5.0. Los resultados de las deformaciones llevaron a concluir que los diseños de pavimentos asfálticos realizados con métodos analíticos pueden estar ligeramente sobredimensionados y en consecuencia elevar los costos de construcción de los pavimentos. Este estudio traza una ruta para analizar la sensibilidad de distintos factores que pueden afectar el diseño de pavimentos asfalticos. Se espera en próximas investigaciones integrar condiciones dinámicas introduciendo resultados obtenidos de pruebas de campo a escala real.

Palabras clave: EverStressFE©1.0, EverStress©5.0, modelado tridimensional de pavimentos, área de contacto, huella de llanta, distribución de presión de inflado, modelado de pavimentos con software libre.

1. Introducción

En la actualidad, en el diseño de estructuras de pavimento se emplean métodos analíticos y/o modelos numéricos definiendo para ello, el eje de diseño –eje simple de 13T de cuatro ruedas (2 en cada extremo)–, el espesor de las capas y las características de los materiales, para calcular las deformaciones a tensión en las fibras inferiores de las capas asfálticas y a compresión en la subrasante, provocadas por la presión de contacto de la carga de diseño que tradicionalmente se aplica de manera homogénea en un área circular sobre la superficie de rodadura como se ilustra en la Fig. 1. Esta variable ha sido objeto de estudio de investigaciones que afirman que la presión de contacto no se distribuye uniformemente, lo que proporciona alguna información para justificar por qué el supuesto de área de contacto convencional está incorrecto [1].

© The author; licensee Universidad Nacional de Colombia.

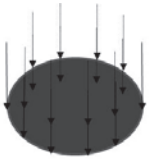

Figura 1. Área de contacto circular
Fuente: Autores

Figura 2. Formas típicas de llanta en el mercado automotor
Fuente: Autores

Figura 3. Huella rectangular
Fuente: Autores

Figura 4. Esquema de la estructura pavimento asfaltico grueso modelada
Fuente: Autores

Tabla 1.
Valores típicos de espesores de capa de una estructura pavimento asfaltico grueso

Capa	Espesor (m)
Capa de rodadura (concreto asfaltico BBSG)	0.060
Base asfáltica (grava asfáltica GB)	0.180
Subrasante	semi-infinita

Fuente: Autores

Tabla 2.
Valores típicos de módulo elástico de las capas constitutivas

Capa	Módulo elástico (MPa)
Capa de rodadura (concreto asfaltico BBSG)	5400
Base asfáltica (grava asfáltica GB)	9300
Subrasante	120

Fuente: Autores

Esta premisa ha sentado las bases de un estudio para evaluar el efecto de la presión de contacto de una carga dual sobre los parámetros de diseño de pavimentos asfalticos (deformaciones horizontales "εxx" y verticales "εzz"). Para este propósito se empleó el modelador tridimensional de elementos finitos EverStressFE 1.0 que permite reproducir de una manera más ajustada la forma de la huella y la intensidad de esfuerzo generados por las llantas de los vehículos de diseño (Figs. 2 y 3) y el software multicapa elástico EverStress© 5.0 para validar los resultados.

2. Métodos

El análisis se abordó por medio de los modeladores computacionales EverStress© 5.0 y EverStressFE1.0; el primero se utilizó para validar los resultados de los modelos de elementos finitos dada su versatilidad y funcionalidad. La estructura de pavimento asfáltico representada es gruesa compuesta por una base de grava asfáltica denotada por GB (Grave Bitume) y una capa de rodadura de concreto asfaltico denotada como BBSG proveniente de la denominación francesa Béton Bitumineux Semi-Grenu como se muestra en la Fig. 4 [2].

Las dimensiones de las capas constitutivas de la estructura de pavimento modelado se presentan en la Tabla 1. La condición de frontera considerada para la subrasante es semi-infinita y como es común en el dimensionamiento de este tipo de estructuras se trabajaron las interfaces ligadas.

Los módulos de elasticidad tomados como referencia para cada una de las capas de acuerdo a las condiciones de trabajo del pavimento se muestran en la Tabla 2. El módulo de elasticidad de la subrasante conocido como resiliente se determina por medio de ensayos triaxiales; el módulo elástico de las capas asfálticas se establece a través de ensayos de módulos resilientes ó dinámicos a temperaturas y frecuencias de diseño [2-4] o a través de tramos experimentales sobre los que se realizan ensayos deflectómetricos Falling Weight Deflectometer (FWD) ó Heavy Weight Deflectometer (HWD) acompañados de análisis inversos o de retro-calculo y corregidos a las condiciones de laboratorio [5-8].

Nótese de la Tabla 2, que el módulo de la Base Asfáltica supera en valor al de la Capa de Rodadura lo cual se encuentra soportado en el hecho de que las deformaciones presentes en las fibras inferiores de la Capa de Rodadura son de compresión contrarias a las que ocurren en la Base Asfáltica, en concordancia con la información contenida en la Guía Francesa de Dimensionamiento de Estructuras de Pavimento del año 94 [2].

Ya que la variación del módulo de Poisson no tiene incidencia considerable en el comportamiento del pavimento [7, 9], se emplearon los valores característicos de la Tabla 3. Los espesores típicos, los módulos elásticos y las relaciones de Poisson fueron tomados de la Guía Francesa para el Diseño de Pavimentos Asfalticos por Metodología Racional "Conception et dimensionnement des structures de chaussée, Guide technique" del antiguo Laboratoire Central des Ponts et Chaussées (LCPC) [2], hoy por hoy, Institut Français des Sciences et Technologies des Transports, de L'aménagement et des Réseaux (IFSTTARs), entidad de investigación reconocida a nivel mundial y líder en Europa.

Tabla 3.
Valores típicos de módulo de Poisson de las capas constitutivas

Capa	Módulo Poisson
Capa de rodadura (concreto asfaltico BBSG)	0.35
Base asfáltica (grava asfáltica GB)	0.35
Subrasante	0.35

Fuente: Autores

La determinación de los parámetros de diseño de pavimentos tienen principio en el diseño racional que consiste en modelar la estructura a partir de la definición de los espesores y las rigideces (módulos resilientes, dinámicos y relaciones de Poisson) de cada capa para calcular las tensiones y compresiones provocadas por una carga tipo e identificar: a) la deformación a tensión máxima (ε_t) capaz de producir la rotura de las capas asfálticas [10]; esta deformación se compara con el límite admisible del material asfáltico (ε_{tadm}) que es función de múltiples factores, entre ellos, el tránsito, coeficientes de calibración y riesgo, efecto de las heterogeneidades locales de rigidez de las capas ligadas y deformación a un millón de solicitaciones con una probabilidad de falla del 50% determinado a 10ºC y 25Hz [2,11]; b) la deformación a compresión máxima (ε_c) sobre la subrasante que se compara con la admisible (ε_{cadm}) y que depende del nivel de tránsito [2].

2.1. Modelo analítico EverStress© 5.0

Se desarrolló el modelo en el programa elástico multicapa de cálculo de esfuerzos y deformaciones para diseño de pavimentos EverStress© 5.0, introduciendo una presión de inflado distribuida uniformemente sobre un área circular de radio 0.125m bajo una presión de 0.662 MPa y distancia entre ejes de 0.375 m. El análisis permite identificar las deformaciones características de control del diseño estructural del pavimento, tales como las deformaciones a tensión en las fibras inferiores de las capas asfálticas y compresión en la parte superior de la subrasante [2]. En la Fig. 5 se indica la ubicación de estos parámetros.

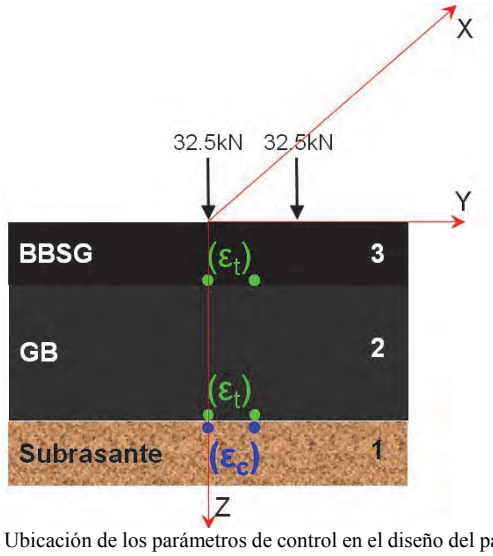

Figura 5. Ubicación de los parámetros de control en el diseño del pavimento EverStress© 5.0
Fuente: Autores

2.2. Modelos de elementos finitos EverStressFE 1.0

Los modelos de elementos finitos con el modelador tridimensional elástico EverStressFE 1.0 fueron validados con el programa EverStress© 5.0. La Fig. 6 muestra el elemento finito que emplea el software; se trata de un elemento tipo BRICK con tres grados de libertad por nodo (UX, UY, UZ). El EverStressFE 1.0 trabaja con mallados de distintos grados de refinamiento y se compone de cinco interfaces que realizan diferentes funciones: a) Geometry and layer properties, contiene una herramienta CAD que permite construir un modelo geométrico e introducir los datos característicos de las capas (espesores y módulos) y definir las fronteras del dominio del modelo, b) Loads, almacena los parámetros de carga, tipo de rueda y eje, contacto, presión, carga, ancho y espaciamiento de las llantas, distancia entre ejes y formas de distribución de la presión de contacto de la rueda, c) Meshing, determina los parámetros de mallado (tipo de malla y refinamiento, división de elementos, condición de interfaz y rigidez) y especificaciones del modelo (número de nodos y elementos finitos), d) Solver, ejecuta el solucionador de elementos finitos, e) Results, permite obtener los resultados del análisis. Los pasos típicos del procedimiento de análisis de un problema de esfuerzo-deformación con EverStressFE 1.0, son: ingresar los datos de dimensionamiento, numero de capas, espesores y parámetros de rigidez (módulos resilientes, dinámicos y de Poisson), condiciones de frontera, valores de presión, carga, ancho y espaciamiento de las llantas (el programa por defecto aplica un cuarto de carga dual según se observa en las Figs. 7, 8 y 9), elegir una combinación de mallado, ejecutar el solucionador y obtener resultados [12 - 14].

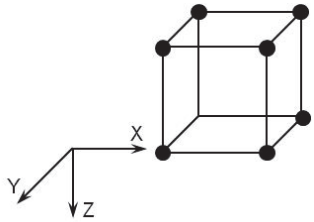

Figura 6. Elemento BRICK.
Fuente: EverStressFE1.0 Theory Manual

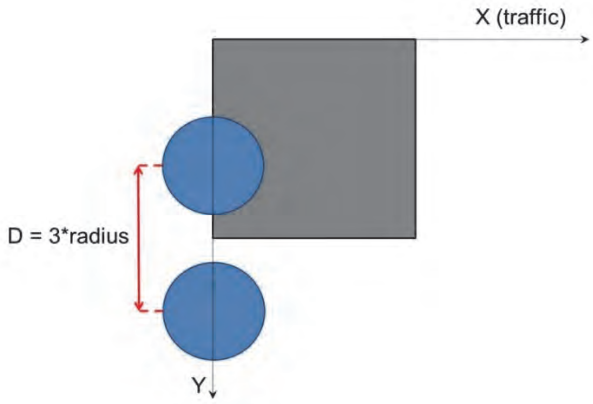

Figura 7. Vista en planta carga dual circular
Fuente: Autores

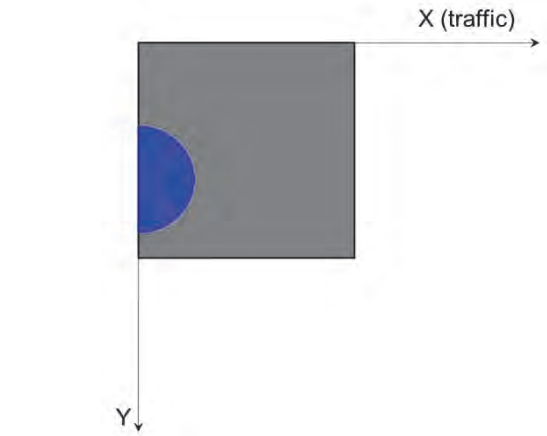

Figura 8. Vista en planta cuarto de carga dual circular
Fuente: Autores

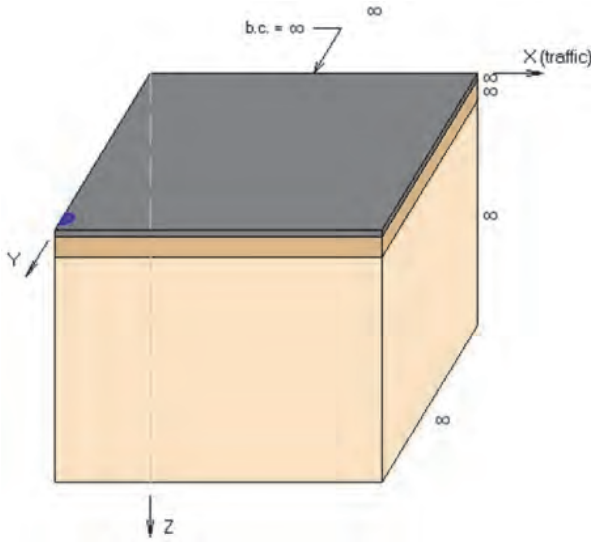

Figura 9. Vista 3D cuarto de carga dual circular
Fuente: Autores

2.2.1. Área de contacto y distribución de la presión

Validado el modelo de elementos finitos con el área de contacto circular, se procedió a desarrollar tres modelos adicionales variando únicamente la distribución de la presión de contacto de la carga dual de manera más ajustada a la realidad (Figs. 2 y 3). Los análisis se desarrollaron con los mismos parámetros de rigidez, espesores, distancia entre ejes y presión de contacto, teniendo en cuenta un área de huella rectangular cuyo ancho de banda "Tire Tread Width" se calcula a partir de las expresiones (1) y (2). La Fig. 10 justifica la procedencia del nuevo dato de cálculo.

$$A_{circular} = \pi r^2 = (\pi)\,(12.5\text{cm})^2 = 490.87\text{cm}^2 \qquad (1)$$

$$A_{rectangular} = 490.87\text{cm}^2 = (5)(25)(x) \Rightarrow x = 3.927\text{cm} \qquad (2)$$

Donde x es el ancho de banda de llanta, A es el área de la huella y r es el radio del área circular.

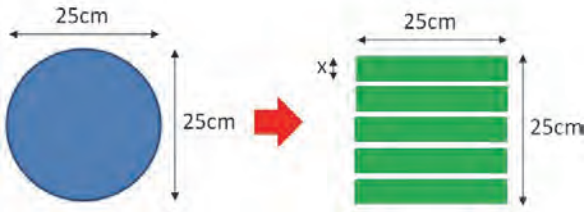

Figura 10. Área de contacto circular y huella rectangular
Fuente: Autores

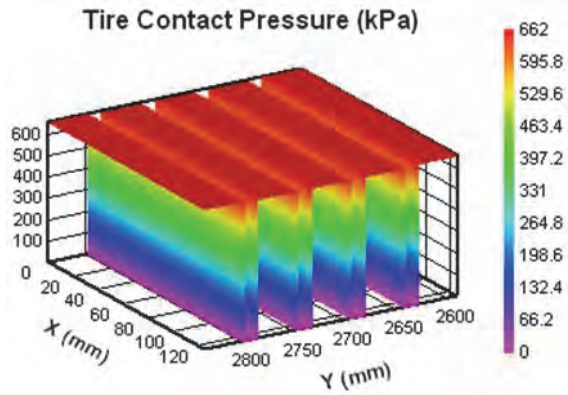

Figura 11. Distribución a lo largo de la llanta presión constante
Fuente: Autores

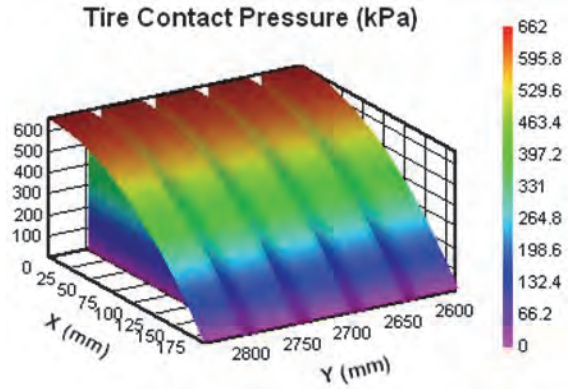

Figura 12. Distribución a lo largo de la llanta presión parabólica y media onda sinusoidal
Fuente: Autores

Definida la forma de la huella, se evaluaron diferentes distribuciones de la presión de contacto: constante, parabólica y media onda sinusoidal como se muestra en las Figs. 11 y 12; destacando que el pulso sinusoidal es característico en la determinación de la curva maestra de ensayos dinámicos de concreto asfaltico, de hecho, *la prueba de módulo dinámico mide la relación esfuerzo-deformación de una muestra bajo un* pulso *de carga sinusoidal continuo* [15-17]. Al igual que en el caso de área de contacto circular, el programa ubica la carga dual a un cuarto (1/4-simétrica) para optimizar el tiempo de cálculo [14]. Las ilustraciones del caso se presentan en las Figs. 13, 14 y 15.

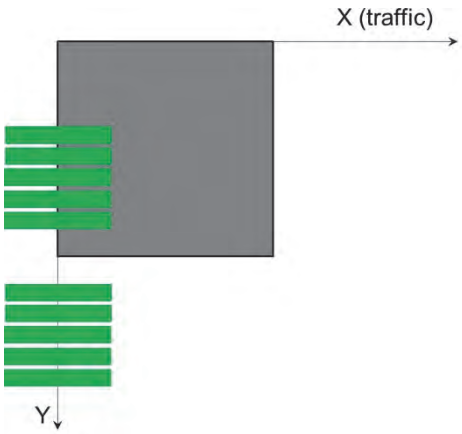

Figura 13. Vista en planta carga dual rectangular
Fuente: Autores

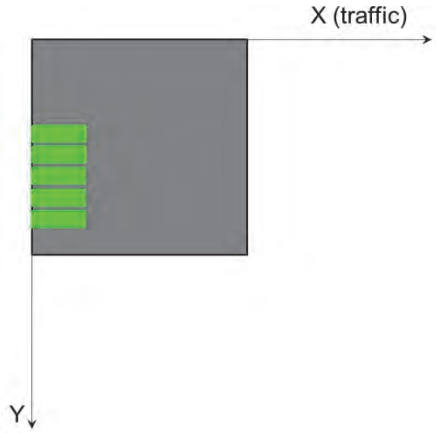

Figura 14. Vista en planta cuarto de carga dual rectangular
Fuente: Autores

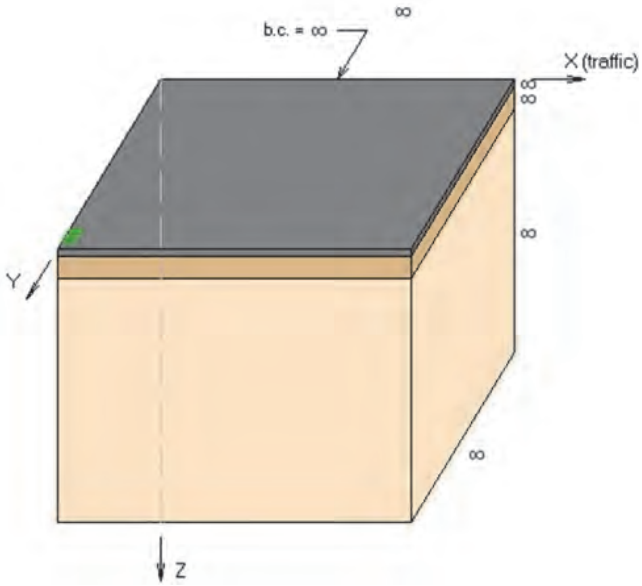

Figura 15. Vista tridimensional cuarto de carga dual rectangular
Fuente: Autores

3. Resultados y Discusión

En la Tabla 4 se presentan los resultados del modelo analítico realizado con EverStress© 5.0 - *utilizado como validador* - y del modelo de elementos finitos EverStressFE 1.0 trabajado con área de contacto circular.

Se observa que los porcentajes de variación del modelo numérico frente al analítico son inferiores al 1% lo cual permite concluir que las decisiones tomadas en la modelación con EverStressFE 1.0 son adecuadas para implementar los modelos que introducen modificaciones en la forma de la huella y la presión de contacto de la llanta. En las Figs. 16 y 17 se presentan los resultados del modelo analítico; los valores subrayados corresponden a los parámetros del diseño racional.

De los resultados contenidos en las Figs. 16 y 17 se verifica que: 1) la deformación máxima a compresión sobre la subrasante en el modelo multicapa elástico está bajo la llanta y no en el centro de la carga dual, 2) las deformaciones máximas en las fibras inferiores de las capas asfálticas BBSG y GB están bajo el centro de la carga dual y no bajo la llanta.

Las Figs. 18, 19 y 20 muestran los resultados gráficos de deformación correspondientes a los parámetros del diseño racional por medio de isocontornos. La Fig. 18 representa las deformaciones εxx situadas en la fibra inferior de la capa asfáltica BBSG; se observa la concentración de esfuerzos en la zona de aplicación de la carga. El semicírculo corresponde a un cuarto de carga dual con la forma típica de la huella empleada por el método racional. Los valores de deformación εxx mostrados en la Fig. 18, sugieren un comportamiento a compresión de la capa asfáltica inclusive en la fibra inferior

Tabla 4.
Validación de los resultados de control de diseño estructura pavimento asfaltico grueso

Capa	Parámetro	Analítico	Elementos Finitos 3D	% Variación
BBSG	εxx → εc	-38.81E-06	-38.83E-06	0.05%
GB	εxx → εt	84.26E-06	84.27E-06	0.01%
Subrasante	εzz → εc	-264.94E-06	-262.96E-06	0.75%

Fuente: Autores

```
Location No:   ZX-Position (cm):     .000  Y-Position (cm):
18.750
Line
cNormal Stresses
Z-Position Layer Sxx   Syy   Szz   Syz   Sxz   Sxy
(cm)  *     (kPa) (kPa) (kPa) (kPa) (kPa) (kPa)

  5.999    1      -361.19    -394.36     -38.89       -.02
.00        .00
 23.999    2      1045.46     785.11     -37.10        .00
.00        .00
 24.001    3        -6.23      -9.59     -37.10        .00
.00        .00
Line
cNormal Strains and Deflections
Z-Position Layer Exx   Eyy   Ezz   Ux    Uy    Uz
(cm)  *     (10^-6)    (10^-6)    (10^-6)    (microns)  (microns)
      (microns)

  5.999    1       -38.81     -47.10      41.77        .000
.000    313.101
 23.999    2        84.26      46.47     -72.88        .000
.001    310.216
 24.001    3        84.27      46.48    -263.06        .000
.001    310.213
Line
```

Figura 16. Resultados de deformación εxx en las fibras inferiores de las capas asfálticas BBSG y GB en EverStress© 5.0 con presión constante circular
Fuente: Autores

Location No: 1X-Position (cm): .000 Y-Position (cm): .000
Line
cNormal Stresses

Z-Position (cm) *	Layer	Sxx (kPa)	Syy (kPa)	Szz (kPa)	Syz (kPa)	Sxz (kPa)	Sxy
5.999	1	-570.01	-526.80	-594.25	39.05	.00	.00
23.999	2	1052.48	888.25	-36.67	4.04	.00	.00
24.001	3	-5.91	-8.03	-36.67	4.03	.00	.00

Line
cNormal Strains and Deflections

Z-Position (cm) *	Layer	Exx (10^-6)	Eyy (10^-6)	Ezz (10^-6)	Ux (microns)	Uy (microns)	Uz (microns)
5.999	1	-32.90	-22.09	-38.96	.000	5.919	309.011
23.999	2	81.12	57.28	-76.98	.000	9.894	301.943
24.001	3	81.13	57.29	-264.94	.000	9.895	301.940

Line

Figura 17. Resultados de deformación εzz sobre la subrasante en EverStress© 5.0 con presión constante circular
Fuente: Autores

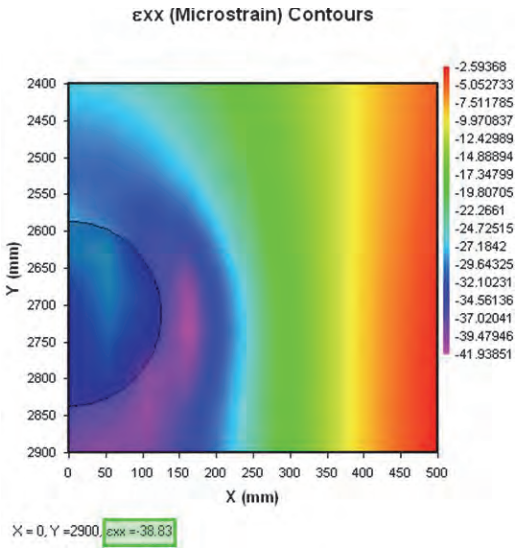

Figura 18. Deformación εxx en la fibra inferior de la capa asfáltica BBSG en EverStressFE 1.0 con presión constante circular
Fuente: Autores

lo cual probablemente es atribuible al módulo de la capa asfáltica de rodadura BBSG, a la rigidez de la capa contigua GB y a la misma condición de liga de las interfaces. El valor de deformación máxima εxx en esta capa se sitúa en el centro de la carga dual (coordenadas: X=0, Y=2900) tal como lo sugiere el modelo multicapa.

La Fig. 19 representa las deformaciones εxx situadas en la fibra inferior de la capa asfáltica GB. Los valores de deformación mostrados en la figura, denotan el típico comportamiento a tensión de la capa asfáltica como lo sugiere el método racional en el control de diseño. El valor de deformación máxima εxx en esta capa se sitúa en el centro de la carga dual (coordenadas: X=0, Y=2900) tal como lo indica el modelo multicapa.

Los isocontornos de deformación vertical de la Fig. 20 siguen el patrón de la huella circular, encontrándose que el valor de deformación máxima vertical εzz en esta capa se

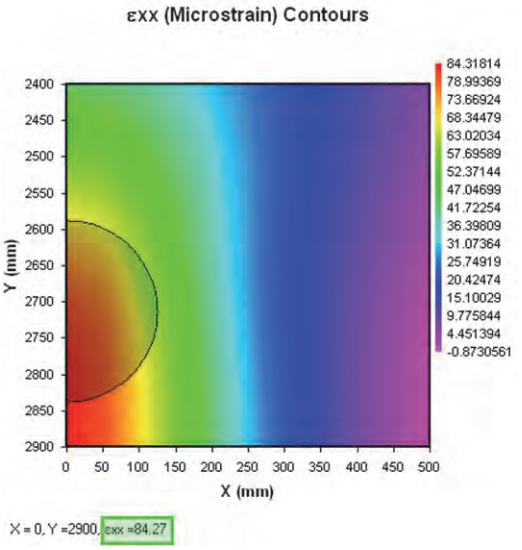

Figura 19. Deformación εxx en la fibra inferior de la capa asfáltica GB en EverStressFE 1.0 con presión constante circular
Fuente: Autores

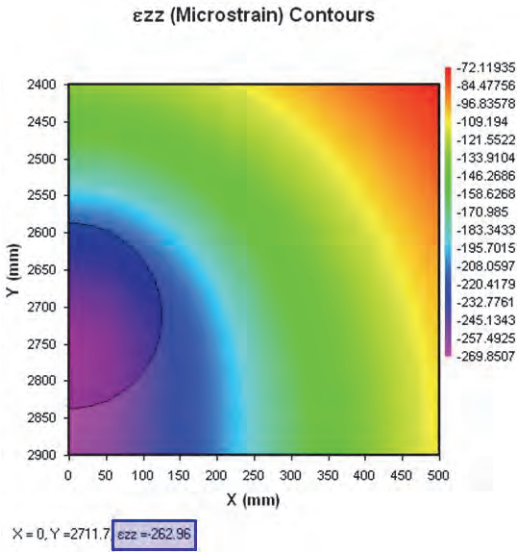

Figura 20. Deformación εzz sobre la subrasante en EverStressFE 1.0 con presión constante circular
Fuente: Autores

sitúa en el centro de la carga dual (coordenadas: X=0, Y=2900) y no en el centro de la llanta como lo sugiere el modelo multicapa, lo cual probablemente es debido a la carga dual y/o a la misma rigidez de la estructura y de la subrasante.

3.1. Modelos de elementos finitos con área de contacto rectangular y otras distribuciones de presión

Se desarrollaron tres modelos para analizar la respuesta a la deformación de la estructura de pavimento cuando se emplea un área de contacto y una distribución de la presión de inflado de las llantas sobre la superficie de manera más ajustada a la realidad. El área de contacto corresponde a la huella típica rectangular mostrada en la Fig. 3 y se evaluaron

las distribuciones de presión constante, parabólica y media onda sinusoidal de las Figs. 11 y 12 respectivamente.

3.1.1. Presión constante

La Fig. 21 presenta el desarrollo de la deformación εxx en la fibra inferior de la capa asfáltica BBSG con presión de inflado constante. En el centro de la carga dual ubicado en las coordenadas X=0, Y=2900 y Z=60 cm se encuentra la máxima deformación normal εxx=-39.77E-06 (-39.77 microstrain). Esta deformación por ser de compresión se considera no representativa en el diseño y señala que el eje neutro de la estructura se encuentra por debajo de la capa de rodadura BBSG. En adelante el análisis de resultados se desarrollará respecto al modelo de referencia de presión constante y área de contacto circular. Al comparar los resultados de isocontornos de deformación εxx con los del modelo de referencia, se observa que el rango de valores de deformación es similar, al igual que la distribución de los isocontornos en el plano. Las deformaciones promedio de mayor valor se encuentran capturadas dentro de la huella rectangular. La distribución de la deformación indica que la huella rectangular es una buena representación del contacto de la llanta con la superficie del pavimento.

La Fig. 22 presenta los resultados de la deformación εxx en la fibra inferior de la capa asfáltica GB. Entendiendo al pavimento como un elemento sometido a flexión, se aprecia que el eje neutro de la estructura se encuentra dentro del dominio de esta capa. La máxima deformación normal εxx es 80.92E-06 (80.92 microstrain), está ubicada en el centro de la carga dual con coordenadas X=0, Y=2900, pero con Z=240 cm y representa el estado de tensión característico del diseño racional.

La Fig. 23 representa la deformación εzz sobre la subrasante. La máxima deformación normal εzz de -253.27E-06 (-253.27 Microstrain) está ubicada en las coordenadas X=0, Y=2900 y Z=240 cm.

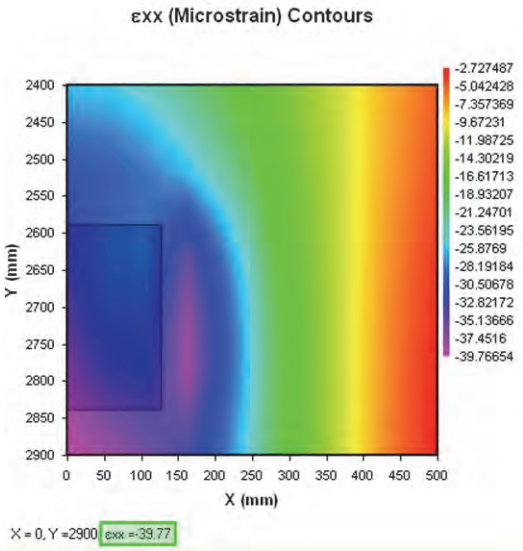

Figura 21. Deformación εxx en la fibra inferior de la capa asfáltica BBSG en EverStressFE 1.0 con presión constante rectangular
Fuente: Autores

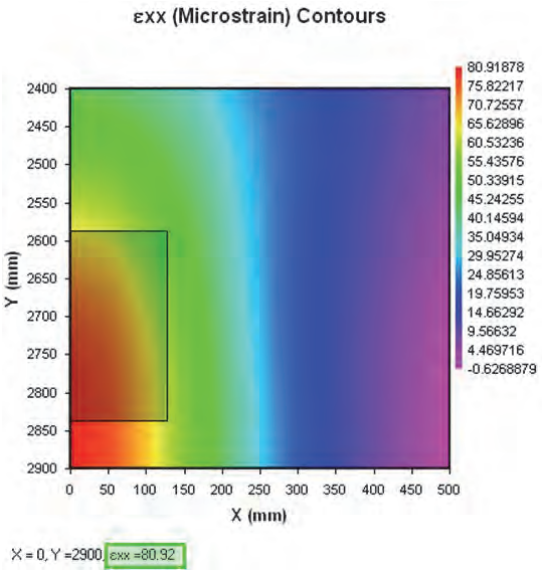

Figura 22. Deformación εxx en la fibra inferior de la capa asfáltica GB en EverStressFE 1.0 con presión constante rectangular
Fuente: Autores

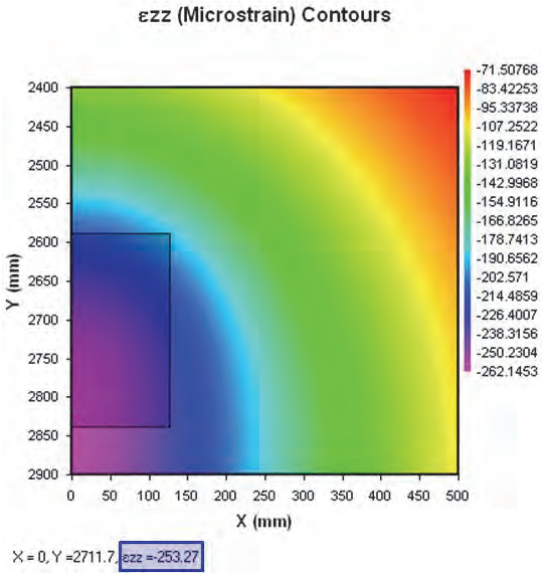

Figura 23. Deformación εzz sobre la subrasante en EverStressFE 1.0 con presión constante rectangular
Fuente: propia

La Tabla 5 contiene el resumen de los resultados comparados con los obtenidos del modelo elástico multicapa EverStress 5.0, determinando porcentajes de variación bajos y poco significativos.

Tabla 5.
Variación de los parámetros de control de diseño estructura pavimento asfaltico grueso mediante una presión constante rectangular

Capa	Parámetro	Analítico	Elementos finitos 3D	% Variación
BBSG	εxx → εc	-38.81E-06	-39.77E-06	2.47%
GB	εxx → εt	84.26E-06	80.92E-06	3.96%
Subrasante	εzz → εc	-264.94E-06	-253.27E-06	4.40%

Fuente: Autores

3.1.2. Presión parabólica

La Fig. 24 indica la deformación εxx en la fibra inferior de la capa asfáltica BBSG. Al comparar los resultados de isocontornos de deformación εxx con los del modelo de referencia, se observa que el rango de valores de deformación es similar, no obstante, la distribución de los isocontornos en el plano es ligeramente diferente, esto es, el contorno de deformación máxima se concentra en el centro de la carga dual, significando menor densidad de deformación normal a compresión alrededor de la huella.

En la Fig. 25 se presenta la deformación εxx en la fibra inferior de la capa asfáltica GB. La máxima deformación normal εxx es 78.95E-06 (78.95 microstrain) y se ubica en las coordenadas X=0, Y=2900 y Z=240 cm.

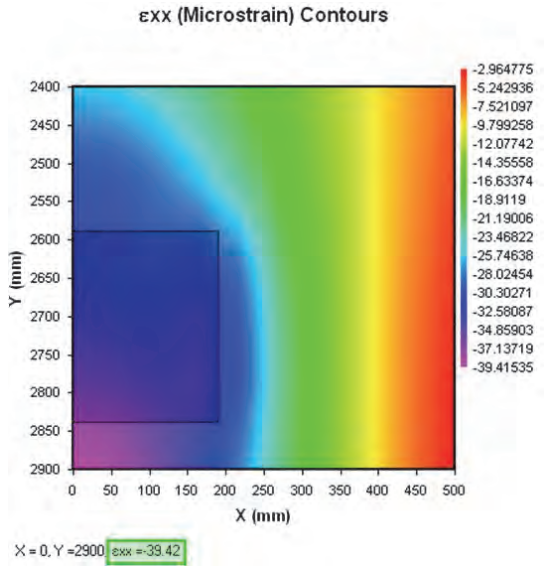

Figura 24. Deformación εxx en la fibra inferior de la capa asfáltica BBSG en EverStressFE 1.0 con presión parabólica rectangular.
Fuente: Autores

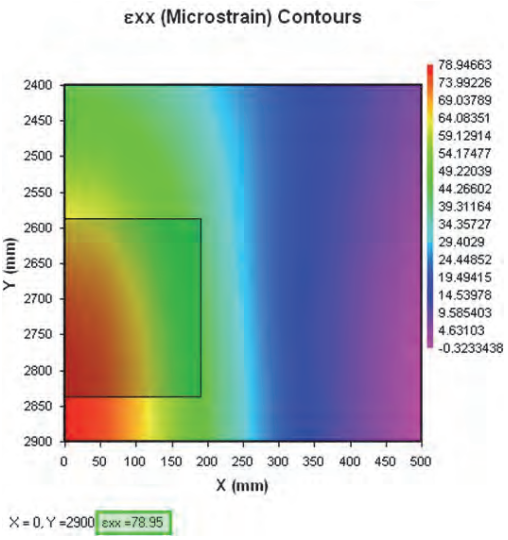

Figura 25. Deformación εxx en la fibra inferior de la capa asfáltica GB en EverStressFE 1.0 con presión parabólica rectangular.
Fuente: Autores

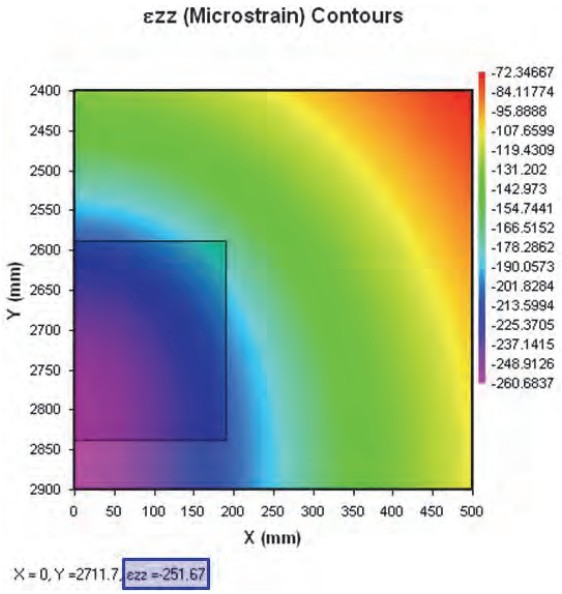

Figura 26. Deformación εzz sobre la subrasante en EverStressFE 1.0 con presión parabólica rectangular.
Fuente: Autores

Tabla 6.
Variación de los parámetros de control de diseño estructura pavimento asfaltico grueso mediante una presión parabólica rectangular.

Capa	Parámetro	Analítico	Elementos finitos 3D	% Variación
BBSG	εxx → εc	-38.81E-06	-39.42E-06	1.57%
GB	εxx → εt	84.26E-06	78.95E-06	6.30%
Subrasante	εzz → εc	-264.94E-06	-251.67E-06	5.01%

Fuente: Autores

La Fig. 26 reproduce la deformación εzz sobre la subrasante. En la coordenada X= 0, Y=2900 y Z=240 cm se ubica la máxima deformación normal a compresión εzz de -251.67E-06 (-251.67 microstrain). Al comparar los resultados de isocontornos de deformación εzz de la Fig. 26 con los del modelo de referencia, se observa que el isocontorno de deformación máxima es más amplio denotando un mayor rango de afectación a compresión. Adicionalmente, dentro de la huella se desarrollan más isocontornos denotando menos homogeneidad o uniformidad de deformación dentro de la misma.

La Tabla 6 contiene el resumen de los resultados comparados con los obtenidos del modelo elástico multicapa EverStress 5.0. Este resultado llama la atención porque las deformaciones εxx y εzz, son variables representativas del diseño y los porcentajes de variación sugieren posibles sobredimensionamientos, por consiguiente mayores costos de la estructura.

3.1.3. Presión media onda sinusoidal

La Fig. 27 nos muestra el mapa de colores de la deformación εxx en la fibra inferior de la capa asfáltica BBSG. La máxima deformación normal εxx es -39.30E-06 (-39.30 microstrain) y se encuentra en las coordenadas X=0, Y=2900 y Z=60 cm.

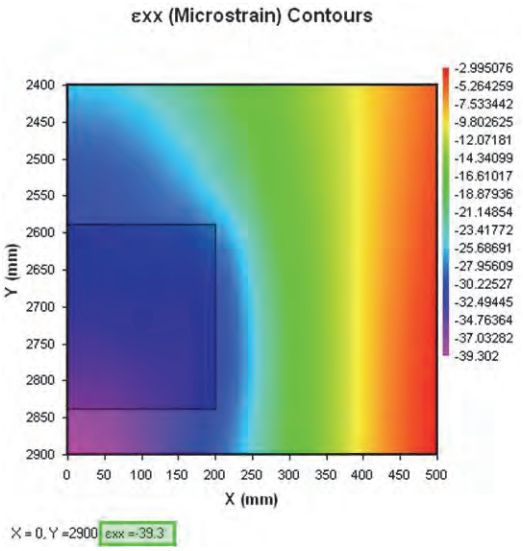

Figura 27. Deformación εxx en la fibra inferior de la capa asfáltica BBSG en EverStressFE 1.0 con presión media onda sinusoidal
Fuente: Autores

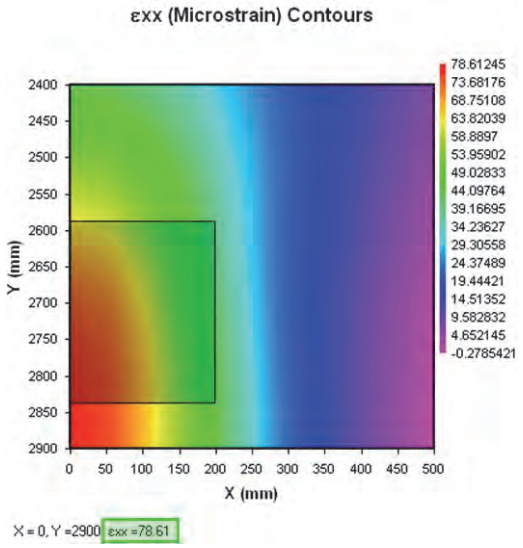

Figura 28. Deformación εxx en la fibra inferior de la capa asfáltica GB en EverStressFE 1.0 con presión media onda sinusoidal
Fuente: Autores

La Fig. 28 expone el mapa de colores de la deformación εxx en la fibra inferior de la capa asfáltica. En las coordenadas X=0, Y=2900 y Z=240 cm se presenta la máxima deformación normal εxx de 78.61E-06 (78.61 microstrain).

En la Fig. 29 se presenta el comportamiento de la deformación εzz sobre la subrasante. La máxima deformación normal εzz es -251.18E-06 (-251.18 microstrain) y se ubica en las coordenadas X= 0, Y=2900 y Z=240 cm.

La Tabla 7 presenta el resumen de los resultados comparados con los valores obtenidos del modelo elástico multicapa EverStress 5.0, encontrándose porcentajes de variación de 1.26% y 6.71% para las capas asfálticas y 5.19% sobre la subrasante. Este escenario también llama la atención, porque las deformaciones εxx y εzz determinadas por el método analítico se encuentran 6.30 y 5.01% por encima de los resultados del modelo de elementos finitos, sugiriendo sobredimensionamiento de la estructura. Probablemente, el diseño racional debería ajustarse a condiciones más reales de área de contacto y distribución de presión.

La Tabla 8 resume los resultados de deformación y esfuerzo de las capas constitutivas de la estructura de pavimento para cada uno de los modelos implementados.

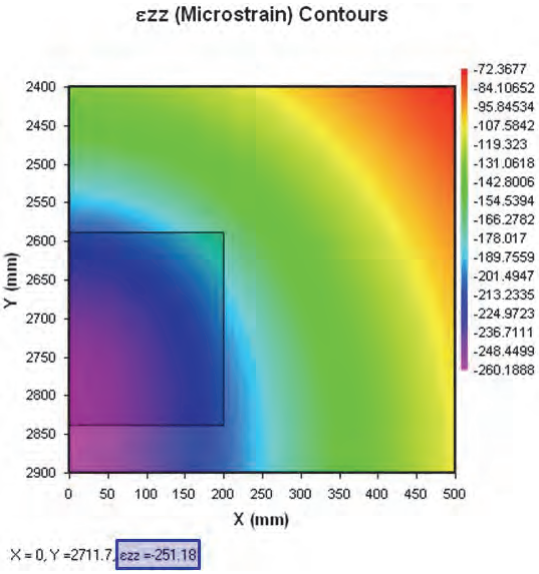

Figura 29. Deformación εzz sobre la subrasante en EverStressFE 1.0 con presión media onda sinusoidal
Fuente: Autores

Tabla 7.
Variación de los parámetros de control de diseño estructura pavimento asfaltico grueso mediante una presión media onda sinusoidal rectangular

Capa	Parámetro	Analítico	Elementos finitos 3D	% Variación
BBSG	εxx → εc	-38.81E-06	-39.30E-06	1.26%
GB	εxx → εt	84.26E-06	78.61E-06	6.71%
Subrasante	εzz → εc	-264.94E-06	-251.18E-06	5.19%

Fuente: Autores

Tabla 8.
Resumen de parámetros de control de diseño estructura pavimento asfaltico grueso

			Elementos finitos 3D		
Capa	Parámetro	Analítico	Presión constante	Presión parabólica	Presión media onda sinusoidal
BBSG	εxx → εc	-38.81E-06	-39.77E-06	-39.42E-06	-39.30E-06
GB	εxx → εt	84.26E-06	80.92E-06	78.95E-06	78.61E-06
Subrasante	εzz → εc	-264.94E-06	-253.27E-06	-251.67E-06	-251.18E-06

Fuente: Autores

4. Conclusiones

Los resultados obtenidos del modelo de elementos finitos desarrollado con el software libre EverStressFE fueron satisfactoriamente validados con el modelo analítico multicapa elástico, lo cual permite analizar el efecto de la presión de contacto de una carga dual sobre los parámetros de diseño de pavimentos asfalticos gruesos.

Los modeladores de elementos finitos de uso libre como el EverStressFE demuestran ser herramientas muy útiles y versátiles, de gran apoyo para análisis como el actual y suficientes frente a herramientas comerciales de alto costo y elevadas curvas de aprendizaje y adiestramiento.

En todos los casos modelados con elementos finitos, la deformación εzz máxima en la subrasante es mayor bajo el centro de la carga dual y no bajo una llanta como lo sugiere el modelo multicapa elástico, probablemente por la carga dual y/o la misma rigidez de la estructura y de la subrasante. Las causas serán estudiadas en futuros análisis.

Si se observa con cuidado los porcentajes de variación reportados en las tablas, es posible concluir que los diseños realizados con métodos analíticos están siendo ligeramente sobredimensionados. Por ejemplo, las deformaciones εxx obtenidas del análisis con presión constante circular y presión media onda sinusoidal en la capa GB son: 84.26E-06 y 78.61E-06 respectivamente, que en términos de número de ejes simples equivalentes con carga dual de 13T corresponde a 3620783 y 5122958 NE con espesores de 0.180m y 0.195m, revelando una diferencia de espesor de 0.015m que constructivamente se traduce en 2 cm adicionales de espesor en el diseño y en consecuencia mayores costos de obra.

El método de los elementos finitos ha demostrado ser muy eficaz y en el caso particular, permitió evaluar el efecto de la presión de contacto de una carga dual sobre los parámetros de diseño de un pavimento, por lo tanto, marca un camino a seguir para estudiar la sensibilidad de distintos factores que pueden afectar el diseño de pavimentos asfalticos.

Generado el interés de profundizar en el efecto de la presión de contacto de una carga dual sobre los parámetros de diseño de pavimentos asfalticos, en próximos estudios se analizarán condiciones dinámicas introduciendo resultados obtenidos de pruebas de campo a escala real.

Referencias

[1] Xia, K., Finite element modeling of dynamic tire/pavement interaction. Pavements and Materials: Testing and Modeling in Multiple Length Scales, pp. 204-214, 2010.

[2] LCPC., Conception et dimensionnement des structures de chaussée, Guide technique. Paris: LCPC and SETRA, 1994.

[3] Kringos, N., Birgisson, B., Frost, D. and Wang, L., Multi-Scale modeling and characterization of infrastructure materials, Proceedings of the International RILEM Symposium: Estocolmo, Springer, 2013.

[4] AASHTO., Mechanistic-empirical pavement design guide, A Manual of Practice. USA: American Association of State Highway and Transportation Officials, 2008.

[5] Rabaiottia, C., Puzrinb, A., Caprezb, M. and Ozanc, C., Pavement structural health evaluation based on inverse analysis of three dimensional deflection bowl. International Journal of Pavement Engineering, 14(4), pp. 374-387, 2013.

[6] Papagiannakis, A.T. and Masad, E.A., Pavement Design and Materials. Texas USA: John Wiley & Sons, 2008.

[7] Rodríguez, W., and Pallares M., Modelado tridimensional de un pavimento bajo carga dual con elementos finitos. DYNA 82(189), pp. 30-38, 2014.

[8] Beltran, G. and Romo, M., Assessing artificial neural network performance in estimating the layer properties of pavements, Ingeniería e Investigación, 34(2), pp. 11-16, 2014. DOI: 10.15446/ing.investig.v34n2.42158

[9] Rodríguez, W. y Pallares M., Desarrollo de un modelo de elementos finitos para el diseño racional de pavimentos. Tecnura, pp. 25-37, 2005.

[10] Tamayo, J., Comportamiento de los materiales bajo carga repetida, Ingeniería e Investigación, pp. 22-29, 1983.

[11] Figueroa, A., Reyes, F., Hernández, D., Jiménez, C. and Bohórquez, N., Análisis de un asfalto modificado con icopor y su incidencia en una mezcla asfáltica densa en caliente, Ingeniería e Investigación, 27(3), pp. 5-15, 2007.

[12] Davids, W.G., EverStressFE1.0 Software for 3D finite-element analysis of flexible pavement structures. Washington USA: The Washington State Department of Transportation, 2009.

[13] Davids, W.G., EverStressFE1.0 Theory Manual. Washington USA: The Washington State Department of Transportation, 2009.

[14] Davids, W.G., EverStressFE1.0 Software for 3D finite-element analysis of flexible pavement structures: Summary of features and capabilities. Maine USA: University of Maine, AEWC Advanced Structures and Composites Center, 2009.

[15] Witczak, M.W., Kaloush, K., Pellinen, T., El-Basyouny, M. and Von Quintus, H., NCHRP Report 465, Simple performance test for superpave mix design. Washington USA: Transportation Research Board, National Research Council, 2002.

[16] Bonaquist, R. and Christensen, D.W., Practical procedure for developing dynamic modulus master curves for pavement structural design. Transportation Research Record, pp. 208-217., 2005.

[17] Brown, E.R., Kandhal, P.S. and Zhang, J., Performance testing for hot mix asphalt. NCAT Report No. 01-05. Auburn Alabama USA: University of Auburn, National Center for Asphalt Technology, 2001.

M.R. Pallares-Muñoz, received the BSc. Eng in Civil Engineering from the UIS in 1998, the MSc. degree on Numerical Methods in Engineering from the UPC in 2004, She has worked as a professor and researcher for over ten years. Currently, she is a full professor in the Civil Engineering Program, Engineering Faculty, Universidad Surcolombiana, Colombia. Her research interests include: simulation and computational modeling.
ORCID: 0000-0003-4526-2357

J.A. Pulecio-Díaz, received the BSc. Eng in Civil Engineering from the USTA in 2008, the MSc. degree on Roadways Construction from the USTA in 2012. He has worked as a professor and researcher for over four years. Currently, he is a full professor in the Civil Engineering Program, Engineering Faculty, Universidad Surcolombiana, Colombia. His research interests include: computational modeling in Roadways.
ORCID: 0000-0001-6924-7034.

UNIVERSIDAD NACIONAL DE COLOMBIA
SEDE MEDELLÍN
FACULTAD DE MINAS

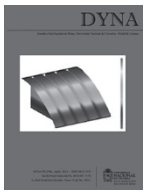

DYNA
http://dyna.medellin.unal.edu.co/

Collaborative goods distribution using the IRP model

Martín Darío Arango-Serna [a], Carlos Andrés-Romano [b] & Julián Andrés Zapata-Cortés [c]

[a] *Escuela Ingeniería de la Organización, Universidad Nacional de Colombia – Sede Medellín, Colombia. mdarango@unal.edu.co*
b Departamento de Organización de Empresas, Universitat Politècnica de València, España. candres@omp.upv.es
c Investigador Grupo GICO, Universidad Nacional de Colombia – Sede Medellín, Colombia. jazapat1@unal.edu.co

Received: August 14th, 2015. Received in revised form: November 01rd, 2015. Accepted: February 10th, 2016.

Abstract
This paper presents a study of the impact that collaboration in inventory has on distribution costs in a network of one supplier and multiple customers. Freight transport is widely studied due to its impact on logistics costs and service levels of enterprises. Looking for network configurations that improve some of these aspects will always be attractive to both academics and businesses. The collaborative distribution system was proposed using the IRP model, and it was compared with the scenarios in which the both supplier or customers optimize their inventory levels. For the IRP model solution a genetic algorithm was used, from which it was obtained a collaborative distribution system with a better performance than if the optimization is made independently.

Keywords: Goods distribution; collaboration; inventory management; IRP; genetic algorithm.

Distribución colaborativa de mercancías utilizando el modelo IRP

Resumen
Este artículo presenta un estudio sobre el impacto que tiene la distribución colaborativa sobre los costos en la toma de las decisiones del inventario entre un proveedor y múltiples clientes, utilizando el modelo IRP para definir el sistema de distribución. El transporte de mercancías es una actividad ampliamente estudiada debido al impacto tiene en los costos logísticos y en el nivel de servicio de las empresas. Buscar redes de distribución que mejoren alguno de estos aspectos siempre será atractivo tanto para académicos como para las empresas. El resultado producido por el modelo IRP fue comparado con los escenarios en que el proveedor y los clientes optimizan sus niveles de inventario. Para la solución del modelo IRP se utilizó un algoritmo genético, a partir del cual se logro obtener un sistema de distribución en colaboración con un mejor desempeño que el correspondiente cuando la optimización se hace de forma independiente.

Palabras clave: Distribución de mercancías; colaboración; manejo de inventario; IRP; algoritmos genéticos.

1. Introducción

La distribución de mercancías consiste en transportar los productos desde uno o múltiples puntos de origen a uno o múltiples puntos de destino, en donde se pueden encontrar varias instancias como zonas de almacenamiento, crossdocking, pasos interurbanos, pasos urbanos, transito internacional, múltiples escalones, entre muchas otras posibilidades que son especificas de la configuración de las empresas participantes y de la relación entre ellas [1]. Estas actividades son especificas a la configuración de la red y condicionan los costos y el cumplimiento de los niveles de servicio del proceso de distribución [2].

Los procesos de distribución de mercancías requieren sistemas de administración que permitan encontrar mejores condiciones de operación para reducir los costos y asegurar el nivel de servicio, de forma que se logren alcanzar las metas estratégicas de la compañía junto con el desempeño financiero propuesto (rentabilidad esperada) [3]. Uno de los elementos críticos en estos sistemas de distribución, es la inclusión de la variable del inventario [4-7].

El presente articulo presenta un esquema en el cual se resuelve de manera conjunta el problema de la asignación del inventario y la determinación de las rutas para un conjunto de clientes atendidos por un mismo proveedor, en el cual, mediante la decisión centralizada por parte del proveedor, se decide la cantidad de mercancía, el momento de enviarlas y la secuencia de las rutas para este proceso de distribución. Para encontrar la configuración de este proceso de distribución se utiliza el modelo de ruteo de inventario IRP (Inventory Routing Problem), el cual fundamenta su enfoque es la estrategia de colaboración VMI [8-10].

© The author; licensee Universidad Nacional de Colombia.

El articulo esta conformado por 4 partes: En la primera se presenta la importancia de incluir la variable inventario en los procesos de distribución y como este proceso puede ser optimizado utilizando el modelo IRP. La segunda parte presenta el enfoque metodológico utilizado para ejemplificar el uso del modelo IRP mediante un algoritmo genético, el cual presenta una nueva forma de representar el individuo. La tercera parte presenta los resultados de la aplicación del modelo y el análisis de resultados, para posteriormente presentar las conclusiones en la cuarta parte.

2. Marco Teórico

Entre las decisiones mas importantes de los procesos de diseño de redes de distribución se encuentra la de asignar adecuadamente el inventario a las instalaciones de la red, lo cual incluye la planificación y determinación de las instancias y el movimiento de los productos en la cadena de distribución [5,7]. Cho et al [11] y Bertazzi y Esperanza [12] mencionan la importancia de incluir dentro de los procesos de distribución de mercancía la variable del nivel de inventario. Estos autores señalan que generalmente los modelos matemáticos implementados para optimizar los costos de transporte se basan en las distancias recorridas y/o en la ubicación de las instalaciones, por lo cual estudiaron la inclusión de los costos de inventario en proveedores y en los clientes, como un elemento fundamental dentro de los procesos de optimización de las redes de transporte.

Para lograr incluir la variable del inventario en los procesos de distribución de mercancías, se hace necesario un proceso de colaboración entre proveedores y clientes, mediante el cual puedan conocerse los pronósticos de demanda y los niveles del inventario y a partir de esto diseñar un esquema de asignación del inventario eficiente para los clientes y para los proveedores [13,14].

La colaboración en la cadena de suministros y particularmente en el manejo del inventario es una estrategia que permite disminuir los costos y mejorar el nivel de servicio en las operaciones de abastecimiento de las empresas y de las propias cadenas [15]. Múltiples autores han estudiado los procesos colaborativos para la toma de decisiones sobre el manejo de inventarios entre empresas [16-21], donde el inventario manejado por el vendedor VMI es la estrategia más comúnmente utilizada a nivel empresarial y mas estudiada a nivel académico [22,23]. El VMI (Vendor Managed Inventory) es el proceso en el cual el vendedor asume la tarea de decidir sobre la asignación del inventario en la cadena de suministros, generando pedidos de compra para el reabastecimiento del inventario de los clientes, mediante un proceso centralizado con el propósito de reducir los costos de almacenamiento y los faltantes de productos en los puntos de distribución [14].

Para resolver el problema de la asignación simultánea de las rutas de transporte y las decisiones del inventario, el modelo mas estudiado es el Problema de Ruteo de Inventario (Inventory Routing Problem - IRP) [22], el cual se basa en la estrategia de inventarios colaborativos manejados por el vendedor (VMI) y que tiene como finalidad combinar el problema de asignación del inventario para reducir los costos de mantener mercancía, al tiempo que optimiza la utilización de los recursos de transporte [9,8,24,25]. El modelo IRP se encarga de asignar el inventario a cada uno de los clientes y a partir de esto asigna las rutas para abastecerlos [10,25,26]. Esto es posible, toda vez que el modelo IRP se basa en el enfoque VMI, en donde las demandas y los niveles del inventarios son conocidos por el proveedor, y es este el responsable de la distribución de las mercancías.

Tabla 1.
Autores que resuelven el IRP y sus variaciones.

Autores	Año	Modelo
Kleywegt et al., [35]	2004	DIRP
Campbell & Savelsbergh, [27]	2004	IRP
Aziz & Moin [38]	2007	MP-IRPMP
Fengjiao Qingnian [37]	2008	IRPSD
Zeng & Wang, [34]	2010	SIRPTW
Archetti et al., [29]	2011	IRP
Coelho et al., [32]	2011	IRPTS
Liu & Lee, [33]	2011	IRPTW
Azuma et al., [9]	2011	IRP
Liu et al., [36]	2011	IRP
Siswanto et al. [39]	2011	IRP
Adulyasak et al.[41]	2012	MIRP
Van Anholt et al. [40]	2013	(PDIRPTW).
Arango et al.[25]	2015	MDIRP

Fuente: Elaboración propia.

Campbell and Savelsbergh [27] estudiaron el modelo IRP para enfoques de decisión de largo plazo, mediante un esquema de descomposición de las decisiones en dos fases: en la primera se asigna el inventario y en la segunda se generan las rutas. Archetti et al.[8] y Solyali y Süral [28] han propuesto métodos exactos para resolver el modelo IRP para un único vehículo, encontrando dificultades para resolver problemas de grandes dimensiones. Para resolver este inconveniente, Archetti et al., [29] y Azuma [30] han utilizado heurísticas y metaheurísticas respectivamente. El problema de múltiples vehículos ha sido resuelto por Coelho et al., [31] y Coelho et al., [32] utilizando metaheurísticas. La Tabla 1 presenta una revisión de algunos otros trabajos encontrados en la literatura especializada, en los que se encuentra solución para diferentes variaciones del modelo IRP.

En su versión mas simple, el modelo IRP para múltiples vehículos puede ser formulado considerando un grafico Hamiltoniano G = (V,A) donde V es el conjunto de nodos $V = \{0, 1, 2, 3, \dots, n\}$ y A es el conjunto de arcos $A = \{(i, j): j, i \in v, i \neq j\}$. El vértice 0 representa el deposito y v' es el subconjunto de vértices en el cual no se incluye el origen. t es el periodo, con τ el conjunto de periodos ($\tau = \{1,2,3, \dots p\}$) y p es el Horizonte de tiempo de la planificación. En el modelo existe un numero limitado de vehículos $k \in K$ $(k = \{1, 2, 3, \dots, n\}$, con capacidad heterogénea. Sea x_{ij}^{kt} es una variable binaria con valor de 1 si el arco i-j es usado en la ruta del vehículo k en el tiempo t, o cero en otro caso, I_0^t y I_i^t el inventario en el proveedor y los clientes respectivamente y h_i, h_0, y c_{ij} los costos de inventario y transporte.

A partir de la formulación presentada por Arango et al. [25], el modelo aquí presentado para la distribución entre un proveedor y múltiples clientes, la función objetivo y el conjunto de restricciones para la minimización de los costos de transporte e inventario se escriben como:

$$minimizar \quad \sum_{i\in v'}\sum_{t\in\tau} h_i I_i^t + \sum_{t\in\tau} h_0 I_0^t + \sum_{t\in\tau}\sum_{i\in v}\sum_{i\in v}\sum_{k\in K} c_{ij} x_{ij}^{kt} \quad (1)$$

Sujeta a las siguientes restricciones:

1. Restricción de inventario en el proveedor.

$$I_0^t = I_0^{t-1} + r_0^{t-1} - \sum_{k\in K}\sum_{i\in v} q_i^{kt-1} \quad (2)$$

$$I_0^t \geq \sum_{k\in K}\sum_{i\in v} q_i^{kt} \quad (3)$$

2. Restricción de inventario en los clientes.

$$I_i^t = I_i^{t-1} + \sum_{k\in K}\sum_{i\in v} q_i^{kt} - d_i^t \quad (4)$$

$$I_i^t \geq 0 \quad (5)$$

$$I_i^t \leq C_i \quad (6)$$

3. Restricciones de política de abastecimiento.

$$q_i^{kt} \geq C_i Y_i^{kt} - I_i^t \quad (7)$$

$$q_i^{kt} \leq C_i - I_i^t \quad (8)$$

$$q_i^{kt} \leq C_i Y_i^{kt} \quad (9)$$

4. Restricciones de capacidad del vehículo.

$$\sum_{i\in v} q_i^{kt} \leq Q_k \quad (10)$$

5. Restricciones de ruteo.

$$\sum_{i\in v} q_i^{kt} \leq Q_k Y_0^{kt} \quad (11)$$

$$\sum_{i\in v, i<j} X_{ij}^{kt} + \sum_{i\in v, j<i} X_{ji}^{kt} = 2y_i^{kt} \quad (12)$$

$$\sum_{i\in S}\sum_{j\in S} X_{ij}^{kt} \leq \sum_{i\in S} y_i^{kt} - y_m^{kt} \quad \forall\, subconjunto\ S \subseteq V \quad (13)$$

6. Restricciones de no-negatividad.

Todas las variables presentadas en el modelo, son mayores o iguales a cero, por lo cual $q_i^{kt} \geq 0$; $Q_k \geq 0$; $I_i^t \geq 0$; $d_i^t \geq 0$; $C_i \geq 0$.

q_i^{kt} es la cantidad enviada al cliente i, Y_i^{kt} es una variable binaria que toma el valor 1 si el nodo i es visitado por el vehículo k en el periodo t, o cero de otra forma. La función objetivo de la eq. (1) busca la minimización del inventario y de los costos de Transporte. Las ecuaciones de política de abastecimiento eq. (7)-(9) aseguran que cuando un cliente es visitado, la cantidad de mercancía que debe recibir sea lo que le falte para llegar a su inventario máximo ($C_i - I_i^t$), Las restricciones de ruteo aseguran que se genere una ruta adecuada en el periodo t, de forma que se visiten todos los clientes que deben ser servidos en dicho periodo. En este sentido, la eq. (11) asegura que si al menos un cliente es visitado, luego la ruta debe visitar al proveedor. La eq. (12) representa que si el nodo (cliente) i es visitado, debe haber un arco para la entrada y un arco para la salida de dicho nodo. La suma de estos arcos debe ser igual a $2y_i^{kt}$, con lo cual se asegura que si y solo si existen dichos arcos. La restricción de la eq. (13) evita la generación de sub-rutas del vehículo k en el tiempo t. Esto quiere decir que para cada subconjunto S, la cantidad de arcos debe ser menor o igual que el numero de nodos menos 1, con lo cual se asegura que solo se cree el tour de la solución.

Otras restricciones pueden ser formuladas para incluir extensiones del problema como ventanas de tiempo, múltiples depósitos, múltiples productos, entregas y recogidas simultaneas, etc. [10,40,42,43]. En la literatura científica especializada es posible encontrar trabajos de investigación que incluyen el inventario en los procesos de distribución de mercancías, que aunque no son enfoques colaborativos, al ser definidos para una única empresa, permiten abordar los procesos de integración de estas variables desde un enfoque mas complejo. Estos trabajos, dentro de los que se encuentran los desarrollados por Chang y Yen [44], Pradhananga et al. [45] y Melián-Batista et al. [46] generalmente utilizan procesos de optimización multiobjetivo para la propuesta de sistemas de transporte que incluyen las decisiones de inventario de forma conjunta con el diseño de las rutas para la distribución de mercancías.

3. Materiales y Métodos

En este artículo se busca evaluar el desempeño del modelo IRP para resolver un problema de distribución de mercancías. Para esto se analiza un problema definido en la literatura científica, a partir del cual se calculan los costos de la distribución optimizando el inventario en las instalaciones de los clientes y en el proveedor, y obteniendo el costo del ruteo con el uso del modelo VRP. Estos resultados son comparados con los costos obtenidos mediante la solución con el modelo IRP. La configuración de la red de distribución corresponde a la instancia de un proveedor, 15 clientes y un horizonte de tiempo de tres periodos, definida por Archetti et al. [8].

Para encontrar la solución tanto al modelo VRP como al IRP, se desarrollaron dos algoritmos genéticos, uno para VRP y otro para IRP. Debido a que el objetivo del modelo aquí presentado (un proveedor con múltiples clientes) es evaluar el IRP, solamente el algoritmo genético desarrollado para su solución será descrito. Ambos algoritmos genéticos fueron programados en Java, utilizando el entorno de desarrollo integrado NetBeans IDE.

3.1. Algoritmo genético para la solución del modelo IRP

Los algoritmos genéticos han demostrado ser herramientas adecuadas para resolver problemas matemáticos complejos [47,48], como es el caso de los problemas de ruteo de vehículos [49-51]. Para resolver el problema IRP, en la literatura científica el numero de trabajos que utilizan algoritmos genéticos o evolutivos es limitado, encontrándose los desarrollados por Azuma [30], Azuma et at. [9], Liu et al. [36], Fengjiao y Qingnian [37], Aziz y Moin [38], Aydin [52] y Cho et al. [11].

La principal diferencia entre estos trabajos se encuentra en la forma de representar el individuo (cromosoma) para su solución. Algunos autores para su solución presentan dos matrices, en las cuales se asigna la cantidad a enviar a cada cliente y la secuencia de las rutas, respectivamente. Otros autores utilizan una matriz en la cual de manera conjunta se representa la asignación del inventario y de las rutas de cada vehículo.

3.1.1. Representación del individuo

En este artículo se adopta la representación conjunta, con la diferencia que directamente el individuo indica la cantidad de mercancía a enviar a cada cliente, así como la secuencia de visita de los clientes que debe seguir cada vehículo. En la Tabla 2 se presenta un ejemplo de la forma del cromosoma utilizado en el algoritmo propuesto, el cual es una matriz en la cual las filas corresponden a los periodos del horizonte de planificación, y en las columnas se genera la asignación del inventario para cada uno de los clientes y luego la secuencia de la ruta a seguir.

En la Tabla 2 se observan las dos partes del cromosoma utilizado para un individuo con cinco clientes y tres periodos de planificación. La parte en gris corresponde a las cantidades asignadas a cada cliente (c) en el respectivo periodo (p). La parte sin sombrear corresponde a las rutas para la distribución de dichas cantidades. El algoritmo determina la mejor ruta con base en las cantidades a distribuir en cada periodo. De esta forma, en el periodo 1 solo se utiliza un vehículo, el cual debe partir del almacén del proveedor (punto cero) visitar los clientes en el respectivo orden 5-1-3 y volver al almacén. Por su parte, para el periodo 2 se requieren dos vehículos debido a que la carga sobrepasa la capacidad de los mismos, con lo cual el vehículo 1 debe visitar los clientes 1 y 4, y el vehículo 2 los clientes 5 y 2 en ese respectivo orden. Cada vez que se realiza una operación de cruce o mutación el algoritmo analiza el individuo y corrige las rutas, con lo cual siempre cada vehículo estará separado por un cero en el cromosoma.

3.1.2. Evaluación del individuo y selección

La evaluación del individuo (Función aptitud) se realiza calculando los costos totales de almacenamiento y transporte para el horizonte de planificación, con base en la eq. (1), que corresponde a la función objetivo del problema IRP. En este caso los mejores individuos son aquellos que presenten los menores valores de la función de aptitud. Los individuos son obtenidos por torneo aleatorio, cuyo tamaño equivale al 20% de la población.

3.1.3. Inicialización de la población

Cada individuo (cromosoma) de la población inicial del algoritmo genético se genera aleatoriamente. En este caso, las cantidades a enviar a cada cliente corresponden a un numero aleatorio entre la demanda del periodo y la cantidad máxima permitida si el cliente requiere ser abastecido, o cero en el otro caso. Las rutas son asignadas aleatoriamente y posteriormente corregidas dependiendo si se envía o no mercancía a todos los clientes.

Tabla 2.
Representación del individuo.

	c1	c2	c3	c4	c5	Secuencia de las rutas						
P1	[10	0	20	0	31	0	5	1	3	0	0	0]
P2	[76	25	0	12	60	0	1	4	0	5	2	0]
P3	[0	27	50	16	0	0	2	3	4	0	0	0]

Fuente: Elaboración propia.

3.1.4. Operador de cruce

El cruce de los cromosomas padres para producir nuevos individuos se realiza con un operador de cruzamiento similar al propuesto por Cho et al.[11], para el cruce vertical en el inventario y cruce de dos puntos para las rutas de un mismo periodo. En este procedimiento de cruce, los nuevos individuos se obtienen intercambiando las cantidades de todos los periodos de un mismo cliente de los padres para la parte del inventario. En la parte de las rutas, mediante cruce de dos puntos para cada periodo se realiza la recombinación para obtener el nuevo individuo. Una vez obtenidos los nuevos individuos, el algoritmo ajusta el cromosoma para obtener secuencia de ruteo factibles.

3.1.5. Operador de mutación

La mutación de individuos se realiza como es habitual de forma aleatoria. En este caso para la parte del inventario se utiliza un operador similar al propuesto por Cho et al.[11], en la cual la cantidad a enviar a un cliente escogido aleatoriamente se modifica, y el restante de la cantidad se compensa en el mismo cliente en los periodos previos o posteriores. Para la parte de las rutas, la mutación se realiza utilizando el método de intercambio simple (Swap) para un punto en cada uno de los periodos, también aleatoriamente. De forma similar a lo realizado con el operador de cruce, una vez la mutación termina, el cromosoma es ajustado para obtener secuencias de ruteo factibles.

4. Resultados

La información de la instancia tomada de Archetti et al. [8] que es utilizada para este articulo se presenta en la Tabla 3, a partir de la cual se obtiene la información requerida para realizar la simulación de los tres escenarios evaluados: Optimización del inventario en las instalaciones de los clientes, optimización del inventario en la instalación del proveedor y colaboración.

El optimo del inventario en las instalaciones de los clientes se obtiene logrando que el inventario en el horizonte de clientes sea el mínimo sin que existan faltantes, mientras que el optimo en el proveedor se logra enviando la mayor cantidad posible a los clientes, hasta que estos alcancen su nivel máximo. De esta forma, la cantidad a enviar a cada uno de los clientes y el inventario en cada periodo para los 2 escenarios mencionados se presenta en la Tabla 4. La Tabla 5 presenta el inventario para el proveedor.

A partir de la asignación del inventario en cada uno de estos dos primeros escenarios se calculan las rutas utilizando el modelo VRP. La Tabla 6 presenta las rutas encontradas

Tabla 3.
Datos de entrada de los tres escenarios.

Proveedor	**Pos. X - Proveedor**		**312**	**Pos. Y - proveedor**			**363**
	Inv. Inicial Proveedor		**2042**	**Costo inventario**			**0,03**
	Cantidad disponible Proveedor por periodo						**826**
	i	xi	yi	Ii0	Ci	di	hi
Clientes	1	237	182	32	64	32	0,02
	2	180	332	72	108	36	0,03
	3	141	388	182	273	91	0,03
	4	163	188	52	104	52	0,02
	5	282	374	152	228	76	0,02
	6	455	296	20	30	10	0,03
	7	326	332	85	170	85	0,04
	8	235	432	79	158	79	0,04
	9	412	488	22	44	22	0,02
	10	113	46	72	108	36	0,04
	11	266	302	136	204	68	0,02
	12	257	23	46	92	46	0,02
	13	363	22	55	110	55	0,02
	14	158	81	65	130	65	0,03
	15	423	95	146	219	73	0,02

Fuente: Elaboración propia. Adaptación de Archetti et al. [8].

utilizando un algoritmo genético para su solución. En esta tabla se observa que con las condiciones de distribución solo se requiere un vehículo para realizar el ruteo de las mercancías. Para todos los casos en que se requiera servir la totalidad de los clientes se asigna la mejor ruta obtenida por el algoritmo.

El tercer escenario, correspondiente a la colaboración entre el proveedor y los clientes se calcula utilizando algoritmo genético propuesto para resolver el modelo IRP. El algoritmo genético utilizado para resolver el problema colaborativo fue probado utilizando 200 individuos y a partir de 150 generaciones no se encontraron resultados que mejoraran la calidad de la solución, tal y como se observa en la Fig. 1.

El mejor individuo encontrado por el algoritmo después de las 150 generaciones presentadas en la Fig. 1 y que corresponden a la mejor solución para el problema de distribución colaborativo, se presenta en la Tabla 7, de la cual se puede observar la asignación del inventario y las rutas para cada uno de los periodos del horizonte de planificación.

A partir del mejor individuo se obtiene las cantidades a enviar y el inventario en cada clientes, como se observa en la Tabla 8. El inventario en el proveedor y las rutas generadas por el algoritmo para el esquema en colaboración se presentan en las Tablas 9 y 10 respectivamente.

Los costos obtenidos en cada uno de los escenarios estudiados son presentados en la Tabla 11, a partir de la cual se puede observar que los costos de la colaboración son inferiores a los obtenidos en cualquiera de los otros escenarios. Cuando se busca optimizar de forma independiente el inventario por

Tabla 4.
Cantidad a enviar e inventario optimizando el inventario en los clientes.

	Cliente		1	2	3	4	5	6	7	8	9	10	11	12	13	14	15
Escenario I. Optimo clientes	Cantidad	P1	0	0	0	0	0	0	0	0	0	0	0	0	0	0	0
		P2	32	0	0	52	0	0	85	79	22	0	0	46	55	65	0
		P3	32	36	91	52	76	10	85	79	22	36	68	46	55	65	73
	Inventario	P1	0	36	91	0	76	10	0	0	0	36	68	0	0	0	73
		P2	0	0	0	0	0	0	0	0	0	0	0	0	0	0	0
		P3	0	0	0	0	0	0	0	0	0	0	0	0	0	0	0
Escenario II. Optimo proveedor	Cantidad	P1	64	72	182	104	152	20	170	158	44	72	136	92	110	130	146
		P2	32	36	91	52	76	10	85	79	22	36	68	46	55	65	73
		P3	32	36	91	52	76	10	85	79	22	36	68	46	55	65	73
	Inventario	P1	64	108	273	104	228	30	170	158	44	108	204	92	110	130	219
		P2	64	108	273	104	228	30	170	158	44	108	204	92	110	130	219
		P3	64	108	273	104	228	30	170	158	44	108	204	92	110	130	219

Fuente: Elaboración propia.

Tabla 5.
Inventario en el proveedor.

	P1	**P2**	**P3**
Escenario I. Optimo clientes	2868	3258	3258
Escenario II. Optimo proveedor	1216	1216	1216

Fuente: Elaboración propia

Tabla 6.
Mejores rutas obtenidas para la distribución en cada periodo para cada escenario

Escenario I. Optimo clientes	P1	No requiere envíos de mercancía
	P2	D-9-8-4-14-12-13-1-7-D
	P3	D-5-2-3-8-9-6-15-13-12-10-14-4-1-11-7-D
Escenario II. Optimo proveedor	P1	D-5-2-3-8-9-6-15-13-12-10-14-4-1-11-7-D
	P2	D-5-2-3-8-9-6-15-13-12-10-14-4-1-11-7-D
	P3	D-5-2-3-8-9-6-15-13-12-10-14-4-1-11-7-D

Fuente: Elaboración propia

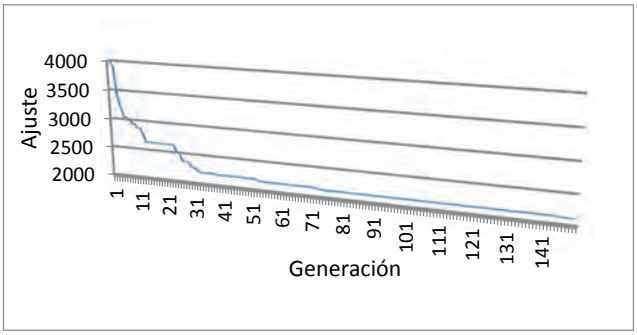

Figura 1. Evolución del mejor individuo obtenido mediante el algoritmo genético.
Fuente: Elaboración propia

Tabla 7.
Mejor individuo obtenido mediante el algoritmo genético.

	INVENTARIO ASIGNADO A LOS CLIENTES															RUTAS															
P1	[0	58	148	0	127	0	0	217	0	0	181	0	0	0	0	0	11	2	3	8	5	0	0	0	0	0	0	0	0	0	0]
P2	[95	0	0	155	0	12	248	0	65	53	0	137	164	149	81	0	1	4	14	10	12	13	15	6	9	7	0	0	0	0	0]
P3	[0	0	0	0	0	0	0	0	0	0	0	0	0	0	0	0	0	0	0	0	0	0	0	0	0	0	0	0	0	0	0]

Fuente: Elaboración propia.

Tabla 8.
Cantidad a enviar e inventario para el esquema en colaboración.

	Cliente		**1**	**2**	**3**	**4**	**5**	**6**	**7**	**8**	**9**	**10**	**11**	**12**	**13**	**14**	**15**
Escenario III. Colabor.	Cantidad	P1	0	58	148	0	127	0	0	217	0	0	181	0	0	0	0
		P2	95	0	0	155	0	12	248	0	65	53	0	137	164	149	81
		P3	0	0	0	0	0	0	0	0	0	0	0	0	0	0	0
	Inventario	P1	0	94	239	0	203	10	0	217	0	36	249	0	0	0	73
		P2	63	58	148	103	127	12	163	138	43	53	181	91	109	84	81
		P3	31	22	57	51	51	2	78	59	21	17	113	45	54	19	8

Fuente: Elaboración propia

alguna de las partes es posible obtener un costo mínimo en cada una de ellas (El inventario es mínimo en los clientes para el escenario I y mínimo en el proveedor en el escenario II), sin embargo ese optimo local genera que las actividades de transporte se intensifiquen para abastecer los clientes con las condiciones definidas para cada escenario, ocasionando que los costos de transporte se incrementen considerablemente y por tanto alejándose del optimo global del sistema. En el esquema colaborativo el inventario en los clientes o en los proveedores no se acerca a los valores óptimos encontrados en los escenarios I o II, sin embargo, debido a la centralización de las decisiones del inventario, los costos de distribución se reducen notablemente, ya que los clientes son visitados el menor numero de veces posible sin generar faltantes de producto, obteniendo en vez del optimo local del inventario, el optimo global del sistema de distribución.

La Fig. 2 presenta el grafico de superficie para el análisis de los costos estudiados, a partir de la cual se observa que los costos que generan mayor impacto son los correspondientes al transporte, ya que los de inventario son muy inferiores en magnitud, y son los que mas influyen para obtener el optimo global del sistema. Esto permite argumentar que las empresas por no realizar acciones colaborativas pueden realizar esfuerzos en actividades que generan poco valor.

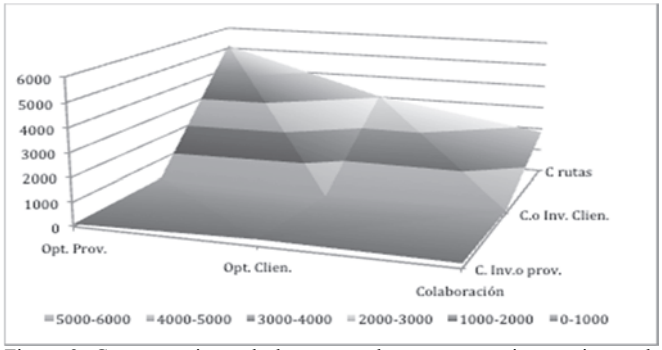

Figura 2. Comportamiento de los costos de transporte e inventario en el proveedor y los clientes.
Fuente: Elaboración propia

Tabla 9.
Inventario en el proveedor para el esquema en colaboración.

	P1	P2	P3
Escenario III. Colaboración	2131	1804	2630

Fuente: Elaboración propia

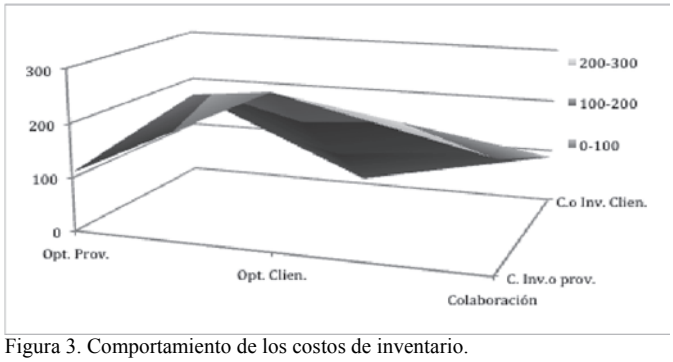

Figura 3. Comportamiento de los costos de inventario.
Fuente: Elaboración propia

Tabla 10.
Rutas para el esquema en colaboración.

Escenario III. Colaboración	P1	D-11-2-3-8-5-D
	P2	D-1-4-14-10-12-13-15-6-9-7-D
	P3	No requiere envío de mercancía

Fuente: Elaboración propia

Tabla 11.
Costos de transporte, inventario y totales de los escenarios evaluados.

Tipo de costo	**Optimo proveedor**	**Optimo clientes**	**Colaboración**
Costo rutas	5128,41	3049,54	1839,17
Costo Inventario proveedor	109,44	281,52	197,13
Costo Inventario clientes	164,91	9,89	86,73
Costo total	5402,76	3340,95	2123,03

Fuente: Elaboración propia

Analizando el comportamiento solo para el inventario en las instalaciones de los proveedores y clientes, tal y como se muestra en la Fig. 3, se observa que al llevar el inventario al menor para alguna parte ocasiona que en la contraparte se obtenga el peor valor del inventario, lo cual influye en el aumento de costos en el sistema. Para el caso en que se realiza la colaboración, como se mencionó anteriormente, no se obtiene el valor mínimo para el proveedor o para los compradores, sino un valor intermedio que no significa deteriorar llevar este valor a condiciones desfavorables para la contraparte, lo cual posibilita que el sistema de distribución sea mas eficiente, tal y como se demostró utilizando el modelo IRP.

Como medida del desempeño del algoritmo genético en este problema en particular, se realiza la comparación de la solución obtenida con otros resultados publicados en la literatura científica. En este mismo problema Azuma [30] reporto una solución con un costo total de 2131.04 y Coelho [53] reporto un costo total de 2236,53. A partir de estos resultados se puede argumentar que el algoritmo presentado arroja buenas soluciones para resolver la instancia utilizada para el ejemplo presentado. Sin embargo antes de poder argumentar que el algoritmo se comporta mejor que los presentados por los autores mencionados, deben realizarse las pruebas con las demás instancias y variaciones propuestas por Archetti et al.[8] o por Archetti et al. [54].

5. Conclusiones

Este artículo presenta una propuesta para optimizar la planificación conjunta de las operaciones de inventario y distribución entre un proveedor y múltiples clientes forma colaborativa. El proceso de distribución colaborativa basado en el IRP y en modelo VMI, permite disminuir significativamente los costos del proceso, comparado con cuando solamente y de forma independiente se busca optimizar los niveles de inventario en las instalaciones de los clientes o en las instalaciones de los proveedores.

En la distribución colaborativa las cantidades del inventario no se acercan a los valores óptimos del proveedor o de los clientes, pero al poder determinar de manera conjunta las cantidades a transportar y los momentos para hacerlo, se obtiene una reducción importante en el transporte, lo que hace que los costos totales del sistema sean inferiores comparados con los óptimos independientes.

EL modelo IRP es una alternativa adecuada para la formulación de problemas en los que los diseñadores de la red de distribución cuentan con la posibilidad de coordinar de manera conjunta los inventarios de los clientes y proveedores, toda vez que este modelo se basa en el modelo de inventarios colaborativos VMI y soporta la decisión de ruteo los enfoques del agente viajero (TSP) cuando se tiene un único vehículo y en el ruteo de vehículos (VRP) para los otros cosos.

Para la solución del modelo IRP presentado se utilizó un algoritmo genético, el cual presenta una representación novedosa de los individuos para este tipo de problemas (Cromosoma). Según el conocimiento de los autores, esta es la primera vez que esta representación es presentada en la literatura especializada para resolver el modelo IRP. Los resultados obtenidos con el algoritmo genético para la instancia analizada, la cual corresponde a una configuración comúnmente estudiada en la literatura científica, demuestra que el algoritmo presenta buenos resultados en la solución del modelo IRP.

Agradecimientos

Los autores agradecen a la Universidad Nacional de Colombia por el apoyo al proyecto *"Optimización de la distribución de mercancías utilizando un modelo genético multiobjetivo de n proveedores con m clientes"*, código Hermes: 29314. Proyecto del cual se deriva este artículo de investigación.

Referencias

[1] Rushton, A., Croucher, P. and Baker, P., The handbook of logistics and distribution management, 3rd edition, Ed. Kogan Page Limited. 2010. ISBN 0-7494-4669-2

[2] Estrada, M.A., Análisis de estrategias eficientes en la logística de distribución de paquetería. Tesis Doctoral. Programa de Doctorado de Ingeniería Civil E.T.S. de Ingenieros de Caminos, Canales y Puertos de Barcelona. Universitat Politècnica de Catalunya, España. 2007.

[3] Adarme, W., Arango, MD. and Balcazar, D.A., Modelo para la coordinación de agentes en un sistema logístico de la industria Astillera Colombiana. Revista Ingeniería e Investigación. 31(2), pp.102-111, 2011

[4] Hernández, S., Peeta, S. and Kalafatas, G., A less-than-truckload carrier collaboration planning problem under dynamic capacities. Transportation Research Part E 47, pp. 933-946, 2011.

[5] Moin, N.H; Salhi, S. and Aziz, N.A.B., An efficient hybrid genetic algorithm for the multi-product multi-period inventory routing problem. Int. J. Production Economics, 133 pp. 334-343, 2011.

[6] Deflorio, F., Gonzalez-Feliu, J., Perboli, G. and Tadei, R., The influence of time windows on the costs of urban freight distribution services in city logistics applications. EJTIR, 12(3), pp. 256-274, 2012.

[7] Antún, J.P., Distribución urbana de mercancías: Estrategias con centros logísticos. Banco Interamericano de Desarrollo. Departamento de Infraestructura y Medio Ambiente. Nota técnica # IDB-TN-167. [Online]. 2013. Available at: http://publications.iadb.org/facet-view?field=type_view.

[8] Archetti, C., Bertazzi, L., Laporte, G. and Speranza, M.G., A branch-and-cut algorithm for a vendor-managed inventory-routing problem. Transportation Science, 1(3), pp 382-391, 2007.

[9] Azuma, R., Coelho, G.P. and Von Zuben, F.J., Evolutionary multi-objective optimization for the vendor-managed inventory routing problem. In EEE Congress on Evolutionary Computation (CEC), pp. 1457-1464. 2011.

[10] Coelho, L.C. and Laporte, G., The exact solution of several classes of inventory-routing problems. Computers & Operations Research 40, pp.558-565, 2013.

[11] Cho, D.W., Hae-Lee, Y., Youn-Lee, T. and Gen, M., An adaptive genetic algorithm for the time dependent inventory routing problema. Journal Intelligent Manufacturing, 25, pp. 1025-1042, 2014.

[12] Bertazzi, L. and Esperanza, M.G., Inventory routing problems with multiple customers. EURO J Transp Logist, 2, pp. 255-275, 2013.

[13] Zhang, D., Liu, X. and Li, S., An optimization model for multi-period collaborative inventory control based on target performance management. Proceedings of the 2012 IEEE 16th International Conference on Computer Supported Cooperative Work in Design, pp. 930-934, 2012

[14] Arango, M.D., Zapata, J.A. and Adarme, W., Aplicación del modelo de inventario manejado por el vendedor en una empresa del sector alimentario colombiano. Revista EIA, 15, pp. 21-32, 2011.

[15] Arango, M.D., Adarme, W. and Zapata, J.A., Inventarios colaborativos en la optimización de la cadena de suministros. DYNA, 80(181), pp. 71-80, 2013. ISSN 0012-7353

[16] Zavanella, L. and Zanoni, S., A one-vendormulti-buyer integrated production-inventory model: The 'ConsignmentStock'case. Intern. Journal of production Economics, 118, pp. 225-232, 2009.

[17] Kwak, C., Choi, J.S., Kim, C.O. and Kwonc, I.-H., Situation reactive approach to Vendor Managed Inventory problema. Expert Systems with Applications, 36(5), pp. 9039-9045, 2009.

[18] Fawcett, S., Waller, M. and Fawcett, A., Elaborating a dynamic systems theory to understand collaborative inventory successes and failures. The International Journal of Logistics Management, 21(3), pp. 510-537, 2010.

[19] Arango-Serna, M.D., Serna-Urán, C.A. and Alvarez-Uribe, K.C., Collaborative autonomous systems in models of urban logistics. DYNA, 79(172). 2012.

[20] Díaz-Batista, J. and Pérez-Armador, D., Optimización de los niveles de inventario en una cadena de suministro, Ingeniería Industrial, 33(2), pp. 126-132, 2012.

[21] Zhang, T., Liang, L., Yu, Y. and Yu, Y., An integrated vendor-managed inventory model for a two-echelon system with order cost

reduction. International Journal of Production Economics, 109(1–2), pp. 241-253, 2007.
[22] Abdelmaguid, T.F. and Dessouky, M.M., A genetic algorithm approach to the integrated inventory-distribution problema. International Journal of Production Research, 44(21), pp. 4445-4464, 2006.
[23] Gonzalez-Feliu, J., Peris-Pla, C. and Rakotonarivo, D., Simulation and optimization methods for logistics pooling in the outbound supply chain. Third International Conference on Value Chain Sustainability. Towards a Sustainable Development and Corporate Social Responsibility Strategies in the 21st Century Global Market, Nov 2010, Spain. pp. 394-401, 2010.
[24] Archetti, C., Bianchessi, N., Irnich, S. and Speranza, M.G., Formulations for an inventory routing problem. Intl. Trans. in Op. Res. 21, pp. 353-374, 2014.
[25] Arango, M.D., Zapata, J.A. and, Gutierrez, D., Modeling the inventory routing problem (IRP) with multiple depots with genetic algorithms. IEEE Latin American Transactions. 13(12), pp. 3959-3965, 2015.
[26] Zeng, Z. and Zhao, J., Study of stochastic demand inventory routing problem with soft time windows based on MDP. Adv. in Neural Network Research & Appli., LNEE(67), pp. 193-200, 2010.
[27] Campbell A.M. and Savelsbergh, M.W.P., A decomposition approach for the inventory-routing problem. INFORMS Transportation Science 38(4), pp. 488-502, 2004
[28] Solyali, O and Süral H., A branch-and-cut algorithm using a strong formulation and an a priori tour based heuristic for an inventory-routing problem. Transportation Science; 45(3), pp. 335-345, 2011.
[29] Archetti, C, Bertazzi, L, Hertz, A. and Speranza, M.G., A hybrid heuristic for an inventory routing problem. INFORMS Journal on Computing, pp. 101-116, 2011.
[30] Azuma, R.M., Otimização multiobjetivo em problema de estoque e roteamento gerenciados pelo fornecedor. Tesis MSc., Departamento de Engenharia de Computação e Automação Industrial, Universidade Estadual De Campinas, Brasil, 2011.
[31] Coelho L.C, Cordeau, J-F. and Laporte, G., Consistency in multi-vehicle inventory- routing. Transportation Research Part C; 24(1), pp. 270-287, 2012.
[32] Coelho, L.C, Cordeau, J.F. and Laporte G., The inventory-routing problem with transshipment. Cirrelt. [Online]. 2011. https://www.cirrelt.ca
[33] Liu, S.C. and Lee, W.T., A heuristic method for the inventory routing problem with time windows. A heuristic method for the inventory routing problem with time Windows, pp. 13223-13231, 2011.
[34] Zeng, Z. and Wang, J., Study of stochastic demand inventory routing problem with soft time windows based on MDP. Adv. in Neural Network Research & Appli., LNEE(67), pp. 193-200, 2010.
[35] Kleywegt, A.J., Nori, V.S. and Savelsbergh, M.W.P., Dynamic programming approximations for a stochastic inventory routing problem. Transportation Science 38(1), pp 42-70, 2004.
[36] Liu, G-S., Lin, K-P., Lee, H-W. and Wang, C-Y., A study of inventory-routing problem for the distribution system by applying genetic algorithm. IEEE International Summer Conference of Asia Pacific, pp. 104-108, 2011.
[37] Fengjiao, W. and Qingnian, Z., The research on the inventory routing problem with split pick-ups based on genetic algorithm. WiCOM '08. 4th International Conference on Wireless Communications, Networking and Mobile Computing, pp. 1-4, 2008.
[38] Aziz, N.A.B. and Moin, N.H., Genetic algorithm based approach for the multi product multi period inventory routing problem. IEEE International Conference on Industrial Engineering and Engineering Management, pp. 1619-1623, 2007
[39] Siswanto, N., Essam, D., and Sarker, R., Multi-heuristics based genetic algorithm for solving maritime inventory routing problem. IEEE International Conference on Industrial Engineering and Engineering Management (IEEM), pp. 116-120, 2011.
[40] van Anholt, R., Coelho, L., Laporte, G. and Vis, I., An inventory-routing problem with pickups and deliveries arising in the replenishment of automated teller machines. CIRRELT. [Online]. 2013. Available at: https://www.cirrelt.ca
[41] Adulyasak, Y., Cordeau, J-F. and Jans, R., Formulations and branch-and-cut algorithms for multi-vehicle production and inventory routing problems. Technical report G-2012-14, GERAD, Montreal, Canada; 2012.
[42] Lien R.W., Iravani S.M.R., Smilowitz, K. and Tzur, M., An efficient and robust design for transshipment networks. Production and Operations Management; 20(5), pp. 699-713, 2011.
[43] Coelho, L.C. and Laporte, G., A branch and cut algorithm for the multi product multi vehicle inventory routing problem. CIRRELT-2012-53. [Online]. 2012. Available at: https://www.cirrelt.ca
[44] Chang, T-S. and Yen, H-M., City-courier routing and scheduling problems. European Journal of Operational Research, 223, pp. 489-498, 2012.
[45] Pradhananga, R., Taniguchi, E., Yamada, T. and Qureshi. A.G., Bi-objective decisión support system for routing and scheduling of hazardous materials. Socio-Economic Planning Sciences, 48, pp. 135-148, 2014.
[46] Melián-Batista, B., De Santiago, A., Bello, F.A. and Alvarez, A., A bi-objective vehicle routing problem with time windows: A real case in Tenerife. Applied Soft Computing, 17, pp. 140-152, 2014.
[47] Vidal, T., Crainic, T.G., Gendreau, M. and Prins, C., Heuristics for multi-attribute vehicle routing problems: A survey and synthesis. Montreal: Cirrelt. 2012.
[48] López, A, Zapotecas S. and Coelho, L.C., An introduction to multiobjective optimization techniques. In Ajith A., Lakhmi J. and Goldberg R. (Eds.), Evolutionary multiobjective optimization: Theoretical advances and applications, pp. 7-32, Springer-Verlag, London, ISBN 1-85233-787-7. 2009.
[49] González, G. y González, F., Metaheurísticas aplicadas al ruteo de vehículos. Un caso de estudio. Parte 2: Algoritmo genético, comparación con una solución heurística. Revista Ingeniería e Investigación. 27(1), pp. 149-157, 2007.
[50] Arango, M.D. and Serna, C.A., A memetic algorithm for the traveling salesman problem. IEEE Latin America Transactions,13(8), 2015. DOI: 10.1109/TLA.2015.7332148.
[51] Arango, M.D., Zapata, J.A. and Andres, C., Metaheuristics for goods distribution. Proceedings of 2015 International Conference on Industrial Engineering and Systems Management (IESM), IEEE Publications, pp.99-107, 2015. DOI. 10.1109/IESM.2015.7380143
[52] Aydın, N., A genetic algorithm on inventory routing problem. Emerging Markets Journal. 3(3), pp. 59-66, 2014.
[53] Coelho, L.C., Inventory-Routing. [Online]. [Date of reference: August 11th of 2015]. Available at: http://www.leandro-coelho.com/instances/inventory-routing/
[54] Archetti, C., Bertazzi, L., Hertz, A. and Speranza, M.G., A hybrid heuristic for an inventory routing problem. INFORMS Journal on Computing, 24(1), pp. 101-116, 2012.

M.D. Arango-Serna, graduado como Ing. Industrial en 1991 en la Universidad Autónoma Latinoamericana,, Colombia, Esp. en Finanzas, Formulación y Evaluación de Proyectos en 1993 por la Universidad de Antioquia, Colombia, Esp. en Docencia Universitaria en 2007 por la Universidad Politécnica de Valencia, España, MaSc. en Ingeniería de Sistemas en 1997 por la Universidad Nacional de Colombia – Sede Medellín, Dr. Ingeniero Industrial en 2001 por la Universidad Politécnica de Valencia, España. Es profesor titular en dedicación exclusiva, adscrito al Departamento de Ingeniería de la Organización, Facultad de Minas, Universidad Nacional de Colombia, sede Medellín. Es Investigador Senior según clasificación Colciencias 2015. Director del Grupo de I+D+i Logística Industrial- Organizacional "GICO", grupo A1. Los temas de trabajo en los cuales se desempeña el profesor Arango-Serna están relacionados con procesos logísticos en la cadena de suministros, Investigación de operaciones, diseños de plantas, técnicas de optimización industrial-Organizacionales, entre otras.
ORCID: 0000-0001-8448-8231

C. Andrés-Romano, graduado como Ing. Industrial en 1995 y como Dr. en Ingeniería Industrial en 2001, en la Universidad Politécnica de Valencia, España. Actualmente se desempeña como profesor titular, en el Departamento de Organización de Empresas de la Universidad Politécnica de Valencia, España. Las temáticas en las que se desenvuelve el profesor Andrés-Romano son en el estudio de tiempos y métodos para el mejoramiento de procesos, programación y administración de proyectos,

desarrollo de metaheurísticas para resolver problemas de optimización industrial, entre otros.
ORCID: 0000-0003-4453-4891

J.A. Zapata-Cortes, graduado como Ing. Químico en 2006, como MSc. en Ingeniería Administrativa en 2011 y candidato a Dr. en Ingeniería – Industria y Organizaciones en la Universidad Nacional de Colombia. Actualmente se desempeña como investigador en el grupo de I+D+I Logística Industrial-Organizacional "GICO" de la Universidad Nacional de Colombia. Investigador Junior según clasificación Colciencias 2015. Los temas en los que se desenvuelve son en la optimización de redes de transporte e inventario, tecnologías de la información y la comunicación aplicadas a la cadena de suministro y a la administración de procesos empresariales, entre otros.
ORCID: 0000-0002-1270-3577

UNIVERSIDAD NACIONAL DE COLOMBIA
SEDE MEDELLÍN
FACULTAD DE MINAS

Área Curricular de Ingeniería Administrativa e Ingeniería Industrial

Oferta de Posgrados

Especialización en Gestión Empresarial
Especialización en Ingeniería Financiera
Maestría en Ingeniería Administrativa
Maestría en Ingeniería Industrial
Doctorado en Ingeniería - Industria y Organizaciones

Mayor información:

E-mail: acia_med@unal.edu.co
Teléfono: (57-4) 425 52 02

UNIVERSIDAD NACIONAL DE COLOMBIA
SEDE MEDELLÍN
FACULTAD DE MINAS

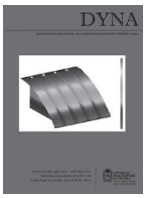

DYNA
http://dyna.medellin.unal.edu.co/

Baseflow analysis using master recession curves and numerical algorithms in mountain basins: Suratá's river and Oro's river (Santander, Colombia)

Sully Gómez-Isidro [a] & Viviana Lucía Gómez-Ríos [b]

[a] *Escuela de Ingeniería Civil, Universidad Industrial de Santander, Bucaramanga, Colombia. sgomez@uis.edu.co*
[b] *Ingeniera Civil, Universidad Industrial de Santander, Bucaramanga, Colombia. vilugori92@gmail.com*

Received: September 26th, 2015. Received in revised form: February 23th, 2016. Accepted: March 17th, 2016.

Abstract
The interaction between groundwater inflow and outflow is complex in streams connected from aquifers located in fractured rock media. The recession curves of hydrographs provide information about these hydrogeological processes and they are useful to assess an insight in the storage-discharge relationship in subsurface reservoirs. In this study, the physic base and the nonlinearity relationship of storage-discharge were analyzed through a mathematical expression which describe a master recession curve. Four numerical algorithms were applied to estimate the baseflow of the Suratá's River basin and the high Oro's River basin, Santander-Colombia. In both cases, master recession curves showed the nonlinearity relationship in storage-discharge. Furthermore, the exponent values and the proportionality constants give additional information about the aquifers in contact to the river and the special scale of recharges that may occur in these aquifers.

Keywords: master recession curve; baseflow separation; numerical filters; nonlinearity.

Análisis de flujo base usando curvas maestras de recesión y algoritmos numéricos en cuencas de montaña: Cuenca del río Suratá y cuenca del Río de Oro (Santander, Colombia)

Resumen
Las interacciones entre flujo de entrada y flujo de salida del agua subterránea en ríos conectados con acuíferos localizados en ambientes de rocas fracturadas son complejas. Las curvas de las recesiones en los hidrogramas ofrecen información sobre estos procesos hidrogeológicos y permiten observar la relación almacenamiento-descarga de los reservorios subterráneos. En este trabajo se estudió la base física y la validez de la forma lineal de la relación almacenamiento-descarga que describe la curva maestra de recesión. Se aplicaron cuatro algoritmos numéricos que estimaron el porcentaje de flujo base en las cuencas del río Suratá y Río de Oro, Santander, Colombia. Las curvas maestras de recesión mostraron que la relación almacenamiento-descarga no es lineal y que los valores del exponente y la constante de proporcionalidad ofrecen información sobre el tipo de acuíferos en contacto con los ríos y la escala espacial en la que puede ocurrir la recarga a estos acuíferos.

Palabras clave: curva maestra de recesión; separación de flujo base; filtros numéricos; no linealidad.

1. Introducción

Los almacenamientos hídricos subterráneos proveen de agua a las corrientes de los ríos en temporadas de precipitaciones bajas o nulas, cuando los niveles freáticos son más altos que los niveles del río y por tanto el río es ganador. Estos almacenamientos en contacto con ríos pueden abastecer comunidades con agua de buena calidad, debido a que por su naturaleza se encuentran libres de turbiedad y patógenos, lo que la hace, en general, apta para el consumo humano.

© The author; licensee Universidad Nacional de Colombia.

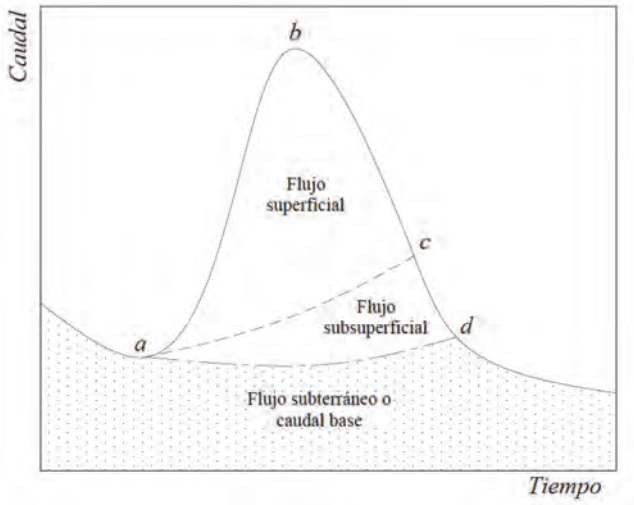

Figura 1. Esquema de separación del hidrograma.
Fuente: Los autores

La fracción de flujo base respecto al flujo total en el río es un valor que puede ser utilizado como indicador de sostenibilidad de la reserva hídrica en cuencas [1]. Es por esto que la literatura científica ha dedicado gran esfuerzo al conocimiento del flujo base de los ríos [2-4].

Los métodos para la separación de flujo base se clasifican principalmente en métodos gráficos, químicos (isótopos estables del agua) y algoritmos numéricos (filtros) con base física, estos últimos utilizan series de tiempo de caudales. En estudios de separación de flujo base conviene aplicar varios métodos para poder contrastar los resultados. Entre algunos de los algoritmos numéricos disponibles se encuentran programas de computador de libre acceso como, *HYSEP* [5], *PULSE* [6], *RECESS* [7], *WHAT* [8] y el método de *BFI* [9], considerados como algoritmos que tienen poca base física. Ellos fueron creados para tener procesos repetibles, fácilmente programables y se han utilizado para tener una primera aproximación al valor del flujo base [10]. En la actualidad las técnicas de filtros han incorporado elementos que incluyen una base física, la mayoría de ellos reflejan la recesión del hidrograma [11], otros hacen algunas simplificaciones considerando un balance de masas en laderas [12] o consideran que la infiltración tiene una componente rápida y otra lenta, como el Modelo IACRES [13].

En la Figura 1 se observa un esquema de separación. El flujo base o flujo subterráneo está representado por la parte baja del hidrograma y la línea formada por el punto ***a*** y el punto ***d*** durante el evento de lluvia, mientras que el flujo subsuperficial es delimitado por la curva anterior y otra entre los puntos ***a*** y ***c***. En este trabajo se enfatiza en la separación del hidrograma en dos componentes: el flujo subterráneo y el flujo superficial. Las curvas de recesión representan la disminución de los almacenamientos subterráneos en contacto con las corrientes, pueden ofrecer información sobre las características físicas e hidrodinámicas de las formaciones geológicas, porosidad, conductividad hidráulica y capacidad especifica. Ellas son utilizadas para estimar recarga a acuíferos, caudales mínimos o de estiaje en ríos y tiempos de recesión. La curva maestra de recesión (CMR) es una curva generalizada de recesiones del flujo en un río que ofrece una percepción de la capacidad y agotamiento del almacenamiento subterráneo.

La curva maestra de recesión ha sido considerada como una herramienta expedita y de uso generalizado en la hidrología, que expresa una función exponencial decreciente. Por lo regular, el uso de la CMR resulta válido en ríos de valles aluviales donde la contribución principal del flujo base proviene de acuíferos aluviales conectados de forma local con el río; en estos casos, las áreas influenciadas por estos acuíferos son importantes para la protección de la calidad del agua superficial. Sin embargo, en condiciones geológicas complejas y topografías fuertes [14] la contribución del flujo base puede provenir de almacenamientos subterráneos localizados en zonas altas (altiplanos y cordilleras) y el caudal base puede estar relacionado con caudales de largo plazo [15].

En este trabajo se estudian e interpretan las curvas de recesión del hidrograma en dos cuencas de montaña localizadas sobre el macizo de Santander (Colombia) que abastecen de agua a través de bocatomas a una comunidad de cerca de un millón de habitantes de la ciudad de Bucaramanga y su área metropolitana. El flujo subterráneo que alimenta el flujo base en estas cuencas presenta algunas particularidades relacionadas con la geología que pudieron ser observadas en el estudio de las curvas de recesión. Se aplican cuatro algoritmos numéricos desarrollados en el programa ***G2*** [16] para obtener la fracción del flujo base y se obtienen parámetros que expresan el concepto de no linealidad en la recesión de los almacenamientos subterráneos. Estos resultados se contrastan con valores obtenidos mediante otros métodos. El flujo base en estas cuencas es una reserva importante que debe ser tenida en cuenta en los planes de manejo y gestión del recurso hídrico y en otorgamiento de licencias ambientales, los cuales deben considerar flujos de larga distancia que alimentan el caudal base de estos ríos, de lo contario el agua de las bocatomas será afectada en cantidad y en calidad.

2. Metodología

Se presenta una revisión y análisis de la forma matemática de la curva de recesión y una breve descripción tanto de los algoritmos numéricos utilizados para realizar la separación del flujo base, de las condiciones hidrogeológicas de la zona de estudio relacionadas con las recesiones de los hidrogramas y métodos utilizados.

2.1. Revisión de la forma matemática de la curva de recesión de los hidrogramas

El hidrograma es una gráfica que representa la variación temporal del caudal medido en un punto de un río o de una corriente. Los parámetros físicos de la cuenca (geomorfología, cobertura, uso del suelo) y las características geológicas de las formaciones acuíferas en contacto con el río, determinan la forma y las magnitudes relativas de las componentes de los hidrogramas.

El descenso o agotamiento del agua almacenada en el acuífero en épocas de estiaje o pocas lluvias da lugar a la

recesión. La CMR es el resultado de la superposición de todas las curvas de recesión que han ocurrido a lo largo de una serie de tiempo de caudales. La pendiente de la recta formada por la CMR en la escala logarítmica es la llamada constante de recesión del río en el punto de interés. La forma matemática de la CMR ha sido interpretada con una función exponencial decreciente como se muestra en la ecuación (1).

$$Q_t = Q_0 e^{-t/\alpha} \quad (1)$$

El valor de Q_t representa el caudal en el tiempo $\boldsymbol{t}$, Q_0 es la caudal inicial y α es el índice de recesión que representa el tiempo de "*vida media*" o tiempo promedio en el que una gota de agua que ingresa al acuífero en contacto con el río [17]. Otro término físico significativo en la evaluación de una CMR es la constante de recesión $\boldsymbol{k}$ en días^{-1}, que representa la pendiente de la curva de caudales en escala semilogarítmica y también corresponde al inverso del índice de recesión. La función exponencial en la ecuación (1) supone que el acuífero reacciona como un simple reservorio lineal donde el volumen almacenado es proporcional a la salida del flujo del acuífero ($S = \alpha Q$, α es una constante de proporcionalidad dependiente del área, porosidad del suelo, conductividad hidráulica y propiedades geomorfológicas, [13]. En la gráfica de Q_t contra *t*, en escala logarítmica, se observa una línea recta. Este comportamiento puede ser característico de cuencas que, principalmente, presentan acuíferos confinados constituidos por formaciones geológicas homogéneas y gradientes hidráulicos suaves. Sin embargo, se conoce que en cuencas donde existen acuíferos heterogéneos conformados por rocas fracturadas, meteorizadas o carbonatadas, con presencia de laderas muy inclinadas, no es posible representar el sistema con la ecuación que representa reservorios lineales y la curva de recesión no se ajusta a un único valor de $\boldsymbol{k}$ [11].

El concepto físico de no linealidad en el flujo subterráneo ha sido estudiado por algunos autores que han desarrollado modelos basados en la combinación de depósitos lineales para proporcionar una mejor forma a la curva de recesión [19, 20], mientras que otros han propuesto una relación no lineal entre el almacenamiento y la descarga, adicionando un exponente $\boldsymbol{b}$ a la ecuación de un reservorio lineal [18, 21], como se muestra en la siguiente ecuación:

$$S = \alpha Q^b \quad (2)$$

Donde S es el volumen de almacenamiento disponible para ser descargado en la corriente y Q es el caudal de descarga, α tiene unidades de medida de $mm^{1-b}d^b$ si el almacenamiento es dado en *mm* y el caudal en mm/d y b es una variable adimensional. La ecuación (1) es un caso particular en el que la ecuación diferencial es despejada teniendo en cuenta que $b = 1$ [11], en este caso se trata de un reservorio lineal y se asume que la salida Q del acuífero es linealmente dependiente del almacenamiento S.

La ecuación (2) puede ser considerada una ecuación cuadrática cuando b toma el valor de 0.5, y en este caso se trata de una aproximación teórica de la salida de flujo desde acuíferos no confinados cuya solución implica la condición de Dupuit-Forcheimer. El caso particular $b=1$ caracteriza un acuífero no confinado horizontal [4]. Variaciones de estos valores implican que la realidad del flujo subterráneo hacia ríos no es representada con las consideraciones teóricas anteriores. Resolviendo la ecuación (2) con la ayuda de la ecuación de continuidad en términos de flujo de salida de un reservorio (esto significa que no hay entradas superficiales de acuíferos, ni precipitación, ni flujos profundos, ni salida por evapotranspiración) $dS/dt = -Q$, la solución para el reservorio no lineal cuyo agotamiento empieza con un valor de descarga inicial Q_o, fue propuesta por [22] y se expresa en la ecuación (3).

$$Q_t = Q_o \left[1 + \frac{(1-b){Q_o}^{1-b}}{ab} t\right]^{\frac{1}{b-1}} \quad (3)$$

Esta es una ecuación que representa en forma general la curva de recesión del hidrograma. Los parámetros $\boldsymbol{a}$ y $\boldsymbol{b}$, representan propiedades o condiciones de los acuíferos en contacto con el río.

En los hidrogramas construidos con los datos de caudales se identifican las temporadas de recesión a través de líneas rectas descritas por la ecuación (4). Las curvas de recesión se agrupan para generar la CMR.

$$Ln(Q_t) = Ln(Q_0) - kt \quad (4)$$

La metodología para obtener la CMR consiste en graficar la serie de datos de caudales junto con los eventos de precipitación registrados en estaciones cercanas a la estación de medición de caudales; esto permite observar la consistencia de las épocas de recesión seleccionadas. En una etapa posterior, se visualizan en una gráfica independiente las recesiones registradas. En este paso se busca tener en una misma Fig., las temporadas de recesión, para ir formando grupos de recesiones alineadas de tal manera que se integren una o varias líneas tangentes a los datos. Por último, se realiza una regresión lineal con todos los datos para identificar el valor de los parámetros de la ecuación (4). Estos valores deben ser analizados en conjunto con las condiciones físicas de la cuenca como son: las características geológicas y topográficas, el tipo de acuífero y las condiciones del suelo.

2.2. Algoritmos numéricos para separación de flujo base

Los algoritmos numéricos basados en las curvas de recesión fueron creados para reproducir, a partir de hidrogramas, señales de alta frecuencia (respuesta de flujo superficial) y señales de baja frecuencia (respuesta del flujo base) en forma repetitiva [14]. El hidrograma está conformado por un flujo rápido que representa el flujo superficial originado por eventos de precipitación, y por un flujo más lento relacionado con el flujo subterráneo. El uso de algoritmos numéricos, es una técnica de separación automática utilizada cuando se cuenta con series de tiempo de caudales, permite que el flujo base se ajuste a la forma del hidrograma en los tramos de recesión.

Los algoritmos también son llamados filtros numéricos, y

hacen referencia a procesos simples con resultados muy sensibles a los parámetros del filtro. Los parámetros son constantes que representan, en su mayoría, condiciones físicas de la cuenca o propiedades del hidrograma. Para que los resultados puedan ser considerados válidos los parámetros deben ser obtenidos mediante un proceso de calibración [23]. Durante el proceso de calibración los parámetros se ajustan haciendo que el hidrograma y el flujo base se asemejen a la curva de recesión. Para ello se escogen tramos de recesiones en las cuales se evalúe la forma del flujo base y se calculen los porcentajes de error relativo en los tramos de las épocas de recesión. Una primera aproximación se realiza utilizando periodos del hidrograma de diez a veinte días, buscando el mejor ajuste según metodología mostrada en [24]. El objetivo de aplicar los algoritmos numéricos es hallar la fracción del flujo base respecto al flujo total y analizar los valores de los parámetros de recesión.

En este trabajo la separación del flujo base se realizó mediante el uso de algoritmos programados en el código de Matlab llamado ***G2*** [16]. Esta herramienta requiere, como datos de entrada, series de tiempo de caudales en escalas horarias o diarias. En la Tabla 1 se describen cuatro de los algoritmos desarrollados en el programa ***G2*** así como los parámetros utilizados en cada uno de ellos. Una descripción más detallada de estos algoritmos se presenta en [14].

2.3. Descripción de la zona de estudio

La metodología anterior fue aplicada a los caudales medidos en el río Suratá y en el Río de Oro, localizados sobre la parte montañosa de la cuenca Superior del Río Lebrija (Figura 2). Estos ríos surten de agua potable a la ciudad de Bucaramanga y al municipio de Piedecuesta, respectivamente, en el departamento Santander. La precipitación en esta zona ocurre a lo largo del año con un óptimo pluviométrico que puede alcanzar 2000 milímetros anuales localizado entre 1800 y 2000 ms.n.m. La precipitación anual presenta una tendencia bimodal acorde con el paso de la Zona de Convergencia Intertropical (ZCIT) que pasa sobre la región generando dos épocas lluviosas en los meses de marzo, abril y mayo, posteriormente en los meses de septiembre, octubre y noviembre, y dos épocas secas o menos lluviosas en los meses de diciembre, enero, febrero, junio y julio [29]. En estas cuencas hasta la fecha no han funcionado proyectos de regulación de caudal y en general son cuencas que no han tenido afectación antrópica drástica, con excepción de las actividades dedicadas a la minería del oro en el páramo de Santurbán.

La cuenca del río Suratá tiene un área de 697 km^2 y está conformada por las subcuentas de los ríos Tona, Charta y Vetas; la altura mínima es de 700 ms.n.m y la cota de elevación

Tabla 1.
Filtros numéricos para la separación de flujo base

Filtro	Ecuación		Condición
Un parámetro (**1-P**)	$Q_{b\,(i)} = \frac{K}{2-\mathrm{K}} Q_{b\,(i-1)} + \frac{1-\mathrm{K}}{2-K} Q_{(i)}$	(5)	El caudal base es el medio ponderado de la escorrentía directa Q_d y el flujo de base $Q_{b\,(i)}$, en el intervalo de tiempo anterior [25]. Debe cumplirse la condición $Q_b(i) < Q(i)$. En [26] proponen que el parámetro de este filtro sea ***k*** (constante de recesión). El flujo base es un promedio entre la escorrentía directa y el flujo base del intervalo anterior, lo cual se ajusta mejor al hidrograma.
Dos parámetros (**2-P**)	$Q_{b(i)} = \frac{K}{1+K} Q_{b(i-1)} + \frac{C}{1+C} Q_{(i)}$	(6)	En este caso el parámetro C proporciona mejor ajuste a la ecuación, y es calibrado gráficamente en zonas del hidrograma de altos eventos de precipitación [27]. Se respeta la condición $Q_{b(i)} \leq Q_{(i)}$. Este algoritmo proporciona mejor ajuste al considerar un segundo parámetro C asociado a una recarga rápida a los acuíferos.
Tres parámetros o IHACRES (**3-P**)	$Q_{b(i)} = \frac{k}{1+C} Q_{b(i-1)} + \frac{C}{1+C}\left[Q_{(i)} + \alpha_q Q_{(i-1)}\right]$ $C = \frac{\beta_s}{\beta_q} \;\; ; \;\; k = -\alpha_s - \alpha_q \frac{\beta_s}{\beta_q}$	(7)	Usa el componente lineal del modelo de lluvia-escorrentía de [13] en el que el flujo es dividido en: el flujo rápido (escorrentía directa) y el flujo lento (flujo base). El parámetro $\alpha_q < 0$. Estos flujos se expresan con subíndices de los nuevos parámetros α y β.
Nathan & McMahon, 1990 (**N&M**)	$Q_{d(i)} = \beta Q_{d(i-1)} + \frac{1+\beta}{2}\left[Q_{(i)} - Q_{(i-1)}\right]$	(8)	El filtro es ejecutado sobre los datos de caudales tres veces: hacia adelante, hacia atrás y hacia adelante (paso 1, paso 2 y paso 3, respectivamente) [28]. Es similar al algoritmo de un parámetro, donde la constante de recesión se reemplaza por un valor β.

Fuente: Los autores

- Q_b es el flujo base en el intervalo de tiempo (i)
- Q es el flujo total en el intervalo de tiempo (i)
- Q_d es la escorrentía directa en el intervalo de tiempo (i)
- $K = e^{-k}$, en el algoritmo de uno y de dos parámetros, es el factor de agotamiento, siendo k la constante de recesión en [días^{-1}].
- C, en el algoritmo de dos parámetros, es una constante adimensional que indica la respuesta rápida del flujo, y es hallada en la inspección de la forma del flujo al final de la escorrentía, en especial para grandes eventos de precipitación.
- α, en el algoritmo de tres parámetros, está relacionada con la pendiente de la línea tangente en el hidrograma o índice de recesión en la CMR de la ecuación (1).
- β, en el algoritmo de tres parámetros, está relacionado con la capacidad de almacenamiento de los acuíferos, es decir, el área bajo la curva de caudales.
- Los sufijos q y s, en el algoritmo de tres parámetros, hacen referencia al flujo lento o flujo base y al flujo rápido o escorrentía directa, respectivamente.
- β, en el filtro de Nathan & McMahon, corresponde a un valor constante de 0.925 para un intervalo de tiempo diario.

máxima está localizada en la parte alta de la microcuenca del río Vetas, a 4200 ms.n.m, con una pendiente media del 7.5%; por su parte, la cuenca del Río de Oro tiene un área de 80 km2, el punto más bajo de la cuenca está localizado 1100 ms.n.m y el más alto en 3500 ms.n.m, con una pendiente media del 10%. El río Suratá nace en la parte alta del páramo de Santurbán y el Río de Oro en cercanía al páramo de Berlín.

Las cuencas se localizan sobre un basamento ígneo metamórfico que comprende las unidades gneis de Bucaramanga, formación Silgará, ortogneis, tonalita y granodiorita, cuarzomonzonita de la Corcova y de Santa Bárbara, así como una franja sedimentaria conformada por las formaciones Los Santos y Rosablanca, principalmente. Las rocas cristalinas se encuentran afectadas por intenso fracturamiento y meteorización, lo que ha llevado a la generación de suelos residuales espesos [30] que favorecen el flujo subterráneo y la formación de acuíferos. Además, la cuenca del río Suratá y la del Río de Oro se encuentran delimitadas en un área de complejidad estructural producto del cruce de las fallas Suratá y Cucutilla [31], así como las fallas de los ríos Charta, La Cristalina, Tona y de Oro entre otras, las cuales generan escarpes con fuertes pendientes presentes en ambas cuencas. Por su parte, en la cuenca del río Suratá se identifica un patrón de fracturamiento en dirección NE en escala regional alineado a las fallas Cucutilla y Suratá, relacionado con corredores formados por rocas que tienen porosidad secundaria y constituyen potenciales canales de flujo de aguas subterráneas. Los levantamientos de campo de las direcciones de diaclasas y estrías de falla, así como la localización de manantiales, sugieren una dirección de flujo que pone en conexión la zona alta del páramo de Santurbán y el páramo de Berlín con las zonas bajas del río Charta [32].

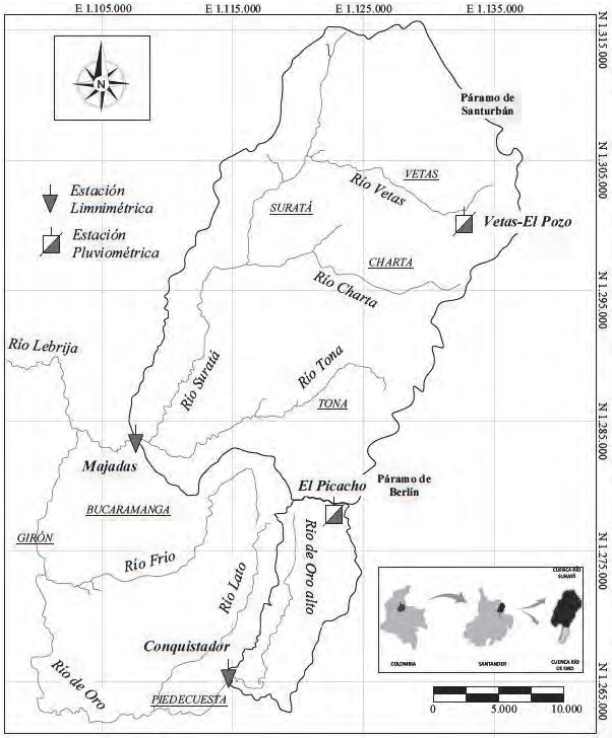

Figura 2. Cauces de la cuenca superior del río Lebrija y delimitación de las cuencas del río Suratá y de Oro.
Fuente: Los autores.

Aunque aún no existen datos geológicos concluyentes, los inventarios de manantiales en la cuenca del río Tona [33] permiten inferir que el sistema de flujo del río Charta puede estar comunicado con sistemas de fracturas presentes en la cuenca del río Tona. Por otro lado, en la parte alta de la cuenca del Río de Oro, en límites con el altiplano de Berlín, se encuentran rocas como la cuarzomonzonita de Santa Bárbara (cristalinas) y las rocas de la formación Rosablanca (calizas); esta última se identifica como una formación hidrogeológica tipo cárstica, donde se localizan numerosos manantiales [34]. Las cuarzomonzonitas presentan suelos residuales arenosos producto de la meteorización, que favorecen el flujo subterráneo y la formación de acuíferos.

El modelamiento hidrológico realizado en la cuenca alta del Río de Oro ha mostrado que puede existir un flujo subterráneo resultante de áreas externas a la cuenca [35], por lo tanto, no se descarta la existencia de flujos subterráneos provenientes del altiplano de Berlín.

A partir de estudios de isótopos estables se ha encontrado que la principal recarga de los acuíferos de la meseta de Bucaramanga proviene de la zona montañosa del macizo de Santander, cuyas zonas de recarga pueden extenderse hasta alturas mayores a los 3000 ms.n.m., asociadas a flujos de larga a media distancia [36]. Valores isotópicos tomados en el flujo base del Río de Oro (estación Conquistador) indican que la parte más alta del macizo contribuye en mayor proporción a la recarga de los acuíferos en contacto con los ríos en la zona de montaña [37]. La parte del flujo base del Río de Oro en la estación Conquistador fue estimado mediante la aplicación de isótopos estables en la ecuación de conservación de masa en una sección del río y equivale a cerca del 80 % del flujo total [38].

En la cuenca del río Suratá se localiza una estación limnimétrica (Majadas) y una estación pluviométrica (Vetas -El Pozo). Asimismo, en la cuenca del Río de Oro se ubica una estación limnigráfica (Conquistador Alto) y una estación pluviométrica (El Picacho). Las estaciones de caudales se encuentran localizadas para ambos casos aguas arriba de bocatomas, con excepción de las bocatomas que se localizan en la cuenca del río Tona desde hace más de 50 años. La información general de estas estaciones se muestra en la Tabla 2.

Las gráficas de las series de tiempo de los caudales en los puntos de cierre de las cuencas de rio Suratá y rio de Oro se muestran en la Fig. 3. y Fig 4. Se observan que las variaciones temporales de caudales altos ocurren durante los años 2010 y 2011. Los caudales mínimos se observan regularmente en las épocas secas.

Tabla 2.

Estación limnigráfica. Estación pluviométrica. *Periodo de tiempo en el que se tiene información de cada estación.

Cuenca	Estación	Tipo	ms.n.m.	Periodo*
Río Suratá	Majadas		700	01/01/1990 31/10/2013
	Vetas-El Pozo		3220	01/01/1993 31/12/2013
Río de Oro	Conquistador Alto		1105	02/10/2008 31/03/2011
	El Picacho		3310	01/07/1967 28/02/2015

Fuente: Los autores

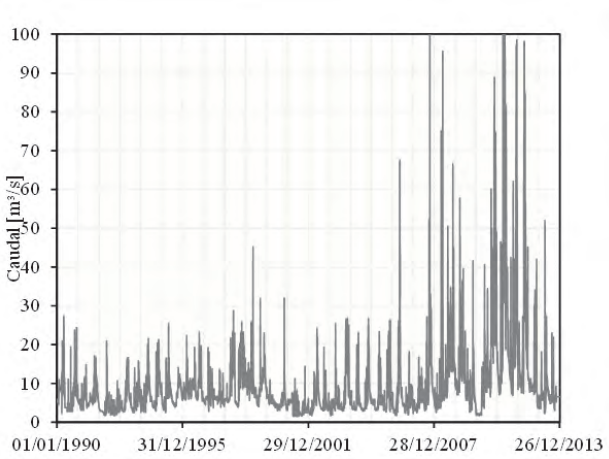

Figura 3. Serie de caudales de la estación Majadas, río Suratá.
Fuente: Los autores

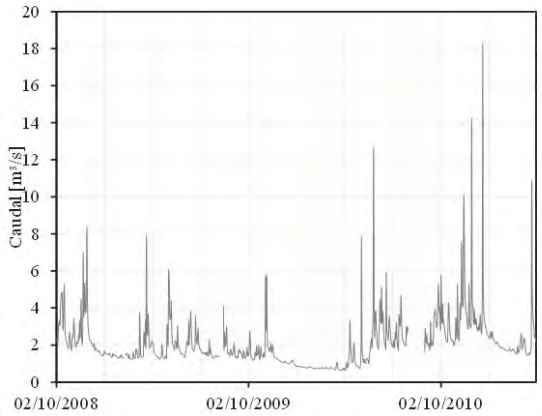

Figura 4. Serie de caudales de la estación Conquistador Alto, Río de Oro.
Fuente: Los autores

2.4. Selección de algoritmos de separación flujo base

Para seleccionar el algoritmo numérico que ofrece mejores resultados se utiliza el coeficiente de determinación, R^2 [39]. Este coeficiente expresa el ajuste entre el caudal del río y el caudal base hallado para cada algoritmo durante las épocas de estiaje; se calcula únicamente con datos de las temporadas de recesión. El análisis se realiza bajo la hipótesis de que todo el flujo en épocas de estiaje proviene de los acuíferos, es decir, el caudal observado Q_t corresponde al flujo base Q_b.

3. Análisis de resultados

A continuación, se presentan los resultados obtenidos en las dos cuencas de estudio después de aplicar la metodología propuesta y los conceptos presentados en este trabajo.

3.1. Curva maestra de recesión

La revisión de la información limnimétrica en la estación Majadas permitió identificar dieciocho periodos de recesión ocurridos entre 1990 y 2013, mientras que para la estación Conquistador Alto se tiene información desde 2008 hasta 2011, y fueron identificadas tres épocas de recesión. En la cuenca del río Suratá se observan recesiones cuya duración varía entre 30 y 101 días, y en el Río de Oro, entre 63 y 120 días. En el Río de Oro, a pesar de tener un periodo de tiempo menos representativo en datos, se encontró la recesión de mayor duración.

La información pluviométrica en ambas cuencas muestra una relación de la lluvia diaria con la respuesta de los caudales diarios, tal como se observa en la Figura 7 y en la Figura 8. Con los datos de las series de caudales de ambos ríos se construyeron las respectivas curvas maestras de recesión.

Se observó que no es posible distinguir una tendencia lineal única en el comportamiento del flujo base de ambos ríos. La CMR obtenida en el río Suratá (Figura 5) muestra que existen tres comportamientos diferenciables, cada uno con una pendiente característica, por lo tanto, la forma de la ecuación lineal (1) no resulta representativa para este río. Por esta razón se optó por realizar un nuevo ajuste a una ecuación no lineal (3) que represente de mejor forma el comportamiento de todas las recesiones encontradas; el resultado del ajuste igualmente se muestra en la Figura 5. El coeficiente de determinación (R^2) obtenido en este caso fue 0.963.

La CMR del Río de Oro (Figura 6) también muestra que existen tres comportamientos diferentes, en consecuencia, la forma de la ecuación lineal tampoco es representativa. El ajuste a una forma no lineal presenta un coeficiente de determinación (R^2) de 0.956.

En el río Suratá y en el Río de Oro las curvas de recesión presentan forma no lineal y en este caso se ajustaron a una forma cóncava (Ecuación (3)). Un análisis de las tendencias permite observar que la respuesta rápida de la descarga del flujo subterráneo (constante de recesión mayor 0.012 1/día para el río de Oro y 0.032 1/día para el río Suratá) puede corresponder a la movilización de flujo proveniente de recargas más locales, mientras que la respuesta lenta (constant de recesión menor,

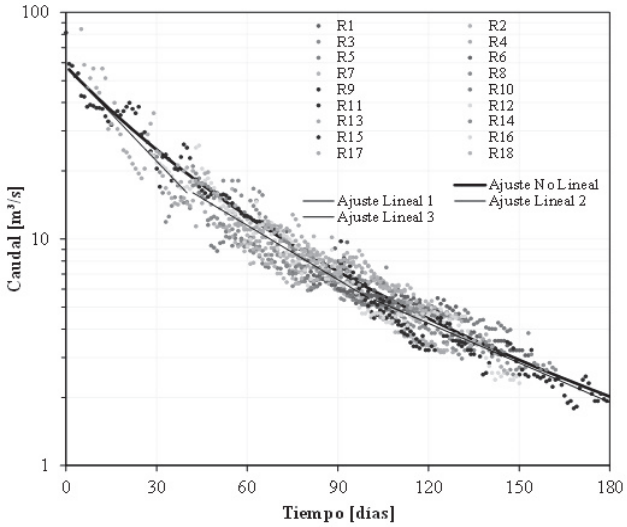

Figura 5. Ajuste a la forma lineal de la CMR, ecuación (1) y a la forma no lineal, ecuación (3). Estación Majadas del río Suratá.
Fuente: Los autores

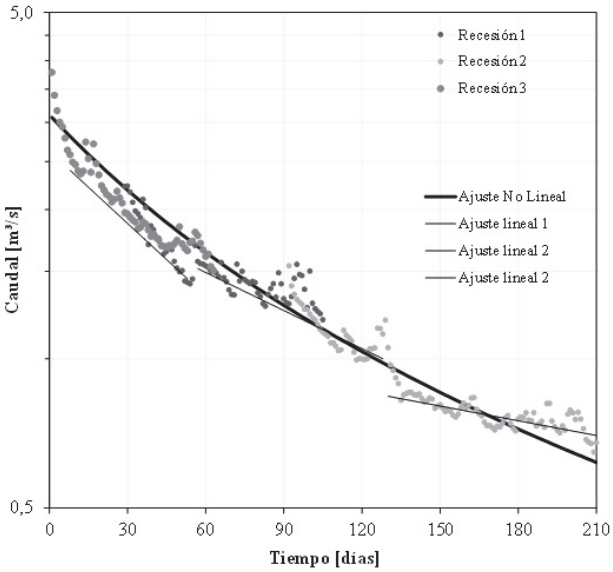

Figura 6. Ajuste a la forma lineal de la CMR, ecuación (1) y a la forma no lineal, ecuación (3). Estación Conquistador Alto, cuenca del Río de Oro. Fuente: Los autores

0.002 para el río de Oro y 0.013 para río Suratá) corresponde a un retardo del flujo generado en los caminos de mayor distancia que comunican a los acuíferos con el río; en este caso el flujo es alimentado con recargas de larga distancia.

La forma general de la curva maestra de recesión muestra los valores obtenidos de los parámetros ***a*** y ***b***, para ambos ríos en la Tabla 3. En el río Suratá y en el Río de Oro el exponente ***b*** toma valores de 0.7 y 0.4 respectivamente. Ambos difieren de los exponentes utilizados en los modelos teóricos, que son $b = 0.5$ (aproximación cuadrática) o $b = 1$ (aproximación lineal). En este caso se deben estudiar las razones para las cuales pueden existir diferencias de estos valores. Valores diferentes significan que en la realidad el flujo no puede ser representado mediante las aproximaciones anteriores. El valor para el Río de Oro es de 0.4, y si bien no es muy diferente a 0.5, puede expresar flujo desde acuíferos libres en contacto con el río. Valores de 0.4 podrían explicarse según [11], en términos de convergencia del flujo subterráneo. Sin embargo, [18] expone otras razones para estos valores, que van desde disminución de conductividad hidráulica con la profundidad, variación espacial de la lluvia y la infiltración, así como el comportamiento transitorio de la relación almacenamiento-descarga, que no son consideradas en las ecuaciones. Esta última razón puede implicar efectos de histéresis o variabilidad del gradiente hidráulico del acuífero. Todas estas condiciones se pueden presentar en la realidad, en particular, en el caso de cuencas de montañas con geologías complejas.

En el río Suratá el exponente ***b*** toma un valor de 0.7, que también difiere de los modelos teóricos, pero en este caso se aleja de la aproximación cuadrática y se acerca al valor de 1 más representativo de acuíferos confinados en contacto con el río. El valor obtenido de 0.7 se puede explicar en términos de una componente de un flujo que quizás se origine en la existencia de macroporos o fracturas.

Tabla 3.
Parámetros de la CMR

Parámetros		Río Suratá Área 697 km^2	Río de Oro Área 80 km^2
Modelo lineal	α_{Prom} *[días]*	53.4	150.8
	k_{prom} *[días^{-1}]*	0.0213	0.007
Modelo no lineal	$a\ [mm^{1-b}d^b]$	150	380
	b	0.7	0.4
	Q_o*[mm/d]*	57.8	3.1

Fuente: Los autores

Por otro lado, el valor del parámetro ***a*** de las cuencas se ha encontrado mediante el proceso de ajuste (ajuste de la forma de la curva a los datos de la CMR). Este parámetro se relaciona con parámetros físicos de los acuíferos como la porosidad y la conductividad hidráulica, o con características generales de las cuencas.

En las cuencas del río Suratá y del Río de Oro se obtuvieron valores, para ***a***, de 150 y 380 respectivamente, como se observa en la Tabla 3. Los promedios de los parámetros corresponden al enfoque lineal

Los valores obtenidos de ***a*** se comparan con valores obtenidos en cuencas de Alemania y China [40], donde se utilizaron resultados de más de veinte cuencas, observándose una relación entre el valor de ***a*** y el área de la cuenca. En este trabajo se advierte que el río Suratá muestra un valor semejante a los encontrados en las cuencas anteriores que tienen áreas semejantes. Sin embargo, el valor de ***a*** obtenido para el Río de Oro difiere considerablemente de los resultados anteriores. De acuerdo con la relación encontrada, el valor de ***a*** correspondería a cuencas con áreas mayores a 1400 km^2. El valor de ***a*** obtenido para la cuenca del Río de Oro también confirma tiempos de viaje bastantes mayores que los que presenta la cuenca del río Suratá.

3.2. Separación de flujo base

La separación del flujo base se realizó aplicando cuatro algoritmos numéricos (capítulo 0) a las series de datos de caudales de los ríos Suratá y de Oro.

El algoritmo numérico de un parámetro requiere de un solo valor de constante de recesión; al existir tres valores diferentes se optó por el procedimiento clásico de utilizar el valor promedio de las constantes de recesión como representativo del valor ***K*** (ver Tabla 3).

El algoritmo de dos parámetros, además del parámetro ***K*** anterior, utiliza el parámetro ***C***, que proporciona mayor flexibilidad a la ecuación del algoritmo. El proceso de calibración permitió observar que el porcentaje de flujo base se incrementa a medida que aumenta el valor de ***C***, lo cual indica que, debido a la permeabilidad de la cuenca, en eventos de lluvia la recarga local ocurre más rápidamente y satura el suelo convirtiendo el exceso de agua en escorrentía directa [16]. Asimismo, el proceso de calibración llevó a escoger $C = 2$ como el mejor valor. Por su parte, la inspección visual del hidrograma y de la línea de separación permitió observar que este algoritmo sobrestima el caudal base en eventos de precipitación y lo subestima en los periodos de estiaje.

En el algoritmo de tres parámetros la disposición de la ecuación (7) permite ver que el factor β_s/β_q expresa el flujo

rápido y el flujo lento, cuya relación puede tener una interpretación similar a la constante ***C*** del algoritmo de dos parámetros.

El algoritmo desarrollado por Nathan & McMahon se desarrolla en tres pasos, cada paso obtiene un valor menor de flujo base como porcentaje del flujo total, debido a que cada uno de estos se basa en los resultados del anterior. Para finalizar, se observó que el paso 1 es el que mejor se acopla a la forma del hidrograma en la recesión.

En la Tabla 4 se observan los valores de los parámetros obtenidos durante la calibración de los diferentes algoritmos numéricos utilizados.

Después de aplicar la técnica de algoritmos numéricos a los datos de caudales se obtuvo el porcentaje de flujo base con respecto al flujo total. Los resultados gráficos de la aplicación de los algoritmos a los dos ríos en una recesión particular que ocurre después de un evento significativo de precipitación, tanto para el Río de Oro, como para el río Suratá, se muestran en la Figura 7 y en la Figura 8. En este caso el evento de lluvia en el Rio de Oro fue de 125 mm en los 5 días anteriores al pico y en Rio Suratá 152 milímetros en 15 días anteriores. En estas gráficas se observa la relación entre el evento de lluvia y el evento del hidrograma, al cual siguen épocas de estiaje importantes (45 días para el caso del río Suratá y 80 días para caso del Río de Oro). Además, en estas figuras, también se puede observar el ajuste al hidrograma de los diferentes algoritmos de separación de flujo base evaluados.

En la Tabla 5 se presentan los resultados obtenidos de porcentaje de separación de flujo base mediante la aplicación de diferentes algoritmos aplicados a las series de tiempo del río Suratá y del Río de Oro.

3.3. Resultados de separación de flujo base

Los porcentajes de error presentados en la Tabla 5 muestran, en general, un resultado más favorable para el ajuste en el Río de Oro que en el río Suratá. Este resultado sugiere que las recesiones analizadas en el Río de Oro, aunque pocas en número, son representativas.

El mayor error para ambos ríos corresponde a la aplicación del algoritmo de un parámetro. Los conceptos analizados y los resultados obtenidos durante este trabajo permiten afirmar que este algoritmo está lejos de representar una estimación confiable para las cuencas en estudio, porque asume una única constante de recesión y desconoce la no linealidad que presenta la relación descarga-almacenamiento del flujo subterráneo en contacto con el río.

Tabla 4.
Parámetros de los algoritmos de separación de flujo base

Método	Parámetro	Río Suratá	Río de Oro
1-P	K	0.979	0.993
2-P	C	0.08	0.06
3-P	α_s	-0.985	-0.98
	α_q	-0.4	-0.12
	β_s	1.5	0.6
	β_q	18	4
N&M	β	0.875	0.875

Fuente: Los autores

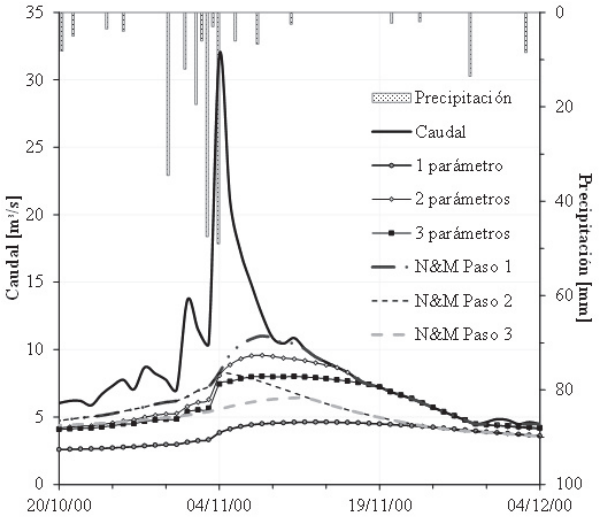

Figura 7. Separación de flujo base en una temporada de recesión típica, río Suratá.
Fuente: Los autores

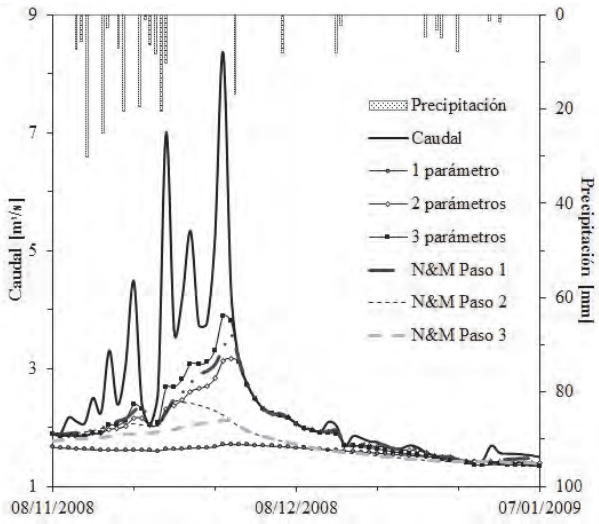

Figura 8. Separación de flujo base en una temporada de recesión típica, Río de Oro.
Fuente: Los autores

Tabla 5.
Resultados de la separación de flujo base (en %) y coeficiente de determinación R^2 en el río Suratá y Río de Oro

	Río Suratá		Río de Oro	
Método	Caudal base	R^2	Caudal base	R^2
1-P	48.6	0.485	52.6	0.757
2-P	72.3	0.787	78.6	0.979
3-P	69.2	0.750	81.0	0.979
N&M Paso 1	82.2	0.873	83.4	0.995
N&M Paso 2	68.3	0.694	73.4	0.914
N&M Paso 3	62.5	0.609	69.4	0.913

Fuente: Los autores

Los valores más altos de coeficientes de determinación hallados para los datos de ambos ríos fueron 0.873 y 0.995, con el algoritmo de Nathan & McMahon, paso 1, el cual es

considerado como un algoritmo que representa en buena forma el fenómeno de recesión de estos ríos. Los valores más bajos de los errores relativos permiten seleccionar el valor de separación de flujo base de 82.2 % para el río Suratá y 83.4 % para el Río de Oro. Estos son resultados de flujo base que reflejan una componente significativa de flujo subterráneo en ambas cuencas. El parámetro β que corresponde a estos resultados es de 0.875.

Un análisis de sensibilidad realizado a estos resultados muestra que, variando ligeramente el parámetro, los mejores coeficientes de determinación corresponden a un rango de porcentaje de flujo base que varía entre 78 y 82.2% para el rio Suratá y entre 80.5 y 83.4% para el rio de Oro, se seleccionan los que corresponden al valor más alto de R^2.

Es importante contar con otras técnicas de separación de flujo base que corroboren los datos obtenidos mediante la aplicación de los algoritmos. Para el caso del Río de Oro, la técnica de isótopos estables reportó un valor de 80 %, casi igual al obtenido mediante los algoritmos numéricos. Hasta el momento no existe otra técnica aplicada que permita contrastar el valor obtenido para el río Suratá.

4. Conclusiones

El estudio de las curvas de recesión en la parte alta de las cuencas del río Suratá y el Río de Oro permitió obtener curvas maestras de recesión que no se ajustan a la forma lineal de la relación almacenamiento-descarga atribuida a un reservorio lineal, en ninguno de los dos casos. Para representar los datos de recesión de estas cuencas fue necesario adicionar un exponente a la ecuación clásica que representa el reservorio lineal. El exponente encontrado, de 0.4, para el Río de Oro, expresa acuíferos libres en contacto con el río y flujos subterráneos en geologías complejas. El exponente de 0.7 para el río Suratá expresa transición entre un acuífero confinado y un acuífero libre.

La constante de proporcionalidad de la relación almacenamiento-descarga fue obtenida, para la cuenca del río Suratá, con un valor (150) bastante cercano a otras cuencas en el mundo que tienen aproximadamente la misma área. Sin embargo, el valor obtenido para el Río de Oro (380) dista de los valores encontrados en otras cuencas. El valor obtenido correspondería a valores encontrados en cuencas con áreas mayores. Acorde con este resultado, la cuenca del Río de Oro (cuya área es de 80 km^2) presenta tiempos de viaje promedio de 150 días, que son mayores que los que presenta la cuenca del río Suratá (53 días), con un área de 690 km^2. Este resultado puede ser interpretado como una evidencia más de que en la cuenca del Rio de Oro existen flujos subterráneos de largas distancias provenientes de otras cuencas.

Los valores de las constantes de recesión en estas cuencas no se pueden representar con un solo valor, sino con un rango amplio, los valores altos expresan respuesta rápida a la descarga del flujo subterráneo proveniente de recargas locales y los valores bajos expresan una respuesta lenta, característica de recargas de larga distancia. Las recargas locales estarían asociadas a eventos de lluvia de corto plazo, y las recargas de larga distancia lo están a eventos de lluvia de largo plazo.

El algoritmo de Nathan & McMahon fue seleccionado en ambas cuencas porque se acopla bastante bien al hidrograma en épocas de recesión y presenta el mejor ajuste; así, se obtuvo para el Río de Oro, un porcentaje de flujo base de 83.4 %, y para el río Suratá de 82.2 %. El resultado de flujo base del Río de Oro se ha podido corroborar con el resultado obtenido mediante la técnica de isótopos estables (80 %). Los valores de flujo base en ambos ríos expresan una reserva de flujo subterráneo importante. Estos resultados deben ser tenidos en cuenta en la realización de planes de ordenamiento y otorgamiento de licencias ambientales, particularmente en cuencas donde se realizan actividades que afectan el flujo subterráneo como es la minería en la cuenca del Rio Suratá. Se recomienda continuar con el estudio de los fenómenos de flujo subterráneo de manera que sea posible identificar zonas de recarga para su protección.

Los algoritmos numéricos o filtros utilizados han incorporado elementos que incluyen una base física y son una herramienta útil para realizar la separación de flujo base, estos resultados siempre deben ser contrastados con resultados obtenidos utilizando otras técnicas, por ejemplo, la aplicación de isótopos estables del agua.

Bibliografía

[1] IAEA. Isotopic age and composition of streamflow as indicators of groundwater sustainability. Results of a 2004-2009 Coordinated Research Project. 261 P., 2010.

[2] Wittenberg, H. and Sivapalan, M., Watershed groundwater balance estimation using streamflow recession analysis and baseflow separation. Journal of Hydrology, 219, pp. 20-33, 1999.

[3] Sophocleous, M., Interactions between groundwater and surface water: The state of the science. Hydrogeology Journal, 10, pp. 52-67, 2002. DOI: 10.1007/s10040-001-0170-8

[4] Sánchez-Murillo, R., Brooks, E.S., Elliot, W.J., Gazel, E., Boll., J. Baseflow recession analysis in the inland Pacific Northwest of the United States. Hydrogeology Journal, 23, pp. 287-303, 2015. DOI: 10.1007/s10040-014-1191-4

[5] Sloto, R.A. and Crouse, M.Y., HYSEP: A computer program for streamflow hydrograph separation and analysis, Water-Resources Investigations Report 96-4040, U.S. Geological Survey, Lemoyne-Pennsylvania, 1996, 46 P.

[6] Rutledge, A.T., Model-estimated ground-water recharge and hydrograph of ground-water discharge to a stream, Water-Resources Investigations Report 97-4253, U.S. Geological Survey, Reston-Virginia, 29 P. 1997.

[7] Rutledge, A.T., Computer programs for describing the recession of ground-water discharge and for estimating mean ground-water recharge and discharge from streamflow records-update, Water-Resources Investigations Report 98-4148, U.S. Geological Survey, Reston-Virginia, 43 P., 1998.

[8] Lim, K.J., Engel, B.A., Tang, Z., Choi, J., Kim, K.-S., Muthukrishnan, S. and Tripathy, D., Automated web GIS based hydrograph analysis tool, WHAT. JAWRA Journal of the American Water Resources Association, 41, pp. 1407-1416, 2005. DOI: 10.1111/j.1752-1688.2005.tb03808.x

[9] Eckhardt, K., How to construct recursive digital filters for baseflow separation. Hydrological Processes, 19, pp. 507-515, 2005. DOI: 10.1002/hyp.5675

[10] Arnold, J.G., Allen, P.M., Muttiah, R., Bernhardt, G., Automated base flow separation and recession analysis techniques. Ground Water, 33, pp. 1010-1018, 1995

[11] Chapman, T., A comparison of algorithms for stream flow recession and baseflow separation. Hydrological Processes, 13, pp. 701-714, 1999.

[12] Furey, P. and Gupta, V., A physically based filter for separating base flow from streamflow time series. Water Resources Research, 37, pp. 2709-2722, 2001.

[13] Jakeman, A. and Hornberger, G., How much complexity in warranted in a rainfall-runoff model. Water Resources Research, 29(8), pp. 2637-2649, 1993.
[14] Gómez, S., Aguas subterráneas en zonas de montaña y trazadores ambientales, Bucaramanga, Universidad Industrial de Santander, ISBN 978-958-8777-77-1, 2014.
[15] Cantafio, L. and Ryan, M., Quantifying baseflow and water-quality impacts from a gravel-dominated alluvial aquifer in an urban reach of a large Canadian river, Hydrogeology Journal, 22(4), pp. 957-970, 2014. DOI: 10.1007/s10040-013-1088-7
[16] Gómez, D. y Gómez, L., Separación de flujo base en la cuenca del Río de Oro en la estación Conquistador alto mediante la programación de algoritmos de no linealidad, Tesis de grado, Escuela de Ingeniería Civil, Universidad Industrial de Santander, Bucaramanga-Colombia, 2012.
[17] Chow, V., Maidment, D. and Mays, L., Applied hydrology, New York, McGraw-Hill, 1998.
[18] Wittenberg, H., Baseflow recession and recharge as nonlinear storage processes. Hydrological Processes, 13, pp. 715-726, 1999.
[19] Griffiths, G.A. and Clausen, B., Streamflow recession in basins with multiple water storages. Journal of Hydrology, 190, pp. 60-74, 1997.
[20] Moore, R., Storage-outflow modelling of streamflow recessions, with application to a shallow-soil forested catchment. Journal of Hydrology, 198, pp. 260-270, 1997.
[21] Tallaksen, L.M., A review of baseflow recession analysis. Journal of Hydrology, 165, pp. 349-370, 1995.
[22] Coutagne, A., Etude générale des variations de débits en fonction des facteurs qui les conditionnent, 2ème partie: Les variations de débit en période non influencée par les precipitations. La Houille Blanche, 3, pp. 416-436, 1948.
[23] Brodie, R. and Hostetler, S., A review of techniques for analysing baseflow from stream hydrographs, Australian National University. 2005.
[24] Gómez, S. and Guzmán, J., Separación de flujo base en la Cuenca superior del río Lebrija. Revista de la Facultad de Ingeniería de la Universidad de Antioquia, 61, pp. 41-52, 2011.
[25] Chapman, T. and Maxwell, A., Baseflow separation – comparison of numerical methods with tracer experiments. 23rd Hydrology and Water Resources Symposium, Hobart-Austria, 1996.
[26] Lyne, V.D. and Hollick, M., Stochastic time-variable rainfall-runnof modelling, in Hydrol and Water Resour. Symp. Institution of Engineers Australia, Perth, pp 89-92, 1979.
[27] Boughton, W., A hydrograph-based model for estimating the water yield of ungauged catchments, Engineering for Hydrology and Water Resources Conference, Newcastle, pp. 317-324. 1993.
[28] Nathan, R. and McMahon, T., Evaluation of automated techniques for base flow and recession analyses. Water Resources Research, 26(7), pp. 1465-1473, 1990.
[29] Ruiz, J.D, y Arenas, J.P., Estudio de la variación del régimen de lluvias en la Cuenca superior del Rio Lebrija. Tesis de Ingenieria Civil. Universidad Industrial de Santander, Colombia, 2005.
[30] Lozano, J., Caracterización del perfil de meteorización de las rocas cristalinas en la cuenca superior del río Lato y sus implicaciones hidrogeológicas, Piedecuesta Santander, Tesis de grado de Geologia. Universidad Industrial de Santander, Colombia, 2012.
[31] Ward, D., Goldsmith, R., Jimeno, A., Cruz, J., Restrepo, H. y Gómez, E., Mapa Geológico del Cuadrángulo H12 Bucaramanga, INGEOMINAS, Bogotá D.C, 1977
[32] Velandia, F., Gómez, S., Cetina, M. y Castellanos, E., Análisis de fracturas como base para estudios hidrogeológicos alrededor de páramos macizo de Santander, Charta-Colombia. Submitted to: Revista Mexicana de Ciencias Geológicas, 2015
[33] INGEOMINAS, Proyecto de investigación geológica e hidrológica en la región central del departamento de Santander, 2007.
[34] Oviedo, R., Gómez, S., Hernández, D. y Castillo, E., Análisis de la calidad del agua subterránea en el macizo de Santander al oriente de Bucaramanga. V Congreso Colombiano de Hidrogeología, Medellín, 2014.
[35] Forero, J., Modelo hidrológico distribuido de la cuenca superior del Río de Oro, Tesis de MSc., Escuela de Ingeniería Civil, Universidad Industrial de Santander, Bucaramanga, Colombia, 2012.
[36] Gómez, S. y Anaya, A., Acercamiento a un modelo conceptual de recarga de los acuíferos de la región de Bucaramanga. Revista Avances en Recursos Hidráulicos, 11, pp. 37-50, 2004.
[37] Gómez, S., Taupin, J. y Rueda, J., Estudio hidrodinámico e isotópico de las formaciones acuíferas de la región de Bucaramanga (Colombia), Revista Peruana Geo-Atmosférica, 4, ISSN 2077-3447, 2015.
[38] Arias, C., Gallego, A. y Sana, C., Separación del flujo base utilizando isótopos estables del agua en la cuenca alta del Río de Oro, en la estación El Conquistador Alto, Tesis de grado, Escuela de Ingeniería Civil, Universidad Industrial de Santander, Bucaramanga, Colombia, 2015.
[39] Kottegoda, N. and Rosso, R., Applied statistics for civil and environmental engineers, Oxford, Blackwell Publishing LTDA, 2008
[40] Wittenberg, H., Nonlinear analysis of flow recession curves, in FRIEND: Flow regimes from international experimental and network data, International Association of Hydrological Sciences IAHS publication No. 221, 1994.

S. Gómez-Isidro, es Ing. Civil de la Universidad Industrial de Santander, Colombia, MSc. en Recursos Hídricos y Dra. en Ingeniería, de la Universidad Nacional de Colombia, sede Medellín, Colombia. Actualmente es profesora titular de la Universidad Industrial de Santander, donde trabaja desde 1991. Es Directora del grupo de investigación en recursos hídricos y saneamiento ambiental - GPH en la Universidad Industrial de Santander. ORCID: 0000-0002-9200-6586.

V.L. Gómez-Ríos, es Ing. Civil de la Universidad Industrial de Santander, Colombia. Ingeniera en proyectos de investigación del grupo GPH -UIS. ORCID: 0000-0001-5975-8201.

UNIVERSIDAD NACIONAL DE COLOMBIA
SEDE MEDELLÍN
FACULTAD DE MINAS

Área Curricular de Ingeniería Civil

Oferta de Posgrados

Especialización en Vías y Transportes
Especialización en Estructuras
Maestría en Ingeniería - Infraestructura y Sistemas de Transporte
Maestría en Ingeniería – Geotecnia
Doctorado en Ingeniería - Ingeniería Civil

Mayor información:

E-mail: asisacic_med@unal.edu.co
Teléfono: (57-4) 425 5172

UNIVERSIDAD NACIONAL DE COLOMBIA
SEDE MEDELLÍN
FACULTAD DE MINAS

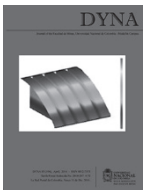

DYNA
http://dyna.medellin.unal.edu.co/

Study of the adsorption capacity of Fe(II) dissolved in water by using a mineral rich in Manganese Dioxide (MnO_2) from Colombia

Jhonnathan Machado-Infante [a], Gustavo Ramírez-Caballero [a] & Martha Barajas-Meneses [a]

[a] *Grupo de Investigación en Polímeros, Escuela de Ingeniería Química, Universidad Industrial de Santander (UIS), Bucaramanga, Colombia.*
marthabm@uis.edu.co

Received: October 14th, 2015. Received in revised form: January 18th, 2016. Accepted: February 15th, 2016.

Abstract
In Colombia, a mineral rich in MnO_2 is extracted from the mines of Mallama, Nariño. In this work we studied the adsorption capacity of this mineral for Fe(II) dissolved in aqueous solution of open systems. The characterization was done through ICP-AES, XRF and Raman spectroscopy. The effect of different pretreatments on the mineral with oxidizing agents such as $KMnO_4$ and NaClO was evaluated. Studies of equilibrium and kinetics of adsorption showed that the mechanism fits well to the Langmuir isotherm and its kinetics to a model of pseudo-second order. At the conditions studied was found that the adsorption capacity for the mineral modified with $KMnO_4$ and NaOCl were 59.209 and 51.279 mg/g respectively. It is concluded that the mineral is a potential alternative in water treatment.

Keywords: Adsorption of Fe (II); Pyrolusite; Maximum adsorption; Kinetics; Isotherms.

Estudio de la capacidad de adsorción de Fe(II) disuelto en agua usando un mineral rico en Dióxido de Manganeso (MnO_2) de origen colombiano

Resumen
En Colombia, un mineral rico en MnO_2 es extraído de las minas de Mallama, Nariño. En este trabajo se estudió la capacidad de adsorción de Fe(II) del agua en sistemas abiertos de este mineral. La caracterización del mineral se hizo a través de ICP-AES, XRF y Espectroscopía Raman. Se evaluó el efecto de diferentes pretratamientos realizados al mineral con agentes oxidantes como $KMnO_4$ y NaClO. Los estudios de equilibrio y cinética de adsorción demostraron que el mecanismo se adapta muy bien a la isoterma de Langmuir y su cinética a un modelo de pseudo-segundo orden. A las condiciones estudiadas se encontró que la capacidad de adsorción del mineral tratado con $KMnO_4$ y NaClO fue 59,209 y 51,279 mg/g respectivamente. Se concluye que el mineral presenta alto potencial en el tratamiento de aguas.

Palabras clave: Adsorción de Fe (II); MnO_2; Adsorción máxima; Cinética; Isotermas.

1. Introducción

El hierro es un elemento esencial en la nutrición. Se estima que el requerimiento mínimo diario de hierro depende de la edad y el sexo. Un rango promedio de la dosis diaria está entre 8 y 18 mg/ día [1]. Sin embargo el hierro es indeseable tanto en el agua potable como en el agua industrial causando problemas en la apariencia del agua y problemas operacionales. Por ejemplo, el hierro imparte un color rojo, amarillo o marrón en el agua, un sabor astringente y hasta turbiedad, dando la impresión de que el agua estuviera contaminada. Adicionalmente, el hierro puede promover el crecimiento de microorganismos que pueden formar una película maloliente, requiriendo altas dosis de cloro para la desinfección [2]. Como aspecto a favor, el hierro puede contribuir a la precipitación de contaminantes tóxicos como Cr(VI), siendo una potencial alternativa para remover cromo de los cuerpos de agua [3–5].

Pero puesto que el hierro es el cuarto elemento más abundante y el segundo metal más abundante en la corteza de la tierra, es un constituyente a altas concentraciones en el agua subterránea. Por lo tanto la remoción de hierro del agua es una principal preocupación para la mayoría de las compañías

© The author; licensee Universidad Nacional de Colombia.

relacionadas con el agua. La American Water Works Association (AWWA) ha sugerido una concentración límite de hierro de 0,05 mg/L para un agua de buena calidad mientras que la World Health Organization (WHO) recomienda que la concentración del hierro en agua potable sea menor de 0,3 mg/L [2].

Es por tales motivos que hay muchos esfuerzos e investigaciones en la remoción de hierro del agua. Por ejemplo, en el año 2005 en Malasia, carbón activado granular (GAC) obtenido de la cáscara del coco macerado a 850 y 1000 μm fue usado para la remoción de Fe (II). Estudios preliminares demostraron que la adsorción de Fe (II) sobre GAC alcanza el equilibrio al cabo de 6 horas. Los datos experimentales se adaptaron mejor a una isoterma de Langmuir. La capacidad máxima de adsorción correspondió a 3,601 mg de Fe (II) por g de GAC [6].

En el 2007 en Turquía, los efectos de pretratamientos de la clinoptilolita en la capacidad de adsorción de Fe (III) fueron evaluados. Los pretratamientos incluyeron lavados con $Na_2S_2O_8$ a 20°C (1), $Na_2S_2O_8$ a 70°C (2), HNO_3 a 20°C (3) y HNO_3 a 70°C (4). Los estudios de la zeolita sin ningún pretratamiento demuestran que la capacidad disminuye de 20 a 15 mg/g desde un pH de 3 a 5. La zeolita sin tratamiento y modificada con los tratamientos (1), (2) y (3) mostraron una capacidad similar de adsorción y más alta que el tratamiento (4). Los datos obtenidos de los estudios cinéticos se adaptaron mejor a una ecuación de pseudo-segundo orden y los de equilibrio se adaptaron mejor al modelo Langmuir [7]

En el 2008 en Jordán, residuos de la oliva verde y negra después de la extracción del aceite fueron usados para la remoción de hierro después de ser lavada varias veces, posteriormente secada y molida. Los estudios de eficiencia en la remoción de hierro se realizaron a 28, 35 y 45° C y a un pH entre 2 y 10. Se observó que un pH de 5 es un pH óptimo de la remoción. Los autores discutieron que a un pH mayor de 5, hay suficientes cargas negativas y el hidróxido de hierro podría empezar a precipitar. También se evidenció que la dosis óptima de adsorbente es de 5 g/L a 28° C. Los datos experimentales se adaptaron bien a las isotermas de Langmuir, Freundlich y Dubinin-Kaganer-Radushkeich, aunque con Freundlich los coeficientes de correlación fueron levemente más altos. La capacidad máxima de adsorción fue de 58.479, 45.249, y 39.370 mg/g a 28, 35 y 45°C, respectivamente. Los estudios termodinámicos demostraron la espontaneidad del proceso y los estudios cinéticos demostraron que la adsorción correspondía a un proceso de pseudo-segundo orden [8].

En el año 2014 la ceniza de la cáscara de arroz fue evaluada como medio adsorbente para la remoción de hierro. La cascarilla de arroz fue molida y lavada con agua destilada. Después fue secada a 105 °C entre 5 y 6 horas. El tamaño de partícula seleccionado para los estudios fue entre 300 y 250 μm. Este material fue calentado en una mufla a 550°C hasta obtener ceniza. Para realizar los estudios de adsorción las muestras de cenizas producidas a partir de la cascarilla de arroz fueron agitadas por 5 horas en soluciones acuosas con diferentes concentraciones iniciales de Hierro y Manganeso. Se observó que a mayor concentración inicial, la capacidad de adsorción del material se incrementó, y que el material fue más selectivo para el Hierro que para el Manganeso. El tiempo tomado para llegar al equilibrio fue de 100 minutos para el Manganeso y 50 minutos para el Hierro. El estudio termodinámico demostró un proceso espontáneo con un delta en la energía libre de Gibbs negativo y un proceso exotérmico dado por un delta de entalpia negativo. Los resultados de los estudios de equilibrio se adaptaron a los modelos de Freundlich, Langmuir, y Temkin, pero el mejor que se adaptó fue la isoterma de Freundlich. Los datos cinéticos demuestran que un pseudo-orden secundario se adapta mejor a los datos, siendo el proceso más rápido para Manganeso que para el Hierro. La capacidad máxima de adsorción fue de 66,66 mg/g para el Hierro [9].

Los sedimentos marinos, altamente ricos en MnO_2, son un intercambiador iónico [10,11] y pueden oxidar Fe(II). Este proceso ha estado bajo estudio y se ha propuesto la siguiente reacción [10] :

$$2\mathrm{Fe}^{2+} + MnO_2 + H_2O \rightarrow 2FeOOH + Mn^{2+} + 2H^+ \qquad (1)$$

Usando MnO_2 soluble en agua se ha encontrado que la reacción es de primer orden con respecto a MnO_2 y Fe(II), siendo el orden total dos [12]. La reacción de oxidación de hierro causada por sedimentos ricos en MnO_2 también fue estudiada a través de curvas de ruptura [10]. Se observó la baja concentración de Mn^{+2} antes de la ruptura de Fe(II). Esta observación fue atribuida a la presencia de manganita MnOOH en los sedimentos, que fue desproporcionada a MnO_2 y Mn^{+2} en presencia de los protones producidos en la reacción dada por eq. (1). Un estudio comparativo de la cinética de este proceso bajo atmósfera de aire y nitrógeno demostró que birnesita, un mineral rico en MnO_2, y sintetizado a través de la reducción de Permanganato de Potasio, mantuvo una alta estabilidad en aire y permitió una rápida remoción de Fe(II) atribuida al oxígeno presente en el aire. Mientras que en condiciones anóxicas la remoción de hierro fue más lenta [13].

Desafortunadamente muy poca información es conocida de de los procesos de oxidación del hierro presente en aguas en sistemas abiertos y por minerales ricos en MnO_2 extraídos de minas. Esta información es básica para el diseño de operaciones continuas para la purificación del agua. De esta manera, este trabajo está enfocado en la caracterización cinética y los procesos de equilibrio de los fenómenos de adsorción de Hierro acuoso usando un mineral rico en MnO_2, extraído de las minas localizadas en Mallama, Nariño. Este material está siendo comercializado por CCM Ingeniería actualmente. Este trabajo presenta un estudio con mucha aplicabilidad puesto que materiales adsorbentes de hierro basados en MnO_2 deben ser importados, como los son Pirolox, Catalox, y Filox. Así que la razón de ser de este trabajo es demostrar las propiedades de adsorción de este mineral de origen colombiano en la remoción de Fe (II), y su potencial para ser usado como una alternativa viable en el tratamiento de aguas.

2. Metodología

2.1. Calibración de equipo de espectrofotometría UV-visible

El espectrofotómetro de UV-vis corresponde a un Spectroquant Pharo 300 de Merck. Para la calibración se preparó una solución madre de Fe (II) de 200 mg/L a partir de la sal Sulfato Amónico Ferroso Hexahidratado ($(NH_4)_2Fe(SO_4)_2.6H_2O$). A partir de la dilución de esta solución madre se obtuvieron 5 soluciones patrón para

calibrar el equipo. Este procedimiento se realizó siguiendo los métodos propuestos en la norma técnica colombiana NTC 4754 [14], y el método 3500-Fe D de la American Public Health Association (APHA), AWWA, y Water Environment Federation (WEF) [15]. Ambos métodos siguen los mismos parámetros con algunas modificaciones.

2.2. Calibración del pH-metro

El pH-metro es un Schott Instruments, referencia Lab 850. Este equipo se calibró utilizando tres soluciones buffer de referencia de pH 4, 7 y 10.

2.3. Caracterización del mineral

El material fue caracterizado por Espectroscopía de Emisión Atómica por Plasma acoplado inductivamente (ICP-AES) que fue usada para realizar el análisis elemental, y Espectroscopía de Fluorescencia por Rayos X (XRF) usada para el análisis de óxidos. Estos análisis fueron llevados a cabo por ALS Minerals de Colombia. Adicionalmente se hicieron estudios de tamaño de partícula a través de tamices para obtener información acerca del tamaño de partícula.

2.4. Pretratamiento de las muestras del mineral rico en MnO_2 con NaClO y $KMnO_4$. Caracterización.

Para retirar posible contaminación sobre la superficie del mineral por efecto de exposición al ambiente, este material fue lavado bajo el siguiente procedimiento. Muestras diferentes fueron tratadas por separado con solución 0,25 molar de $KMnO_4$ y solución de NaClO al 1% en volumen. Luego fueron enjuagadas con abundante agua destilada para retirar residuos de los químicos usados para el lavado. Posteriormente fueron sometidas a secado en un horno a 60 °C durante 24 horas para su activación. Muestras de mineral sin tratar y tratadas con los dos agentes oxidantes fueron caracterizadas a través de Espectroscopía Raman utilizando un láser de 532 nm y una potencia de 10 mW.

2.5. Estudio del efecto de pH sobre la adsorción

El estudio de pH se realizó para determinar el pH óptimo de adsorción de Fe (II) sobre la superficie del mineral. Se preparó una solución de 100 mg/L de Fe (II) a partir de Sulfato Amónico Ferroso Hexahidratado ($(NH_4)_2Fe(SO_4)_26H_2O$) y se dispuso en 5 matraces de 100 ml previamente cargados con 0,015 g de de mineral modificado con $KMnO_4$. El pH de los matraces fue ajustado con ácido sulfúrico a valores de 2, 3, 4, 5, 6 y 7. Los matraces fueron sometidos a agitación durante 8 horas y 230 rpm en un Shaker Heidolph Unimax 2010. Las soluciones obtenidas después de filtración fueron sometidas a análisis de absorbancia UV-vis para medir la concentración de Fe (II) en la solución.

2.6. Estudio de la cinética de adsorción

El principal objetivo de los estudios cinéticos fue determinar el tiempo de contacto de equilibrio y cuál era el modelo cinético que mejor describía el fenómeno de adsorción. Para esto se puso en contacto 0,04 g del mineral modificado con $KMnO_4$ en un matraz con 250 ml de solución de Fe (II) de 200 mg/L a una temperatura de 23 °C con agitación constante de 230 rpm. La primera muestra se tomó 30 minutos después de iniciar la agitación y las siguientes cada 60 minutos, con un total de 8 muestras. Todas las muestras fueron analizadas en el espectrofotómetro UV-vis donde se obtuvo la concentración final de cada una de ellas. El procedimiento anterior fue repetido para el mineral modificado con NaClO.

2.7. Estudio de distribución de Fe (II) en equilibrio

La distribución del Fe(II) entre las fases sólida y líquida es de gran importancia para tener una noción aproximada de como interactúa el Fe(II) con el mineral rico en MnO_2. En esta etapa se dispusieron en 5 matraces 0,015 g de mineral modificado con $KMnO_4$ con 50 ml de solución de Fe(II) de concentración inicial 5, 10, 20, 40 y 60 mg/L a pH=4, 23°C y con agitación constante de 230 rpm durante 8 horas. Todas las muestras fueron analizadas en el espectrofotómetro UV-vis donde se obtuvo la concentración final de cada una de ellas. Se repitió el procedimiento anterior pero esta vez para la muestra de mineral modificado con NaClO.

3. Resultados y análisis

A continuación, se muestran los resultados obtenidos de los estudios de caracterización y adsorción adsorción de Fe (II) del mineral tratado con $KMnO_4$, NaClO y sin tratamiento como adsorbentes. Estos ensayos permitieron comparar la efectividad de los tratamientos previamente mencionados.

3.1. Caracterización del mineral rico en MnO_2

3.1.1. Espectroscopía de Fluorescencia por Rayos X (XRF)

El análisis de óxidos por Espectroscopía de Fluorescencia por Rayos X mostrado en la Tabla 1 evidencia un alto porcentaje de MnO_2. Este óxido es el responsable de la oxidación del Fe (II) a Fe (III).

Este análisis demuestra que además de que el material presenta un contenido muy alto de MnO2, también presenta un contenido importante de óxido de Silicio (9.24%). En una proporción menor están los óxidos de Bario, Aluminio y Hierro. (2.34, 1.38, y 1.47%).

Tabla 1.
Óxidos presentes en el mineral rico en MnO_2

Óxido	Porcentaje en peso
SiO_2	9.24
Al_2O_3	1.38
Fe_2O_3	1.47
CaO	0.28
MgO	0.05
Na_2O	0.06
K_2O	0.21
Cr_2O_3	0.01
TiO_2	0.02
MnO_2	82.87
P_2O_5	0.13
SrO	0.03
BaO	2.34

Fuente: Análisis de ALS Minerals Colombia Ltda, suministrado por CCM Ingeniería S.A.

Tabla 2.
Análisis Elemental del mineral rico en MnO_2

Elemento	Concentración mg/Kg	Elemento	Concentración mg/Kg
Ag	0.30	Mn	>50000
Al	<0.001	Mo	0.96
As	120.00	Na	<0.001
Au	<0.2	Nb	0.17
B	<10	Ni	28.4
Ba	>10000	P	500
Bi	0.48	Pb	3.5
Ca	<0.001	Rb	4.5
Cd	1.60	Re	<0.001
Ce	3.49	S	<0.001
Co	20.40	Sb	17
Cr	1.00	Sc	2
Cs	0.44	Sn	0.2
Cu	390.00	Sr	360
Fe	0.001	Ta	<0.01
Ga	7.57	Te	0.14
Ge	1.41	Ti	<0.001
Hf	0.06	Tl	0.05
Hg	10.00	U	1.81
In	0.05	V	26
K	<0.001	W	25.7
La	4.70	Y	16.35
Li	11.2	Zn	192
Mg	<0.001	Zr	2

Fuente: Análisis de ALS Minerals Colombia Ltda, suministrado por CCM Ingeniería S.A.

3.1.2. Espectroscopía de Emisión Atómica por Plasma Acoplado Inductivamente (ICP-AES)

El análisis elemental es mostrado en la Tabla 2. Este muestra que el contenido de Manganeso es el más alto con respecto a todos los demás elementos, con un contenido mayor de 50000 mg/Kg, seguido por un contenido de Bario mayor de 10000 mg/Kg.

3.1.3. Tamaño de partícula

El estudio de tamaño de partícula del mineral rico en MnO2 mediante el uso de tamices estándar para ensayos mostró que el material pasa a través de la malla Nº 325 con un porcentaje de retención de aproximadamente 7%, lo que indica que aproximadamente el 93% del material corresponde a un tamaño de partícula no mayor a 45 µm. Este resultado indica que el material fue finamente pulverizado lo que representa una mayor área expuesta para la adsorción.

3.1.4. Caracterización de las muestras después del tratamiento con KMnO4 y NaClO

Los estudios de Espectroscopía Raman demuestran que la banda observada en 646 cm^{-1} en el mineral sin tratamiento fue desplazada hacia 632 cm^{-1} después de que el mineral fuera tratado con ambos agentes oxidantes. Ver Fig. 1. La banda presente a 646 cm^{-1} está muy cerca a la banda característica reportada para manganosita (MnO), de 647 cm^{-1} [16]. Esta observación puede confirmar que el MnO presente se oxidó hacia MnO_2 debido a los tratamientos con $KMnO_4$ y NaClO. También se observa la desaparición del pico correspondiente a 461 cm^{-1}. Este pico puede ser relacionado con el Óxido de Silicio, SiO_2 presente [17]. La desaparición del SiO2 puede ser debida a la formación de silicatos solubles en agua producidos por la oxidación.

3.2. Efecto del pH sobre la adsorción

El efecto del pH de la solución en la adsorción de Fe (II) sobre el mineral se muestra en la Fig. 2. La adsorción de Fe (II) en el material presenta un máximo en un pH de 4. Esto puede ser debido a que a pH por debajo de 4, donde hay una alta proporción de protones, se presenta una densidad de carga positiva alta en la superficie del mineral lo que conlleva una alta repulsión electrostática entre el adsorbente y Fe (II), disminuyendo la eficiencia de la remoción. Al aumentar el pH, la densidad de carga positiva disminuye, aumentando la eficiencia de la remoción. Sin embargo, por encima de un pH de 4 se presenta la precipitación de hidróxidos de hierro [8].

3.3. Cinética de adsorción de Fe (II)

La Fig. 3 muestra la relación entre la capacidad de adsorción (q) de Fe (II) y el tiempo de contacto (t) del mineral modificado con $KMnO_4$ y el modificado con NaClO. La concentración inicial de la solución de Fe (II) fue 200 mg/L. La capacidad de adsorción en equilibrio máxima (q_e) del modificado con $KMnO_4$ fue de 148,745 mg/g, alcanzada después de 6,5 horas. Teniendo en cuenta las concentraciones iniciales y finales de hierro, el porcentaje de eficiencia de remoción de hierro después de 6,5 horas, puede ser calculado así:

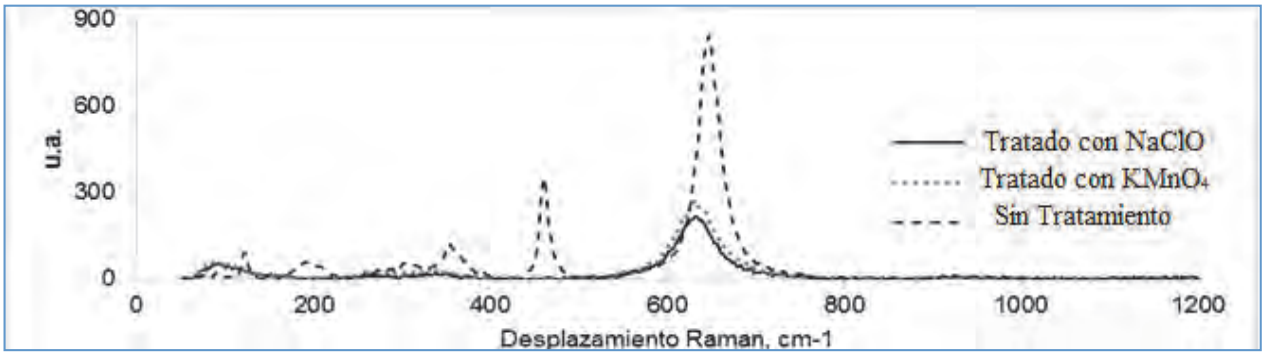

Figura 1. Espectros Raman para Mineral tratado con NaClO, tratado con KMnO4 y sin tratamiento. (Los espectros fueron tomados en el Laboratorio de Espectroscopia Parque Tecnológico Guatiguará - Universidad Industrial de Santander)
Fuente: Autores.

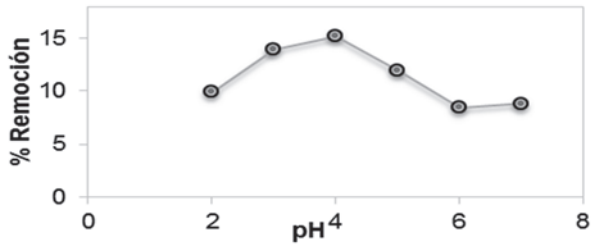

Figura 2. Efecto de pH sobre la remoción de Fe (II) en el mineral modificado con $KMnO_4$. Fuente: Autores

$$\%\ Eficiencia = \frac{Concentración\ inicial - Concentración\ final}{Concentración\ inicial} * 100 \quad (2)$$

Puesto que la concentración final de hierro en la solución es de 176.201 mg/L, la eficiencia de remoción es de 11.90%. La adsorción de equilibrio máxima (q_e) en el mineral modificado con NaClO fue de 140,236 mg/g, siendo esta alcanzada después de 6,5 horas. Este valor es obtenido teniendo en cuenta que la concentración final de hierro en la solución fue de 177.562 mg/L. Así que la eficiencia de remoción corresponde a un porcentaje de 11.21%, muy similar al anterior. Estos porcentajes pueden ser aumentados incrementando la razón de la masa de mineral a volumen de solución. También se observa que durante la primera media hora de contacto la adsorción fue rápida pero después de este tiempo el proceso se hace más lento hasta alcanzar el punto de equilibrio. La rapidez inicial de adsorción se debe a que hay mayor cantidad de sitios inicialmente disponibles en la superficie del adsorbente (significa que la superficie esta insaturada), pero luego se ralentiza debido a la falta de disponibilidad de estos sitios ya ocupados en su mayoría y así el tiempo de contacto aumenta gradualmente hasta que se alcanza el equilibrio. También se observa una leve diferencia en la capacidad de adsorción del modificado con $KMnO_4$ frente al modificado con NaClO.

Los resultados obtenidos al aplicar los modelos de pseudo-primer orden y pseudo-segundo orden se muestran en las Tablas 3 y 4 respectivamente. Mediante la revisión del parámetro de ajuste lineal r^2 para cada modelo se puede observar que los resultados obtenidos con el modelo de pseudo-segundo orden son más cercanos a los experimentales, evidenciando esto que la cinética de adsorción de Fe (II) en el mineral rico en MnO_2 modificado con ambos tratamientos se ajusta a un modelo de pseudo-segundo orden.

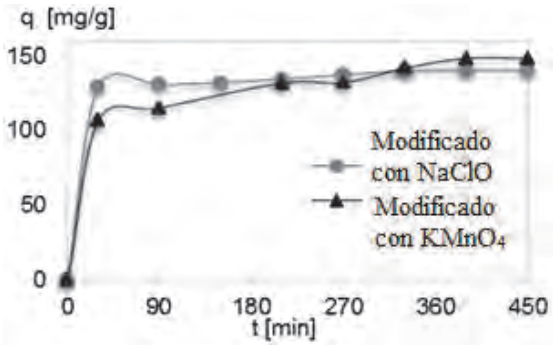

Figura 3. Perfil de adsorción de Fe (II) en el tiempo. Fuente: Autores

Tabla 3.
Parámetros cinéticos de Pseudo-primer orden de adsorción de Fe (II).

Adsorbente	$q_{e\ (exp)}$ (mg/g)	Pseudo-Primer orden		
		$q_{e\ (Teor.)}$ (mg/g)	K_1 (min-1)	r^2
Tratado-$KMnO_4$	148.745	53.543	0.0055	0.9143
Tratado-NaClO	140.236	25.556	0.0104	0.7378

Fuente: Autores

Tabla 4.
Parámetros cinéticos de Pseudo-segundo orden de adsorción de Fe (II).

Adsorbente	$q_{e\ (exp)}$ (mg/g)	Pseudo-Segundo orden		
		$q_{e\ (Teor.)}$ (mg/g)	K_2 (g/mg min)	r^2
Tratado-$KMnO_4$	148.745	151.515	0.0004	0.9892
Tratado-NaClO	140.236	142.857	0.0009	0.9993

Fuente: Autores

3.4. Estudios de distribución de Fe (II) en equilibrio.

Se utilizaron los modelos de adsorción de equilibrio de Langmuir y Freundlich para la descripción cuantitativa de la adsorción de Fe (II).

Se calcularon las constantes y coeficientes de correlación para las isotermas de adsorción de Fe(II) y los resultados presentados la Tabla 5. Los coeficientes de correlación r^2 del modelo de Langmuir para el mineral modificado con $KMnO_4$, el modificado con NaClO y sin tratamiento fueron 0.999, 0.993 y 0.977 respectivamente, mientras que los coeficientes de correlación del modelo de Freundlich para los mismos adsorbentes fueron de 0.823, 0.848 y 0.588 respectivamente. Estos resultados permitieron concluir que el proceso de equilibrio se describe mejor por el modelo de Langmuir lo que indica la adsorción a través una monocapa.

La Tabla 5 muestra la capacidad máxima de remoción (q_m) para el mineral modificado con $KMnO_4$, NaClO y sin tratar. Estos valores fueron 59.209, 51.279 y 0.233 mg/g, respectivamente. A través de este estudio se evidenció la favorabilidad del proceso de adsorción para los minerales modificados con $KMnO_4$ y NaClO. Estos materiales presentaron mayor capacidad de adsorción que el mineral sin tratamiento. Esto en gran medida debido a que el proceso de lavado remueve impurezas en la superficie del mineral y a su vez la acción oxidante del $KMnO_4$ y del NaClO promueve la reacción de oxidación de MnO a MnO_2. El MnO se presenta probablemente por efecto de exposición del mineral a agentes reductores en el ambiente durante los procesos de pulverización, transporte y manipulación del mismo. También, y al igual que el estudio cinético, se obtuvo mejor resultado de remoción para el mineral modificado con $KMnO_4$ comparado con el modificado con NaClO aunque ambos resultados no distan en gran proporción.

Los factores de separación adimensional (R_L), se muestra en la Tabla 5. Los valores de R_L están en el rango de 0-1, indicando que la adsorción de Fe (II) en el mineral es favorable.

Tabla 5.
Parámetros de isotermas de adsorción de Langmuir y Freundlich.

Adsorbente	Parámetros Modelo Langmuir				Parámetros Modelo Freundlich	
	q_m (mg/g)	K_L (L/mg)	r^2	R_L	K_F(mg/g) (L/mg)$^{1/n}$	r^2
Tratado-$KMnO_4$	59.209	1.238	0.999	0.013	29.799	0.823
Tratado-NaClO	51.279	0.682	0.993	0.024	23.812	0.848
No tratado*	0.233	0.776	0.977	0.061	0.113	0.588

Condiciones: pH 4; T 296 ± 2 K; 230 rpm; tiempo de contacto 8 horas
*Esta es una muestra de mineral sin pretratamiento, pH=2. Fuente: Autores

4. Conclusiones

El material estudiado corresponde a un material con excelentes propiedades de adsorción de Fe (II) y es una alternativa viable para ser usado en tratamientos de agua. Este material es de origen colombiano lo que ahorraría costos de importar materiales patentados del mismo tipo como Pirolox, Catalox, y Filox. El mineral rico en MnO_2, utilizado en este trabajo debió ser tratado a través de lavados con agentes oxidantes como $KMnO_4$ ó NaClO para favorecer el proceso de adsorción de Fe (II) en tratamiento de aguas. Las muestras del mineral tratadas con $KMnO_4$ y NaClO presentan capacidades de adsorción de Fe (II) de 59.209 mg/g y 51.279 mg/g, respectivamente. Estas capacidades de adsorción están en el mismo rango de otros materiales que han mostrado excelentes propiedades de adsorción. Los estudios de adsorción en equilibrio permiten concluir que el mineral presenta afinidad por el Fe (II) y que su adsorción se realiza en un solo tipo de sitio sobre el mineral rico en MnO_2 formando una monocapa que puede atribuirse a una quimisorción para este caso en particular.

Referencias

[1] Benito-Peinado, P.J., Calvo-Bruzos, S.C. and Gómez-Candela, C., Alimentación y nutrición en la vida activa: Ejercicio físico y deporte, UNED Ciencias de la Salud, Madrid 2014.

[2] Sharma, S.K., Adsorptive iron removal from groundwater, in Intemational Inst. Infrastructural, Hydraul. Environ. Eng., Academic Board of Wageningen University 2001.

[3] Vargas-Nieto, C., Carriazo, J.G. and Castillo, E., Estudio de materiales adsorbentes de bajo costo para remover Cr (VI) de efluentes acuosos. Ingeniería e Investigación, 31(1), pp. 154-162, 2011.

[4] Higuera-Cobos, O.F., Florez García, L.C. and Arroyave-Londoño, J.F., Estudio de la biosorción de cromo con hoja de café. Ingeniería e Investigacion, 29(2), pp. 59-64, 2009.

[5] Buerge, I.J. and Hug, S.J., Kinetics and pH dependence of chromium(VI) reduction by iron(II). Environmental Science and Technology 31(5), pp. 1426-1432, 1997. DOI:10.1021/es960672i

[6] Jusoh, B.A., Cheng, W.H., Low, W.M., Nora'aini, A. and Noor, M.M. M.J., Study on the removal of iron and manganese in groundwater by granular activated carbon. Desalination, 182(1-3), pp. 347-353, 2005.

[7] Öztaş, N.A., Karabakan, A. and Topal, Ö., Removal of Fe(III) ion from aqueous solution by adsorption on raw and treated clinoptilolite samples. Microporous and Mesoporous Materials, 111(1-3), pp. 200-205, 2008. DOI: 10.1016/j.micromeso.2007.07.030

[8] Al-Anber, Z.A. and Al-Anber, M.A.S., Thermodynamics and kinetic studies of iron(III) adsorption by olive cake in a batch system. Journal of the Mexican Chemical Society, 52(2), pp. 108-115, 2008.

[9] Adekola, F.A., Hodonou, D.S.S. and Adegoke, H.I., Thermodynamic and kinetic studies of biosorption of iron and manganese from aqueous medium using rice husk ash. Applied Water Science, pp. 1-12, 2014. DOI: 10.1007/s13201-014-0227-1

[10] Postma, D. and Appelo, C.A.J.,Reduction of Mn-oxides by ferrous iron in a flow system: Column experiment and reactive transport modeling. Geochimica et Cosmochimica Acta, 64(7), pp. 1237-1247, 2000. DOI: 10.1016/S0016-7037(99)00356-7

[11] Appelo, C.A.J. and Postma, D., A consistent model for surface complexation on birnessite (delta-MnO2) and its application to a column experiment. Geochimica et Cosmochimica Acta, 63(19), pp. 3039-3048, 1999. DOI: 10.1016/s0016-7037(00)00480-4

[12] Siebecker, M., Madison, A.S. and Luther, G.W., Reduction kinetics of polymeric (soluble) Manganese (IV) Oxide (MnO_2) by Ferrous Iron (Fe2+). Aquatic Geochemistry, 21, pp. 143-158, 2015. DOI: 10.1007/s10498-015-9257-z

[13] Gao, T., Shen, Y., Jia, Z., Qiu, G., Liu, F., Zhang, Y., Feng, X. and Cai, C., Interaction mechanisms and kinetics of ferrous ion and hexagonal birnessite in aqueous systems. Geochemical Transactions, 16, [Online]. 2015. DOI: 10.1186/s12932-015-0031-3

[14] Instituto Colombiano de Normas Técnicas y Certificación, ICONTEC, Norma Técnica Colombiana-NTC 4754 Calidad del agua. Determinación de Hierro, Bogotá, Colombia 2000.

[15] APHA, AWWA, and WEF, Method 3500- Fe D, in Stand. Methods Exam. Water Wastewater.

[16] Julien, C., Massot, M., Baddour-Hadjean, R., Franger, S., Bach, S. and Pereira-Ramos, J.P., Raman spectra of birnessite manganese dioxides. Solid State Ionics, 159(3-4), pp. 345-356, 2003. DOI: 10.1016/S0167-2738(03)00035-3

[17] Holder, J., Wynn-Williams, D., Rull-Perez, F. and Edwards, H.G., Raman spectroscopy of pigments and oxalates in situ within epilithic lichens: Acarospora from the Antarctic and Mediterranean. The New Phytologist, 145(2), pp. 271-280, 2000. DOI: 10.1046/j.1469-8137.2000.00573.x

J. Machado -Infante, recibió su título de pregrado en Ing. Química en el año 2015 de la Escuela de Ingeniería Química de la Universidad Industrial de Santander, Colombia. Desarrolló su proyecto de investigación con el aval del grupo de investigación en polímeros de la Universidad industrial de Santander. Sus intereses se centran en el estudio de nuevas alternativas en el tratamiento de aguas.
ORCID: 0000-0002-1791-914X

G.E. Ramírez-Caballero, recibió su título de pregrado de la Universidad Industrial de Santander, Colombia en el año 2006, y su grado de Dr. en Filosofía, PhD en Ingeniería y Ciencia de los Materiales de Texas A&M University, USA. Se unió a la Escuela de Ingeniería Química desde al año 2012 y es líder del Grupo de Investigación en Polímeros. Sus intereses están en la síntesis y caracterización de polímeros biodegradables.
ORCID:0000-0001-9665-4022

M.J. Barajas-Meneses, recibió su título de pregrado en Ing.Química de la escuela de Ingeniería Química en el año 2001 de la Universidad Industrial de Santander, Colombia, el título de MSc. en Ciencias de la Universidad de Puerto Rico en Mayagüez y el título de Dr. en Filosofía, PhD en el año 2013 de Michigan Technological University. Ella ha estado trabajando con el Grupo de Investigación en Polímeros de la Escuela de Ingeniería Química de la Universidad Industrial de Santander desde inicios del año 2014. Sus intereses en investigación son Polímeros, degradación termal de polímeros, Espectroscopía y aplicaciones ambientales, específicamente, tratamiento de aguas.
ORCID: 0000-0001-6954-9526

UNIVERSIDAD NACIONAL DE COLOMBIA
SEDE MEDELLÍN
FACULTAD DE MINAS

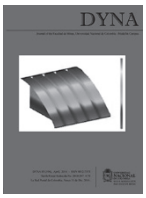

DYNA
http://dyna.medellin.unal.edu.co/

Preliminary studies on hydrated cement for its reuse in geopolymers

Yasna Pamela Segura-Sierpe [a,b], María Victoria Borrachero-Rosado [b], José María Monzó-Balbuena [b] & Jordi Payá-Bernabeu [b]

[a] *Facultad de Ingeniería, Universidad de Magallanes, Punta Arenas, Chile. yasna.segura@umag.cl*
[b] *Instituto de Ciencia y Tecnología del Hormigón, Universitat Politècnica de Valencia, Valencia, España. vborrachero@cst.upv.es, jmmonzo@cst.upv.es, jjpaya@cst.upv.es.*

Received: November 15th, 2015. Received in revised form: February 24th, 2016. Accepted: March 2nd, 2016.

Abstract
The carbonation of hydrated ordinary Portland cement (OPC) allows the transformation of hydrated calcium aluminates and silicates into calcium carbonate and amorphous silica/ alumina. These carbonated materials are appropriate to being used as inorganic precursors for alkaline activation. The use of sodium silicate and hydroxide solutions enables the production of cementitious gels. Two ways of carbonation of hydrated cement were studied: in a dry environment, where relative humidity did not exceed 70% and in an aqueous medium at a temperature of 5 ± 1 ° C. Both materials were micro-structurally characterised and they have been used for the manufacturing of geopolymeric mortars. These mortars reached mechanical strength between 10 and 20 MPa, depending on the activating solution, the water/binder ratio and curing time/temperature. These results show the feasibility of reusing hydrated cement contained in construction and demolition wastes.

Keywords: Alkali activation; carbonation; geopolymer; hydrated cement; mechanical strength; microstructure; waste.

Estudios preliminares sobre cemento hidratado para su reutilización en geopolímeros

Resumen
La carbonatación de cemento Pórtland hidratado permite la transformación de los silicatos y aluminatos cálcicos hidratados en carbonato cálcico y sílice/alúmina amorfas. Estos materiales carbonatados son susceptibles de ser usados como precursores inorgánicos para su activación alcalina. El uso de disoluciones de hidróxido y silicato sódico permite la obtención de geles cementantes. Se han estudiado dos vías de carbonatación de cemento hidratado: en un ambiente seco, donde la humedad relativa no sobrepasaba el 70 % y en un medio acuoso a temperatura de 5 ± 1 o C. Ambos materiales se han caracterizado microestructuralmente y han sido utilizados para la fabricación de morteros geopoliméricos. Estos morteros alcanzaron resistencias mecánicas entre 10 y 20 MPa, dependiendo de la disolución activadora, la relación agua/binder y del tiempo/temperatura de curado. Estos resultados demuestran la viabilidad de la reutilización de cemento hidratado presente en los residuos de construcción y demolición.

Palabras clave: Activación alcalina; carbonatación; cemento hidratado; geopolímero; microestructura; residuo; resistencia mecánica.

1. Introducción

El cemento Pórtland (del inglés: ordinary Portland Cement, OPC) es uno de los materiales de mayor producción a nivel mundial. En su fabricación se emiten grandes cantidades de gases de efecto invernadero. Se calcula que 1 ton de clínker de OPC produce aproximadamente 1 ton de CO_2 que se emite a la atmósfera y, además también se consume en el proceso una gran cantidad de energía y de recursos naturales (aproximadamente 1.5 ton de materia prima es necesaria para producir 1 ton de clínker) [1-2].

En la industria de la construcción se generan residuos en gran volumen, como son los residuos de construcción y demolición (CDW). En España se estima que se producen alrededor de 2 kg por habitante y día de dichos residuos [3]. La composición de los CDW es muy heterogénea están formados, en su mayor parte, por mezclas de áridos, hormigones, piedra, materiales cerámicos, gravas y arenas,

© The author; licensee Universidad Nacional de Colombia.

suelo y, en menor medida, metales, vidrios y plásticos, entre otros [4]. Además, en algunas plantas de reciclaje, debido al lavado de los residuos, se obtienen 5-8 ton por hora de limo, dependiendo del tamaño de la planta y la cantidad de material a procesar, siendo este residuo un problema importante [5].

A partir de estos problemas ambientales, los científicos y la industria del cemento están estudiando la forma de disminuir las emisiones de CO_2, y además, están valorando la reutilización y aprovechamiento de los residuos sólidos, provenientes de los distintos sectores industriales y, por supuesto, de la construcción. Así, una posible vía alternativa está encaminada hacia la sustitución parcial del OPC por residuos los cuales están compuestos mayoritariamente de sílice (SiO_2) y/o alúmina (Al_2O_3); los residuos más usados son: la ceniza volante, humo de sílice, puzolanas naturales o el catalizador de craqueo catalítico [6-7] o el uso de otros tipos de conglomerantes como los geopolímeros o conglomerantes de activación alcalina. En este sentido, se ha demostrado que estos últimos conglomerantes son más sostenibles y contaminan menos que el cemento tradicional [8-10] Uno de los puntos clave en este tipo de conglomerantes es que no requieren la descarbonatación de la caliza para su elaboración [11] y, además, se pueden obtener prestaciones mecánicas similares a las obtenidas con OPC [12].

Los conglomerantes de activación alcalina se preparan a partir de una sustancia precursora de composición silicoaluminosa y de una disolución activadora fuertemente alcalina [8]. Se ha investigado con éxito la fabricación de este tipo de conglomerantes utilizando como precursores residuos tales como escorias [13], cenizas volantes [14-15], catalizador de craqueo catalítico [16-17], residuos cerámicos [18-19] y residuos del vidrio [20].

De acuerdo con lo anterior, los CDW podrían ser usados como precursor mineral en la preparación de morteros y hormigones, dado su carácter silicoaluminoso. Por ejemplo, el residuo de ladrillo de arcilla roja presentan un alto contenido de SiO_2 (49.9 %) y Al_2O_3 (16.6 %) esenciales para la activación alcalina [18]. Está aceptado por la normativa española (EHE-08) que parte de los residuos de hormigón pueden reutilizarse como áridos reciclados (fracción mayor de 4 mm) [21-25]. Sin embargo, la fracción más fina de hormigón, que está compuesta en su mayoría por cemento hidratado y parcialmente carbonatado, de momento tiene una aplicación muy limitada como árido reciclado, debido fundamentalmente a la elevada porosidad de las partículas. Esta fracción suele provenir de los procesos mecánicos de trituración y cribado del hormigón.

En estudios previos, se ha utilizado el limo generado en las plantas de lavado de áridos reciclados, como material precursor para elaborar conglomerante activado alcalinamente, obteniendo resultados aceptables. Además se realizaron mezclas de este limo con metacaolín y con ceniza volante, logrando aumentar significativamente la resistencia mecánica [5]. También esta fracción fina de limo se ha estudiado como componente del crudo en la preparación de nuevo clínker para el OPC. Los hormigones fabricados con este cemento han alcanzado, a los seis meses, 54 MPa [26]. Otros investigadores trabajaron con la fracción fina del CDW, la cual sometieron a tratamiento térmico. El material tratado se combinó con OPC y ceniza volante, llegando a resistencias de hasta 18 MPa [27].

El objetivo de esta investigación se centra en la preparación de cemento hidratado y carbonatado para simular un residuo fino de demolición. Dicho material se utilizó como precursor inorgánico en la fabricación de geopolímero. Con esto se consigue cerrar el ciclo de vida del material ¨hormigón¨ puesto que se aprovecha una fracción de difícil reutilización.

2. Experimental

2.1. Materiales, equipos y métodos

2.1.1. Materiales

El material de partida utilizado es el cemento Pórtland (OPC) del tipo CEM I 52.5R, clasificado de acuerdo con la norma EN 197-1:2011 [28], cuya composición química y pérdida al fuego (P.F.) se especifican en la Tabla 1. Este cemento posee un diámetro medio aproximado de 15.81 µm. Para preparar los morteros geopoliméricos se utilizó una arena silícea (módulo de finura 3.05) y una proporción arena:cemento 3:1 y la solución alcalina se preparó con hidróxido de sodio (98% pureza) y silicato sódico (28%SiO_2;8% Na_2O; 64% H_2O).

El cemento Pórtland (OPC) de partida se hidrató de acuerdo con el estudio de Tashima et al. [29], donde se mezcló 1000 g de OPC en 5 L de agua desionizada y se agitó 2 veces al día durante un mes. A continuación se separó la parte líquida del sólido y se secó al aire a temperatura ambiente. De esta manera se obtuvo el cemento hidratado (HydC) de partida. En la parte de resultados y discusión se detallan los procedimientos de carbonatación realizados. Se prepararon dos cementos hidratados carbonatados, uno por vía seca (HCC Dry) y otro por vía húmeda (HCC Wet-Cold). El CO_2 usado en la carbonatación fue provisto en cilindro con una presión de 57.3 bar y pureza de 99.9 %.

2.1.2. Equipos

La composición química del OPC, HCC Dry y HCC Wet-Cold se determinó por fluorescencia de rayos X (XRF) en un equipo Philips MAGIC PRO, modelo PW2400 equipado con

Tabla 1.
Composición química del cemento de Pórtland, tipo CEM I-52,5R, HCC Dry y HCC Wet-Cold. (% de peso).

Óxidos	CEM I 52,5 R	HCC Dry	HCC Wet-Cold
SiO_2	20.80	11.47	12.14
Al_2O_3	4.60	2.90	2.79
Fe_2O_3	4.80	2.29	2.46
CaO	65.60	44.26	43.02
MgO	1.20	1.04	1.46
SO_3	1.70	1.64	0.88
K_2O	1.00	0.51	0.35
Na_2O	0.07	0.23	0.17
TiO_2	---	0.25	0.24
P_2O_5	---	0.15	0.18
Cl^-	---	0.06	0.04
P.F.[a]	2.02	35.21	36.26

[a] P.F: Pérdida al fuego.
Fuente: Los autores.

tubo de rodio y ventana de berilio. Las características granulométricas se determinaron por difracción de rayos láser (ADL) por medio del equipo Mastersizer 2000 de Malvern Instruments. Para el análisis termogravimétrico (TGA) se utilizó un equipo modelo TGA 850 Mettler-Toledo. El difractómetro de rayos X utilizado es un modelo Brucker AXS D8 Advance, donde la intensidad y voltaje del tubo generador de rayos X se ha ajustado a 20 mA y 40 kV respectivamente. Se registraron los difractogramas para el intervalo 2θ entre 5º y 70º, con un ángulo de paso de 0.05 grados y un tiempo de acumulación de 2 s. La microscopía de los materiales se obtuvo por medio del equipo JEOL JSM6300 aplicando a la muestra un voltaje de 20 kV.

2.1.3. Preparación de pastas

Para poder analizar el comportamiento de los cementos hidratados carbonatados (HCC Dry y HCC Wet-Cold) como material geopolimérico, se prepararon pastas activadas con hidróxido de sodio y silicato de sodio con relaciones de agua/binder de 0.45 y de 0.50 (donde el binder corresponde al precursor a utilizar HCC Dry o HCC Wet-Cold). Las soluciones activadoras se prepararon con mezcla de hidróxido de sodio (NaOH) y silicato de sodio (waterglass).

Se realizaron pruebas preliminares, utilizando concentraciones de Na^+ entre 5 y 9 molal (molalidad en mol/kg de disolvente), y relaciones molar de Na_2O/SiO_2 entre 0.34 y 1.23. Las mezclas que se prepararon se caracterizaron por tener una adecuada fluidez y al ser curadas a temperatura ambiente fraguaron a las 24 h. A partir de ello se eligieron las siguientes relaciones resumidas en la Tabla 2 donde la nomenclatura X/Y/Z corresponde a: "X" la molalidad (mol/kg) en Na^+ en la disolución alcalina, "Y" es la relación molar SiO_2/Na_2O utilizada en la preparación de la solución y "Z" corresponde a la relación agua/binder (a/b).

2.1.4. Preparación de morteros

En los morteros activados alcalinamente de HCC Dry y de HCC Wet-Cold se mezcló el binder con solución alcalina por 1.5 min, luego se adicionó arena silícea y se mezcló de forma continua por 2.5 min. El mortero se colocó en moldes de 40 x 40 x 160 mm y fue vibrado por 3 min. Las probetas se curaron en: a) baño térmico de 65 ºC con una HR de 90 - 95% por 3 y 7 días; y b) cámara húmeda a 20 ºC y humedad relativa superior 95 %, a edades de 7 y 28 días (este curado sólo para los morteros con HCC Dry).

3. Resultados y Discusión

En la fracción fina del hormigón de demolición, existe fundamentalmente arena fina y cemento hidratado (y posiblemente también parcialmente carbonatado). En nuestro caso, se ha realizado una simulación, partiendo de un cemento puro hidratado (HydC). La reacción de activación alcalina requiere de la disponibilidad de sílice y alúmina reactivas. Sin embargo, en el cemento hidratado ambas se encuentran combinadas químicamente con calcio, fundamentalmente en forma de silicato cálcico hidratado ($C_xS_yH_z$), y de aluminato cálcico hidratado ($C_{x'}A_{y'}H_{z'}$).

Para que en el material precursor que se va a utilizar en la elaboración del conglomerante de activación alcalina, la sílice y alúmina estén disponibles, realizamos la carbonatación del cemento hidratado HydC. En este proceso se neutraliza en primer lugar la portlandita, generando carbonato cálcico de acuerdo con la ec. (1):

$$Ca(OH)_2 + CO_2 \rightarrow CaCO_3 + H_2O \qquad (1)$$

El proceso de carbonatación de los productos de hidratación del cemento no se detiene en este punto. Los geles cementantes son alterados, formando gel de sílice y alúmina amorfa según ecs. (2) y (3):

$$C_xS_yH_z + xCO_2 + nH_2O \rightarrow xCaCO_3 + ySiO_2 + (n+z)H_2O \qquad (2)$$

$$C_{x'}S_{y'}H_{z'} + x'CO_2 + n'H_2O \rightarrow x'CaCO_3 + y'Al_2O_3 + (n'+z')H_2O \qquad (3)$$

3.1. Carbonatación en seco

El proceso de carbonatación del cemento hidratado (HydC) se llevó a cabo con el objeto de carbonatar la portlandita presente en este material y además descomponer los silicatos y aluminatos cálcicos hidratados para obtener un material con sílice y alúmina amorfas. Para ello se siguió el procedimiento siguiente: El HydC es colocado en un desecador estanco; junto a una solución de glicerina y agua (al 30 %) y gel de sílice a fin de mantener una HR entre 60 - 70 %. Esta humedad relativa es la más apropiada, ya que se conoce que si la HR sobrepasa el 70 % la carbonatación se reduce debido a que la tasa de difusión del CO_2 es más lenta, mientras que con HR menores al 50 % la carbonatación no se produce por falta de humedad suficiente en el sistema [30]. Posteriormente se ingresa CO_2 al 95 % en volumen, creando una atmósfera rica en este gas. Todo este proceso se realiza a temperatura ambiente. Cada día, se hace pasar CO_2 puro en el interior del desecador durante 15 min. Este proceso de renovación se repite durante 15 días. El producto obtenido es el cemento hidratado carbonatado (HCC Dry). En la Fig. 1 se observa el esquema del proceso de carbonatación en seco.

En la Fig. 2 se muestran las curvas TGA y DTG de HydC, donde se puede observar una pérdida continua en todo el intervalo de calentamiento (35-1000 ºC). En el primer intervalo de temperatura (100-300 ºC) la pérdida de masa es debida a la evaporación de agua de los compuestos presentes en el cemento hidratado, como la etringita, silicatos cálcicos hidratados y aluminatos cálcicos hidratados (C-S-H y C-A-H). En el segundo tramo (450-550 ºC) la pérdida de masa detectada es la debida al agua de la descomposición de la portlandita, según la ec. (4):

Tabla 2.
Condiciones de las mezclas en pastas activadas alcalinamente fabricadas con HCC Dry y HCC Wet-Cold.

Mezcla	Na^+	Na_2O/SiO_2	(%) respecto al conglomerante		
(X/Y/Z)	(mol/kg)		Na_2O	SiO_2	H_2O
7/1.56/0.45	7	0.64	9.77	14.77	45
7/1.56/0.50	7	0.64	10.85	16.41	50
9/1.22/0.45	9	0.82	12.56	14.77	45
9/1.22/0.50	9	0.82	13.95	16.41	50

Fuente: Los autores.

$$Ca(OH)_2 \rightarrow CaO + H_2O \quad (4)$$

Por último, en el tercer tramo (700-850 ºC, con un pico en la curva DTG a 806 ºC) se obtiene la pérdida debida a la eliminación de CO_2, correspondiente a la reacción de descomposición de los carbonatos, según la ec. (5):

$$CaCO_3 \rightarrow CaO + CO_2 \quad (5)$$

En la Tabla 3 se listan los valores de las pérdidas en los diversos intervalos de temperatura así como los porcentajes de $Ca(OH)_2$ y $CaCO_3$ presentes en el material de partida.

Debemos destacar que el porcentaje tan elevado de carbonato cálcico que aparece en HydC es debido por una parte a la presencia de una pequeña cantidad de caliza en el cemento de partida (CEM I contiene aproximadamente 4.6 % de $CaCO_3$). Además, en el proceso de secado al aire se ha producido una importante carbonatación, lo cual da lugar a un contenido de 33 % de $CaCO_3$.

En la Fig. 3 se representan las curvas TGA/DTG de la muestra HCC Dry. En este caso podemos observar una pérdida total mayor que la obtenida para la muestra sin carbonatar (ver Tabla 3). En el intervalo de temperatura entre 100 - 300 ºC existe una pérdida del orden del 7 % (Tabla 3), atribuida al agua y grupos OH residuales de la sílice y alúmina amorfas generadas, ya que debido a la carbonatación de la muestra los productos hidratados del cemento (C-S-H y C-A-H) se han descompuesto parcialmente. Obviamente, también puede solaparse la pérdida de agua de los geles cementantes no descompuestos. Se ha producido una disminución de la pérdida en ese intervalo, porque parte de los geles cementantes han sido descompuestos por la carbonatación.

Por otra parte, la pérdida de masa entre los 450 - 550 ºC supone solamente un 0.11%. A pesar de que la carbonatación ha sido intensa, no ha sido completa la transformación de la portlandita, probablemente debido a que los cristales de $Ca(OH)_2$ que se carbonatan dan lugar a una película de $CaCO_3$ que impide la carbonatación completa de las partículas, quedando en el interior de los mismos una pequeña cantidad de $Ca(OH)_2$ sin carbonatar.

La pérdida de masa correspondiente al carbonato aumenta considerablemente (Tabla 3) y la curva DTG presenta un pico centrado a 841 ºC, con un pico de menor intensidad a temperaturas ligeramente menores (742 ºC). Esa pérdida equivaldría en carbonato cálcico a un 63.95 %.

A partir de los datos termogravimétricos se puede calcular el porcentaje de CaO que forma parte de las distintas fases en el cemento carbonatado. Para ello (ver Tabla 4) se calcula el porcentaje de CaO en forma de $Ca(OH)_2$ (CaO^{CH}), en forma de $CaCO_3$ (CaO^{Cc}) y el que está combinado en otras fases, tales como silicatos y aluminatos cálcicos hidratados (CaO^{of}). Este último óxido de calcio combinado se determina a partir de la diferencia entre la base calcinada y la suma de CaO^{CH} y CaO^{Cc} y del resto de óxidos (Ox^{rest}), teniendo en cuenta que el cemento de partida tiene un contenido de CaO en base calcinada de 66.95% (este valor se obtiene a partir de la base calcinada de CEM I, 97.98%, y del contenido de CaO

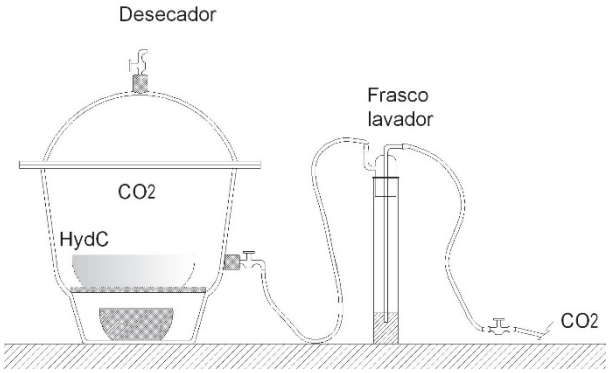

Figura 1. Proceso de carbonatación en seco (HCC Dry).
Fuente: Los autores.

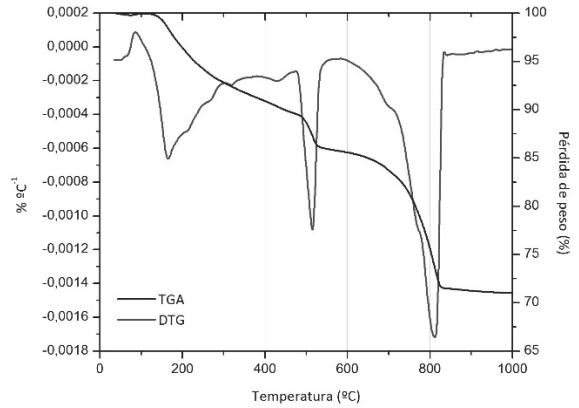

Figura 2. Curvas TGA y DTG del material de partida cemento hidratado (HydC).
Fuente: Los autores.

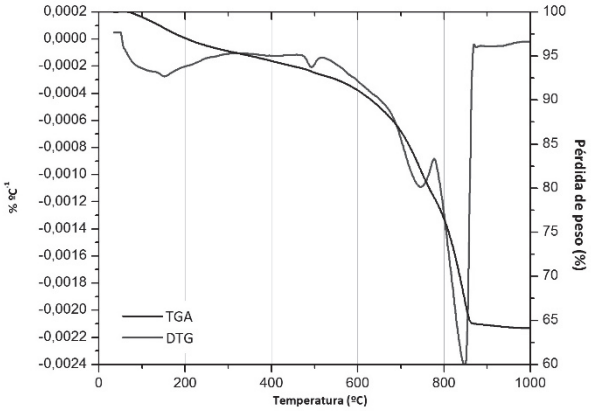

Figura 3. Curvas TGA/DTG para HCC Dry.
Fuente: Los autores.

Tabla 3.
Resumen de los datos termogravimétricos para HydC, HCC Dry y HCC Wet-Cold.

Material	HydC	HCC Dry	HCC Wet-Cold
Pérdida total (TG)	28.72	35.26	35.43
100-300 ºC	10.02	7.00	8.61
450-550 ºC	4.18	0.11	0.00
700-850 ºC	14.53	28.14	26.82
$Ca(OH)_2$	17.21	0.44	0.00
$CaCO_3$	33.04	63.95	60.95

Fuente: Los autores.

del 65.60% según Tabla 1). Para los cálculos sobre los materiales antes y después de la carbonatación se parte de la base calcinada, esto es teniendo en cuenta la pérdida total según el termograma (ver Tabla 3). Se calcula también el porcentaje de $Ca(OH)_2$ transformado en carbonato ($CaO^{CH\text{-}tr}$) y el porcentaje de CaO en otras fases transformado en carbonato ($CaO^{of\text{-}tr}$). Se puede observar que en el caso de HCC Dry la carbonatación ha supuesto una disminución desde el 18.24% de CaO^{CH} hasta el 0.53%, lo que supone una reducción del 17.71%, o lo que es lo mismo, la carbonatación ha supuesto una transformación del 95.52% de la portlandita.

Además, la carbonatación ha supuesto un incremento muy importante de los carbonatos, de modo que se ha producido un aumento de CaO^{Cc} desde el 25.95% al 55.31%, en parte debido a la carbonatación de $Ca(OH)_2$. Pero una parte importante de los carbonatos generados provienen de la transformación de los silicatos y aluminatos cálcicos hidratados [31]. En este caso, se ha producido un 11.66% de carbonato (en base CaO) por esta transformación, lo que supone que se ha descompuesto el 51.20% del CaO proveniente de los C-S-H/C-A-H para generar carbonato de calcio y geles de sílice y alúmina.

3.2. Carbonatación en húmedo y en frío

El proceso de carbonatación anterior es muy lento, por lo que se ha buscado un método alternativo más rápido y con similar eficiencia; para ello, se consideró que el proceso por vía húmeda podría ser más rápido. De esa forma, se diseñó un proceso de carbonatación de HydC, donde se mezcló 2,5 L de agua potable con 200 g de HydC y se agita continuamente, mientras que se burbujea CO_2 en la suspensión. A la mezcla se le adiciona unas gotas del indicador ácido-base fenolftaleína para poder detectar el final del proceso de carbonatación con el cambio de color de la fenolftaleína: cuando se produzca un grado de neutralización importante que genere un pH por debajo de 9 unidades, el cambio de color desde rojo a incoloro indicará el final del proceso. Además, el matraz con la suspensión (agua+HydC), se rodea de hielo manteniendo una temperatura de 5 ± 1 ºC, de modo que se solubilice la mayor cantidad de CO_2 en agua. De esta manera se burbujea CO_2 a la suspensión durante 3 horas hasta observar el cambio de color en la mezcla por medio del indicador. En la Fig. 4 se observa el esquema del proceso de carbonatación en frío y húmedo (HCC Wet-Cold).

El nuevo material se deja decantar por 24 h, se seca en la estufa a una temperatura entre 100 ± 5 ºC por 24 h y se muele hasta tamaño adecuado (ver Sección 3.3). En la Fig. 5 se representa la curva TGA/DTG de la muestra obtenida en este proceso y en la Tabla 3 se recogen los datos de pérdidas de masa asociadas. Se puede distinguir una primera pérdida en el rango de temperatura entre 100-300 ºC que muestra el agua asociada a los hidratos del cemento hidratado presentes, así como los grupos hidroxilos residuales de los productos amorfos formados (geles de SiO_2 y Al_2O_3). En este caso, no se detecta en la curva DTG ningún pico asociado a la descomposición de la portlandita entre 450-550 ºC lo que demuestra su completa carbonatación. Por último, en el intervalo 700-850 ºC de la curva DTG se muestra la descomposición de los carbonatos (pico en la curva DTG a 830 ºC). La pérdida de masa es de 26.82 %, que corresponde estequiométricamente a un contenido en carbonato cálcico del 60.95 %, valor muy parecido al obtenido en la carbonatación en seco (Ver Tabla 3).

Para esta carbonatación, se ha observado (ver Tabla 4) que CaO de otras fases (CaO^{of}) se ha reducido de 22.77 a 14.04%, una reducción ligeramente menor que la observada para la carbonatación en seco. Esta reducción supone el 8.68% de CaO de C-S-H/C-A-H que ha sido transformado, es decir, solamente 38.12% (frente a 51.20% para el método en seco). Por tanto, podemos afirmar que el método en húmedo es más efectivo en la carbonatación de la portlandita, pero menos efectivo en la carbonatación de C-S-H/C-A-H, y por ello menos efectivo en la formación de geles de alúmina y sílice, que son los de mayor interés para la activación alcalina.

Tabla 4.
Porcentaje en base calcinada de las distintas formas de CaO (CaO^{CH}, CaO^{Cc}, CaO^{of}) y del resto de óxidos (Ox^{rest}) en HydC, HCC Dry y HCC Wet-Cold, y porcentaje de $Ca(OH)_2$ y otras fases cálcicas transformadas en carbonato durante la carbonatación ($CaO^{CH\text{-}tr}$ y $CaO^{of\text{-}tr}$).

Material	HydC	HCC Dry	HCC Wet-Cold
CaO^{CH}	18.24	0.53	0.00
CaO^{Cc}	25.95	55.31	52.86
CaO^{of}	22.77	11.11	14.04
Ox^{rest}	33.05	33.05	33.05
($CaO^{CH\text{-}tr}$)	---	17.71	100
($CaO^{of\text{-}tr}$)	---	11.66	8.68

Fuente: Los autores.

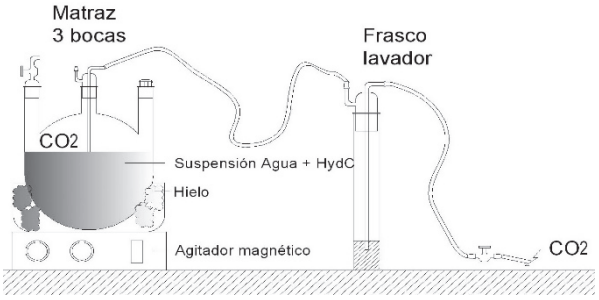

Figura 4. Proceso de carbonatación en húmedo y frío (HCC Wet-Cold).
Fuente: Los autores.

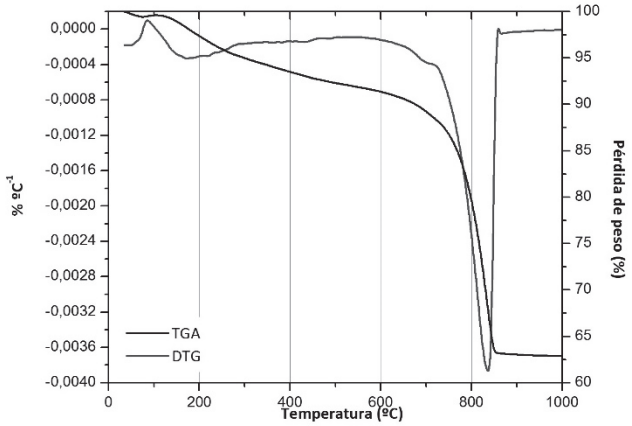

Figura 5. Curvas TGA/DTG para HCC Wet-Cold.
Fuente: Los autores.

3.3. Caracterización físico - química de las muestras de HCC Dry y HCC Wet-Cold.

La composición química de las muestras de HCC Dry y HCC Wet-Cold se determinó por un análisis de fluorescencia de rayos X (XRF). Como se muestra en la Tabla 1, se puede observar que ambos materiales presentan un elevado contenido en CaO. Además, se aprecia un porcentaje considerable de $SiO_2 + Al_2O_3 + Fe_2O_3$, superior al 17 %. El valor de la pérdida al fuego (P.F.) para ambos caso es cercana a un 36 %, valor lógico, teniendo en cuenta el elevado contenido en carbonatos de ambas muestras.

El espectro de difracción de rayos X de ambas muestras se presenta en la Fig. 6. El compuesto mineralógico mayoritario en ambos materiales es la calcita ($CaCO_3$, PDFcard050586) y debido a las elevadas cantidades de material cristalino, no es posible distinguir una desviación de la línea base entre 15-30 grados 2 θ. Por ello la presencia de sustancias amorfas relacionadas con la sílice y la alúmina no puede ser detectada. Además, para ambos materiales se observa la presencia de trazas de un carbosilicato cálcico, la fukalita ($Ca_4Si_2O_6(CO_3)(OH)_2$, PDFcard 290308) y de cuarzo (SiO_2, PDFcard 331161). En el caso del HCC Dry se aprecian trazas de portlandita ($Ca(OH)_2$, PDFcard 040733), lo que corrobora los resultados obtenidos por TGA. Es importante destacar que no se aprecia, en ninguna de las dos muestras, compuestos hidratados del cemento de origen como la etringita.

Los materiales HCC Dry y HCC Wet-Cold se molieron en un molino de bolas planetario durante 10 minutos y se midió su granulometría por análisis de difracción láser; el HydC tiene un diámetro medio de 38 µm. El diámetro medio del HCC Dry es de 22 µm y del HCC Wet-Cold es de 9 µm. Como podemos observar existe una diferencia importante entre ambos materiales carbonatados. A pesar de haber estado molidos de la misma manera, HCC Wet-Cold es más fino, lo cual puede ser atribuido a que dicho material se produjo bajo agitación constante en suspensión acuosa. De esta forma, las partículas generadas, tanto de carbonatos como de gel de sílice y alúmina, son más pequeñas.

En la Fig. 7, se observan las micrografías SEM de ambos materiales. Se detectan partículas irregulares y de textura rugosa; además se observa que en general los agregados obtenidos en la carbonatación en seco presentan un tamaño mayor que los obtenidos en el proceso en frío y húmedo.

3.4. Pasta activadas alcalinamente

Las mezclas activadas alcalinamente de HCC Dry y HCC Wet-Cold, se curaron en baño de 65 ºC y se analizaron a 3 y 7 días. En la Tabla 2 se muestran sus dosificaciones y las condiciones de activación del sistema geopolimérico.

3.4.1. Estudios de difracción de rayos X (DRX)

En la Fig. 8 se muestran los difractogramas de rayos X de la pasta 7/1.56/0.50 de HCC Dry a 3 y 7 días curadas en baño a 65 ºC. Se detectan los compuestos presentes en el material carbonatado de partida, siendo el componente principal la calcita ($CaCO_3$, PDFcard050586). También se detecta la fukalita ($Ca_4Si2O_6(CO_3)(OH)_2$, PDFcard290308).

Por otra parte se han observado trazas de vaterita ($CaCO_3$, PDFcard040030), y también de hidrotalcita ($Mg_6Al_2CO_3(OH)_{16}$, PDFcard140191), que probablemente se hayan generado debido al ambiente alcalino de la activación. Además, en la pasta a 7 días se detecta trazas de un silicato cálcico hidratado tipo girolita ($Ca_8Si_{12}O_{30}(OH)_4 \cdot 7H_2O$, PDFcard120217).

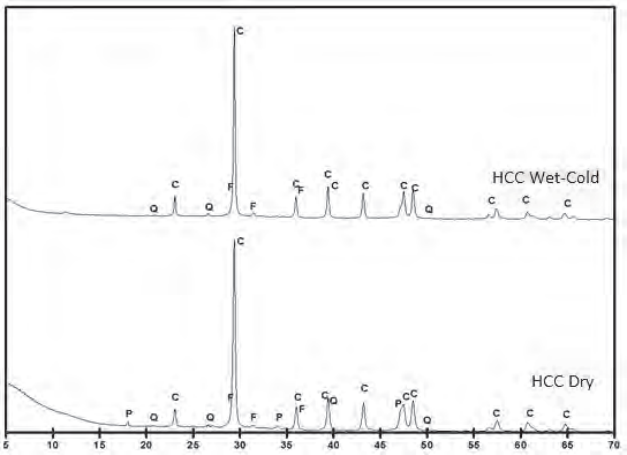

C: Calcita ($CaCO_3$); P: Portlandita ($Ca(OH)_2$); F: Fukalita ($Ca_4Si_2O_6(CO_3)(OH)_2$); Q: Cuarzo (SiO_2).

Figura 6. Difractogramas de rayos X para HCC Dry y HCC Wet-Cold.
Fuente: Los autores.

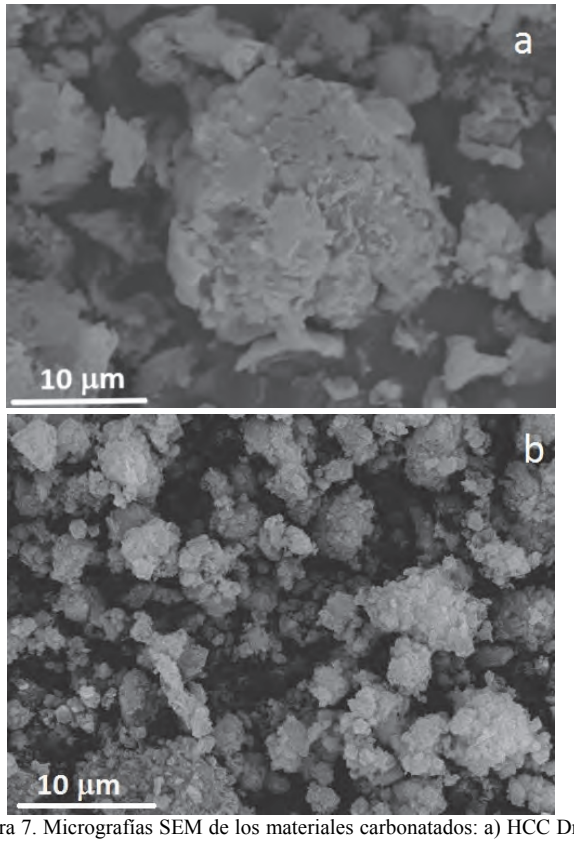

Figura 7. Micrografías SEM de los materiales carbonatados: a) HCC Dry y b) HCC Wet-Cold.
Fuente: Los autores.

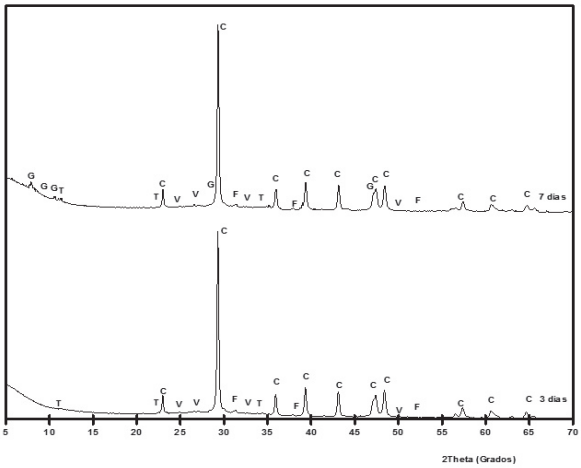

G: Girolita ($Ca_8Si_{12}O_{30}$ $(OH)_4 \cdot 7H_2O$), T: Hidrotalcita ($Mg_6Al_2CO_3$ $(OH)_{16}$), C:Calcita ($CaCO_3$), V: Vaterita ($CaCO_3$), F: Fukalita ($Ca_4Si_2O_6(CO_3)(OH)_2$)

Figura 8. Difractogramas de rayos X para las pastas con HCC Dry, con dosificación 7/1.56/0.50, curadas en baño 65 ºC a edades de 3 y 7 días.
Fuente: Los autores.

La pasta de HCC Dry 9/1.22/0.50, presenta difractogramas de rayos X muy similares a los anteriores, aunque la presencia de girolita en la pasta curada a 7 días es más difícil de detectar, ya que los picos son menos intensos que en el caso anterior. Respecto a las pastas con HCC Wet-Cold, se muestra en la Fig. 9, a modo de ejemplo, el difractograma de la pasta 9/1.22/0.45 a 7 días a 65 ºC: donde se observan, igualmente, como compuesto mayoritario, la calcita con trazas de fukalita, hidrotalcita y vaterita. Además se observan en el espectro trazas de un carbonato sódico, la natrita (Na_2CO_3) (PDFcard 370451), y compuestos de tipo zeolítico como la natrolita ($Na_2Al_2Si_3O_{10} \cdot 2H_2O$; PDFcard200759), que son productos de la evolución de los geles N-A-S-H formados durante la activación alcalina.

3.4.2. Estudios termogravimétricos

En la Fig. 10 se muestra las curvas TGA/DTG de una mezcla de HCC Dry activada alcalinamente con una relación SiO_2/Na_2O de 1.22 y relación a/b de 0.45, curada a 7 días en baño de 65 ºC. Se observan dos zonas de descomposición:

a) Entre 35 y 300 ºC: Pérdidas de peso a temperaturas inferiores a 90 ºC están asociadas al agua libre o evaporable presente en la muestra (proceso de secado). Por su parte, las pérdidas de peso comprendidas entre 90 y 200 ºC son atribuidas al agua químicamente combinada en los geles de N-A-S-H y C-A-S-H [32]. Dichos geles se han formado por reacción entre los geles de sílice y alúmina y el sodio y calcio presentes en el medio.
b) Entre 400 y 800 ºC: Esta segunda zona está relacionada con la descomposición de los carbonatos. Debe destacarse que ahora el pico que aparece a 830 ºC en el HCC Dry en la curva DTG se ha movido a temperaturas más bajas. A menor temperatura, se descomponen los carbosilicatos (fukalita) y carboaluminatos (hidrotalcita), mientras que a temperaturas mayores se descomponen los carbonatos cálcicos (calcita y vaterita) [33]. Ahora, la activación alcalina ha producido una reducción en la temperatura de descomposición de la calcita, con respecto a la muestra HydC: se puede observar que los picos DTG en la Fig. 10 que aparecen por debajo de 800 ºC, mientras que para HydC ese pico se encontraba a 830 ºC.

Además, se ha cuantificado en las curvas TGA las pérdidas de peso para cada uno de los sistemas evaluados, obteniéndose datos de pérdida total (35-1000 ºC), pérdida de masa debida a productos de activación alcalina tipo C-A-S-H y N-A-S-H (entre 35-300 ºC) y la pérdida de peso debida a la presencia de carbonatos (entre 400-800 ºC). En la Tabla 5 se listan estos datos. Además, en la Fig. 11 se representan las curvas DTG de todas las pastas analizadas a 7 días de curado.

La activación alcalina con mayor concentración de Na^+ produce un mayor número de hidratos, tal y como demuestran las pérdidas en el intervalo 35-300 ºC: para HCC Dry activado con 7 molal de Na^+, las pérdidas están en el intervalo 4.68-4.74 % mientras que para las muestras activadas con 9 molal se incrementó la pérdida a 5.54-6.05%. Lo mismo se puede observar para HCC Wet-Cold, que se pasa de 6.36-3.48 % para 7 molal a 8.02-8.43 % para 9 molal.

A la vista de los datos obtenidos se puede concluir que en los procesos de activación alcalina ha habido una reacción de los carbonatos presentes en la muestra original con la disolución alcalina, formando probablemente carbosilicatos y carboaluminatos [33-34]. Las pérdidas asociadas en el intervalo entre 400-800 ºC, son similares para ambos precursores, ligeramente mayores para HCC Dry, debido a que el material de partida tenía una mayor cantidad de carbonatos.

La forma de las curvas DTG asociadas a carbonatos es distinta, dependiendo del material carbonatado como se puede observar en las curvas DTG de la Fig. 11. Así, para las muestras con HCC Dry, la pérdida en el intervalo 400-600 ºC es mayor que la encontrada para HCC Wet-Cold. Probablemente este hecho puede ser debido a la distinta finura del material de partida.

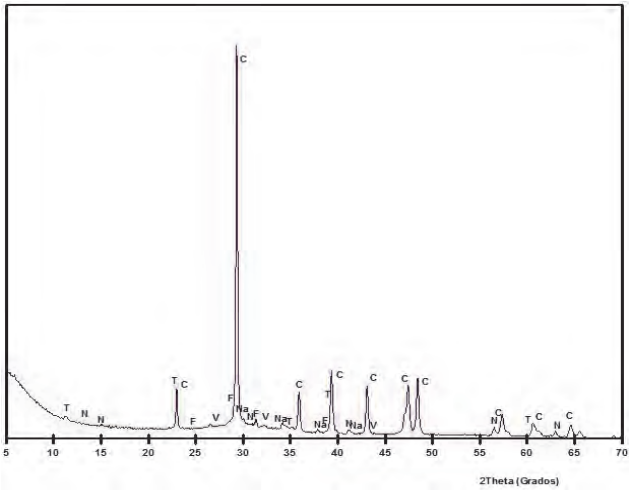

T: Hidrotalcita ($Mg_6Al_2CO_3(OH)_{16}$), N: Natrita (Na_2CO_3), C:Calcita ($CaCO_3$), V:Vaterita ($CaCO_3$), F: Fukalita ($Ca_4Si_2O_6(CO_3)(OH)_2$), P:Natrolita ($Na_2Al_2Si_3O_{10} \cdot 2H_2O$).

Figura 9. Difractograma de rayos X para la pasta con HCC Wet-Cold, con dosificación 9/1.22/0.45, curada 7 días en baño 65 ºC.
Fuente: Los autores.

3.4.3. Microscopía electrónica de barrido (SEM)

En la Fig. 12 se muestras las micrografías SEM para las pastas de HCC Dry y de HCC Wet-Cold, con una dosificación 9/1.22/0.45 y curadas a 65 ºC durante 7 días. Se identifica una gran cantidad de gel, que se atribuye a los compuestos N-A-S-H y C-A-S-H. Este gel presenta una forma poco regular (Fig. 12a) para el HCC Dry, mientras que en el caso de HCC Wet-Cold presenta una cierta estructura fibrosa (Fig.12b), lo cual se puede atribuir a la presencia de zeolitas, que podrían ser producto de la evolución de los geles N-A-S-H: recordemos que fue detectada natrolita por difracción de rayos X.

3.4.4. Resistencia a compresión

Se prepararon morteros de activación alcalina mezclando el precursor, HCC Dry o HCC Wet-Cold, con la solución alcalina y arena fina de módulo de finura 3.05. A continuación las probetas se curaron cámara húmeda a 20 ºC de temperatura y HR superior al 95 %, a edades de 7 y 28 días (sólo para HCC Dry) y también se curaron en baño a 65 ºC con una HR de un 95 %, por 3 y 7 días.

Las dosificaciones analizadas para morteros con HCC Dry curados a 20 ºC corresponden a las concentraciones de Na^+ 7 y 9 mol/kg y las relaciones SiO_2/Na_2O de 1.22 y 1.56. De acuerdo con lo observado en la Tabla 6, se aprecia un aumento de su resistencia a compresión, para las distintas dosificaciones, a medida que se incrementa el tiempo de curado, no observándose diferencias significativas con el aumento de sodio en la dosificación, para una misma relación a/b. Si parece que influya la relación a/b, encontrando que el aumento desde 0.45 a 0.50 supone una ligera reducción en el valor de la resistencia a compresión.

En la Tabla 6 se detallan los valores de las resistencias mecánicas a compresión para 3 y 7 días de morteros con HCC Dry curados a 65 ºC. Se puede observar que la mayor resistencia se obtiene con la dosificación 9/1.22/0.45, alcanzando los 20.18 MPa a los 7 días. Los otros morteros presentan resistencias en el intervalo 14 - 16 MPa. Debe destacarse que no existe una evolución importante al incrementar el curado de 3 a 7 días. Aparentemente, la reacción de geopolimerización se ha desarrollado en los tres primeros días a la temperatura de 65 ºC.

También en la Tabla 6 se relacionan las resistencias a compresión correspondientes a las activaciones alcalinas de HCC Wet-Cold (9 mol/kg de Na^+ y SiO_2/Na_2O=1.22). En este caso, también se produce un ligero descenso de la resistencia mecánica con el incremento de la relación a/b para 3 días, pero a 7 días el mortero con relación a/b de 0.50 presenta una mayor resistencia (19.04 MPa) que para la relación 0.45 (16.74 MPa). Los valores de resistencia a 3 días

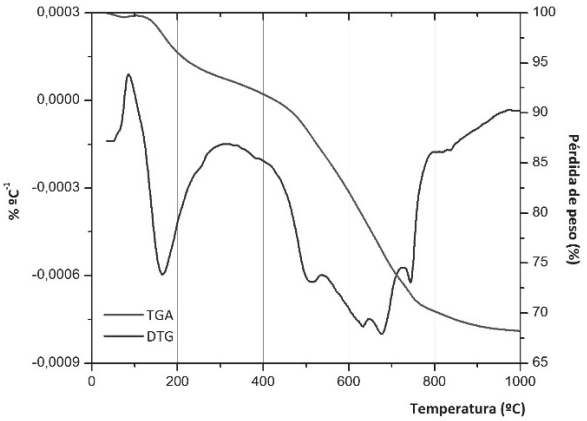

Figura 10. Curvas DTG/TGA correspondientes a la pasta 9/1.22/0.45 con HCC Dry curada durante 7 días a 65 ºC.
Fuente: Los autores.

Tabla 5.
Sistemas geopoliméricos con HCC Dry y HCC Wet-Cold: datos termogravimétricos de las pastas.

Mezcla	HCC	Pérdida de peso		
		Total	35-300 ºC	400-800 ºC
7/1.56/0.45	Dry	30.79	4.74	23.91
	Wet-cold	29.73	6.36	21.22
7/1.56/0.50	Dry	29.62	4.68	22.38
	Wet-cold	29.47	6.48	20.23
9/1.22/0.45	Dry	31.78	6.05	21.71
	Wet-cold	31.81	8.43	19.06
9/1.22/0.50	Dry	30.76	5.54	21.80
	Wet-cold	30.39	8.02	19.92

Fuente: Los autores.

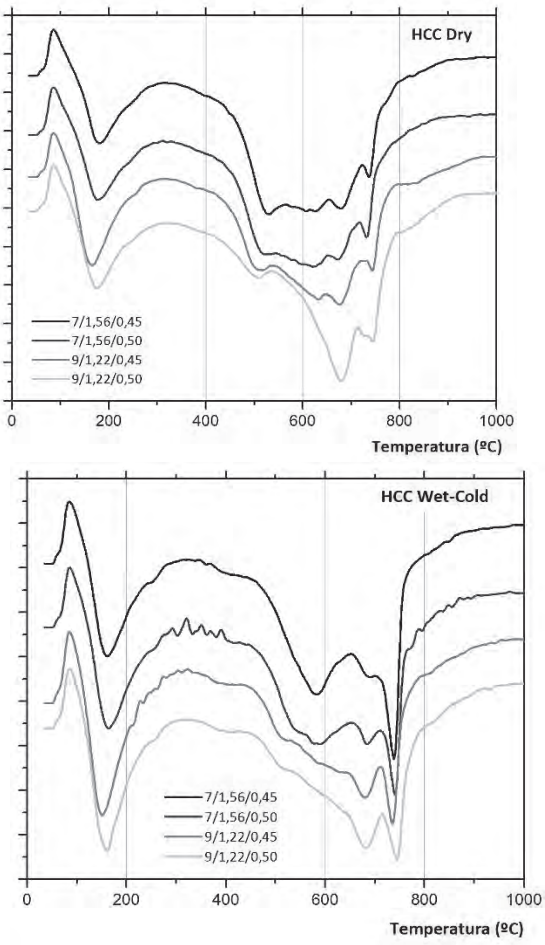

Figura 11. Curvas DTG de las pastas geopoliméricas con HCC Dry y con HCC Wet-Cold, para las distintas dosificaciones a 7 días.
Fuente: Los autores.

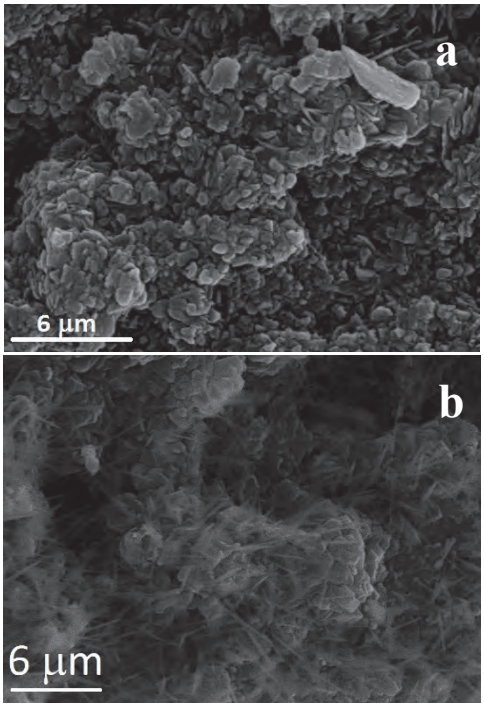

Figura 12. Micrografías SEM de las pastas geopoliméricas curadas 7 días a 65 ºC: a) HCC Dry y b) HCC Wet-Cold. Fuente: Los autores.

Tabla 6.
Resistencias a compresión de morteros HCC Dry y HCC Wet-Cold, curados en cámara húmeda y en baño térmico.

Cámara húmeda, R_c (MPa)				
	a/b	Material	7 días	28 días
7/1.56	0.45	HCC Dry	10.05 ± 0.28	13.35 ± 0.44
	0.50		9.07 ± 0.15	11.52 ±0.26
9/1.22	0.45		9.47 ± 0.25	13.94 ± 0.29
	0.50		7.76 ± 0.33	10.60 ± 0.23
Baño térmico, R_c (MPa)				
	a/b	**Material**	**3 días**	**7 días**
7/1.56	0.45	HCC Dry	16.38 ± 0.78	15.96 ± 0.79
	0.50		15.93 ± 0.39	14.23 ± 0.45
9/1.22	0.45	HCC Dry	19.52 ± 0.94	20.18 ± 1.02
		HCC Wet-Cold	15.85 ± 0.96	16.74 ± 0.66
	0.50	HCC Dry	16.33 ± 0.65	16.16 ± 1.04
		HCC Wet-Cold	13.25 ± 0.88	19.04 ± 0.94

Fuente: Los autores.

para HCC Wet-Cold son ligeramente inferiores a los encontrados para HCC Dry: Ello puede atribuirse a que el precursor HCC Wet-Cold está inicialmente menos carbonatado, de modo que contendrá una menor cantidad de sílice y alúmina amorfas.

4. Conclusiones

El material de partida, cemento hidratado (HydC) fue carbonatado bajo distintas condiciones con el fin de buscar un tiempo óptimo de carbonatación y unas características químicas que hagan del material resultante un buen precursor para activación alcalina. El método en seco (HCC Dry) suponía un tiempo muy largo de obtención, mientras que por la vía húmeda (HCC Wet-Cold) el proceso se redujo en tiempo de forma drástica. Ambos materiales carbonatados pudieron ser activados por medio de una disolución de NaOH y silicato sódico, generando geles cementantes. Las prestaciones mecánicas obtenidas fueron significativas (entre 10 y 20 MPa, dependiendo de las condiciones de curado y de la dosificación). Las matrices geopoliméricas obtenidas fueron caracterizadas microestructuralmente, destacando la formación de nuevas fases conglomerantes y la alteración en las temperaturas de descomposición de los carbonatos presentes con respecto a los materiales carbonatados de partida. Los resultados obtenidos demuestran que es viable la reutilización de fases de cemento hidratadas en sistemas de activación alcalina, por medio de la carbonatación previa.

Agradecimientos

Los autores agradecen al Ministerio de Ciencia e Innovación español por apoyar este estudio a través del Proyecto BIA2011-26947 y financiación FEDER. También agradecen a la Universidad de Magallanes, por apoyar esta investigación a través de la estancia de investigación concedida a Yasna Segura.

Bibliografía

[1] Ahmari, S., Ren, X., Toufigh, V. and Zhang, L., Production of geopolymeric binder from blended waste concrete powder and fly ash. Construction and Building Materials, 35, pp. 718-729, 2012. http://dx.doi.org/10.1016/j.conbuildmat.2012.04.044

[2] Hoenig, V., Hoppe, H. and Emberger, B., Carbon capture technology-options and potentials for the cement industry. PCA R&D Serial Nº 3022, 98 P., 2007.

[3] Del Río, M., Izquierdo, P., Salto, I. y Santa Cruz, J., La regulación jurídica de los residuos de construcción demolición (RCD) en España. El caso de la Comunidad de Madrid. Informes de la Construcción, 62(517), pp. 81-86, 2010. DOI: 10.3989/ic.08.059

[4] Morán-del Pozo, J.M., Valdés, A., Aguado, P.J., Guerra, M.I. y Medina, C., Estado actual de la gestión de residuos de construcción y demolición: Limitaciones. Informes de la Construcción, 63(521), pp. 89-95, 2011. DOI: 10.3989/ic.09.038

[5] Lampris, C., Lupo, R. and Cheeseman, C.R., Geopolymerisation of silt generated from construction and demolition waste washing plants. Waste Management, 29(1), pp. 368-373, 2009. DOI: 10.1016/j.wasman.2008.04.007

[6] Torres, N., Izquierdo, S., Torres, J. and Mejía-de Gutiérrez, R., Resistance of blended concrete containing an industrial petrochemical residue to chloride ion penetration and carbonation. Ingeniería e Investigación, 34(1), pp.11-16, 2014. DOI: 10.15446/ing.investig. v34n1. 38730

[7] Torres, N. and Torres, J., Using spent fluid catalytic cracking (FCC) catalyst as pozzolanic addition - a review. Ingeniería e Investigción, 30(2), pp. 35-42, 2010.

[8] Khale, D. and Chaudhary, R., Mechanism of geopolymerization and factors inuencing its development: A review. Journal of Materials Science, 42(3), pp. 729-746, 2007. DOI: 10.1007/s10853-006-0401-4

[9] Zhang, Z., Provis, J.L., Reid, H. and Wang, A., Geopolymer foam concrete: An emerging material for sustainable construction. Construction and Building Materials, 56, pp. 113-127, 2014. DOI: 10.1016/j.conbuildmat.2014.01.081

[10] Duxson, P., Provis, J., Lukey, G.C. and van Deventer, J., The role of inorganic polymer technology in the development of "green concrete". Cement and Concrete Research, 37(12) pp. 1590-1597, 2007. DOI: 10.1016/j.cemconres.2007.08.018

[11] Tailby, J. and MacKenzie, K., Structure and mechanical properties of aluminosilicate geopolymer composites with Portland cement and its

constituent minerals. Cement and Concrete Research, 40(5), pp. 787-794, 2010. DOI: 10.1016/j.cemconres.2009.12.003
[12] Duxson, P., Fernández-Palomo, A., Provis, J.L., Lukey, G.C., Palomo, A. and van Deventer, J., Geopolymer technology: The current state of the art. Journal of Materials Science, 42(9), pp. 2917-2933, 2006. DOI: 10.1007/s10853-006-0637-z
[13] Puertas, F. and Torres-Carrasco, M., Use of glass waste as an activator in the preparation of alkali-activated slag. Mechanical strength and paste characterisation. Cement and Concrete Research, 57, pp. 95-104, 2014. DOI: 10.1016/j.cemconres.2013.12.005
[14] Kovalchuk, G., Fernández-Jiménez, A. and Palomo, A., Alkali-activated fly ash: Effect of thermal curing conditions on mechanical and microstructural development - Part II. Fuel, 86(3), pp. 315-322, 2007. DOI: 10.1016/j.fuel.2006.07.010
[15] Molina, D., Arcila, J and Gutiérrez, R., Mechanical and thermal performance of a geopolymeric and hybrid material based on fly ash. DYNA, 83(195), pp. 216-223, 2016. DOI: 10.15446/dyna.v83n195.50824
[16] Tashima, M., Akasaki, J., Castaldelli, V.N., Soriano, L., Monzó, J., Payá, J. and Borrachero, M.V., New geopolymeric binder based on fluid catalytic cracking catalyst residue (FCC). Materials Letters, 80, pp.50-52, 2012. DOI: 10.1016/j.matlet.2012.04.051
[17] Tashima, M., Akasaki, J., Melges, J., Soriano, L., Monzó, J., Payá, J. and Borrachero, M.V., Alkali activated materials based on fluid catalytic cracking catalyst residue (FCC): Influence of SiO_2/Na_2O and H_2O/FCC ratio on mechanical strength and microstructure. Fuel, 108, pp. 833-839, 2013. DOI: 10.1016/j.fuel.2013.02.052
[18] Reig, L., Tashima, M.M., Borrachero, M.V., Monzó, J., Cheeseman, C.R. and Payá, J., Properties and microstructure of alkali-activated red clay brick waste. Construction and Building Materials, 43, pp. 98-106, 2013. DOI: 10.1016/j.conbuildmat.2013.01.031
[19] Reig, L., Tashima, M.M, Soriano, L., Borrachero, M.V., Monzó, J. and Payá, J., Alkaline activation of ceramic waste materials. Waste and Biomass Valorization, 4(4), pp. 729-736, 2013. DOI: 10.1007/s12649-013-9197-z
[20] Tashima, M.M, Soriano, L., Borrachero, M.V., Monzó, J. and Payá, J., Effect of curing time on microstructure and mechanical strength development of alkali activated binders based on vitreous calcium aluminosilicate (VCAS). Bulletin of Materials Science, 36(2), pp. 245-249, 2013. DOI: 10.1007/s12034-013-0466-z
[21] UNE-EN12620:2003+A1:2009., Áridos para hormigón, AENOR. 2009.
[22] UNE-EN933-11:2009., Ensayos para determinar las propiedades geométricas de los áridos. Parte 11: Ensayo de clasificación de los componentes de los áridos gruesos reciclados, AENOR. 2009.
[23] López-Gayarre, F., Serna, P., Domingo-Cabo, A., Serrano-López, M.A. and López-Colina, C., Influence of recycled aggregate quality and proportioning criteria on recycled concrete properties. Waste management, 29(12), pp. 3022-3028, 2009. DOI: 10.1016/j.wasman.2009.07.010
[24] Ulloa, V., García-Monzó, J.M., Pelufo, M.J., Domingo, A. and Serna, P., New views on effect of recycled aggregates on concrete compressive strength. Materials Journal, 110(6), pp.687-696, 2013.
[25] Secretaria General Técnica. EHE - 08 Instrucción de hormigón estructural, 2011.
[26] Gastaldi, D., Canonico, F., Capelli, L., Buzzi, L., Boccaleri, E. and Irico, S., An investigation on the recycling of hydrated cement from concrete demolition waste. Cement and Concrete Composites, 61, pp. 29-35, 2015. DOI: 10.1016/j.cemconcomp.2015.04.010
[27] Shui, Z., Xuan, D., Wan, H. and Cao, B., Rehydration reactivity of recycled mortar from concrete waste experienced to thermal treatment. Construction and Building Materials, 22(8), pp. 1723-1729, 2008. DOI: 10.1016/j.conbuildmat.2007.05.012
[28] UNE-EN197-1:2011., Cemento. Parte 1: Composición, especiaciones y criterios de conformidad de los cementos comunes. AENOR. 2011.
[29] Payá, J., Borrachero, M.V., Monzó, J., Soriano, L. and Tashima, M.M., A new geopolymeric binder from hydrated-carbonated cement. Materials Letters, 74, pp. 223-225, 2012. DOI: 10.1016/j.matlet.2012.01.132
[30] Basheer, P.A.M., Rankin, G.I.B., Long, A.E. and Russell, D., Effect of relative humidity and air permeability on prediction of the rate of carbonation of concrete. Proceedings of the ICE - Structures and Buildings, 146(3), pp. 319-326, 2001. DOI: 10.1680/stbu.2001.146.3.319
[31] Liu, J., Xu, D., Xiong, L., Hills, C., Carey, P. and Gardner, K., Comparison of properties of traditional and accelerated carbonated solidified/stabilized contaminated soils. Journal of Environmental Sciences, 20(5), pp. 593-598, 2008. DOI: 10.1016/S1001-0742(08)62099-9
[32] Rodríguez-Martínez, E., Efecto de incorporación de materiales basados en sílice sobre las propiedades de matrices de cemento Pórtland y activadas alcalinamente, Tesis Dr., Universitat Politècnica de Valencia, Valencia, España, 2012, 452 P. DOI: 10.4995/Thesis/10251/17400
[33] Rodríguez, E., Bernal, S., Provis, J., Payá, J., Monzó, J. and Borrachero, M.V., Structure of portland cement pastes blended with sonicated silica fume. Journal of Materials in Civil Engineering, 24(10), pp. 1295-1304, 2012. DOI: 10.1061/(ASCE)MT.1943-5533.0000502
[34] Ismail, I., Bernal, S., Provis, J., Hamdan, S. and van Deventer, J., Drying - induced changes in the structure of alkali - activated pastes. Journal of Materials Science, 48(9), pp. 3566-3577, 2013. DOI: 10.1007/s10853-013-7152-9

Y.P. Segura-Sierpe, es MSc. de una Universitat Politècnica de València, España y profesora del Dpto. de Ingeniería en Construcción de la Universidad de Magallanes, Chile. Sus intereses de investigación incluyen la valoración de los residuos de construcción y morteros geopoliméricos.
ORCID: 0000-0001-6394-5392

M.V. Borrachero-Rosado, es Dra. de la Universidad de Murcia, España y profesora del Instituto de Ciencia y Tecnología del Hormigón de la Universitat Politècnica de València, Valencia, España. Sus intereses de investigación incluyen subproductos industriales utilizados como reemplazo de cemento Pórtland.
ORCID: 0000-0002-7873-0658

J.M. Monzó-Balbuena, es Dr. de la Universitat de València, Valencia, España y profesor de química de los materiales de construcción en el Instituto de Ciencia y Tecnología del Hormigón en la Universitat Politècnica de València, España. Sus intereses de investigación incluyen química analítica, materiales de construcción, el reciclaje y los materiales de construcción no convencionales para los países en desarrollo.
ORCID: 0000-0002-3657-3076

J. Payá-Bernabeu, es Dr. de la Universitat de València, España y profesor de química de los materiales de construcción en el Instituto de Ciencia y Tecnología del Hormigón en la Universitat Politècnica de València, España. Sus intereses de investigación incluyen el uso de subproductos industriales y residuos, hormigón geopolimérico y ensayos no destructivos aplicados a hormigón.
ORCID: 0000-0001-7425-5311

DYNA
83 (196), April 2016
is an edition consisting of 250 printed issues
which was finished printing in the month of January of 2016
in Todograficas Ltda. Medellín - Colombia

The cover was printed on Propalcote C1S 250 g,
the interior pages on Hanno Mate 90 g.
The fonts used are Times New Roman, Imprint MT Shadow

- Variation in risk category in methods of calculation of the modified fire load density
- Application of the Delphi Method for the inclusion of externalities in occupational safety and health analysis
- Occupational risk assessment at Olive Oil Mills: Limitations and new perspectives
- Absenteeism and presenteeism costs from occupational accidents with WRMSDs in a Portuguese hospital
- Identification of areas of intervention for public safety policies using multiple correspondence analysis
- A qualitative analysis on occupational health and safety conditions at small construction projects in the Brazilian construction sector
- Emerging risk in the construction industry: Recommendations for managing exposure to nanomaterials
- Differences in muscular activity between obese and non-obese workers during manual lifting
- Impact of a workplace exercise program on neck and shoulder segments in office workers
- Occurrence of a skarn-type mineralogy found in Ciénaga Marbles, located in the NW foothills of the Santa Marta Massif (Colombia)
- Decontamination of industrial textile wastewater using photocatalysis
- Nutritional composition of meals at work and its relationship with manufacturing workers' anthropometric profile and energy expenditure
- Study of a repair technique in carbonated blended mortars: Electrochemical re-alkalization
- The manufacture of a maxillofacial prosthesis from an axial tomography using simulation technologies with a virtual machine tool and four-axis machining
- The influence of design methodology on a designer's emotional parameters and on design results
- Computational simulation of laminar heat convection of nanofluids in a circular tube and squared duct
- Viscoelastic behavior of yellow pitahaya treated with 1-MCP
- Adopting Ecodesign Management Systems in the construction sector. Analysis from the perspective of stakeholders
- Numerical experimentation for the optimal design of reinforced rectangular concrete beams for singly reinforced sections
- A study of co-movements between U.S. and Latin American stock markets: A cross-bicorrelations perspective
- A comparative study for the design of rectangular and circular isolated footings using new models
- Developing a self-regulating soldering iron based on induction heating
- Microstructure and electrical properties of solid electrolytes of fully stabilized zirconia with rare earth mixed oxides
- Analysis of working nanofluids for a refrigeration system
- Synthesis and modification of beta zeolite for use in toluene disproportionation reaction
- Effect of a dual tire pressure on the design parameters of thick asphalt pavements using finite element freeware
- Collaborative goods distribution using the IRP model
- Baseflow analysis using master recession curves and numerical algorithms in mountain basins: Suratá's river and Oro's river (Santander, Colombia)
- Study of the adsorption capacity of Fe(II) dissolved in water by using a mineral rich in Manganese Dioxide (MnO_2) from Colombia
- Preliminary studies on hydrated cement for its reuse in geopolymers

- Variación de la categoría de riesgo en los métodos de cálculo de la densidad de carga de fuego ponderada
- Aplicación del método Delphi para la inclusión de las externalidades en análisis de seguridad y de salud laboral
- Evaluación de riesgos laborales en Almazaras: Limitaciones y nuevas perspectivas
- Costos de accidentes de trabajo con TMOL consecuencia de absentismo y presentismo en un hospital portugués
- Identificación de aéreas de intervención de políticas públicas en seguridad laboral usando análisis de correspondencias múltiple
- Un análisis cualitativo de las condiciones de salud y seguridad en el trabajo en pequeños proyectos de construcción en el sector de la construcción brasileña
- Riesgo emergente en la industria de la construcción: Recomendaciones para controlar la exposición a nanomateriales
- Diferencias en la actividad muscular entre trabajadores obesos y no obesos durante la elevación manual de cargas
- Impacto de un programa de ejercicio en el trabajo en los segmentos de cuello y hombros en los trabajadores de oficina
- Ocurrencia de una mineralogía tipo skarn reconocida en los Mármoles de Ciénaga, estribaciones NW del Macizo de Santa Marta (Colombia)
- Descontaminación de aguas de desecho de la industria textil usando Fotocatálisis
- La alimentación de los trabajadores en la industria y su relación con los datos antropométricos y el gasto energético
- Estudio de una técnica de reparación aplicada a morteros adicionados carbonatados: Realcalinización electroquímica
- Manufactura de una prótesis maxilofacial, a partir de una tomografía axial, usando tecnologías de simulación en una máquina herramienta virtual y maquinado de cuatro ejes
- Influencia de la metodología de diseño en los parámetros emocionales del diseñador y en los resultados del diseño
- Simulación computacional de convección de calor laminar de nanofluidos en tubo circular y ducto cuadrado
- Comportamiento viscoelástico de pitahaya amarilla tratada con 1-MCP
- Adopción de Sistemas de Gestión de Ecodiseño en el sector de la construcción. Análisis de la perspectiva de los diferentes agentes involucrados
- Experimentación numérica para el diseño óptimo de vigas rectangulares de concreto reforzado para secciones simplemente reforzadas
- Un estudio de comovimientos entre las bolsas de valores de Estados Unidos de Norteamérica y América Latina: Una perspectiva de la bicorrelación cruzada
- Un estudio comparativo para diseño de zapatas aisladas de forma rectangular y circular usando nuevos modelos
- Desarrollo de un cautín autorregulable basado en calentamiento por inducción
- Microestructura y propiedades eléctricas de electrólitos sólidos de circonia totalmente estabilizada con óxidos mixtos de tierras raras
- Análisis de nanofluidos para un sistema de refrigeración
- Síntesis y modificación de la zeolita beta para su uso en la reacción de desproporción de tolueno
- Efecto de la presión de contacto de una carga dual sobre los parámetros de diseño de pavimentos asfalticos gruesos usando software libre de elementos finitos
- Distribución colaborativa de mercancías utilizando el modelo IRP
- Análisis de flujo base usando curvas maestras de recesión y algoritmos numéricos en cuencas de montaña: Cuenca del río Suratá y cuenca del Río de Oro (Santander, Colombia)
- Estudio de la capacidad de adsorción de Fe(II) disuelto en agua usando un mineral rico en Dióxido de Manganeso (MnO_2) de origen colombiano
- Estudios preliminares sobre cemento hidratado para su reutilización en geopolímeros

DYNA
Publication admitted to the
Sistema Nacional de Indexación y Homologación de
Revistas Especializadas CT+I - PUBLINDEX, Category A1

Red Colombiana de Revistas de Ingeniería

UNIVERSIDAD NACIONAL DE COLOMBIA
SEDE MEDELLÍN
FACULTAD DE MINAS